

## A I C h E

*Published by the American Institute of Chemical Engineers*

## CONTENTS

Heats of Mixing of Liquids

Rate Studies in Tubular Reactors

Performance of Packed Columns: Part IV

Densities of Liquid-acetone—water Solutions up to Their Normal Boiling Points

Absorption and Stripping-factor Functions for Distillation Calculation by Manual- and Digital-computer Methods

A Study of Laminar-flow Heat Transfer in Tubes

Dynamics of Liquid Agitation in the Absence of an Air-liquid Interface

Foam-frothate Concentration Relations in Foam Fractionation

Ion Exclusion Equilibria in the System Glycerol—sodium chloride—water—Dowex-50

Equilibrium in the System  $\text{Cu}^{++}$ — $\text{Na}^{+}$ —Dowex-50Vapor-liquid Equilibria of Benzene—*n*-hexane and Benzene-cyclohexane Systems

Diffusion in Three-component Gas Mixtures

Simplified Flow Calculations for Tubes and Parallel Plates

Separation of Liquids by Thermal Diffusion

Radioisotope Technique for the Determination of Flow Characteristics in Liquid-liquid Extraction Columns

Reaction Kinetic Studies: Catalytic Dehydrogenation of Sec-butyl Alcohol to Methyl Ethyl Ketone

Phase Behavior of Hydrogen—light-hydrocarbon Systems

Effect of Wall Roughness on Convective Heat Transfer in Commercial Pipes

Control of Continuous-flow Chemical Reactors

Volumetric and Phase Behavior of the Hydrogen—*n*-hexane System

Flow of Steam-water Mixtures in a Heated Annulus and Through Orifices

Hydraulics of Wetted-wall Columns

Some Remarks on Longitudinal Mixing or Diffusion in Fixed Beds

Mass Transfer in a Continuous-flow Mixing Vessel

Ion Exchange Separation of Gram Quantities of Americium from a Kilogram of Lanthanum

Approximate Operational Calculus in Chemical Engineering

Fluidization and Sedimentation of Spherical Particles

H. W. Schnaible, H. C. Van  
Ness, and J. M. Smith  
Eric Weger and H. C. Hoelscher  
H. L. Shulman and  
J. E. Margolis  
K. T. Thomas and  
R. A. McAllisterWayne C. Edmister  
Joseph F. Gross and  
H. C. Van NessDavid S. Laity and  
Robert E. TreybalVictor Kevorkian and  
Elmer L. Gaden, Jr.Edward L. Shurts and  
Robert R. WhiteH. C. Subba Rao and  
M. M. DavidV. N. Kumarkrishna Rao, D. R.  
Swami, and M. Narasinga Rao

H. L. Toor

R. R. Rothfus, D. H. Archer,  
I. C. Klimas, and K. G. Sikchi

John E. Powers and C. R. Wilke

S. E. Markas and  
R. B. BeckmannJoseph J. Perona and  
George ThodosA. L. Benham, D. L. Katz, and  
R. B. WilliamsJ. W. Smith and Norman Epstein  
Oleg Bilous, H. D. Block, and  
E. L. PiretW. B. Nichols, H. H. Reamer,  
and B. H. Sage

John W. Hoopes, Jr.

E. R. Michalik

Rutherford Aris and  
Neal R. AmundsonD. W. Humphrey and  
H. C. Van NessD. E. Armstrong, L. B. Asprey,  
J. S. Coleman, T. K. Keenan,  
L. E. LaMar, and  
R. A. Penneman

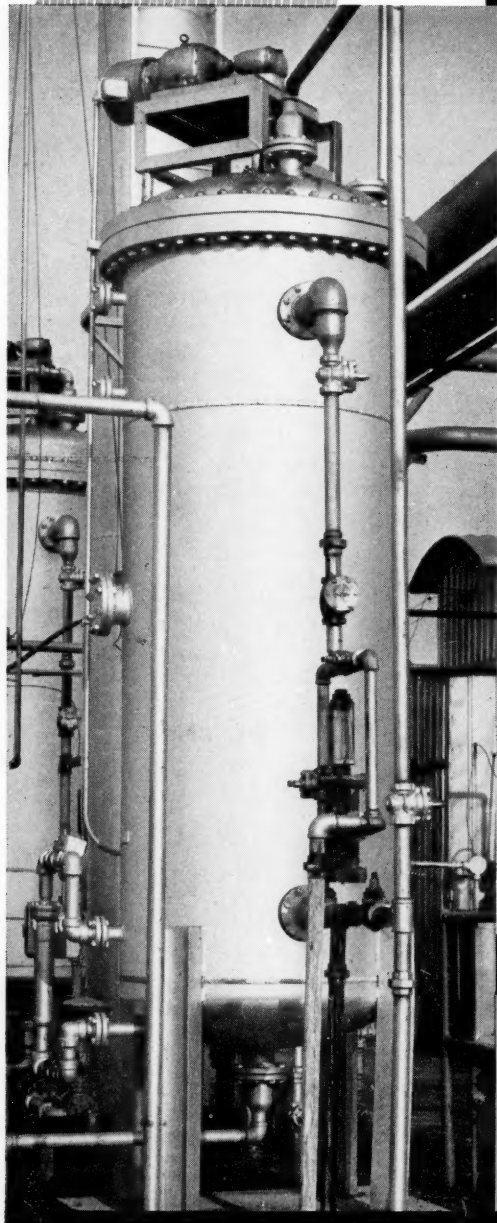
Stuart W. Churchill

Thomas J. Hanratty and  
Abdemannan Bandukwala

# Practical, Efficient, and Economical **SOLVENT EXTRACTION**

with

## **YORK-SCHEIBEL LIQUID-LIQUID EXTRACTORS**



The YORK-SCHEIBEL patented multi-stage extraction column:

- Is ideal for the common multi-stage, countercurrent extractions in which the feed material is contacted with a single solvent.
- Is effective and efficient for fractional liquid extraction in which the feed material is contacted with two selective and immiscible solvents flowing countercurrent through the column.
- May be designed for liquid streams carrying solids in suspension.

The columns employ agitators in each stage to insure complete liquid-liquid contacting. The phase separating sections between the mixing zones consist of wire mesh packing, a new arrangement of baffles, or both baffles and packing.

High stage efficiencies are obtained even with difficult-to-separate materials. Here are a few of the extractions for which York-Scheibel columns have no equal:

- close boiling mixtures
- non-volatile mixtures
- structural isomers
- materials from dilute solutions
- azeotropic mixtures
- impurities and color bodies
- heat sensitive materials

Check these outstanding features:

- ✓ Single, compact column
- ✓ High efficiency
- ✓ High throughput capacity
- ✓ Low cost per stage
- ✓ Efficient laboratory, pilot plant and large scale performance
- ✓ Low stage height

SEND INFORMATION on your requirements and let York engineers recommend the best design for your conditions.

# **YORK**

**YORK PROCESS EQUIPMENT CORP.**  
4 Central Avenue, West Orange, N. J.

Send for latest literature giving complete details



# A I C h E JOURNAL

JUNE 1957 • VOL. 3, NO. 2

## PUBLISHER

F. J. Van Antwerpen

## EDITOR

Harding Bliss

## ADVERTISING MANAGER

L. T. Dupree

## ADVISORY BOARD

C. M. Cooper, O. E. Dwyer, W. C. Edmister, E. R. Gilliland, A. N. Hixson,  
H. F. Johnstone, W. R. Marshall, Jr., R. H. Newton, R. L. Pigford,  
E. L. Piret, J. M. Smith, Theodore Vermeulen, R. R. White, R. H. Wilhelm

The A.I.Ch.E. Journal, an official publication of the American Institute of Chemical Engineers, is devoted in the main to theoretical developments and research in chemical engineering and allied branches of engineering and science. Manuscripts should be submitted to the New York office.

Computing Machines and the Patterns of Research . . . . .	145
Heats of Mixing of Liquids . . . . . <i>H. W. Schnaible, H. C. Van Ness, and J. M. Smith</i>	147
Rate Studies in Tubular Reactors . . . . . <i>Eric Weger and H. C. Hoelscher</i>	153
Performance of Packed Columns: Part IV . . . . . <i>H. L. Shulman and J. E. Margolis</i>	157
Densities of Liquid-acetone—water Solutions up to Their Normal Boiling Points <i>K. T. Thomas and R. A. McAllister</i>	161
Absorption and Stripping-factor Functions for Distillation Calculation by Manual- and Digital-computer Methods . . . . . <i>Wayne C. Edmister</i>	165
A Study of Laminar-flow Heat Transfer in Tubes . . . . . <i>Joseph F. Gross and H. C. Van Ness</i>	172
Dynamics of Liquid Agitation in the Absence of an Air-liquid Interface . . . . . <i>David S. Laity and Robert E. Treybal</i>	176
Froth-frothate Concentration Relations in Foam Fractionation . . . . . <i>Victor Kevorkian and Elmer L. Gaden, Jr.</i>	180
Ion Exclusion Equilibria in the System Glycerol—sodium chloride—water—Dowex-50 <i>Edward L. Shurts and Robert R. White</i>	183
Equilibrium in the System $\text{Cu}^{++}$ — $\text{Na}^{+}$ —Dowex-50 . . . . . <i>H. C. Subba Rao and M. M. David</i>	187
Vapor-liquid Equilibria of Benzene— <i>n</i> -hexane and Benzene-cyclohexane Systems <i>V. N. Kumarkrishna Rao, D. R. Swami, and M. Narasinga Rao</i>	191
Diffusion in Three-component Gas Mixtures . . . . . <i>H. L. Toor</i>	198
Simplified Flow Calculations for Tubes and Parallel Plates <i>R. R. Rothfus, D. H. Archer, I. C. Klimas, and K. G. Sikchi</i>	208
Separation of Liquids by Thermal Diffusion . . . . . <i>John E. Powers and C. R. Wilke</i>	213
Radioisotope Technique for the Determination of Flow Characteristics in Liquid-liquid Extraction Columns <i>S. E. Markas and R. B. Beckmann</i>	223
Reaction Kinetic Studies: Catalytic Dehydrogenation of Sec-butyl Alcohol to Methyl Ethyl Ketone <i>Joseph J. Perona and George Thodos</i>	230
Phase Behavior of Hydrogen—light-hydrocarbon Systems . . . . . <i>A. L. Benham, D. L. Katz, and R. B. Williams</i>	236
Effect of Wall Roughness on Convective Heat Transfer in Commercial Pipes . . . . . <i>J. W. Smith and Norman Epstein</i>	242
Control of Continuous-flow Chemical Reactors . . . . . <i>Oleg Bilous, H. D. Block, and E. L. Piret</i>	248
Volumetric and Phase Behavior of the Hydrogen— <i>n</i> -hexane System <i>W. B. Nichols, H. H. Reamer, and B. H. Sage</i>	262
Flow of Steam-water Mixtures in a Heated Annulus and Through Orifices . . . . . <i>John W. Hoopes, Jr.</i>	268
Hydraulics of Wetted-wall Columns . . . . . <i>E. R. Michalik</i>	276
Some Remarks on Longitudinal Mixing or Diffusion in Fixed Beds . . . . . <i>Rutherford Aris and Neal R. Amundson</i>	280
Mass Transfer in a Continuous-flow Mixing Vessel . . . . . <i>D. W. Humphrey and H. C. Van Ness</i>	283
Ion Exchange Separation of Gram Quantities of Americium from a Kilogram of Lanthanum <i>D. E. Armstrong, L. B. Asprey, J. S. Coleman, T. K. Keenan, L. E. LaMar, and R. A. Penneman</i>	286
Approximate Operational Calculus in Chemical Engineering . . . . . <i>Stuart W. Churchill</i>	289
Fluidization and Sedimentation of Spherical Particles . . . . . <i>Thomas J. Hanratty and Abdemannan Bandukwala</i>	293
Communications to the Editor . . . . .	8J
Exchange . . . . .	10J

Publication Office, Richmond, Virginia. Published quarterly in March, June, September, and December by the American Institute of Chemical Engineers, 25 West 45 Street, New York 36 New York. Manuscripts and other communications should be sent to the New York office. Correspondence with the editor may be addressed to him at Yale University, 225 Prospect Street, New Haven 11, Connecticut. Statements and opinions in the *A.I.Ch.E. Journal* are those of the contributors, and the American Institute of Chemical Engineers assumes no responsibility for them. Subscriptions: one year, member \$4.50, nonmember \$9.00; two years, member \$7.50, nonmember \$15.00; additional yearly postage, Canada 50 cents, Pan American Union \$1.50, other foreign \$2.00 (foreign subscriptions payable in advance). Single copies: \$3.00. Second-class mail privileges authorized at Richmond, Virginia. Copyright 1957 by the American Institute of Chemical Engineers. National headquarters of A.I.Ch.E. is concerned about nondelivery of copies of the *A.I.Ch.E. Journal* and urgently requests subscribers to give prompt notification of any change of address. Sixty days must be allowed for changes to be made in the records.



## New Title for Chemical Engineers

### PROJECT ENGINEERING of PROCESS PLANTS

By Howard F. Rase, *The University of Texas*; and M. H. Barrow, *Foster Wheeler Corporation*. A guide to the practical application of process design principles in industry, this book is written in accordance with modern techniques of project organization, planning, and execution. The authors first describe the steps and methods of plant design in the logical sequence followed in industry, discussing as well the business phases of the project which must be understood by all who are involved. They then give practical details on the design and selection of the major items of equipment used in a process plant. 1957. 692 pages. \$14.25.

### PROPERTIES of PETROLEUM RESERVOIR FLUIDS

By Emil J. Burcik, *The Pennsylvania State University*. A logical and detailed coverage of the fundamental concepts on which petroleum engineering is based—as they pertain to reservoir fluids. It describes not only the properties of ideal fluids but also provides empirical correlations necessary for a more realistic approach to the complex systems that exist in petroleum reservoirs. Practical applications of the concepts and principles are presented and illustrated with many example calculations. The author incorporates all data, tables, and correlation charts needed to solve a wide variety of problems commonly encountered in this phase of petroleum engineering. 1957. 190 pages. \$7.50.

### THERMAL POWER from NUCLEAR REACTORS

By A. Stanley Thompson, *General Atomic Division of General Dynamics Corp.*, and Oliver E. Rodgers, *Studebaker-Packard Corp.* Discusses expertly the three most important factors of nuclear power: the generation of heat in reactors; the removal of heat from reactors; and the use of this heat in thermal power plants. Without overstressing familiar background materials, it covers reactor design thoroughly, building upon engineering method, and uses techniques familiar to the engineer to solve problems in the field of nuclear power. "... well written and easy to follow ... presents an excellent starting point for the many complex problems of nuclear power plants."—M. A. Schultz, in the *Review of Scientific Instruments*. 1956. 229 pages. \$7.25.

### HIGH-TEMPERATURE TECHNOLOGY

Edited by I. E. Campbell, *Battelle Memorial Institute*, and sponsored by *The Electrochemical Society*. Thirty-five experts give a succinct picture of the new materials, new methods of production, and new measuring techniques which have been discovered in the development of special materials of construction for use at very high temperatures. "This volume makes a very substantial contribution to the literature of high-temperature technology. ... Of particular value are the many hundreds of literature references. The work should be of special interest to engineers and others engaged in the more conventional high-temperature processes and in the newer fields of jet reactions." E. W. Slocum, in the *A.I.Ch.E. Journal*. 1956. 526 pages. \$15.00.

### VACUUM DEPOSITION of THIN FILMS

By L. Holland, *W. Edwards & Co., London*. This work covers in detail: plant design, film production, and the physical properties of thin films, irrespective of the particular purpose for which the film is required. 1956. 541 pages. \$10.00.

### SCIENTIFIC FRENCH:

#### A Concise Description of the Structural Elements of Scientific and Technical French

By William N. Locke, *The Massachusetts Institute of Technology*. 1957. 112 pages. \$2.25.

### SCIENTIFIC GERMAN:

#### A Concise Description of the Structural Elements of Scientific and Technical German

By George E. Condoyannis, *Saint Peter's College*. 1957. 163 pages. \$2.50.

Send for on-approval copies.

JOHN WILEY & SONS, Inc., 440 Fourth Avenue, New York 16, N. Y.



## *Computing Machines and the Patterns of Research*

Certainly one of the most important developments of recent times is the computing machine that can accomplish detailed calculations of enormous intricacy in a very short time. These machines are now becoming available in such a wide variety of places and at such reasonable cost that they are bound to have a great influence on chemical engineering generally and on research in particular. One aspect of this consequence seems very much worth considering. A computing machine, at least at present, cannot examine experimental results for the fundamental parameters or constants of the problem. It cannot analyze; it can only synthesize. If the appropriate equations and known values of the basic parameters are fed to the machine, it can put them all together and present us quickly with results to be expected in an experiment or for a given set of design conditions. It is important to recognize this distinction between analysis and synthesis because it will have a vital bearing on future trends in research programs.

The simplified experiment, the clean-cut determination of one dependent variable or one measurable quantity, may be coming back into prominence. In the relatively recent past the simplified experiment has been somewhat discredited because it did not closely approximate a real application with which an engineer might be faced. Since this application was often of paramount importance, experiments have been developing into closer and closer approaches to the exact problem at hand until the difference between experiment and design is essentially only that of size.

As an example, one may cite the study of mass transfer phenomena in fixed beds. We have always recognized that the mechanism of this process involves both solid and fluid diffusion, and it is becoming more and more apparent that axial diffusion, as well, plays a big part. Yet, despite this recognition, there have been very few attempts to measure separately these funda-

mental quantities. We have preferred, in the past, to set up and solve (with many simplifying assumptions) the appropriate differential equations, to devise an elaborate experiment which closely resembles the ultimate application, and to determine the fundamental parameters by careful and detailed studies of the experimental results, in this case the "break-through" curves. This procedure has proved to be very difficult, and there have been many areas of disagreement in methods and results. It is also noteworthy that the addition of axial diffusion complicates the problems so much that the appropriate differential equations have not been solved, at least for finite bed lengths, and this approach becomes impossible. While the fixed-bed problems are particularly good examples of this difficulty, there are certainly several more which come to mind such as the treatment of consecutive and simultaneous reactions and of nonisothermal reactions, the analysis of shock-tube results, and heat and mass transfer in catalytic converters.

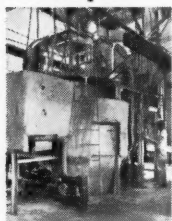
Perhaps it is time to abandon this analytical experimental approach and return to the simplest possible experiments. Equipment and procedure should be devised to permit the measurement of solid diffusivities alone, fluid-phase transfer coefficients or even "film" thicknesses under simplified circumstances, axial diffusion coefficients without transfer and without any other effects. The last approach, incidentally, has been begun by several research groups and is proving interesting indeed.

These simplified experiments should yield values of the basic constants and their dependence on such operating variables as flow rates, temperature, and pressure. For a given set of operating conditions, one has only to evaluate the parameters and "plug them into" the machine. The machine can tell us what results are to be expected probably as accurately as we could measure them and certainly a great deal more quickly.

H.B.

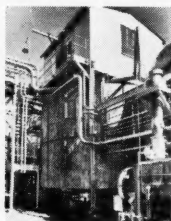
*Spray Drying is the modern labor-saving process used to produce products with greater sales appeal, often at reduced production costs. Numerous processes in use today are subject to the same modernization as has been applied, with Bowen cooperation, in many leading industries:*

Electronic industry benefits by a high quality finely blended homogeneous Titania material which is easily extruded for special dielectric parts . . .



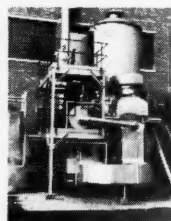
**FIRST  
SPRAY DRIED  
BY  
American  
Lava**

Evaporation loss of crude oil can now be reduced by 80-90 per cent with nitrogen-filled microscopic phenolic spheres which form vapor seal on stored crude oil . . .



**FIRST  
SPRAY DRIED  
BY  
Bakelite**

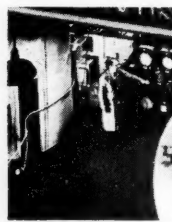
New sterile Plasma Volume Expander for intravenous injections has saved countless lives in both military and civilian use . . .



**FIRST  
SPRAY DRIED  
BY  
Commercial  
Solvents**

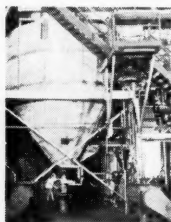
## Developing New Products on Bowen SPRAY DRYERS

Patented Bowen air cooling features made possible the large production of thermoplastic and thermosetting resin powders . . .



**FIRST  
SPRAY DRIED  
BY  
Plaskon**

Controlled spherical shape, free-flowing characteristics and high density of spray dried Ferrites, makes possible superior performance of electrical cores . . .



**FIRST  
SPRAY DRIED  
BY  
Stackpole  
Carbon**

And, many other companies with whom Bowen has worked have pioneered with Bowen Equipment to produce a FIRST-of-its-kind product. Bowen engineers are available to work with you to incorporate Spray Drying in the production of your products. Whether you are producing a high cost quality product or a basic material in quantity where low cost is the determining factor, you should investigate Spray Drying.



*Write for this  
Interesting Book*

**THE BOWEN  
LABORATORY  
SPRAY DRYER**

*We will be glad to  
send it - No obligation*

**BOWEN ENGINEERING, INC.**  
NORTH BRANCH 12, NEW JERSEY

**BOWEN SPRAY DRYERS**  
*Always Offer You More!*

**Recognized Leader in Spray Dryer Engineering Since 1926**



# Heats of Mixing of Liquids

H. W. SCHNAIBLE, H. C. VAN NESS, and J. M. SMITH

Purdue University, Lafayette, Indiana

Experimental data are presented for the heats of mixing of liquids at 25°C. and 1 atm. pressure for ten binary and five ternary systems. For nonpolar binary systems a two-constant equation has been developed which correlates the data within experimental accuracy. Several equations which have been proposed for the calculation of ternary heats of mixing from binary data are tested for the systems studied. The method of Jost and Röck (4) for determining the constants in power-series functions from experimental data is considered.

Most of the many recent studies of the heats of mixing of liquids have been carried out to establish new theories or to test existing theories about the nature of liquids and solutions. Heat-of-mixing data are of practical value in industrial design; Tsao and Smith (13) have pointed out that for solutions which deviate appreciably from ideal behavior the heat of mixing may be of considerable importance. Moreover, with the development of extractive and azeotropic distillation processes, a demand has arisen for heat-of-mixing data for ternary systems. Since such data are more difficult to obtain than data for binary systems, it is desirable to develop methods for the prediction of heats of mixing for ternary systems from binary data.

This paper is a continuation of the work of Tsao and Smith and has the following objectives: (1) to evaluate and develop correlation procedures for binary systems, (2) to present experimental data for binary and ternary mixtures, and (3) to evaluate the different methods of predicting heats of mixing for ternary systems from binary data. The term *heat of mixing* as used in this paper is defined as the change in enthalpy per mole of mixture (or per unit volume of mixture) when the pure components are mixed at constant temperature and pressure.

The experimental apparatus has been described by Tsao and Smith (13), and only very minor modifications were made for the present work. The measurements were made in an isothermal calorimeter suitable for determining heats of mixing for endothermic systems. All data were taken at 25°C. and atmospheric pressure.

## MATERIALS

The materials used in the present work and their specifications are listed below:

Methanol—99.5% pure, distilled with zinc dust and caustic soda  
Toluene—boiling range 0.2°C.; residue after evaporation, 0.001%  
*n*-Heptane—boiling range 0.2°C.

H. W. Schnaible is with Gulf Research and Development Company, Pittsburgh, Pennsylvania; H. C. Van Ness at Rensselaer Polytechnic Institute Troy, New York; and J. M. Smith at University of New Hampshire, Durham, New Hampshire.

Benzene—thiophene free  
*n*-Hexane—99 mole % pure, minimum  
*n*-Octane—99 mole % pure, minimum  
*n*-Nonane—99 mole % pure, minimum  
Cyclohexane—99 mole % pure, minimum

Ethanol—absolute, distilled with zinc dust and caustic soda.

## EXPERIMENTAL RESULTS

Heat-of-mixing data were obtained for the ten binary systems cyclohexane-benzene, toluene-cyclohexane, heptane-

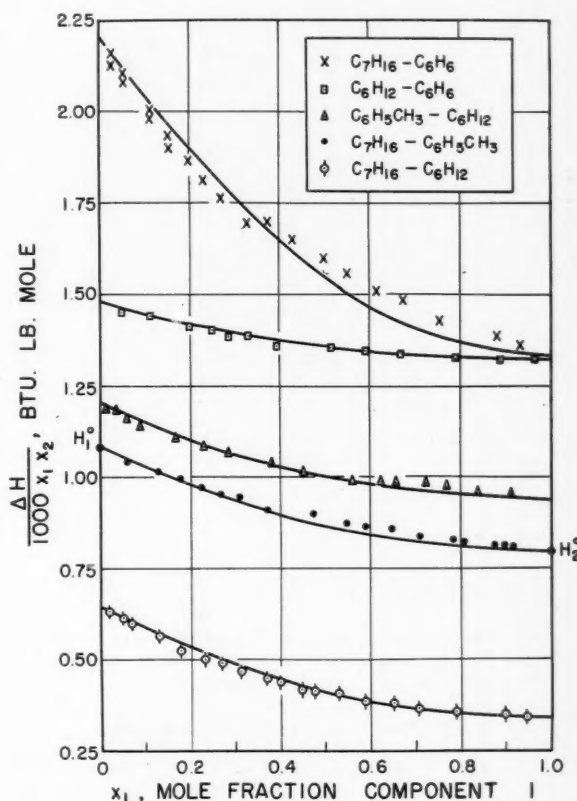


Fig. 1. Heats of mixing for five binary hydrocarbon systems at 25°C.

TABLE 1. HEATS OF MIXING FOR FOUR ALCOHOL-HYDROCARBON SYSTEMS

Values of  $H_{12}/x_1x_2$ , B.t.u./lb. mole, 25°C., 1 atm.

Mole fraction component 1 (alcohol)	Ethanol-benzene	Ethanol-cyclohexane	Ethanol-toluene	Methanol-benzene
0	7,420	12,000	7,200	7,000
0.05	4,460	3,160	4,350	3,980
0.10	3,250	2,120	3,010	2,820
0.20	2,300	1,560	2,120	1,925
0.40	1,610	1,210	1,460	1,260
0.60	1,280	1,165	1,180	985
0.80	1,060	1,220	990	845
1.00	865	1,340	830	760

cyclohexane, heptane-benzene, heptane-toluene, hexane-benzene, ethanol-benzene, ethanol-toluene, ethanol-cyclohexane, and methanol-benzene. Data for five of the hydrocarbon binaries are shown in Figure 1, and smoothed results for the polar binary systems are tabulated in Table 1. In addition to these results, heats of mixing were obtained for the binary systems formed by mixing benzene and toluene with the normal hydrocarbons hexane, heptane, octane, and nonane. The results of this series of experiments are given in Figure 8. Data for five ternary systems: ethanol-toluene-cyclohexane, heptane-toluene-cyclohexane, heptane-benzene-cyclohexane, ethanol-

benzene-cyclohexane, and methanol-benzene-cyclohexane, are plotted on five ternary diagrams in Figures 2 through 6.

Since hexane and methanol are not completely miscible at 25°C., an isothermal solubility curve was determined for the methanol-benzene-hexane system. This was accomplished by cooling a pycnometer which contained weighed amounts of the three components in a variable-temperature bath and noting the temperature at which the solution became cloudy. The solubility at 25°C. was determined by interpolation after this operation had been repeated several times with solutions of different concentrations.

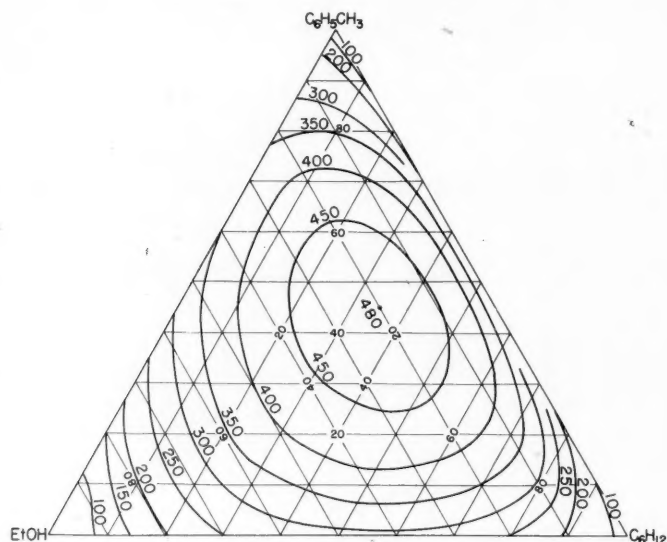


Fig. 2. Heats of mixing for the ethanol-toluene-cyclohexane systems at 25°C. Isenthalpic lines in B.t.u./lb. mole; compositions in mole %.

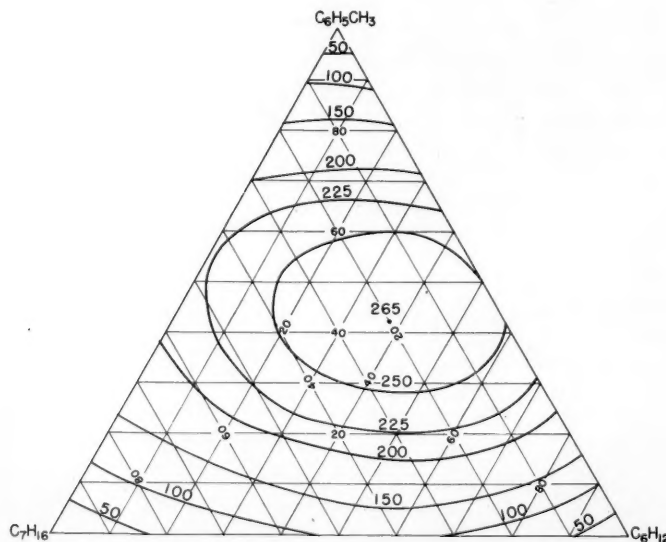


Fig. 3. Heats of mixing for the heptane-toluene-cyclohexane system at 25°C. Isenthalpic lines in B.t.u./lb. mole; compositions in mole %.

## PRECISION AND ACCURACY OF MEASUREMENTS

The main sources of error in isothermal calorimetry, the vaporization and condensation effects of volatile liquids, are diminished by keeping the vapor space in the calorimeter as small as possible.

In order to check the accuracy of the apparatus used in this investigation, measurements were made first on the cyclohexane-benzene system. Since the two components in this system have approximately the same vapor pressures and heats of vaporization, errors due to the vaporization and condensation effects of mixing should be negligible. Moreover, data of several other investigators (1, 6, 10) are available for this system, and when they are compared with the present results (Figure 7), the agreement is good. As a further check on the accuracy of the results, measurements were made for several systems with different volumes of vapor space. Since the magnitude of the error involved when two substances are mixed is a function of the amount of vapor space, it should be possible to detect errors if several different vapor spaces are used. Finding that the size of the vapor space had no appreciable effect on the results, the authors concluded that vaporization and condensation effects introduced no appreciable error in the results.

The accuracy of the heat-of-mixing measurements is believed to be well within 5%. The excellent reproducibility of the data suggests that this is probably a very conservative estimate. For example, the maximum deviation of the data from the smoothed results of Table 1 is less than 1%.

Data are available in the literature for several of the binary systems studied, and agreement with the present work ranges from excellent to poor. For the methanol-benzene system, which has been studied more extensively than the others, Tsao and Smith (13) compared all available results. The present data agree almost exactly with those of Tsao and Smith.

## CORRELATION OF BINARY DATA

For many years there have been attempts to correlate binary heat-of-mixing data by the use of equations based on certain theoretical assumptions. As early as 1906 van Laar (14) gave a treatment based on the van der Waals equation for the mixture and the pure components. Since that time Scatchard (9), Hildebrand (3), Longuet-Higgins (5), and Prigogine (7) have also developed equations which ultimately take the same form as the van Laar equation. The fact that all these equations reduce to essentially the same form has been shown in detail by Scott (12).

The "regular"-solution equation can be written in the following form:

$$\Delta E = z_1 z_2 A_{12} V_m \quad (1)$$

where  $\Delta E$  is the energy change of mixing,  $z$  is volume fraction of the component in solution,  $V_m$  is the molal volume of the mixture, and

$$A_{12} = c_{11} + c_{22} - 2c_{12} \quad (2)$$

If a relationship can be assumed between the interaction energy density  $c_{12}$  and the cohesive energy densities of the pure components  $c_{11}$  and  $c_{22}$ , it becomes possible by Equations (1) and (2) to predict heats of mixing from data for the pure components alone. It is usually assumed that

$$c_{12} = \sqrt{c_{11}c_{22}} \quad (3)$$

What is often not pointed out, however, is that  $c_{12}$  is so near in value to  $(c_{11} + c_{22})/2$  that only a very small change in the value of  $c_{12}$  will make a significant change in the heat of mixing. If it is assumed that

$$c_{12} = (c_{11}c_{22})^n \quad (4)$$

where  $n$  can be any value near 0.5, it is found that for the benzene-heptane system, for example, a change in the value of  $n$  by only 0.08% causes changes in the heat of mixing by as much as 23%. Thus general methods such as this for predicting heats of mixing from data for the pure components alone do not appear promising.

Nevertheless such general equations are useful for correlating experimental data. An equation which has been used for the correlation of heats of mixing for nonpolar systems is (10)

$$\begin{aligned} \frac{\Delta H_{12}}{x_1 x_2} &= A_0 + A_1(x_1 - x_2) \\ &+ A_2(x_1 - x_2)^2 \\ &+ A_3(x_1 - x_2)^3 + \dots \quad (5) \\ &= \sum_w A_w(x_1 - x_2)^w \\ &= \sum_w A_w(2x_1 - 1)^w \end{aligned}$$

where  $w$  takes the integral values, 0, 1, 2, 3, etc.

A particularly convenient method for determining the constants in Equation (5) from experimental data is through the use of Vettin's discontinuous orthogonal polynomials as suggested by Jost and Röck (4). The polynomials are defined so that

$$\lim_{\Delta y \rightarrow 0} V(y/\Delta y) = P(y)$$

$$\Delta y \rightarrow 0$$

where

$V(y/\Delta y)$  = Vettin's polynomial in  $y/\Delta y$   
 $P(y)$  = Legendre's polynomial in  $y$   
 $y$  = the variable

$\Delta y$  = increment chosen between discrete values of  $y$

An expansion of  $\Delta H/x_1 x_2$  in Vettin's polynomial where  $y = x_1 - x_2 = 2x_1 - 1$  and  $\Delta y = 2\Delta x_1 = 0.2$  is represented as follows:

$$\begin{aligned} \frac{\Delta H}{x_1 x_2} &= \sum_k a_k V\left(\frac{y}{0.2}\right) \\ &= a_0 V_0 + a_1 V_1 + a_2 V_2 \\ &+ a_3 V_3 + \dots \end{aligned}$$

$$\begin{aligned} &= a_0(1) + a_1(y) \\ &+ a_2 \frac{5}{9}(3y^2 - 6/5) \\ &+ a_3 \frac{25}{72}\left(10y^3 - \frac{178}{25}y\right) \\ &+ a_4 \frac{125}{504}(35y^4 - 35y^2 \\ &+ 504/125) + \dots \quad (7) \end{aligned}$$

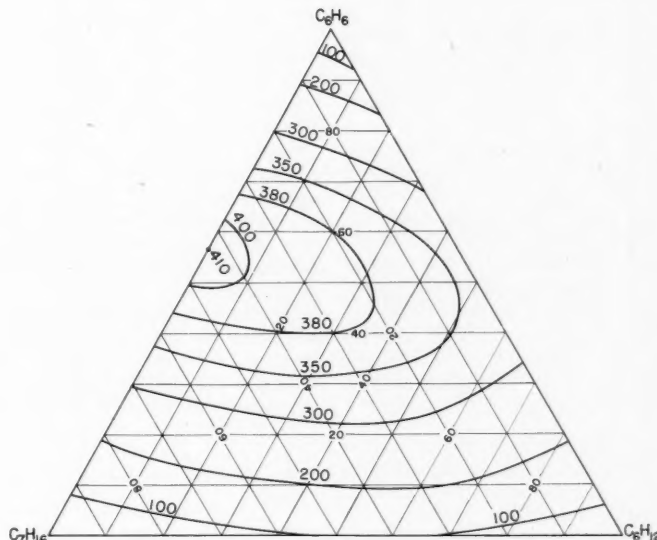


Fig. 4. Heats of mixing for the heptane-benzene-cyclohexane system at 25°C. Isenthalpic lines in B.t.u./lb. mole; compositions in mole %.

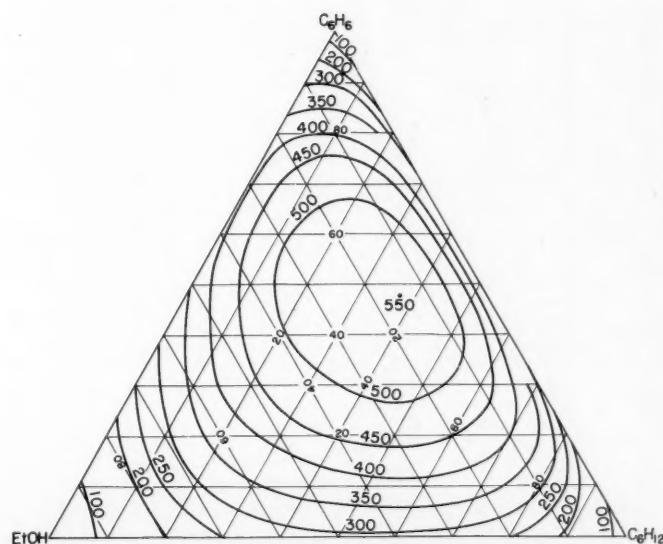


Fig. 5. Heats of mixing for the ethanol-benzene-cyclohexane system at 25°C. Isenthalpic lines in B.t.u./lb. mole; compositions in mole %.

The constants,  $a_0, a_1, a_2, a_3$ , etc., are readily determined (4), and they have the advantage of being independent of the number of terms in the expansion.

Equation (7) may be rearranged to give a simple power series, and it is therefore equivalent to Equation (5). A comparison of Equations (5) and (7) shows the two sets of constants to be related as follows for a series of five terms:

$$\begin{aligned}A_0 &= a_0 - (2/3)a_2 + a_4 \\A_1 &= a_1 - (89/36)a_3 \\A_2 &= (5/3)a_2 - (625/72)a_4 \\A_3 &= (125/36)a_3 \\A_4 &= (625/72)a_4\end{aligned}$$

This method is recommended for the determination of the constants for Equation (5).

It should be mentioned that if one component of the binary system is a polar material, the heat-of-mixing curve will be skewed. Therefore, more terms are necessary in Equation (5) to obtain a good fit to the experimental data than is the case where nonpolar components are mixed. For example, it was possible to fit the cyclohexane-benzene binary data with an average deviation of only 0.1% with an equation of three terms; whereas five terms were not sufficient to correlate the ethanol-benzene binary data with an average deviation of even 5%.

Actually, for nonpolar systems a two-constant equation is sufficiently accurate for engineering purposes. An especially convenient equation was developed by Boissonnas and Noordtzig (2):

$$\frac{\Delta H_{12}}{x_1 x_2} = H_1^\infty x_2 + H_2^\infty x_1 \quad (8)$$

It is seen from Equation (8) that when  $x_2 = 0$  and  $x_1 = 1$ ,  $\Delta H_{12}/x_1 x_2 = H_2^\infty$  and when  $x_2 = 1$  and  $x_1 = 0$ ,  $\Delta H_{12}/x_1 x_2 = H_1^\infty$ . Thus  $H_1^\infty$  and  $H_2^\infty$  represent the end points of the curves of  $\Delta H_{12}/x_1 x_2$  vs.  $x_1$  as shown in Figure 1. Moreover, it can readily be shown that  $H_1^\infty$  is the heat of mixing when one mole of component 1 is mixed with an infinite amount of component 2, and  $H_2^\infty$  is the heat of mixing when 1 mole of component 2 is mixed with an infinite amount of component 1. Thus,  $H_1^\infty$  is the heat of solution per mole of component 1 at infinite dilution. It may also be regarded as the relative partial molal enthalpy of component 1 at infinite dilution or as the partial molal enthalpy of component 1 at infinite dilution when the pure component is considered to have zero enthalpy. Experimentally, these values may be determined from measurements of the heat effect when a few drops of one pure component are mixed with a relatively large volume of the other pure component.

An empirical modification of Equation (8) was found to give an excellent correlation for nonpolar systems. Thus the following expression, containing but two constants, fits the data within two or three per cent.

$$\begin{aligned}\frac{\Delta H_{12}}{x_1 x_2} &= H_1^\infty x_2 + H_2^\infty x_1 \\&\quad - x_1 x_2 [H_1^\infty - H_2^\infty]\end{aligned} \quad (9)$$

where  $[H_1^\infty - H_2^\infty]$  represents the absolute value of  $H_1^\infty - H_2^\infty$  taken as positive regardless of the actual sign.

It is seen that for nonpolar systems only  $H_1^\infty$  and  $H_2^\infty$  are needed for the complete determination of the heat-of-mixing curve by Equation (9). The values of  $H_1^\infty$  and  $H_2^\infty$  for the six hydrocarbon binary systems studied are listed in Table 2. The curves shown in Figure 1 were determined by Equation (9) with the constants as given by Table 2. For clarity, the hexane-benzene system has been omitted from Figure 1.

TABLE 2. VALUES OF  $H_1^\infty$  AND  $H_2^\infty$  FOR EQUATION (9)

System Component 1-Component 2	$H_1^\infty$ B.t.u./lb. mole	$H_2^\infty$ B.t.u./lb. mole
Heptane-benzene	2,210	1,335
Hexane-benzene	2,040	1,370
Cyclohexane-benzene	1,480	1,320
Toluene-cyclohexane	1,200	940
Heptane-toluene	1,080	800
Heptane-cyclohexane	640	340

In addition, the experimental data show that the heats of mixing of the normal aliphatic hydrocarbons (hexane, heptane, octane, and nonane) with benzene are the same within experimental error at the same volume fractions of the hydrocarbons if the heats of mixing are based on a unit volume of mixture. This was also true for systems of the aliphatic hydrocarbons and toluene. These hydrocarbon correlations for mixing with both benzene and toluene are shown in Figure 8. Deviations from this correlation for the systems investigated are never more than 5% and in most cases are less than 2%.

There are several reasons for the difficulties in the prediction of the heats of mixing of polar systems. The "regular"-solution equation [Equation (1)] is based on the assumption that the intermolecular attractions are due entirely to dispersion forces. However, unlike dispersion forces, the dipole moments of polar substances in a nonpolar solvent depend on the solvent and on concentration. Furthermore, the magnitudes of the dipole moments alone do not provide a basis for an understanding of their influence upon intermolecular forces. In addition the actual geometry of the molecules must be considered.

Since equations with a large number of constants are necessary to represent data for polar systems and since all the necessary correlations can be presented graphically, it would seem that a graphical correlation would be more expedient than an analytical one. Hence, no equation is recommended for the polar systems studied. The minimum number of points necessary to establish the curve with sufficient accuracy is about six;  $H_1^\infty$ ,  $H_2^\infty$ , and four other points at the mole fractions 0.1, 0.2, 0.4, and 0.75 of the polar component. It is essential that data be

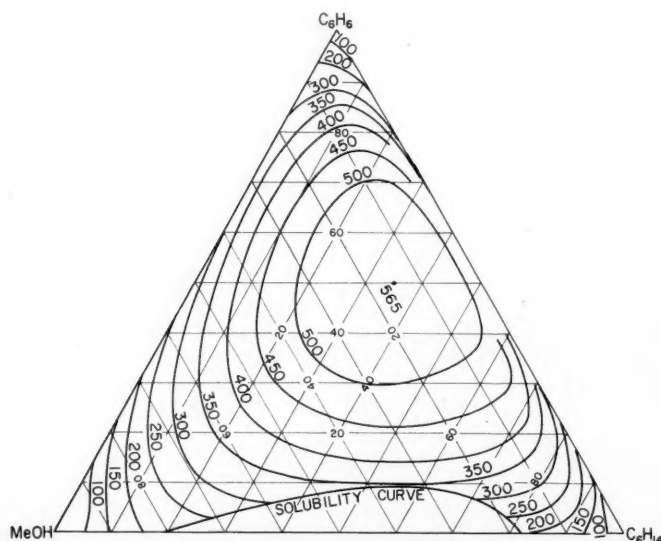


Fig. 6. Heats of mixing for the methanol-benzene-hexane system at 25°C. Isenthalpic lines in B.t.u./lb. mole; compositions in mole %.



taken in the region of low concentration of the polar component.

#### PREDICTION OF TERNARY HEATS OF MIXING FROM BINARY DATA

Three equations for predicting heats of mixing of ternary systems from binary data have been analyzed for the four completely miscible systems studied in this investigation.

The first equation was proposed by Redlich and Kister (7) and further developed by Scatchard and coworkers (9) for three substances which have similar binary heats of mixing:

$$\Delta H_{123} = x_1 x_2 \sum_w A_{w12}(x_1 - x_2)^w + x_1 x_3 \sum_w A_{w13}(x_1 - x_3)^w + x_2 x_3 \sum_w A_{w23}(x_2 - x_3)^w \quad (10)$$

Scatchard (9) modified Equation (10) to apply to mixtures containing one polar component (component 1):

$$\Delta H_{123} = x_1 x_2 \sum_w A_{w12}(2x_1 - 1)^w + x_1 x_3 \sum_w A_{w13}(2x_1 - 1)^w + x_2 x_3 \sum_w A_{w23}(x_2 - x_3)^w \quad (11)$$

Tsao and Smith (13) suggested the following equation:

$$\Delta H_{123} = x_1 x_2 \sum_w A_{w12}(2x_1 - 1)^w + x_1 x_3 \sum_w A_{w13}(2x_1 - 1)^w + (1 - x_1)(x_2^*)(1 - x_2^*) \sum_w A_{w23}(2x_2^* - 1)^w \quad (12)$$

In these equations  $\Delta H_{123}$  is the heat of mixing of the ternary mixture based on zero enthalpy for the three pure components and  $A_{w12}$ ,  $A_{w13}$ , and  $A_{w23}$  are the coefficients of Equation (5) for the individual systems, 1-2, 1-3, and 2-3. In Equation (12) the special function  $x_2^*$  is introduced. It is defined as  $x_2^* = x_2/(x_2 + x_3)$ .

Equations (10), (11), and (12) may be readily solved if the constants in Equation (5) are known for the three binary mixtures of the components. However, it is frequently more convenient to rearrange these equations so that the binary heats of mixing may themselves be used. This procedure is particularly advantageous when the binary data appear only in tabular or graphical form or are correlated by equations of different form than Equation (5).

In Equations (10), (11), and (12) the coefficients are those resulting from Equation (5) for the binary mixtures. Hence each summation term of Equations (10), (11), and (12), for example,

$$\sum_w A_{w12}(x_1 - x_2)^w \quad \text{or} \quad \sum_w A_{w12}(2x_1 - 1)^w$$

must be related to a binary heat of mixing for the two components involved at a binary composition equivalent to the compositions of the two components in the ternary mixture. If the equivalent binary compositions are represented by  $x_1'$ ,  $x_2'$ , and  $x_3'$ , the binary heats of mixing at these equivalent compositions are given by

$$\frac{\Delta H_{12}}{x_1' x_2'} = \sum_w A_{w12}(2x_1' - 1)^w \quad (5a)$$

$$\frac{\Delta H_{13}}{x_1' x_3'} = \sum_w A_{w13}(2x_1' - 1)^w \quad (5b)$$

$$\frac{\Delta H_{23}}{x_2' x_3'} = \sum_w A_{w23}(2x_2' - 1)^w \quad (5c)$$

It should be noted that the values of  $x_1'$ ,  $x_2'$ , and  $x_3'$  will be different in the two equations in which each appears. If  $x_1'$  in Equation (5a) is selected so that  $2x_1' - 1 = x_1 - x_2$ , then the first summation term of Equation (10) may be replaced by the equivalent term in Equation (5a) or by  $\Delta H_{12}/x_1' x_2'$ . Similarly,  $x_1'$  in Equation (5b) is chosen so that  $2x_1' - 1 = x_1 - x_3$ , and  $x_2'$  in Equation (5c) is taken so that  $2x_2' - 1 = x_2 - x_3$ .

In this way the second and third summation terms of Equation (10) may be replaced by their equivalent values from Equation (5b) and (5c). Equation (10) can then be expressed as

$$\Delta H_{123} = x_1 x_2 \left( \frac{\Delta H_{12}}{x_1' x_2'} \right) + x_1 x_3 \left( \frac{\Delta H_{13}}{x_1' x_3'} \right) + x_2 x_3 \left( \frac{\Delta H_{23}}{x_2' x_3'} \right) \quad (13)$$

The values of  $\Delta H_{12}/x_1' x_2'$ , for example, can be obtained from a graph of  $\Delta H_{12}/x_1' x_2'$  vs.  $x_1'$  at a value of  $x_1'$  given by the relation  $2x_1' - 1 = x_1 - x_2$ . (See Figure 1, for example; of course, on this graph  $x_1$  and  $x_2$  are identical with  $x_1'$  and  $x_2'$  used in the preceding discussion.)

In a like fashion Equation (11) may be transformed to give

$$\Delta H_{123} = \frac{x_2 \Delta H_{12}}{1 - x_1} + \frac{x_3 \Delta H_{13}}{1 - x_1} + x_2 x_3 \left( \frac{\Delta H_{23}}{x_2' x_3'} \right) \quad (14)$$

In this case  $\Delta H_{12}$  and  $\Delta H_{13}$  are obtained at a value of  $x_1' = x_1$ , since  $x_1'$  is selected so that  $2x_1' - 1 = 2x_1 - 1$ . On the other hand,  $\Delta H_{23}$  is read at a value of  $x_2'$  such that  $2x_2' - 1 = x_2 - x_3$ .

Equation (12) may be written

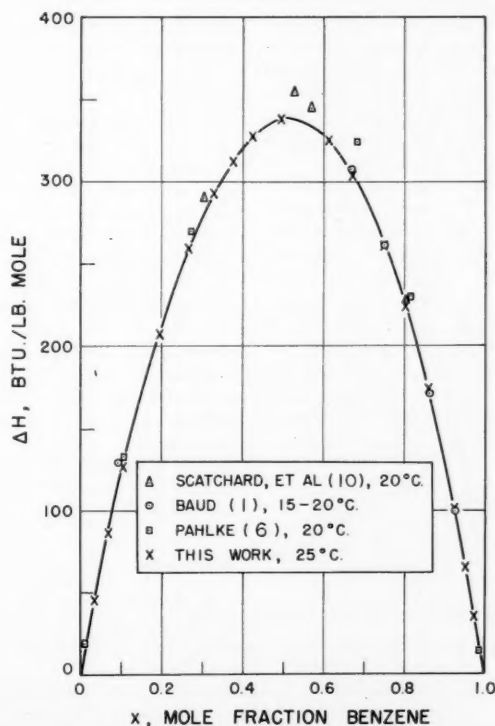


Fig. 7. Heats of mixing for the benzene-cyclohexane system.

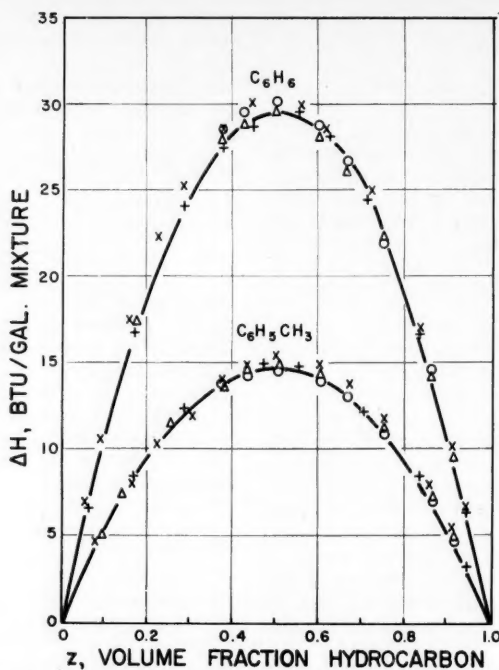


Fig. 8. Correlation for aliphatic hydrocarbons with benzene and toluene at 25°C. ×-hexane, +heptane, Δ-octane, O-nonane.

$$\Delta H_{123} = \frac{x_2 \Delta H_{12}}{1 - x_1} + \frac{x_3 \Delta H_{13}}{1 - x_1} + (1 - x_1) \Delta H_{23} \quad (15)$$

Here  $\Delta H_{12}$  and  $\Delta H_{13}$  are read at a value of  $x_1' = x_1$  and  $\Delta H_{13}$  is obtained at a value of  $x_2' = x_2^* = x_2/(x_2 + x_3)$ .

A comparison of the experimental heat-of-mixing data for the four completely miscible ternary systems with the values calculated by Equations (13), (14), and (15) gave the results shown in Table 3. Equations (10), (11), and (12) were not used for the prediction of ternary heats of mixing because of the fact that it was not possible to represent the binary data accurately for polar systems by an equation containing a reasonable number of constants. It seemed better to use the graphical correlations of binary data so as to base the predictions for ternary systems on the actual experimental results for the binary systems.

TABLE 3. AVERAGE DEVIATION OF EQUATIONS FROM EXPERIMENTAL DATA

	Two nonpolar systems, %	Two systems having one polar component, %
Equation (13)	2.4	12.0
Equation (14)	1.6	4.7
Equation (15)	5.9	10.9

On the basis of these results, it appears that Equation (14) is satisfactory for the

prediction of ternary heats of mixing from binary data for both polar and nonpolar systems. Equation (13) also gives satisfactory results for nonpolar systems. The maximum deviations of the predicted values from the experimental results were generally about twice the average deviation.

It should be mentioned that whereas Equation (13) is symmetrical, Equations (14) and (15) are not. It is necessary, therefore, that the proper component be selected as component 1 in the application of Equations (14) and (15). The simplest procedure is to select as components 2 and 3 the components which make up the binary having the lowest heat of mixing. Component 1 will then be the most dissimilar chemical in the ternary. If all three binaries have approximately equal heats of mixing, Equation (13) should probably be used.

The results given for the ternary systems in Figures 2 through 6 are experimental values and are not based on any assumed relation of the ternary values to binary data. Complete data are given by Schnaible (11).

#### CONCLUSIONS

In summary, it would appear that no satisfactory general method is available for the prediction of heats of mixing from data for the pure components alone. On the other hand, a satisfactory empirical equation does exist for the prediction of ternary heats of mixing from binary data at least for systems containing no more

than one polar component. The correlation of binary data for nonpolar systems may be readily accomplished by a simple two-constant equation. However, data for polar binary systems are probably still best represented graphically. For this purpose a plot of  $\Delta H_{12}/x_1 x_2$  is most convenient.

#### ACKNOWLEDGMENT

The authors are indebted to the Visking Corporation for support of this work through a fellowship.

#### NOTATION

- $a$  = a constant
- $A$  = a constant
- $c$  = cohesive energy density or interaction energy density
- $\Delta E$  = energy change of mixing
- $\Delta H$  = heat of mixing at constant temperature and pressure
- $H^\infty$  = heat of solution per mole of solute at infinite dilution
- $n$  = an exponent in Equation (4)
- $P$  = Legendre's polynomial
- $V$  = Vettin's polynomial
- $V_m$  = molal volume of mixture
- $w$  = a power or subscript taking values, 0, 1, 2, 3, etc.
- $x$  = mole fraction
- $x'$  = mole fraction in binary mixture equivalent to that of a ternary mixture
- $x_2^* = x_2/(x_2 + x_3)$
- $y$  = variable, equal to  $x_1 - x_2$
- $z$  = volume fraction

#### LITERATURE CITED

- Baud, E., *Bull. soc. chim. France*, **17**, 329 (1915).
- Boissonnas, C. G., and R. M. A. Noordtzig, *Helv. Chim. Acta.*, **37**, 1060 (1954).
- Hildebrand, J. H., and S. E. Wood, *J. Chem. Phys.*, **1**, 817 (1933).
- Jost, W., and H. Röck, *Chem. Eng. Sci.*, **3**, 17 (1954).
- Longuet-Higgins, H. C., *Proc. Roy. Soc. (London)*, **205A**, 247 (1951).
- Pahlke, H., Dissertation, Univ. Kiel, Germany (1936).
- Prigogine, I., and V. Mathot, *J. Chem. Phys.*, **20**, 49 (1952).
- Redlich, Otto, and A. T. Kister, *Ind. Eng. Chem.*, **40**, 345 (1948).
- Scatchard, G., *Chem. Rev.*, **8**, 321 (1931).
- , L. B. Ticknor, J. R. Goates, and E. R. McCartney, *J. Am. Chem. Soc.*, **74**, 3721 (1952).
- Schnaible, H. W., Ph.D. thesis, Purdue Univ., Lafayette, Ind. (1955).
- Scott, R. L., *Discussions Faraday Soc.*, **15**, 44 (1953).
- Tsao, C. C., and J. M. Smith, *Chem. Eng. Progr. Symposium Series No. 7*, **49**, 107 (1953).
- Van Laar, J. J., "Sechs Vortage über das Thermodynamische Potential," Braunschweig (1906).

Presented at A.I.Ch.E. Pittsburgh meeting

# Rate Studies in Tubular Reactors

ERIC WEGER and H. E. HOELSCHER, The Johns Hopkins University, Baltimore, Maryland

The tubular reactor, as the term is used in the present paper, is a cylindrical tube on the inner surface of which a catalyst is deposited. The reacting mixture flows through this tube, the reaction components diffuse to the wall, where reaction takes place, and the products diffuse back into the main gas stream.

Damkohler (6) first analyzed this type of system and presented the basic differential equations describing the process. Baron, Manning, and Johnstone (1), utilizing this analysis in their studies of the oxidation rates of sulfur dioxide in a tubular reactor, solved the diffusion equation by assuming a first-order kinetic mechanism at the tube wall as a boundary condition. The experimental work was limited to low flow rates. The catalytic oxidation of ammonia in tubular reactors was studied by Johnstone, Houvouras, and Schowalter (10), who used the same type of analysis. The maximum Reynolds number was 150.

Rossberg and Wicke (14) measured the rate of combustion of graphite tubes when nitrogen-oxygen mixtures were passed through them. The flow rates were in the laminar region and temperatures between 500° and 1,400°C. were used. The mechanism which controlled the process was found to depend on the operating temperature.

Satterfield and coworkers (15), studied the decomposition of hydrogen peroxide in a tubular reactor by means of the classical diffusion techniques, using  $j$  factors and the Chilton-Colburn equation (2, 3).

The present study was undertaken in order to extend the theory and technique necessary for the use of tubular reactors in kinetic investigations. The reaction between hydrogen and the olefin-1 hydrocarbons has been investigated extensively, and a review of these studies has been presented by Hoelscher, Poynter, and Weger (8). Because of the availability of these kinetic data, the aforementioned reaction was chosen to be studied. The catalyst used was palladium black on carbon.

## EXPERIMENTAL WORK

### Reaction Apparatus

The experimental apparatus used in this study was quite standard and is shown schematically in Figure 1. Complete details regarding the apparatus and its design are available elsewhere (9, 16). Electrolytic hydrogen and olefin of c.p. grade were fed from two commercial high-pressure cylinders through a series of pressure-regulating and flow-stabilizing devices into the gas-purification system. After passing through the purifiers, the gases were metered and mixed

intimately prior to entering the heat exchanger section of the constant-temperature bath. Insulated Pyrex manifolds permitted the selection of any one of four reactor-tube assemblies for a particular trial. Temperatures of the catalyst tube during the reaction were measured by means of thermocouples embedded in the tube wall at various points along the tube length. The exit gas stream from the reactor was passed through a flow divider where a small portion of the gas was taken for analysis by a thermal conductivity unit. The remainder was vented to the atmosphere. A blank reactor-tube assembly permitted analysis of the gas entering the catalyst tubes. All outlet streams from the system were sealed from the atmosphere by means of dioctyl-phthalate bubblers.

From the mixing chamber the feed stream passed through a preheater tube and then into an insulated inlet manifold which exhausted through stopcocks into four individual reactor sections. The preheater and the reactor sections were maintained in a constant-temperature bath through which water from a thermostatically controlled supply was pumped continuously. The reactor sections were connected to an exit manifold to which was attached a manometer for measuring pressures in the catalyst tubes.

Each reactor section consisted of a catalyst tube (of different lengths, as explained later) preceded by a calming section at least 100 diameters in length and followed by a tail section. These two sections consisted of tubes identical in diameter (0.44 cm.) with the catalyst tube but not impregnated with catalyst. The purpose of the calming section was to produce a well-developed velocity profile in the feed stream before it entered the catalyst tube. The purpose of the tail section was to prevent any downstream disturbances which might regress into the catalyst tube.

The palladium black catalyst was deposited in the carbon tubes by drawing a 5% palladous chloride solution into them. The tubes absorbed the solution, were dried, and then fired at 500°C. with a stream of nitrogen passing through them. This method gave a very uniform deposit of palladium black. Spectrophotometric analysis of six different catalyst-tube sections yielded a palladium-to-carbon weight ratio of 0.0090 with an average deviation of  $\pm 0.3\%$ .

The problem of sealing the catalyst tubes was solved by the use of brass tubing with an inside diameter almost identical to the outside diameter of the graphite tubes. It was found that by turning the tubes down a few thousandths of an inch on a lathe they could be made to fit snugly inside the brass tubing (Figure 2). The calming section, catalyst tube, and tail section were butted together inside the brass tubing, which in turn was fastened to the glass-ball joints on either end with Cerroseal, a special indium solder that adheres to both glass and metal. The glass-ball joints provided the connections to the manifolds.

### Analytical Apparatus

The apparatus used for gas analysis was a Leeds and Northrup Thermal Conductivity Unit especially constructed so that an accuracy of at least one part in ten thousand might be obtained. Complete details including the circuit diagram for this apparatus are available elsewhere (9, 16).

The conductivity unit was calibrated for the hydrogen-olefin mixtures used in this study by running a large number of samples of known composition through the unit and measuring the resulting bridge unbalance. In a study of the characteristics of Leeds and Northrup thermal-conductivity cells Collier (4), using the system hydrogen, ethylene, ethane, found that ethane was not differentiated from ethylene as long as the hydrogen concentration was kept above 35%. Since the lowest hydrogen concentration used in the present study was 58%, it was felt that the result cited above could safely be applied in this case and generalized to other olefin-alkane combinations.

The logarithm of the mole percentage of hydrogen in the gas stream was found to be directly proportional to the bridge unbalance.

### Experimental Conditions

The main factors which influence the rate of reaction in a tubular reactor are flow rate, temperature, and composition of the reacting system (other factors, such as catalyst activity, being constant).

These primary variables covered as wide a range as possible while still retaining the differential characteristics of the tubular reactor. Thus, since the palladium black is a highly active hydrogenation catalyst, it was possible to run the reaction at relatively low temperatures. The experimental temperature range finally chosen was 30° to 45°C. The range of Reynolds numbers for which experimental data was obtained was 125 to 2,300. At the lower Reynolds number limit and at the higher temperature limit the percentage conversions of the reactants were as high as they could be permitted to become in a differential reactor. At those extreme limits the molar flow rate was decreased by 7% over the reactor length, owing to reaction. At the upper Reynolds number limit and the lower temperature limit the conversions were just high enough to permit accurate measurement.

The composition range used in the experimental work was 58 to 95 mole % hydrogen in the inlet gases. The factor which fixed the lower limit was the possibility of olefin polymerization at high olefin concentrations. The operating range of temperatures was low enough to prevent any polymerization, but the high exothermicity of the reaction could have produced local thermal effects which might have caused polymerization unless an excess of hydrogen had been present.

The length of the reactor tube was varied over a twofold range in order to determine the effect of variation of contact time. The three tube lengths which were

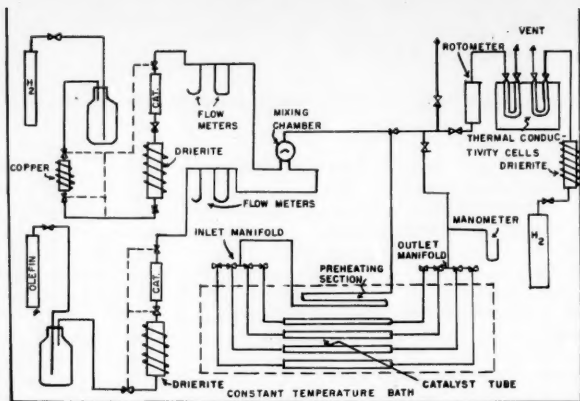


Fig. 1. Schematic flow diagram.

used to obtain all the final data were 22.9, 34.3, and 45.7 cm.

As was mentioned previously, temperature measurements were made at various points along the catalyst tube by means of thermocouples, so that it was possible to determine how closely the reaction adhered to the desired isothermal conditions. Owing to the highly exothermal character of the reaction being studied, a small temperature rise at the catalyst surface was to be expected, but this rise was generally observed to be constant—ranging from 2° to 3°C. above the bath temperature.

The complete experimental data are available in a detailed report to the Office of Ordnance Research by the present authors (9).

#### ANALYSIS OF DATA

The physical system used in this work, the range of parameters investigated, and the extensive information available on the highly active nature of the catalyst used combined to suggest initially that the process should be diffusion controlled. On this assumption, a model involving the existence of a boundary layer of product along the tube wall was set up and used as the basis for an analytical description of the process (9, 16).

More thorough study of the data has indicated that this model is not correct. The conversion was noted to be affected markedly by slight changes in temperature; an "over-all" energy of activation was computed by plotting the logarithm of the conversion vs. the reciprocal of the absolute temperature for any one set of conditions and was found always to be in the range of 6,000 to 7,000 cal./mole. Such a value is much too high to indicate diffusion control. In addition, the rate of the hydrogenation reaction was observed to be of the same order of magnitude for all the olefins used. Yet the diffusivity of ethylene in a hydrogen-ethylene mixture is more than ten times as great as the diffusivity of butene in a hydrogen-butene mixture. Had diffusion been the controlling factor, one would have expected a sharp decrease in measured rate with increasing chain length of

the olefin. Thus a chemical-reaction mechanism was assumed to be controlling the process.

Available evidence seems to indicate that the Langmuir-Hinshelwood mechanism best describes the hydrogenation of olefins (11, 12). This mechanism postulates a reaction between an adsorbed olefin molecule and hydrogen adsorbed in either the molecular or atomic form. The olefin is strongly adsorbed and the hydrogen is weakly adsorbed. The differential rate equation for this model is developed by Laidler (11), who assumes that the Langmuir form of the adsorption isotherm holds:

$$r = \frac{k'b'y_A y_B}{(1 + b y_A)^2} \quad (1)$$

The constant  $b'$  was assumed to be the same for the hydrogenation of the three olefins used in the present work. The kinetic constant which was therefore determined was  $k'b'$ . Equation (1) then takes the form

$$r = \frac{k b y_A y_B}{(1 + b y_A)^2} \quad (2)$$

The form of Equation (2) indicates that the rate will pass through a maximum at some intermediate olefin concentration. The results of Constable (5) and Pease (13) confirm this for the hydrogenation of ethylene on copper. The data of Constable, for example, show that for a reaction temperature of 0°C. the rate passes through a maximum at 0.18 mole fraction ethylene and drops to 90% of this maximum rate at 0.09 and 0.33 mole fraction ethylene. This represents only a 10% change in the rate over a mole fraction of ethylene change of 0.24. Similar conclusions can be drawn from the data of Farkas and Farkas (7) on platinum. In the present work the ethylene concentration was varied only over a mole fraction range of 0.17.

As a consequence, hydrogenation data obtained in the region of this maximum can usually be correlated satisfactorily on the basis of an assumed zero-order reaction. The assumption made in this

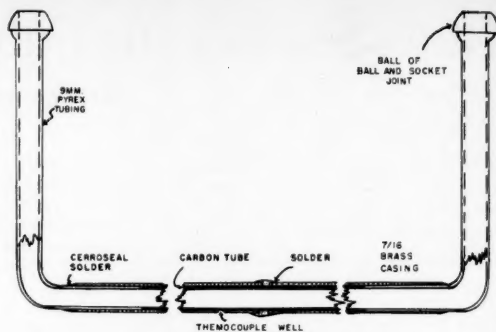


Fig. 2. Catalyst-tube-assembly detail.

work, that the same mechanism applies to the hydrogenation of propylene and butene-1 as to the hydrogenation of ethylene, is probably justified because of the close structural similarity of the three molecules.

#### DERIVATION OF RATE EQUATIONS

$n_A$  and  $n_B$  represent the number of moles of olefin and the number of moles of hydrogen per unit time, respectively. Then by a material balance over a differential section of the tubular reactor one obtains

$$dn_A = -\pi D r dL \quad (3)$$

Since the rate is proportional to the mole fractions of the materials present, the problem is to express  $dn_A$  in terms of mole fractions.

In the reaction  $A + B \rightarrow R$  the following stoichiometric relations will be valid reaction when there is no product in the feed stream:

$$n_A = \frac{y_A n_{B_0}}{(1 - y_A)} \quad (4)$$

and

$$y_B = \frac{y_{B_0} - y_{A_0}(1 - y_A)}{y_{B_0}} \quad (5)$$

(The subscript  $_0$  indicates inlet quantities)

$$\text{Then } dn_A = \frac{F y_{B_0} dy_A}{(1 - y_A)^2} \quad (6)$$

Combining Equations (2), (3), (5), and (6) yields

$$\frac{y_{B_0}^2 (1 + b y_A)^2 dy_A}{y_A (1 - y_A)^2 (\gamma + y_{A_0} y_A)} = -k b \frac{\pi D dL}{F} \quad (7)$$

This equation is integrated over the length of the reactor tube to yield the following result:

$$2.303 \left[ \frac{y_{B_0}^2}{\gamma} \log \left( \frac{\gamma}{y_A} + y_{A_0} \right) + (b + 1)(b\gamma - 1) \log \frac{(1 - y_A)}{y_{B_0}} \right]$$



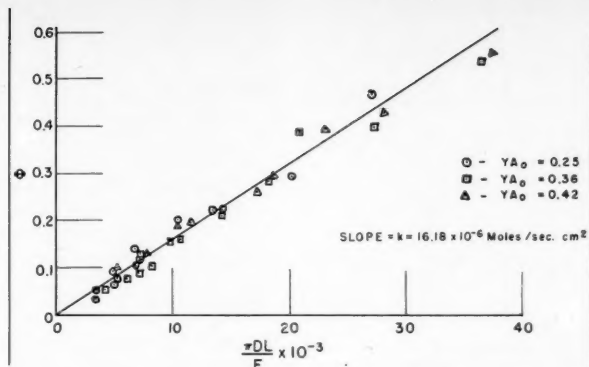


Fig. 3. Typical plot of  $\phi$  vs.  $\pi DL/F$  data for  $C_2H_4 + H_2$  at  $45^\circ C$ . [See Equation (9).]

$$\left[ \frac{\left( \frac{\gamma}{y_{A_0}} + y_{A_0} \right)}{\left( \frac{\gamma}{y_{A_0}} + y_A \right)} \right] + (b+1)^2 \frac{(y_{A_0} - y_A)}{(1 - y_A)} = kb \frac{\pi DL}{F} \quad (8)$$

$[y_A$  in Equation (8) is the exit mole fraction of olefin]

or

$$\phi = kb \frac{\pi DL}{F} \quad (9)$$

where  $\phi$  = the left-hand side of Equation (8). Since no independent adsorption data were available, the adsorption constant  $b$  had to be evaluated before use could be made of Equation (9).

The ethylene hydrogenation runs were made with three values for the inlet ethylene mole fraction (0.25, 0.36, 0.42). As a first approximation it was assumed that the ethylene mole fractions were near the value corresponding to the maximum rate mentioned before. To check this assumption the ethylene data were correlated by use of a zero-order kinetic equation. The data correlated well on this basis, and kinetic constants derived from it checked closely with those derived later from the more elaborate analysis.

Since the reaction at the ethylene mole-fraction values used was determined to be approximately zero order, the initial rates at the extremes of the inlet compositions were now equated and the adsorption constant was evaluated, as follows:

$$r_0 = \frac{kby_{A_0}y_{B_0}}{(1 + by_{A_0})^2}$$

where

$r_0$  = initial rate

and

$$r_0(y_{A_0} = .25) = \frac{kb(0.75)(0.25)}{(1 + 0.25b)^2}$$

$$r_0(y_{A_0} = 0.42) = \frac{kb(0.58)(0.42)}{(1 + 0.42b)^2}$$

Then

$$\frac{(0.75)(0.25)}{(1 + 0.25b)^2} = \frac{(0.58)(0.42)}{(1 + 0.42b)^2}$$

and

$$b \cong 1.0$$

To check the validity of this procedure, the value of  $r_0/k$  was calculated for all three of the compositions used in the ethylene hydrogenation studies. The following values were obtained.

$$\frac{r_0}{k} (y_{A_0} = 0.25) = 0.1200$$

$$\frac{r_0}{k} (y_{A_0} = 0.36) = 0.1240$$

$$\frac{r_0}{k} (y_{A_0} = 0.42) = 0.1210$$

As was to be expected,  $r_0/k$  is practically a constant at the compositions under discussion. It should be noted also that the rate constant evaluated independently by means of the zero-order rate equation is approximately 0.12 of the rate constant which was evaluated by means of the equation making use of the Langmuir-Hinshelwood expression. This is also supported by the preceding values.

Since hydrogenation data for propylene and butene were not obtained in the region of a rate maximum (and the available data could not be correlated by a zero-order equation), the same methods could not be applied to the determination of  $b$  for these cases. Hydrogenation runs were made with butene at two initial compositions. The constant  $b$  was evaluated by a trial-and-error method. Values of  $\phi$  were calculated by use of various assumed values for  $b$ , and the  $\phi$ 's were then plotted vs. their respective  $(\pi DL)/F$

TABLE 1. RATE CONSTANTS

Hydrogenation of	$k \times 10^6$ , moles/(sec.)(sq. cm.)		
	30°C.	40°C.	45°C.
Ethylene	9.23	13.37	16.18
Propylene	4.33	6.04	8.13
Butene-1	2.21	3.57	4.67

TABLE 2. FREQUENCY FACTORS AND ACTIVATION ENERGIES

Hydrogenation of	$A$ , moles/(sec.)(sq. cm.)	$E$ , cal./g. mole
Ethylene	1.62	7,140
Propylene	2.76	8,130
Butene-1	10.6	9,330

groups. The value of  $b$  which gave the best correlation independent of initial composition was chosen as the applicable one. For butene-1 this was found to be  $b = 14$ .

Since propylene hydrogenation runs were made at only one composition, a value of  $b = 10$  was chosen arbitrarily for this case. It was found that the rate constant was not too sensitive to the exact value of  $b$ ; for instance,  $b = 10 \pm 2$  for the case of propylene would not have altered  $k$  appreciably.

## RESULTS

The rate constants for the hydrogenation of ethylene, propylene, and butene-1 were evaluated by plotting  $\phi$  vs.  $(\pi DL)/F$ . A typical plot is presented in Figure 3, and activation energies and frequency factors were obtained by means of the conventional Arrhenius plots shown in Figure 4, the results being presented in Tables 1 and 2.

The derived rate equation is based on mixed mean mole fractions at inlet and outlet of the tubes. The composition of the gas at the catalytic surface is obviously somewhat different owing to the gradients existing across the tube radius. A fully rigorous derivation would involve the solution of the diffusion equation with the Langmuir-Hinshelwood equation as a boundary condition.

The values obtained for the rate constant could not be compared directly with other published data as they depend on many factors unique to the particular system and apparatus used in the investigation. It will be observed that the rate constants are of the same order of magnitude for the hydrogenation of all three olefins. This lends support to the previous arguments in favor of a reaction-controlled process.

The activation energies show an interesting trend in that they increase regularly as the number of carbon atoms in the hydrocarbon increases, probably owing to steric effects. The energies reported are within the range of values

commonly found for catalysis by the higher molecular weight transition-state metals. Since values shown in Table 2 include the hydrogen adsorption equilibrium constant, comparison with other data is impossible. However, the trend is expected. It may be shown that the frequency factor for a heterogeneous catalytic reaction of this type is inversely proportional to the product of the partition functions and directly proportional to the concentration of available active sites. An estimate of these terms for this problem indicates that the frequency factor should increase with increasing molecular weight and, moreover, that the ratio of the values found is of the right order of magnitude.

It had been expected that the geometry of the tubular reactor, i.e., a high volume-to-surface ratio, would permit the rate of diffusion of reactants to the catalyst surface to become the controlling step in the reaction—at least at low Reynolds numbers. This is a reasonable expectation, since lateral transport occurs only by the mechanism of molecular diffusion in the laminar flow range. It seems likely therefore that a certain amount of turbulence occurred in the tubes, even at low Reynolds numbers, which would greatly increase the lateral diffusion rate, as the mechanism of eddy diffusivity would then be available for reactant and product transport. That such turbulence existed seems probable.

In recent work which required the preparation of a palladium black catalyst on the outer surface of carbon tubes identical to those used in this study, visual observation of the surface was possible, and it was evident that despite care in providing a carbon surface which is initially smooth, the process of impregnation and firing to the amorphous metal results in a highly roughened surface. Furthermore, the process is known to be exothermic; wall temperatures along the reactor tube were measured and found to be as much as 2° to 3° above the bath temperature, and the radial temperature gradient through the gas stream, although not measured because of the small tube diameter, could easily have been appreciable. Such a gradient would cause a convective process at the wall which would, in turn, contribute to gas-phase mixing and a radial-diffusion resistance lower than expected from pure molecular diffusion.

In retrospect it therefore seems likely that considerable turbulence, or lateral mixing, was introduced into the gas stream by surface roughness and convective (thermal) mixing. This accounted for the rapid lateral diffusion rates which caused the over-all process to be rate controlled.

The use of a tubular reactor in kinetic research, however ideal it may seem at first consideration, has several severe drawbacks.

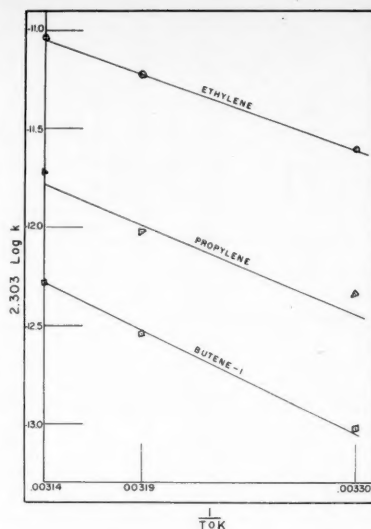


Fig. 4. Arrhenius plots. (See Table 2 for values of  $A$  and  $E$ .)

One of the seemingly attractive features of using a hollow tube is the possibility of maintaining easily describable velocity and concentration gradients in the laminar region; however, two conditions peculiar to a chemical reactor of this type nullify these advantages. First, an active catalyst surface is by its very nature a rough surface. This roughness tends to destroy the usual streamline character of flow at low Reynolds numbers. Second, since the catalyst must be highly active owing to the high volume-to-surface ratio of a tubular reactor, there is a pronounced temperature rise at the wall for exothermic reactions. This temperature rise can cause additional turbulence in the fluid and is hard to control.

Even were it possible to control these factors so as to obtain truly laminar flow, the possible development of concentration boundary layers at the tube wall would cause difficulties in any attempt at rigorous mathematical analysis of the system.

An experimental difficulty inherent in tubular reactors is that the large free volume makes it necessary for economical reasons to restrict the tube diameter to rather small values. This makes it almost impossible to obtain velocity or concentration gradients experimentally.

#### ACKNOWLEDGMENT

The authors express their gratitude to the Office of Ordnance Research of the Department of the Army for financial support of this work.

W. G. Poynter was responsible for the glass-blowing and many other constructional details of the apparatus, and the authors

wish to take this opportunity to express appreciation for his assistance.

#### NOTATION

- $A$  = Arrhenius frequency factor, moles/(sq. cm.)(sec.)
- $b$  = adsorption equilibrium constant for olefin, dimensionless
- $b'$  = adsorption equilibrium constant for hydrogen, dimensionless
- $D$  = inside diameter of reactor, cm.
- $E$  = energy of activation, cal./g.-mole
- $F$  = inlet total molal flow rate, moles/sec.
- $k$  =  $k'b'$ , modified rate constant, moles/(sq. cm.)(sec.)
- $k'$  = rate constant, moles/(sq. cm.)(sec.)
- $L$  = length of reactor, cm.
- $n_A$  = molal flow rate of olefin, moles/sec.
- $n_{A_0}$  = inlet molal flow rate of olefin, moles/sec.
- $n_B$  = molal flow rate of hydrogen, moles/sec.
- $n_{B_0}$  = inlet molal flow rate of hydrogen, moles/sec.
- $r$  = rate of reaction, moles/(sq. cm.)(sec.)
- $r_0$  = initial rate, moles/(sq. cm.)(sec.)
- $y_A$  = mole fraction of olefin
- $y_{A_0}$  = inlet mole fraction of olefin
- $y_B$  = mole fraction of hydrogen
- $y_{B_0}$  = inlet mole fraction of hydrogen
- $\gamma$  =  $y_{B_0} - y_{A_0}$
- $\phi$  = left-hand side of Equation (8)

#### LITERATURE CITED

1. Baron, T., W. R. Manning, and H. F. Johnstone, *Chem. Eng. Progr.*, **48**, 125 (1952).
2. Chilton, T. H., and A. P. Colburn, *Ind. Eng. Chem.*, **26**, 1183 (1935).
3. Colburn, A. P., *Trans. Am. Inst. Chem. Engrs.*, **29**, 174 (1933).
4. Collier, D. W., Ph. D. dissertation, Princeton Univ., Princeton, N. J. (1944).
5. Constable, F. H., *Z. Elektrochem.*, **35**, 105 (1929).
6. Damkohler, Gerhard, *ibid.*, **42**, 846 (1936).
7. Farkas, Adalbert, and Ladislaus Farkas, *J. Am. Chem. Soc.*, **60**, 22 (1938).
8. Hoelscher, H. E., W. G. Poynter, and Eric Weger, *Chem. Rev.*, **54**, 575 (1954).
9. Hoelscher, H. E., and Eric Weger, *Final Report, OOR Project 698, Contract DA 36-03A-ORD-1619 RD*, Johns Hopkins Univ., Baltimore, Md. (1955).
10. Johnstone, H. F., E. T. Houvouras, and W. R. Schowalter, *Ind. Eng. Chem.*, **46**, 702 (1954).
11. Laidler, K. J., "Chemical Kinetics," p. 161, McGraw-Hill Book Company, Inc., New York (1950).
12. ———, *Discussions Faraday Soc.*, **8**, 47 (1950).
13. Pease, R. N., *J. Am. Chem. Soc.*, **45**, 1196 (1923).
14. Rossberg, M., and Ewald Wicke, *Chem. Ing. Tech.*, **28**, 181 (1956).
15. Satterfield, C. N., H. Resnick, and R. L. Wentworth, *Chem. Eng. Progr.*, **50**, 460 (1954).
16. Weger, Eric, D. Eng. dissertation, Johns Hopkins Univ., Baltimore, Md. (1955).

# Performance of Packed Columns

H. L. SHULMAN and J. E. MARGOLIS

Clarkson College of Technology, Potsdam, New York

## IV. Effect of Gas Properties, Temperature, and Pressure on Gas-phase Mass Transfer Coefficients

To test the applicability, over a wide range of temperatures, pressures, and gas physical properties, of the mass transfer correlation presented earlier, 0.5-in. naphthalene Berl saddles were vaporized into air, carbon dioxide, and Freon-12 in a 4.0-in. column. Temperatures from 15° to 73°C. and pressures from 0.26 to 1 atm. were covered.

The correlation was found to represent all the experimental data when the surface temperature of the naphthalene was used to evaluate the correct driving force.

This correlation, when combined with effective interfacial areas presented previously, makes it possible to estimate the volumetric mass transfer coefficient,  $k_G a$ , for any gas-liquid-solute system.

In the first three papers (10, 11, 12) of this series devoted to packed columns, a method was proposed for predicting over-all mass transfer coefficients  $K_G a$  from gas- and liquid-phase coefficients  $k_G$  and  $k_L$  and the effective interfacial area  $a$ . The correlation presented for estimating  $k_G$

$$j_D = \left[ \frac{k_G M_M P_{BM}}{G} \right] \left[ \frac{\mu}{\rho D_e} \right]^{2/3} \\ = 1.195 \left[ \frac{D_p G}{\mu(1 - \epsilon)} \right]^{-0.36} \quad (1)$$

was based on data obtained with air as the inert gas at atmospheric pressure and room temperatures. Although this equation correlated the data of several previous investigators, obtained under similar conditions, there were no data to provide a suitable check on the ability of the equation to predict  $k_G$  over the wide range of temperatures, pressures and gas physical properties that may be encountered in design problems.

The object of this work is to study the effect of gas physical properties, temperature, and pressure on gas-phase mass transfer coefficients and the usefulness of Equation (1) for predicting coefficients under a variety of conditions.

An examination of the terms in Equation (1) indicates that  $k_G$  should be almost independent of temperature, being approximately proportional to  $T^{0.11}$ . The methods for estimating effective interfacial areas  $a$  presented previously (10, 11, 12) also predict small changes

with temperature. For water systems  $k_G a$  should be independent of temperature because small increases in  $k_G$  are counterbalanced by small decreases in  $a$  as temperature increases.

Decreases in  $k_G a$  with increasing temperature for ammonia absorption work have been reported by Kowalko, Hougen, and Watson (7), Dodge and Dwyer (3), and Molstad, McKinney, and Abbey (9), these decreases ranging from 0.2 to 0.8 %/°C. based on the outlet water temperature. These data cannot be used for predicting the effect of temperature or checking Equation (1) because the gas temperatures were not varied over a wide range and the water temperature variations are peculiar to the conditions under which the columns were operated. In ammonia absorption it is possible to obtain a rise in water temperature when the ammonia dissolves and a fall in water temperature if the air used is not saturated. It should be pointed out that the effect of temperature on  $k_G$  should be determined by employing varying gas-phase temperatures rather than temperatures based on conditions in the liquid phase.

For low concentrations of the solute in the carrier gas, Equation (1) predicts that  $k_G$  should be inversely proportional to total pressure. This has been found to hold for absorption in packed columns over the range of 1 to 14 atm. by Zabban and Dodge (14). Goodman's (4) unpublished data for the vaporization of naphthalene Berl saddles into air, shown in Figure 5, cover the range 0.26 to 1 atm. and show the expected effect of pressure. Both sets of data mentioned were obtained at low solute concentration, thus leaving in doubt the use of  $P_{BM}$  in Equation (1) in place of the total pressure.

In the third paper of this series (12) it was shown that Equation (1) combined with effective interfacial areas made

possible the correlation of packed-column data for absorption in water as well as the vaporization of several liquids when air was used as the inert gas. This implies that the correct exponent on the Schmidt number is  $\frac{2}{3}$ . Recently two sets of data have become available for the vaporization of water into several inert gases, which raise the question as to whether or not the dimensionless groups of a correlating equation, such as Equation (1), satisfactorily represent the physical properties of all inert gases. Lynch and Wilke (8) vaporized water from a wet-bulb thermometer and 1-in. Raschig rings into helium, air, and Freon-12. They concluded that  $k_G a$  was proportional to the Schmidt number raised to the  $-0.47$  to  $-0.50$  power and recommended that the H.T.U.  $[G/(k_G a M_M P_{BM})]$  be compared at equal values of  $\rho u^2$  rather than at equal values of a Reynolds number. At equal values of Reynolds number, the H.T.U. was proportional to the Schmidt number raised to the 0.9 power. Yoshida (13) also vaporized water from 1-in. Raschig rings employing helium, air, and carbon dioxide as the inert gases. He concluded that the H.T.U.  $[G/(k_G a M_M P_{BM})]$ , when compared at equal values of Reynolds number, was proportional to the Schmidt number raised to the 0.77 power although the  $\frac{2}{3}$  power was also satisfactory.

To answer the questions which have been raised as to the usefulness of Equation (1) for predicting values of  $k_G$  over a wide range of temperatures, pressures, and physical properties of the inert gas, an experimental program was carried out to provide the required data. The temperature extremes were 15° and 73°C. Data are reported for pressures from 0.26 to 1 atm., and air, carbon dioxide, and Freon-12 were used to vaporize naphthalene 0.5-in. Berl saddles in a 4.0-in.-diam column.

Tabular material has been deposited as document 5211 with the American Documentation Institute, Photoduplication Service, Library of Congress, Washington 25, D. C., and may be obtained for \$1.25 for photoprints or 35-mm. microfilm.

Parts I, II, and III appeared in the *A.I.Ch.E. Journal*, 1, 247 (1955).

TABLE 1. PACKING CHARACTERISTICS

Nominal size, in.	0.5
Void fraction, dry	0.660
Number of pieces/cu. ft.	15,000
Surface area/piece, sq. ft.	0.00888
Surface area, sq. ft./cu. ft.	133
Diameter of equivalent sphere, ft.	0.0532

## EQUIPMENT

The equipment shown in Figure 1 was used in studying the temperature variation of  $k_g$  and that shown in Figure 2 in the study of the variation of  $k_g$  with gas properties. In the equipment used to study  $k_g$  temperature variations, the air was circulated by means of a U. S. Hoffman centrifugal blower. The air rate was measured with rotameters reading from 2 to 32 and 24 to 244 lb. air/hr. The rotameters were calibrated to read to within 2% of the actual flow rate. A thermometer and manometer were located at the rotameter exit so that corrections might be made for deviations from the conditions at which the rotameters were calibrated. The air rate was adjusted by means of valves beneath the rotameters. Since the blower heated up during operation, a packed humidifier was used to cool the air. The temperature was set with three 500-watt bayonet heaters connected to variable transformers.

The heated air was passed through an aluminum column 6 in. high by 4.0 in. in diameter. The column was packed with about 2.5 in. of 0.5-in. naphthalene Berl saddles. During a run the column usually contained 200 naphthalene saddles. A 1-in. layer of 0.5-in. ceramic saddles was located at the bottom of the column to insure characteristic gas distribution to the bottom layer of naphthalene saddles. The column was held in place with three quick-releasing, spring-loaded clamps and was gasketed at top and bottom.

Temperatures were indicated on two thermometers, one located 2 in. below the column and the other approximately 0.5 in. from the top layer of naphthalene. The thermometers read from  $-1.0^\circ$  to  $101.0^\circ\text{C}$ . in tenths of a degree. Weighings were made on a torsion balance sensitive to a tenth of a gram in the range employed.

The naphthalene saddles, which were molded by Maurice A. Knight, have the same dimensions as the porcelain saddles supplied by this company and the characteristics given in Table 1. The naphthalene used was crushed refined Polar naphthalene

Gas	Viscosity $\mu$ , lb./ft. (hr.)	Density $\rho$ , lb./cu. ft.	Diffusivity* $D$ , sq. ft./hr.	Schmidt No. ( $\mu/\rho D$ )
Air	0.0439	0.0752	0.210	2.57
Carbon dioxide	0.0355	0.113	0.160	1.96
Freon-12	0.0299	0.313	0.085	1.12

\*Diffusivities are reported for the naphthalene-gas systems.

from the Barrett Division of Allied Chemical and Dye Corporation.

The column was insulated by being wrapped with two electric heating pads. Running the column with 4 in. of ceramic packing at high gas rates at various temperatures ensured no heat loss from the column. A section of rubber hose was located above the column to facilitate its removal. After passing through the column the air was exhausted.

The equipment used to study the variation of  $k_g$  with gas properties was, unlike the equipment previously described, a closed system. The gas, either air, carbon dioxide, or Freon-12, was blown through the rotameters by means of a Roots-Connorsville gas pump. Coarse adjustments of the flow rate were made by means of a variable-speed motor drive and fine adjustments were made with the valves under the rotameters. The gas from the pump was cooled in a 13-ft. double-pipe heat exchanger with a 2-in.-diam. shell. The tube, supplied by the Brown Fintube Company, was 0.75-in. pipe with twenty 0.5-in. high axial fins. A thermometer and manometer were again located at the rotameter exit. The column packing and thermometers were the same as in the equipment described previously. The column was held between the top plate and bottom support with three 8-in. C clamps.

To make it possible to recycle the gas, the naphthalene was removed by means of activated carbon. The tank containing the carbon was 28 in. in diameter by 5.5 ft. high. It was filled with 220 lb. of 4- by 10-mesh activated carbon for the Freon and carbon dioxide runs. Before the Freon runs were made, the carbon was saturated with Freon.

The capacity of this activated carbon for

naphthalene was roughly 15% by weight, or 33 lb. naphthalene in the carbon dioxide and Freon runs. Since the total weight of naphthalene vaporized was only 0.75 lb. for all the runs, it was assumed that the naphthalene concentration in the recycled gas could be taken as zero.

The compressed gas was supplied by the Matheson Chemical Company. The Freon-12 was at least 97% pure, and the carbon dioxide at least 99.8% pure. Atmospheric pressures were obtained from a Taylor recording barometer, and vacuum was obtained from a Cenco Hyvac pump.

## PROCEDURE

The variation of  $k_g$  with temperature was studied by vaporizing naphthalene Berl saddles into air at temperatures from  $20^\circ$  to  $70^\circ\text{C}$ . Runs were made as follows.

A cardboard tube was inserted in the equipment in place of the aluminum column and the gas rate was adjusted. The temperature of the gas was set with the three bayonet heaters. The column, containing 1 in. of ceramic packing covered by a brass plate, was weighed in an insulated box. The naphthalene packing was then added and the column plus packing was put in an oven and heated to the temperature of the air passing through the cardboard tube.

When the naphthalene reached the proper temperature, the column was transferred into the insulated box, covered by the brass plate to eliminate vaporization, and weighed. The cardboard tube was then removed and the column inserted in its place. The necessary time, temperature, and pressure data were then taken. Temperatures were recorded every 2 min. for the first 10 min., every 5 min. for the next 20 min., and every 10 min. after that. At

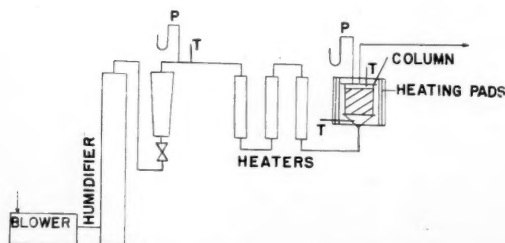


Fig. 1. Schematic diagram of apparatus, I.

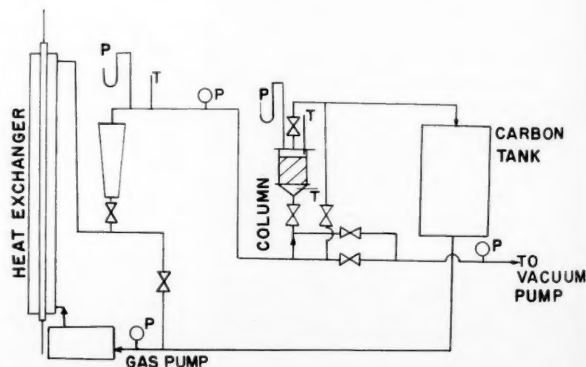


Fig. 2. Schematic diagram of apparatus, II.



the end of the run the column was covered by the brass plate, returned to the insulated box, and weighed.

In the work with various carrier gases, the system was first evacuated to 27 in. Hg. below atmospheric pressure, filled with gas, evacuated again, and refilled with gas. The pressure at the suction end of the gas pump was always slightly above atmospheric pressure. During runs the pressure would fall slightly because of leakage past the stuffing boxes on the pump. To compensate, gas was continuously introduced.

The column plus the ceramic and naphthalene packing was weighed before and after each run. The equipment was set up so that the section containing the column might be isolated from the rest of the system and evacuated separately. When the column was replaced in the equipment after the initial weighing, it was evacuated to 28 in. Hg. below atmospheric pressure before the valves connecting it to the rest of the system were opened. The weight loss during this evacuation period was not detectable on the balance used.

#### METHOD OF CALCULATION

The expression used to calculate  $k_G$  is

$$k_G = \frac{N_A}{A(\Delta p)_{lm}} \quad (2)$$

where

$$(\Delta p)_{lm} = \frac{(p_{s1} - p_1) - (p_{s2} - p_2)}{\ln \left[ \frac{(p_{s1} - p_1)}{(p_{s2} - p_2)} \right]} \quad (3)$$

Since the inlet gas did not contain naphthalene,  $p_1$  was always taken as zero and  $p_2$  was calculated from a naphthalene material balance.

It can be shown that when equilibrium conditions are reached in the column, the surface temperature of the naphthalene packing will be lower than the bulk temperature of the gas passing the surface. At room temperature this temperature difference is small enough to be neglected and the partial pressure of the naphthalene at the surface of the packing can be taken as equal to the vapor pressure of naphthalene at the bulk gas temperature. For the runs at the higher temperatures, however, it was necessary to calculate the surface temperatures at the bottom and top of the naphthalene packing in order to evaluate the true driving force. This was done by writing an equation for the wet-bulb temperature of naphthalene in terms of the bulk temperature  $t$  and bulk partial pressure  $p$  of the gas passing the surface:

$$p_s = 0.642(t - t_s) + p \quad (4)$$

The constant, 0.642, was obtained by using the psychrometric ratio for the naphthalene-air system reported by Beddingfield and Drew (1). The surface temperature  $t_s$  and partial pressure  $p_s$  can be obtained by solving Equation (4) simultaneously with the equation for the

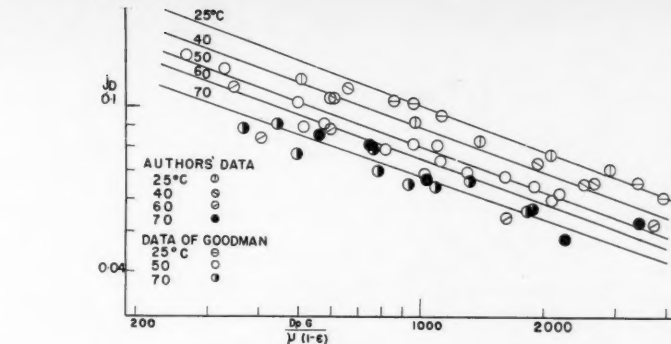


Fig. 3. Effect of temperature on  $j_D$  based on bulk-gas temperature.

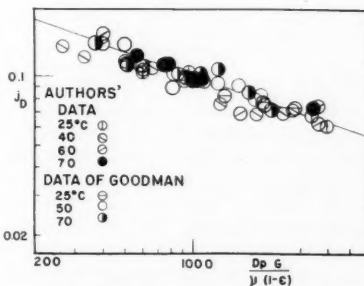


Fig. 4. Effect of temperature on  $j_D$  based on naphthalene-surface temperature.

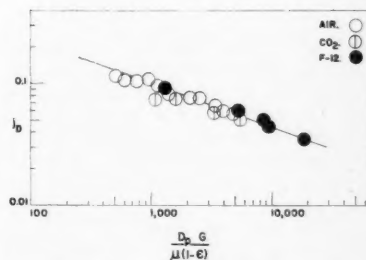


Fig. 6. Effect of carrier gas on  $j_D$ .

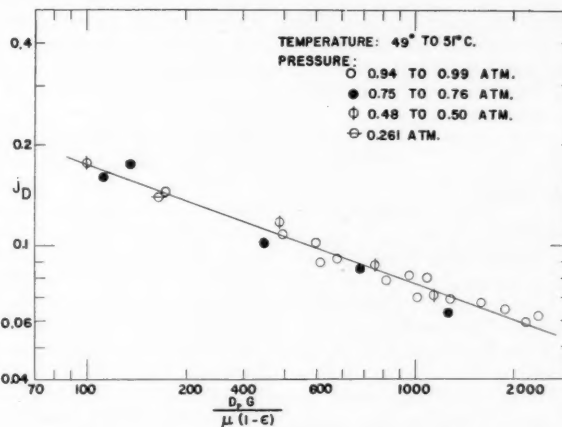


Fig. 5. Effect of pressure on mass transfer factor.

vapor pressure of naphthalene reported in the "International Critical Tables" (6).

$$\log p_s = -\frac{3,729}{t_s + 273.1} + 11.450 \quad (5)$$

The constants in Equations (4) and (5) require temperatures to be expressed in

degrees centigrade and pressures in millimeters of mercury. These equations were solved simultaneously either by the use of charts which were prepared for this purpose or by trial and error.

An experimental value of the diffusivity is available for the naphthalene-air system (6) but not for the naphthalene-

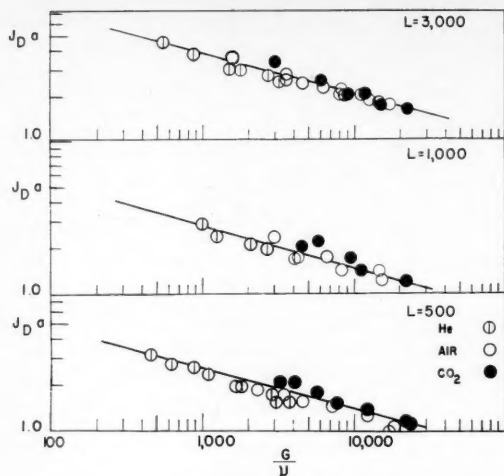


Fig. 7. Data of Yoshida.

carbon dioxide and naphthalene-Freon-12 systems. These diffusivities were estimated by the method suggested by Hirschfelder, Bird, and Spotz (5) using the collision radius for Freon-12 reported by Buddenburg and Wilke (2) and a force constant estimated from the critical temperature. The collision radius of naphthalene was estimated from its critical volume, and a force constant was estimated from the critical temperature.

The viscosities of Freon-12 and carbon dioxide are reported by Buddenburg and Wilke (2). The physical properties of the gases employed are tabulated for 20°C. in Table 2.

The naphthalene saddles retained their shape even when more than one quarter of their weight was lost by vaporization. This made it possible to assume constant surface area during a run.

## EXPERIMENTAL RESULTS

### Effect of Temperature

The experimental data obtained with air as the inert gas at temperatures from 25° to 70°C. are shown in Figures 3 and 4 with some similar data of Goodman (4). For Figure 3 the data have been calculated with driving forces based on bulk gas temperatures. The same data are shown in Figure 4 with driving forces based on naphthalene surface temperatures obtained as outlined under the discussion of the method of calculation. The solid line through the data in Figure 4, as well as the 25°C. line in Figure 3, represents Equation (1), which satisfactorily correlates these data when the true driving force is employed. Figure 3 is an excellent illustration of how false conclusions can be reached as to the effect of temperature if the bulk gas temperature is employed instead of the temperature existing at the phase boundary.

These results raise some questions as to the evaluation of driving forces in packed absorption columns. If the surface temperature of the liquid differs substantially from the bulk liquid temperature, which is commonly used as the basis for evaluating the driving force, there may appear to be some effect of temperature. The direction of this effect will depend upon the heat effects at the surface and, as pointed out for ammonia absorption, the surface temperature may be above or below the bulk liquid temperature for different operating conditions. Unfortunately, nothing is known about the temperature gradient in the liquid phase in packed columns, and so it is impossible to estimate actual surface temperatures except for special cases.

### Effect of Pressure

Figure 5 presents the previously unpublished data of Goodman (4) obtained by vaporizing 0.5-in. naphthalene Berl saddles into air at approximately 50°C. and pressures varying from 0.261 to 0.99 atm. As data are based on bulk gas temperatures, the line corresponds to the 50°C. line of Figure 3. If these points were corrected for surface temperature, they would fall on the line representing Equation (1) in Figure 4. It is obvious that on a  $j_D$  vs. modified-Reynolds-number plot there is no effect of pressure. This means that  $k_G$  is inversely proportional to pressure as observed by Zabban and Dodge (14), who used packed columns for absorption at pressures above 1 atm.

### Effect of Properties of Inert Gas

The data obtained with air, carbon dioxide, and Freon-12 as carrier gases are shown in Figure 6. The solid line, again, represents Equation (1), and it can be seen that this equation satisfactorily represents the data for inert gases of different physical properties.

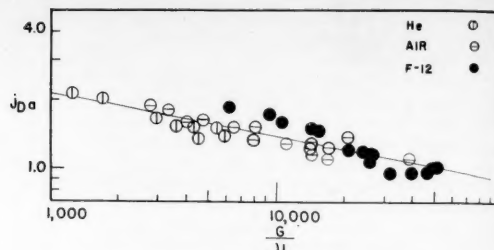


Fig. 8. Data of Lynch and Wilke.

Tests of this method of correlation for packed columns are shown in Figures 7 and 8. The product of  $j_D$  and the effective interfacial area  $j_D a$  is plotted vs.  $G/\mu$ , which is proportional to the Reynolds number for any one packing. In Figure 7 the water-vaporization data of Yoshida (13) are brought together for three different inert gases. Similar results are shown in Figure 8 for the data of Lynch and Wilke (8).

There is always difficulty in correlating  $k_G a$  data because  $k_G$  and  $a$  are not affected by the same variables in the same way. For example, at a given liquid rate  $a$  is relatively independent of  $G$ , up to the loading point. Lynch and Wilke (8), using a 1-ft.-diam. column packed with 1-in. rings, operated at gas rates up to and in the neighborhood of the loading point. Yoshida (13), by using the same packing in a 4-in. column, avoided loading conditions although he operated at similar gas and liquid rates. For a given liquid rate, therefore, Yoshida could maintain a constant effective interfacial area, whereas Lynch and Wilke could not. Yoshida's data, therefore, are brought together better than the data of Lynch and Wilke on  $j_D a$  vs. modified Reynolds-number plots such as Figures 7 and 8.

For design purposes the  $k_G$ , obtained from Equation (1), can be combined with the effective interfacial areas  $a$  obtained from the plots of  $a$  vs.  $G$  reported previously (11). For inert gases other than air these plots should be taken as  $a$  vs.  $G/\sqrt{\rho/0.075}$  because loading and flooding points as well as pressure drops can be correlated for various gases with this term.

## SUMMARY OF RESULTS AND CONCLUSIONS

The equation

$$j_D = \left[ \frac{k_G M_M P_{BM}}{G} \right] \left[ \frac{\mu}{\rho D_e} \right]^{2/3} = 1.195 \left[ \frac{D_p G}{\mu(1 - \epsilon)} \right]^{-0.36} \quad (1)$$

has been shown to correlate mass transfer data for a wide variety of packings, operating conditions, and physical properties of the solute and inert gases.

A design method is now available whereby the  $k_G$  obtained from Equation (1) can be combined with effective interfacial areas  $a$  reported previously (10, 11, 12) to obtain a  $k_G a$  for any desired gas-liquid-solute system for which physical properties are available.

#### ACKNOWLEDGMENT

The authors wish to acknowledge support of this work under Contract No. AT (30-1)-1463 of the Atomic Energy Commission.

#### NOTATION

- $A$  = total surface area of packing, sq. ft.  
 $a$  = effective interfacial area, sq. ft./cu. ft.  
 $D_g$  = diffusivity of solute in gas, sq. ft./hr.  
 $D_p$  = diameter of sphere possessing the same surface area as a piece of packing, ft.  
 $G$  = superficial gas rate, lb./(hr.) (sq. ft.)  
H.T.U. = height of a gas-phase transfer unit, ft., ( $G/k_G a M_M P_{BM}$ )  
 $j_D$  = mass transfer factor, defined by Equation (1)  
 $K_G$  = over-all mass transfer coefficient, lb. moles/(hr.) (sq. ft.) (atm.)

- $k_G$  = gas-phase mass transfer coefficient, lb. moles/(hr.) (sq. ft.) (atm.)  
 $k_L$  = liquid-phase mass transfer coefficient, lb. moles/(hr.) (sq. ft.) (lb. moles/cu. ft.)  
 $M_M$  = mean molecular weight of gas, lb./lb. mole  
 $N_A$  = rate of mass transfer, lb. moles/hr.  
 $p$  = partial pressure of naphthalene in the gas, atm.  
 $(\Delta p)_{lm}$  = logarithmic mean driving force, atm.  
 $P_{BM}$  = mean partial pressure of inert gas in the gas phase, atm.  
 $T$  = absolute temperature, °K.  
 $t$  = temperature of the gas, °C.  
 $u$  = gas velocity, ft./sec.

#### Greek Letters

- $\epsilon$  = void fraction, cu. ft./cu. ft.  
 $\mu$  = gas viscosity, lb./(hr.) (ft.)  
 $\rho$  = gas density, lb./cu. ft.

#### Subscripts

- $S$  = at the naphthalene surface  
 $S_1$  = at the naphthalene surface, bottom of packing  
 $S_2$  = at the naphthalene surface, top of packing  
1 = bottom of packing  
2 = top of packing

#### LITERATURE CITED

1. Bedingfield, C. H., and T. B. Drew, *Ind. Eng. Chem.*, **42**, 1165 (1950).
2. Buddenburg, J. W., and C. R. Wilke, *J. Phys. Colloid Chem.*, **55**, 1491 (1951).
3. Dodge, B. F., and O. E. Dwyer, *Ind. Eng. Chem.*, **33**, 485 (1941).
4. Goodman, E. L., M.S. thesis, Clarkson College of Technology, Potsdam, N. Y. (1954).
5. Hirschfelder, J. O., R. B. Bird, and E. L. Spotz, *Trans. Am. Soc. Mech. Engrs.*, **71**, 921 (1949).
6. "International Critical Tables," McGraw-Hill Book Company, Inc., New York (1928).
7. Kowalke, O. L., O. A. Hougen, and K. M. Watson, *Bull. Univ. Wisc. Eng. Expt. Sta. Ser. No. 68* (1925).
8. Lynch, E. J., and C. R. Wilke, *A. I. Ch. E. Journal*, **1**, 9 (1955).
9. Molstad, M. C., J. F. McKinney, and Abbey, R. G., *Trans. Am. Inst. Chem. Engrs.*, **39**, 605 (1943).
10. Shulman, H. L., C. F. Ullrich, and N. Wells, *A. I. Ch. E. Journal*, **1**, 247 (1955).
11. Shulman, H. L., C. F. Ullrich, A. Z. Proulx, and J. O. Zimmerman, *A. I. Ch. E. Journal*, **1**, 253 (1955).
12. Shulman, H. L., C. F. Ullrich, N. Wells, and A. Z. Proulx, *A. I. Ch. E. Journal*, **1**, 259 (1955).
13. Yoshida, F., *Chem. Eng. Progr. Symposium Ser.*, No. 16, **51**, 59 (1955).
14. Zabban, W., and B. F. Dodge, *Chem. Eng. Progr. Symposium Ser. No. 10*, **50**, 61 (1954).

## Densities of Liquid-acetone-water Solutions up to Their Normal Boiling Points

K. T. THOMAS and R. A. McALLISTER,

North Carolina State College, Raleigh, North Carolina

The densities of acetone-water liquid solutions have been measured over the entire composition range from 20°C. to within 3° to 7°C. of the normal boiling point of the mixture. The density was measured with a Robertson pycnometer (13), which was modified slightly. The density values are thought to be accurate to within  $\pm 0.00005$  density units. The technique for determining density values of the volatile mixture near the boiling temperature is given in some detail. The refractive index ( $n_D^{25}$ ) of pure acetone has been redetermined and equals  $1.35596 \pm 0.00003$ .

In a study of the effect of the physical properties on the efficiency of distillation in the binary acetone-water system, physical properties such as density, viscosity, molecular diffusivity, and surface tension were needed at the boiling temperature. No density data of acetone-water mixtures above 25°C. could be found in the literature; furthermore, no reliable method

was known whereby the density data could be extrapolated 30° to 75°C. to the boiling points with confidence. It was resolved to measure the density precisely (at least to  $\pm 0.01\%$ ) from 20°C. to within a few degrees of the boiling temperature. These data could then be used to extrapolate accurately to the boiling points. Measurements and correlations of other physical properties such as the absolute viscosity, the surface tension, and molecular diffusivity require accurate

density values, and the density data would also be useful in this respect.

Several early investigators (8, 10) have reported the densities of acetone-water mixtures at 15°, 20°, and 25°C. Their results, however, scatter considerably, probably because of the inferior quality of the acetone available to them. The most recent, and presumably the best, determinations of the densities of acetone-water mixtures were done by Young (16) at 20°C. and by Griffiths (5) at 25°C.

K. T. Thomas is with Indian Rare Earths, Ltd., Bombay, India.

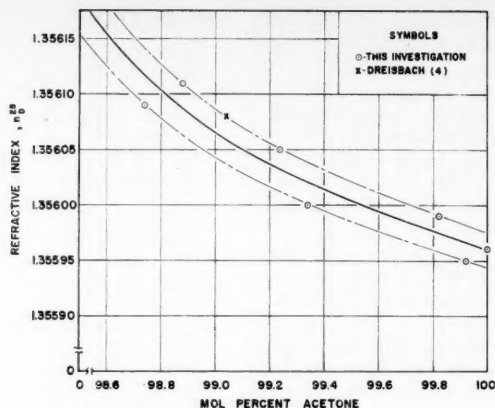


Fig. 1. Refractive index of acetone-water solutions, high acetone concentration.

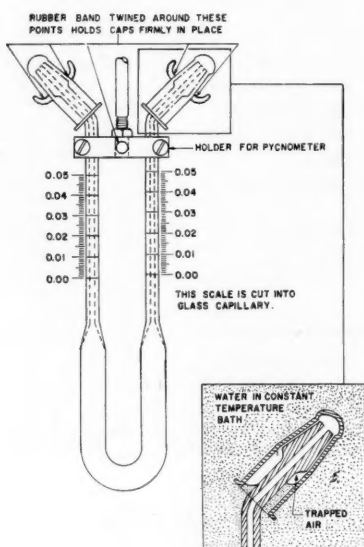


Fig. 2. Modified Robertson pycnometer.

TABLE 1. DENSITY OF "PURE" ACETONE AT 20.00°C.

Density, g./ml.	Reference
0.792	7
0.79082	15
0.79079 (99.70 wt. %)	4
0.79061	16
0.79060	15
0.79053	15
0.78990	14
0.7895	2
0.7894	12
0.7894	6

The density of pure water is, of course, known very accurately, but not the density of pure acetone. Density values for "pure" acetone at 20.00°C. are listed

in Table 1. The agreement of density values of acetone at other temperatures is no better (15). Thirion and Craven (14) made a careful study of the density and dryness of acetone and concluded that the most accurate density of pure acetone at 20.00°C. was 0.78990 g./ml. Small amounts of water increase the density, while isopropyl ether, a probable contaminant if the acetone is manufactured from isopropanol, will reduce the density. Careful measurements of the density of acetone-water mixtures in the range of 0 to 5 wt. % of water were made by Young (16) at 20°C. The acetone that Young used as pure, however, had been dried over calcium chloride for one week and had a density

of 0.79061, an indication that it was not yet completely anhydrous. Tests in the authors' laboratory show that the water content of acetone continues to decrease even after 6 months with calcium sulfate as the desiccant. Using Thirion's (14) 100.00% density value of 0.78990 g./ml. and drawing a curve parallel to Young's in the region of 0 to 5 wt. % water in acetone is an accurate means of predicting the water content of acetone samples from precision density measurements. This was the primary standard by which the water content of the acetone used in this work was determined. Dreisbach's (4) density value for 99.70 wt. % acetone (99.04 mole %) is 0.79079. The value read from the aforementioned curve at 99.04 mole % is 0.79078, showing excellent agreement with this method. The secondary standard was the refractive-index vs. water-composition curve. A record was made of the refractive indexes of the acetone samples the water contents of which had been determined by density measurements. These data are given in Table 2 and Figure 1.

TABLE 2. REFRACTIVE INDEXES AND DENSITIES OF CONCENTRATED ACETONE-WATER SOLUTIONS

Mole % acetone	Density at 20°C., g./ml.	Refractive index, $n_D^{25}$
99.92	0.78998	1.35595
99.82	0.79007	1.35599
98.74	0.79106	1.35609
98.88	0.79093	1.35611
99.24	0.79061	1.35605
99.34	0.79059	1.35600
100.00	0.78990	1.35596*

\*This value was extrapolated from the data of Figure 1.

The dashed curves in the figure are approximately  $\pm 0.00002$  refractive index units from the solid, median curve. The instrument with which the measurements was made is accurate to  $\pm 0.00003$  unit. It is seen from the figure that Dreisbach's (4) point at 99.04 mole % acetone is well within the rated accuracy. From this graph the water content of the "pure" acetone was checked each time an acetone-water mixture was made up. In this way the mole percentages of acetone reported are thought to be accurate to within  $\pm 0.1\%$  of the value of the composition.

#### EXPERIMENTAL PROCEDURE

A 10-ml. Robertson pycnometer (13), obtained from the Scientific Glass Apparatus Company of Bloomfield, New Jersey, was modified as shown in Figure 2. The modification consisted of putting a skirt on the caps which would allow the entire pycnometer, including the caps, to be immersed in the constant-temperature bath without the ground glass of the tips being wetted. When the bath temperature was above room temperature, it was necessary to immerse the entire pycnometer to prevent condensation of the acetone-water mixture in the caps.



Bauer's (1) technique for precision pycnometric measurements was followed carefully except for a few modifications which became necessary. The standard liquid used for calibrating the pycnometer was tap water that had been distilled once in a Barnstead still and redistilled in an all-quartz apparatus (9).

The acetone used in this investigation was Baker Analyzed Reagent Grade, Baker and Adamson Reagent Grade, and Fisher Certified Reagent, Spectroanalyzed. Thirion and Craven's (14) test for isopropyl ether indicated that this impurity was not present. The three acetone sources were also analyzed in a Fisher-Gulf Partitioner (a gas chromatography unit) and the results showed that water was the only contaminant, a finding that was supported by distillation studies in a laboratory still (1- by 90-cm. reflux section packed with 1/8-in. Pyrex helices). The boiling point range was 56.1° to 56.2°C. (749 to 750 mm. Hg). The water content of the acetone was determined from density and refractive-index measurements as described.

All weights used in the calibration, in the density determinations, and in making up the mixtures were corrected to the vacuum weight. The brass weights used were compared with National Bureau of Standards calibrated weights and the corrections noted. The constant-temperature bath controlled the temperature to  $\pm 0.01^\circ\text{C}$ . and the thermometer used was calibrated by the National Bureau of Standards.

The method of filling the pycnometer is shown in Figure 3. Using the ball joint as shown in the figure avoided air locks in the filling and flushing of the pycnometer. Especially at the higher temperatures it was found convenient to fill the pycnometer completely and immediately after filling to immerse it partially in an auxiliary bath  $3^\circ$  to  $10^\circ$  above the temperature at which the density was to be measured. The liquid which was forced out of the pycnometer was wiped off quickly with a dry chamois,

and the caps were set in place. Enough liquid had overflowed from the pycnometer so that when it was put in the main constant-temperature bath at the test temperature, the liquid contracted and the menisci fell into the graduated range of the capillary arms. From the completion of filling until the pycnometer was placed in the main constant-temperature bath was a matter of less than 1 min. Evaporation in handling the pycnometer was negligible. Some evaporation from the liquid necessarily took place in the constant-temperature bath. The vapors filled the upper arms of the capillaries and the small volumes of the caps. It was estimated that this amount of evaporation changed the mole percentage of the liquid in the pycnometer less than 0.002 unit. The density differences resulting from this were completely unimportant to the accuracy of the measurements.

After the volume had been read in the constant-temperature bath, the pycnometer was removed and carefully wiped dry and clean on the outside with a chamois. The

caps were removed, the portion of the arm under the cap skirt was quickly wiped, and clean dry caps were inserted immediately. At  $37.78^\circ\text{C}$ . and higher the pycnometer was removed from the bath and straightway carried to a refrigerator, where the wiping and replacement of the caps took place. In

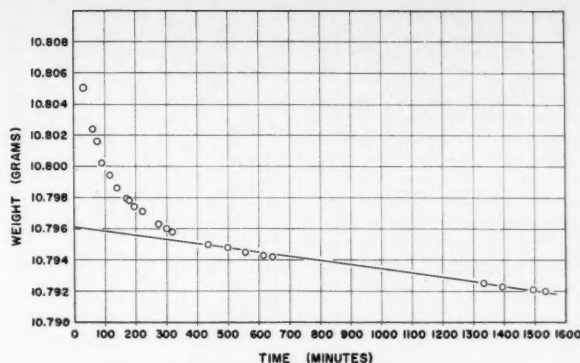


Fig. 4. Pycnometer weight as a function of time.

TABLE 3. DENSITY OF LIQUID-ACETONE-WATER SOLUTIONS

Temperature, $^\circ\text{C}$ .	Mole % acetone	Density, g./ml.
20.00	100.00	0.78990*
	99.92	0.78998
	99.82	0.79007
	99.34	0.79050
	99.24	0.79061
	98.88	0.79093
	98.74	0.79106
	78.84	0.81344
	49.06	0.85953
	25.10	0.91613
	14.50	0.94833
25.00	0.00	0.99823
	99.58	0.78482
	80.31	0.80626
	48.21	0.85617
	38.02	0.87836
	25.30	0.91103
	14.55	0.94446
	6.935	0.97033
37.78 (100.00°F.)	99.58	0.77015
	76.46	0.79646
	50.12	0.83921
	37.22	0.86742
	25.02	0.90015
	14.52	0.93483
	7.166	0.96247
50.05	99.58	0.75556
	78.13	0.78003
	48.55	0.82888
	24.86	0.88911
	14.40	0.92542
	7.152	0.95486
60.11	11.00	0.93104
70.20	4.716	0.95218
	2.063	0.96482
80.35	2.109	0.95971

\*Reference 14.

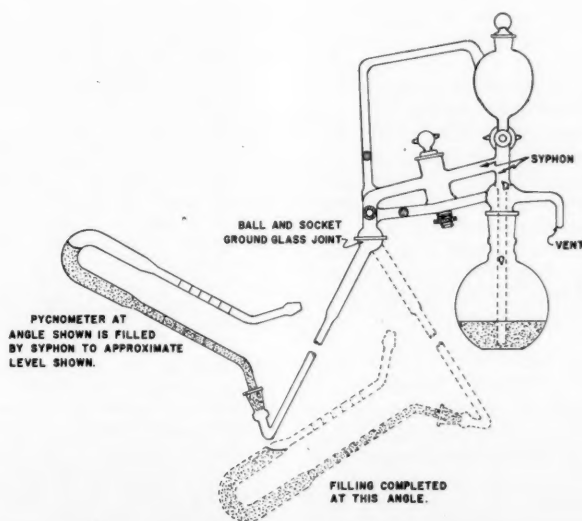


Fig. 3. Pycnometer filling procedure and apparatus.

this way vaporization losses were held to a minimum. The pycnometer was suspended in the left arm of the balance, a tare (dummy pycnometer) being in the right arm, and the weighings were begun. Weight-vs.-time curves, such as shown in Figure 4, were prepared. Zero time corresponded to the time of reading the volume just before the pycnometer was removed from the constant-temperature bath. The first portion of the curve represented the time period when water evaporation and water-vapor adsorption on the outside of the pycnometers were coming to their equilibrium

TABLE 4. DENSITIES OF LIQUID-ACETONE-WATER SOLUTIONS AT THE NORMAL BOILING POINTS

Mole % acetone	Boiling temperature*, °C.	Density, g./ml.
0	100.00	0.9584
2	86.50	0.9551
5	75.00	0.9472
7.5	70.20	0.9385
10	66.72	0.9298
20	62.17	0.8949
30	61.01	0.8623
40	60.40	0.8368
50	59.84	0.8155
60	59.30	0.7983
70	58.81	0.7823
80	58.20	0.7678
90	57.43	0.7560
100	56.20	0.7476

\*Averaged values from References 2, 3, and 11.

values. At the same time some weight was being lost owing to evaporation of the liquid in the pycnometer. The former effects no longer changed the apparent weight after about 300 min., but the latter effects continued as long as weighings were made. The straight-line portion of Figure 4 represented that time period when only evaporation caused a weight change. Extrapolation of this line to zero time represented the accurate apparent weight at the time of reading the volume. The continued loss in weight must indicate the fugitive nature of acetone-water vapors in spite of tightly placed ground-glass caps. In the water-calibration runs the weight-vs.-time curve soon fell to a constant weight.

## RESULTS

The results of the density measurements are given in Table 3 and Figure 5. The isotherms are shaped in a smooth curve and display a small inflection near 15 mole %. Density values read at fixed compositions from enlarged plots of Figure 5 were cross-plotted as functions of temperature from which the densities at the boiling temperature were obtained by extrapolation. The values are listed in Table 4 and shown in Figure 6. Boiling-point temperatures as functions of composition in the liquid phase were determined from the average values from several sources (2, 3, 11). More weight

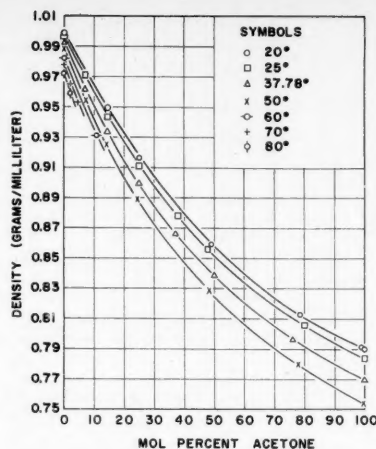


Fig. 5. Density of liquid-acetone-water solutions.

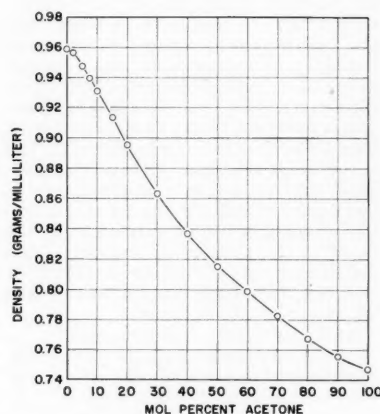


Fig. 6. Densities of liquid-acetone-water solutions at the normal boiling points.

was given to the boiling-point data of Brunjes (2), as they seemed to have more internal consistency. The boiling-point temperatures are probably no more accurate than  $\pm 0.1^\circ\text{C}$ . The extrapolated density values therefore lack precision. Should more accurate boiling-point temperatures become available, corresponding density values can be extrapolated with a precision to match that of the measured density values.

## DISCUSSION

The pycnometer was calibrated at  $20^\circ$ ,  $25^\circ$ , and  $60^\circ\text{C}$ . Two runs were made at each temperature, one run with water at a low level in the calibrated arms of the pycnometer and another at a high level. If the milliliters per scale division in each arm were assumed to be equal at

the given temperature, the volume of the pycnometer with both menisci at the zero scale reading was a straight-line function of temperature and was expressed as an equation derived by the method of least squares.

Calculation of the difference of the calibration points from the least-squares calibration curve gave the average expected error in the volume readings as  $\pm 0.000175$  ml. With  $\pm 0.0002$  g. allowed as the maximum error in the vacuum weights calculated along with the volume deviation mentioned above, the error in the density measurements was estimated as  $\pm 0.00003$  density unit. The figure given in the abstract for the accuracy of the density values of  $\pm 0.00005$  is a conservative one.

The accuracy of the reported mole percentage is discussed above and estimated as  $\pm 0.1\%$  of the reported composition.

## ACKNOWLEDGMENT

This work was carried out in connection with Research Project 1, "Tray Efficiencies in Distillation Columns," sponsored by the American Institute of Chemical Engineers. The authors gratefully acknowledge the support and encouragement of the A. I. Ch. E. Research Committee during the course of this investigation.

## LITERATURE CITED

- Bauer, Norman, in A. Weissberger, ed., "Technique of Organic Chemistry," vol. 1, 2 ed., pp. 267ff, Interscience Publishers, Inc., New York (1949).
- Brunjes, A. S., and M. J. P. Bogart, *Ind. Eng. Chem.*, **35**, 257 (1943).
- Chu, J. C., "Distillation Equilibrium Data," p. 24, Reinhold Publishing Corporation, New York (1950).
- Dreisbach, R. R., and R. A. Martin, *Ind. Eng. Chem.*, **41**, 2876 (1949).
- Griffiths, V. S., *J. Chem. Soc.*, 1326 (1952).
- Griswold, J., and C. B. Buford, *Ind. Eng. Chem.*, **41**, 2347 (1949).
- Hodgeman, C. D., ed., "Handbook of Chemistry and Physics," 30 ed., p. 597, Chemical Publishing Company, Cleveland (1948).
- "International Critical Tables," vol. III, p. 113, 5 references, McGraw-Hill Book Company, Inc., New York (1928).
- Kendall, J., *J. Amer. Chem. Soc.*, **38**, 2460 (1916).
- Naville, P., *Helv. Chim. Acta*, **9**, 913 (1926).
- Othmer, D. F., and R. F. Benenati, *Ind. Eng. Chem.*, **37**, 299 (1945).
- Othmer, D. F., and F. Morley, *Ind. Eng. Chem.*, **38**, 751 (1946).
- Robertson, G. R., *Ind. Eng. Chem., Anal. Ed.*, **11**, 464 (1939).
- Thirion, R., and E. C. Craven, *J. Appl. Chem.*, **2**, 210 (1952).
- Timmermans, J., "Physico-Chemical Constants of Pure Organic Compounds," p. 355, Elsevier Publishing Company, Inc., New York (1950).
- Young, W., *J. Soc. Chem. Ind.*, **52**, T449 (1933).

# Absorption and Stripping-factor Functions for Distillation Calculation by Manual- and Digital-computer Methods

WAYNE C. EDMISTER, California Research Corporation, Richmond, California

New absorption- and stripping-factor functions have been developed for use in computing multicomponent separations in fractionators, reboiled absorbers, refluxed strippers, and columns with side-stream strippers. Charts of fraction not absorbed vs.  $A$  factor and fraction not stripped vs.  $S$  factor are included with the equations for these operations.

These functions and procedures are of particular advantage in computing complex columns, i.e., two or more feeds and three or more products, where the proposed  $A$  and  $S$  factor equations provide a method for converging on a solution.

Distillation calculations for multicomponent mixtures are so tedious that process engineers have long been seeking a labor-saving method or device that will give them the required answers rapidly and with a minimum of effort. The high-speed digital computer is such a device. Its use in solving distillation problems requires careful and complete programming to obtain an automatic machine operation that duplicates rigorous manual calculations.

Experience with manual plate-to-plate and short-cut calculations is valuable in developing the machine programs. Absorption and stripping factors have been used in short-cut and in manual plate-to-plate calculations and are also useful in digital-computer distillation calculations. An advantage in using  $A$  and  $S$  factors in machine calculations is that the mathematical language is already familiar to process engineers. This makes it easier to interpret machine results and to extrapolate to different conditions as the same equations are used in hand and machine calculations.

Absorption and stripping factors have been used in distillation calculations for many years (1 to 10). New and more convenient relationships of these factors were required for present purposes. General functions of the  $A$  and  $S$  factors are developed and arranged for application to four distillation operations frequently used in the petroleum industry, i.e., (a) fractionator, (b) reboiled absorber, (c) refluxed strippers, and (d) fractionators with side-stream strippers. The fact that the same functions of  $A$  and  $S$  may be applied to all these columns manually or by machine is advantageous.

## BASIC CONCEPTS

Component distributions in multicomponent distillation are determined by the number of theoretical stages, the interstage vapor and liquid quantities, and the vapor-liquid  $K$  values. Three of these variables are frequently grouped in absorption ( $A = L/KV$ ) or stripping ( $S = KV/L$ ) factors. Functions of these

factors and the number of stages may be used to compute the component distributions.

Calculation methods using absorption and stripping factors may be rigorous or approximate depending upon the evaluation of the separation functions. These functions of  $A$  and  $S$  for separation calculations will be derived for two evaluation procedures: (a) plate-to-plate and (b) effective factors. Both of these may be done by hand or with a computer.

For design-calculation purposes it is convenient to consider all multistage separation processes as combinations of five separation zones: (1) condensing, (2) absorbing, (3) feed flash, (4) stripping, and (5) reboiling. Zones 1, 3, and 5 are each single-stage equilibrium flash separations, and zones 2 and 4 are multistage separations. There are two feeds to each of these multistage zones, i.e., the liquid entering the top and the vapor entering the bottoms. Likewise, there are two products: the liquid from the bottom and the vapor from the top.

It is convenient to regard both of these as separation operations where the liquid feed is subject to stripping by the rising vapors and where the vapor feed is subject to absorption by liquid flowing down the column. Thus zones 2 and 4 have both absorption and stripping taking place simultaneously, with absorption predominating in 2 and stripping in 4.

Absorption calculations are made with functions of the absorption factor, and stripping calculations are made with functions of the stripping factor for the same sections of plates. Values of  $A$  and  $S$  on individual plates may be used in some cases, but effective values of  $A$  and  $S$  for sections of plates are generally used in manual calculations. Effective values of  $A$  and  $S$  are also useful in the iterations of digital computer calculations which must be revised between trials.

## COMPONENT-DISTRIBUTION EQUATIONS

Rigorous functions of absorption and stripping factors are derived for multicomponent distribution in the four basic

multistage sections that constitute distillation columns: absorber, enricher, stripper, and exhauster.

### Absorber (Figure 1)

A component material balance around the top of the absorber to include plates 1 through  $i$  gives

$$l_i + v_1 = v_{i+1} + l_0$$

Combining this with the equilibrium relation  $l_{i+1} = A_{i+1}v_{i+1}$  and rearranging gives

$$l_{i+1} = (l_i - l_0 + v_1)A_{i+1} \quad (1)$$

Equation (1) is the basic relationship by which the liquid leaving plate  $i+1$  is found from the liquid leaving plate  $i$ .

An equation for the multistage absorption operation is obtained by combining relationships similar to Equation (1) for each plate:

$$l_n = v_1(A_1A_2A_3 \cdots A_n + A_2A_3 \cdots A_n + A_3 \cdots A_n + \cdots + A_n) - l_0(A_2A_3 \cdots A_n + A_3 \cdots A_n + \cdots + A_n) \quad (2)$$

Equation (2) will be used in later developments.

### Enricher (Figure 1)

A component material balance around the top of the enricher to include the condenser and Plate  $i$  gives

$$l_i + d = v_{i+1}$$

Combining with the equilibrium relation  $l_{i+1} = A_{i+1}v_{i+1}$  and rearranging gives

$$l_{i+1} = [l_i + d]A_{i+1} \quad (3)$$

Equation (3) is the basic relationship between the liquid leaving plate  $i+1$  and plate  $i$ . For the partial condenser, indicated in Figure 1, this relationship becomes

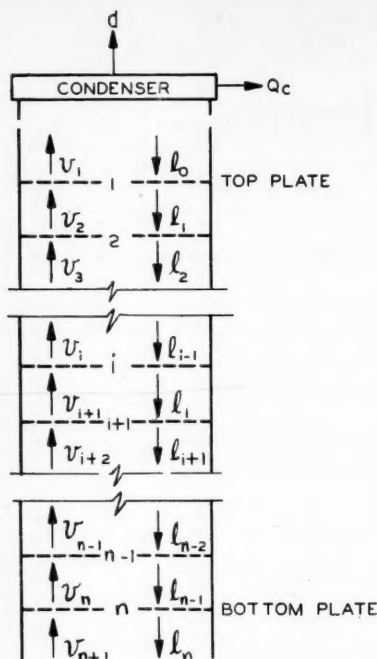
$$l_0 = dA_0 \quad (3a)$$

where

$$A_0 = \frac{L_0}{DK_0}$$

For a total condenser, where reflux and distillate are of same composition,  $l_0/d$  equals the reflux ratio, and so  $A_0 = R_{LD}$ .

An equation for the multistage enriching operation shown in Figure 1 is obtained by combining Equation (3a) and relationships like Equation (3) for each stage, to obtain





and

$$\psi_A = 1 - \phi_S$$

$$\psi_S = 1 - \phi_A$$

In other words both  $\psi_A$  and  $(1 - \phi_S)$  represent the fraction of a component in the liquid feed to the top of a section of plates that is stripped off into the residue gas leaving the top. Likewise,  $\psi_S$  and  $(1 - \phi_A)$  represent the fraction of a component in the gas feed to the bottom of a section of plates that is absorbed into the rich oil leaving the bottom. Thus a given section of plates is regarded as an absorber for finding  $\phi_A$  and  $\psi_A$  and as a stripper for finding  $\phi_S$  and  $\psi_S$ .

The foregoing can be shown to be mathematically equivalent. For simplicity take a three-plate absorber, where the plates are identified by subscripts  $a$ ,  $b$ , and  $c$  from the top. From definitions of  $\psi_A$  and  $\phi_S$

$$\psi_A = 1 - \frac{\left(\frac{L}{KV}\right)_a \left(\frac{L}{KV}\right)_b \left(\frac{L}{KV}\right)_c}{\left(\frac{L}{KV}\right)_a \left(\frac{L}{KV}\right)_b \left(\frac{L}{KV}\right)_c + \left(\frac{L}{KV}\right)_b \left(\frac{L}{KV}\right)_c + \left(\frac{L}{KV}\right)_c + 1}$$

$$\phi_S = \frac{1}{\left(\frac{KV}{L}\right)_c \left(\frac{KV}{L}\right)_b \left(\frac{KV}{L}\right)_a + \left(\frac{KV}{L}\right)_b \left(\frac{KV}{L}\right)_a + \left(\frac{KV}{L}\right)_a + 1}$$

Writing  $\psi_A = 1 - \phi_S$  in terms of the above  $A$  and  $S$  factor functions and clearing fractions proves the equivalencies.

These identities permit writing Equations (10) and (11) in terms of the  $\phi$  fraction:

$$v_1 = \phi_A v_{n+1} + (1 - \phi_S) l_0 \quad (12)$$

$$l_1 = \phi_S l_{n+1} + (1 - \phi_A) v_0 \quad (13)$$

where

$$\phi_A = \frac{1}{A_1 A_2 A_3 \cdots A_n + A_2 A_3 \cdots A_n + A_3 \cdots A_n + \cdots + A_n + 1} = 1 - f_a$$

$f_a$  = fraction absorbed

$$\phi_S = \frac{1}{S_1 S_2 S_3 \cdots S_m + S_2 S_3 \cdots S_m + S_3 \cdots S_m + \cdots + S S_m + 1} = 1 - f_s$$

$f_s$  = fraction stripped

Plates are numbered from the top down in evaluating the  $\phi_A$  functions for both equations and from the bottom up in evaluating the  $\phi_S$  functions.

Equations (12) and (13) are generalized separation functions that express the physical operation in terms of fractions absorbed and stripped. These fractions are functions of the absorption and stripping factors.

These functions are applicable to sections of any type of column, i.e., absorber, stripper, fractionator, etc. The values of  $\phi_A$  and  $\phi_S$  are always between zero and unity regardless of the magnitude of the  $A$  and  $S$  values. This is an advantage in evaluating and using the functions.

#### ENRICHING AND EXHAUSTING EQUATIONS

Component distribution functions of

$\phi_A$  and  $\phi_S$  for the enriching and exhausting sections (Figures 1 and 2) of a fractionator may be derived from Equations (4) and (8) and the definitions of  $\phi_A$  and  $\phi_S$ . Alternatively they may be derived from Equations (12) and (13) plus component material balances around the condenser and the reboiler.

An enriching equation may be derived from the absorber equation [Equation (12)] by making the lean oil equal zero, i.e.,  $l_0 = 0$ , and letting the top plate be a partial condenser. Equation (12) then reduces to Equation (4b). In like manner Equation (8b) may be obtained from Equation (13). Development of enriching and exhausting equations by combination follows.

An equation for the entire enriching section is readily obtained from Equation

section to the amount in the distillate. This will be called the "enriching ratio." The functions  $\phi_{SE}$  and  $\phi_{AE}$  will be between zero and unity for all components.

A similar equation may be written for the exhausting section by combining Equation (13) with the equivalents:

$$l_1 = v_0 + b \quad (\text{component material balance around reboiler})$$

$$v_0 = S_0 b \quad (\text{vapor-liquid equilibria for partial reboiler operation})$$

$$l_{m+1} = v_m + b \quad (\text{over-all component material balance})$$

This combination, followed by rearranging, gives

$$\frac{V_m}{b} = \frac{S_0 \phi_{AX} + 1}{\phi_{SX}} - 1 \quad (15a)$$

or

$$\frac{l_{m+1}}{b} = \frac{S_0 \phi_{AX} + 1}{\phi_{SX}} \equiv \frac{S_0 \phi_{AX}}{\phi_{SX}} + \frac{1}{\phi_{SX}} \quad (15b)$$

where the second subscript  $X$  designates the exhausting section.

When the reboiler vapor is of the same composition as bottoms product,  $S_0 = V_0/B = \text{boilup ratio}$ .

Equation (15) gives the "exhausting ratio" as a function of this boilup ratio and the functions  $\phi_{AX}$  and  $\phi_{SX}$ , which are also between 0 and 1.

Equations (14a) and (4a) both give  $l_n/d$  as a function of the  $L$ ,  $V$ , and  $K$  values for each plate. The different arrangements of the variables make these two equations suitable for different calculation purposes, but both are useful. Likewise, Equations (15a) and (8a) both give  $v_m/b$  as a function of the  $L$ ,  $V$ , and  $K$  values for each plate. These equations are also used for different kinds of calculations. The applications of these four equations will be taken up further after "effective"  $A$  and  $S$  factors are defined and the  $\phi_A$  and  $\phi_S$  functions evaluated.

#### EFFECTIVE FACTORS

The recovery fractions,  $\phi_A$  and  $\phi_S$  in Equations (12), (13), (14), and (15), may be evaluated from assumed or previous trial values of  $K$ ,  $V$ , and  $L$  on each plate. When the correct values of  $A$  and  $S$  are used, this method is rigorous. In some calculations (by hand and machine) it is convenient to use effective absorption and stripping factors,  $A_e$  and  $S_e$ .  $A_e$  is a mean value of the absorption factor that will give the same value of  $\phi_A$  that is obtained from using the values of  $A$  on each plate.  $A_e$  is defined as follows:

$$\phi_S = \frac{1}{A_e^n + A_e^{n-1} + \cdots + A_e^2 + A_e + 1} = \frac{A_e - 1}{A_e^{n+1} - 1} \quad (16a)$$

For  $A_e = 1.0$  the value of  $\phi_A$  is

$$\phi_A = \left[ \frac{1}{1+n} \right]_{A=1.0}$$

For an infinite number of plates and  $A_e \geq 1.0$ , the value of  $\phi_A$  is zero.

$$\phi_A = [0]_{A \geq 1.0, n=\infty}$$

For infinite plates and less-than-unity  $A_e$  factors

$$\phi_A = [1 - A_e]_{A_e < 1.0, n=\infty}$$

Analogous (effective) stripping-factor relationships can be written by inspection; i.e.,

$$\phi_S = \frac{1}{S_e^m + S_e^{m-1} + \dots + S_e^2 + S_e + 1} = \frac{S_e - 1}{S_e^{m+1} - 1} \quad (16b)$$

$$\phi_S = \left[ \frac{1}{1+m} \right]_{S=1.0}$$

$$\phi_S = [0]_{S \geq 1.0, m=\infty}$$

$$\phi_S = [1 - S]_{S < 1.0, m=\infty}$$

Figure 3 is a plot of  $\phi_A$  vs.  $A_e$  and  $n$  and of  $\phi_S$  vs.  $S_e$  and  $m$ . A probability scale is used for  $\phi_A$  and  $\phi_S$  and a logarithmic scale for  $A_e$  and  $S_e$ . This chart and Figures 3A and 3B were prepared from Equation (16). Rectangular coordinates for  $\phi_A$  and  $A_e$  would give a plot similar in appearance to the Kremser-Brown absorption-factor-vs.-fraction (or per cent) extraction plot. (See Figure 3A.) Figure 3B is an expanded plot on logarithmic scales of the lower right-hand corner of Figure 3A. Hull and Raymond (6) used such a Kremser-Brown chart, plotting  $(A^{n+1} - A)/(A^{n+1} - 1) = 1 - (A - 1/A^{n+1} - 1)$ .

For two plates the effective factors are given by the relations previously proposed (2).

$$A_e = \sqrt{A_B(A_T + 1) + 0.25} - 0.5 \quad (17a)$$

$$S_e = \sqrt{S_T(S_B + 1) + 0.25} - 0.5 \quad (17b)$$

Subscripts  $B$  and  $T$  designate the bottom and top plates, respectively. In many cases the effective factors are functions of terminal (top and bottom plates) conditions only and independent of the number of plates. In these cases correct values of  $A_e$  and  $S_e$  are obtained by these simple relations. Even where this simplification is not justified for final calculation, it may be used as a first approximation.

In some calculations both  $A_e$  and  $S_e$  are required for the same group of plates. For absorption factors the plates are numbered from the top down, and for stripping factors from the bottom up. For this reason  $A_1 = A_T$  and  $S_1 = S_B$  (subscripts  $T$  and  $B$  refer to top and

bottom). Also  $S_T = 1/A_T$  and  $S_B = 1/A_B$ . Another method of finding the values of  $A_e$  and  $S_e$  is by a proportionality rela-

tionship based upon the method proposed by Horton and Franklin (5) for locating the effective factor. The location of the

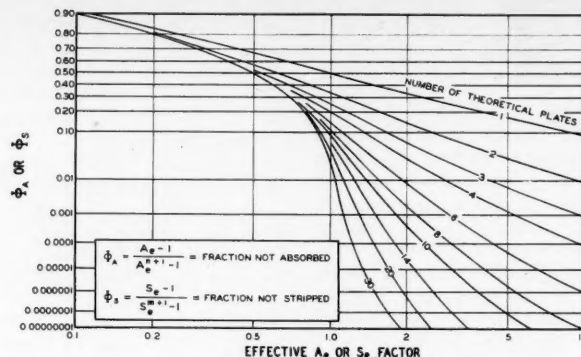


Fig. 3. Functions of absorption and stripping factors.

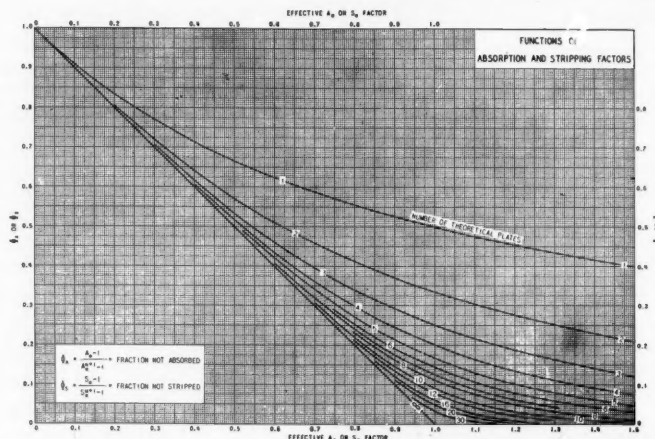


Fig. 3a. Functions of absorption and stripping factors.

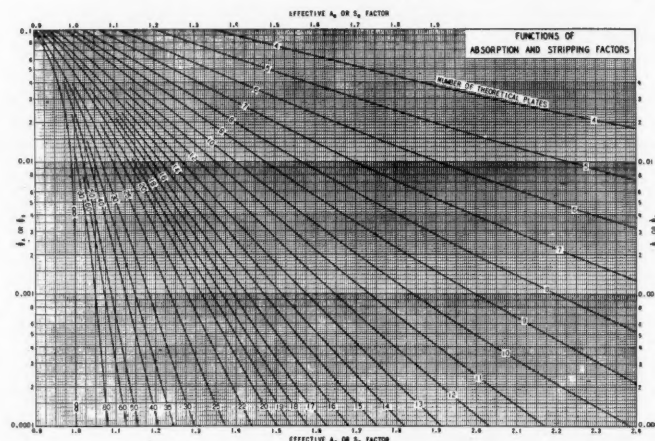


Fig. 3b. Functions of absorption and stripping factors.

effective factor depends upon the value of  $A$  (or  $S$ ). Assuming a linear relationship between  $A$  (or  $S$ ) and the number of theoretical plates and using the locations given by Horton and Franklin, one can write the following equations for  $A_e$  and  $S_e$ .

Value of $A$ (or $S$ )	$A_e =$	$S_e =$
0 to 0.1	$A_B$	$S_T$
0.1 to 0.4	$A_B + 0.1 (A_T - A_B)$	$S_T + 0.1 (S_B - S_T)$
0.4 to 1.0	$A_B + 0.2 (A_T - A_B)$	$S_T + 0.2 (S_B - S_T)$
1.0 to 4.0	$A_B + 0.3 (A_T - A_B)$	$S_T + 0.3 (S_B - S_T)$
4.0 to $\infty$	$A_B + 0.4 (A_T - A_B)$	$S_T + 0.4 (S_B - S_T)$

These proportionality relationships give essentially the same values of  $A_e$  and  $S_e$  that are found by Equation (17). It will be noted that  $A_e$  is always nearer to  $A_B$  and that  $S_e$  is always nearer to  $S_T$ . These relationships for effective factors must be modified for absorbers with intercoolers and distillation columns with intermediate reflux. For  $A_e$  and  $S_e$  they are accurate for two theoretical plates only but are convenient approximations for more plates. A rigorous solution for  $A_e$  or  $S_e$  is an iterative calculation requiring starting values of  $A$  and  $S$  and revision methods to converge on the satisfactory values.

In hand calculations the starting values may be approximated from the column terminals. For computer work plate-to-plate calculations may be made from the column terminals, starting with the desired products and the given or assumed reflux ratio. From the results of these calculations, values of  $A_e$  and  $S_e$  may be found by inverting the functions developed above.

Equation (16) may be inverted to find  $A_e$  for known values of  $\phi_A$  and  $n$  by an iterative procedure which is readily handled on a computer. In the following equation the single primes designate any trial value of  $A_e$  and the double primes

designate the  $A_e$  for the next trial.

$$A_e'' = A_e' - \left[ \frac{1 + (A_e') + (A_e')^2 + (A_e')^3 + \cdots + (A_e')^{n-1} + (A_e')^n - (1/\phi_A)}{1 + 2(A_e') + 3(A_e')^2 + \cdots + (n-1)(A_e')^{n-2} + (A_e')^{n-1}} \right] \quad (18a)$$

This equation is from the series equation for  $1/\phi_A$ . The numerator of the fraction gives the difference between starting and calculated values of  $1/\phi_A$ . The denominator is the first derivative of the series solution for  $1/\phi_A$ . Solution of this equation is repeated until the value of  $A_e$  is constant for successive trials; i.e.,  $A_e'' = A_e'$ . Cyclic solutions such as this are readily handled on digital computers.

Equation (16) may be solved for  $n$  for known values of  $A_e$  and  $\phi_A$  by the following equation:

$$n = \frac{\log \left[ \frac{1 + \frac{1}{\phi_A} (A_e - 1)}{A_e} \right]}{\log A_e} \quad (19a)$$

The solution of Equation (19a) is more

straightforward than the solution of Equation (18a), no cycling with successive approximations being required.

Analogous equations for  $S_e$  and  $m$  may be written by inspection. Graphical solution of these relationships are convenient for hand calculations and illustrate the functions. (See Figures 3, 3A, and 3B.)

The enriching and exhausting equations, i.e. Equations (4) and (8) and Equations (14) and (15), may also be written in terms of effective factors, giving an enriching equation in terms of  $A_e$  and an exhausting equation in terms

of  $S_e$ . For the enricher

$$\frac{v_{n+1}}{d} = A_0 A_e^n + A_e^n + A_e^{n-1} + \cdots + A_e^2 + A_e + 1 \quad (20a)$$

$$\frac{v_{n+1}}{d} = A_0 A_e^n + \frac{A_e^{n+1} - 1}{A_e - 1}$$

For the exhauster

$$\frac{l_{m+1}}{b} = S_0 S_e^m + S_e^m + S_e^{m-1} + \cdots + S_e^2 + S_e + 1 \quad (20b)$$

$$\frac{l_{m+1}}{b} = S_0 S_e^m + \frac{S_e^{m+1} - 1}{S_e - 1}$$

Equation (20a) may be inverted to

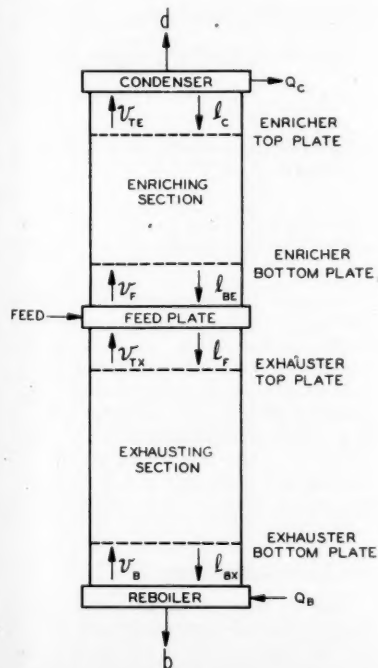


Fig. 4. Schematic diagram of fractionator.

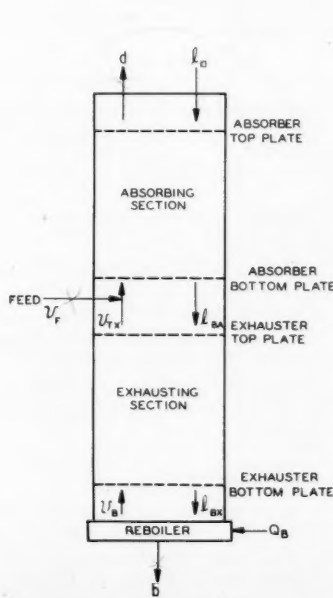


Fig. 5. Reboiled absorber.

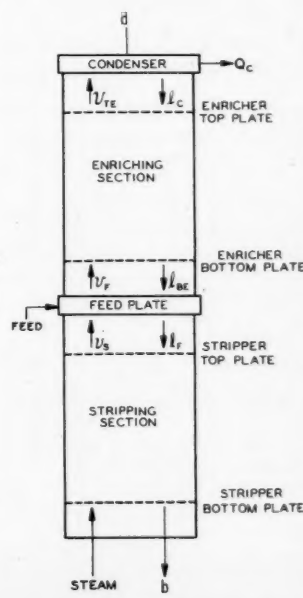


Fig. 6. Refluxed steam stripper.

give  $A_e$  in terms of  $v_{n+1}/d$ ,  $A_0$ , and  $n$  by the following:

$$A_e'' = A_e' - \left[ \frac{1 + (A_e') + (A_e')^2 + (A_e')^3 + \cdots + (A_e')^{n-1} + (1 + A_0)(A_e')^n - \frac{v_{n+1}}{d}}{1 + 2(A_e') + 3(A_e')^2 + \cdots + (n-1)(A_e')^{n-2} + n(1 + A_0)(A_e')^{n-1}} \right] \quad (18b)$$

The value of  $n$  for known values of  $A_e$ ,  $A_0$ , and  $v_{n+1}/d$  is found by the following equation:

$$n = \frac{\log \left[ \frac{1 + \frac{v_{n+1}}{d} (A_e - 1)}{(1 + A_0)A_e - A_0} \right]}{\log A_e} \quad (19b)$$

Analogous equations may be written for  $S_e$  and  $m$ .

The foregoing equations in effective factors are useful in making revisions in starting conditions for plate-to-plate calculations. These revisions are handled by a computer. Equations for fractionators, absorbers, and other columns are obtained by combining equations for the various sections.

#### FRACTIONATOR

Figure 4 is a schematic diagram of a fractional distillation column. This apparatus is obtained by combining the enricher of Figure 1 and the exhauster of Figure 2 with a feed plate, which is an equilibrium stage where vapor from the exhausting section and liquid from the enriching section join and mix with the fresh feed and then flash to give equilibrium vapor and liquid which go to enriching and exhausting sections, respectively (Figure 4).

By definition  $A_F = l_F/v_F$ . From this definition it follows that

$$\frac{b}{d} = A_F \left( \frac{v_F/d}{l_F/b} \right) \quad (22)$$

Separation functions for the enricher and exhauster are written in terms of  $l_F$  and  $v_F$ .

The vapor leaving the feed plate is the vapor going to plate  $n$ , and so Equation (14b) may be written

$$\frac{v_F}{d} = \frac{A_0 \phi_{SE} + 1}{\phi_{AE}} \quad (14c)$$

Likewise, the liquid leaving the feed plate is the liquid going to plate  $m$ , and so Equation (15b) may be written

$$\frac{l_F}{b} = \frac{S_0 \phi_{AX} + 1}{\phi_{SX}} \quad (15c)$$

Combining Equations (22), (14c), and (15c) gives

$$\frac{b}{d} = A_F \left( \frac{\frac{A_0 \phi_{SE} + 1}{\phi_{AE}}}{\frac{S_0 \phi_{AX} + 1}{\phi_{SX}}} \right) \quad (23)$$

A similar equation is obtained by combining Equations (20a), (20b), and (22) in like manner.

by combining Equation (12) for the absorber and Equation (15a) for the exhauster. For this case Equation (12) may be written

$$d = \phi_{AA}(v_{TX} + v_F) + (1 - \phi_{SA})l_0 \quad (25)$$

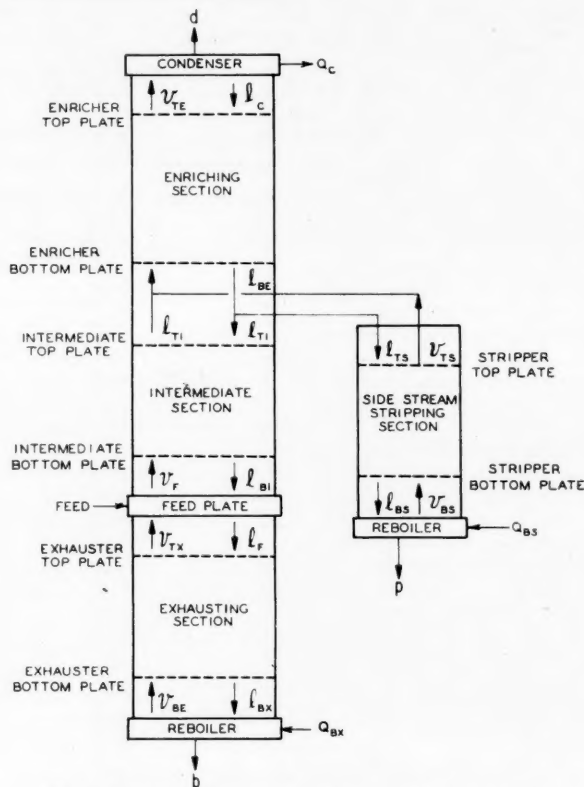


Fig. 7. Schematic diagram of fractionator with side stream.

Equation (15a) for this case becomes

$$\frac{v_{TX}}{b} = \frac{S_0 \phi_{AX} + 1}{\phi_{SX}} - 1 \quad (26)$$

Combining Equations (25) and (26) and rearranging gives

$$\frac{d}{b} = \frac{\phi_{AA} \left( \frac{S_0 \phi_{AX} + 1}{\phi_{SX}} \right) + (1 - \phi_{SA} - \phi_{AA}) \frac{l_0}{b}}{(1 - \phi_{AA})} \quad (27)$$

Equation (27) is solved for a given theoretical column with assumed temperature and  $L$  and  $V$  values at the key points. An over-all material balance,  $d + b = l_0 + v_F$ , is used with these equations to find the values of  $d$  and  $b$  that satisfy the given and the assumed conditions. Machine calculations for reboiled absorbers will utilize Equation (27) for making revisions in terminal-product assumptions.

#### REFLUXED STEAM STRIPPER

Figure 6 is a schematic diagram of a refluxed steam stripper. This is a combination of the enricher of Figure 1, the stripper of Figure 2, and an equilibrium feed plate.

#### REBOILED ABSORBER

Figure 5 is a schematic diagram of a reboiled absorber, which is a combination of the absorber of Figure 1 and the exhauster of Figure 2. An all-vapor feed with an equilibrium flash of feed is shown. An equation for this operation is obtained



With steam as the stripping medium  $v_0 = 0$ ,  $l_1 = b$  in Equation (13), so that  $l_F = b/\phi_{SX}$  for the stripper. This relationship and the feed-plate relationship  $l_F = A_F v_F$  are combined with Equation (14c) to give the following equation for this operation:

$$\frac{b}{d} = A_F \left( \frac{\phi_{SS}}{\phi_{AE}} \right) (A_0 \phi_{SE} + 1) \quad (29)$$

This equation and the over-all material balance,  $b + d = f$ , are solved with assumed temperatures and liquid-vapor traffics for a given column. The results are used to check starting conditions and make revisions.

$$d = \frac{f}{1 + \left( \frac{l_{BE}/d}{(l_{TS}/p)} X + \frac{A_F}{(l_F/b)\phi_{AI}} \left[ 1 + \left( \frac{l_{BE}/d}{(l_{TS}/p)} X + (1 - X)(l_{BE}/d)\phi_{SI} \right] \right)} \quad (38)$$

#### FRACTIONATOR WITH SIDE STREAM STRIPPER

Figure 7 is a schematic diagram of a fractionator with a side stream stripper. This apparatus splits the feed into three products. There are four sections of plates, two reboilers, one condenser, and a feed plate.

Component distributions for this operation may be found by solving simultaneously

over-all component balance:

$$d + b + p = f \quad (29)$$

for the feed plate:

$$l_F/v_F = A_F \quad (30)$$

for the exhausting section:

$$\frac{l_F}{b} = \left[ \frac{S_0 \phi_{AX} + 1}{\phi_{SX}} \right] = \left[ S_0 S_e^m + \left( \frac{S_e^{m+1} - 1}{S_e - 1} \right) \right] \quad (31)$$

$$v_{TX} = l_F - b \quad (32)$$

for the intermediate section:

$$v_{TI} = \phi_{AI} v_F + (1 - \phi_{SI}) l_{TI} \quad (33)$$

for the side stream stripper:

$$\frac{l_{TS}}{p} = \left[ \frac{S_0 \phi_{AS} + 1}{\phi_{SS}} \right] = \left[ S_0 S_e^m + \left( \frac{S_e^{m+1} - 1}{S_e - 1} \right) \right] \quad (34)$$

$$v_{TS} = l_{TS} - p = X l_{BE} - p \quad (35)$$

where  $X$  = fraction of liquid from enriching-section bottom plate going to side stream stripper.

for the enriching section:

$$\frac{l_{BE}}{d} = \left[ \frac{A_0 \phi_{SE} + 1}{\phi_{AE}} - 1 \right]$$

$$= \left[ A_0 A_e^n + \left( \frac{A_e^{n+1} - 1}{A_e - 1} \right) - 1 \right] \quad (36)$$

$$l_{BE} + d = v_{TS} + v_{TI} \quad (37)$$

With the nine equations above it is possible to solve for the amounts of all components in the three products that would come from an assumed column with given temperatures and liquid and vapor traffics.

Combining these equations and rearranging gives the following relationship for the amount of any component in the distillate from its amount in the feed and the values of the different separation functions:

$K = y/x$ , by definition

$y$  and  $x$  = mole fractions in vapor and liquid phases in equilibrium

$y = v/V$  and  $x = l/L$

$A = L/KV$  and  $S = KV/L$ , by definition.

$l/v = L/KV$  for any component at any equilibrium stage

$R_{LD} = L_0/D$  = reflux ratio

$R_{VB} = V_0/B$  = boilup ratio

$\Sigma A = A_1 A_2 A_3 \cdots A_n + A_2 A_3 \cdots A_n + \cdots + A_n$

$\Sigma S = S_1 S_2 S_3 \cdots S_m + S_2 S_3 \cdots S_m + \cdots + S_m$

$\pi_A = A_1 A_2 A_3 \cdots A_n$

$\pi_S = S_1 S_2 S_3 \cdots S_n$

$\phi_A = 1/\Sigma A + 1 = (A_e - 1)/(A_e^{n+1} - 1) = 1 - f_a$  = fraction of any wet-gas component not recovered in an absorber

$\phi_S = 1/\Sigma S + 1 = (S_e - 1)/(S_e^{m+1} - 1) = 1 - f_s$  = fraction of any rich-oil component not recovered in a stripper

$\phi_{AE}$  = value of  $\phi_A$  for enriching section

$\phi_{SE}$  = value of  $\phi_S$  for enriching section

$\phi_{AX}$  = value of  $\phi_A$  for exhausting section

$\phi_{SX}$  = value of  $\phi_S$  for exhausting section

$\psi_A = [1 - \pi_A/(\Sigma A + 1)]$  = fraction of any lean-oil component leaving an absorber in the off gas

$\psi_S = [1 - \pi_S/(\Sigma S + 1)]$  = fraction of any stripping-gas component leaving a stripper in the lean oil

$f_a$  = fraction absorbed

$f_s$  = fraction stripped

$Q_c$  = heat removed by condenser

$Q_B$  = heat added in reboiler

#### Subscripts

$i$  = any plate in enricher or absorber

$n$  = bottom plate in enricher or absorber

$j$  = any plate in exhauster or stripper

$m$  = top plate in exhauster or stripper

$\infty$  = pinch point

#### LITERATURE CITED

1. Brown, G. G., Mott Souders, Jr., and W. W. Hesler, *Trans. A. I. Ch. E.*, **30**, 438 (1933-34).
2. Edmister, W. C., *Ind. Eng. Chem.*, **35**, 837 (1943).
3. ———, *Trans. A. I. Ch. E.*, **42**, 15 (1946).
4. ———, *Chem. Eng. Progr.*, **44**, 615 (1948).
5. Horton, George, and W. B. Franklin, *Ind. Eng. Chem.*, **32**, 1384 (1940).
6. Hull, R. J., and Knight Raymond, *Oil & Gas J.* (Nov. 9, 16, 23, and 30, Dec. 7, 14, and 28, 1953).
7. Hummel, H. H., *Trans. A. I. Ch. E.*, **40**, 445 (1944).
8. Kremser, Alois, *Natl. Petroleum News*, **22**, No. 21, 48 (May 21, 1930).
9. Shiras, R. N., D. N. Hanson, and C. H. Gibson, *Ind. Eng. Chem.*, **42**, 871 (1950).
10. Souders, Mott, and G. G. Brown, *ibid.*, **24**, 519 (1932).
11. Underwood, A. J. V., *Chem. Eng. Progr.*, **44**, 603 (1948).

Presented at A.I.Ch.E. Pittsburgh meeting

# A Study of Laminar-flow Heat Transfer in Tubes

JOSEPH F. GROSS and H. C. VAN NESS

Purdue University, Lafayette, Indiana

The general problem of heat transfer to fluids in laminar flow in tubes is discussed, a new procedure for the measurement of local laminar-flow heat transfer coefficients is described, and an empirical equation is presented for the correlation of data for local heat transfer rates to liquids flowing upward in laminar flow in vertical tubes under conditions of constant heat flux at the tube wall.

The study of laminar-flow heat transfer in tubes has continued both experimentally and analytically ever since the pioneer work of Graetz (1) in 1883. Most such work has been directed toward describing this phenomenon through the use of arbitrarily defined heat transfer coefficients which apply to a finite length of tube and include entrance effects. The purpose of this paper is to describe a new experimental technique for the measurement of local heat transfer rates in laminar flow and to present a preliminary correlation of such data for the heating of liquids in tubes.

Heat transfer to fluids in fully developed turbulent flow has long been adequately handled by means of heat transfer coefficients, primarily because of the existence of a laminar boundary layer or film at the tube wall. In the core of the fluid the temperature varies but little over a cross section because of the high degree of turbulence. Only in the laminar film does the temperature rise sharply to the wall temperature. Thus for the case of turbulent flow the bulk temperature of the fluid is essentially the temperature of the turbulent core. Heat transferred to the core must pass through the laminar boundary layer. Since mixing does not occur in this film, the mechanism of heat transfer through it is conduction, which occurs at a rate given by the basic equation

$$dq = -k \left( \frac{dt}{ds} \right) dA \quad (1)$$

where  $dq$  is the differential rate of heat transfer across the differential area  $dA$ ,  $k$  is the thermal conductivity, and  $dt/ds$  is the temperature gradient in the direction of heat transfer, perpendicular to the plane of  $A$ .

For the case of turbulent flow, the temperature gradient in the laminar film is approximately  $\Delta t/\delta$ , where  $\Delta t$  is the difference between the wall temperature and the bulk temperature of the fluid and  $\delta$  is the film thickness. Thus

$$-\frac{dt}{ds} = \frac{dt}{dr} = \frac{t_w - t_b}{\delta} = \frac{\Delta t}{\delta} \quad (2)$$

where  $t_w$  is the wall temperature, and  $t_b$  is the bulk temperature of the flowing fluid.

If Equations (1) and (2) are combined, the resulting equation for heat transfer to a fluid in turbulent motion is

$$dq = \frac{k(\Delta t)}{\delta} dA \quad (3)$$

Because of the difficulty of measuring film thicknesses, this equation is put on an empirical basis by defining a local heat transfer coefficient as  $k/\delta$ . The result is the familiar equation

$$dq = h\Delta t dA \quad (4)$$

A similar approach to laminar-flow heat transfer is not so easily justified because the temperature of the fluid at a given cross section varies continuously from the tube wall to the axis of flow, and there is no dissimilar region of flow at the boundary which can be used to account for the major part of the resistance to heat transfer. Nevertheless, the practice has been to define heat transfer coefficients for laminar flow exactly as for turbulent flow. In this case the bulk temperature of the fluid does not correspond even approximately to the temperature of any large segment of the fluid, and the  $\Delta t$ , defined as the wall temperature minus the bulk temperature, has no physical significance as a driving force. The bulk temperature of a flowing fluid is defined as the temperature which would be measured if the fluid were run into an adiabatic cup and completely mixed. It is sometimes called the *mixing-cup* temperature.

Experimental values of the local heat transfer coefficient for laminar flow are virtually nonexistent in the literature. Almost all measurements made in the past have been of *mean* values of  $h$  for finite lengths of tubing. In the absence of any known relationship among the variables, integration of Equation (4) is carried out to give

$$q = h_m(\Delta t)_m A \quad (5)$$

The apparent simplicity of this equation is misleading. The main point is that the mean values of  $h$  defined by this equation have no significance except in relation to the kind of mean used for  $(\Delta t)_m$ . Since no method has been available for determining the *proper* mean to be used, the universal practice has been to define  $(\Delta t)_m$  arbitrarily as the arithmetic mean of the values at the ends of the section considered.

Another important point to be kept in mind when the mean values of  $h$  reported in the literature are considered is that the finite lengths of tubing over which they apply invariably include the entrance length, i.e., the length of tube beyond the entrance which is required for the development of complete velocity and temperature profiles in the fluid. This length is usually small for turbulent flow and is relatively unimportant. In laminar flow, however, it has a large influence. The temperature changes which occur as a fluid enters and moves along a heated tube may be considered here. At the entrance the fluid temperature is uniform over the cross section. As the fluid passes into the heated tube, temperature changes occur first in the fluid adjacent to the wall. Gradually the effect of heating progresses to the center of the tube, and as the fluid moves away from the entrance the zone of temperature uniformity narrows until it has only a differential diameter at the center of the tube. The length required for the complete temperature profile to be developed is known as the *thermal entrance length*. For the

J. F. Gross is with the RAND Corporation, Santa Monica, California, and is presently on leave, studying under a Fulbright grant at the Technische Hochschule München, Munich, Germany. H. C. Van Ness is at Rensselaer Polytechnic Institute, Troy, New York.

case of fluids having properties independent of temperature and flowing in a circular tube with constant heat flux at the wall, Levy (3) has derived an equation giving this length as

$$(L)_t = \frac{(112)(D)(N_{Pr})}{(N_{Re})(f/2)^{0.5}} \quad (6)$$

where  $N_{Pr}$  is Prandtl number,  $N_{Re}$  is Reynolds number,  $D$  is tube diameter, and  $f$  is the Fanning friction factor.

The mechanism of heat transfer to a fluid in laminar flow is conduction. The basic equation is Equation (1), and this fact should not be lost sight of when empirical equations involving arbitrary heat transfer coefficients are substituted for it. At a given cross section the temperature profile in a fluid being heated or cooled in laminar flow depends on the mode of heating or cooling and not alone on the bulk properties of the flowing fluid. Thus the value of  $h$  at a given location along a heated tube with a constant wall temperature throughout its length is different from the local value of  $h$  measured in another tube at exactly the same conditions of fluid bulk temperature and tube-wall temperature but with a constant heat flux at the wall rather than a constant wall temperature.

Many attempts have been made to solve the problem of laminar-flow heat transfer analytically, but no general solution has been achieved, and the equations which have been developed are based on assumptions which make them unreliable for general application. The basic work has been described by Drew (4); however, analytical solutions have served the purpose of suggesting functional relationships among the variables involved. Thus the Graetz solution (1) indicates that the mean Nusselt number should be a function of the mean Reynolds number, the mean Prandtl number, and the ratio of the tube diameter to the heated length as follows:

$$(N_{Nu})_m = \phi[(N_{Re})_m(N_{Pr})_m(D/L)]$$

The case considered is for a fluid with properties independent of temperature, for a constant tube-wall temperature, and for a tube length which includes the entrance length.

Sieder and Tate (5) were indeed able to correlate the data for liquids flowing in laminar flow inside tubes of constant wall temperature by an equation of this form. In order to bring the data for heating and cooling runs together, they found it necessary to include a viscosity-ratio term,  $(\mu/\mu_w)_m$ , where  $\mu$  is the bulk viscosity of the fluid and  $\mu_w$  is the viscosity of the fluid at the temperature of the tube wall. Their final correlation was

$$(N_{Nu})_m = 1.62[(N_{Re})_m(N_{Pr})_m(D/L)]^{1/3} \cdot \left(\frac{\mu}{\mu_w}\right)_m^{0.14} \quad (7)$$

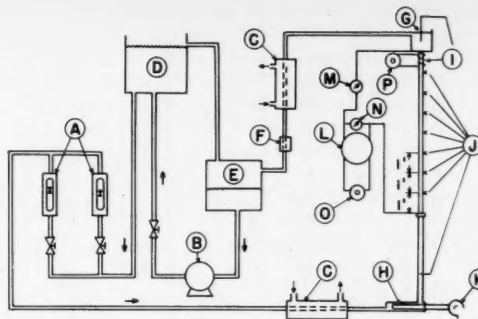


Fig. 1. Experimental apparatus: A, rotameters; B, pump; C, coolers; D, constant-head tank; E, storage tank; F, filter; G, mixing cup; H, I, heaters; J, thermocouples; K, O, P, variable transformers; L, welding transformer; M, ammeter; N, voltmeter.

This equation has the advantage of being dimensionless. It is similar in form to equations used for the turbulent region and has been used in the preparation of a single graph which represents heat transfer data for all three regions of flow. In the laminar region separate lines are shown for different values of  $L/D$ . In the turbulent region a single line represents all the data. In the transition region lines are sketched in to connect the separate lines for various values of  $L/D$  in the laminar region with the single line of the turbulent region. This graph has been widely published in the chemical engineering literature. In using it, one should keep in mind that the values of the heat transfer coefficient which it correlates in the laminar region are average values based on arithmetic-mean temperature differences and that they are valid only when the wall temperature is constant and when  $L$  includes the entrance length. The values of  $h$  correlated in the turbulent region are essentially local values, subject to none of the foregoing restrictions. The significance of the values of  $h$  predicted for the transition region by this correlation is open to speculation, for the lines in this region merely connect a correlation for mean values of  $h$  subject to severe restriction to a line for local values subject to none.

An alternative approach to the problem of laminar-flow heat transfer would be a return to the basic equation for heat conduction, Equation (1). Since all heat transferred to or from the fluid must pass through a differential lamina of fluid adjacent to the wall, the temperature gradient in the fluid at the wall may be used in Equation (1) together with the cylindrical surface area of the tube to give the heat transfer rate to the fluid. This equation for the case of heating becomes

$$dq = k_w \left( \frac{dt}{dr} \right)_w dA \quad (8)$$

where the subscript  $w$  denotes values adjacent to the tube wall. Thus the local

heat transfer rate at any location along the tube can be calculated from the thermal conductivity of the fluid and the radial temperature gradient in the fluid adjacent to the wall. Laminar-flow heat transfer should be considered in relation to a temperature gradient of physical significance rather than with respect to an abstract coefficient and a meaningless  $\Delta t$ . The experimental problem is that of measuring and correlating the radial temperature gradients at the wall.

An energy balance over a differential length of tube  $dx$  in which the bulk temperature of the fluid increases by  $dt_b$  gives

$$dq = mc dt_b \quad (9)$$

where  $m$  is mass flow rate and  $c$  is specific heat. Also

$$dA = \pi D dx \quad (10)$$

Equations (8), (9), and (10) combine to give

$$\left( \frac{dt}{dr} \right)_w = \frac{mc}{\pi D k_w} \left( \frac{dt_b}{dx} \right) \quad (11)$$

Experimentally, the problem is to determine values of the bulk temperature  $t_b$  at various locations along the tube so that  $dt_b/dx$  may be evaluated. The technique developed for this purpose involves a series of measurements in which successively shorter heat transfer sections are used. The conditions in each shorter length of tube exactly match those in an equal length from the entrance of the preceding longer tube. The measurement of the bulk temperatures of the fluid flowing from these various lengths amounts to the measurement of the bulk temperatures of the fluid at various points in the original full-length tube. From these measurements, values of the derivative  $dt_b/dx$  are readily calculated for use in Equation (11).

#### EXPERIMENTAL

The general technique just described is applicable in various types of experiments. The particular measurements made in this

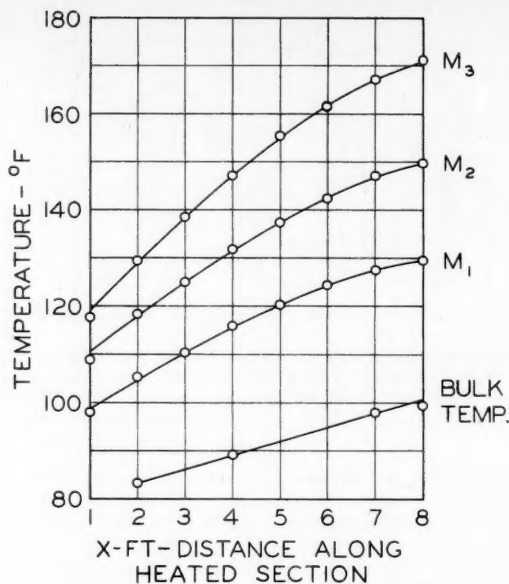


Fig. 2. Experimental data: runs made with 50% aqueous ethylene glycol in the 0.305-in. tube;  $M_1 = 0.0148$  lb./sec.,  $M_2 = 0.0288$  lb./sec.,  $M_3 = 0.0428$  lb./sec.

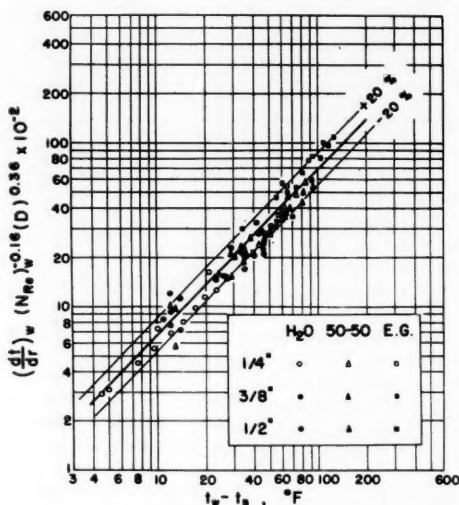


Fig. 3. Correlation of results: 1/4, 3/8, and 1/2 in. are the nominal tube sizes referring respectively to tubes having internal diameters of 0.224, 0.305, and 0.432 in.

work to test the utility of the method involved the heating of three liquids flowing upward in vertical tubes with constant heat flux at the wall. The three liquids used were water, ethylene glycol, and a 50%-by-weight aqueous ethylene glycol solution. The properties of water are readily available, and those of ethylene glycol and its aqueous solutions are given by Cragoe (6). Three tube sizes were used: 0.224 in. I.D., 0.305 in. I.D., and 0.432 in. I.D. All were made of austenitic stainless steel. The equipment is shown schematically in Figure 1. The test section of stainless steel tubing, shown at the right, was initially 12 ft. long. Thermo-

couples were attached to the tube at 1-ft. intervals, and the entire tube was enclosed in a Vermiculite-filled box. An adiabatic mixing cup was fastened to the top of the test section, and a thermocouple was used to measure the bulk temperature of the fluid after complete mixing. The stainless steel tube was heated by passing a high current at low voltage directly through the tube wall, thus giving a constant rate of heat input with length. A welding transformer was used to supply power. Current was fed to the tube through clamps, one attached to the top of the tube and the other at a point 8 ft. lower. The initial 4-ft.

length of tube was used as a calming section. Heat losses from the upper clamp were compensated by winding it with electrical heating wire. Heat was supplied at a rate such that no temperature gradient existed in the clamp.

The fluid to the test section, supplied from a constant-head tank, was metered in calibrated rotameters and controlled by regulating valves. Before entering the test section, it passed through a cooler and a heater so that its initial temperature might be adjusted to any desired value. The fluid from the mixing cup was cooled and returned to the system. Runs were made with the full length of tube for each fluid at three mass-flow rates and for three bulk-temperature increases between the tube entrance and the mixing cup. These initial runs were made primarily to establish the wall-temperature profiles along the tube.

The tube was then cut 1 ft. from the top, and the mixing cup was remounted. All runs were repeated with the new tube length. In each case the original entrance conditions of the fluid were duplicated, and the power supplied to the tube and top clamp was adjusted to give wall-temperature profiles along the remaining tube identical with those originally observed. Thus the temperature histories of the fluid in the tube up to the point where the tube was cut were made to duplicate those for the initial runs up to the same point. For each cutting of the tube this procedure was repeated. For the case of constant heat input along the tube length, only one additional cut was needed because intermediate bulk temperatures could be calculated by an energy balance. In the present work, therefore, the only other cut made in most instances was at a point 5 ft. below the first one. In a few cases another cut was made to provide a check on the calculations for intermediate points.

## RESULTS

As an example of the data, Figure 2 shows the results of one set of runs taken for the 0.305-in. I.D. tube with 50% aqueous ethylene glycol as the fluid. The three upper curves represent wall-temperature profiles for three different mass-flow rates. The bottom line represents the bulk temperature of the fluid, which was made the same for all three flow rates by adjusting the power input. The wall temperatures are those at the inside of the tube and are average values. They were calculated from the values measured at the outside of the tube by Equation (12):

$$t_{in} = t_{out} + \left( \frac{E}{L} \right)^2 \frac{(r_2^2 - r_1^2) - 2r_2^2 \ln(r_2/r_1)}{4k_t \rho_t} \quad (12)$$

where  $E/L$  is the voltage drop per unit length of tube and  $r_2$  and  $r_1$  are the outside and inside radii of the tube. This equation is readily derived from an energy balance if  $k_t$  and  $\rho_t$  are assumed constant and if heat losses from the outside of the tube are assumed negligible. The bulk-temperature line shown in Figure 2 is based



on the measured values at  $x = 2$  and  $x = 7$  ft. only. If constant heat input is assumed, the heating rate per foot of length may be determined from two bulk-temperature measurements. Temperatures at other points are then easily calculated if the specific heat is known as a function of temperature. The complete data are given by Gross (2).

The slopes of the bulk-temperature curves taken from data such as those shown in Figure 2 were used with Equation (11) to calculate values of  $(dt/dr)_w$ . Eighty-five separate sets of runs were made under steady state conditions. With this amount of data it was not thought necessary to use more than one value of  $(dt/dr)_w$  from each set of runs for purposes of correlation. Hence the correlation of results is based on data for the 5-ft. point in the tubes. This point was far enough from the entrance to lie beyond the thermal entrance length in most cases and far enough from the end not to be influenced by possible end effects. A purely empirical correlation of the values of  $(dt/dr)_w$  was attempted. It was postulated that the radial temperature gradient in the fluid at the wall should be a function of  $N_{Re}$ ,  $N_{Pr}$ ,  $D$ ,  $\mu/\mu_w$ , and  $\Delta t$ . Therefore it was assumed that

$$\left(\frac{dt}{dr}\right)_w = B(N_{Re})^a(N_{Pr})^b(D)^c(\mu/\mu_w)^d(\Delta t)^e$$

where  $B$ ,  $a$ ,  $b$ ,  $c$ ,  $d$ , and  $e$  are constants. On this basis the data were correlated by a multiple linear-regression analysis based on the method of least squares. The computations were carried out by an Electrodata digital computer. The correlation was successful, but suggested a change in the postulated functional relationship. The following dimensional equation was the final result:

$$\left(\frac{dt}{dr}\right)_w = 68(N_{Re})^{0.16}(D)^{-0.36}(\Delta t) \quad (13)$$

where

$$\begin{aligned} (dt/dr)_w &= \text{temperature gradient in the fluid at the wall, } ^\circ\text{F./ft.} \\ (N_{Re})_w &= \text{Reynolds number of the fluid evaluated at the wall temperature} \\ D &= \text{inside tube diameter, in.} \\ \Delta t &= t_w - t_b, ^\circ\text{F.} \end{aligned}$$

The correlation is shown graphically in Figure 3. It will be seen that most of the points lie within 20% of the line representing Equation (13).

If a local heat transfer coefficient is defined in the usual way, the correlation may be expressed in an alternative form. By Equations (4) and (8),

$$h = \frac{k_w(dt/dr)_w}{\Delta t}$$

It follows from Equation (13) that

$$h = 68k_w(N_{Re})^{0.16}(D)^{-0.36} \quad (14)$$

where  $h$  is a local value of the heat transfer coefficient in B.t.u./(hr.)(sq. ft.)( $^\circ\text{F.}$ ) and  $k_w$  is the thermal conductivity of the fluid at the wall temperature in B.t.u./(hr.)(sq. ft.)( $^\circ\text{F./ft.}$ ).

#### DISCUSSION

If  $f$  in Equation (6) is replaced by  $16/N_{Re}$  for laminar flow, the result is

$$(L)_t = (39.5)(D)(N_{Pr})(N_{Re})^{-0.5} \quad (15)$$

Calculations of the thermal entrance lengths by Equation (15) for the runs made showed the 5-ft. point to be within the entrance region for five of the ethylene glycol runs. These points failed to fit the correlation and were discarded, but all other points are included. On the basis of excellent energy balances, the data are thought to be accurate to within 10%.

The correlation of results applies specifically to liquids flowing upward in vertical tubes under conditions of constant heat flux at the wall and gives local values for the case of fully developed temperature profiles. It is not suggested that this correlation should be valid under any other circumstances. It was thought that liquids heated in upward flow would be less susceptible to the effects of free convection than in any other arrangement. The heating of liquids in horizontal tubes or in downward flow in vertical tubes should follow the present correlation provided that free-convection effects are negligible.

It has not been possible to compare the present results with those of any previous work. No data are available in the literature for local heat transfer rates to liquids in laminar flow. Furthermore, the results of this work are applicable only in the region of fully developed temperature and velocity profiles. All mean values of  $h$  reported in the literature include the entrance region. Since the results of this work do not apply to this region, it is not possible to integrate to get mean values of  $h$  comparable with those given in the literature. It might be added that most data available from previous work are for the case of constant wall temperatures, whereas the present work was concerned with the case of constant heat flux at the wall.

The results presented are thus seen to be of limited practical utility. However, it is hoped that the presentation of this experimental method will stimulate efforts toward further research on laminar-flow heat transfer. The method is by no means limited to the case of constant heat flux at the wall, and it should not be difficult to devise experiments for the study of other cases. An interrelation among the local heat transfer rates for different modes of heating and cooling may be found, and it is possible that a single correlation of such rates might be made through the introduction of other

factors. The entrance region might well be treated separately from the region of fully developed profiles. A detailed study of entrance effects is also possible by this method. In addition, point values of heat transfer rates in the transition region might be investigated. However, this may involve added experimental difficulties. In the course of the present work the region of transition flow was inadvertently entered several times, and it was noted that the temperatures fluctuated wildly, a result that would be expected because of the unstable nature of transition flow. Certainly, further work on these problems is needed.

#### ACKNOWLEDGMENT

Thanks are due E. I. du Pont de Nemours and Company for support of this work through a fellowship and to the Carpenter Steel Company, Alloy Tube Division, for supplying the stainless steel tubing used as test sections.

#### NOTATION

$A$	= area
$c$	= specific heat
$D$	= tube diameter
$E$	= voltage drop
$f$	= Fanning friction factor
$h$	= local heat transfer coefficient
$k$	= thermal conductivity of fluid
$k_t$	= thermal conductivity of the tube wall
$L$	= tube length
$L_t$	= thermal entrance length
$m$	= mass flow rate
$N_{Nu}$	= Nusselt number, $hD/k$
$N_{Pr}$	= Prandtl number, $c\mu/k$
$N_{Re}$	= Reynolds number, $D\rho v/\mu$
$q$	= rate of heat transfer
$r$	= tube radius
$s$	= distance in the direction of heat flow
$t$	= temperature
$t_w$	= tube-wall temperature
$t_b$	= bulk temperature of fluid
$v$	= velocity of fluid
$x$	= distance along tube
$\delta$	= film thickness
$\rho$	= density of fluid
$\rho_t$	= electrical resistivity of tube
$\mu$	= viscosity of fluid at bulk temperature
$\mu_w$	= viscosity of fluid at wall temperature

#### LITERATURE CITED

1. Graetz, L., *Ann. Physik* (N.F.), **18**, 79 (1883).
2. Gross, J. F., Ph.D. thesis, Purdue University, Lafayette, Ind. (1956).
3. Levy, S., A.S.M.E. Paper No. 54-A-142.
4. Drew, T. B., *Trans. Am. Inst. Chem. Engrs.*, **26**, 26 (1931).
5. Sieder, E. N., and G. E. Tate, *Ind. Eng. Chem.*, **28**, 1429 (1936).
6. Cragoe, C. S., "Properties of Ethylene Glycol and its Aqueous Solutions," Cooperative Research Council Report.

# Dynamics of Liquid Agitation in the Absence of an Air-liquid Interface

DAVID S. LAITY and ROBERT E. TREYBAL

New York University, New York, New York

The dynamics of agitating single- and two-phase liquid mixtures in the absence of an air-liquid interface was compared with that of similar systems with an interface. Two geometrically similar cylindrical vessels, 12 and 18 in. in diameter respectively, were used, each fitted with a similar six-bladed, disk-turbine impeller.

New general correlation curves of power number with Reynolds number are presented which show that elimination of the air-liquid interface makes it possible to attain dynamic similarity in scale-up in unbaffled vessels but makes little difference in baffled vessels.

In the study of the dynamics of liquid agitation, particular attention has been given to open baffled vessels operated batchwise with a single liquid phase (2, 6). Where study or design of such a system as a continuously operated, multiple-stage, liquid-liquid extractor must be considered, there is little information available on the effect of operation with continuous flow of two liquid phases in the absence of an air-liquid interface above the impeller.

Olney (4) recently reported that in mass transfer studies in such an extractor, higher stage efficiencies were obtained with no baffles than with baffles at the same power input. However, earlier agitation studies based on open unbaffled vessels indicate that with turbulent agitation it is not possible to scale up an unbaffled extractor and obtain dynamic similarity in a larger system (3, 5). The flow dynamics giving optimum results in a pilot plant therefore could not be reproduced in plant-scale equipment which is geometrically similar.

In an open unbaffled vessel, turbulent agitation will result in a vortex. The flow characteristics are affected by the geometry of the vessel and the impeller, the impeller speed, and the properties of the liquid. These can be related for geometrically similar systems by

$$\frac{P g_c}{D^5 N^3 \rho} = K \left( \frac{D^2 N \rho}{\mu} \right)^m \left( \frac{D N^2}{g} \right)^n \quad (1)$$

or

$$N_p = K(N_{Re})^m (N_F)^n \quad (2)$$

where the values of  $K$ ,  $m$ , and  $n$  are characteristics of the type of impeller (6). Here a dimensionless power number,  $N_p$ , is expressed as a function of the dimensionless agitation Reynolds number (for viscous forces in the liquid) and the Froude number (for gravitational forces producing the vortex). It can be shown mathematically that dynamic similarity cannot be obtained in scale-up of a

system with both these forces controlling the flow pattern (5).

The vortex is eliminated by adding radial baffles to the vessel. With the gravitational forces negligible, the flow dynamics are controlled by the viscous forces in the liquid, and Equation (2) becomes (6)

$$N_p = K(N_{Re})^m \quad (3)$$

Thus for baffled vessels dynamic similarity is obtained in two geometrically similar vessels operated at the same Reynolds number.

In a covered unbaffled vessel with no air-liquid interface the swirl flow pattern characteristic of unbaffled operation is obtained; however, there is no vortex. The equations derived for open vessels do not describe this type of agitation.

In the determination of the Reynolds and power numbers for agitation of two-phase liquids, mean values of density and viscosity are used. Miller and Mann (3) recommended the use of a weighted geometric mean viscosity, derived from studies in open unbaffled vessels:

$$\mu_a = \mu_x^x \mu_y^y \quad (4)$$

TABLE 1. PHYSICAL PROPERTIES OF LIQUIDS STUDIED

Liquid	Temperature, °F.	Density, g./ml.	Viscosity, centipoises
Water	68	0.9982	1.000
S.A.E. 10 motor oil	68	0.8914	96.35
Kerosene I	68	0.8132	2.271
Kerosene II	68	0.8144	2.121
Blend A (kerosene and oil)	68	0.8600	21.22
Water saturated with sec-butanol	77	0.9720	1.931
Sec-butanol saturated with water	77	0.8742	4.367
Glycerine (aq.)	86	1.134	4.62
S.A.E. 30 motor oil	77	0.9292	368.5
Blend D (kerosene and oil)	86	0.9032	35.94

Vermeulen and associates (7) have recommended another relationship, derived from studies in baffled vessels with no air-liquid interface:

$$\mu_m = \frac{\mu_c}{1 - x_d} \left[ 1 + \frac{(1.5)(x_d)(\mu_d)}{\mu_c + \mu_d} \right] \quad (5)$$

Vermeulen also recommends for density the use of a weighted arithmetic mean, originally used by Miller and Mann:

$$\rho_a = x \rho_x + y \rho_y \quad (6)$$

These empirical equations may be satisfactory for the physical systems for which they were derived, but there is no theoretical basis to evaluate their reliability for open baffled vessels or covered unbaffled vessels with no air-liquid interface.

No information has been published on the quantitative effect of continuous flow on the power characteristics of impellers.

It is apparent that a need exists for the basic correlations necessary to define the dynamics of agitation in the absence of an air-liquid interface. Flynn (1) started the investigation with a study of mass transfer rates in covered baffled extractors. This investigation continues that work with the emphasis on liquid dynamics.

## APPARATUS AND SCOPE OF EXPERIMENTS

Correlations are based on power-speed measurements taken with batch and continuous-flow operation with both single- and two-phase liquids. All runs in unbaffled vessels were made in the absence of an air-liquid interface. For baffled vessels runs were made with and without an interface for comparative purposes. The liquids and mixtures studied are listed in Tables 1, 2, and 3 along with the range of operating conditions (1a).

The vessel and impeller are shown in Figure 1. Two geometrically similar cylindrical vessels 12 and 18 in. in diameter respectively were used. Each was fitted with a similar six-bladed, disk-turbine impeller, manufactured by the Mixing Equipment Company of Rochester, New York. This type of impeller was selected because of its wide application in liquid-liquid extractors. All data were taken with the impeller at the midpoint of the vessel, except where the effect of impeller height was under study.

Baffles, when used, were 16.7% of the vessel diameter. This choice of baffle width was dictated by the results obtained by Flynn (1), who measured the effect on power of operation with and without an

David S. Laity is at present with E. I. du Pont de Nemours and Company, Inc., Newark, Delaware.

TABLE 2. SUMMARY OF SYSTEMS AGITATED UNDER BATCH CONDITIONS

Liquid system	Volumetric phase ratio	Air-liquid interface	Impeller C/D	Impeller speed, rev./sec.
<i>Unbaffled 12-in. vessel with 4-in. impeller</i>				
Water	—	No	1.5	6.30-25.20
S.A.E. 10 motor oil	—	No	1.5	5.86-22.00
Kerosene I	—	No	1.5	11.11-24.84
Blend A	—	No	1.5	7.89-22.52
Water-S.A.E. 10 motor oil	0.5-6	No	1.0-2.0	5.81-24.60
Water-kerosene-I	0.178-10	No	1.5-2.0	8.33-24.94
Water-Blend-A	1.04	No	1.5	10.06-22.94
<i>Unbaffled 18-in. vessel with 6-in. impeller</i>				
Water	—	No	1.5	4.46-9.50
Kerosene II	—	No	1.5	5.08-10.50
Glycerine (aq.)	—	No	1.5	3.50-9.42
S.A.E. 30 motor oil	—	No	1.5	2.85-7.60
Water-kerosene-II	0.35-2.65	No	1.5	4.16-11.60
<i>Baffled 12-in. vessel with 4-in. impeller</i>				
Water	—	Yes	1.5	4.09-8.37
S.A.E. 10 motor oil	—	Yes	1.5	5.02-8.36
Kerosene I	—	No	1.5	5.12-19.62
Blend A	—	No	1.5	5.91-19.05
Water-S.A.E.-10 motor oil	0.5-2.0	No	1.5-2.0	6.24-18.11
Water-kerosene-I	0.5-1.13	Yes	1.5	6.07-17.44
Water-Blend-A	0.49-4.25	No	1.5	6.12-15.10
Water-Blend-A	1.06	No	1.5	4.42-16.37
Water-Blend-A	1.20	Yes	1.5	4.42-15.72
Water-Blend-A	1.20	Yes	1.5	5.04-16.41
Water-Blend-A	1.20	No	1.5	5.25-15.57
Water-Blend-A	1.20	Yes	1.5	6.38-11.62
<i>Baffled 18-in. vessel with 6-in. impeller</i>				
Blend D	—	No	1.5	2.43-6.05
Water-Blend-D	0.56-0.85	No	1.5	3.75-5.72

TABLE 3. SUMMARY OF SYSTEMS AGITATED UNDER CONTINUOUS-FLOW CONDITIONS (No Air-liquid Interface, C/D = 1.5)

Liquid system	Volumetric phase ratio	Impeller speed, rev./sec.	Flow rate, lb./min.
<i>Unbaffled 12-in. vessel with 4-in. impeller</i>			
Water	—	10.90-20.72	76
Water-kerosene-II	1.22-1.44	10.82-22.90	6.4
<i>Unbaffled 18-in. vessel with 6-in. impeller</i>			
Water	—	4.26-7.79	77
<i>Baffled 12-in. vessel with 4-in. impeller</i>			
Water	—	5.13-13.03	79
<i>Baffled 18-in. vessel with 6-in. impeller</i>			
Water-blend-D	0.51-0.79	3.74-5.76	12

air-liquid interface and with 10, 16.7, and 25% baffles. He found that 16.7% baffles were the largest for which differences in power requirements were obtained for the two methods of operation. It was one of the objectives of this study to confirm and refine Flynn's results by use of larger vessels, the power requirements of which could be measured more accurately. When, as will be shown, no difference was found between operation with and without an air-liquid interface at 16.7% baffles, it

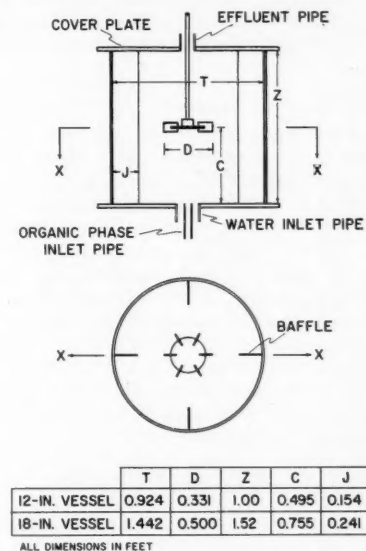


Fig. 1. Mixing vessel and disk-turbine impeller.

was not considered justified to pursue this part of the study further with the more customary 10% baffles.

Power was measured with a torque-table dynamometer, similar to that employed by previous investigators. It consisted of the motor supported by a thrust bearing and

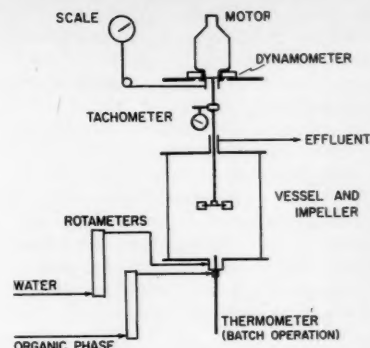


Fig. 2. Diagram of equipment.

restrained by a cord attached to a dynamometer scale and auxiliary weights (Figure 2).

Continuous flow was provided by a suitable arrangement of feed tanks, piping, a pump, rotameters, and receiving tanks. Runs were made with batch operation except where the effect of continuous flow was evaluated.

#### UNBAFFLED VESSELS

For turbulent agitation of a liquid in an open, unbaffled vessel, a plot of power number against the Reynolds number alone gives a family of curves with speed as the parameter (6). The Froude number must be included to provide a single, continuous curve.

All power measurements in this study of unbaffled vessels were taken with a full covered vessel without an air-liquid interface or a vortex. A review of all such measurements for any given liquid agitated at a number of different speeds showed that the correlation of power number with Reynolds number alone resulted in a smooth, continuous curve. The use of the Froude number was not required as it is for open unbaffled vessels. This observation is valid for all the data for unbaffled vessels, regardless of liquids, phase ratios, impeller height, flow conditions, or vessel size.

In addition, a general correlation of power number with Reynolds number for all batch systems resulted in a single, general curve which described all the single-phase and most of the two-phase liquids studied. This curve is shown in Figure 3 as it was derived from the data points for single-phase liquids in both the 12- and 18-in. vessels.

The significance of these observations is considerable. Until now Rushton and other investigators have emphasized the necessity of studying agitation only in baffled vessels because of the impracticability of scale-up with both gravitational and viscous forces controlling the flow pattern (5). The results of this study now show that laboratory studies of mass or heat transfer need not be limited to baffled systems. By operation without an air-liquid interface, the possible



advantages of unbaffled agitation can be evaluated. The flow dynamics giving optimum results on the small scale can be reproduced in a larger system which is geometrically similar.

Of the general equations relating the Reynolds and power numbers, Equation (2), originally derived for baffled vessels, can be used, as the effect of gravitational forces is eliminated. Between  $N_{Re} = 10^3$  and  $N_{Re} = 10^5$ , the general correlation curve is approximately straight, and so the constant  $K$  and slope  $m$  can be evaluated to give

$$N_p = 14.86(N_{Re})^{-0.2545} \quad (7)$$

For other values of  $N_{Re}$ , as the slope is variable, single quantitative values cannot be substituted for  $m$  and  $K$ .

## Two Liquid Phases

Neither the weighted geometric mean viscosity  $\mu_a$  of Miller and Mann nor the mean viscosity  $\mu_m$  of Vermeulen was satisfactory in the correlation of data for two-phase liquids with data for single-phase liquids for this investigation. The average deviation of the power numbers from those given by the curve for single-phase liquids in these cases were 23.2% (for  $\mu_a$ ) and 16.1% (for  $\mu_m$ ). Instead, modifications of Vermeulen's viscosity were found to fit the data best as follows:

For water more than 40% by volume:

$$\mu_L = \frac{\mu_w}{x_w} \left[ 1 + \frac{6.0x_o\mu_o}{\mu_w + \mu_o} \right] \quad (8)$$

For water less than 40% by volume:

$$\mu_L = \frac{\mu_o}{x_o} \left[ 1 - \frac{1.5x_w\mu_w}{\mu_w + \mu_o} \right] \quad (9)$$

These equations cover cases where the impeller was located both above, below, and at the liquid-liquid interface for the system at rest. In Figure 4 the two-phase liquid data points calculated with  $\rho_a$  and  $\mu_L$  are superimposed on the general correlation curve for single-phase liquids. The average deviation of the power numbers from those given by the curve is 7.7%.

It is noted that individual points at  $N_{Re} = 10^4$  show greater deviation than those at  $N_{Re} = 10^5$ . These deviations are attributed to lack of uniformity of the two-phase mixture at low impeller speeds. In every case the points coincide with or approach the general curve at higher speeds.

## Effect of Impeller Height

The effect of the impeller height with relation to the liquid-liquid interface was evaluated by moving the impeller in steps from the heavy to light phase of various two-phase systems. Between heights of one to two impeller diameters from the bottom, substantially no effect was found.

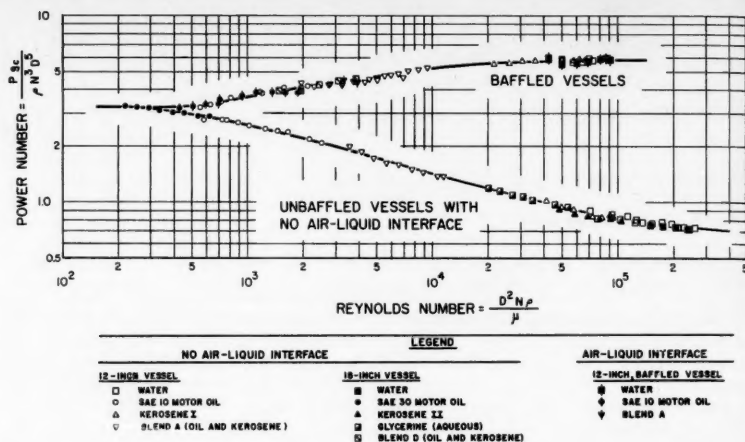


Fig. 3. General correlation of power number with Reynolds number for single-phase liquids agitated by batches in baffled and unbaffled vessels.

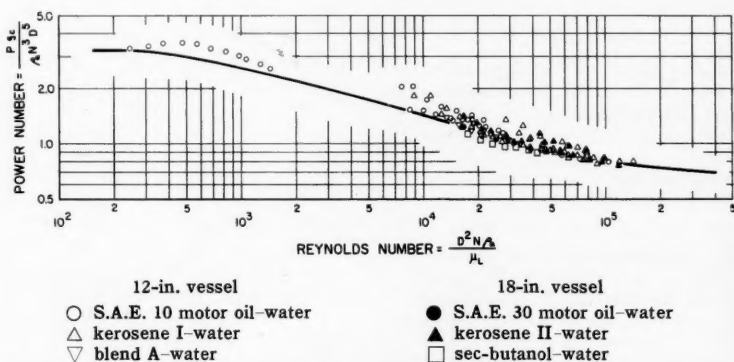


Fig. 4. Correlation of two-phase liquid data points with the general curve for single-phase liquids, agitated by batches in unbaffled vessels with no air-liquid interface.

## Continuous-flow Operation

Flow through the vessel was found to have a small but measurable effect on power number. The deviations in the 12- and 18-in. vessels can be related linearly to (water flow rate)/(vessel diameter) as in Figure 5. The flow rates employed in water runs were high, corresponding to a retention time as low as 32 sec. Measurements with kerosene-water at the more normal retention time of 7 min. agreed with those for batch operation. For most applications, therefore, the effect of continuous flow on agitation dynamics can be ignored.

## BAFFLED VESSELS

Essentially all data taken in baffled vessels operated batchwise were correlated by a single general curve similar to that developed by Rushton for single liquids in open vessels (6). The only exceptions were deviations caused by air entrainment in open vessels with agitation at power inputs (20 to 80 hp./1,000 gal.) far above those normally encountered in practice.

The correlation obtained from this study is shown in Figure 3 as it was

derived from the measurements with single-phase liquids. It should be noted that this curve includes runs made both with and without an air-liquid interface.

It is concluded, therefore, that there is substantially no effect on liquid dynamics between operation with and without an air-liquid interface in a vessel with 16.7% baffles.

## Two Liquid Phases

Power measurements for two phase liquids in baffled vessels were correlated with the general curve with the mean viscosity of Vermeulen [Equation (5)] and the weighted arithmetic mean density [Equation (6)]. In Figure 6 the calculated values of  $N_p$  and  $N_{Re}$  for two-phase liquids are shown superimposed on the general curve derived for single-phase liquids. The continuous phase, for the purpose of calculating  $\mu_m$ , was taken as that phase in which the impeller was located when at rest.

The weighted geometric mean viscosity [Equation (4)] of Miller and Mann was in no case completely satisfactory for correlation of two-phase liquid measurements in baffled vessels. When a high-viscosity phase such as oil is continuous,



the deviations resulting from use of this function are large.

#### Effect of Impeller Height

In contrast to unbaffled vessels, in baffled vessels impeller height in relation to the liquid interface was found to have a significant effect.

Though the data taken on the effect of impeller height were too limited to warrant completely general conclusions, it was observed that the continuous phase

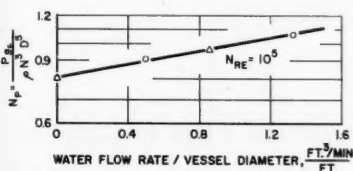


Fig. 5. Deviation of power number with water flow rate through unbaffled vessels.

○ 12-in. vessel, △ 18-in. vessel.

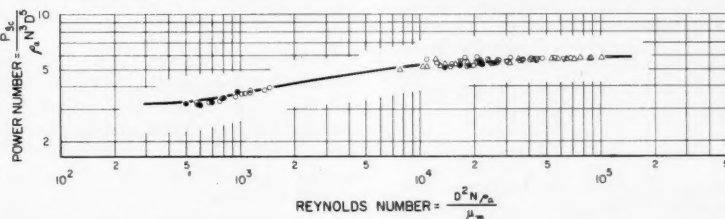


Fig. 6. Correlation of two-phase liquid data points with the general curve for single-phase liquids, agitated batchwise in baffled vessels. 12-in. vessel: no air-liquid interface: same legend as in Fig. 4; air-liquid interface: ● S.A.E. 10 motor oil-water, ▼ blend A-water.

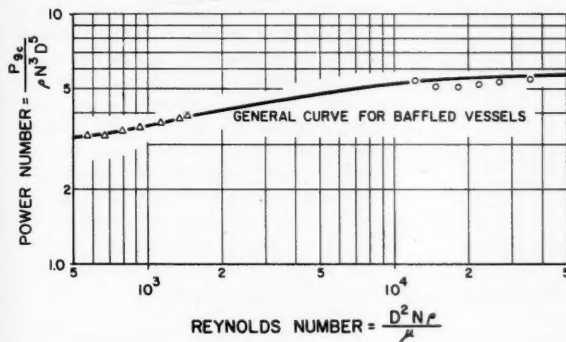


Fig. 7. Effect of impeller position on Reynolds number and power numbers for two-phase liquids, agitated batchwise in baffled vessels. Water-41%, S.A.E. 10 motor oil-59%; ○  $C = 1.5 D$ , impeller at liquid-liquid interface; △  $C = 2.0 D$ , impeller in oil phase.

was that phase in which the impeller was located when at rest. When the impeller was located at the liquid-liquid interface, the water phase was found to be continuous for oil-water systems and the organic phase for kerosene-water systems.

In Figure 7 the effect is shown of moving the impeller from the light phase to the interface of an oil-water system. The change from a water-in-oil to an oil-in-water dispersion resulted in a lower mixture viscosity, which in turn increased the Reynolds number, the measure of turbulence, by more than twenty-fold.

#### Continuous-flow Operation

Measurements taken with continuous flow of water and Blend-D-water systems showed negligible deviations from those taken with batch agitation of the same system. Flow was from the bottom to the top of the vessel and the impeller was located above the interface of the two-phase liquid when at rest.

#### CONCLUSIONS

In summary, the following conclusions are drawn based on agitation in unbaffled vessels with no air-liquid interface and in baffled vessels with four radial baffles each 16.7% of the vessel diameter.

1. Dynamic similarity is obtained in geometrically similar, unbaffled vessels by operating with no air-liquid interface and equal Reynolds numbers.

2. For such unbaffled vessels, a single general curve of  $N_p$  plotted against  $N_{Re}$  will describe all single-phase and most two-phase liquid data.

3. With minor exceptions, all power measurements in baffled vessels can also be correlated with a single general curve of  $N_p$  plotted against  $N_{Re}$ .

4. Elimination of the air-liquid interface in a baffled vessel has little effect on the dynamics of agitation.

5. Measurements for two-phase liquids in unbaffled vessels are best correlated with those for single-phase liquids with the weighted arithmetic mean density and a new relationship for mean viscosity,  $\mu_L$  [Equations (8) and (9)].

6. Data for two-phase liquids in baffled vessels can be similarly correlated

with the same mean density and the mean viscosity recommended by Vermeulen [Equation (5)].

7. Impeller height in relation to the liquid-liquid interface of two-phase systems has little effect between one and two impeller diameters from the bottom of an unbaffled vessel.

8. Impeller height in baffled vessels is important in agitation of two-phase liquids. For more effective agitation, the vessel should be operated, if possible, with the impeller in the low-viscosity phase.

9. Continuous flow of liquid through an unbaffled vessel has a small effect on the power characteristics of the impeller. For low flow rates the foregoing conclusions for batch systems can be applied. For baffled vessels the effect of continuous flow is negligible.

#### NOTATION

- $C$  = impeller distance off tank bottom (to midpoint of blade), ft.
- $D$  = impeller diameter, ft.
- $g$  = acceleration due to gravity, ft./sec.<sup>2</sup>
- $g_c$  = conversion factor, (ft./sec.<sup>2</sup>) (lb. mass/lb. force)
- hp. = horsepower
- $J$  = baffle width, ft.
- $K$  = a constant
- $N$  = rotation rate of the impeller, rev./sec.
- $N_F$  = Froude number,  $DN^2/g$
- $N_p$  = power number,  $Pg_c/D^5N^3\rho$
- $N_{Re}$  = Reynolds number,  $D^2N\rho/\mu$
- $P$  = power, ft.-lb./sec.
- $T$  = vessel diameter, ft.
- $x$  = volume fraction of phase  $x$
- $x_c$  = volume fraction of continuous phase
- $x_d$  = volume fraction of dispersed phase
- $y$  = volume fraction of phase  $y$
- $Z$  = liquid depth, ft.
- $\mu$  = liquid viscosity, lb. mass/(ft. sec.)
- $\mu_m$  = weighted geometric mean viscosity [Equation (4)]
- $\mu_L$  = mean viscosity derived in this study [Equations (8) and (9)]
- $\mu_m$  = mean viscosity of Vermeulen [Equation (5)]
- $\rho$  = liquid density, lb. mass/cu. ft.
- $\rho_a$  = average density [Equation (6)]

#### Subscripts

- $c, d$  = continuous and dispersed phases
- $o, w$  = organic and water layers
- $x, y$  = phases  $x$  and  $y$

#### Exponents

- $m$  = exponent of the Reynolds number
- $n$  = exponent of the Froude number
- $x$  = volume fraction of phase  $x$
- $y$  = volume fraction of phase  $y$

# LITERATURE CITED

1. Flynn, A. W., and R. E. Treybal, *A. I. Ch. E. Journal*, **1**, No. 3, 324 (1955).
- 1a. Laity, D. S., Ph.D. thesis, New York Univ. (1956).
2. Mack, D. E., and A. E. Kroll, *Chem. Eng. Progr.*, **44**, 189 (1948).
3. Miller, S. A., and C. A. Mann, *Trans. Am. Inst. Chem. Engrs.*, **40**, 709 (1944).
4. Overcashier, R. H., H. A. Kingsley, Jr., and R. B. Olney, *A. I. Ch. E. Journal*, **2**, 529 (1956).
5. Rushton, J. H., *Chem. Eng. Progr.*, **47**, 485 (1951).
6. Rushton, J. H., E. W. Costich, and H. J. Everett, *Chem. Eng. Progr.*, **46**, 395, 467 (1950).
7. Vermeulen, Theodore, G. M. Williams, and G. E. Langlois, *Chem. Eng. Progr.*, **51**, No. 2., 85F (1955).

Presented at A.I.Ch.E. Pittsburgh meeting

## Froth-frothate Concentration Relations in Foam Fractionation

VICTOR KEVORKIAN and ELMER L. GADEN, JR.

Columbia University, New York, New York

Concentration relations between foams and their residual liquids (frothates) have been examined.

Clean air streams of 88, 91, and 96% water saturation were bubbled into aqueous solutions of isobutyl alcohol. The concentration of the alcohol in the collected and collapsed foam was plotted against its concentration in the bulk liquid.

Varying the saturation of the air stream resulted in both positive and negative enrichment of the foam with the surface-active alcohol. This suggests that where froth-frothate-concentration relations are unfavorable, a change in operating conditions may advantageously affect these relations and allow the mixture to be foam separated.

Foam formation is often undesirable—for example, in stills, boilers, or fermenters. As a result, industrial study of foams has largely been directed toward (a) preventing their formation and (b) destroying them once formed. A foam, however, possesses qualities which can be usefully employed in certain instances. One of these is the fractionation of liquid mixtures.

Foaming may be used to separate the components of a homogeneous liquid mixture if one, or more, of them is surface active. When such a liquid is formed, these components may be preferentially adsorbed in the foam layer (froth) and their concentration there will be greater than in either the residual liquid (frothate) or the original solution.

Foaming therefore offers a means of separating positively adsorbed substances from solutions the other components of which are adsorbed to a lesser degree. As such it deserves investigation for it may provide a convenient means of fractionating liquid mixtures, particularly those containing complex, heat-sensitive, and chemically unstable materials. In such cases the more conventional methods, like distillation and extraction, are frequently unsatisfactory.

A few examples of foam separation have been reported. These include the separation of ricinic acids from fatty acids (2), fractionation of fatty acids (1), and the purification of enzymes (5). Ore flotation (7), though apparently quite similar, involves a somewhat different

principle in that the materials being separated are not present in a homogeneous single phase.

### PRINCIPLES

Gibbs (3) formulated from thermodynamic considerations an adsorption equation predicting the surface excess of a solute which is in equilibrium with its bulk concentration. In modified form this relationship is

$$\Gamma = -\frac{a}{RT} \left( \frac{d\gamma}{da} \right) \quad (1)$$

where

$\Gamma$  = excess solute per unit surface

$a$  = solute activity

$\gamma$  = surface tension of the solution

$R$  = universal gas constant

$T$  = absolute temperature

For sufficiently dilute solutions the mass concentration,  $x$ , may be substituted for activity and the equation becomes

$$\Gamma = -\frac{x}{RT} \left( \frac{d\gamma}{dx} \right) \quad (2)$$

Equation (1) says that if the solute is surface active—that is, if it lowers the surface tension of the solvent when added—it will concentrate in the surface layer. Conversely, a surface-inactive solute is negatively adsorbed (or “desorbed”) and its concentration in the interior of the solution is therefore greater than at the surface. In any case, then,

where the addition of solute to a solvent alters the surface tension of that solvent the surface layer of molecular depth will differ in concentration from the solution bulk.

In the work reported here, concentration relationships existing between foams and the bulk liquids from which they were formed have been measured by the rising-bubble technique. Solutions of isobutyl alcohol and water were studied and the results expressed in plots of alcohol concentration in the collected and collapsed foam (froth) vs. concentration in the residual liquid (frothate).

It is important to note that the rising-bubble method does not give equilibrium data. The values obtained are dependent upon the manner in which the bubbling apparatus is operated. Furthermore, in the case reported here the concentrations of froth and frothate were constantly changing, owing to the preferential evaporation of water by the entering air stream. Thus the data presented are for a particular arbitrary operating time (30 min.); longer or shorter periods would have given numerically different results. This point will be considered more completely in the discussion of the experimental data.

With this essential limitation of the rising-bubble technique recognized, it is still the simplest and most direct approach by far.

### EXPERIMENTAL DETAILS

Filtered air was bubbled into isobutyl alcohol-water solutions in the apparatus shown in Figure 1. The resulting foam was collected, collapsed, and continuously returned to the solution to be refoamed. This method provides recirculation, making it possible to keep the bubble-retention time constant. If the foam were removed, retention time would continually decrease during the run period. Retention time is defined here as the total fluid volume

(liquid chamber)

Apparatus

Dust filter  
A pressure liquid constant enter

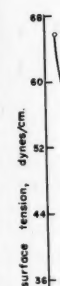


Fig. 2

degree may flow C co This pack chron therm the p a ca man stati Th diam A r diam the bubb An a chan liqui

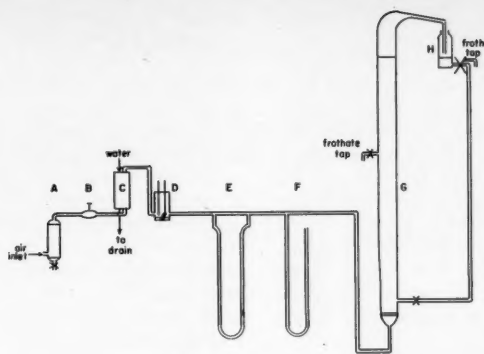


Fig. 1. Apparatus.

(liquid plus entrapped air) in the foaming chamber divided by the volumetric gas rate.

#### Apparatus

Dust in the air stream is removed in the filter *A*, which is packed with glass wool. A pressure regulator *B* maintains the liquid-foam interface in the column *G* at a constant height even if the pressure of the entering air stream should vary. Any

flow to the base of the column, where it is reformed.

#### Procedure

Runs were made at 27°C. with solutions ranging in alcohol mole fraction from zero to concentrated solutions approaching the saturation value. The concentration curves are extrapolated to this latter value, for as the solutions approach saturation the foam

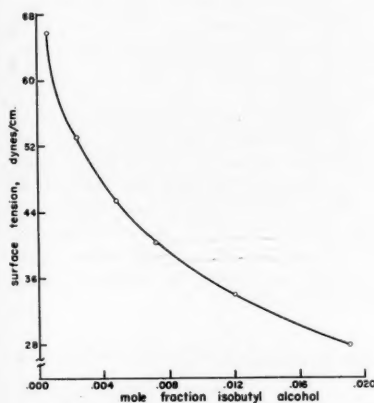


Fig. 2. Surface tension of aqueous solutions of isobutyl alcohol, 15°C.

degree of saturation of the inlet air stream may be obtained by varying the rate of flow of water trickling down the saturator *C* countercurrent to the rising air stream. This saturation column is a glass cylinder packed with 1/2-in. Raschig rings. A psychrometer *D*, with wet- and dry-bulb thermometers, permits the determination of the percentage of saturation of the air and a calibrated flow meter *E* and mercury manometer *F* indicate the rate of flow and static pressure of the air respectively.

The foaming column *G* has an inside diameter of 0.67 in. and a height of 47 in. A medium fritted-glass disk (capillary diameters: 10 to 15 $\mu$ ) at its base disperses the air in the solution, forming small bubbles of approximately 1/2-mm. diameter. An adapter leads the foam to the collecting chamber *H*, where it collapses. The resulting liquid is continuously recycled by gravity

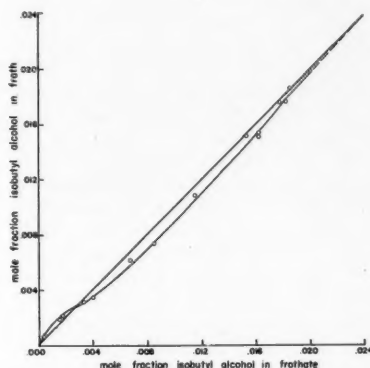


Fig. 3. Froth-frothate-concentration relations of isobutyl alcohol-water; air stream is 88% saturated at entrance.

persistence decreases sufficiently to prevent foam from being collected.

The air-stream velocity was kept constant during a given run to provide an average retention time of 3.6 min. for the air bubbles in the solution.

The humidity of the entering air could be varied in the saturation column *C* and measured in the psychrometer *D* before the foam column. Air streams of 88, 91, and 96% water saturation were used to note the effect of this variable. The degree of saturation of the air leaving the foam column was not measured. For the purposes of this study it was important only that it was equal to (unlikely) or greater than the entering value.

After the column was filled and the air rate adjusted, an arbitrary half-hour operating period was allowed before samples of froth and frothate (bulk liquid) were

removed and analyzed for alcohol content with the Abbe refractometer.

## RESULTS

### Solution Surface Tensions

A surface-tension-concentration diagram for aqueous isobutanol solutions at 15°C. is shown in Figure 2. These data are taken from the literature (4) and show the trend even though the temperature is different from that used in the experiments reported here. Isobutyl alcohol is clearly surface active and, from the adsorption theorem [Equation (2)], adsorption should always be positive with the surface concentration exceeding that of the bulk.

### Froth-frothate-concentration Relations

The froth-frothate-concentration relations actually obtained with the rising-bubble apparatus are tabulated (Table 1) and plotted in Figures 3, 4, and 5 for the different values used for air-stream saturation. They are obviously at least partially in disagreement with what one would expect from the Gibbs relationship (1).

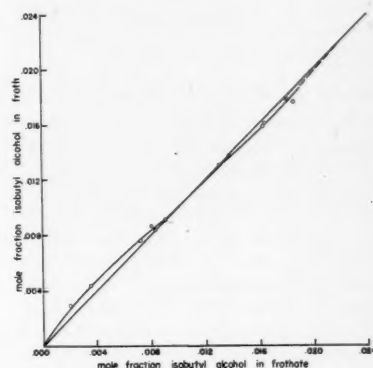


Fig. 4. Froth-frothate-concentration relations of isobutyl alcohol-water; air stream is 91% saturated at entrance.

The froth-frothate-concentration relations have been plotted here in the familiar  $y$ - $x$  manner for convenience. They are not, of course, equilibrium curves, and the chosen method of plotting is not meant to imply this.

Since  $dy/dx$  is always negative, surface adsorption should never be zero or negative and the froth should always be richer in alcohol than the frothate. The runs reported were made randomly rather than by continuously increasing or decreasing the initial concentration. Thus the possibility that negative adsorption has been erroneously reported is discounted by the sizable negative adsorptions frequently observed and the continuous nature of the curves.

As a final check, a test of significance

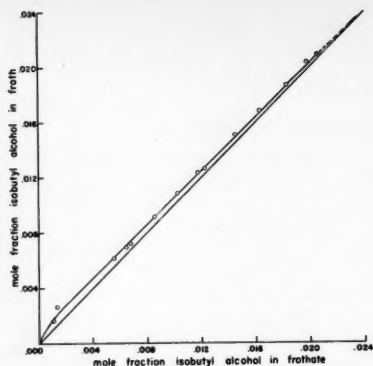


Fig. 5. Froth-frothate-concentration relations of isobutyl alcohol-water; air stream is 96% saturated at entrance.

was applied to the data of Table 1. This established the minimum difference between froth and frothate concentrations which must be equal or exceeded before it may be said that a concentration change has actually taken place. At the 95% confidence level this difference is 0.00025 mole fraction of isobutyl alcohol. The data of Table 1 testify that significant differences in concentration between foam and residue did, in fact, occur.

#### Interpretation of Froth-frothate Curves

The apparent anomaly in these curves relating alcohol concentrations in froth and frothate is believed to be due to the preferential evaporation of water into the air stream during foaming. Evidently two processes were occurring during foaming. On one hand surface adsorption tended to concentrate alcohol in the foam "phase" as predicted. At the same time, however, preferential evaporation of water caused the alcohol concentration in the bulk liquid to increase. The actual froth-frothate-concentration relation ob-

served depends on the relative rates of these two competing processes.

In dilute solutions  $dy/dx$ , the slope of the surface tension curve (Figure 2), is large and the former effect, surface adsorption, is greater. Positive adsorption results, and froth alcohol concentrations exceed those in the frothate. As the solution concentration is increased, however,  $dy/dx$  decreases in absolute magnitude and adsorption falls off accordingly. At some point for each degree of air-stream saturation the two effects become equal and there is no apparent enrichment of the froth.

Support for the foregoing interpretation is afforded by the facts that the vapor pressure of water at 27°C. is twice that of alcohol and its mass transfer coefficient in air is about three times as large (6). A test to check this point was also made by bubbling unsaturated air through an alcohol-water solution in a bottle. After  $\frac{1}{2}$  hr. the alcohol concentration had increased from 0.005 to 0.00585 mole fraction.

#### Effect of Air-stream Saturation

If the previous interpretation is true, then the more completely saturated the air stream is with water vapor, the less will be the evaporation effect. As air-stream saturation increases, positive adsorption and alcohol enrichment of the foam should occur over a wider concentration range. This does in fact occur, as Table 1 and the curves show.

At very dilute concentrations foam enrichment results in all three degrees of saturation. As saturation increases, this enrichment is observed over a greater range of concentration before the adsorption effect is equaled by evaporation. When the air stream is least saturated (88%), zero and negative enrichment occur at a lower concentration than for higher saturations (91%). For the same reasons the degree of apparent "negative

adsorption" observed at 88% saturation is greater than for 91%. When the air stream is 96% saturated (Figure 5), the adsorption effect seems to be always greater than evaporation, giving positive adsorption, or enrichment, over practically the entire concentration range.

The fact that varying saturation of the air stream permitted, in effect, both positive and negative adsorption of a surface-active agent, which should be only positively adsorbed, is extremely interesting. These results suggest that in cases where froth-frothate-concentration relations are unfavorable, alterations in operating conditions like temperature and the nature and degree of saturation of the gas with the solvent may propitiously affect these relations and permit the mixture to be separated by foaming.

#### SUMMARY

A clean air stream of 88, 91, and 96% water saturation was bubbled into solutions of isobutyl and water. The resulting foam was collected, collapsed, and continuously returned to the solution to be refoamed. Runs were made at 27°C. for solutions ranging in concentration from 0 mole fraction alcohol to near saturation.

The concentration of the alcohol in the collected and collapsed foam was plotted against its concentration in the bulk liquid.

Varying the saturation of the air stream resulted in both positive and negative enrichment of the foam with the surface-active alcohol. This suggests that where froth-frothate-concentration relations are unfavorable, a change in operating conditions may advantageously affect these relations and allow the mixture to be foam separated.

#### ACKNOWLEDGMENT

The work reported here was supported in part by a grant from the Esso Research and Engineering Company, and this assistance is acknowledged with appreciation.

#### LITERATURE CITED

1. Aenlle, E. O., and S. G. Fernandez, *Analales fis. y quim.*, **45B**, 217 (1949).
2. Dubrisay, René, *Bull. soc. chim. France*, **280** (1953).
3. Gibbs, J. W., "Collected Works," Vol. I, Longmans, Green and Company, New York (1928).
4. "International Critical Tables," Vol. IV, 468, McGraw-Hill Book Company, Inc., New York (1928).
5. London, M., M. Cohen, and P. B. Hudson, *J. Am. Chem. Soc.*, **75**, 1746 (1953).
6. Perry, J. H., "Chemical Engineers' Handbook," 3 ed., Table II, p. 539, McGraw-Hill Book Company, Inc., New York (1950).
7. Taggart, A. F., "Handbook of Ore Dressing," p. 779, John Wiley & Sons, New York (1928).

TABLE 1.

AIR-STREAM MOISTURE, % SATURATION

88		91		96	
$x$	$y$	$x$	$y$	$x$	$y$
0.0004	0.0006	0.0021	0.00285	0.0011	0.0016
0.0016	0.00185	0.0036	0.00435	0.0014	0.0026
0.00185	0.0021	0.0073	0.0076	0.0056	0.0061
0.0034	0.0031	0.0081	0.0086	0.0065	0.00685
0.0041	0.0034	0.00835	0.00835	0.00685	0.0071
0.0088	0.0061	0.0091	0.0091	0.0086	0.0091
0.0086	0.00735	0.01305	0.01305	0.0103	0.0108
0.0116	0.0108	0.01635	0.0158	0.0118	0.0123
0.0154	0.0151	0.0165	0.01605	0.0123	0.0126
0.01635	0.0153	0.0181	0.01785	0.0145	0.01505
0.01635	0.01505	0.0186	0.0176	0.01635	0.0168
0.01785	0.0176			0.01835	0.0186
0.01835	0.0176			0.01985	0.02035
0.0186	0.0186			0.0206	0.0208
0.0201	0.01985				

$x$  = mole fraction isobutyl alcohol in frothate.  
 $y$  = mole fraction isobutyl alcohol in froth.



# Ion Exclusion Equilibria in the System Glycerol-sodium Chloride-water-Dowex-50

EDWARD L. SHURTS and ROBERT R. WHITE

University of Michigan, Ann Arbor, Michigan

Ion exclusion is an operation in which an ion exchange resin is used to separate an electrolyte from a nonelectrolyte in a polar solvent. An ion exchange resin tends to absorb a nonelectrolyte and to exclude an electrolyte. This is described quantitatively by the equilibrium distribution of the electrolyte, the nonelectrolyte, and the solvent between the resin phase and the liquid phase surrounding the resin.

As no ternary distribution data applicable to ion exclusion are available, and only a few binary data have been published, a principal purpose of this investigation was to determine the distribution data for a typical system: glycerol-sodium chloride-water-Dowex-50.

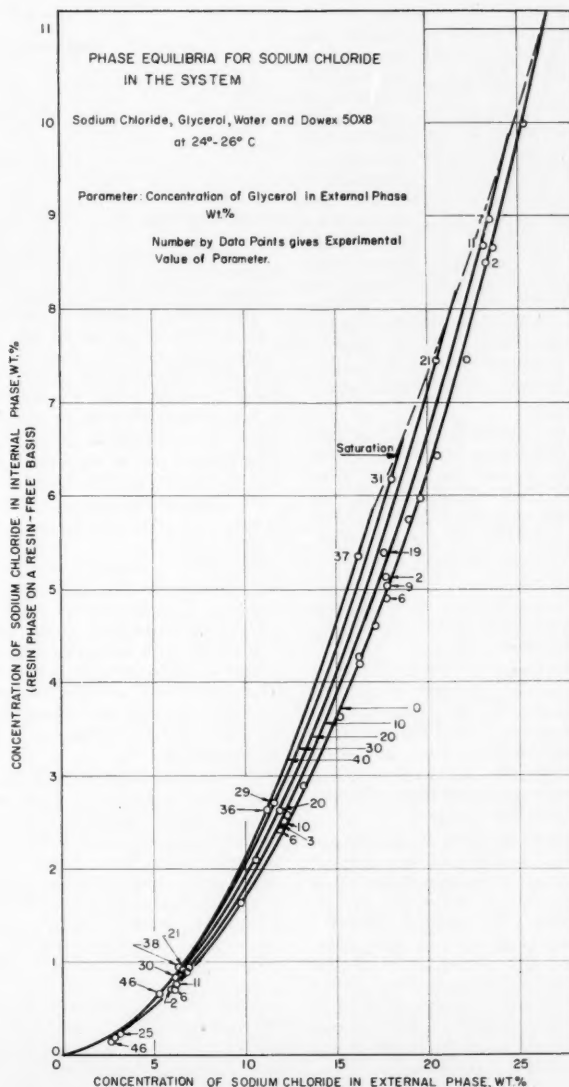


Fig. 1. →

E. L. Shurts is with E. I. du Pont de Nemours and Company, Inc., Wilmington, Delaware.

Of these five quantities, all but  $V_s''$ , the final solution volume, can be measured directly and accurately. The initial volumes of the resin and solution can be determined from their weight and density. The final volume of the resin is a function of the initial weight of air-dry resin and the composition of the final external solution. It can be accurately determined by swelling measurements conducted independently of equilibrium experiments. Likewise the correction to additive volumes  $\Delta V_T$  can be correlated as a function of the composition of the external solution by independent measurements. Once the final solution volume  $V_s''$  has been calculated, the weight of every component in both phases may be determined by difference.

#### Methods of Analysis

It was necessary to analyze accurately for sodium chloride and glycerol in aqueous solutions, as errors were magnified when differences were taken in the material-balance equations. A combination of density measurements and titration for the chloride ion was developed for this purpose.

The densities of ternary mixtures in the system sodium chloride-glycerol-water were determined by a careful pycnometer technique to a precision of  $\pm 0.00003$  g./ml. The compositions of binary mixtures of sodium chloride-water and glycerol-water were determined from density data. The sodium chloride content of dilute solutions was determined by a Beckman Flame Photometer and spectrophotometer, both of which could be read to several parts per million. They were calibrated by diluting standard salt solutions the concentration of which had been determined by density. The sodium chloride content of the ternary solutions was determined by Fajan's method of analysis (14).

The glycerol concentration in ternary mixtures was determined from the sodium chloride titrations and the density data. The precision of the ternary analysis was calculated to be  $\pm 0.02$  wt. % for sodium chloride and  $\pm 0.04$  wt. % for glycerol.

The resin contained  $17.79 \pm 0.10$  wt. % water and had a density of  $1.4673$  g./ml. in the sodium form. It had an equivalent weight, milliequivalents/gram, of  $5.00 \pm 0.06$  in the hydrogen form.

The initial volume of the air-dry resin was calculated from its initial weight and density, determined by the displacement of xylene. The decrease in the total volume of both resin and solution phases caused by the equilibration  $\Delta V_T$  was measured in a pycnometer, the results of these measurements being shown in Figure 1.

The increase in volume of the air-dry resin caused by equilibration with various final concentrations of sodium chloride and glycerol solutions was measured by observing with Barker's technique (1) the swelling of resin beads under a microscope. [Each diameter ratio at a given concentration required at least twenty observations on ten beads to give a precision for  $D/D_0$  of  $\pm 0.0004$ . The results of the swelling measurements are shown in Figure 2 and the data are available elsewhere (11)].

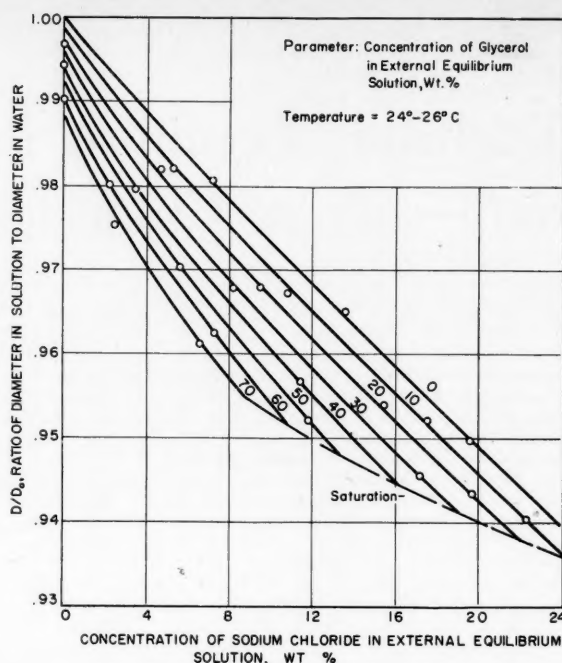


Fig. 2. Swelling of the resin.

#### Distribution Data

A weighed quantity of air-dry resin of known composition was equilibrated with a weighed quantity of a solution containing a known concentration of sodium chloride and glycerol. A portion of the equilibrium solution phase was analyzed to determine the sodium chloride and glycerol concentrations. These data enable accurate material-balance calculations to be made to determine the resin-phase composition. The experimental results are shown in Figures 3 and 4 and in Tables 1 and 2.

The data were correlated by the method of least squares to give the curves of Figures 3 and 4. Salt is seen to have a pronounced effect upon the distribution of glycerol, but the effect of glycerol upon salt is considerably less. The distribution coefficient  $Y/X$  for salt varies between 0.03 and 0.40 and that for glycerol between 0.6 and 1.3. The difference between their distribution coefficients makes their separation possible by ion exclusion, and the strong influence of the salt upon the glycerol is beneficial to this separation.

The sodium chloride distribution data were correlated with a standard residual error of  $\pm 0.07$  weight % and the glycerol data with an error of  $\pm 0.15$  weight %. It is enlightening to study the experimental errors which will cause deviations of the aforementioned magnitude. Table 3 summarizes the most important experimental errors. The controlling error in both cases appears to be the analysis of the external phase. The swelling error is probably next in importance. Table 3 serves as a minimum standard that must be met to take equilibrium data of the same precision when a 40-g. sample of resin is used.

TABLE 1. PHASE EQUILIBRIA DATA FOR BINARY EXTERNAL SOLUTIONS

Resin: Dowex-50, DVB content = 8.7, sodium form  
Temperature:  $24^\circ$  to  $26^\circ\text{C}$ .

Notation:  $X_s$ ,  $X_g$  concentration of sodium chloride of glycerol in the external phase, respectively, weight per cent.  $Y_s$ ,  $Y_g$  concentration of sodium chloride or glycerol in the internal phase, respectively, weight per cent. The internal phase is defined as the solution in the resin phase on a resin-free basis.

Sodium chloride-water		Glycerol-water	
$X_s$	$Y_s$	$X_g$	$Y_g$
6.74	0.91	17.94	11.68
9.79	1.64	32.50	22.87
12.35	2.55	52.62	42.50
15.27	3.61	72.11	65.88
17.17	4.60	84.25	82.88
20.54	6.43		
23.10	8.16	12.41	7.71
		22.18	14.70
6.95	0.93	32.70	23.22
10.58	2.10	43.12	32.85
13.20	2.88	49.55	39.28
15.96	4.03	62.45	53.81
19.01	5.72	74.38	68.81
19.70	5.95	88.63	84.85
22.15	7.45		
23.63	8.64	2.24	1.52
		6.73	4.42
16.28	4.17		
16.25	4.27		
2.82	0.18		

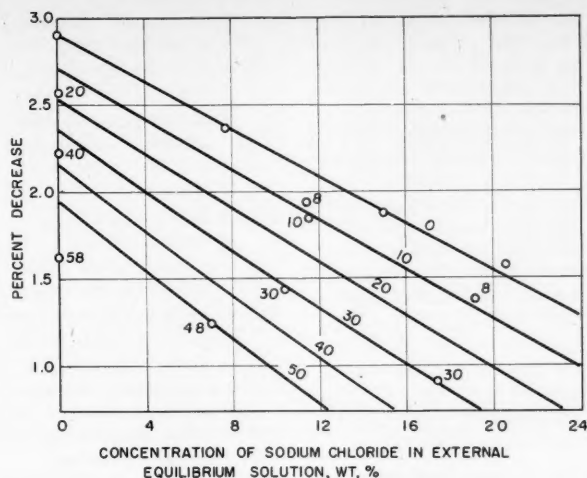


Fig. 3. Change of total volume during swelling. Basis: initial volume of air-dry resin; parameter: concentration of glycerol in external solution, wt. %.

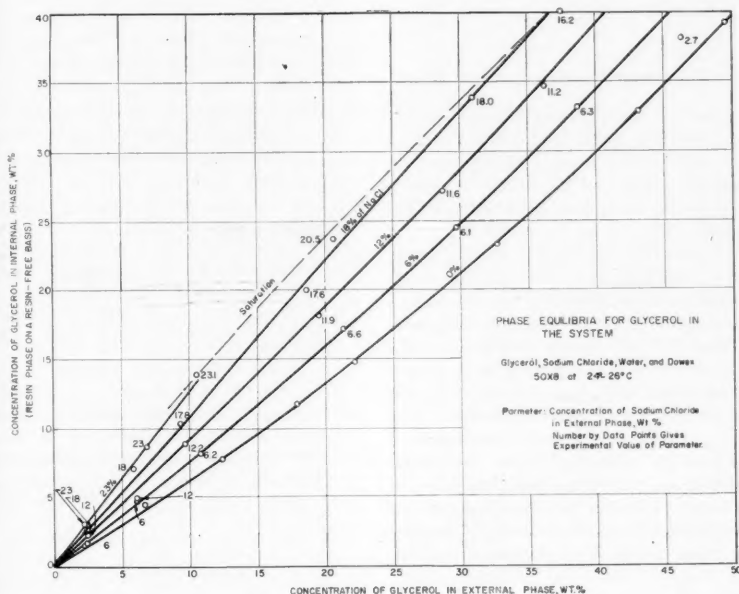


Fig. 4.

terms were added to a correlating equation by trial and error until the deviations of the points showed no bias when plotted against the variables. The results of this process, which is reported in detail elsewhere (10), were for glycerol

$$Y_G = 0.5687X_G + 0.004472X_G^2 + 0.023023X_GX_S - 0.000113X_G^2X_S + 0.000661X_G^{0.5}X_S^2 \quad (2)$$

Standard residual error = 0.149

TABLE 2. PHASE EQUILIBRIA DATA FOR TERNARY EXTERNAL SOLUTIONS

Resin: Dowex-50, DVB content = 8.7, sodium form  
 Temperature: 24° to 26°C.  
 System: Sodium chloride-glycerol-water-Dowex-50  
 Notation:  $X_S$ ,  $X_G$  concentration of sodium chloride or glycerol in the external phase, respectively, weight per cent  
 $Y_S$ ,  $Y_G$  concentration of sodium chloride or glycerol in the internal phase, respectively, weight per cent. The internal phase is defined as the solution in the resin phase on a resin-free basis.

External phase		Internal phase	
$X_S$	$X_G$	$Y_S$	$Y_G$
6.21	10.81	0.75	8.17
11.19	36.16	2.62	34.73
16.21	37.45	5.34	40.13
17.79	9.38	5.01	10.32
6.15	29.78	0.83	24.46
11.61	28.69	2.70	27.08
11.86	19.59	2.61	18.02
17.63	18.65	5.38	19.94
12.20	9.70	2.51	8.92
6.59	21.35	0.91	17.05
6.32	38.63	0.95	33.19
18.03	30.93	6.17	33.82
12.11	2.58	2.50	2.27
23.23	2.33	8.50	3.02
5.98	2.49	0.72	1.72
17.77	2.54	5.12	2.61
23.44	6.85	8.95	8.64
23.09	10.51	8.68	13.90
6.13	6.18	0.69	4.70
11.93	6.15	2.41	4.90
17.77	5.90	4.88	7.02
3.18	25.27	0.21	19.14
2.70	46.32	0.16	38.17
20.49	20.63	7.45	23.61
5.31	45.76	0.65	40.49

TABLE 3. EFFECT OF ERRORS ON EQUILIBRIUM RESULTS

The following errors will cause the residual error of correlation.

	Sodium chloride	Glycerol
Residual error of correlation	±0.07 wt. %	±0.15 wt. %
Weight of component in resin phase	14 mg.	30 mg.
Analysis of component in external phase	0.02 wt. %	0.04 wt. %
Swelling ratio, $D/D_0$	0.0007	0.0007
Total volume change	0.2 vol. %	0.2 vol. %
Moisture content of reagent	0.05 wt. % $H_2O$	0.05 wt. % $H_2O$

#### CORRELATION OF THE DATA

It was impractical to make equilibrium determinations at a constant concentration parameter. Thus the data require that a family of curves be fitted to the points. The precision of the data seemed to justify developing suitable equations rather than drawing curves interpolated by eye through the points. A method reported by Ezekiel (4) was used in which

For sodium chloride

$$Y_s = 0.0286X_s + 0.01408X_s^2 + 0.0001102X_sX_g \quad (3)$$

Standard residual error = 0.066

Where

$X_g, X_s$  = weight per cent in external phase of glycerol and sodium chloride respectively

$Y_g, Y_s$  = weight per cent in resin phase on a resin-free basis of glycerol and sodium chloride respectively

## DISCUSSION

The equilibrium data of Figures 3 and 4 indicate that glycerol is absorbed by resin in preference to sodium chloride when a solution of glycerol-sodium chloride-water is equilibrated with resin. Thus resin can be used as a fractionation medium for separating glycerol from sodium chloride. The analysis of the performance of a continuous ion exclusion column using the equilibrium data of this investigation will be the subject of a future paper.

It has been shown previously (5, 6, 13) that the basic equation for ion exclusion is

$$RT \ln a_{j,e}^* = RT \ln a_{j,r}^* + P_r \bar{V}_{j,r} \quad (4)$$

The glycerol-water binary is especially suited for the study of activity coefficients in the resin phase. Equation (4) may be so arranged that the only unknown variable is  $a_{g,r}^*$ , the activity of glycerol in the resin phase at zero (or atmospheric) pressure. The activity coefficients of glycerol in water at 0°C. are reported by Lewis and Randall (10). These values were estimated to change by not more than  $\pm 0.003$  at 25°C. by vapor-pressure data from Carr, Townsend, and Badger (2). The osmotic pressure for this case was reported to be 200 atm. by Glueckauf (5) and 75 atm. by Gregor (7). The partial molal volume of glycerol can be calculated from density data, and the concentrations at equilibrium from Figure 4. The resulting stoichiometric molal activity coefficients for glycerol in the resin phase are given in Table 4.

TABLE 4. ACTIVITY COEFFICIENTS OF GLYCEROL IN THE RESIN PHASE

Glycerol molality in resin phase	Activity coefficients $\gamma_{g,r}^*$		
	Osmotic pressure $P_r$ , atm.		
	200	75	1
0.26	0.973	1.456	1.756
0.12	0.976	1.460	1.761
0.29	0.990	1.480	1.787
0.59	1.007	1.508	1.820
1.20	1.048	1.567	1.889
3.12	1.197	1.790	2.160

Thus it is seen that the activity coefficient in the resin phase is sensitive to the value assigned to the osmotic pressure. This observation emphasizes that fundamental data in the form of activities and osmotic pressure are not available to permit quantitative application of the theoretical equation.

The usefulness of this equation for predicting the qualitative behavior of phase equilibria will be illustrated. The following data show the effect of glycerol upon the activity coefficient of hydrochloric acid (9).

TABLE 5. MEAN ACTIVITY COEFFICIENT OF HYDROCHLORIC ACID IN GLYCEROL-WATER SOLUTIONS AT 25°C.

Molality of hydrochloric acid	Activity coefficients of hydrochloric acid, weight % of glycerol in solvent	
	3.1	21.2
0.01	0.902	0.885
0.1	0.798	0.775
1.0	0.810	0.810
2.0	1.019	1.030
4.0	1.792	1.914

Thus for molalities of 2.0 and 4.0 the concentration of the hydrochloric acid in the resin phase would be expected to increase slightly as glycerol is added to the solvent. This same effect is noted for sodium chloride in Figure 3. However for concentrations of less than 1 molal the reverse happens. The salt data tends to confirm this below 5%, but the results are not conclusive. A similar comparison of the effect of the electrolyte upon the distribution of the nonelectrolyte should be more striking, but activity data are not available for the comparison.

It would be convenient to extend these equilibrium data to other Dowex-50 resins. The structure and properties of Dowex 50 indicate that the fundamental properties of the resin that can be changed are resin capacity (equivalent weight) and cross linkage (divinyl benzene content). These properties should be sufficient to fix the variables pertaining to the resin in Equation (4). Since Dowex 50 can usually be assumed to possess one sulfonic acid group per styrene molecule (3), the resin capacity can also probably be correlated as a function of divinyl benzene content. Therefore, the latter should be sufficient to correlate these equilibrium data to other Dowex 50 resins. Correlations of this type have been reported for ethylene glycol and water (12) and potassium chloride and water (8).

## NOTATION

$a_{j,e}^*$  = activity of component  $j$  in the external phase at zero pressure

$a_{j,r}^*$  = activity of component  $j$  in the resin phase at zero pressure  
 $D$  = diameter of a resin bead immersed in a specified solution  
 $D_0$  = diameter of the same bead immersed in pure water  
 $P_r$  = osmotic pressure of the resin phase  
 $R$  = gas constant  
 $T$  = temperature  
 $\bar{V}_{j,r}$  = partial molal volume of component  $j$  in the resin phase  
 $V_R$  = initial volume of the air-dry resin  
 $V_s'$  = initial volume of the solution added to the cell  
 $V_R''$  = final volume of the resin at equilibrium  
 $V_s''$  = final volume of the external solution at equilibrium  
 $\Delta V_T$  = change in total volume  
 $X_s$  = concentration of sodium chloride in the external phase, wt. %  
 $X_g$  = concentration of glycerol in the external phase, wt. %  
 $Y_s$  = concentration of sodium chloride in the internal phase, wt. %  
 $Y_g$  = concentration of glycerol in the internal phase, wt. %, where the internal phase is defined as the solution in the resin phase on a resin-free basis  
 $\gamma_{g,r}^*$  = stoichiometric molal activity coefficient for glycerol in the resin phase at zero pressure

## LITERATURE CITED

- Barker, G. E., Ph.D. thesis, Univ. Michigan, Ann Arbor (1952).
- Carr, A. R., R. E. Townsend, and W. L. Badger, *Ind. Eng. Chem.*, **17**, 643 (1925).
- Duncan, J. F., *Nature*, **169**, 22 (1952).
- Ezekiel, M., "Methods of Correlation Analysis," John Wiley and Sons, New York (1930).
- Glueckauf, E., *Proc. Roy. Soc. (London)*, **A214**, 207 (1952).
- Gregor, H. P., *J. Am. Chem. Soc.*, **73**, 642 (1951).
- Gregor, H. P., and M. Frederick, *Ann. N. Y. Acad. Sci.*, **57**, Art. 3, 87 (1953).
- Gregor, H. P., and M. H. Gottlieb, *J. Am. Chem. Soc.*, **75**, 3539 (1953).
- Harned, H. S., and B. B. Owen, "The Physical Chemistry of Electrolytic Solutions," 2 ed., p. 551, Reinhold Publishing Company, New York (1950).
- Lewis, G. N., and Merle Randall, "Thermodynamics," p. 288, McGraw-Hill Book Company, Inc., New York (1923).
- Shurts, E. L., Ph.D. thesis, Univ. Michigan, Ann Arbor (1955).
- Wheaton, R. M., and W. C. Bauman, *Ann. N. Y. Acad. Sci.*, **57**, Art. 3, 159 (1953).
- Whitcombe, J. A., Ph.D. thesis, Univ. Michigan, Ann Arbor (1952).
- Willard, H. H., and N. H. Furman, "Elementary Quantitative Analysis," 3 ed., 182, D. Van Nostrand Company, New York (1940).



# Equilibrium in the System Cu<sup>++</sup>-Na<sup>+</sup>-Dowex-50

H. C. SUBBA RAO and M. M. DAVID

University of Washington, Seattle, Washington

Equilibrium isotherms are presented for the cation exchange of copper and sodium on Dowex-50 resin in solutions from 0.01 to 4*N* in chloride content, and the equilibrium data are correlated on the basis of the Donnan equilibrium. Data are also given on the water content of the resin and the diffusible ions present in this water.

Although extensive equilibrium data for univalent cation exchange are available, the published data for unipolyvalent cation exchange are relatively sparse. Gregor et al. (7) have listed the majority of unipolyvalent equilibrium studies, practically all of which cover only a limited concentration range and are concerned principally with relatively dilute solutions. More complete investigations have been made by Bauman and coworkers (2) for Ca<sup>++</sup>-Na<sup>+</sup> exchange and by Gregor et al. (7) for Mg<sup>++</sup>-K<sup>+</sup> exchange. These are valuable both in furthering the understanding of the fundamental mechanisms of cation exchange and in providing data for the design of ion exchange processes. Accordingly equilibrium data were obtained for the system Cu<sup>++</sup>-Na<sup>+</sup>-Dowex-50, a system of interest particularly at high concentrations, in various waste-treatment and recovery processes (4, 14). Selke and Bliss (14) have presented a small amount of equilibrium data for copper-hydrogen exchange at two solution concentrations, and Nayak (11) has studied copper-sodium and copper-hydrogen exchange at three different solution concentrations. The present investigation covered the concentration range from 0.01 to 4*N*.

## THEORY

Methods for explaining and correlating ion exchange equilibrium data have generally been based on the law of mass action, adsorption theory (including statistical approaches), or Donnan equilibrium theory. As pointed out by Schubert (13) and Gaines and Thomas (5), one approach does not necessarily have a greater fundamental validity than another, as long as not too many simplifying assumptions are made. All three approaches lead to the same general form of equilibrium equation. The Donnan equilibrium principle was used to interpret the experimental data of the present

investigation, because it can account for the presence of diffusible anions in the resin phase when the resin is in equilibrium with an external solution. As developed by Bauman and Eichorn (1), the Donnan membrane principle leads to the following expression for equilibrium in the system Cu<sup>++</sup>-Na<sup>+</sup>-Dowex-50:

$$\frac{a_{Na}^2 A_{Cu}}{a_{Cu} A_{Na}^2} = 1 \quad (1)$$

If activity coefficients are used, Equation (1) becomes

$$\frac{x_{Na}^2 X_{Cu} \gamma_{Na}^2 f_{Cu}}{x_{Cu} X_{Na}^2 \gamma_{Cu} f_{Na}^2} = 1 \quad (2)$$

where

$$\frac{\gamma_{Na}^2}{\gamma_{Cu}} = \frac{\gamma_{Na}^2 \gamma_{Cl}^2}{\gamma_{Cu} \gamma_{Cl}^2} = \frac{\gamma_{NaCl}^4}{\gamma_{CuCl_2}} \quad (3)$$

Nearly all the theoretical equations proposed for ion exchange equilibria, including those above, require data on the activities or activity coefficients of the ions in the resin and solution phases, and it is this requirement which generally limits the utility of the equations. Some data are available on the activity coefficients of single chemical compounds in aqueous solutions, and the mean ionic activity coefficients of the components in a solution containing more than one solute may be obtained from the activity coefficients of the pure components by applying the Lewis ionic-strength principle (10). Activity coefficients for ions in the resinous phase of an ion exchange system are exceedingly scarce; however, Schubert (13) has noted for several electrolytes that if the activity coefficient for the resin phase is plotted as a function of the solution strength computed from the water content of the resin, the curve for the resin-phase activity coefficient has the same shape as, but lies below, the corresponding curve for aqueous solutions of the electrolyte. If it may therefore be assumed that activity coefficients for the cations in the resin phase are proportional to the activity coefficients of these same cations in an

aqueous solution of the same ionic strength as that in the resin phase, Equation (2) may be modified to

$$\frac{x_{Na}^2 X_{Cu} \gamma_{NaCl}^4 f_{CuCl_2}^3}{x_{Cu} X_{Na}^2 \gamma_{CuCl_2}^3 f_{NaCl}^4} = K \quad (4)$$

Equation (4) requires for its use only activity coefficients in the aqueous phase.

Simplified forms of Equation (4) may be obtained by neglecting the activity coefficients in the solid phase, the activity coefficients in both phases, or the activity coefficients in both phases and the change in water content of the resin. The last of these possibilities is frequently encountered as the definition of the selectivity coefficient  $K'_c$ :

$$K'_c = \frac{x_{Na}^2 M_{Cu}}{x_{Cu} M_{Na}} \quad (5)$$

Equation (5) predicts that the equilibrium will strongly favor the copper form of the resin for dilute external solutions but that this selectivity for copper will decrease as the external solution concentration increases (2).

## APPARATUS AND PROCEDURE

Commercial-grade Dowex-50 cation exchange resin, 20 to 50 mesh size, 8% cross linkage, was used in the study. The resin was thoroughly pretreated, and the capacity measured with both copper and hydrogen was  $5.1 \pm 0.05$  meq./g. of the dry hydrogen form, exclusive of "unattached" cations which might be present in the resin pores. Reagent grade copper chloride and sodium chloride were used to furnish the copper and sodium ions.

The equilibrium data were determined by the columnar technique, wherein solution of known composition is passed through a sample of the resin until equilibrium is attained, and the resin was then analyzed for chloride, copper, and water content. The resin was held in a small Pyrex tube containing a coarse fritted-glass disk near one end to serve as a resin support. The entire resin-bed unit could be attached to or removed at will from a system supplying the necessary liquid solutions. Two beds, each containing approximately 1 g. of resin, were used in the study. An accurately

H. C. Subba Rao is at present with the General Petroleum Corporation, Los Angeles, California.

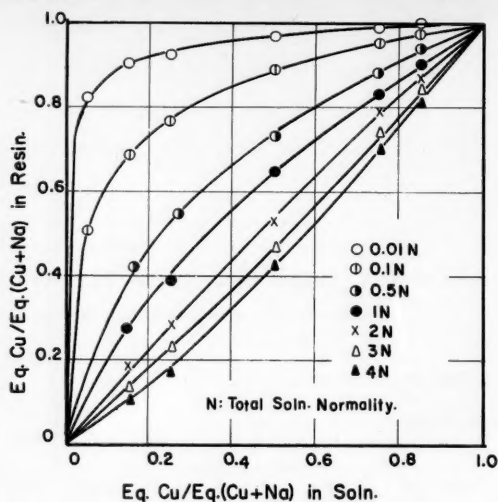


Fig. 1. Exchange isotherms (resin composition after washing).

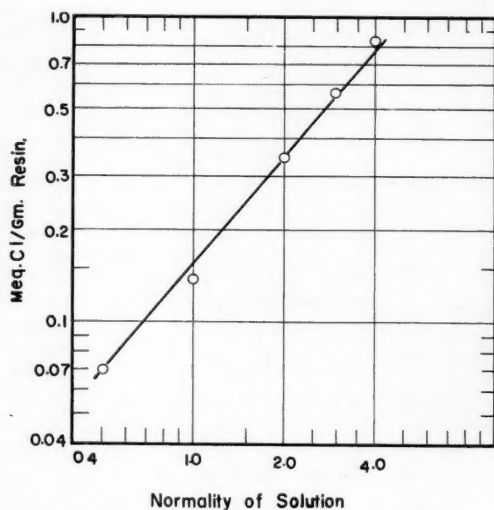


Fig. 3. Chloride content of resin (in pore solution).

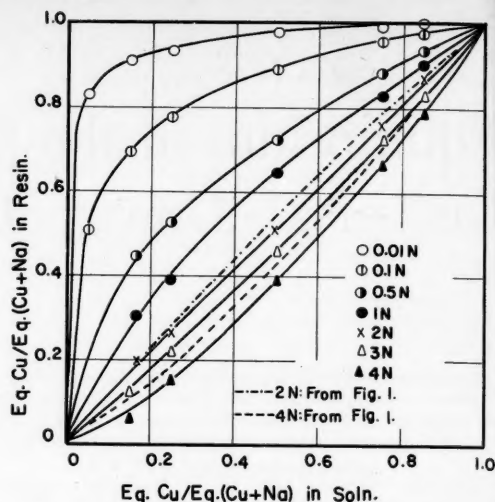


Fig. 2. Exchange isotherms (pore solution included in resin composition).

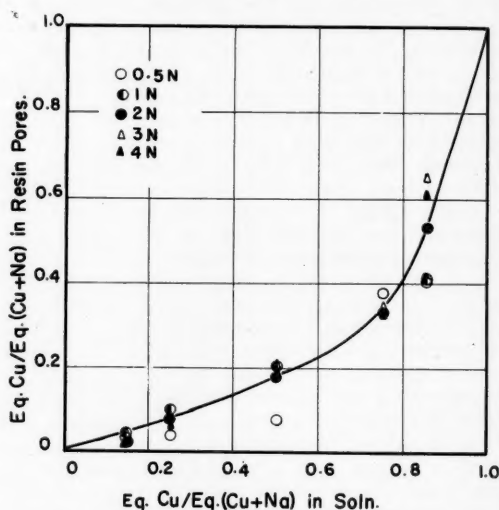


Fig. 4. Indicated copper content of pore solution.

weighed quantity of resin was placed in each bed and remained in that bed throughout the entire series of experiments.

For a given determination, 2 liters of solution of desired composition were passed through the bed at a low flow rate. Preliminary tests showed that the volume of solution and the flow rate used were generously adequate for the resin to reach equilibrium with the solution. After saturation the bed was detached from the feed system and the solution in the tube permitted to drain. The two ends of the bed were then sealed with rubber caps and the bed was centrifuged at approximately 2,000 rev./min. for 3 min., a time determined by preliminary experiments. Solution sticking to the lower end of the tube was removed by drying with filter paper and the bed was quickly weighed. After the weighing 200 ml. of distilled water was passed through the bed to elute the solution present in the pores of the resin, and the effluent wash water was analyzed for copper and chloride ions. The copper chemically combined with

the resin was next eluted with 2 liters of 1N sodium chloride solution, which was sufficient to remove all copper from the resin. This regenerant solution was analyzed for copper content, the resin was again washed with distilled water, and the bed was ready for reuse.

The pH of the regenerant solutions was not measured, but solubility data, weight checks on the resin samples, and resin capacity measurements all indicated that there was no copper precipitation within the resin during regeneration.

All copper determinations were made colorimetrically, with tetraethylene pentamine as the reagent, and the chloride ion was measured turbidimetrically, with silver nitrate as the reagent.

The data obtained in the foregoing procedure, with a knowledge of the weights of the resin and Pyrex tube, are sufficient to permit calculation of the complete composition of the resin phase if electroneutrality of the resin phase is assumed and the capacity of the resin is known.

All runs were made at room temperature (22° to 25°C.). The equilibrium solution normality was varied from 0.01 to 4.0 total normality. The copper to chloride normality ratios used at each solution concentration were varied from 0.15 to 0.85, except at the 0.01 and 0.10 normality concentrations, where the copper to chloride normality ratio was extended to 0.05 to permit more accurate determination of the equilibrium isotherms. Results were computed on the basis of the oven-dry hydrogen form of the resin.

#### EXPERIMENTAL RESULTS AND DISCUSSION

The experimental results of the study are presented in Figures 1 through 5. A complete tabulation of the original experimental data, the values used for intermediate calculations and the final results shown in Figures 1 to 6, is available in reference 15.

Figures 1 and 2 contain the primary

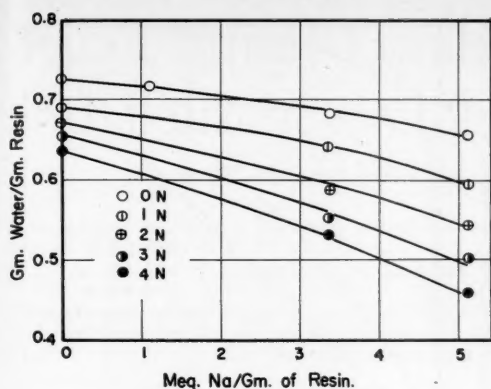


Fig. 5. Water content of resin.

results and show resin composition as a function of the equilibrium-solution composition and concentration. The two figures differ only in that the exchange isotherms in Figure 2 include the ionic contents of the resin pores as part of the resin composition; whereas those of Figure 1 do not. Equivalent fractions are used as the ordinates in both figures, since cation exchange is essentially a constant normality process (at least in dilute solutions), and the data are thus presented in a form useful for design calculations and rate studies. As predicted by Equation (5), the "adsorption" of the copper is strongly favored at low solution concentrations, but this selectivity decreases as total solution normality increases and at high solution concentrations the selectivity is actually reversed. These results are also in accord with those of previous investigators of unipolyvalent exchange (2, 7, 14). The ionic content of the liquid in the resin pores has negligible effect on the equilibrium isotherms at low solution concentrations but becomes important at high concentrations, as may be noted from the comparative isotherms included in Figure 2. This effect could be significant in the design of ion exchange recovery or separations processes utilizing strong regenerants.

The magnitude of the ionic holdup in the pores of the resin is shown in Figure 3. The chloride content of the pore solution was found to be dependent only upon the total normality of the external solution and not upon the ratio of copper to sodium in the external solution. At high solution normalities the cations in the pore solution are a sizable fraction of the resin capacity. The data in Figure 3 may be expressed by the relation

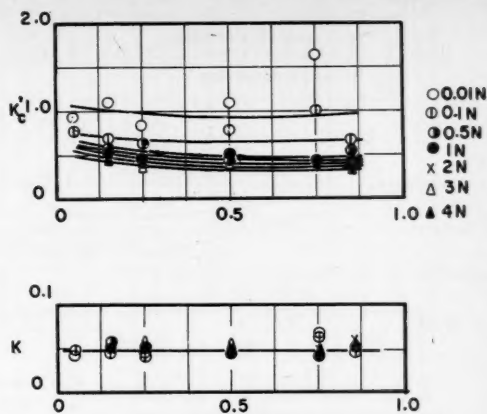
$$\log q_{Cl} = \log (0.198N)^{1.14} \quad (6)$$

Whitcome et al. (16) found similar relations for the chloride ion content of Dowex 50 in equilibrium with pure sodium and potassium chloride solutions.

The cation composition of the pore solution as indicated by the analysis of

the wash water used to elute the pore material is shown in Figure 4. Determination of the true composition of the pore solution is difficult, as the equilibrium between the resin and external solution is effectively a three-way equilibrium, involving the ions "attached" to the resin, the ions in the pore solution, and the ions in external solution. Replacement of the external solution with wash water disturbs this equilibrium and effectively brings the resin in contact with a very dilute solution. This in turn would tend to promote further take-up of copper from the pore solution by the resin. That this action does take place is possibly indicated by the data of Figure 4, which show that the copper-to-total-normality ratio is always less in the solution eluted from the pores than in the original equilibrium solution. Within the limits of experimental error for the very dilute solutions analyzed, the ratio of copper to sodium in the wash water was found to be independent of the total normality of the original equilibrium solution.

The water content of the resin (i.e., inside the resin pores) at equilibrium is shown in Figure 5 as a function of the external solution composition. The water content is higher for the copper form of the resin, and for a given total external solution normality the water content varies almost linearly with the resin composition. The water content decreases as the normality of the external solution increases. These results are in agreement with the trends found by other investigators (3, 8, 12), and the effect of solution concentration observed is to be expected from the Donnan equilibrium theory (6). The water content of the resin is a guide to the degree of swelling of the resin, and data on it are needed for thermodynamic analysis of the ion exchange process. In the present study the water-content data were used only for the computation of activity coefficients in the resin phase.



Eq. Cu/Eq.(Cu+Na) in Soln.

Fig. 6. Correlation of experimental data.

#### CORRELATION OF DATA AND USE IN DESIGN

Substitution of the experimental data into Equations (4) and (5) produces the results shown in Figure 6. A very good correlation of the data is obtained from Equation (4) (lower graph). The equilibrium constant  $K$  shows an average deviation of 8.5% and a maximum deviation of 15% from the average value of 0.047, except for four cases at high copper fractions (for the reason discussed below). The pore solution was included as part of the resin phase in computing  $K$ , as this inclusion was found to produce better constancy of  $K$ . Although  $K$  was found to vary as described above, use of Equation (4), taking the average value for  $K$ , would permit very accurate computation of equilibrium compositions, as this reverse calculation is relatively insensitive to small variations in  $K$ .

The selectivity coefficient  $K'_c$  exhibits a much greater variance than the equilibrium constant  $K$ .  $K'_c$  varies with the total solution normality and, to a lesser degree, with the copper-to-sodium ratio of the solution. Values of  $K'_c$  have an average deviation of 34% from the mean value of 0.59. The largest deviations are for the lowest normality solutions, and it may be noted that the  $K'_c$  values for these solutions show considerable scattering in the high copper region. This latter effect is caused by relatively small errors in observed copper content of the resin producing large percentage errors in the computed sodium content.  $K'_c$  is very sensitive to small changes in the value used for the sodium content of the resin, since this factor enters to the second power.

Equations intermediate to Equations (4) and (5) were also tested with the experimental data. Modification of Equation (5) by use of molalities rather than mole fractions in the resin phase actually provided a somewhat less satisfactory correlation than Equation (5). Correction

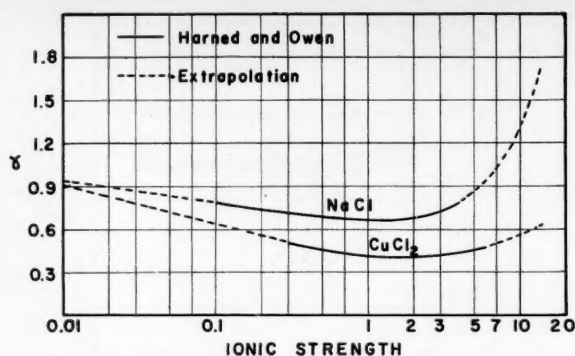


Fig. 7. Activity coefficients used in data correlation.

for both the water content of the resin (i.e., use of molalities in the resin phase) and activity coefficients in the external solution phase resulted in a small improvement over Equation (5).

Calculation of  $K$  requires activity-coefficient data for the resin and external phases. As discussed earlier, activity coefficients in the resin phase were taken as proportional to activity coefficients in an aqueous phase having the same solution strength (based on the water content of the resin) as the resin phase. Accordingly, only activity coefficients for aqueous solutions were needed. The activity coefficients for copper and sodium chloride are available in the literature (9) for ionic strengths up to 6.5 and 4 respectively. These data were extrapolated as shown in Figure 7. The extrapolation was performed on a linear coordinate plot, essentially by eye, and the upward curvature of the sodium chloride curve is accentuated by the transfer of the original extrapolation to the semilog plot used in Figure 7. Relatively little attempt was made to adjust the extrapolations at high solution strengths to provide optimum agreement of  $K$  values. Such adjustment, however, could be viewed as an empirical method for defining the activity coefficient values in the resin phase. It is of interest to note that the ionic strength in the resin phase is sometimes as high as 13.6, a concentration which would not exist in an aqueous solution at room temperature.

Although values of  $K_e'$  computed from the experimental data show considerable variation, use of Equation (5) with a value of 0.5 for  $K_e'$  is generally satisfactory for design purposes. Exchange isotherms using this relation are compared with experimental results in Figure 8. The equilibrium distribution of ions between the resin and the solution predicted by this equation has a maximum error of 10% for that ion which is present in the larger amount on the resin. To obtain better agreement with experimental data,  $K_e'$  of 0.6 for solutions with concentrations up to 0.5N and  $K_e'$  of 0.4 for higher solution concentrations may be used. If still more accuracy is desired, Equation (4) may be used, with the proper activity coefficient corrections.

However, this last procedure involves tedious trial and error.

For solution concentrations of 2N and higher, even simpler relations can be used to express the equilibrium for many cases. At high solution concentrations, the exchange isotherms are nearly linear, with an approximate slope of unity, as shown in Figures 1 and 2. The isotherms in Figure 1 may be approximated by the equation

$$\frac{q_{Cu}}{q_0} = \frac{N_{Cu}}{N_{total}} + B \quad (7)$$

$B$  is a constant for a particular solution normality, with the values 0.03, -0.02, and -0.05 for solution normalities of 2, 3, and 4 respectively. Equation (7) gives results with reasonable accuracy for  $N_{Cu}/N_{total}$  between 0.1 and 0.9.

#### NOTATION

- $A$  = activity of ion in resin phase
- $a$  = activity of ion in solution
- $B$  = constant in Equation (7)
- $f$  = activity coefficient of ion in resin phase
- $f^\circ$  = activity coefficient of ion in a solution whose ionic strength is the same as that in the resin phase
- $K$  = equilibrium constant defined by Equation (4)
- $K_e'$  = selectivity coefficient defined by Equation (5)
- $M$  = moles of ion per unit weight of dry hydrogen form of resin
- $N$  = normality of solution
- $q_{Cl}$  = equivalents of chloride ion per gram of dry hydrogen form of resin
- $q_{Cu}$  = equivalents of copper per gram of dry hydrogen form of resin
- $q_0$  = total exchange capacity, equivalent per gram of dry hydrogen form of resin (exclusive of cations in the pore solution)

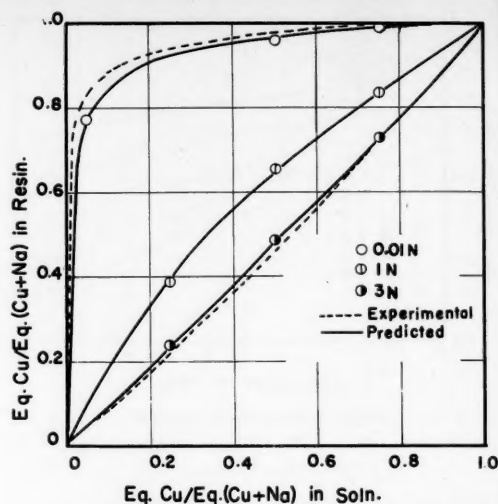


Fig. 8. Prediction of exchange isotherms from the selectivity coefficient.

- $X$  = molality of ion in resin
- $x$  = molality of ion in solution
- $\gamma$  = activity coefficient of ion or compound in solution

#### LITERATURE CITED

1. Bauman, W. C., and J. Eichhorn, *J. Am. Chem. Soc.*, **69**, 2830 (1947).
2. Bauman, W. C., J. R. Skidmore, and R. H. Osmun, *Ind. Eng. Chem.*, **40**, 1350 (1948).
3. Bonner, O. D., A. W. Davidson, and W. J. Argersinger, Jr., *J. Am. Chem. Soc.*, **74**, 1044 (1952).
4. David, M. M., and Harding Bliss, *Trans. Indian Inst. Chem. Eng.*, **5**, 1 (1952-53).
5. Gaines, G. L., and H. C. Thomas, *J. Chem. Phys.*, **21**, 714 (1953).
6. Gregor, H. P., *J. Am. Chem. Soc.*, **70**, 1293 (1948).
7. ———, O. R. Abolafia, and M. H. Gottlieb, *J. Phys. Chem.*, **58**, 984 (1954).
8. Gregor, H. P., Fradelle Guttoff, and J. I. Bregman, *J. Colloid Science*, **6**, 245 (1951).
9. Harned, H. S., and B. B. Owen, "The Physical Chemistry of Electrolytic Solutions," Reinhold Publishing Company, New York (1950).
10. Lewis, G. N., and Merle Randall, "Thermodynamics and Free Energy of Chemical Substances," McGraw-Hill Book Company, Inc., New York (1953).
11. Nayak, M. V., "A.I.I.S. Thesis," Indian Institute of Science, Bangalore (1954).
12. Pepper, K. W., D. Reichenberg, and D. K. Hale, *J. Chem. Soc.*, 3129 (1952).
13. Schubert, Jack, *Annual Rev. Phys. Chem.*, **5**, 413 (1954).
14. Selke, W. A., and Harding Bliss, *Chem. Eng. Progr.*, **47**, 529 (1951).
15. Subba Rao, H. C., M.S. thesis, Univ. Washington, Seattle (1956).
16. Whitcombe, J. A., J. T. Banchemo, and R. R. White, *Chem. Eng. Progr. Symposium Ser. No. 14*, **50**, 73 (1954).



# Vapor-liquid Equilibria of Benzene-*n*-hexane and Benzene-cyclohexane Systems

V. N. KUMARKRISHNA RAO, D. R. SWAMI, and M. NARASINGA RAO, Andhra University, Waltair, India

Vapor-liquid equilibria of two binary systems, benzene-*n*-hexane and benzene-cyclohexane, were measured at pressures from 4 to 18 atm. The three-constant Redlich-Kister equation was found satisfactory for correlation.

With the benzene-*n*-hexane system no azeotrope occurred; with the benzene-cyclohexane system an azeotrope appeared, and the mole fraction of cyclohexane in it diminished with increase in pressure. Lack of correction for fugacity in the vapor phase introduced a maximum error of 4% in activity coefficients at highest pressure.

Previously published data on these two systems have been restricted to measurements at atmospheric pressure and have conflicted as to the occurrence or absence of an azeotrope in the benzene-*n*-hexane system. Tonoberg and Johnston (11) reported vapor-liquid-equilibria data on the benzene-*n*-hexane system at atmospheric pressure and found no azeotrope; Other investigators (13, 5, 7, 6) reported the formation of an azeotrope. Griswold and Ludwig (2), in commenting on the data of Tonoberg and Johnston, stated that the azeotrope perhaps escaped detection because of the small temperature difference, 0.1°C., between the

normal boiling points of the azeotrope and *n*-hexane.

Vapor-liquid equilibria and thermodynamic properties of the benzene-cyclohexane system have been established by Scatchard, Wood, and Mochel (10) and by Wood and Austin (12), who attribute the highly irregular behavior of this system to the

large entropy of mixing. Richards and Hargreaves (9) established similar data on this system at atmospheric pressure and found the azeotrope composition to be 50.2 mole % benzene at a normal boiling point of 77.4°C. As the boiling points of the pure components are close together, a slight deviation from ideality readily produces a minimum boiling azeotrope (3).

#### APPARATUS AND EXPERIMENTAL PROCEDURE

The apparatus used for measuring vapor-liquid equilibria was a continuous liquid-recirculating still similar to that used by Griswold et al. (1), as shown in Figure 1. It consisted of a still, condenser *C*, reboiler leg *B*, condensate reservoir *CR*, and calibrated spring-loaded nonreturn valve *N* (Figure 2).

Temperature measurements were made with an iron-constantan thermocouple with its cold junction at the melting point of ice.

Temperatures recorded by the thermocouples, being slightly lower than the true values owing to heat losses along the thermocouple wires, were made by use of the following equation for the size of wire used:

$$t_0 = 0.000\,15686\,t^2 + 0.9996\,t + 0.856 \quad (1)$$

where  $t_0$  = true temperature and  $t'$  = observed temperature. Pressures were measured by a Bourdon gauge having a scale range of 0 to 600 lb./sq. in. and a dial 8 in. in diameter with divisions marked at 2 lb./sq. in. intervals. This gauge was calibrated periodically against a dead-weight gauge. A Doran potentiometer in conjunction with a multiflux-spot galvanometer was used to record potentials (Figure 3). Vapor-pressure-temperature relationships were measured for three pure compounds, benzene (b.p. 80.1°C.), cyclohexane (b.p. 80.7°C.), and methanol (b.p. 64.7°C.)

The three reagents, benzene, *n*-hexane, and cyclohexane, were obtained from the British Drug Houses.

## Benzene

### Analytical quality

Boiling point 80.1°C.

Density at 30°C., 0.8059 g./ml.

Density at 28°C., 0.8077 g./ml.

## N-Hexane

The *n*-hexane of laboratory quality was dried with anhydrous calcium chloride and fractionated in a glass column. The fraction collected between 67° and 69°C. was fractionated, and the final cut selected had a normal boiling point of 68.6°C. and density of 0.6228 g./ml. at 30°C.

V. N. Kumarkrishna Rao at present is with Caltax Oil Refining (Ltd.) India, Visakhapatnam, India, and D. R. Swami and M. Narasinga Rao are at Indian Institute of Technology, Kharagpur, India.

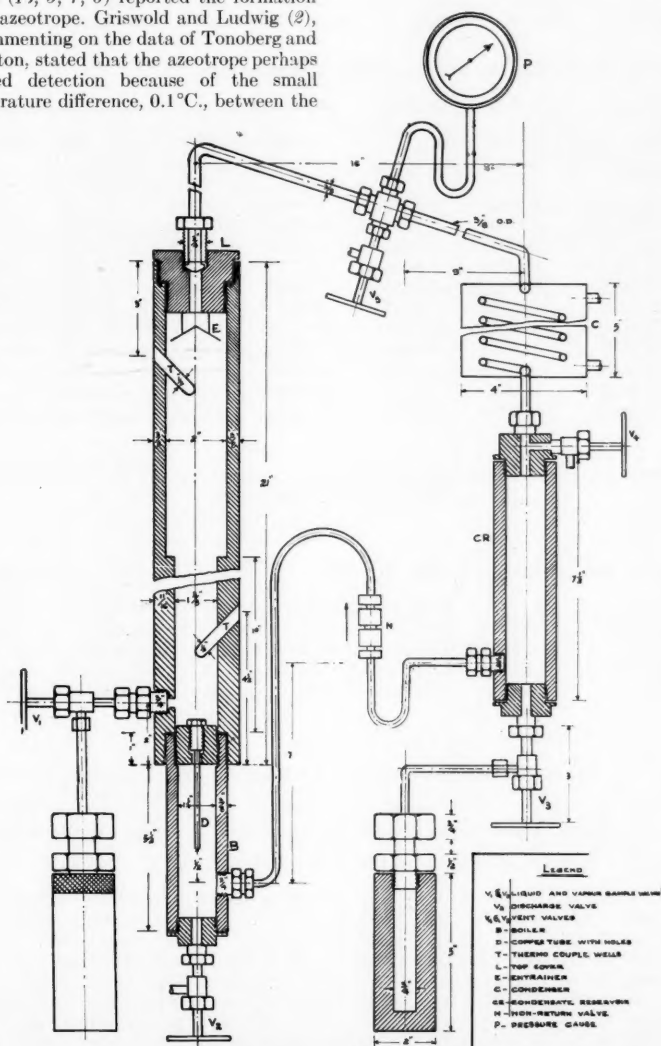


**Fig. 1. Continuous liquid-recirculating still.**

## Cyclohexane

Laboratory reagent quality  
Normal boiling point, 80.7°C.  
Density at 28°C., 0.7181 g./ml.

The vapor pressures of the three pure components were measured and plotted on large-scale graphs (18 by 28 in.) to facilitate accurate interpolation. Owing to the large differences in the densities of these components the compositions of each binary system could be established with accuracy from density measurements.

## CORRELATION OF EXPERIMENTAL DATA

Benzene-*n*-Hexane System

To establish with certainty the presence or absence of an azeotrope in the benzene-*n*-hexane system experiments were made at high pressures, where a possible azeotrope in the system would be more readily observed. Since the heat of vaporization of *n*-hexane is less than that of benzene, the *n*-hexane content of a possible azeotrope in this system would diminish with increased pressure; accordingly studies were made at pressures up to 10 atm.

TABLE 8. BENZENE-*n*-HEXANE SYSTEM; REDLICH-KISTER CORRELATIONS

$x_1$	58.8 lb./sq. in. abs.		88.6 lb./sq. in. abs.		117.6 lb./sq. in. abs.		147 lb./sq. in. abs.	
	$\log \gamma_1/\gamma_2$		$\log \gamma_1/\gamma_2$		$\log \gamma_1/\gamma_2$		$\log \gamma_1/\gamma_2$	
	Exp.	Calc.	Exp.	Calc.	Exp.	Calc.	Exp.	Calc.
0.0	0.141	0.132	0.111	0.125	0.101	0.119	0.079	0.107
0.1	0.104	0.100	0.083	0.090	0.076	0.085	0.059	0.074
0.2	0.071	0.070	0.055	0.058	0.052	0.054	0.041	0.046
0.3	0.041	0.040	0.031	0.031	0.036	0.028	0.022	0.022
0.4	0.014	0.013	0.007	0.007	0.006	0.005	0.003	0.002
0.5	-0.012	-0.012	-0.014	-0.014	-0.014	-0.014	-0.014	-0.014
0.6	-0.033	-0.034	-0.032	-0.031	-0.031	-0.030	-0.028	-0.027
0.7	-0.048	-0.043	-0.045	-0.045	-0.043	-0.043	-0.037	-0.037
0.8	-0.062	-0.068	-0.056	-0.057	-0.053	-0.052	-0.044	-0.044
0.9	-0.074	-0.078	-0.065	-0.064	-0.060	-0.059	-0.049	-0.048
1.0	-0.085	-0.084	-0.074	-0.071	-0.063	-0.063	-0.052	-0.051

TABLE 9. BENZENE-*n*-HEXANE SYSTEM, CORRELATION OF REDLICH-KISTER CONSTANTS WITH PRESSURE

$\pi$ , lb./sq. in. abs.	$B$		$C$		$D$	
	Exp.	Calc.	Exp.	Calc.	Exp.	Calc.
58.8	0.1131	0.1131	-0.024	-0.024	-0.0049	-0.0049
88.6	0.0958	0.0958	-0.027	-0.026	0.0021	-0.0023
117.6	0.0891	0.0815	-0.028	-0.028	0.0014	0.0014
147.0	0.0757	0.0692	-0.028	-0.030	0.0033	0.0070

TABLE 17. BENZENE-CYCLOHEXANE SYSTEM, REDLICH-KISTER CORRELATIONS

$x_1$	66.7 lb./sq. in. abs.		116.5 lb./sq. in. abs.		165.9 lb./sq. in. abs.		217 lb./sq. in. abs.		268.7 lb./sq. in. abs.	
	$\log (\gamma_1/\gamma_2)$		$\log (\gamma_1/\gamma_2)$		$\log (\gamma_1/\gamma_2)$		$\log (\gamma_1/\gamma_2)$		$\log (\gamma_1/\gamma_2)$	
	Exp.	Calc.	Exp.	Calc.	Exp.	Calc.	Exp.	Calc.	Exp.	Calc.
0.0	0.0780	0.0785	0.0560	0.0529	0.0400	0.0382	0.0360	0.0345	0.0337	0.0309
0.1	0.0720	0.0720	0.0517	0.0508	0.0365	0.0359	0.0326	0.0372	0.0314	0.0312
0.2	0.0650	0.0651	0.0450	0.0456	0.0314	0.0312	0.0282	0.0342	0.0273	0.0277
0.3	0.0560	0.0561	0.0362	0.0374	0.0240	0.0243	0.0225	0.0267	0.0210	0.0212
0.4	0.0430	0.0438	0.0255	0.0262	0.0160	0.0156	0.0140	0.0157	0.0126	0.0124
0.5	0.0265	0.0265	0.0120	0.0120	0.0052	0.0052	0.0030	0.0030	0.0024	0.0024
0.6	0.0027	0.0030	-0.0043	-0.0051	-0.0080	-0.0064	-0.0104	-0.0105	-0.0103	-0.0082
0.7	-0.0297	-0.0285	-0.0218	-0.0249	-0.0213	-0.0209	-0.0240	-0.0235	-0.0234	-0.0188
0.8	-0.0662	-0.0693	-0.0434	-0.0476	-0.0378	-0.0320	-0.0355	-0.0346	-0.0331	-0.0281
0.9	-0.1034	-0.1208	-0.0685	-0.0732	-0.0545	-0.0455	-0.0435	-0.0432	-0.0400	-0.0356
1.0	-0.1390	-0.1845	-0.0955	-0.1009	-0.0730	-0.0590	-0.0480	-0.0465	-0.0443	-0.0405

Activity coefficients in the liquid phase were calculated from the ratio  $\gamma_1 = y_1\pi/x_1P_1$ . No corrections were made for lack of ideality in the vapor phase. Vapor pressures of pure *n*-hexane and benzene are tabulated in Tables 1\* and 2\* and density-composition relations for the binary solutions in Table 3\*. In Tables 4 through 7\* experimental values of activity coefficients for the benzene-*n*-hexane system are tabulated. With the benzene-*n*-hexane system no azeotrope was found.

The experimental values of  $t$ ,  $y$  and  $\log \gamma$  are shown graphically in Figure 4 for a pressure of 58.8 lb./sq. in. abs. and the experimental  $y$ - $x$  data at all pressures are shown in Figure 5.

The experimental data on activity coefficients were correlated with the Van Laar equation and on activity-coefficient ratios by the Redlich-Kister (8) equation. The latter equation gave

TABLE 18. BENZENE-CYCLOHEXANE SYSTEM, CORRELATION OF REDLICH-KISTER CONSTANTS WITH PRESSURE

$\pi$ , lb./sq. in. abs.	$B$		$C$		$D$	
	Exp.	Calc.	Exp.	Calc.	Exp.	Calc.
66.7	0.1162	0.0934	0.0530	0.0493	0.0153	0.0143
116.5	0.0775	0.0778	0.0240	0.0240	-0.0006	0.0055
165.9	0.0518	0.0648	0.0104	0.0117	-0.0032	-0.0025
217.0	0.0537	0.0537	0.0060	0.0056	-0.0132	-0.0100
268.7	0.0441	0.0444	0.0048	0.0026	-0.0084	-0.0174

TABLE 19. BENZENE-CYCLOHEXANE SYSTEM  $x$ - $y$  CORRELATIONS

$x_1$	66.7 lb./sq. in. abs.		116.5 lb./sq. in. abs.		165.9 lb./sq. in. abs.		217 lb./sq. in. abs.		268.7 lb./sq. in. abs.	
	$y_1$	$y_1/y_2$	$y_1$	$y_1/y_2$	$y_1$	$y_1/y_2$	$y_1$	$y_1/y_2$	$y_1$	$y_1/y_2$
0.1	0.111	0.116	0.131	0.111	0.125	0.112	0.126	0.106	0.119	0.105
0.2	0.250	0.227	0.294	0.220	0.282	0.217	0.277	0.212	0.269	0.208
0.3	0.429	0.335	0.504	0.322	0.475	0.320	0.471	0.317	0.464	0.318
0.4	0.667	0.433	0.764	0.420	0.724	0.420	0.724	0.418	0.718	0.419
0.5	1.000	0.519	1.079	0.513	1.053	0.513	1.053	0.512	1.049	0.511
0.6	1.500	0.602	1.519	0.605	1.532	0.608	1.561	0.607	1.545	0.606
0.7	2.333	0.689	2.215	0.696	2.289	0.700	1.333	0.701	2.344	0.703
0.8	4.000	0.770	3.348	0.790	3.762	0.790	3.762	0.797	3.926	0.798
0.9	9.000	0.885	7.696	0.890	8.091	0.890	8.091	0.894	8.434	0.897

\*Tabular matter may be ordered as document 5214 from the American Institute of Documentation Auxiliary Publications, Photoduplication Service, Library of Congress, Washington 25, D. C., for \$2.50 for photoprints or \$1.75 for 35-mm. microfilm.

the better results. The three-constant Redlich-Kister equation (8) was found to be satisfactory, namely,

$$\log \frac{\gamma_1}{\gamma_2} = B(1 - 2x_1) + C[6x_1(1 - x_1) - 1] + D(1 - 2x_1)[1 - 8x_1(1 - x_1)] \quad (2)$$

The constants  $B$ ,  $C$ , and  $D$  were obtained from data taken at constant pressures with temperatures fixed by pressure and composition. Values of individual coefficients thus calculated at a given pressure differ slightly from those based upon constant temperature and pressure. These constants were evaluated at each pressure and correlated in terms of pressure by the following relations:

$$\log B = -0.00242\pi - 0.8043 \quad (3)$$

$$\log (-C) = 0.00114\pi - 1.6868 \quad (4)$$

$$\log (D + 0.01) = 0.00594\pi - 2.6416 \quad (5)$$

where  $\pi$  = total pressure, lb./sq. in. abs.

A comparison of experimental values of  $\gamma_1/\gamma_2$  with calculated values is given in Table 8 and Figure 6 for a pressure of 58.8 lb./sq. in. abs.

The experimental values of  $B$ ,  $C$ , and  $D$  are plotted in Figure 7 and a comparison of calculated with experimental values is tabulated in Table 9. At high concentrations of  $n$ -hexane the  $y$ - $x$  vapor-liquid lines nearly coincide with the  $y$ - $x$  line but this is not proof of azeotrope formation. The two lines must cross to establish such proof.

#### Benzene-cyclohexane System

The vapor pressures of pure cyclohexane are tabulated in Table 10\* and density-composition relationships for the benzene-cyclohexane system in Table 11\*.

Since the  $y$ - $x$  differences for this system are small, interpolations of the density-composition data were made by the following equation rather than from graphs.

$$x = 4.004 d^3 - 101.08 d^2 + 17.096 d \quad (6)$$

\*See footnote on page 192.

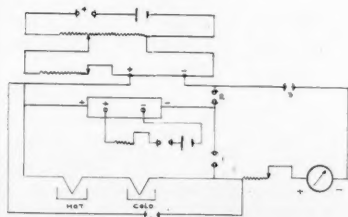


Fig. 3. Multiflux circuit.

where

$x$  = mole fraction of benzene  
 $d = d_m - d_c$

$d_m$  = density of mixture  
 $d_c$  = density of cyclohexane

Equilibrium data and activity coeffi-

TABLE 21. BENZENE-CYCLOHEXANE SYSTEM, CORRELATION AND PREDICTION OF AZEOTROPIC DATA

$\pi$ , lb./ sq. in. abs.	$m$		$c$		$x_{1az}$		$t_{az}$ , °C.		$\sigma'$	$\sigma''$
	Exp.	Calc.	Exp.	Calc.	Exp.	Calc.	Exp.	Calc.	Devia- tion in $x_{1az}$	Devia- tion in $t_{az}$
14.7	—	—	—	—	0.505	0.522	77.3	74.8	3.4	3.2
66.7	0.8373	0.8496	0.0331	0.0248	0.615	0.594	137.1	140.6	3.0	2.6
116.5	0.9214	0.9122	0.0234	0.0234	0.665	0.649	165.7	168.0	2.4	1.4
165.9	0.9364	0.9372	0.0224	0.0220	0.700	0.691	185.5	186.2	1.3	0.4
217.0	0.9521	0.9511	0.0207	0.0206	0.730	0.725	201.7	200.5	0.7	0.6
268.7	0.9609	0.9597	0.0191	0.0191	0.755	0.763	215.7	212.3	1.0	1.1

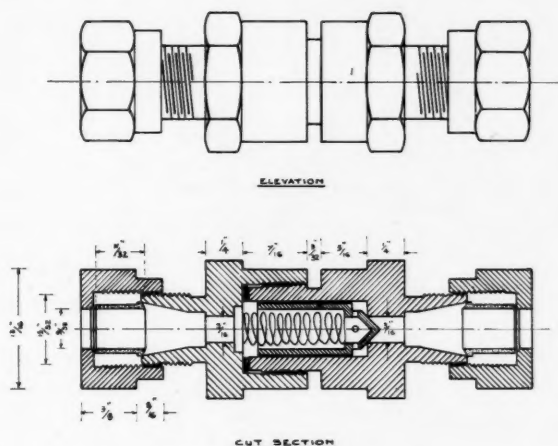


Fig. 2. Spring-loaded nonreturn valve N.

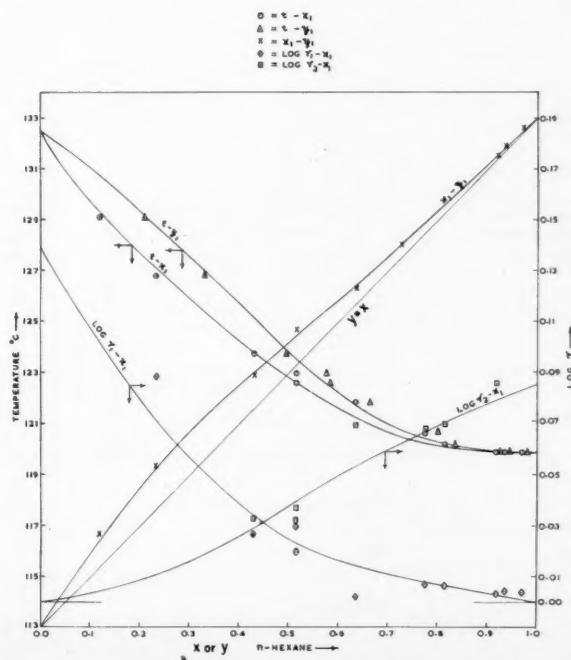


Fig. 4.  $\gamma$ ,  $t$ ,  $x$ ,  $y$  diagram at 58.8 lb./sq. in. abs., benzene- $n$ -hexane system.

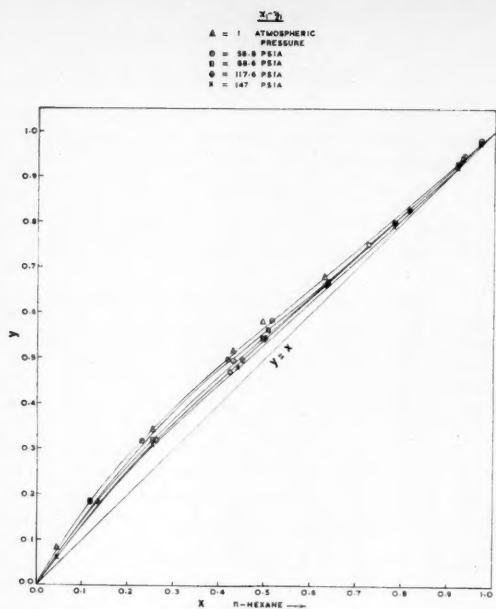


Fig. 5. Benzene-*n*-hexane system  $y$ - $x$  diagram at four pressures.

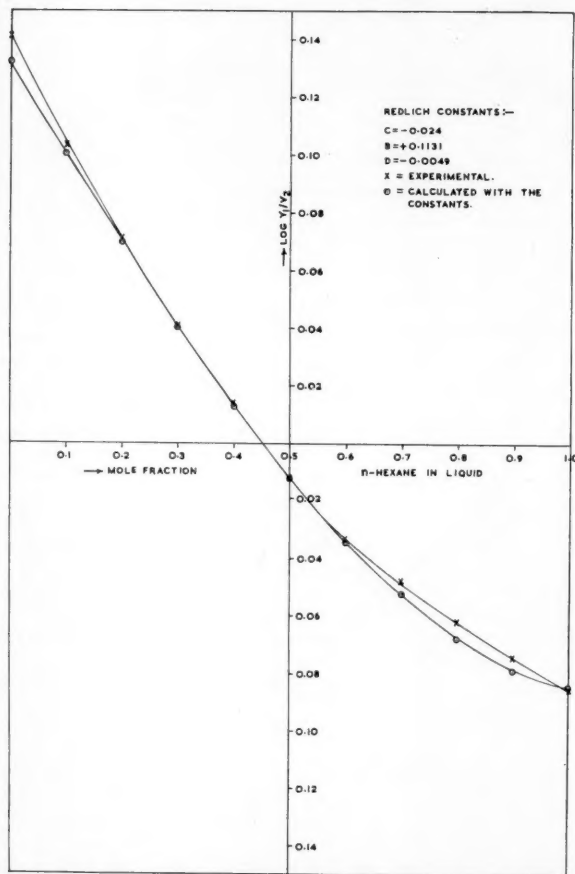


Fig. 6. Benzene-*n*-hexane system  $\log \gamma_1/\gamma_2$  vs.  $x$  at 58.8 lb./sq. in. abs.

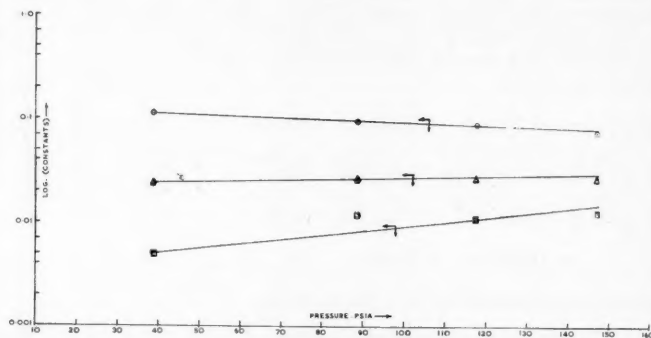


Fig. 7. Benzene-*n*-hexane Redlich-Kister constants vs. pressure.

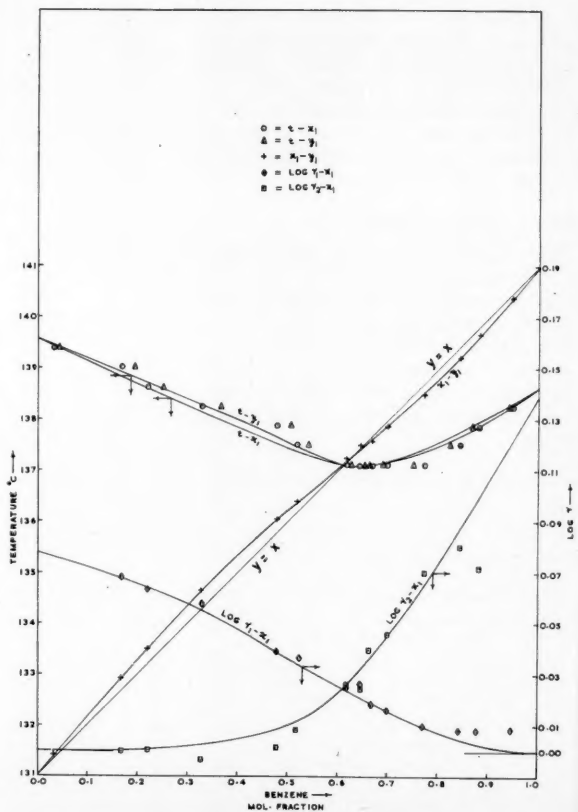


Fig. 8. Benzene-cyclohexane  $\gamma$ ,  $t$ ,  $x$ ,  $y$  at 66.7 lb./sq. in. abs.

coefficients are tabulated in Tables 12\* to 16\* for pressures of 66.7, 116.5, 165.9, 217, and 268.7 lb./sq. in. abs., respectively. Experimental data of  $t$ ,  $x$ ,  $y$ , and  $\log \gamma$  are shown in Figure 8 for a pressure of 66.7 lb./sq. in. abs. and the  $y$ - $x$  data at all pressures are shown in Figure 9. The shift of the azeotrope composition with temperature is shown as the dotted straight line in Figure 10.

The activity coefficients of this system were correlated with the three-constant

\*See footnote on page 192.

○ CONSTANT B  
△ CONSTANT (C)  
□ CONSTANT (D+D₂)

Redlich  
the co  
being

$\log B$

$\log C$

$\log (L$

Exp

$\log \gamma_1$

shown

pressu

pariso

$B$ ,  $C$ ,

tabula

The

the b

with

equat

where

$x_{az} =$

$t_{az} =$

Simpli

For

these

in m

$x_1/x_2$

Hirat

cyclo

A st

press

benz

66.7

On u

a 45

to t

given

secti

C

comp

Equ

The

with

give

A



Redlich-Kister equation, the values of the constants as a function of pressure being related as follows:

$$\log B = -0.0016\pi - 0.9228 \quad (7)$$

$$\log C = -0.0063\pi - 0.8866 \quad (8)$$

$$\log (D + 0.1) = -0.0007\pi - 0.8948 \quad (9)$$

Experimental and calculated values of  $\log \gamma_1/\gamma_2$  are tabulated in Table 17 and shown graphically in Figure 11 for a pressure of 66.7 lb./sq. in. abs. A comparison of calculated values of constants  $B$ ,  $C$ , and  $D$  with experimental values is tabulated in Table 18.

The composition of the azeotrope in the benzene-cyclohexane system shifted with temperature according to the equation

$$t_{az} = 581.1x_{az} - 220.7 \quad (10)$$

where

$x_{az}$  = mole fraction of benzene in the azeotrope

$t_{az}$  = temperature of the azeotrope, °C.

#### Simplified Presentation of $y$ - $x$ data

For simplicity in use the  $y$ - $x$  data for these two binary systems were presented in modified form by plotting  $y_1/y_2$  vs.  $x_1/x_2$  on log-log scales as suggested by Hirata (4). The values for benzene-cyclohexane are tabulated in Table 19. A straight line was obtained for each pressure as shown in Figure 13 for benzene-cyclohexane at a pressure of 66.7 lb./sq. in. abs.; thus

$$\log \frac{y_1}{y_2} = m \log \frac{x_1}{x_2} + c \quad (11)$$

On uniform log scales each line intersects a 45-deg. line at a point corresponding to the azeotropic composition at the given pressure. At this point of intersection

$$\log \frac{x_{1az}}{x_{2az}} = \frac{c}{1 - m} \quad (12)$$

Comparison of experimental azeotropic compositions with those obtained by Equation (12) are tabulated in Table 20. The constants  $m$  and  $c$  were correlated with pressure as shown in Figure 14 to give the following:

TABLE 20.  
AZEOTROPE COMPOSITIONS FOR THE  
BENZENE-CYCLOHEXANE SYSTEM

$\pi$ lb./sq. in. abs.	$x_{1az}$ Exp.	$x_{1az}$ Calc.
66.7	0.615	0.615
116.5	0.665	0.665
165.9	0.700	0.692
217.0	0.730	0.726
268.7	0.755	0.755

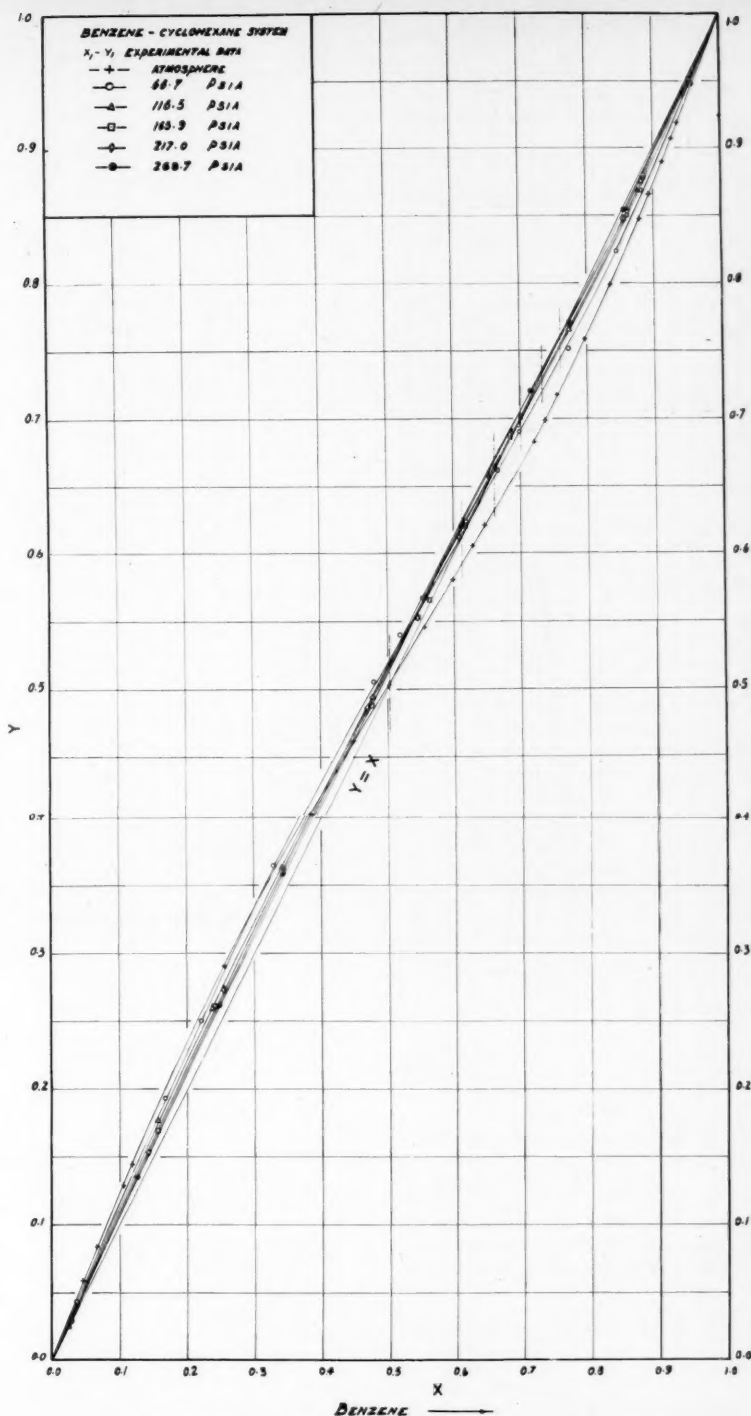


Fig. 9. Benzene-cyclohexane  $y$ - $x$  diagram for five pressures.

$$m = \frac{9.7727}{\pi} + 0.9961 \quad (13)$$

$$c = -2.825(10^{-5})\pi + 0.0267 \quad (14)$$

#### Correlation of Azeotrope Data

The relation between the temperature and pressure of the azeotrope in the

benzene-cyclohexane system is shown in Figure 15 and expressed by the equation

$$\log T = 2.4074 + 0.1147 \log \pi \quad (15)$$

where

$T$  = boiling point of azeotrope in °K.

$\pi$  = pressure, lb./sq. in. abs.

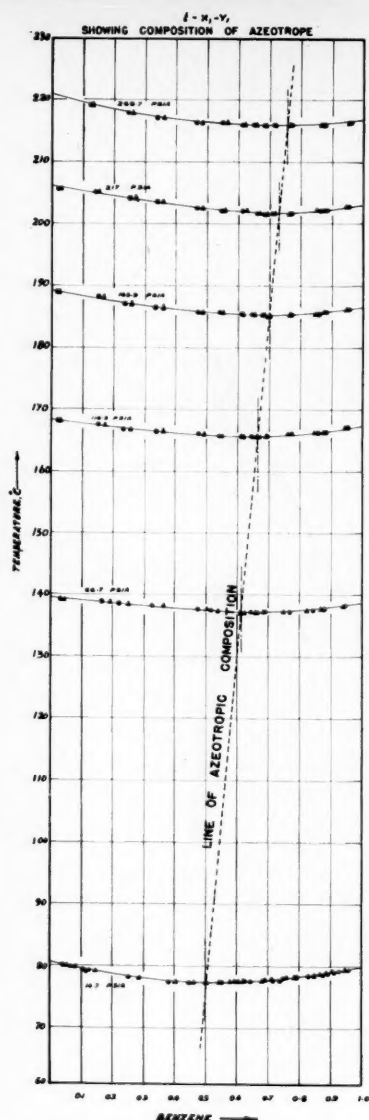


Fig. 10. Benzene-cyclohexane  $t$ ,  $x$ ,  $p$  for azeotrope.

At any pressure  $\pi$  the composition of the azeotrope may be derived from Equations (12), (13), and (14) to give

$$x_{1az} = \frac{1}{1 + 10^k} \quad (16)$$

where

$$k = 0.00724\pi \left[ \frac{\pi - 945.1}{\pi + 2505.8} \right] \quad (17)$$

The azeotropic temperature at the same pressure may also be calculated from Equation (15). A comparison of experimental with calculated values of  $x_{1az}$  and  $t_{az}$  are tabulated in Table 21.

#### SUMMARY AND CONCLUSIONS

Vapor-liquid equilibria data are reported on the two binary systems

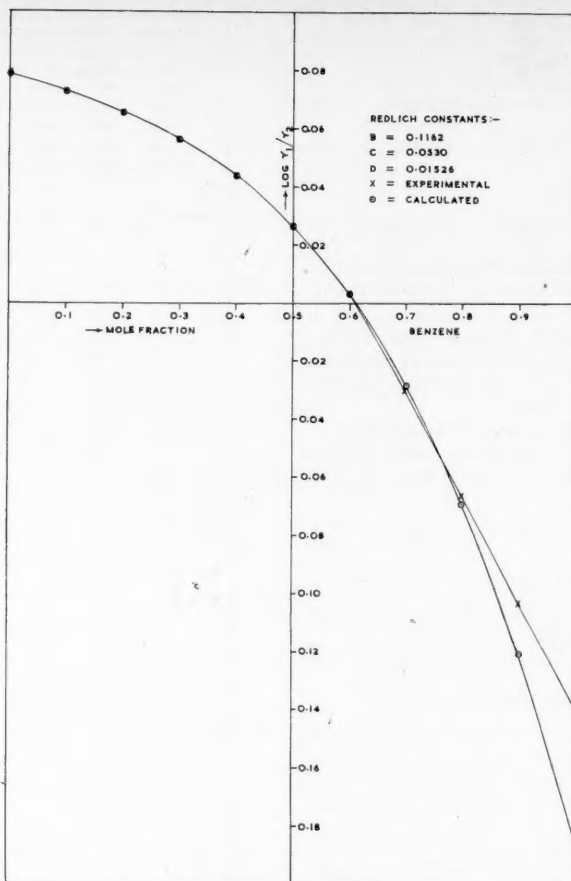


Fig. 11. Benzene-cyclohexane  $\log \gamma_1/\gamma_2$  vs.  $x$  at 66.7 lb./sq. in. abs.

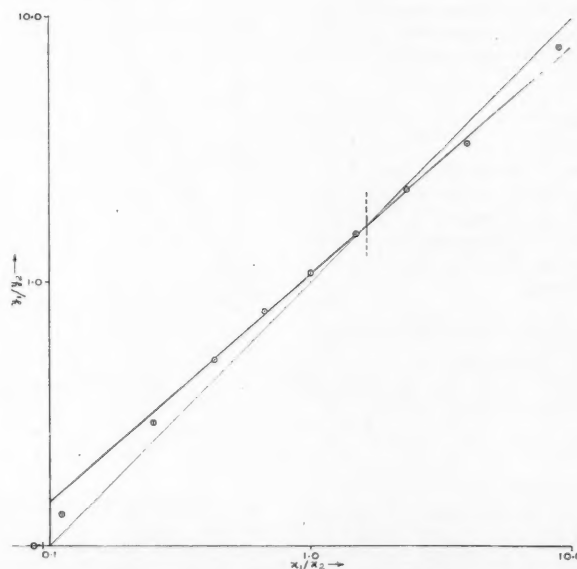


Fig. 12. Benzene-cyclohexane Redlich-Kister constants vs. pressure.

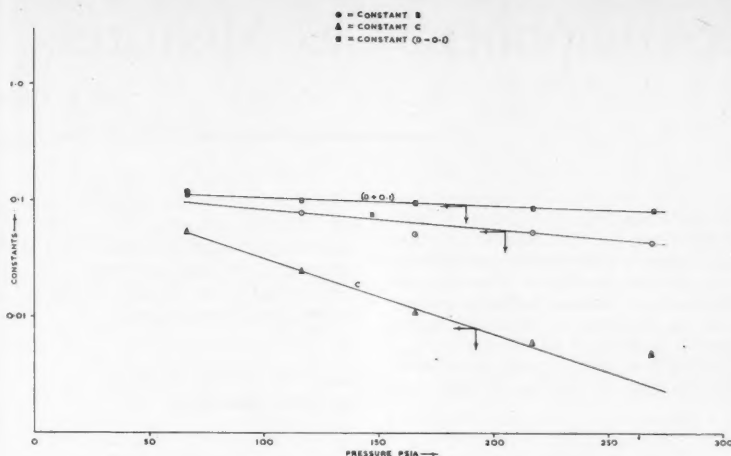


Fig. 13. Benzene-cyclohexane  $\log y_1/y_2$  vs.  $\log x_1/x_2$  at 66.7 lb./sq. in. abs.

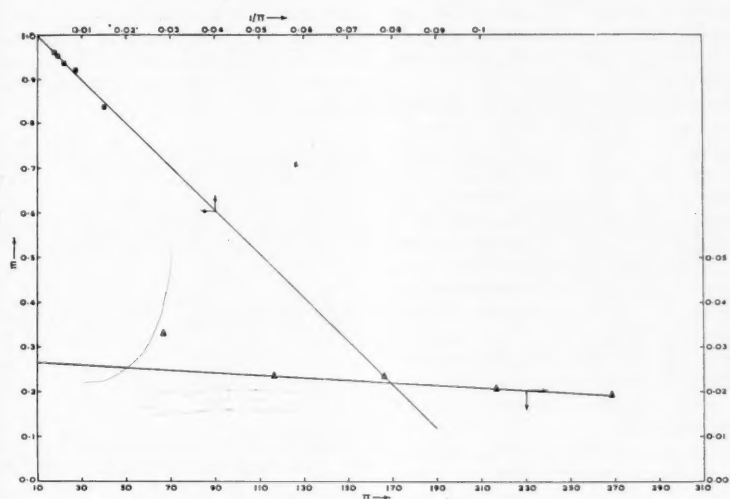


Fig. 14 Benzene-cyclohexane  $m$  and  $c$  vs. pressure.

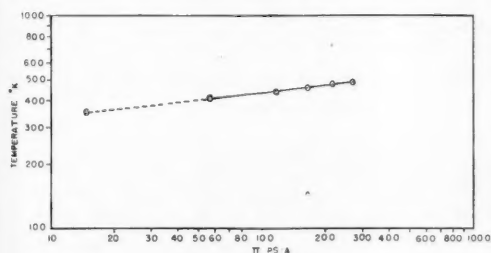


Fig. 15. Effect of pressure upon temperature of azeotrope of benzene-cyclohexane.

benzene-*n*-hexane and benzene-cyclohexane for the pressure range from 4 to 18 atm. Lack of correction for the fugacities in the vapor phase introduces a maximum error of 4% in activity coefficients. The three-constant Redlich-Kister equation satisfactorily represents the ratio of activity coefficients of both binary systems:

$$\log \frac{\gamma_1}{\gamma_2} = B(1 - x_1) + C[6x_1(1 - x_1) - 1] + D(1 - 2x_1)[1 - 8x_1(1 - x_1)]$$

With the benzene-*n*-hexane system no azeotrope was found. The values of  $B$ ,  $C$ , and  $D$  are reported as functions of pressure by the following:

For benzene-*n*-hexane

$$\begin{aligned} \log B &= -0.00242\pi - 0.8043 \\ \log (-C) &= 0.00114\pi - 1.6868 \\ \log (D + 0.01) &= 0.00594\pi - 2.6416 \end{aligned}$$

For benzene-cyclohexane

$$\begin{aligned} \log B &= -0.0016\pi - 0.9228 \\ \log C &= -0.0063\pi - 0.8866 \\ \log (D + 0.01) &= -0.0007\pi - 0.8948 \end{aligned}$$

For the benzene-cyclohexane system empirical correlations are given for the change of the azeotrope composition with temperature and pressure.

A simple modified method is given for representing the  $y$ - $x$  data of these two binary systems.

#### ACKNOWLEDGMENTS

The authors wish to express their grateful thanks to Professor O. A. Hougen for taking a continuing interest in and providing the necessary background for this work.

#### NOTATION

- $B, C, D$  = constants of the Redlich-Kister equation  
 $c$  = empirical constant  
 $m$  = empirical constant  
 $P_1, P_2$  = vapor pressures of the pure components 1 and 2, lb./sq. in. abs.  
 $t_0$  = true temperature, °C.  
 $t$  = temperature recorded by the thermocouple, °C.  
 $x_1, x_2$  = mole fraction of components 1 and 2 in the liquid phase  
 $y_1, y_2$  = mole fractions of components 1 and 2 in the vapor phase  
 $\gamma$  = activity coefficient  
 $\pi$  = total pressure, lb./sq. in. abs.

#### LITERATURE CITED

- Griswold, J., D. Andres, and V. A. Klein, *Trans. Am. Inst. Chem. Engrs.*, **39**, 223 (1943).
- Griswold, J., and E. E. Ludwig, *Ind. Eng. Chem.*, **35**, 117 (1943).
- Hildebrand, J. H., "Solubility of Non-electrolytes," Reinhold Publishing corporation, New York (1948).
- Hirata, M., *Ind. Eng. Chem.*, **45**, 1815 (1953); *Chem. Eng. (Japan)*, **13**, 138 (1949).
- Jackson, D. M., et al., *ibid.*, **73**, 922 (1898).
- Lecat, M., *Ann. Soc. Sci. Bruxelles.*, **63**, 58 (1949).
- Marshner, R. F., and W. P. Cropper, *Ind. Eng. Chem.*, **38**, 262 (1946).
- Redlich, Otto, and A. T. Kister, *ibid.*, **40**, 345 (1948).
- Richards, A. R., and E. Hargreaves, *ibid.*, **36**, 805 (1944).
- Scatchard, G., S. E. Wood, and J. M. Mochel, *J. Phys. Chem.*, **43**, 119 (1939).
- Tonoberg, C. O., and F. Johnston, *Ind. Eng. Chem.*, **25**, 733 (1933).
- Wood, S. E., and A. F. Austin, *J. Am. Chem. Soc.*, **67**, 480 (1945).
- Young, S., et al., *J. Chem. Soc.*, **83**, 45, 68, 77, (1903).

# Diffusion in Three-component Gas Mixtures

H. L. TOOR

Carnegie Institute of Technology, Pittsburgh, Pennsylvania

A solution to the Stefan-Maxwell diffusion equations for equimolar countercurrent diffusion in a three-component gas mixture is obtained which is similar in form to Gilliland's equation for diffusion of two gases through a third inert gas. The important features of both types of diffusion are investigated and the conditions under which the following phenomena occur are determined: (1) diffusion barrier (the rate of diffusion of a component is zero even though its concentration gradient is not zero); (2) osmotic diffusion (the rate of diffusion of a component is not zero even though its concentration gradient is zero); (3) reverse diffusion (a component diffuses against the gradient of its concentration).

A generalized driving force which describes these phenomena is introduced, and approximate equations are developed which give the individual rates of diffusion directly.

## PART I

Almost all the theories of mass transfer are based to some extent on molecular diffusion (5, 6, 18). Although binary-diffusion theory is well understood, the theory for multicomponent diffusion is less satisfactory, even though the basic diffusion equations have long been available. This paper will be restricted to the study of steady state diffusion in the simplest multicomponent gas, the ternary.

The equations for diffusion in ideal multicomponent gases were developed by Stefan (16, 17) and Maxwell (11, 12). For ideal binary gas mixtures the more rigorous Chapman-Enskog (2) equations can be shown to reduce to the Maxwell equations when the temperature and total pressure are constant. Similarly, under the same conditions the Curtiss-Hirschfelder (4) extension of the Chapman-Enskog equations can be shown to reduce to the Maxwell-Stefan equations for ideal multicomponent gas mixtures. The predictions of the Maxwell equations for three-component mixtures have been shown to be in good accord with experiment for various types of diffusion (7, 10).

For the general  $n$ -component system there are  $n$  Maxwell equations of the form

$$-\frac{P}{RT} \frac{dy_A}{dx} = \frac{N_A y_B - N_B y_A}{D_{AB}} + \frac{N_A y_C - N_C y_A}{D_{AC}} + \dots \quad (1)$$

When the total pressure is constant, as assumed in the equation, the number of equations is reduced to  $n - 1$ . For steady state diffusion in the  $x$  direction only, these  $n - 1$  differential equations can be solved to give  $n - 1$  algebraic equations relating the rates of diffusion of the  $n$  different molecular species. Therefore the resulting equations will be indeterminate, and one more restriction is necessary to make the system determinate. This restriction is obtained by fixing the rate of diffusion of any one of the components or by relating any two or more of the diffusion rates.

For a binary system the two simplest and most useful special cases of these

general restrictions are the stagnant-gas case and the equimolar countercurrent diffusion case. The former sets the rate of diffusion of one component equal to zero by placing a barrier to the transfer of this component (which will be called an absorption barrier), and the latter usually sets the total net rate equal to zero by an energy balance.

These two restricted types of diffusion appear to be of most utility in multicomponent systems as well as in binary systems. The case of one stagnant gas corresponds to absorption in which one component of the mixture is insoluble in the liquid phase, and equimolar countercurrent diffusion (hereafter referred to as *equimolar diffusion*) corresponds to distillation of a multicomponent mixture. Equimolar diffusion is closely approximated (14) when the distillation column is adiabatic, molar heats of vaporization are approximately the same for all components, etc.

Gilliland (15) solved the diffusion equations for a ternary system by setting the rate of diffusion of one of the components equal to zero, and Hoopes (10) solved the same equation with the rates of transfer unrestricted. Hoopes also presented a solution for the case of equimolar diffusion. Solutions for other special cases of ternary diffusion have been obtained by Benedict and Boas (1) and Cichelli, Weatherford, and Bowman (3).

The integrated equations, even for a three-component system, are highly complex and numerical results usually can be calculated from the equations only by trial-and-error. In addition, the physical significance of the equations is not at all apparent. Wilke (19) has developed approximate methods of solving Maxwell's equations, but his method necessitates a trial-and-error solution and consequently does not bring out the important features of the diffusion process.

This paper will be concerned with the two types of diffusion in three-component gas mixtures: diffusion of two gases through a third stagnant gas and equimolar diffusion. The object is to deter-

mine the important characteristics of the diffusion process and to develop approximate equations which will show these characteristics and still retain, as far as possible, the familiar forms of the binary-diffusion equations.

## SOLUTIONS OF THE MAXWELL DIFFUSION EQUATIONS

It is simplest and most informative to obtain directly the desired solution for equimolar diffusion.

For a three-component system Equation (1) can be written for each component, and since the summation of the mole fractions is 1, the equation for component C can be eliminated. At a constant total pressure  $D_{ij} = D_{ji}$  and the equations become

$$-\frac{P}{RT} \frac{dy_A}{dx} = -\left(\frac{N_B}{D_{AB}} + \frac{N_A + N_C}{D_{AC}}\right)y_A + \left(\frac{1}{D_{AB}} - \frac{1}{D_{AC}}\right)N_A y_B + \frac{N_A}{D_{AC}} \quad (2)$$

$$-\frac{P}{RT} \frac{dy_B}{dx} = -\left(\frac{N_A}{D_{AB}} + \frac{N_B + N_C}{D_{BC}}\right)y_B + \left(\frac{1}{D_{AB}} - \frac{1}{D_{BC}}\right)N_B y_A + \frac{N_B}{D_{BC}} \quad (3)$$

Since  $D_{ij}P$  is independent of  $P$  it can be seen that the diffusion rates are independent of the total pressure and proportional to  $1/RTx$ , where  $x$  is the length of the diffusion path. This is also true for an  $n$ -component mixture.

For equimolar diffusion

$$N = N_A + N_B + N_C = 0 \quad (4)$$

and with this restriction Equations (2) and (3) reduce to

$$-\frac{P}{RT} \frac{dy_A}{dx} = -\left(\frac{1}{D_{AB}} - \frac{1}{D_{AC}}\right)N_B y_A + \left(\frac{1}{D_{AB}} - \frac{1}{D_{AC}}\right)N_A y_B + \frac{N_A}{D_{AC}} \quad (5)$$

$$-\frac{P}{RT} \frac{dy_B}{dx} = -\left(\frac{1}{D_{AB}} - \frac{1}{D_{BC}}\right)N_A y_B + \left(\frac{1}{D_{AB}} - \frac{1}{D_{BC}}\right)N_B y_A + \frac{N_B}{D_{BC}} \quad (6)$$

Part of the solution to these equations may be obtained directly by first multiplying both sides of Equation (5) by  $(1/D_{AB}) - (1/D_{BC})$ , both sides of Equations (6) by  $(1/D_{AB}) - (1/D_{AC})$ , and



then adding the resulting equations:

$$-\frac{P}{RT} \left[ \left( \frac{1}{D_{AB}} - \frac{1}{D_{BC}} \right) \frac{dy_A}{dx} + \left( \frac{1}{D_{AB}} - \frac{1}{D_{AC}} \right) \frac{dy_B}{dx} \right] = \left( \frac{1}{D_{AB}} - \frac{1}{D_{BC}} \right) \frac{N_A}{D_{AC}} + \left( \frac{1}{D_{AB}} - \frac{1}{D_{AC}} \right) \frac{N_B}{D_{BC}} \quad (7)$$

This may be integrated in terms of the variable

$$\left( \frac{1}{D_{AB}} - \frac{1}{D_{BC}} \right) y_A + \left( \frac{1}{D_{AB}} - \frac{1}{D_{AC}} \right) y_B$$

from  $x = 0$  where  $y_A = y_{A_1}$  and  $y_B = y_{B_1}$  to  $x = x$  where  $y_A = y_{A_2}$  and  $y_B = y_{B_2}$  (8)

to give

$$\frac{1}{D_{AC}} \left( \frac{1}{D_{AB}} - \frac{1}{D_{BC}} \right) N_A + \frac{1}{D_{BC}} \left( \frac{1}{D_{AB}} - \frac{1}{D_{AC}} \right) N_B = \frac{P}{RTx} \left[ \left( \frac{1}{D_{AB}} - \frac{1}{D_{BC}} \right) (y_{A_1} - y_{A_2}) + \left( \frac{1}{D_{AB}} - \frac{1}{D_{AC}} \right) (y_{B_1} - y_{B_2}) \right] \quad (9)$$

The second part of the solution may be obtained by use of the Laplace Transform. (13), and the result is

$$\left( \frac{1}{D_{AB}} - \frac{1}{D_{BC}} \right) N_A + \left( \frac{1}{D_{AB}} - \frac{1}{D_{AC}} \right) N_B = \frac{P}{RTx} \ln \left[ \frac{\frac{y_{A_2} - y_{B_2}}{N_A - N_B} - \frac{\frac{1}{D_{AC}} - \frac{1}{D_{BC}}}{\left( \frac{1}{D_{AB}} - \frac{1}{D_{BC}} \right) N_A + \left( \frac{1}{D_{AB}} - \frac{1}{D_{AC}} \right) N_B}}{\frac{y_{A_1} - y_{B_1}}{N_A - N_B} - \frac{\frac{1}{D_{AC}} - \frac{1}{D_{BC}}}{\left( \frac{1}{D_{AB}} - \frac{1}{D_{BC}} \right) N_A + \left( \frac{1}{D_{AB}} - \frac{1}{D_{AC}} \right) N_B}} \right] \quad (10)$$

Equations (9) and (10) together satisfy Equations (5) and (6) as well as the boundary conditions (8), and  $N_A$  and  $N_B$  may be obtained from them by trial and error;  $N_C$  is then fixed by Equation (4).

The parametric solution to the ternary-diffusion problem obtained by Gilliland (15) when one gas is stagnant ( $N_C = 0$ ) is given below:

$$\frac{N_A}{D_{AC}} + \frac{N_B}{D_{BC}} = \frac{P}{RTx} \ln \frac{y_{C_2}}{y_{C_1}} \quad (11)$$

If  $y_A$  and  $y_B$  are assumed small, Equations (2) and (3) may be integrated separately:

$$N_A = \frac{D_{AC}P}{RTx} (y_{A_1} - y_{A_2}) \quad (13)$$

$$N_B = \frac{D_{BC}P}{RTx} (y_{B_1} - y_{B_2}) \quad (14)$$

Although these are the equations for binary equimolal diffusion, as well as the limiting forms for diffusion of one dilute gas through a second stagnant gas, Equation (13) applies to a system consisting of A and C, and Equation (14) applies to a system consisting of B and C. Thus, when gases A and B are dilute they diffuse through the third gas with no interaction among themselves.

The differences in mole fraction in these equations can be conveniently considered to be the driving forces for diffusion in binary systems, and with this picture the first terms on the right of the equations may be considered to be reciprocal resistances. Since mole fraction is proportional to concentration in ideal gases, this is the same as considering a concentration difference to be the driving force.

#### DIFFUSION BARRIER

##### Equimolal Diffusion

If  $N_C$  is set equal to zero,  $N_A + N_B = 0$  from Equation (4), and the equimolal

However, they also yield the additional equation

$$\left( 1 - \frac{D_{AB}}{D_{BC}} \right) (y_{A_1} - y_{A_2}) + \left( 1 - \frac{D_{AB}}{D_{AC}} \right) (y_{B_1} - y_{B_2}) = \ln \frac{y_{C_2}}{y_{C_1}} \quad (16)$$

This indicates, as expected, that  $N_C$  could not be arbitrarily set equal to zero, as all the degrees of freedom were removed by fixing  $N = 0$ . Thus Equation (15) gives the rate of transfer of components A and B when  $N_C = 0$  but  $N_C = 0$  only when the mole fractions are related in such a way that they satisfy Equation (16). This result throws light on Gilliland's solution to the ternary diffusion problem where  $N_C$  is fixed equal to zero. As pointed out by Wilke (19), Equations (11) and (12) are always satisfied by  $N_A + N_B = 0$  and there are usually at least two solutions to the equations. Consequently, as  $N_A$  approaches  $N_B$ , it becomes more and more difficult to determine the correct solution. This difficulty occurs because when  $N_A + N_B = 0$ , Gilliland's equation is a special case of equimolal diffusion.

Although the same physical situation is described regardless of the order in which the limit  $N_A + N_B = N_C = 0$  is approached, Gilliland's solution in the limit gives Equation (15), but it fails to give Equation (16). It can be shown by substituting  $N_A + N_B = N_C = 0$  into the original differential equations, (2) and (3), that Equations (15) and (16) are the correct solutions for this situation. Therefore, when  $N_C$  is fixed equal to zero, by a solubility barrier, for example, equimolal diffusion of the remaining two components occurs when Equation (16) is satisfied and the rate is given by Equation (15). Equation (16) thus complements Gilliland's solution. When it is not satisfied, the solution  $N_A + N_B = 0$  is a fictitious one.

When  $N$  is set equal to zero, by an energy balance, for example, then when Equation (16) is satisfied  $N_C$  goes to zero and Equation (15) gives the rate of diffusion of the other two components. The interesting result is that if component C is not in equilibrium its rate of diffusion, even if there is no apparent barrier to its transfer, will be zero if the com-

$$N_A + N_B = \frac{D_{AB}P}{RTx} \ln \left[ \frac{\frac{N_A + N_B}{N_A} y_{A_2} - \frac{\frac{1}{D_{AB}} - \frac{1}{D_{AC}}}{\frac{1}{D_{AB}} - \frac{1}{D_{BC}}} \frac{N_A + N_B}{N_B} y_{B_2} - \frac{\frac{1}{D_{AB}} - \frac{1}{D_{BC}}}{\frac{1}{D_{AB}} - \frac{1}{D_{AC}}}}{\frac{N_A + N_B}{N_A} y_{A_1} - \frac{\frac{1}{D_{AB}} - \frac{1}{D_{AC}}}{\frac{1}{D_{AB}} - \frac{1}{D_{BC}}} \frac{N_A + N_B}{N_B} y_{B_1} - \frac{\frac{1}{D_{AB}} - \frac{1}{D_{BC}}}{\frac{1}{D_{AB}} - \frac{1}{D_{AC}}}} \right] \quad (12)$$

ponents are distributed so that Equation (16) is satisfied.

(The concept of equilibrium is being used in a restricted sense to indicate the condition when  $y_{i_1} = y_{i_2}$ ; i.e., the ordinary binary driving force is zero. This is really a pseudoequilibrium for each component.) Using the ordinary concept of diffusion in a binary gas, one might say the resistance of the gas to the transfer of component  $C$  is infinite, and this condition will be defined as a *diffusion barrier* to differentiate it from the *solubility barrier*, which exists in gas absorption.

The physical situation is clarified if one considers the theoretical situation in which the two independent restrictions,  $N_C = 0$  and  $N_A + N_B = 0$ , are simultaneously placed in the system. Maxwell's equations then yield Equations (15) and (16); the first equation gives the rates of diffusion and the second describes the manner in which the gases arrange themselves. If either of the original restrictions is placed separately on the system, the preceding situation is reproduced identically if a second restriction is that the compositions must satisfy Equation (16).

When  $D_{AC} = D_{BC}$  it can be shown that the only physically possible solution to Equation (16) is  $y_{C_1} = y_{C_2}$ , and so Equation (15) does not go to infinity, but becomes indeterminate under this restriction. The rates of diffusion of  $A$  and  $B$  under these conditions are shown below to be given by Equations (43) and (44).

Figure (1) shows some concentration relationships which cause diffusion barriers in the system  $H_2$ ,  $H_2O$ , and  $CO_2$ . These curves were determined from Equation (16) by use of binary diffusion coefficients from Table 1. The curves are

TABLE 1.

BINARY-DIFFUSION COEFFICIENTS

(sq. cm./sec.)

$i = CO_2$	$D_{ij} = 0.9220$
$j = H_2O$	$D_{jk} = 2.7064$
$k = H_2$	$D_{ik} = 3.4576$

Approximate values at 40°C. and 155 mm. Hg. from Wilke (19).

independent of the total pressure. All the subsequent calculations are based on these same diffusion coefficients. Equation (16), which gives the conditions for  $N_C = 0$ , was applied to each of the components in turn. Two of the four independent variables were removed by setting the mole fraction of one of the diffusing gases equal to zero at point 1 and setting the mole fraction of the other diffusing gas equal to zero at point 2. This allows the compositions at points 1 and 2 to be given by one point on a curve and also shows the greatest effect of the diffusion barrier.

A point on any of the curves gives the compositions of that component at the terminal points when that component is stopped from diffusing by a diffusion barrier. The 45-deg. line indicates the absence of a diffusion barrier, for this line corresponds to no diffusion when  $y_{C_1} = y_{C_2}$ . The difference between any of the curves and the 45-deg. line therefore gives the driving force,  $y_{C_1} - y_{C_2}$ , for the component which is not diffusing. This difference can be considered in a sense as the strength of the diffusion barrier. The curves show that the maximum strength of the diffusion barrier for hydrogen, the light component, is considerably less than the maximum strength of the barriers for the two heavier components.

Just as in Gilliland's equation, the equations for equimolar diffusion also contain a solution which is usually fictitious for it can be seen that Equation (10) is always satisfied by

$$N_A \left( \frac{1}{D_{AB}} - \frac{1}{D_{BC}} \right) + N_B \left( \frac{1}{D_{AB}} - \frac{1}{D_{AC}} \right) = 0 \quad (17)$$

Under these conditions Equation (9) gives

$$N_A = \frac{P/RTx}{\left( \frac{1}{D_{AB}} - \frac{1}{D_{BC}} \right) \left( \frac{1}{D_{AC}} - \frac{1}{D_{BC}} \right)} \cdot \left[ \left( \frac{1}{D_{AB}} - \frac{1}{D_{BC}} \right) (y_{A_1} - y_{A_2}) + \left( \frac{1}{D_{AB}} - \frac{1}{D_{AC}} \right) (y_{B_1} - y_{B_2}) \right] \quad (18)$$

As before, this solution is true for only one particular relationship among the mole fractions and here the extra equation must be obtained by solving the original differential equations with restrictions given by Equations (17) and (4). The solution gives Equation (18) and the additional relationship

$$\left( \frac{1}{D_{AB}} - \frac{1}{D_{AC}} \right) (y_{B_1} - y_{B_2}) = \left( \frac{1}{D_{AB}} - \frac{1}{D_{BC}} \right) (y_{A_1} - y_{A_2})$$

$$= - \frac{\left( \frac{1}{D_{AB}} - \frac{1}{D_{BC}} \right) (y_{A_1} + y_{A_2}) + \left( \frac{1}{D_{AB}} - \frac{1}{D_{AC}} \right) (y_{B_1} + y_{B_2}) + \frac{2}{D_{BC}}}{\left( \frac{1}{D_{AB}} - \frac{1}{D_{BC}} \right) (y_{A_1} + y_{A_2}) + \left( \frac{1}{D_{AB}} - \frac{1}{D_{AC}} \right) (y_{B_1} + y_{B_2}) + \frac{2}{D_{AC}}} \quad (19)$$

The solution to the equimolar diffusion equations given by Equation (18) is correct only when Equation (19) is satisfied.

One Gas Stagnant

The previous results suggest the possibility of a diffusion barrier when two gases are diffusing through a third gas

which cannot diffuse because of a solubility barrier. If  $N_B$  is set equal to zero in Equation (11),

$$N_A = \frac{D_{AC}P}{RTx} \ln \frac{y_{C_2}}{y_{C_1}} \quad (20)$$

Equations (11) and (12) together also yield

$$\frac{y_{B_2}}{y_{B_1}} = \left( \frac{y_{C_2}}{y_{C_1}} \right)^{D_{AC}/D_{AB}} \quad (21)$$

and so a diffusion barrier exists here also. Gas  $C$  therefore cannot diffuse because of a solubility barrier and when Equation (21) holds, gas  $B$  cannot diffuse, because of a diffusion barrier.

It can be shown (10) that Equations (20) and (21) are the solutions to the diffusion equations, (2) and (3), when  $N_B$  and  $N_C$  are both set equal to zero. Therefore, when two of the three gases are stagnant, the stagnant gas concentrations adjust themselves to satisfy Equation (21), and the diffusion rate is given by Equation (20). If only one gas is initially stagnant owing to a solubility barrier, the system containing two stagnant gases can be exactly reproduced by fixing the compositions of the components at both ends of the diffusion path so that Equation (21) is satisfied.

The fact that two stagnant gases will partially separate when a third gas is passed through them, as shown by Equation (21), is the basis of the sweep-diffusion separation process (3). Hellund (9) has considered the unsteady state analogue of the sweep-diffusion process using his extension of the Chapman-Enskog theory.

Figure 2 shows some concentration relationships when  $H_2O$  is restrained by a diffusion barrier. The terminal concentrations of the diffusing component have been fixed at 0 at point 1 and 0.5 at point 2. The conditions when  $CO_2$  is diffusing and  $H_2$  is stagnant are shown by curve  $a$ , and curve  $b$  shows the conditions when  $H_2$  is diffusing and  $CO_2$  is stagnant. It can be seen that  $CO_2$  is more effective than  $H_2$  in stopping the diffusion of the  $H_2O$ .

When  $y_{B_1}$  approaches 1,  $y_{C_1}$  approaches

$$0 \text{ and } y_{B_2} \text{ must approach } 0.5 \text{ in order for a solution to exist. At this limit the system is reduced to a binary gas and this binary system is indeterminate as the removal of the stagnant gas removes the determinancy condition. Since Equation (21) gives the conditions under which } N_B = 0, \text{ it yields } y_{B_2} = 0.5 \text{ when } y_{B_1} = 1.0, \text{ the}$$

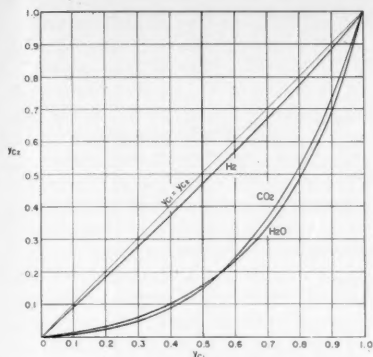


Fig. 1. Diffusion-barrier conditions for component C, equimolal diffusion.

$H_2 = C$	$CO_2 = C$	$H_2O = C$
$\frac{1}{H_2O}$	$\frac{2}{CO_2}$	$\frac{1}{H_2}$
$\frac{2}{H_2}$	$\frac{1}{CO_2}$	$\frac{2}{H_2O}$

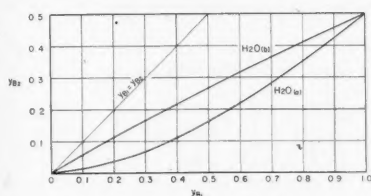


Fig. 2. Diffusion-barrier conditions for component B; component C is stagnant.

$$y_{A1} = 0 \quad y_{A2} = 0.5$$

$$y_{C1} = 1 - y_{B1} \quad y_{C2} = 0.5 - y_{B2}$$

Curve	A	Component B	C
a	CO <sub>2</sub>	H <sub>2</sub> O	H <sub>2</sub>
b	H <sub>2</sub>	H <sub>2</sub> O	CO <sub>2</sub>

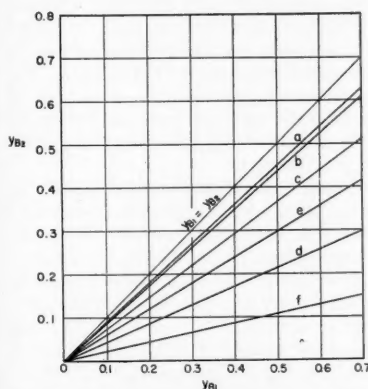


Fig. 3. Diffusion-barrier conditions for component B; component C is stagnant.

$$y_{A1} = 0.7 - y_{B1} \quad y_{A2} = 0.8 - y_{B2}$$

$$y_{C1} = 0.3 \quad y_{C2} = 0.2$$

Curve	A	Components B	C
a	H <sub>2</sub> O	H <sub>2</sub>	CO <sub>2</sub>
b	CO <sub>2</sub>	H <sub>2</sub>	H <sub>2</sub> O
c	H <sub>2</sub>	H <sub>2</sub> O	CO <sub>2</sub>
d	CO <sub>2</sub>	H <sub>2</sub> O	H <sub>2</sub>
e	H <sub>2</sub>	CO <sub>2</sub>	H <sub>2</sub> O
f	H <sub>2</sub> O	CO <sub>2</sub>	H <sub>2</sub>

only composition at point 2 which can exist in this binary system.

Figure 3 shows the diffusion-barrier conditions when the terminal concentrations of the stagnant gas are held constant. There are six different combinations of CO<sub>2</sub>, H<sub>2</sub>O and H<sub>2</sub>, all of which are shown. The strength of the diffusion barrier clearly increases as the mass of the restrained and diffusing components increases.

#### GENERALIZED DRIVING FORCE

When a diffusion barrier exists for a particular component, it cannot diffuse even though it is distributed nonuniformly in the gas. This can be pictured as a dynamic equilibrium between the tendency of the restrained component to diffuse in the direction of decreasing concentration because of the usual concentration driving force and the tendency of the component to be forced in the reverse direction by interactions with the other two diffusing components.

A small increase in the driving force at this point, therefore, should allow it to overcome the interactions and cause the transfer to take place in the direction of the driving force (high to low concentrations) and a small decrease in the driving force should make the transfer take place in the direction opposite to the driving force.

#### Equimolal Diffusion

This conclusion has been tested numerically for equimolal diffusion by use of Equations (9), (10), (4), and (16). Figure 4 shows the rate of diffusion of CO<sub>2</sub> as a function of its mole fraction at point 2, when its mole fraction at point 1 is constant at 0.5. It is assumed for simplicity that the mole fraction of H<sub>2</sub>O is zero at point 1 and the mole fraction of H<sub>2</sub> is zero at point 2. The rates of diffusion of H<sub>2</sub>O and H<sub>2</sub> are also shown on the figure. The dotted lines are approximate equations developed in a later section.

It can be seen that the rate of diffusion of CO<sub>2</sub> is close to a linear function of  $y_{A2}$ . At  $y_{A2} = 0.159$ ,  $N_A$  is zero, as this is the diffusion-barrier concentration. As  $y_{A2}$  decreases from this value, the driving force  $y_{A1} - y_{A2}$  increases and overcomes the interactions and  $N_A$  increases in the positive direction. As  $y_{A2}$  increases from the diffusion-barrier value, the driving force decreases, the interactions overcome the driving force, and the diffusion increases in the negative direction. The direction of diffusion is now opposite to the direction of the driving force.

As  $y_{A2}$  continues increasing the driving force decreases and the magnitude of  $N_A$  increases. At  $y_{A2} = 0.5 = y_{A1}$ , the driving force is now zero but  $N_A$  is not zero. This point is labeled *osmotic diffusion* and is considered later. When  $y_{A2}$

becomes greater than  $y_{A1}$ , the direction of diffusion is unchanged, but the direction of the driving force is reversed so that the diffusion is again in the direction of the driving force. When  $y_{A2}$  equals 1 the system is reduced to a binary gas consisting of CO<sub>2</sub> and H<sub>2</sub>.  $N_A = -N_B$  and the rates are the same as those given by the usual equation for binary equimolal diffusion.

The same conclusions can be reached analytically for the special case of diffusion in which two of the binary-diffusion coefficients are equal. [See Equation (36).]

No diffusion barrier occurs for H<sub>2</sub>O and H<sub>2</sub> because of the way the compositions were fixed.

There are two separation processes which take advantage of the phenomenon of diffusion from regions of low to high concentrations. They differ from themselves, and from the conditions considered here, by the restrictions placed on  $N$ . One has been defined as *mass diffusion* (1) or *atmolysis*, and the other as *sweep diffusion* (3).

It seems useful to define as *reverse diffusion* the diffusion of a constituent of a multicomponent gas from a region where its concentration is low to a region where it is high when it is caused by the action of the other constituents of the gas. The region in which reverse diffusion takes place is indicated in Figure 4.

In one sense the diffusion-barrier concentrations of the restrained component correspond to a zero concentration gradient in a binary gas. When the restrained component is at the concentrations corresponding to a diffusion barrier, its rate of transfer is zero, just as it is zero in a binary gas when  $y_1 = y_2$ . In the ternary gas mixture the diffusion of a component is from point 1 to point 2 when the concentration of the component at 1 is greater than the concentration at 2 corresponding to the diffusion barrier, just as the diffusion in a binary system is from 1 to 2 when  $y_1$  is greater than the value corresponding to zero concentration gradient  $y_2$ . As the displacement from the barrier condition increases, the rate of diffusion increases; therefore, the driving force in a ternary gas which should correspond to  $y_1 - y_2$  in a binary gas is, for component  $i$ ,

$$(y_{i1} - y_{i2}^*) \quad (22)$$

or

$$(y_{i2}^* - y_{i1}) \quad (23)$$

where  $y_{i2}^*$  is the mole fraction which would have to exist at point 1 for a diffusion barrier to exist for component  $i$  when the mole fractions at point 2 are held constant and  $y_{i2}^*$  is the mole fraction necessary at point 2 for a diffusion barrier to exist when the mole fractions at point 1 are held constant.

Equation (16), when  $A$  and  $C$  are

interchanged, gives for component A

$$\frac{y_{A_2}}{y_{A_1}} = \exp \left[ \left( 1 - \frac{D_{BC}}{D_{AB}} \right) (y_{C_1} - y_{C_2}) + \left( 1 - \frac{D_{BC}}{D_{AC}} \right) (y_{B_1} - y_{B_2}) \right] = \delta_A \quad (24)$$

and either  $y_{A_1}$  or  $y_{A_2}$  can be considered to be the starred value. When  $y_{A_1}$  is taken as  $y_{A_1}^*$ , Equation (22) becomes for component A

$$\frac{1}{\delta_A} (\delta_A y_{A_1} - y_{A_2}) \quad (25)$$

and when  $y_{A_2}$  is taken as  $y_{A_2}^*$  Equation (23) yields for component A

$$\delta_A (y_{A_1} - y_{A_2}) \quad (26)$$

There are similar equations for the other two components obtained by interchanging subscripts in the above equations. It can be shown that

$$\delta_i = \delta_i^{D_{jk}/D_{ik}} \quad (27)$$

It is immaterial whether Equation (25) or (26) is considered to represent the generalized driving force; so, for simplicity, the second one will be used. The function defined by Equation (26) satisfies the necessary conditions for a driving force. First, it gives the correct direction of diffusion; when it is positive the direction of diffusion is positive and when it is negative the direction of diffusion is negative. Second, the rate of diffusion is zero when the function is zero. Since the relationship between the rate of diffusion and the generalized driving force must be single valued, the first two conditions require that the rate of diffusion be a monotonic increasing function of the generalized driving force.

A final condition which is desirable but not necessary is that the rate of diffusion should be proportional, or approximately proportional, to the driving force. The rate of diffusion of each of the three components is plotted against its generalized driving force in Figure 5. The curves were obtained by the use of Figure 4 and Equations (24) and (26) and the curves are close to straight lines. In this example no diffusion barrier occurs for H<sub>2</sub> and H<sub>2</sub>O since the composition of both components is fixed at zero at one or the other end of the diffusion path. The rates of diffusion of these two components are roughly proportional to their binary driving forces, and their generalized driving forces are essentially the same as their binary ones. However, CO<sub>2</sub>, for which a diffusion barrier exists, diffuses quite independently of its binary driving force, and its diffusion rate is closely proportional to its generalized driving force. It can be seen that reverse diffusion takes place when the generalized

driving force is of opposite sign to the binary driving force, and this would be expected to be the case in general.

The reciprocal slopes of the curves in Figure 5 are a measure of the generalized resistances to the diffusion of each component (the generalized driving force divided by the diffusion rate). The mean slopes of the lines decrease with increasing molecular weight, an indication, at least for this example, that the generalized resistances increase with the mass of the component. Since the curves for CO<sub>2</sub> and H<sub>2</sub>O have opposite curvatures, their generalized resistances approach each other when the generalized driving forces are small.

In general, the relationship between the rates of diffusion and the generalized driving forces would not be expected to be as linear as in this particular case, and so the generalized resistances for each component would vary more with the composition of the system. In this instance the generalized driving force has the same utility as the one used in the diffusion of one gas through a second inert gas, quantitatively it can be somewhat misleading, but it always gives the correct direction of diffusion and the correct zero condition.

#### One Gas Stagnant

The generalized-driving-force viewpoint can also be applied to transfer when one gas is stagnant by using the displacement

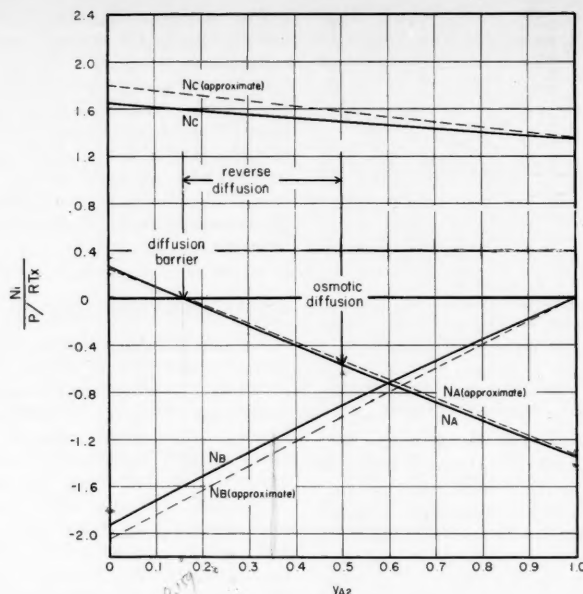


Fig. 4. Diffusion rates as a function of  $y_{A_2}$ , equimolar diffusion.

$$\begin{aligned} y_{A_1} &= 0.5 \\ y_{B_1} &= 0 \\ y_{C_1} &= 0.5 \end{aligned}$$

$$\begin{aligned} y_{A_2} &= 1 - y_{A_1} \\ y_{B_2} &= 1 - y_{A_2} \\ y_{C_2} &= 0 \end{aligned}$$

A  
CO<sub>2</sub>

B  
H<sub>2</sub>O

C  
H<sub>2</sub>

from a diffusion barrier as a measure of the driving force.

Figure 6 shows the rates of diffusion of CO<sub>2</sub> and H<sub>2</sub>O through stagnant H<sub>2</sub> as a function of the mole fraction of CO<sub>2</sub> at point 2. The solid curves were calculated from Equations (11) and (12) and the dotted ones are approximations developed in a later section. The terminal concentrations are fixed as shown in the figure. The inert-gas concentrations are fixed at both ends of the diffusion path, and the concentrations of CO<sub>2</sub> and H<sub>2</sub>O are fixed only at point 1.

These curves bear a resemblance to those shown in Figure 4 for equimolar diffusion, although the conditions are quite different. There is no diffusion barrier for H<sub>2</sub>O, as its concentration at point 1 is zero, but the CO<sub>2</sub> diffusion barrier occurs at  $y_{B_2} = 0.152$ . At this point the tendency for CO<sub>2</sub> to diffuse in the direction of decreasing CO<sub>2</sub> concentration is just balanced by collisions with H<sub>2</sub>O, which is diffusing in the opposite direction.

In this system, contrary to the equimolar one previously discussed, there is a net molal transfer for all values of  $y_{B_2}$ .  $N_A$  never equals  $-N_B$  since Equation (16), the criterion for this condition, cannot be satisfied by any physically possible value of  $y_{B_2}$  in this example.

When  $y_{B_2}$  is less than the diffusion-barrier concentration,  $N_B$  is positive and in the direction of decreasing CO<sub>2</sub> con-



centration. When  $y_{B_2}$  is between the diffusion-barrier concentration and  $y_{B_1}$ , 0.7,  $N_B$  is negative and reverse diffusion takes place. When  $y_{B_1}$  is greater than  $y_{B_2}$ , the diffusion is again in the direction of decreasing  $\text{CO}_2$  concentration. When  $y_{B_2} = 0.8$ , the system reduces to a binary one in which  $\text{CO}_2$  is diffusing through stagnant  $\text{H}_2$  and the rate of diffusion of  $\text{CO}_2$  is given by the binary equation.

Since the diffusion phenomena when one gas is stagnant are similar to the phenomena when the transfer is equimolar, the generalized driving force given by Equation (23) applies here also. The only difference is that  $y_{i*}$  is now given by Equation (21). Thus for component B,

$$\frac{y_{B_2}^*}{y_{B_1}} = \left( \frac{y_{C_2}}{y_{C_1}} \right)^{D_{AC}/D_{AB}} = \delta_B' \quad (28)$$

and the generalized driving force for component B is obtained by combining Equations (23) and (28),

$$(\delta_B' y_{B_1} - y_{B_2}) \quad (29)$$

The equation for component A is obtained by interchanging the A and B subscripts in the preceding equations.  $\delta_A'$  and  $\delta_B'$  are related to each other in the same way as  $\delta_i$  and  $\delta_j$  [Equation (27)]. As before, the generalized driving force gives the correct direction of diffusion as well as the correct zero condition.

The rate of diffusion of both components is shown plotted against their generalized driving forces in Figure 7. The data are from Figure 6 and Equations (28) and (29). The generalized driving force for component A,  $\text{H}_2\text{O}$ , reduces to the binary one because of the terminal concentrations which were used and the rate of diffusion of  $\text{H}_2\text{O}$  is approximately proportional to this quantity. The generalized driving force for  $\text{CO}_2$ , however, is markedly different from the binary one, and only the generalized driving force has the characteristics of a driving force.

The generalized resistances to the diffusion of the two components are not the same although they approach one another as the generalized driving forces approach zero, and the generalized resistance for  $\text{CO}_2$  is greater than that for  $\text{H}_2\text{O}$ .

Simplified approximate equations for the rates of diffusion, developed in a later section both when the diffusion is equimolar and when one gas is stagnant, allow analytic confirmation of the conclusions reached in this section.

## NOTATION

- $D_{ij}$  = diffusion coefficient for binary mixture of components  $i$  and  $j$ , sq. cm./sec.  
 $D_m$  = mean diffusion coefficient defined by Equation (56), sq. cm./sec.

- $N$  = total net diffusion rate, g.-mole/(sq. cm.)(sec.)  
 $N_i$  = diffusion rate for component  $i$ , g.-mole/(sq. cm.)(sec.)  
 $P$  = total pressure, atm.  
 $R$  = gas constant, (cc.)(atm.)/(g.-mole)(°K.)  
 $T$  = temperature, °K.  
 $x$  = distance in direction of diffusion or length of diffusion path, cm.  
 $y_i$  = mole fraction of component  $i$   
 $y_i^*$  = value of  $y_i$  when component  $i$  is restrained by a diffusion barrier  
 $y_{im}$  = log mean of  $y_i$

## Greek Letters

- $\delta, \delta_i, \delta_m, \varphi_C$  = functions used in equimolar diffusion equations, defined by Equations (35), (24), (59), and (60), respectively  
 $\delta', \delta_i', \delta_m', \varphi_C'$  = functions used in stagnant-gas diffusion equations, defined by Equations (49), (28), (65), and (66), respectively

## Subscripts

- A, B, C = components of a mixture  
 $i, j, k$  = indexes which refer to components A, B, or C  
 1, 2 = terminal conditions of the diffusion path

## PART II

### OSMOTIC DIFFUSION

It has been shown that a component not in equilibrium under certain conditions may not diffuse even if there is no barrier to its diffusion, and it has also been shown for a particular example that the converse is true, i.e., that a component which is in equilibrium may diffuse.

#### Equimolar Diffusion

It has already been demonstrated that Equation (16) must be satisfied for  $N_C$  to equal zero when  $N = 0$ . If component C is in equilibrium,  $y_{C_1} = y_{C_2}$ , and since the sum of the mole fractions at any point is equal to 1, Equation (16) is satisfied with these restrictions only if one of the following conditions is satisfied:

$$y_{A_1} = y_{A_2} \quad (30)$$

and consequently

$$y_{B_1} = y_{B_2}$$

or

$$D_{AC} = D_{BC} \quad (31)$$

The first condition is trivial, as it gives the obvious result that there is no transfer if there is complete equilibrium in the system. The second condition shows that  $N_C = 0$  only when the diffusivity of A through C equals the diffusivity of B through C (when  $y_{C_1} = y_{C_2}$ ). When this

condition holds, Equation (15) is indeterminate and the diffusion equations reduce to Equations (43) and (44). When  $D_{AC}$  does not equal  $D_{BC}$ , the rates of diffusion are given by the general equations.

From the generalized-driving-force viewpoint,  $N_C = 0$  for  $y_{C_1} = y_{C_2} = 0$  only when the generalized driving force,  $\delta_C y_{C_1} - y_{C_2}$ , is equal to the usual binary driving force, that is, when  $y_{C_1} = y_{C_2}$ , and Equation (30) or (31) is satisfied. The point at which osmotic diffusion occurs is shown in Figures 4 and 5.

The phenomenon of diffusion of a component which is in equilibrium was predicted by Hellund (8), who extended the Chapman-Enskog equations to a ternary system and obtained a solution for diffusion in the unsteady state. He named the phenomenon *osmotic diffusion* by analogy to liquids.

#### One Gas Stagnant

When  $N_C$  is fixed equal to zero by a solubility barrier,  $N_B$  is zero when Equation (21) holds. If component B is in equilibrium,  $y_{B_1} = y_{B_2}$ , and the condition for  $N_B = 0$  becomes  $y_{C_1} = y_{C_2}$ . This is the condition which reduces the generalized driving force to the binary driving force as well as the condition for complete equilibrium, and so in this system a component which is in equilibrium will always diffuse unless the entire system is in equilibrium. The point at which osmotic diffusion occurs is shown in Figures 6 and 7.

In general, reverse diffusion, both in equimolar diffusion and diffusion with one gas stagnant, would be expected to occur when the generalized driving force lies between zero and the value corresponding to osmotic diffusion.

### TWO DIFFUSION COEFFICIENTS EQUAL

By setting two of the three binary diffusion coefficients equal to each other, one may obtain simplified forms of the diffusion equations.

#### Equimolar Diffusion

If  $D_{AC} = D_{BC}$  Equations (9) and (10) reduce to

$$N_A + N_B = \frac{D_{AC}P}{RTx} \cdot [(y_{A_1} + y_{B_1}) - (y_{A_2} + y_{B_2})] \\ = \frac{D_{AC}P}{RTx} (y_{C_2} - y_{C_1}) \quad (32)$$

and

$$\left( \frac{1}{D_{AB}} - \frac{1}{D_{AC}} \right) (N_A + N_B) \\ = \frac{P}{RTx} \ln \frac{\frac{y_{A_1} - y_{B_1}}{N_A} - \frac{y_{B_2} - y_{A_2}}{N_B}}{\frac{y_{A_1} - y_{B_1}}{N_A} - \frac{y_{B_2} - y_{A_2}}{N_B}} \quad (33)$$

equating the last two equations yields

$$\frac{N_A}{N_B} = \frac{\delta y_{A_1} - y_{A_2}}{\delta y_{B_1} - y_{B_2}} \quad (34)$$

where

$$\delta = \exp \left[ \left( 1 - \frac{D_{AC}}{D_{AB}} \right) (y_{C_1} - y_{C_2}) \right] \quad (35)$$

Substituting Equation (34) into Equation (32) leads to

$$N_A = \frac{y_{C_1} - y_{C_2}}{(1 - y_{C_2}) - \delta(1 - y_{C_1})} \cdot \frac{D_{AC}P}{RTx} (\delta y_{A_1} - y_{A_2}) \quad (36)$$

and

$$N_B = \frac{y_{C_1} - y_{C_2}}{(1 - y_{C_2}) - \delta(1 - y_{C_1})} \cdot \frac{D_{BC}P}{RTx} (\delta y_{B_1} - y_{B_2}) \quad (37)$$

Equation (32) with the equimolal condition gives

$$N_C = \frac{D_{AC}P}{RTx} (y_{C_1} - y_{C_2}) \quad (38)$$

This is the equation for equimolal diffusion in a binary system consisting of *A* and *C*. Hence the rate of diffusion of component *C* is the same as it would be if *A* and *B* were one gas; indeed, as far as *C* is concerned *A* and *B* are the same gas, for their interactions with *C* were assumed identical. Equation (32) shows that the hypothetical gas consisting of *A* and *B* also diffuses through *C* as if it were the second gas in a binary mixture.

In a sense the ternary mixture has been reduced to a binary one in which part of the molecules of one component are tagged to distinguish them from the other part of the same component. The diffusion coefficient  $D_{AB}$  then represents the coefficient of self-diffusion of components *A* and *B*. Although the net rate of diffusion of the tagged and untagged molecules, *A* and *B*, follows the binary equation, the individual components deviate from the binary equation as shown by Equations (36) and (37).

If the composition of the gas *A* and *B* is the same at both ends of the diffusion path,

$$\frac{y_{A_1}}{y_{B_1}} = \frac{y_{A_2}}{y_{B_2}} \quad (39)$$

and Equations (36) and (37) show that

$$\frac{N_A}{N_B} = \frac{y_{A_1}}{y_{B_1}} = \frac{y_{A_2}}{y_{B_2}} \quad (40)$$

Equation (32) then yields

$$N_A = \left( \frac{y_{A_1}}{y_{A_1} + y_{B_1}} \right) \cdot \frac{D_{AC}P}{RTx} (y_{C_2} - y_{C_1}) \quad (41)$$

$$N_B = \left( \frac{y_{B_1}}{y_{A_1} + y_{B_1}} \right) \cdot \frac{D_{BC}P}{RTx} (y_{C_2} - y_{C_1}) \quad (42)$$

so that components *A* and *B* deviate from the binary rate of diffusion of gas *A* and *B* by their mole fractions in the mixture *A* and *B*, and the composition of the gas *A* and *B* is unchanged by the diffusion through component *C*.

As  $D_{AB}$  approaches  $D_{AC}$ ,  $\delta$  approaches 1 and Equations (36) and (37) approach the binary equimolal equations (13) and (14), as expected. When  $y_{C_1}$  approaches  $y_{C_2}$ , Equations (36) and (37) reduce to

$$N_A = \frac{D_{AC}P/RTx}{y_C \left( 1 - \frac{D_{AC}}{D_{AB}} \right) + \frac{D_{AC}}{D_{AB}}} \cdot (y_{A_1} - y_{A_2}) \quad (43)$$

$$N_B = \frac{D_{BC}P/RTx}{y_C \left( 1 - \frac{D_{BC}}{D_{AB}} \right) + \frac{D_{BC}}{D_{AB}}} \cdot (y_{B_1} - y_{B_2}) \quad (44)$$

and this is the special case discussed previously where  $N_C$  is zero and  $N_A = -N_B$ . The presence of component *C* under these conditions merely causes the rates of diffusion of the other two components to deviate from the binary rates by a constant amount.

When gas *C* is dilute, the equations further simplify to the equimolal diffusion equations for the binary system consisting of *A* and *B*. When *A* and *B* are dilute,  $y_C$  approaches 1 and the binary equimolal diffusion equations are again obtained, although in this case the diffusion coefficient  $D_{AC}$  or  $D_{BC}$  replaces the coefficient  $D_{AB}$ , giving Equations (13) and (14). If either *A* or *B* alone is dilute, the rate of diffusion of the other component is given by Equation (13) or (14).

Equations (36) and (37) are very closely related to the idea of a generalized driving force. The last terms on the right of the equations are special cases of the generalized driving force defined by Equations (24) and (26) since  $\delta_A$  and  $\delta_B$  are both equal to  $\delta$ . The remaining terms on the right of the equations are therefore reciprocals of the generalized resistances for this special case. The generalized resistance is the same for components *A* and *B* and, for any particular system, is a function of the concentration of component *C* only. When the terminal concentrations of component *C* are held constant, the generalized resistance is constant and the diffusion rates are directly proportional to the generalized driving forces, but when the concentrations of component *C* are allowed to vary

this proportionality does not exist. It can be shown that the generalized resistance in Equations (36) and (37) is always positive, finite, and nonzero, as indeed is necessary if the driving-force viewpoint is to be meaningful.

The rate of diffusion of component *C*, which is given by the binary-diffusion equation, (38), apparently is not a function of its generalized driving force. To determine the cause of this inconsistency it is necessary to consider the original derivation of the generalized driving force. Applying Equation (24) to component *C* with  $D_{AC} = D_{BC}$  yields

$$\delta_C = \frac{y_{C_2}}{y_{C_1}} = \exp \left[ \left( \frac{D_{AB}}{D_{AC}} - 1 \right) (y_{C_1} - y_{C_2}) \right] \quad (45)$$

and  $y_{C_1}$ , which can be taken as  $y_{C_2}^*$ , is the mole fraction of *C* at point 2, which causes a diffusion barrier. If this equation is combined with Equation (23) as usual, it does not yield the binary driving force which appears in Equation (38), because there is only one solution to Equation (45) which has any physical significance and that solution is  $y_{C_2} = y_{C_1}$ , or  $y_{C_2}^* = y_{C_1}$ . Therefore,  $\delta_C$  must always be 1 and Equation (23) does yield  $y_{C_1} - y_{C_2}$  as the generalized driving force for this limit. There can be no diffusion barrier for component *C* and the only condition for zero diffusion is  $y_{C_1} = y_{C_2}$ .

#### One Gas Stagnant

When  $D_{AC} = D_{BC}$  Equations (11) and (12) yield

$$N_A + N_B = \frac{D_{AC}P}{RTx} \ln \frac{y_{C_2}}{y_{C_1}} \quad (46)$$

and

$$N_A + N_B = \frac{D_{AB}P}{RTx} \ln \frac{\frac{y_{A_2}}{N_A} - \frac{y_{B_2}}{N_B}}{\frac{y_{A_1}}{N_A} - \frac{y_{B_1}}{N_B}} \quad (47)$$

and by equating these the counterpart of Equation (34) is obtained,

$$\frac{N_A}{N_B} = \frac{\delta' y_{A_1} - y_{A_2}}{\delta' y_{B_1} - y_{B_2}} \quad (48)$$

where

$$\delta' = \left( \frac{y_{C_2}}{y_{C_1}} \right)^{D_{AC}/D_{AB}} \quad (49)$$

and so

$$N_A = \frac{\ln \frac{y_{C_2}}{y_{C_1}}}{(1 - y_{C_2}) - \delta'(1 - y_{C_1})} \cdot \frac{D_{AC}P}{RTx} (\delta' y_{A_1} - y_{A_2}) \quad (50)$$

$$N_B = \frac{\ln \frac{y_{C_1}}{y_{C_2}}}{(1 - y_{C_2}) - \delta'(1 - y_{C_1})} \cdot \frac{D_{BC}P}{RTx} (\delta'y_{B_1} - y_{B_2}) \quad (51)$$

Equation (46) shows that the hypothetical gas  $A + B$  diffuses through the stagnant gas  $C$  at the same rate that one gas diffuses through a second inert gas, but Equations (50) and (51) indicate that components  $A$  and  $B$  individually do not follow the binary equations.

When the ratio of  $A$  to  $B$  is the same at both ends of the diffusion path,

$$N_A = \left( \frac{y_{A_1}}{y_{A_1} + y_{B_1}} \right) \frac{D_{AC}P}{RTxy_{Cm}} \cdot (y_{C_2} - y_{C_1}) \quad (52)$$

$$N_B = \left( \frac{y_{B_1}}{y_{A_1} + y_{B_1}} \right) \frac{D_{BC}P}{RTxy_{Cm}} \cdot (y_{C_2} - y_{C_1}) \quad (53)$$

where

$$y_{Cm} = \frac{y_{C_1} - y_{C_2}}{\ln \frac{y_{C_1}}{y_{C_2}}} \quad (54)$$

At this limit the diffusion rates when one gas is stagnant differ from the rates for equimolar transfer by the term  $y_{Cm}$ , just as in binary diffusion. Under these conditions the composition of the gas  $A + B$  is unchanged by its diffusion through gas  $C$ .

Equations (50) and (51) differ from the analogous equimolar equations in that they do not reduce to the binary equations when all the diffusion coefficients are equal.

When  $y_{C_1}$  approaches  $y_{C_2}$ , Equations (50) and (51) reduce to Equations (43) and (44), as do the equimolar equations, since  $N_A = -N_B$ . When the diffusing gases are dilute, Equations (13) and (14) are again obtained, and when only one of the diffusing gases is dilute, the binary stagnant gas equation applies to the other gas.

When the stagnant gas is dilute, the limiting forms of the equations depend, in this case, on how the limit is approached. This would be expected since when component  $C$  is removed, the restriction which makes the system determinate is removed and the resulting binary system is indeterminate. Thus, when  $y_{C_1} = y_{C_2} = 0$ , Equation (47) reduces to the general equation for binary diffusion,

$$N_A + N_B = \frac{D_{AB}P}{RTx} \cdot \ln \left[ \frac{1 - \frac{N_A + N_B}{N_A} y_{A_2}}{1 - \frac{N_A + N_B}{N_A} y_{A_1}} \right] \quad (55)$$

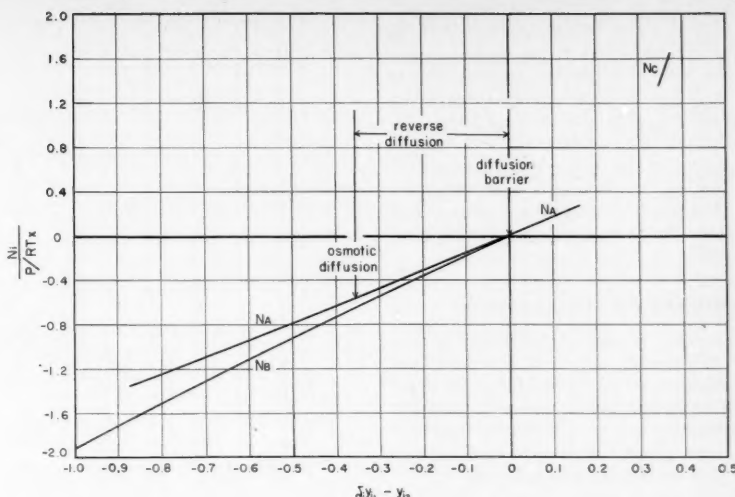


Fig. 5. Diffusion rates as a function of the generalized driving forces, equimolar diffusion.

$$\begin{array}{lll} y_{A_1} = 0.5 & y_{A_2} = 0.5 & y_{A_2} = 1 - y_{A_1} \\ y_{B_1} = 0 & y_{B_2} = 0 & y_{B_2} = 1 - y_{A_2} \\ y_{C_1} = 0.5 & y_{C_2} = 0.5 & y_{C_2} = 0 \end{array}$$

A	B	C
CO <sub>2</sub>	H <sub>2</sub> O	H <sub>2</sub>

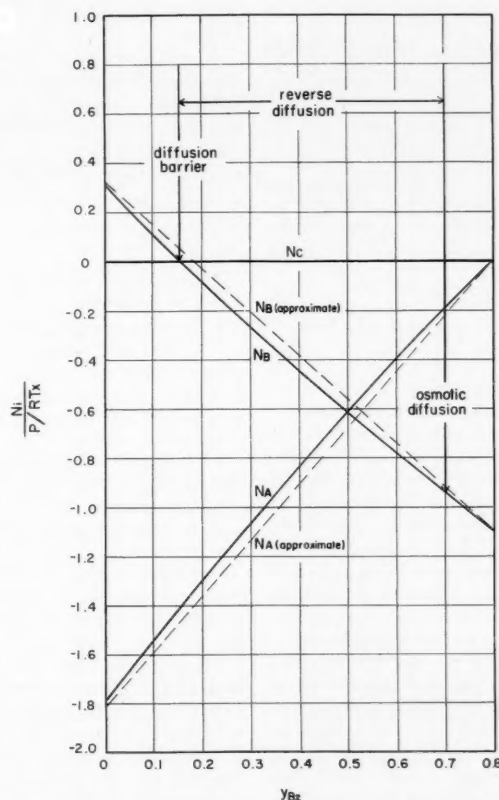


Fig. 6. Diffusion rates as a function of  $y_{B_2}$ ;  $H_2$  is stagnant.

$$\begin{array}{lll} y_{A_1} = 0 & y_{A_2} = 0.8 - y_{B_2} & y_{A_2} = 0.8 - y_{B_2} \\ y_{B_1} = 0.7 & y_{B_2} = 0.2 & y_{B_2} = 0.2 \\ y_{C_1} = 0.3 & y_{C_2} = 0.2 & y_{C_2} = 0.2 \end{array}$$

A	B	C
H <sub>2</sub> O	CO <sub>2</sub>	H <sub>2</sub>

and another restriction is now needed to define  $N_A$  and  $N_B$ .

The last terms on the right of Equations (50) and (51) are special cases of the generalized driving force defined by Equations (28) and (29) and the remaining terms on the right are the generalized resistances, which are the same for both components. This generalized resistance is positive, finite, and nonzero for all conditions of physical significance.

#### APPROXIMATE DIFFUSION EQUATIONS

Since the equations developed in the last two sections apply to a ternary gas in which two of the three binary-diffusion coefficients are equal, it seems possible that they could be modified to approximate the general equations when all the diffusion coefficients are unequal.

#### Equimolar Transfer

The simplest useful modifications of Equations (35) to (37) are obtained by replacing  $D_{AC}$  in Equation (35) by

$$D_m = \frac{D_{AC} + D_{BC}}{2} \quad (56)$$

so that

$$N_A = \frac{D_{AC}P}{RTx} \varphi_C (\delta_m y_{A_1} - y_{A_2}) \quad (57)$$

$$N_B = \frac{D_{BC}P}{RTx} \varphi_C (\delta_m y_{B_1} - y_{B_2}) \quad (58)$$

where

$$\delta_m = \exp \left[ \left( 1 - \frac{D_m}{D_{AB}} \right) (y_{C_1} - y_{C_2}) \right] \quad (59)$$

and

$$\varphi_C = \frac{y_{C_1} - y_{C_2}}{(1 - y_{C_2}) - \delta_m(1 - y_{C_1})} \quad (60)$$

Once  $N_A$  and  $N_B$  are obtained,  $N_C$  can be determined from Equation (4). Although the equations are symmetrical with respect to A and B, they are not symmetrical with respect to C. Therefore, the results obtained from them depend on which of the three components is chosen to be component C. The most accurate results should be obtained when component C is chosen so that  $D_{AC}$  and  $D_{BC}$  are the two diffusion coefficients which are closest to each other, since this choice makes the system approximate as closely as possible the conditions under which Equations (57) and (58) are exact.

The preceding approximate equations are compared with the exact ones in Figure 4, where the approximate equations are shown by dotted lines. The error for  $\text{CO}_2$  is very small and the diffusion-barrier conditions predicted by Equation (57) are close to the true diffusion-barrier conditions. This may not be the case in general, and when  $y_{A_2}$  is between the approximate and exact diffusion barrier values the direction of diffusion given by Equation (57) is incorrect. In

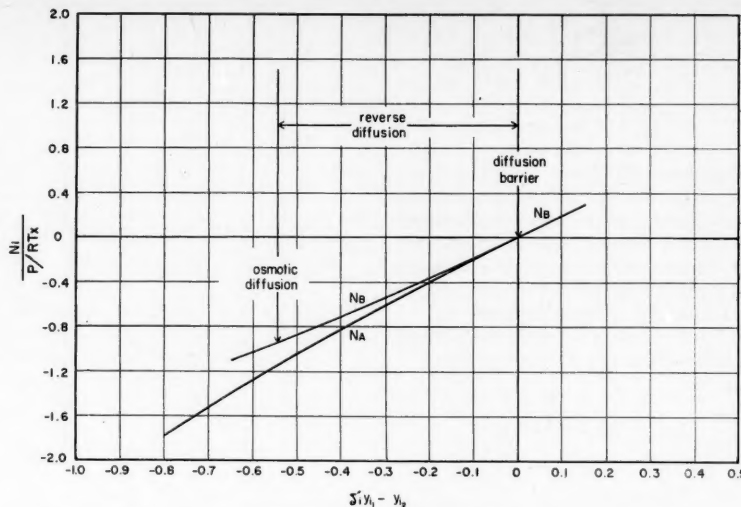


Fig. 7. Diffusion rates as a function of the generalized driving forces;  $\text{H}_2$  is stagnant.

$y_{A_1} = 0$	$y_{A_2} = 0.8 - y_{B_2}$
$y_{B_1} = 0.7$	$y_{B_2} = 0.2$
$y_{C_1} = 0.3$	$y_{C_2} = 0.2$
A H <sub>2</sub> O	B CO <sub>2</sub>
	C H <sub>2</sub>

this example this region is extremely narrow.

If more accurate values are desired near the diffusion barrier, the approximate generalized driving force in Equation (57) may be replaced by the true generalized driving force given by Equations (24) and (26). Thus, for component A

$$N_A = \frac{D_{AC}P}{RTx} \varphi_C (\delta_A y_{A_1} - y_{A_2}) \quad (61)$$

This equation is not symmetrical with respect to positions 1 and 2. The equation can be made symmetrical by replacing  $\delta_m$  by  $\delta_A$  in Equation (60), although better results are obtained by taking the average of the two values given by interchanging points 1 and 2 in Equation (61),

$$N_A = \frac{D_{AC}P}{RTx} \varphi_C \left( \frac{\delta_A + \delta_m}{2 \delta_m} \right) (\delta_A y_{A_1} - y_{A_2}) \quad (62)$$

The equation can be written for the other components by interchanging subscripts. It is a good approximation when the generalized driving force is not too large, as it gives the correct zero condition, but it is usually less accurate than (57) when the generalized driving force is large. For the conditions of Figure 4 it is actually a better approximation to  $N_A$  than Equation (57) over a large part of the range of  $y_{A_2}$ .

The difference between the approximate and true diffusion rates for  $\text{H}_2\text{O}$  is larger than that for  $\text{CO}_2$  and the rate of diffusion of  $\text{H}_2$  is fixed by the equimolar condition, Equation (4). Consequently if  $\text{H}_2$  were diffusing at a relatively low rate compared with that of the other two

components, calculating  $\text{H}_2$  by difference could lead to large relative errors in  $N_C$ .

In order to test the methods under other conditions, the test examples set up by Wilke (19) were used. The system is  $\text{H}_2$ ,  $\text{CO}_2$ , and  $\text{H}_2\text{O}$ , as before, and the results obtained by use of Equations (56) to (60) and (4), defined as method 1, in most cases check those calculated from the exact equations within 10%. They are tabulated in Tables 2 and 3.\* However, when the generalized driving force for  $\text{H}_2$ , which is the recommended choice for component C, is much smaller than the other generalized driving forces, this method causes large errors. (The direction as well as the magnitude is incorrect.) This is due to the fact that  $\text{H}_2$  is obtained by difference. Calculating  $\text{H}_2$  directly by this method also gives poor results because the generalized driving forces are small. In this case Equation (62) is a much better approximation since it uses the correct generalized driving force (method 2). With both methods, the maximum error is 20% although the absolute errors are generally very small.

At present the recommended procedure for equimolar diffusion is to use method 1 in all cases where the generalized driving force is not small and method 2 if the generalized driving force for a component is small. The results may be checked for consistency by use of Equations (4) and (9) without solving the general equations.

The errors in the approximate methods should increase as the difference between the diffusion coefficients increases.

\*Tables 2, 3, and 4 have been deposited as document 5210 with the American Documentation Institute, Photoduplication Service, Library of Congress, Washington 25, D. C., and may be obtained for \$2.50 for photoprints or \$1.75 for 35-mm. microfilm.



## One Gas Stagnant

In this case the approximate diffusion equations are obtained by replacing  $D_{AC}$  in Equation (49) by  $D_m$ ; so from Equations (49) to (51):

$$N_A = \frac{D_{AC}P}{RTx} \varphi_c'(\delta_m' y_{A_1} - y_{A_2}) \quad (63)$$

$$N_B = \frac{D_{BC}P}{RTx} \varphi_c'(\delta_m' y_{B_1} - y_{B_2}) \quad (64)$$

where

$$\delta_m' = \left( \frac{y_{C_2}}{y_{C_1}} \right)^{D_m/D_{AB}} \quad (65)$$

and

$$\varphi_c' = \frac{\ln \frac{y_{C_2}}{y_{C_1}}}{(1 - y_{C_2}) - \delta_m'(1 - y_{C_1})} \quad (66)$$

Since there are only two diffusion rates which are unknown, there is no problem with the third component as there was in equimolal diffusion. The equations are now completely symmetrical, but here there is no freedom in choosing the constituent which is to be considered as component C: it must be the stagnant gas. Therefore, the accuracy of the approximate equations would be expected to decrease as the dissimilarity between the two diffusing gases increases.

The approximate equations are compared with Gilliland's equation in Figure 6, where  $H_2$  is the stagnant gas. When  $y_{B_2} = 0.8$ , the system reduces to a binary gas and the approximate equations are exact at this point. At  $y_{B_2} = 0$ , the approximate equations differ very slightly from the exact ones, but between these two extremes the error is larger because of the curvature in the correct curves.

The diffusion rates are reproduced quite well by the approximate equations, except for  $CO_2$  near its diffusion barrier. The diffusion barrier predicted by the approximate equations occurs at a value of  $y_{B_2}$  slightly different from the correct diffusion barrier, so that in this region the percentage error in  $N_B$  can be very large, although the absolute error is small. In addition, when  $y_{B_2}$  is between the values corresponding to the two diffusion barriers, the approximate equation gives the wrong direction of diffusion for  $CO_2$ .

If the correct generalized driving force is used to replace the approximate one in Equation (63), the equation can be made to yield the correct diffusion-barrier conditions, and when the equation is made symmetrical as in the equimolal case,

$$N_A = \frac{D_{AC}P}{RTx} \varphi_c' \left( \frac{\delta_A' + \delta_m'}{2\delta_A'} (\delta_A' y_{A_1} - y_{A_2}) \right) \quad (67)$$

The equation for  $N_B$  is similar.

It is interesting to note here that

$$\delta_m' = \sqrt{\delta_A' \delta_B'} \quad (68)$$

As Equation (67) is exact when  $N_A = 0$ , it should be a good approximation when the generalized driving force is small. If it is applied to  $CO_2$  in Figure (6) by interchanging A and B, it reproduces the correct diffusion rate very accurately in the vicinity of the diffusion barrier and it is a better approximation than Equation (64) over the range of  $y_{B_2}$  from 0 to 0.5.

The previous test examples were used here also.  $N_C$  instead of  $N$  is set equal to zero and method 1, with Equations (63) to (66), is generally very accurate—appreciably more so than the analogous method for equimolal diffusion. The average error is a few per cent and the maximum error is 18%. This error is very small compared with the total diffusion rate. Method 2, which uses the correct generalized driving force, Equation (67), is in general less accurate than method 1 in these examples. The results are in Table 4.\*

The recommended procedure for calculating the rates of diffusion of two gases through a third stagnant gas is to use method 1 except when the generalized driving force is very small, a point at which method 2 should be more reliable.

Wilke's (19) approximate methods for solving Maxwell's equations have not been checked extensively, but it appears that the equations are not inconsistent with the phenomena discussed above if the negative partial film pressure factors which occur in the procedure are not rejected as he suggested, but are retained. This makes the average effective diffusion coefficient used by Wilke negative in the reverse diffusion region.

## CONCLUSIONS

It is clear that in general there are marked qualitative as well as quantitative differences between binary and ternary diffusion. The approximate Equations (57) and (63) show explicitly that in both equimolal diffusion and diffusion of two gases through a third stagnant gas, the usual concept of a driving force,  $(y_{A_1} - y_{A_2})$ , is inapplicable and the rate of transfer of one component is not only a function of its own concentration gradient but is also a function of the concentrations of the other components. This interaction is the cause of the diffusion barriers, reverse diffusion, and osmotic diffusion which are predicted by the more rigorous diffusion equations as well as by the new approximate equations.

How great an effect these results have on mass transfer in operations such as ternary distillation or in the absorption of two gases from a third stagnant gas

depends both on whether an actual region exists in which steady state molecular diffusion controls the transfer rate (i.e., the usual laminar film) and on what percentage of the total resistance to transfer resides in this region if it does exist.

Without going too far astray from the purposes of this paper, one might point out that if a laminar gas film exists at all, even if it is so thin that it would have no over-all effect in binary transfer, it would still stop the transfer of any component which is prevented from diffusing by a diffusion barrier. In other words, if a diffusion barrier exists, then the resistance of the film, no matter how thin it is, is infinite as far as one component is concerned, and the film then completely stops the transfer of this component. Thus a laminar film may be controlling in the usual sense for one component only while the transfer of the other components is controlled by some other resistance in the system.

## NOTATION

The notation for this article appears on Page 203.

## LITERATURE CITED

1. Benedict, Manson, and Arnold Boas, *Chem. Eng. Progr.*, **47**, 51 (1951).
2. Chapman, S., and T. G. Cowling, "Mathematical Theory of Non-Uniform Gases," Cambridge University Press, Cambridge (1939).
3. Cichelli, M. T., W. D. Weatherford, Jr., and J. R. Bowman, *Chem. Eng. Progr.*, **47**, 63 (1951).
4. Curtiss, C. F., and J. O. Hirschfelder, *J. Chem. Phys.*, **17**, 550 (1949).
5. Danckwerts, P. V., *Ind. Eng. Chem.*, **43**, 1460 (1951).
6. ———, *A. I. Ch. E. Journal*, **1**, 456 (1955).
7. Fairbanks, D. F., and C. R. Wilke, *Ind. Eng. Chem.*, **42**, 471 (1950).
8. Hellund, E. J., *Phys. Rev.*, **57**, 737 (1940).
9. *Ibid.*, p. 743.
10. Hoopes, J. W., Jr., Ph.D. thesis, Columbia Univ., New York (1951).
11. Maxwell, J. C., *Scientific Papers*, **2**, p. 57, Dover Publications, Inc., New York (1952).
12. *Ibid.*, p. 625.
13. Pipes, L. A., "Applied Mathematics for Engineers and Physicists," McGraw-Hill Book Company, Inc., New York (1946).
14. Robinson, C. S., and E. R. Gilliland, *Elements of Fractional Distillation*, 2 ed., McGraw-Hill Book Company, Inc., New York (1950).
15. Sherwood, T. K., "Absorption and Extraction," 1 ed., McGraw-Hill Book Company, Inc., New York (1949).
16. Stefan, J., *Sitzber. Akad. Wiss. Wien.*, **63** (Abt. II), 63 (1871).
17. *Ibid.*, **65** (Abt. II), 323 (1872).
18. Whitman, W. G., *Chem. & Met. Eng.*, **29**, 147 (1923).
19. Wilke, C. R., *Chem. Eng. Progr.*, **46**, 95 (1950).

\*See footnote on page 206.

# Simplified Flow Calculations for Tubes and Parallel Plates

R. R. ROTHFUS, D. H. ARCHER, I. C. KLIMAS, and K. G. SIKCHI

Carnegie Institute of Technology, Pittsburgh, Pennsylvania

The effective correlations of turbulent velocities and friction losses for tubes and parallel plates recently published have been analyzed further in order to simplify their use and to extend the range of Reynolds number.

Working diagrams have been developed from which turbulent friction losses and local velocities for tubes and parallel plates can be calculated without interpolation or trial-and-error procedures. Tentative values of parallel-plate friction factors and average-to-maximum velocity ratios in the transition region are also included, and new experimental values of the velocity ratio in smooth tubes are reported. The working diagrams permit more rapid, accurate, and consistent calculations of fluid behavior to be made over a wider range of operating conditions than was previously possible.

Successful use of the concept of hydraulic radius in calculating the friction head associated with turbulent flow in noncircular conduits hinges on the proper choice of an "equivalent" tube with which to compare the noncircular cross section. The most commonly used method is based on the assumption that a tube having the same ratio of cross-sectional area to wetted perimeter as the noncircular conduit is hydrodynamically equivalent to the noncircular configuration when operated at the same bulk average linear velocity with the same fluid.

Since there is much more reliable experimental information available about turbulent phenomena in tubes than in noncircular conduits, it is a practical necessity to base working correlations for the latter on a comparison of the two types of ducts. This fact does not, in itself, detract from utility and accuracy if a truly equivalent tube can be found. The results of recent experimental investigations of pressure drop and velocity distribution in annuli (3, 9, 10) have indicated, however, that the tube postulated in the usual hydraulic-radius concept is not the correct one, although its use often yields a good approximation to the actual friction head. It is therefore reasonable to believe that the hydraulic-radius method is based on an empiricism which in many cases is not far removed from the true situation.

In a recent article Rothfus and Monrad (8) presented correlations of pressure drop and velocity distribution in fluids flowing in turbulent motion between

parallel flat plates. Their method involves the concept of an equivalent tube somewhat different from the one used in the method of hydraulic radius. The notable data of Sage and associates (1, 6, 7) show the new correlations to be effective for both pressure drop and velocity distribution. The equivalent tube used by Rothfus and Monrad is consistent with viscous-flow theory and appears to have some general significance in the handling of flow through noncircular ducts.

In order to use the new parallel-plate correlations for the prediction of friction losses and local velocities, it is necessary to perform a number of intermediate calculations which are troublesome and time consuming. This paper presents the Rothfus and Monrad correlations in a readily usable form, based on the best experimental data available, in which the intermediate calculations are implicit. To this end, some additional experimental values of the ratio of average-to-maximum velocity in smooth tubes are also presented.

## BASIS FOR PARALLEL-PLATE CORRELATIONS

In truly viscous motion the velocity profile in a fluid of constant density flowing steadily and isothermally between two smooth, parallel, infinite, flat plates is a parabola. The same is true for similar flow in a smooth tube. Rothfus and Monrad have shown that the local velocities in the two types of conduits must be coincident if

1. The radius  $r_0$  of the tube is equal to the half clearance  $b$  of the plates
2. The fluids have the same kinematic viscosity in each case

3. The friction velocity  $\tau_{0g}/\rho$  in the tube is equal to the friction velocity between the parallel plates.

The latter stipulation is equivalent to stating that the maximum (center-line) local velocities must be equal.

Rothfus and Monrad postulated that the same behavior might occur under comparable conditions in fully turbulent flow. On this basis they concluded that the friction velocity parameters as well as the friction distance parameters were the same in the two conduits at the same distance from the wall; that is,

$$(u^+)_p = (u^+)_F \quad (1)$$

and

$$(y^+)_p = (y^+)_F \quad (2)$$

whenever  $\tau_0 = b$ ,  $(\mu/\rho)_p = (\mu/\rho)_F$ , and  $(\sqrt{\tau_{0g}/\rho})_p = (\sqrt{\tau_{0g}/\rho})_F$ . Also, in view of the restrictions placed on the densities and skin frictions, the Fanning friction factors were observed to be related through the equation

$$\frac{\sqrt{f_F}}{\sqrt{f_p}} = \frac{(V/u_m)_p}{(V/u_m)_F} \quad (3)$$

Finally, the Reynolds numbers defined in the usual manner as  $(N_{Re})_F = 4bV_F\rho/\mu$  and  $(N_{Re})_p = 2r_0V_p\rho/\mu$  were found to be related through the equation

$$\frac{(N_{Re})_F}{(N_{Re})_p} = \frac{2(V/u_m)_F}{(V/u_m)_p} \quad (4)$$

It is apparent that if the Reynolds number for the parallel-plate case under consideration is known, the Reynolds

I. C. Klimas is at present with Columbia-Southern Chemical Corporation, Natrium, West Virginia.

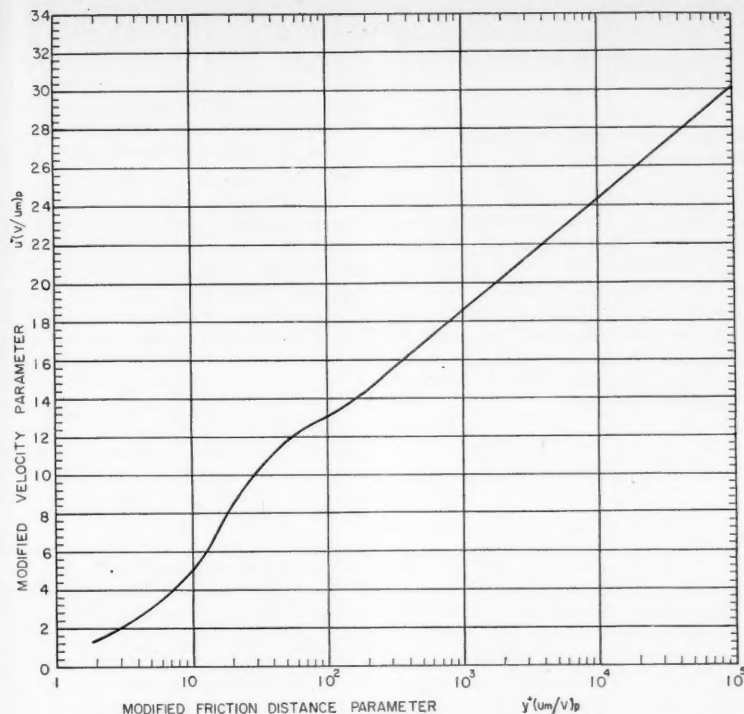


Fig. 1. Correlation of mean local velocities for steady, isothermal, turbulent flow in smooth tubes and between smooth, parallel, flat plates.

number at which the equivalent tube must be operated can be obtained from Equation (4) provided that the relationship between  $(V/u_m)$  and Reynolds number is available for each conduit. The friction factor for the tube is then obtained in the usual way at the tube Reynolds number and the friction factor for the parallel-plate case is calculated by means of Equation (3). The pressure drop

TABLE 1		$U^+$			
$Y^+$	From	Deissler (tubes)		Sage (parallel plates)	
		Min.	Max.	Min.	Max.
	Fig. 1				
2	1.4	1.5	1.5		
4	2.6	2.3	2.9	2.0	2.5
6	3.4	3.3	4.0	3.1	3.7
10	5.1	4.9	5.6	4.7	5.9
20	8.4	8.1	9.1	8.2	8.9
40	11.1	10.4	11.1	10.1	11.0
60	12.1	11.3	12.3	11.6	12.2
100	13.1	12.5	13.4	12.7	13.4
200	14.4	13.8	14.8	14.0	14.5
400	16.2	16.2	17.1	15.4	16.2
600	17.2	16.9	17.5	16.8	17.3
1,000	18.7	18.5	19.1		
2,000	20.3	20.3	21.0		

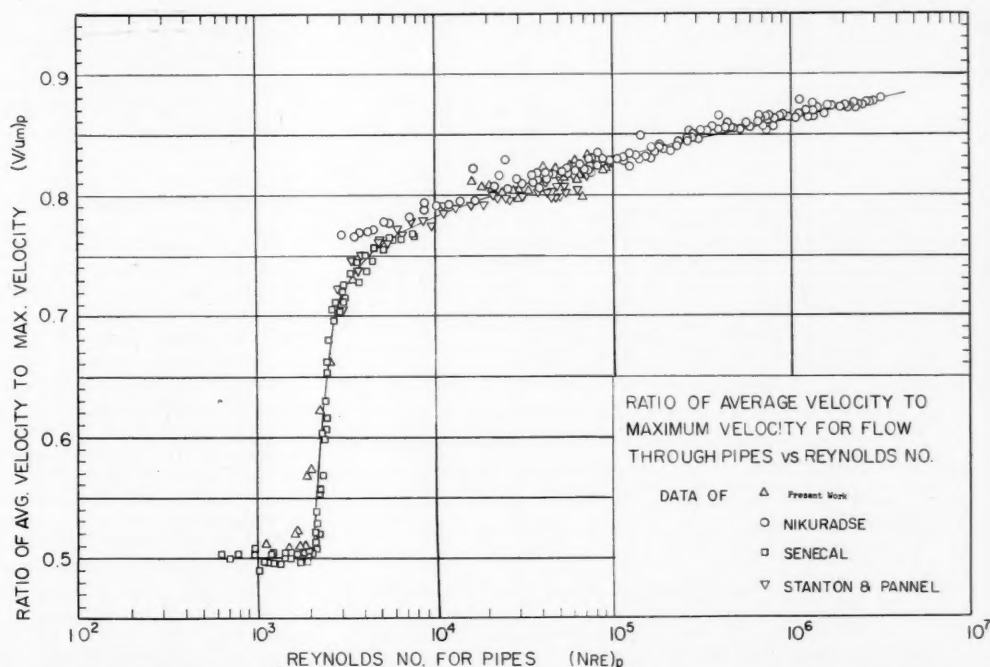


Fig. 2. Effect of Reynolds number on the ratio of bulk average to maximum velocity in smooth tubes.

due to friction can immediately be calculated from the Fanning equation written in terms of the clearance,  $2b$ , between the plates, namely

$$(\Delta p)_F = \frac{f_F \rho V_F^2 L}{g_0(2b)} \quad (5)$$

If it is desired to obtain a value of the local velocity at some point in the stream, the friction velocity can be calculated by means of the equation

$$(u_*)_F = V_F \sqrt{f_F/2} \quad (6)$$

and the values of  $(y^+)_F$  and  $(u^+)_F$  can be read directly from the  $u^+$ ,  $y^+$  correlation for smooth tubes, as indicated in Equations (1) and (2).

Unfortunately, two factors contribute to the difficulty of the calculations. In the first place, Equation (4) must be solved by means of trial and error if only the usual graph of  $(V/u_m)_p$  against  $(N_{Re})_p$  is available. In the second place, the  $u^+$ ,  $y^+$  relationship for smooth tubes is not unique but varies considerably with Reynolds number. This makes it necessary in some cases to perform a difficult interpolation.

The calculation of pressure-drop and velocity distribution can be simplified a great deal if the following diagrams are made available:

1. An accurate velocity correlation which does not require interpolation
2. Accurate values of the friction factor for parallel plates as a function of the Reynolds number for parallel plates.

In addition, it is sometimes convenient to have a working graph of the velocity ratio  $(V/u_m)_F$  against the Reynolds number for parallel plates.

#### VELOCITY DISTRIBUTIONS FOR TUBES AND PARALLEL PLATES

Rothfus and Monrad have shown that the effect of Reynolds number can effectively be removed from the ordinary  $u^+$ ,  $y^+$  correlation for smooth tubes by empirical means. They have observed that a unique correlation can be obtained when the coordinates are modified to account for the change of  $(V/u_m)$  ratio with Reynolds number. Their modified coordinates are simply

$$U^+ = u^+ \left( \frac{V}{u_m} \right)_p = \frac{u}{u_*} \left( \frac{V}{u_m} \right)_p \quad (7)$$

and

$$Y^+ = y^+ \left( \frac{u_m}{V} \right)_p = \frac{y u_* \rho}{\mu} \left( \frac{u_m}{V} \right)_p \quad (8)$$

It follows from Equations (1) and (2) that the modified correlation must be equally valid for both tubes and parallel plates if the velocity profiles are actually coincident, as originally postulated. It should be noted that the  $(V/u_m)_p$  term in the modified coordinates is that for the equivalent tube at the tube Reynolds number, since in view of Equations (1) and (2) the same correction must be made whether the tube case or parallel-plate case is being calculated.

As originally presented, the modified velocity correlation was based on the

data of Nikuradse (5) and of Senecal and Rothfus (11) for the most part. Relatively few of the data were in the range of low  $Y^+$  values (i.e., close to the tube wall), however; so there was considerable uncertainty attached to the portion of the experimental curve lying below a  $Y^+$  of 30.

The extensive data of Deissler (2) have since been found to form a unique curve on  $U^+$ ,  $Y^+$  coordinates in the questionable range of  $Y^+$  values. The resultant correlation, based on all the cited data for smooth tubes, is shown in Figure 1. The data of Sage and associates (1, 6, 7) on velocity distributions between parallel plates are in close agreement with Deissler's tube data as shown in Table 1.

Figure 1 is therefore equally applicable to both smooth tubes and smooth parallel plates and adequately represents the best available experimental data in each case. Its use is limited to the range of fully turbulent motion. On the basis of current information, it appears that the modified correlation is valid at Reynolds numbers greater than 3,000 for tubes and greater than 7,000 for parallel plates. It should be noted that the velocity curve cannot retain its unique character all the way to the tube wall, for viscous-flow theory predicts that  $U^+$  must equal  $[(V/u_m)_p^2 Y^+ (1 - y/2r_0)]$  in the laminar film adjacent to the solid surface.

The supporting data for tubes fully cover the Reynolds-number range from 3,000 to 3,240,000. Their average deviation from the curve shown in Figure 1 is essentially independent of the Reynolds number. The supporting data for parallel plates cover Reynolds numbers from 6,960 to 53,200. It appears reasonable, however, to predict that Figure 1 can be used for parallel plates up to Reynolds numbers of about ten million without appreciable error.

#### VELOCITY RATIOS IN TUBES

It is obvious that the modified velocity correlation requires accurate knowledge of the ratio of average to maximum velocity in smooth tubes over the entire turbulent range. The ratio is implicit in the correlation, of course, since integration of the velocity profile at any given Reynolds number must yield a consistent value of the bulk average velocity. The region near the tube wall, however, is a difficult one in which to obtain accurate measurements of the local velocity. Unfortunately, this region substantially influences the values of the bulk average velocity obtained by means of integration. Consequently, the average velocities obtained from experimental velocity profiles are often from 1 to 4% higher than those measured directly by means of flow-metering devices. In addition, there is an abundance of directly measured data in the literature on which a

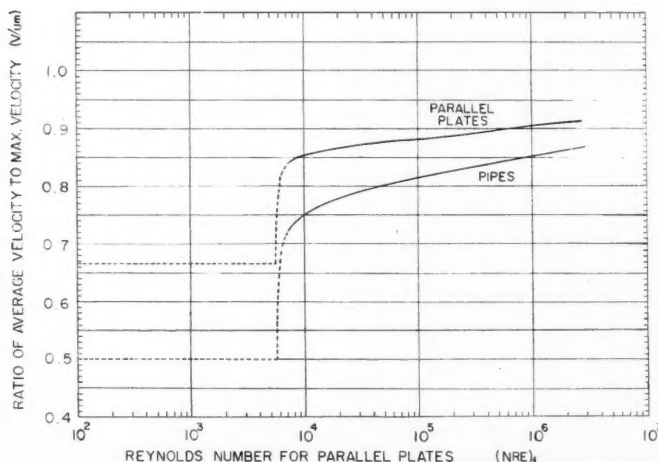


Fig. 3. Velocity ratios for parallel plates and "equivalent" smooth tubes as functions of the parallel-plate Reynolds number.



correlation of  $(V/u_m)_p$  as a function of Reynolds number can be based.

Taken together, the data of Nikuradse (5), Stanton and Pannell (12), and Senecal and Rothfus (11) furnish experimental values of  $(V/u_m)_p$  over the entire range of Reynolds numbers from 600 to 3,240,000. The viscous, transition, and turbulent regimes are therefore included and a complete picture of the effect of Reynolds number is available. There is only one portion of the flow range in which the data are inconsistent. At Reynolds numbers between 4,000 and 100,000 Nikuradse's values are significantly higher than those of Stanton and Pannell. Inconsistencies in Nikuradse's local velocity data in the lower turbulent region lend the impression that the Stanton and Pannell data are more reliable below a Reynolds number of, say, 50,000. This view is supported by the fact that the latter data agree with Senecal's data in the low turbulent region where the two overlap. On the other hand, Stanton's data terminate at a Reynolds number of about 100,000 and cannot be extrapolated to agreement with Nikuradse's high Reynolds-number values.

In order to reconcile the differences, experimental values of  $(V/u_m)_p$  have been obtained at Reynolds numbers between 20,000 and 100,000 in a brass tube having an inside diameter of 1.00 in. The test fluid was water at room temperature. The bulk average velocity was obtained by means of a calibrated orifice meter. The maximum local velocity was measured by means of an impact tube made from hypodermic tubing having an outside diameter of 0.042 in. It was found that the data thus obtained formed a satisfactory connection between the low Reynolds-number data of Stanton and Pannell and the high Reynolds-number data of Nikuradse.

Figure 2 summarizes the effect of Reynolds number on the ratio of average to maximum velocity in smooth tubes. The solid line indicates the recommended values of  $(V/u_m)_p$  to be used in conjunction with the velocity correlation shown in Figure 1. In order to present the complete correlation on the same set of coordinates, the recommended line has been extended through the transition region. It should be remembered, however, that Figure 1 is valid only at Reynolds numbers greater than 3,000.

#### VELOCITY RATIOS BETWEEN PARALLEL PLATES

In order to apply the velocity correlation shown in Figure 1 to flow between smooth parallel plates, it is necessary to determine the Reynolds number in the equivalent tube. The reason for this stems directly from the fact that  $(V/u_m)_p$  must be evaluated at the tube Reynolds number. It would therefore prove con-

venient to have available a diagram showing  $(V/u_m)_p$  as a function of the parallel-plate Reynolds number since the latter is usually a known starting point for velocity computations.

Since the velocity profiles for the tube and parallel plates are coincident at the conditions under which the comparison is made, it is possible to develop the relationship between the tube and parallel-plate Reynolds numbers in the following manner.

By definition,

$$V_p = 2 \int_0^1 u_p \left(1 - \frac{y}{r_0}\right) d\left(\frac{y}{r_0}\right) \quad (9)$$

and

$$\begin{aligned} V_F &= \int_0^1 u_F d\left(\frac{y}{b}\right) \\ &= \int_0^1 u_F d\left(\frac{y}{r_0}\right) \end{aligned} \quad (10)$$

Therefore

$$\begin{aligned} (N_{Re})_p &= \frac{4r_0\rho}{\mu} \int_0^1 u_p d\left(\frac{y}{r_0}\right) \\ &\quad - \frac{4r_0\rho}{\mu} \int_0^1 u_p \left(\frac{y}{r_0}\right) d\left(\frac{y}{r_0}\right) \end{aligned} \quad (11)$$

and similarly,

$$(N_{Re})_F = \frac{4r_0\rho}{\mu} \int_0^1 u_F d\left(\frac{y}{r_0}\right) \quad (12)$$

But the velocity profiles are coincident, and so the local velocity  $u_p$  is equal to the local velocity  $u_F$ . Consequently

$$\begin{aligned} (N_{Re})_F &= (N_{Re})_p \\ &\quad + \frac{4r_0\rho}{\mu} \int_0^1 u_p \left(\frac{y}{r_0}\right) d\left(\frac{y}{r_0}\right) \end{aligned} \quad (13)$$

The last equation can be combined with Equations (7) and (8) to yield an expression for the Reynolds-number relationship in terms of the modified friction velocity parameter and friction distance parameter, namely

$$\begin{aligned} (N_{Re})_F &= (N_{Re})_p \\ &\quad + \frac{4}{Y_m^+} \int_0^{Y_m^+} U^+ Y^+ dY^+ \end{aligned} \quad (14)$$

where  $Y_m^+$  is the maximum (or center-line) value of the modified friction distance parameter.

The integration indicated in Equation (14) has been performed by means of Simpson's rule. In the fully turbulent range corresponding values of  $U^+$  and  $Y^+$  were taken from Figure 1. The velocity ratio  $(V/u_m)_p$  was obtained from Figure 2. Fanning friction factors  $f_p$  were evaluated by means of Koo's equation for smooth tubes (4).

Almost nothing is known about the transition behavior of fluids flowing between parallel plates. On the other hand, the velocity distribution and friction data of Senecal and Rothfus cover the transition range for smooth tubes. Since the method of comparing tubes and parallel plates suggested by Rothfus and Monrad appears to be equally valid for viscous and fully turbulent flow, it might be reasonable to postulate its validity in the transition range as well.

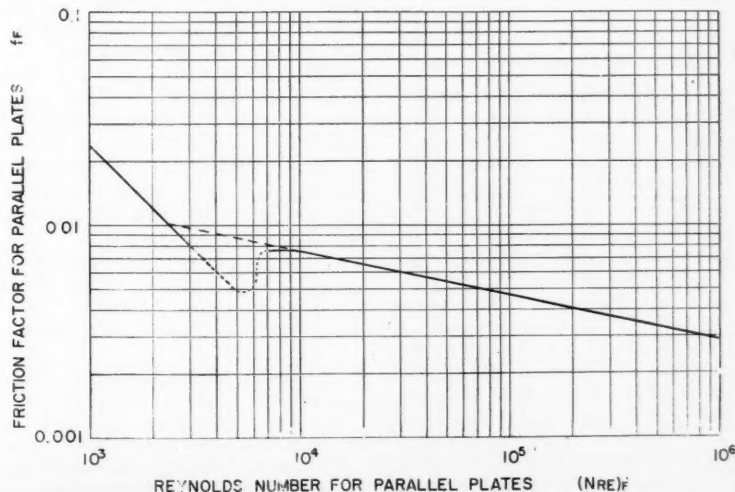


Fig. 4. Effect of Reynolds number on the Fanning friction factor for parallel plates.

It is recognized that such an assumption must be considered highly tentative, subject to future experimental investigation. On this basis the velocity data of Senecal and Rothfus have been integrated as indicated in Equation (14). Friction factors were obtained from their friction data in the transition range and  $(V/u_m)_p$  values were again taken from Figure 2.

The resultant diagram of  $(V/u_m)_p$  against the parallel-plate Reynolds number is shown in Figure 3. The transition relationship is shown as a dashed line to emphasize its tentative nature. In the fully turbulent region, the values of  $(V/u_m)_p$  to be used in conjunction with Figure 1 can be read directly at the parallel-plate Reynolds number.

It is sometimes convenient to have a diagram of  $(V/u_m)_F$  against  $(N_{Re})_F$  immediately available. Such a curve is also included in Figure 3. It was obtained through combination of Equations 4 and 14 into the expression

$$\left(\frac{V}{u_m}\right)_F = \frac{1}{2} \left(\frac{V}{u_m}\right)_p + \frac{\sqrt{f_p/2}}{(Y_m^+)^2} \cdot \int_0^{Y_m^+} U^+ Y^+ dY^+ \quad (15)$$

from which  $(V/u_m)_F$  was calculated at various tube Reynolds numbers. The transition range has been treated in the manner previously described, and the resultant relationship is shown as the dashed portion of the curve.

Both curves in Figure 3 are made consistent with theory in the viscous-flow range. Senecal's data indicate that the ratio of average to maximum velocity in smooth tubes deviates negligibly from the viscous-range value of 0.500 at Reynolds numbers below 2,100. Since the theoretical value of  $(V/u_m)_F$  is 0.667 in the viscous range, Equation (4) suggests that this value should be maintained up to a Reynolds number of 5,600 in the parallel-plate case.

#### FRICTION FACTORS FOR PARALLEL PLATES

The Fanning friction factors for parallel plates have been calculated by means of Equation (3) and are presented as functions of the parallel-plate Reynolds number in Figure 4. The indicated values are based on velocity ratios from Figure 3, Koo's friction factor equation in the turbulent range, and Senecal's friction data in the transition range. The theoretical value of  $24/(N_{Re})_F$  is shown in the viscous region. The transition range is again indicated by a dashed line since the validity of Equation (3) in this region has been assumed without supporting data. A few experimental points have been obtained in rectangular ducts (13) and these lie within the triangular area bounded by the transition curve and the extension of the turbulent line.

The transition region appears to extend upward to a Reynolds number of about 7,000. The same upper limit has been found to exist at the outer walls of annuli by Rothfus, Monrad, Sikchi, and Heideger (10).

#### USE OF THE CORRELATIONS

Figures 1 through 4 afford accurate and consistent means by which to calculate friction losses and local velocities associated with isothermal turbulent flow in smooth tubes and between smooth parallel plates. The correlations can be used directly without any necessity for intermediate calculations involving trial-and-error procedures.

If it is desired to calculate the pressure drop caused by fluid friction between parallel plates, the friction factor obtained from Figure 4 at the parallel-plate Reynolds number can be inserted directly into Equation (5). If the local velocity at some point between the plates is desired, the proper value of  $(V/u_m)_p$  can be read from Figure 3 at the parallel-plate Reynolds number. Figure 1 can then be used in conjunction with the friction factor from Figure 4 to obtain the desired velocity. If a local velocity within a smooth tube is to be calculated,  $(V/u_m)_p$  can be obtained from Figure 2 and the velocity can be determined by means of Figure 1 and appropriate friction factors.

Although tentative values of the friction factor and velocity ratio for parallel plates are presented in the transition range, such values must be used with caution until experimental data are made available.

Since  $(V/u_m)_p$  varies only from 0.80 at a Reynolds number of 25,000 to 0.88 at a Reynolds number of 3,000,000, it is apparent that the Reynolds-number effect on the unmodified  $u^+$ ,  $y^+$  diagram is very small in the higher turbulent range. The modified correlation is therefore most useful at Reynolds numbers between 3,000 and 25,000 where the main-stream velocity profile is appreciably affected by the Reynolds number. If it is desired to obtain local velocities close to the wall at high Reynolds numbers, however, the modified correlation affords a reasonable means of extrapolating main-stream data into the wall region where no reliable experimental information is available at such Reynolds numbers.

#### NOTATION

- $b$  = half clearance between parallel plates, ft.  
 $f$  = Fanning friction factor  $[= (2R_H \Delta p g_0) / (\rho V^2 L)]$ , dimensionless  
 $g_0$  = conversion factor = 32.2 (lb.mass)(ft.)/(lb.force)(sec.)(sec.)  
 $L$  = length of conduit over which  $\Delta p$  is measured, ft.

- $N_{Re}$  = Reynolds number  $(= 4R_H V \rho / \mu)$ , dimensionless  
 $\Delta p$  = pressure drop caused by fluid friction, lb. force/sq. ft.  
 $r_0$  = radius of experimental or "equivalent" tube, ft.  
 $R_H$  = hydraulic radius  $(= r_0/2$  for tubes and  $= b$  for parallel plates), ft.  
 $u$  = local fluid velocity, ft./sec.  
 $u_m$  = maximum local fluid velocity, ft./sec.  
 $u_*$  = friction velocity  $(= \sqrt{\tau_0 g_0 / \rho} = V \sqrt{f/2})$ , ft./sec.  
 $u^+$  = friction velocity parameter  $(= u/u_*)$ , dimensionless  
 $U^+$  = modified friction velocity parameter defined by Equation (7), dimensionless  
 $V$  = bulk average linear velocity, ft./sec.  
 $y$  = distance from the conduit wall at which the local velocity  $u$  is measured, ft.  
 $y^+$  = friction distance parameter  $(= y u_* / \mu)$ , dimensionless  
 $Y^+$  = modified friction distance parameter defined by Equation (8), dimensionless  
 $Y_m^+$  = maximum value of the friction distance parameter, dimensionless  
 $\mu$  = fluid viscosity, lb. mass/(sec.)(ft.)  
 $\rho$  = fluid density, lb. mass/cu. ft.  
 $\tau_0$  = skin friction at the conduit wall, lb. force/sq. ft.

#### Subscripts

- $F$  = flow between parallel plates  
 $p$  = flow in tubes

#### LITERATURE CITED

- Corcoran, W. H., F. Page, Jr., W. G. Schlinger, and B. H. Sage, *Ind. Eng. Chem.*, **44**, 410 (1952).
- Deissler, R. G., *Trans. Am. Soc. Mech. Engrs.*, **73**, 101 (1951).
- Knudsen, J. G., and D. L. Katz, *Proc. Midwestern Conf. on Fluid Dynamics, 1st Conf.*, No. 2, 175 (1950).
- McAdams, W. H., "Heat Transmission," 3 ed., p. 155, McGraw-Hill Book Company, Inc., New York (1954).
- Nikuradse, J., *V.D.I.-Forschungsheft*, **356**, 1 (1932).
- Page, F., Jr., W. H. Corcoran, W. G. Schlinger, and B. H. Sage, *Ind. Eng. Chem.*, **44**, 419 (1952).
- Page, F., Jr., W. G. Schlinger, D. K. Breaux, and B. H. Sage, *ibid.*, p. 424.
- Rothfus, R. R., and C. C. Monrad, *ibid.*, **47**, 1144 (1955).
- Rothfus, R. R., C. C. Monrad, and V. E. Senecal, *ibid.*, **42**, 2511 (1950).
- Rothfus, R. R., C. C. Monrad, K. G. Sikchi, and W. J. Heideger, *ibid.*, **47**, 913 (1955).
- Senecal, V. E., and R. R. Rothfus, *Chem. Eng. Progr.*, **49**, 533 (1953).
- Stanton, T. E., and J. R. Pannell, *Trans. Roy. Soc. (London)*, **A214**, 199 (1914).
- Washington, Lawrence and W. M. Marks, *Ind. Eng. Chem.*, **29**, 337 (1937).

# Separation of Liquids by Thermal Diffusion

JOHN E. POWERS and C. R. WILKE

University of California, Berkeley, California

Data were obtained in flat-plate continuous-flow thermogravitational columns to check the theory developed by Furry, Jones, and Onsager and a modification of this theory proposed by the authors. Separations of ethyl alcohol-water and benzene-*n*-heptane mixtures were measured, flow rate, column length, temperature difference, spacing between plates, and inclination of the plates being varied in the experiments. Theory and data are in qualitative agreement for the range of variables studied. Quantitative agreement exists between theory and experiment in the region of practical design for liquid-thermal-diffusion plants.

Equations to aid in the design of thermal-diffusion plants are developed, and a plant to treat 1,000 bbl./day of a liquid aromatic-aliphatic mixture is designed and costs are estimated.

During the past quarter century the need for new separation methods, particularly for commercial application, has given strong impetus to the investigation of irreversible processes. For example, most of the work on irreversible processes involving nonisothermal-solution behavior has been reported in the past several decades, although this effect was first noted almost one hundred years ago.

Nonisothermal solution behavior has two manifestations, one the inverse of the other. If two gases of different composition and initially at the same temperature are allowed to diffuse together, a transient temperature gradient results from the ordinary diffusion process. This phenomenon was first noted by Dufour (4) in 1873, and bears his name. Conversely, if a temperature gradient is applied to a homogeneous solution, a concentration gradient is usually established. The name *thermal diffusion* (or *thermodiffusion*) is generally applied to this second effect.

Obviously only the nonisothermal-solution phenomena relating to thermal diffusion can be used for the separation of solutions, as the Dufour effect is the result of a mixing process. Two methods of utilizing thermal diffusion for the separation of solutions have been proposed. In the static method the thermal gradient is established in such a manner that convection is eliminated and there is no bulk flow. When applied to liquid or solid solutions the static method is called the Ludwig-Soret, or the Soret, effect. No special name has been given to the phenomenon in gases. The extent of the separation obtainable by the static method is generally very slight. The thermogravitational method multiplies the separation achieved in the static method by utilizing convection currents

to produce a cascading effect. The apparatus that is used to produce the cascading effect is called a *thermogravitational* column or, commonly, a Clusius-Dickel column (3). Thermogravitational columns have been used to bring about separations in both gas and liquid solutions and have been operated in both batch (not to be confused with static) and continuous manners. The terms *continuous* and *batch* indicate, respectively, the presence or absence of a net bulk flow through the thermogravitational column.

Numerous reviews on thermal diffusion are available (1, 5, 10). The diversity of nationality represented by these publications attests to the widespread attention given to the subject. Several of these reviews merit particular discussion.

DeGroot (5) has presented a very comprehensive study of thermal diffusion in condensed phases (liquids and solids). His review of the theories that have been applied to the fundamental problem of the Soret effect is excellent, although he recognizes that these theories have met with very limited success, an article by Jones and Furry (10), which contains a resume of the theories and experimental work published before 1946, is especially noteworthy because of its excellent summary of column theory. Theoretical treatments of hot-wire, concentric-cylinder, and flat-plate columns are included, and the transient and steady state behavior of batch columns with and without reservoirs are discussed. The results obtained from the theoretical treatment of a batch column are extended to continuous-flow apparatus, and both single- and multistage processes are considered. The authors point out that the equations developed by Furry, Jones, and Onsager (7) for gas separations are equally applicable to the treatment of liquids.

Continuous-flow thermogravitational columns would most certainly be used

in any large-scale commercial application of thermal diffusion. The equations for such columns reviewed by Jones and Furry incorporate a large number of assumptions and yet no critical comparison of theory and experimental data has appeared in the literature. It is the purpose of this study to compare theory with experimental data on continuous-flow columns and to improve on the theory where possible.

## COLUMN THEORY

The temperature gradient applied between the plates of a thermogravitational column has two effects: (1) a flux of one component of the solution relative to the other (or others) is brought about by thermal diffusion, and (2) convective currents are produced parallel to the plates owing to density differences. The combined result of these two effects is to produce a concentration difference between the two ends of the column which is generally much greater than that obtainable by the static method. Figure 1 illustrates the flows and fluxes prevailing in a continuous-flow column.

In an ideal column a temperature gradient exists only in the direction normal to the plates. The flux of component 1 due to thermal diffusion,  $J_{x-TD}$ , is given by (10)

$$J_{x-TD} = \frac{\alpha D}{T} C_1 C_2 \frac{dT}{dx} \quad (1)$$

The choice of sign is arbitrary and is taken as positive in order to be consistent with the notation of Jones and Furry (10). Equation (1) was developed to represent the behavior of isotopic gas mixtures. In this case  $\alpha$  is essentially independent of temperature, pressure, and composition. Although nonisotopic liquid solutions may bear little resemblance to isotopic mixtures of gases,

J. E. Powers is at present at The University of Oklahoma, Norman, Oklahoma.

Equation (1) can be used to define the thermal-diffusion constant  $\alpha$  for liquids.

The concentration gradient produced by the combined effects of thermal diffusion and convection acts to oppose thermal diffusion and limits the separation. By combining the thermal-diffusion flux with simultaneously acting fluxes due to ordinary diffusion and convective flow the general differential equation applicable to any point in the column may be formulated:

$$\frac{\partial C_1}{\partial t} = D \left[ \frac{\partial^2 C_1}{\partial x^2} + \frac{\partial^2 C_1}{\partial y^2} \right] - \frac{\alpha D}{T} \frac{dT}{dx} \frac{\partial(C_1 C_2)}{\partial x} - v(x) \frac{\partial C_1}{\partial y} \quad (2)$$

Only the steady state solution of this equation ( $\partial C_1 / \partial t = 0$ ) is considered in this article.

The net flow due to thermal diffusion and ordinary diffusion must be zero at both walls. Therefore a solution to Equation (2) must be found subject to the boundary conditions

$$-D \frac{\partial C_1}{\partial x} + \frac{\alpha D}{T} C_1 C_2 \frac{dT}{dx} = 0 \quad (3)$$

at  $x = \pm \omega$

In addition to the conditions expressed in Equation (3), a solution to Equation (2) must satisfy material balances made around any section of the column. Equation (4) represents a material balance made around the end of the enriching section.

$$\sigma_e C_e = +B_e \int_{-\omega}^{+\omega} \rho C_1 v(x) dx - B_e \int_{-\omega}^{+\omega} \rho D \frac{\partial C_1}{\partial y} dy \quad (4)$$

Equation (5) expresses a similar condition existing in the stripping section:

$$-\sigma_s C_s = +B_s \int_{-\omega}^{+\omega} \rho C_1 v(x) dx - B_s \int_{-\omega}^{+\omega} \rho D \frac{\partial C_1}{\partial y} dy \quad (5)$$

The velocity distribution  $v(x)$  appearing in Equations (2), (4), and (5) is determined by applying the Navier-Stokes relations for laminar flow. For the enriching section:

$$v(x) = \frac{\beta_T g \cos \theta \Delta T}{12 \omega \eta} (\omega^2 x - x^3) + \frac{3}{4} \frac{\sigma_e}{B_e \rho \omega^3} (\omega^2 - x^2) \quad (6)$$

In obtaining a solution to these equations for a batch column ( $\sigma_e = \sigma_s = 0$ ) Furry, Jones, and Onsager (7) assumed  $\partial C / \partial y$  in Equations (2), (4), and (5) to

be independent of  $x$ . (For a complete listing of the assumptions see reference 14.) Based on this assumption the following relation was obtained:

$$q = \exp \left[ \frac{H^{(0)} L_T}{K^{(0)}} \right] \quad (7)$$

$$H^{(0)} = \frac{\alpha \beta_T \rho g \cos \theta (2\omega)^3 B_e (\Delta T)^2}{6! \eta T} \quad (7a)$$

$$K^{(0)} = K_e^{(0)} + K_d \quad (7b)$$

$$K_e^{(0)} = \frac{\beta_T^2 \rho g^2 \cos^2 \theta (2\omega)^7 B (\Delta T)^2}{9! D \eta^2} \quad (7c)$$

$$K_d = 2\omega D B_e \rho \quad (7d)$$

The assumption that  $\partial C / \partial y$  is independent of  $x$  is incompatible with the boundary conditions, Equation (3), in the case of a continuous-flow column. To obtain a solution for this case it was necessary (7) to set  $\sigma_e = 0$  in Equation (6) but not in Equation (4). For these conditions Jones and Furry (10) list a general solution and a number of restricted solutions. For the conditions of this experimental investigation, namely,

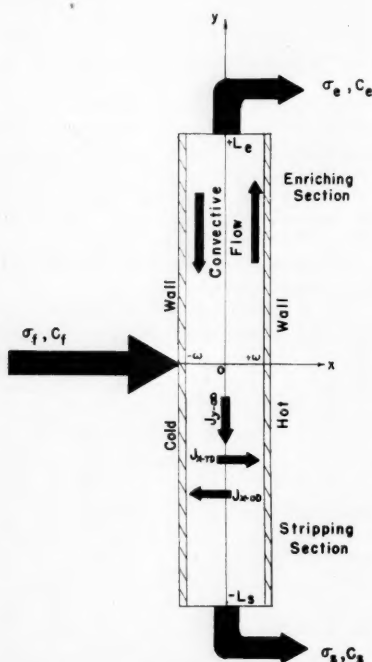


Fig. 1. Schematic diagram of a continuous-flow thermogravitational column.

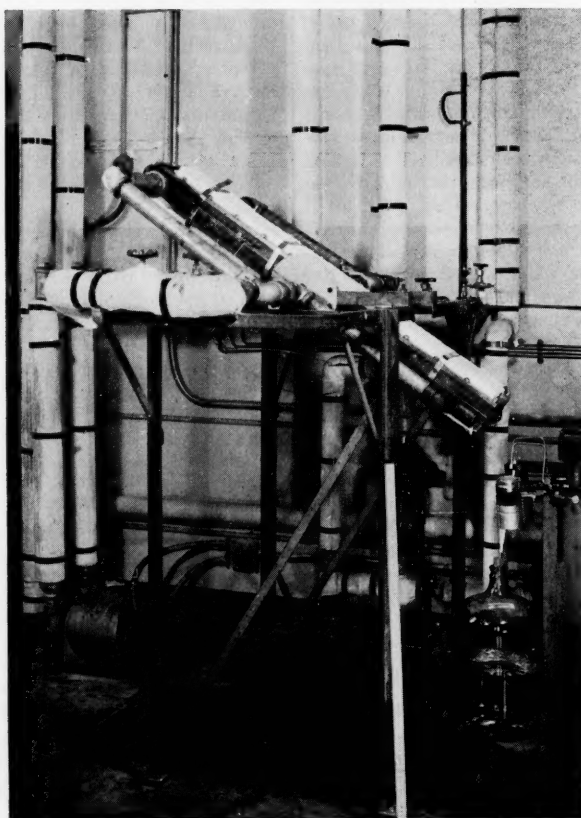


Fig. 2. Thermogravitational column (4 ft.) at an angle of 45 deg.



$$C_1 C_2 = \cong 0.25; \text{ i.e., } 0.7 > C_1 > 0.3$$

$$\sigma_e = \sigma_s = \sigma$$

$$L_e = L_s = L_T/2$$

$$B_e = B_s$$

the solution for a continuous-flow column is\*

$$\Delta = C_e - C_s$$

$$= \frac{H^{(0)}}{2\sigma} \left( 1 - \exp \frac{-\sigma L_T}{2K^{(0)}} \right) \quad (8)$$

In an attempt to improve on the equations for the continuous-flow thermogravitational column, it was assumed in the course of this work that  $\partial C/\partial y$  was not independent of  $x$  but varied linearly; i.e.,

$$\partial C/\partial y = (1 + \gamma x)\psi(y) \quad (9)$$

This assumption made it possible to include the bulk-flow-rate term in Equations (4) and (6) and to satisfy the boundary conditions imposed by Equation (3). Completing the derivation yields an equation similar to (8):

$$\Delta = \frac{H}{2\sigma} \left( 1 - \exp \frac{-\sigma L_T}{2K} \right) \quad (10)$$

where

$$H = H^{(0)}h(\omega\gamma) \quad (11)$$

$$h(\omega\gamma) = 1 - 18 \quad (12)$$

$$\sum_{\lambda=0}^{\infty} \frac{(\omega\gamma)^{2\lambda}}{(2\lambda-1)(2\lambda+1)(2\lambda+3)(2\lambda+5)}$$

$$K = K_e^{(0)}k(\omega\gamma) + K_d \quad (13)$$

\*More generally over any interval for which  $C_1 C_2$  can be assumed constant at  $C_1 C_2$ ,

$$\Delta = \frac{2C_1 C_2 H^{(0)}}{\sigma} \left( 1 - \exp \frac{-\sigma L_T}{2K^{(0)}} \right)$$

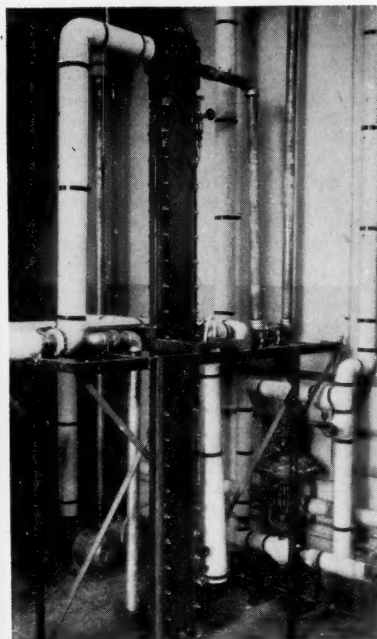


Fig. 3. Thermogravitational column (8 ft.) in the vertical position.

TABLE 1. SEPARATION AND FLOW-RATE MEASUREMENTS FOR THE SYSTEM ETHYL ALCOHOL-WATER

	$\sigma_e$	$\sigma_s$	$\sigma$	$C_e$	$C_s$	$\Delta$	$\Delta T$
	Flow rate, g./min.			Composition, weight fraction EtOH			
Experiment and group	Top product	Bottom product	$(\sigma_e + \sigma_s)/2$ , g./min.	Top product	Bottom product	$C_e - C_s$ , weight fraction EtOH	Temp. diff., °C.
94-Q	10.55	9.5	10.025	0.3982	0.3913	0.0069	35.4
102-R	9.95	9.9	9.9	0.4026	0.3910	0.0116	36.4
111-S	1.71	1.47	1.59	0.4090	0.3851	0.0239	35.7
134-W	13.55	14.3	13.9	0.3986	0.3982	0.0004	36.2
139-X	0.853	0.814	0.834	0.4087	0.3893	0.0194	18.0

TABLE 2. SEPARATION AND FLOW-RATE MEASUREMENTS FOR THE SYSTEM *n*-HEPTANE-BENZENE

	$\sigma_e$	$\sigma_s$	$\sigma$	$C_e$	$C_s$	$\Delta$	$\Delta T$
	Flow rate, g./min.			Composition, mole fraction $nC_7$			
Experiment and group	Top product	Bottom product	$(\sigma_e + \sigma_s)/2$ , g./min.	Top product	Bottom product	$C_e - C_s$ , Mole fraction $nC_7$	Temp. diff., °C.
177-BA	2.03	1.90	1.96	0.528	0.461	0.067	38.9
178-BA	1.37	1.04	1.20	0.529	0.456	0.073	38.9
186-BB	1.45	1.90	1.67	0.531	0.482	0.049	42.2
187-BB	8.7	9.2	8.95	0.522	0.487	0.035	42.2
193-BC	9.5	9.9	9.7	0.511	0.490	0.021	43.7
194-BC	1.9	1.8	1.85	0.549	0.452	0.097	43.2

$$k(\omega\gamma) = 1 - 0.39636(\omega\gamma)^2$$

$$+ 0.09844(\omega\gamma)^4 \sum_{\lambda=0}^{\infty} (\omega\gamma)^{2\lambda}$$

$$\sum_{n=0}^6 \frac{\binom{6}{n}(-1)^n}{2n + 2\lambda + 1} \quad (14)$$

$$\gamma = \frac{-6! \eta \sigma_e}{(2\omega)^4 \beta_T \rho g \cos \theta B_s \Delta T} \quad (15)$$

The infinite series in Equations (12) and (14) converge in the interval  $|\omega\gamma| \leq |1|$ .

Equations (8) and (10) referred to as the *uncorrected* and the *corrected* equations respectively, are compared with experimental data in a later section. These equations have the simplest form of any of the solutions presented by Jones and Furry and are as valid as the more general equation in the region for which they were developed.

## EXPERIMENTS

### Continuous-flow Thermogravitational Column

**Equipment.** The two thermogravitational columns used in the course of this investiga-

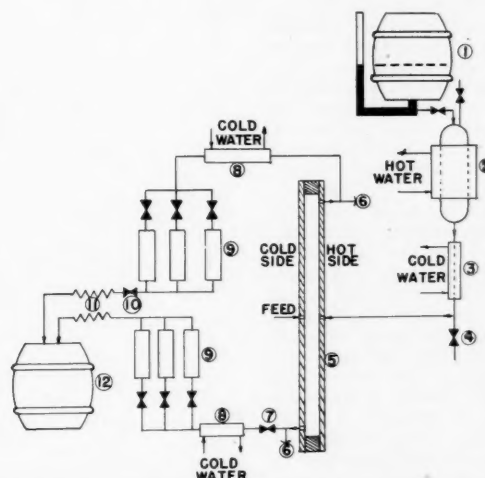


Fig. 4. Gravity-flow feed system: (1) feed barrel, (2) out-gasser, (3) feed cooler, (4) feed-sample tap, (5) thermogravitational column, (6) product-sample taps, (7) control valve, (8) product coolers, (9) rotameters, (10) control valve, (11) shunted capillary tubes, and (12) product barrel.

tion were constructed in the form of parallel plates (rather than concentric cylinders) in order to facilitate changes in the plate spacing ( $2\omega$ ) and to permit operation of the column at angles other than vertical. The working space between the plates measured approximately 6 in. by 4 ft. in the smaller column and 6 in. by 8 ft. in the larger. The transfer plates were constructed of 1/8-in. stainless steel sheet that was relatively free of scratches. The surfaces of these plates were given no special finishing treatment, as grinding caused excessive warpage of the plates. Two thermocouples were located on the surface of each transfer plate. The column was supported on an iron frame by means of support arms, to one of which a pointer was attached to indicate the angle of the column on a large metal protractor connected to the frame. Figure 2 is a view of the 4-ft. column inclined at an angle of 45 deg. and Figure 3 is a photograph of the 8-ft. column.

The gravity-flow feed system that provided steady flows through the columns is diagrammed in Figure 4. All material other than the gasket contacted by the feed was either stainless steel, glass, or Teflon. The feed supply was kept in a barrel (1) 14 ft. above the floor. The liquid level in the barrel could be seen in a glass side tube. The feed was raised to the temperature of the heating water in a 1-liter glass cylinder (2) just below the feed barrel. The gases released by this heating process were periodically vented from the cylinder. The feed was cooled on passing through a small heat exchanger (3), and a sample tap (4) was located between the feed cooler and the thermogravitational column (5). The feed entered the column through holes drilled centrally in both transfer plates. The top product was removed through the hot plate and the bottom product through the cold plate. Product sample taps (6) were located as close to the working space as possible.

Temperature-controlled water was circulated through jacketed sections on either side of the transfer plates to control the temperature at the hot and cold walls.

**Procedure.** In experiments with the continuous-flow thermogravitational columns, the separation was determined as a function of flow rate. The plate spacing  $2\omega$ , column length  $L_T$ , angle of plates from the vertical  $\theta$ , and temperature difference between the plates  $\Delta T$  were treated as parameters. Changes in  $\theta$  and  $\Delta T$  could be made easily. Two separate columns were used to investigate the effect of column length. The plate spacing was varied by using gaskets of different thicknesses between the transfer plates. After a new gasket had been installed the plate spacing had to be determined accurately before the more useful experimental data could be taken. As the plate spacing appears in the theory as  $(2\omega)^3$ ,  $(2\omega)^4$ , and  $(2\omega)^7$ , interpretation of the data is extremely sensitive to any error in this measurement. The method of measuring the plate spacing is discussed in detail elsewhere (14). Table 3 lists typical measured values of the column parameters, as well as average values of the feed composition and column width.

After necessary plate-spacing determinations had been made, a series of experiments was conducted to determine the separation

TABLE 3. MEASURED VALUES OF COLUMN PARAMETERS

Group	Included runs	Plate spacing from direct measure $2\omega$ , cm.	Mean temp. diff. $\Delta T_m$ , °C.	Angle† from vertical $\theta$ , °	Total column height $L_T$ , cm.	Column width $B$ , cm.	Feed conc. $C_F$
{	Q 94-101	0.1356-0.1344*	35.2	+1.0	115.8	15.32	0.3933-0.3962
	R 102-110	0.1454-0.1378*	37.0	+1.0	237.8	15.30	0.3977
	S 111-115	0.1344†	35.9	+1.0	237.8	15.30	0.3982
{	W 134-138, 145						
	149-152, 164	0.0908†	36.0	+1.0	237.8	15.17	0.3986
{	X 139-142	0.0908†	18.1	+1.0	115.8	15.17	0.3986
{	BA 177-184	0.0813	41.1	+1.0	115.8	15.17	0.492
	BB 186-192	0.1078†	42.1	+1.0	115.8	15.59	0.502
	BC 193-200	0.0805†	43.0	+1.0	115.8	15.66	0.500

\*Extremes of measured values.

†Average value (data self-consistent).

‡Positive angles indicate hot plate on top.

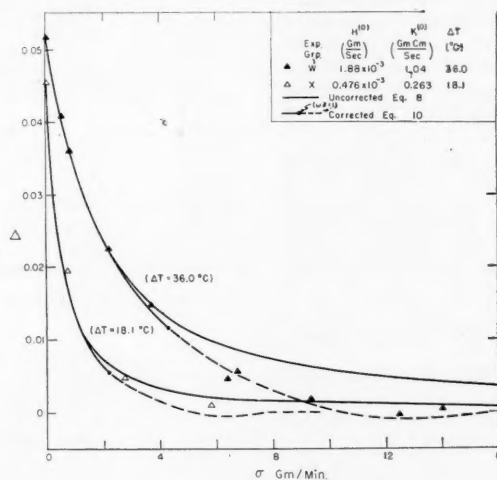


Fig. 5. Separation in a continuous-flow thermogravitational column as a function of flow rate.

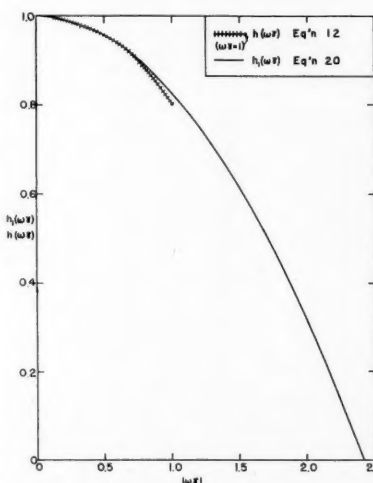


Fig. 6.  $h(\omega\gamma)$  and  $h_1(\omega\gamma)$  as functions of  $|\omega\gamma|$ .

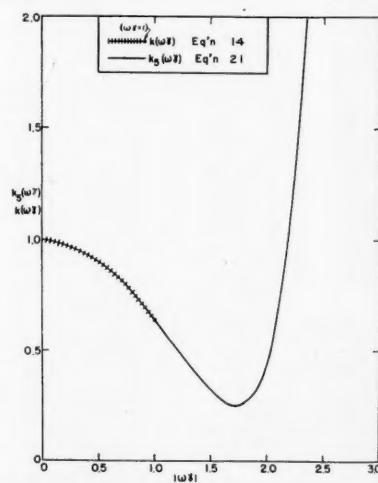


Fig. 7.  $k(\omega\gamma)$  and  $k_0(\omega\gamma)$  as functions of  $|\omega\gamma|$ .

as a function of the flow rate. The column and all lines were purged with the mixture to be investigated. The rotameters were used to set approximate flow rates through the working space, and samples from both

product streams were analyzed periodically. Sufficient time was allowed between sets of samples to purge the headers and eliminate any disturbances introduced by the sampling procedure. The separation was

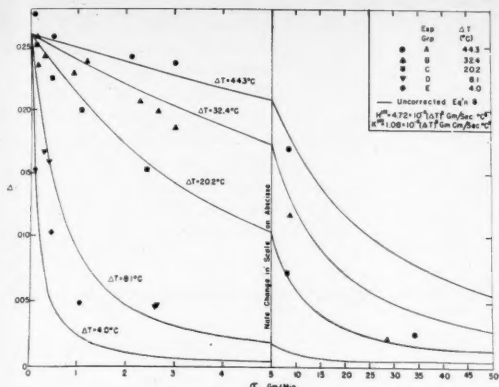


Fig. 8. Separation as a function of flow rate with temperature difference as parameter.

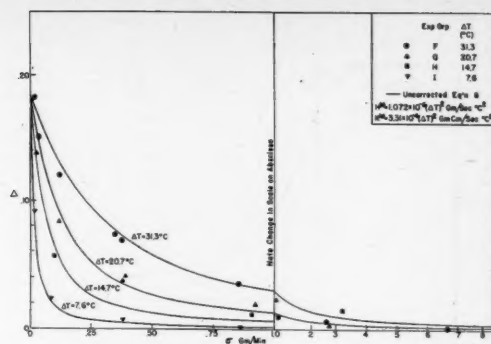


Fig. 9. Separation as a function of flow rate with temperature difference as a parameter.

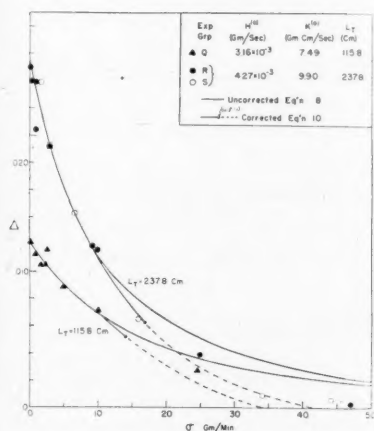


Fig. 10. Separation as a function of flow rate with column length as parameter.

plotted as a function of the time to determine the steady-state separation when the relaxation time was large compared with the time between samples. Several analyses were made with the column operating under steady state conditions, and the average of these analyses was reported. During the time interval between samples taken under steady state conditions, rotameter readings were taken, and the actual product-flow rates were measured by collecting and weighing samples. Other readings taken at this time included the temperatures of the water entering and leaving the column, manometer readings (water flow rate), controller readings, index of refraction of the feed, feed-barrel level, and the potentials of the four thermocouples located at the surfaces of the transfer plates. A record of these four potentials was made by a Brown electronic multipoint recorder.

All experiments with the ethyl alcohol-water system were made at a mean temperature level of 120°F., and those made with the *n*-heptane-benzene mixtures were at a mean temperature of 108°F. These mean temperatures were taken as the average of the temperatures indicated on the temperature recorder-controllers. Physical properties of the materials are given in Table 4. Concentrations were determined

from refractive-index measurements of the solutions based upon calibration data obtained on reference solutions of the materials used in the columns.

## RESULTS

Typical results are given in Table 1 for the ethyl alcohol-water system and

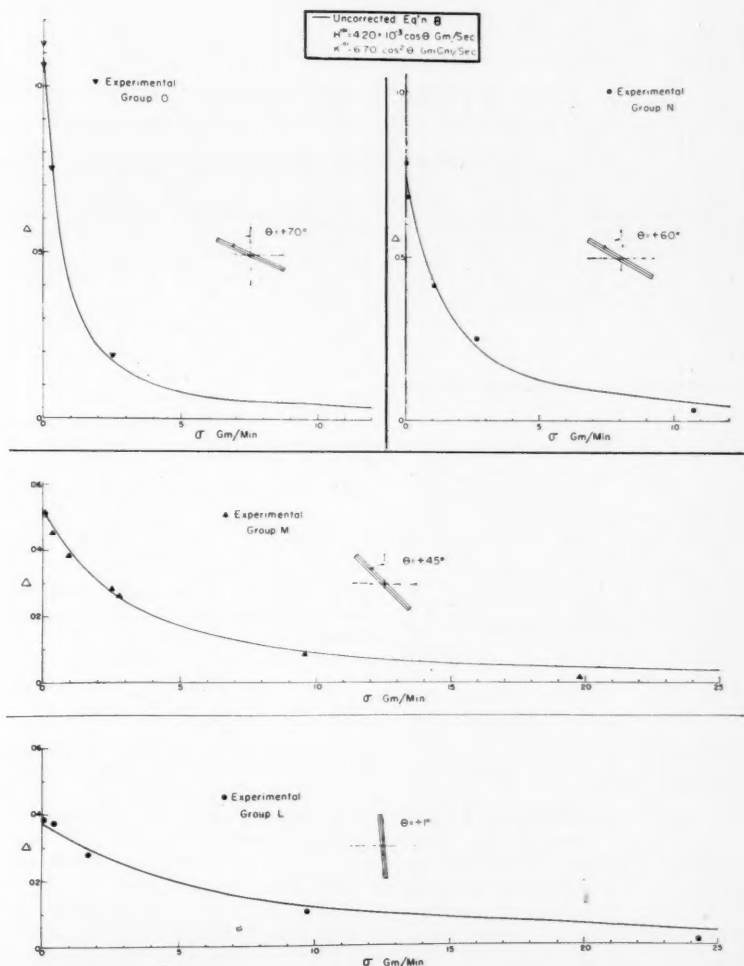


Fig. 11. Separation as a function of flow rate with column inclined at various angles.

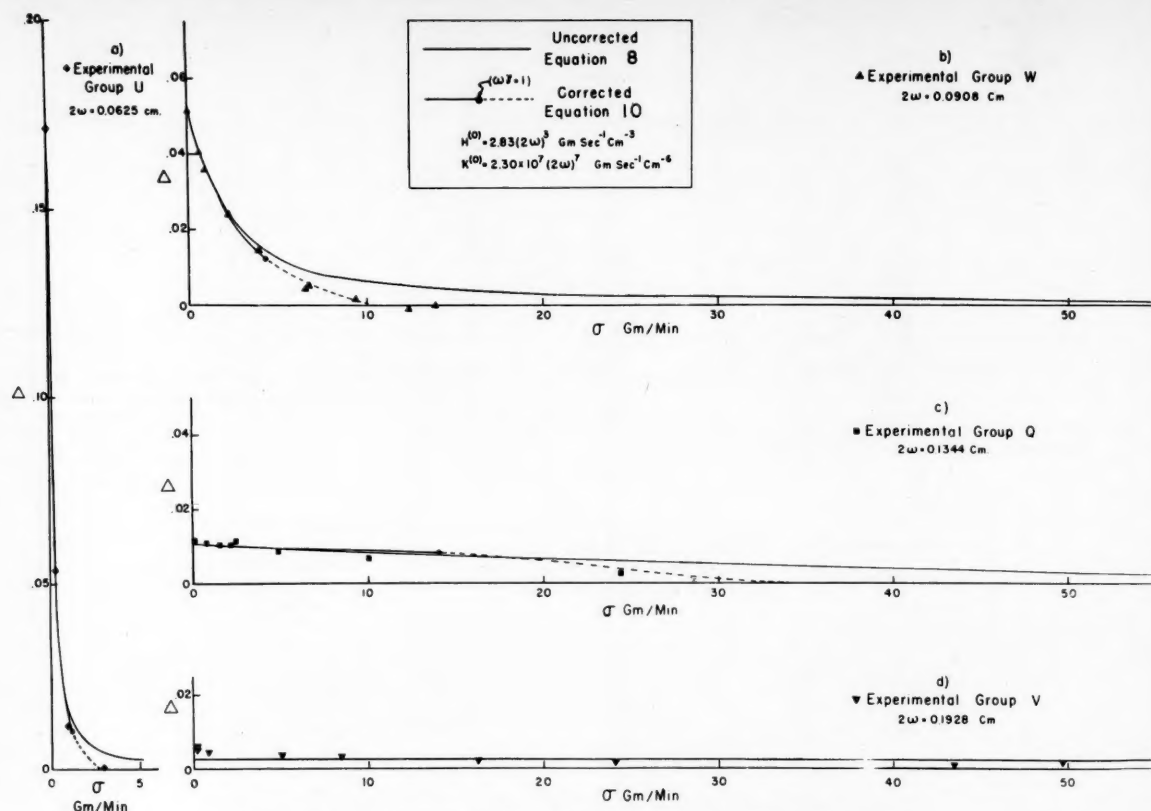


Fig. 12. Separation as a function of flow rate for four different plate spacings.

in Table 2 for the *n*-heptane-benzene system. (A complete listing of the data is on file.)\* Included in the original thesis (14) are data on the column heat load and approach to steady state in the columns.

#### INTERPRETATION OF EXPERIMENTAL RESULTS

The mixtures investigated in the continuous-flow thermogravitational columns were all relatively concentrated binary liquid solutions. This type of mixture was chosen for several reasons: (a) there are relatively few data on such systems reported in the literature; (b) the maximum separation of any ideal binary mixture should occur when the feed is composed of equal amounts of each component; and (c) for the conditions  $0.7 > C_1 > 0.3$ , i.e., for  $C_1 C_2 \cong \frac{1}{4}$ , the solution to the transport equation is of the simple form given by Equations (8) and (10).

#### Flow-rate Dependence

Two of the first questions to be resolved were whether the flow-rate dependence predicted by Equations (8) and (10) corresponded to the experimental results and

over what range the uncorrected equations of Jones and Furry (10) were applicable. Since the flow-rate dependence is here considered to be of prime importance, values of  $H^{(0)}$  and  $K^{(0)}$  in Equations (8) and (10) were determined empirically in such a manner that  $\Delta$  values calculated from these equations agreed with experimental data in the region  $\sigma \rightarrow 0$ . The following procedure was used to obtain empirical values of  $H^{(0)}$  and  $K^{(0)}$ . If Equation (10) is expanded in series, Equation (16) results:

$$\Delta = \frac{HL_T}{4K} - \frac{HL_T^2}{8K^2} \sigma + \frac{HL_T^3}{16K^3} \sigma^2 \dots \quad (16)$$

In the limit  $\sigma \rightarrow 0$ , the intercept  $\Delta_0$  and the initial slope  $m_0$  are obtained from Equation (16) by inspection.

$$\Delta_0 = \frac{H^{(0)} L_T}{4K^{(0)}} \quad (17)$$

$$m_0 = -\frac{H^{(0)} L_T^2}{8(K^{(0)})^2} \quad (18)$$

Equations (17) and (18) can thus be solved simultaneously for  $H^{(0)}$  and  $K^{(0)}$  values that will satisfy the experimental values of  $\Delta_0$  and  $m_0$ .

Some typical data are presented in Figure 5. The complete solid lines represent values of the separation  $\Delta$  calculated from uncorrected Equation (8) with values of  $H^{(0)}$  and  $K^{(0)}$  determined in the

manner described in the preceding paragraph. The solid lines ending in a dot represent separations calculated from the corrected Equation (10) by use of these same  $H^{(0)}$  and  $K^{(0)}$  values. For relatively low flow rates the corrected and uncorrected equations give almost identical results and agree very well with the data. At higher flow rates the uncorrected equation deviates markedly from the data and predicts separations larger than those found experimentally. The corrected equation gives values that compare very well with the experimental data. However, for values of  $\omega\gamma > 1$  (dots indicate  $\omega\gamma = 1$ ) the series appearing in Equations (12) and (14) diverge and lead to the indeterminate expression  $\Delta = \infty \cdot 0$ .

It is of interest to note that in all cases tested the unmodified theory, Equation (8), is in fair agreement with the data up to a flow rate corresponding to  $\omega\gamma = 1$  and in poor agreement for higher flow rates. Thus the limit of applicability of Equation (8) is given by

$$(\sigma)_l = \frac{2(2\omega)^3 \beta_T g \cos \theta B_s \Delta T}{6! \eta} \quad (19)$$

This further suggests that the  $\omega\gamma$  term might be used to correlate correction factors similar to Equation (12) and (14) outside of the region of convergence of these series.

\*Tabular material has been deposited as document 5209 with the American Documentation Institute, Photoduplication Service, Library of Congress, Washington 25, D. C., and may be obtained for \$1.25 for photoprints or 35-mm. microfilm.



The dashed lines drawn as a continuation of the corrected curves on Figure 5 represent the use of correction terms  $h_1(\omega\gamma)$  and  $k_5(\omega\gamma)$ . Values of  $h_1(\omega\gamma)$  are calculated by ignoring all terms but the first in the series appearing in Equation (12), and  $k_5(\omega\gamma)$  values are calculated by considering only the first five terms of the series in Equation (14). These relations are given by Equations (20) and (21) and are represented graphically in Figures 6 and 7.

$$h_1(\omega\gamma) = 1 - 0.17143(\omega\gamma)^2 \quad (20)$$

$$\begin{aligned} k_5(\omega\gamma) = & 1 - 0.39636(\omega\gamma)^2 \\ & + .033567(\omega\gamma)^4 + 2.2378 \\ & \times 10^{-3}(\omega\gamma)^6 + 3.949 \\ & \times 10^{-4}(\omega\gamma)^8 + 1.0392 \\ & \times 10^{-4}(\omega\gamma)^{10} + 3.464 \\ & \times 10^{-5}(\omega\gamma)^{12} \end{aligned} \quad (21)$$

Values of  $h(\omega\gamma)$  and  $k(\omega\gamma)$  for  $|\omega\gamma| \leq 1$  are included in Figures 6 and 7 for comparison.

The term  $h_1(\omega\gamma)$  becomes negative at large flow rates, and the separations predicted for  $\omega\gamma > 2.43$  are opposite in sign to  $\Delta_0$ . The net result of the use of  $k_5(\omega\gamma)$  is to limit the separations calculated for  $\omega\gamma > 2.43$  to very small values. Negative separation values are shown in Figure 5. In other figures the dotted line representing the corrected Equation (10) is terminated at  $\omega\gamma = 2.43$  because separations of opposite sign at higher flow rates have no physical significance. In most cases both calculated and measured separation values are equal to zero within experimental accuracy for  $\omega\gamma > 2.43$ . The agreement with experimental data for  $2.43 > \omega\gamma > 1.0$  that is obtained by using these approximations is remarkable, as the use of the first several terms in these divergent series is entirely empirical.

Equations (17) and (18) were used to determine empirical values of  $H^{(0)}$  and  $K^{(0)}$  for most of the groups of experimental data which were obtained. The variation of the separation  $\Delta$  with flow rate was properly accounted for by use of Equation (10). In general the corrected equation with the terms  $h_1(\omega\gamma)$  and  $k_5(\omega\gamma)$  was superior to the uncorrected equation in representing the data.

The separation-flow-rate data successfully represented by Equation (10) were obtained for a variety of operating conditions. The theory predicts the effect of changes in the operating conditions, and the empirical  $H^{(0)}$  and  $K^{(0)}$  values can be used to check these predictions. The functional dependence of the term  $H^{(0)}$  is given by Equation (7a).  $K^{(0)}$  is composed of three additive terms:  $K_c^{(0)}$ , representing the remixing effects due to the convective flow;  $K_d$ , which accounts for

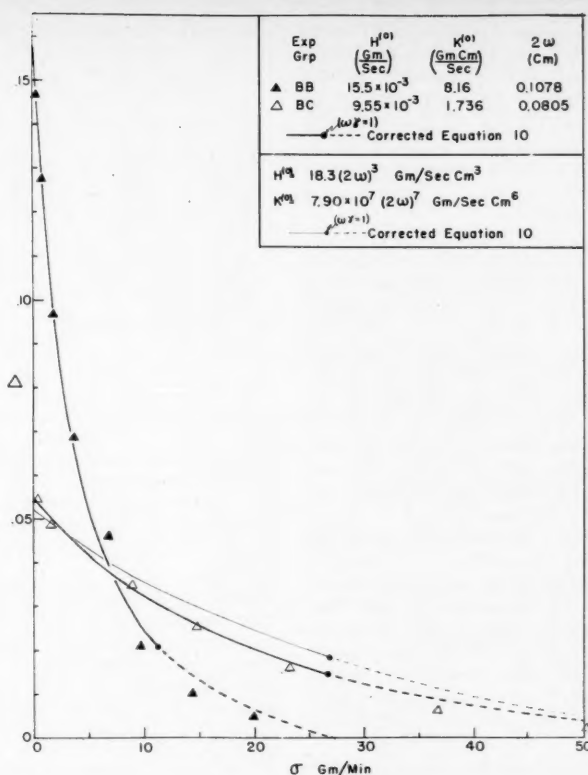


Fig. 13. Separation as a function of flow rate with plate spacing as parameter.

vertical diffusion; and  $K_p$ , a term appended to the theory to account for parasitic remixing effects. Fortunately, for the range of variables investigated in connection with this research, both  $K_d$  and  $K_p$  appear to be negligible when compared with  $K_c^{(0)}$ . In this case the functional dependence of  $K^{(0)}$  is essentially given by Equation (7c), i.e., that for  $K_c^{(0)}$ .

#### Temperature Difference ( $\Delta T$ )

According to Equations (7a) and (7c), both  $H^{(0)}$  and  $K^{(0)}$  are proportional to  $(\Delta T)^2$ . Values of  $H^{(0)}$  and  $K^{(0)}$  used in Equation (10) were obtained from relations of the form  $H^{(0)} = a(\Delta T)^2$  and  $K^{(0)} = b(\Delta T)^2$  where  $a$  and  $b$  are empirical constants determined from the data. These relations seem to satisfy the data presented in Figures 5, 8, and 9 over a wide range of  $\Delta T$  and for three different values of the plate spacing,  $2\omega$ .

In Figures 8 and 9 and subsequent figures in which no curve (or curves) representing the corrected equation appears, the measurement of the plate spacing was too inaccurate to permit a proper evaluation of the correction.

#### Length ( $L_T$ )

The theory predicts that  $H^{(0)}$  and  $K^{(0)}$  are independent of the column length. From Equation (17)  $\Delta_0$  should be proportional to  $L_T$  and, according to Equation (10), the separation should become

independent of height at high flow rates. These theoretical predictions are definitely substantiated by the data presented in Figure 10. The difference between the values of  $H^{(0)}$  and  $K^{(0)}$  used to represent the two experimental groups and the deviation of the theoretical curves at high flow rates is due in part to slight differences in the plate spacing and  $\Delta T$ .

#### Effective Gravitational Field ( $g \cos \theta$ )

The effective gravitational field was changed by tilting the column in the manner illustrated in Figure 2. This variation is accounted for in the theory by the product  $g \cos \theta$ . The results of experiments made with the hot plate on top (positive angles) are presented in Figure 11. The curves drawn on Figure 11 represent separations calculated using values of  $H^{(0)}$  and  $K^{(0)}$  obtained from relations of the form  $H^{(0)} = a \cos \theta$  and  $K^{(0)} = b \cos^2 \theta$  as predicted by theory.

#### Plate Spacing ( $2\omega$ )

According to the theory the separation should show a strong dependence on the plate spacing with  $H^{(0)} = a(2\omega)^3$  and  $K^{(0)} = b(2\omega)^7$ . The magnitude of this effect is even more clearly emphasized by the fact that  $m_0$ , the initial slope, is inversely proportional to  $(2\omega)^{11}$ . The tremendous effect of the plate spacing is illustrated in Figure 12 by retaining the same relative scales on the four graphs. The curves on Figure 12 represent values

calculated from Equation (10) with values of  $H^{(0)}$  and  $K^{(0)}$  determined from the foregoing relations. Values of  $a$  and  $b$  were determined from the data taken for  $2\omega = 0.0908$  cm. (Figure 12b), and slight corrections were made for variations in  $\Delta T$ . The agreement appears to be quantitative largely because the scales are small.

Actually some discrepancies exist between the theoretical and experimental values for data taken at the larger plate spacings. Figure 13 represents other data taken to investigate the effect of plate spacing and will serve to illustrate the nature of these discrepancies. If the constants  $a$  and  $b$  in the relations  $H^{(0)} = a(2\omega)^3$  and  $K^{(0)} = b(2\omega)^7$  are evaluated from the data taken at the smaller plate spacing (larger  $\Delta_0$ ), values of  $H^{(0)}$  and  $K^{(0)}$  calculated from these relations fail to represent the data taken at the larger plate spacing (light line). The predicted value of  $\Delta_0$  is somewhat smaller than that found experimentally, and experimental values of the separation at high flow rates are substantially smaller than the calculated values. On the other hand, values of  $H^{(0)}$  and  $K^{(0)}$  obtained empirically from each individual set of data serve to represent the data very well (heavy lines).

Jones (9) has reported some qualitative conclusions based on an extensive investigation of the separation of liquids in continuous-flow thermogravitational columns. Although he does not indicate the nature of the dependence of the separation on the flow rate, his conclusions with regard to other variables are in general agreement with the theory and with the results of this investigation.

## PROCESS DESIGN

In order to obtain quantitative agreement between the theory and experimental data it was necessary to apply empirical correction factors to the terms  $H^{(0)}$  and  $K^{(0)}$ . The correlation of these correction factors which was developed incorporates the data of Drickamer and his coworkers on the separation of mixtures of gases as well as mixtures of liquids. Details have been presented previously (14). From an engineering standpoint the most important conclusion to be reached from the correlation is that no correction or modification of the theory as originally proposed by Furry, Jones, and Onsager (7) and Jones and Furry (10) is necessary when their equations are used as the basis for design of thermal-diffusion plants for separation of liquid mixtures, because optimum design relations dictate the use of small plate spacings and low flow rates. The theory is in quantitative agreement with the data for these conditions.

Krasney-Ergen (11) has developed equations for estimating optimum dimensions in the design of thermal-diffusion

TABLE 4. VALUES OF PHYSICAL PROPERTIES USED IN THE CALCULATIONS

System		Fraction	Average	Density	$-\partial\rho/\partial T$	Diff.	Coefficient
A	B	A	temp.	$\rho$ , g./cc.	$\beta \times 10^4$ , g./ (cc.)(°C.)	coef. $D \times 10^5$ , sq. cm./sec.	of viscosity $\eta$ , centipoise
EtOH	H <sub>2</sub> O	0.3986*	322.1	0.9133†	8.11	1.04††	1.14**
EtOH	H <sub>2</sub> O	0.3913*	322.1	0.9150†	8.08	1.06††	1.12**
EtOH	H <sub>2</sub> O	0.3322*	322.1	0.9273‡	7.80	1.262††	1.09**
n-Heptane	Benzene	0.500†	315.4	0.7363**	9.44	3.21††	0.351¶

\*Weight fraction.

†Mole fraction.

‡References 8 and 15.

\*\*Reference 8.

††References 6, 12, and 16.

‡‡Reference 18.

¶Reference 17.

processes based on the equations of Furry, Jones, and Onsager. Krasney-Ergen was interested principally in the concentration of relatively rare isotopes and treated the case in which the relative amount of the substance being concentrated,  $C_1$ , is very small throughout the apparatus ( $C_1 \ll 1$ ). The equations "tested" in the present work, on the other hand, were based on the assumption that the materials being separated are present in almost equal amounts ( $C_1 C_2 \cong 1/4$ ). In the next section the method of Krasney-Ergen will be applied to develop a design procedure for the case  $C_1 C_2 \cong 1/4$ .

## EQUATIONS FOR DETERMINING THE OPTIMUM DIMENSIONS OF A THERMAL-DIFFUSION APPARATUS ( $C_1 C_2 \cong 1/4$ )

The optimum dimensions are the cheapest. Costs are considered in two categories only: (1) fixed charges, mainly depreciation of the capital investment, and (2) power costs, which are defined so as to include the cost of both fuel and cooling water. The notation  $S$  is used to denote the amount of fixed charges per unit area (square centimeters) per unit time (day). The amount of heat transferred is inversely proportional to the plate spacing, and therefore the power cost per square centimeter per day is designated by  $p_c/2\omega$ . The total cost  $\pi$  is given by

$$\pi = [S + p_c/2\omega] \int_A dA \\ = [S + p_c/2\omega] BL_T \quad (22)$$

From Equation (10),

$$L_T = \frac{2K}{\sigma} \left[ -\ln \left( 1 - \frac{2\sigma\Delta}{H} \right) \right] \quad (23)$$

If the angle of the plates from the vertical  $\theta$  is set arbitrarily and the temperature difference  $\Delta T$  and temperature level  $\bar{T}$  are dictated by the available heating and cooling media, for any particular system the terms  $H^{(0)}$  and  $K^{(0)}$  can be considered to be functions of the column width  $B$  and the plate spacing  $2\omega$ . [The terms  $h(\omega\gamma)$  and  $k(\omega\gamma)$  are ignored in this development.]

$$H^{(0)} = aB(2\omega)^3 \quad (24)$$

$$K^{(0)} = a'B(2\omega)^7 + b'B(2\omega) \quad (25)$$

Equation (22) is obtained by combining Equations (26) through (25):

$$\pi = \frac{2B^2}{\sigma} [a'S(2\omega)^7 + a'p_c(2\omega)^6 \\ + b'S(2\omega) + b'p_c] \\ \cdot \left\{ -\ln \left[ 1 - \frac{2\sigma\Delta}{aB(2\omega)^3} \right] \right\} \quad (26)$$

In general, the required separation  $\Delta$  and the average flow rate  $\sigma$  are designated. The total cost  $\pi$  is then a function of  $2\omega$  and  $B$  only. From Equation (26) it can be shown that the costs are infinite in both of the limits  $B \rightarrow \infty$  and  $(2\sigma\Delta)/aB(2\omega)^3 \rightarrow 1.0$ . Clearly then at least one minimum must exist between the limits defined by

$$0 > \frac{2\sigma\Delta}{aB(2\omega)^3} > 1.00 \quad (27)$$

In order for the total cost to be minimized these conditions must be satisfied:

$$\frac{\partial\pi}{\partial B} = 0 = \frac{\partial\pi}{\partial(2\omega)} \quad (28)$$

By differentiating Equation (26) with respect to  $B$  and combining with Equation (28), one obtains

$$-2 \ln \left( 1 - \frac{2\sigma\Delta}{aB^*(2\omega)^3} \right) = \frac{1}{\frac{aB^*(2\omega)^3}{2\sigma\Delta} - 1} \quad (29)$$

$B^*$  refers to the optimum value of the column width for any plate spacing.

The optimum plate spacing as a function of the various parameters is obtained by differentiating Equation (26) with respect to  $2\omega$  and combining the resulting equation with Equations (28) and (29):

$$(2^* \omega)^7 - 5 \frac{b'}{a'} (2^* \omega) - 6 \frac{b'}{a'} \frac{p_c}{S} = 0 \quad (30)$$

Equation (30) is identical to the relation developed by Krasney-Ergen for the case  $C_1 \ll 1$ .

If  $\Gamma$  is defined by

$$\Gamma = \frac{2\sigma\Delta}{a(2\omega)^3} \quad (31)$$

Equation (29) can be reduced to

$$-2 \ln(1 - \Gamma/B^*) = \frac{1}{B^*/\Gamma - 1} \quad (32)$$

The solution to Equation (32) is

$$B^* = 1.39\Gamma \quad (33)$$

which is considerably more simple than the analogous relation developed by Krasney-Ergen.

#### DESIGN ILLUSTRATION

Both Krasney-Ergen (11) and Jones and Furry (10) have included numerical examples of the design of processes for concentrating dilute mixtures of isotopic gases. It is interesting to apply the equations developed in the preceding section to the design of a single-state apparatus for the separation of a concentrated liquid mixture.

For purposes of illustration a thermal-diffusion plant to process 1,000 bbl./day of a 50 mole % *n*-heptane-benzene mixture will be designed. This particular design would have no commercial significance, as *n*-heptane-benzene is easily separated by distillation. However, the process is indicative of separations of aromatics and aliphatics, a difficult separation when applied to lubricating oils.

Equation (10) used in this development was restricted to the range  $0.7 > C_1 > 0.3$  and to equal flow rates in each section. On the basis of these restrictions the following product specifications were arbitrarily designated:

top product—

500 bbl./day 70 mole % *n*-heptane

bottom product—

500 bbl./day 30 mole % *n*-heptane

From these specifications it follows that  $\Delta = 0.40$ . The problem is further defined by setting  $\cos \theta = 1.00$ ,  $\Delta T = 100^\circ\text{C}$ . and  $T = 315^\circ\text{K}$ .

The power costs  $p_c$  were approximated by considering the cost of heating and cooling media to be twice the cost of fuel at 30 cents/million B.t.u. A value of  $\$7.32 \times 10^{-6}/(\text{day})(\text{sq. cm.}/\text{cm.})$  was obtained for  $p_c$ .

The equipment costs were assumed to be independent of  $2\omega$  and the cost per square foot of area of one plate was estimated to be \$60/sq. ft. This is ten times the value obtained from Chilton's (2) cost curves for heat exchange surface and is intended to include cost of auxiliary equipment, design, etc. On this basis a value of  $\$3.91 \times 10^{-5}/(\text{day})(\text{sq. cm.})$  was obtained for  $S$ .

These cost data and values of the other system parameters were used in Equations (30), (31), (33), and (23) to obtain the dimensions for the "optimum" design listed in Table 5. Estimates of the total heat load, capital investment, and operating costs are included.

Even though a column 1.43 cm. long and 82.7 miles wide with a plate spacing of 0.182 mm. may be optimum, it would hardly seem practical. An increase in the plate spacing would decrease the column width and increase the column length. The cost would also be increased by any increase in plate spacing. (Actually a decrease in fabrication cost with an increase in  $2\omega$  would probably offset the predicted increase in cost.) A plate spacing of 0.793 mm. (1/32 in.) was arbitrarily chosen as a minimum practical plate spacing, and values of  $B$  and  $L_T$  were calculated from Equations (33) and (23). The results of these calculations are listed under Practical Design in Table 5 for comparison with the optimum design. The values of the column length (17 ft.) for this arbitrary plate spacing represent a practical construction, and thus no other designs were considered.

The cost data used in these estimates are certainly only approximate, and yet the results should indicate the order of magni-

tude of the costs. As pointed out previously, thermal diffusion is an expensive process; however, with motor oil selling for 60 cents a quart the process may become economically feasible in the near future.

#### SUMMARY OF DESIGN PROCEDURES

##### Equations

Although there is some doubt as to the usefulness of the equations developed above in their application to liquids, they are summarized here for convenient reference.

##### Optimum Plate Spacing ( $2^*\omega$ )

$$(2^*\omega)^7 - 5 \frac{b'}{a} (2^*\omega) - 6 \frac{b' p_c}{a' S} = 0 \quad (30)$$

$$\frac{b'}{a'} = 9! \left( \frac{D\eta}{\beta \tau g \cos \theta \Delta T} \right)^2 \quad (34)$$

##### Optimum Column Width ( $B^*$ )

$$B^* = 1.39\Gamma = \frac{2.78\sigma\Delta}{a(2\omega)^3} \quad (33a)$$

$$a = \frac{\alpha \beta \tau g \cos \theta (\Delta T)^2}{6! \eta T} \quad (35)$$

##### Column Length ( $L_T^*$ )

$$L_T^* = \frac{2K^{(0)}}{\sigma} \left[ -\ln \left( 1 - \frac{2\sigma\Delta}{H^{(0)}} \right) \right] = \frac{2.54K^{(0)}}{\sigma} \quad (23a)$$

$$K^{(0)} = 2\omega DB^* \rho \left[ \frac{a'}{b'} (2\omega)^6 + 1 \right] \quad (36)$$

##### Determination of Design Constants

The equations listed above are most useful when applied to the separation of binary mixtures for which all the required data on the physical properties including the ordinary and thermal-diffusion coefficient are known. Under these conditions the application of the equations is straightforward, as was shown in the design illustration.

In general, not many of the required physical data are available even for binary systems. This is especially true of thermal-diffusion data. In this more general case the terms  $a$ ,  $a'$ ,  $b'$ , and  $K^{(0)}$  can be evaluated empirically from data taken with either the continuous-flow or the batch-type thermogravitational column.

In the treatment of continuous-flow thermogravitational-column data, values of  $H^{(0)}$  and  $K^{(0)}$  would be obtained by use of Equations (17) and (18) as described. Values of  $H^{(0)}$  and  $K^{(0)}$  for batch columns are obtained from data on the approach to steady state in the column by applying the transient-state equations (10). (See also reference 13.) In either case these  $H^{(0)}$  and  $K^{(0)}$  values can be used to determine  $a$ ,  $a'$ , and  $b'$  by applying Equations (24) and (25). Constants  $a'$  and  $b'$  can be determined from Equation

TABLE 5. SUMMARY OF DESIGN ESTIMATES

Plant to process 1,000 bbl./day of 50 mole % *n*-heptane-benzene

	Optimum design	Practical design
$2\omega$ cm.	0.0182	0.0793
(in.)	(0.0072)	(1/32)
$B$ , cm.	$1.33 \times 10^{+7}$	$1.60 \times 10^{+5}$
(ft.)	$(4.36 \times 10^{+5})$	$(5.25 \times 10^{+3})$
(miles)	(82.7)	(1.0)
$L$ , cm.	1.43	514
(ft.)	(0.0468)	(16.9)
Total area		
$(B \times L)$ , sq. cm.	$1.90 \times 10^{+7}$	$8.23 \times 10^{+7}$
(sq. ft.)	$(2.05 \times 10^4)$	$(8.88 \times 10^{+4})$
Heat load, B.t.u./hr.	$5.27 \times 10^{+8}$	$5.27 \times 10^{+8}$
Capital investment	\$1,230,000	\$5,320,000
Operating costs		
Fuel and cooling water	\$7,670	\$ 7,670
Fixed charges	743	3,230
Total	\$8,413	\$10,900
Cost per barrel of feed processed	\$8.41	\$10.90
Cost per gallon of feed processed	\$0.20	\$ 0.26

(25) by making several determinations at two different plate spacings.

In the light of present results it would appear that determination of  $H^{(0)}$  and  $K^{(0)}$  values to be used in any final design should be made in an apparatus with approximately the same plate spacing  $2\omega$  as that to be used in the plant. Further, when these constants are determined empirically, this design procedure can be applied also to the treatment of multicomponent mixtures.

#### ACKNOWLEDGMENT

The authors have become indebted to many people during the course of the work on this project. J. L. Fick prepared most of the figures appearing in the text, and H. Stapp and R. J. Riddell gave many helpful suggestions in the development of the modified theory.

The assistance of E. J. Lynch, C. d'A. Hunt, W. Dong, E. I. Motte, A. W. Peterson, L. J. Hov, and Mr. and Mrs. R. B. Waite, Harriet Powers, Esther Fenske, H. N. Pratt and C. E. Bacon and support to J. E. Powers by Socony Mobil Oil Corporation during part of the work are gratefully acknowledged.

This work was conducted under the sponsorship of the Radiation Laboratory.

#### NOTATION

$a, a', a''$  = general constants  
 $A$  = area of the working space in a thermogravitational column ( $BL_T$ )  
 $B$  = column width when  $B_e = B_s$   
 $B^*$  = optimum value of the column width, obtained from Equation (33a)  
 $B_e, B_s$  = column width in the enriching section, stripping section  
 $b, b'$  = general constants  
 $C_1, C_2$  = fraction of component 1, 2 in a binary solution  
 $C_e, C_s$  = fraction of component 1 in the product stream exiting from the enriching section, stripping section  
 $C_F$  = fraction of component 1 in the feed stream  
 $D$  = ordinary-diffusion coefficient  
 $e$  = subscript used to identify variables in enriching section ( $y > 0$ )  
 $F$  = subscript used to identify feed properties  
 $g$  = acceleration due to gravity  
 $H$  = parameter evaluated by Equation (11)  
 $H^{(0)}$  =  $H$  for a column with no net flow of material through the working space [Equation (7a)]  
 $h(\omega\gamma)$  = correction term Equation (12)  
 $h_s(\omega\gamma)$  = use of the first term in the series defined by Equation (12)  
 $J_{x-TD}$  = flux of component 1 in the  $x$  direction due to thermal diffusion  
 $J_{x-OD}, J_{y-OD}$  = flux of component 1 in the  $x, y$  direction due to ordinary diffusion

$K$  =  $K_e + K_d + K_P$   
 $K_e$  =  $K_e^{(0)}k(\omega\gamma)$   
 $K_e^{(0)}$  =  $K_e$  for a column with no net flow of material through the working space  
 $K_d$  = parameter defined and evaluated by Equation (7d)  
 $K_P$  = a term appended to the mathematical treatment to account for the effects of parasitic remixing  
 $k(\omega\gamma)$  = correction term Equation (14)  
 $k_s(\omega\gamma)$  = use of the first five terms in the series defined by Equation (14)  
 $L_e, L_s$  = length of the enriching, stripping section  
 $L_T$  = total column length  
 $m_0$  =  $(\partial\Delta/\partial\sigma)_{\sigma=0}$   
 $n$  = index number used in Equation 14  
 $p_e$  = power costs per unit area (sq. cm.) per unit time (day) for an apparatus with transfer plates at unit distance (cm.)  
 $q$  = equilibrium separation factor for a thermogravitational column,  $C_e(1 - C_s)/C_s(1 - C_e)$   
 $S$  = amount of fixed charges per unit area (sq. cm.) per unit time (day)  
 $s$  = subscript used to identify variables in the stripping section ( $y < 0$ )  
 $T$  = absolute temperature  
 $\bar{T}$  = arithmetic average of the hot- and cold-plate temperatures  
 $t$  = time  
 $v(x)$  = general velocity distribution function  
 $x$  = axis normal to the plates  
 $y$  = axis parallel to the plates in the direction of normal convective flow

#### Greek Letters

$\alpha$  = thermal-diffusion constant  
 $\beta_T$  =  $-\partial\rho/\partial T$   
 $\gamma$  = parameter defined by Equation (9) and evaluated by Equation (15)  
 $\Delta$  = difference of concentrations at the ends of a thermogravitational column at steady state  
 $\Delta_0$  = difference of concentrations at the ends of a thermogravitational column at steady state with no net flow of material through the working space  
 $\Delta T$  = difference in temperature of the hot and cold plate  
 $\eta$  = coefficient of viscosity  
 $\theta$  = angle of the plates of a thermogravitational column from the vertical  
 $\lambda$  = index number used in Equations (12) and (14)  
 $\pi$  = total cost of operating a thermal-diffusion plant per unit time (day)  
 $\rho$  = density  
 $\sigma$  =  $(\sigma_e + \sigma_s)/2$

$\sigma_e, \sigma_s$  = mass flow rate out the enriching, stripping section  
 $\sigma_F$  = mass flow rate of the feed stream  
 $(\sigma)_1$  = mass flow rate beyond which Equation (8) does not represent the data  
 $\psi(y)$  = relation defined by Equation (9)  
 $\omega$  = one half of the distance between the plates of a thermogravitational column  
 $2^*\omega$  = optimum value of the plate spacing obtained from Equation (30)

#### LITERATURE CITED

1. Bijl, A., *Ned. Tijdschr. Natuurk.*, **7**, 147 (1940); B. N. Cacciapuoti, *Nuovo cimento*, **18**, 114 (1941); R. H. Davis and J. T. Kendall, *Proc. Intern. Congr. Pure and Appl. Chem. (London)*, **11**, 429 (1947); H. Fleischmann and H. Jensen, *Ergeb. exakt. Naturw.*, **20**, 121 (1942); K. E. Grew and T. L. Ibbs, "Thermal Diffusion in Gases," Cambridge University Press, Cambridge (1952); G. S. Hartley, *Trans. Faraday Soc.*, **27**, (1931); Kozo Hirota, *J. Chem. Soc. (Japan)*, **63**, 292 (1942); J. A. Hveding, *Tidsskr. Kjemi Bergvesen Met.*, **1**, 110 (1941); H. Hensen, *Angew. Chem.*, **54**, 405 (1941); R. E. Kirk and D. F. Othmer, "Encyclopedia of Chemical Technology," pp. 115-124, The Interscience Encyclopedia Company, New York (1950); A. N. Murin, *Uspekhi Khim.*, **10**, 671 (1941); T. H. Osgood, *J. Appl. Phys.*, **15**, 89 (1944); K. Schafer, *Naturwissenschaften*, **34**, 104, 137, 166 (1947); Eiichi Takeda, *Bull. Tokyo Inst. Technol.*, **13**, 137; A. J. E. Welch, *Sci. J. Roy. Coll. Sci.*, **11**, 19 (1941).
2. Chilton, C. H., *Chem. Eng.*, **56**, no. 6, 97 (June, 1949).
3. Clusius, K., and G. Dickel, *Naturwissenschaften*, **26**, 546 (1938).
4. Dufour, L., *Arch. Sci. phys. et nat.*, **45**, 9 (1872); *Pogg. Ann.*, **148**, 490 (1873); *Ann. Physik* [5], **28**, 490 (1873).
5. DeGroot, S. R., thesis, Univ. Amsterdam (1945).
6. Franke, G., *Ann. Physik*, **14**, 675 (1932).
7. Furry, W. H., R. C. Jones, and L. Onsager, *Phys. Rev.*, **55**, 1083 (1939).
8. "International Critical Tables," McGraw-Hill Book Company, Inc., New York (1928).
9. Jones, A. L., *Petroleum Processing*, **6**, 132 (February, 1951).
10. Jones, R. C., and W. H. Furry, *Rev. Modern Phys.*, **18**, 151 (1946).
11. Krasney-Ergen, William, *Phys. Rev.*, **58**, 1078 (1940).
12. Lemonde, H., *Compt. rend.*, **202**, 468, 731, 1069 (1936).
13. Nier, A. O., *Phys. Rev.*, **57**, 30 (1940).
14. Powers, J. E., Univ. Calif. Radiation Lab. Rept., UCRL-2618 (August, 1954).
15. Rakshit, J. N., *Z. Elektrochem.*, **32**, 276 (1926).
16. Smith, I. E., and J. A. Starrow, *J. Appl. Chem. (London)*, **2**, 225 (1952).
17. Trevo, D. J., and H. G. Drickamer, *J. Chem. Phys.*, **17**, 582 (1949).
18. *Ibid.*, 1117 (1949).

Presented at A.I.Ch.E. Detroit meeting



# Radioisotope Technique for the Determination of Flow Characteristics in Liquid-liquid Extraction Columns

S. E. MARKAS and R. B. BECKMANN

Carnegie Institute of Technology, Pittsburgh, Pennsylvania

A radioisotope technique has been utilized to study the point holdup of the dispersed phase and some operational flow characteristics in a packed countercurrent liquid-liquid extraction tower. The system used was toluene-water and the packing was Raschig rings. The toluene dispersed phase was tagged with gamma-radiating iodine-131.

The study revealed that holdup experiences a hysteresis cycle with variations of the continuous-phase flow rate. Correlating equations are presented for "total" and permanent holdup, below loading, to account for this hysteresis. Entrance effects and flow maldistribution effects are readily determined by the method utilized. Displacement studies demonstrated that no simple "operational" dispersed-phase flow holdup exists, but rather a complex dispersed-phase movement, which involves all the "nonhysteresis" permanent holdup.

During recent years the widespread use of packed dispersed-solvent-extraction columns as a means of separating the components of solutions has shown the need for fundamental information on the extraction mechanism of the column. This investigation was undertaken to elucidate the phenomena of dispersed-liquid-phase holdup\* within a randomly packed extraction column in a partial attempt to determine the interfacial area of contact of the two phases. Holdup information, along with drop-size information, for a given system and packing provides a means of calculating the interfacial-contact area.

The effect of (1) flow rates and (2) packing size upon the point holdup of a toluene dispersed phase flowing countercurrent to a continuous water phase in a packed liquid-liquid extraction column

was studied by means of a radioisotope technique which entailed the measurement of gamma radiation emitted from the "tagged" toluene droplets containing iodine-131.

In general, the available holdup data in the literature can be classified into two principal categories, depending upon the manner in which the data were obtained: (1) holdup data in which the volume of holdup was measured by draining the column and separating the desired phase and (2) holdup data obtained by simultaneously closing all streams to and from the column and then measuring the volume of continuous phase needed to restore the altered two-phase interface to its initial position.

Row, Koffolt, and Withrow (6) obtained holdup data during their study of the rate of mass transfer of benzoic acid from water to toluene in an 8.75-in. I.D. packed column. Their holdup data on  $\frac{1}{2}$ -in. Berl saddles,  $\frac{1}{2}$ -in. Raschig rings, and knitted-copper-cloth packing indicate a sharp increase in the liquid holdup as flooding was approached. Allerton, Strom, and Treybal (1) measured holdup in a 3.56-in. I.D. column packed with  $\frac{1}{2}$ -in. carbon rings with

benzoic acid as the solute in the kerosene-water system. Their results indicated an increase in holdup with increasing rates of both phases. Gier and Hougen (5) reported similar results in their holdup measurements made in a 6.0-in. I.D. column packed with  $\frac{1}{2}$ - and  $\frac{3}{4}$ -in. Raschig rings. Their holdup data, which were obtained by determining the volume alteration in the lowering of the interfacial level, were found to be a linear function of the dispersed-phase rate when the continuous-phase rate was constant.

Gayler and coworkers (3 and 4) conducted an extensive study of dispersed-phase holdup using 3-, 6-, and 12-in. I.D. columns with a packed height of 10 ft. The packing used were  $\frac{1}{4}$ -,  $\frac{3}{8}$ -,  $\frac{1}{2}$ -,  $\frac{3}{4}$ -, 1- and 1 $\frac{1}{2}$ -in. ceramic Raschig rings and  $\frac{1}{4}$ -,  $\frac{1}{2}$ -, and 1-in. ceramic Berl saddles. The continuous phase in each of the systems studied was water; methyl isobutyl ketone, butyl acetate, dibutyl carbide, benzene, and isooctane were each used as the dispersed phase. The normal holdup data used by the authors in developing their conclusions were obtained by determining the volume alteration in the lowering of the interfacial level. During the course of the investiga-

S. E. Markas is with California Research Corporation, Richmond, California.

This paper is based on the thesis of S. E. Markas submitted in partial fulfillment of the requirements for the doctorate of philosophy. Original data and calibrations are available on interlibrary loan from Carnegie Institute of Technology, Pittsburgh, Pennsylvania.

\*In liquid-extraction columns the term *holdup* will be used to designate the fractional holdup of the dispersed phase in the portion of the total column volume which may be occupied by liquid.

tion it was found that an additional volume of the dispersed phase was also present in the column, presumably in the form of droplets trapped in the packing. The quantity of permanent holdup present was determined by draining the column after removing the normal holdup from the column. The authors concluded that only the normal holdup was involved in the mass transfer operation; consequently, the normal holdup data were correlated by means of the following equation:

$$V_D + \frac{X}{1-X}(V_C) = F\bar{v}_0X(1-X) \quad (1)$$

Where  $V_D$  and  $V_C$  are the superficial velocity of the dispersed phase and the continuous phase respectively.  $X$  is the fractional holdup,  $F$  is the fractional voidage of packing, and  $\bar{v}_0$  is a velocity characteristic of a given packing.

Wicks and Beckmann (7) conducted a study of dispersed-phase holdup using three extraction columns and six different sized packings. The columns were 3-, 4-, and 6-in. I.D., and the packings consisted of  $\frac{1}{4}$ -,  $\frac{3}{8}$ -,  $\frac{1}{2}$ -,  $\frac{5}{8}$ -,  $\frac{3}{4}$ -, and 1-in. unglazed porcelain Raschig rings. One liquid-liquid system was used, with toluene as the dispersed and water as the continuous phase, the experimental technique being the same as that utilized by Gayler and Pratt (3). The normal holdup, denoted as *free* holdup, was obtained by returning the interface to its initial position; permanent holdup was measured by drainage of the column. An empirical correlation was presented for total holdup (i.e., the summation of free and permanent holdup):

$$X_T = A_1(V_D)^r + B_1(V_D)(V_C)^s \quad (2)$$

where  $X_T$  is the total holdup,  $V_D$  and  $V_C$  are the dispersed- and continuous-phase flow rates, respectively, and the other terms represent constants characteristic of a given packing size and column diameter.

## APPARATUS

A schematic flow diagram of the equipment is shown in Figure 1. Basically the equipment utilized was the same as reported earlier by Wicks (7) with the addition of the counting equipment to measure the gamma radiation from the tagged toluene dispersed phase.

### Scintillation-counting Circuit

A diagram of the scintillation-counting circuit is illustrated in Figure 2. The scintillation counter *A* and the rate meter and high-voltage supply *B* were Nuclear-Chicago models. The recorder *C* was manufactured by the Esterline-Angus Company.

The a.c. input *F* to the rate meter was standard, 110 to 115 volts, 60 cycle. The rate meter *B* was capable of producing voltages up to 1,500 volts and registering

counting rates to 50,000 counts/min. Cable *D* supplied the high voltage to the scintillation counter. The cathode follower input cable *E* transmits the necessary low voltages and also receives the negative ionization pulses produced by the counter. Cables *H* represent the chart drive to the recorder and carry alternating current (110 to 115 volts, 60 cycle). The final component of the circuit *G* denotes cables, through which the counting rate is transmitted to the recorder by means of a d.c. milliamperage signal.

The scintillation counter is shown in detail in Figure 3. The detector consisted of a sodium iodide thallium-activated crystal *B*, a Lucite light pipe *D*, a DuMont 5819 photomultiplier tube *H*, and a preamplifier *I*, for effective coupling of the signal to the count-rate meter. The gamma radiation from iodine-131, entered the detector and caused scintillation within the crystal. These gamma photons are channeled by the light pipe, and the signal is in turn amplified by the multiplier tube.

As shown in Figure 3, an appreciable quantity of lead was utilized for shielding and collimation. The sensitive scintillation counter thus shielded is capable of detecting gamma activities in samples as low as  $10^{-10}$  curie. The collimating shield permitted sharp discrimination against activities more than 15 deg. off the axis of the probe. Scattered and extraneous gamma radiation were filtered from the counter by means of a 1/32-in. lead absorber, and consequently only the 0.364-mev. primaries of iodine-131 were predominately measured.

The scintillation counter and lead shield rested on a mounting, which in turn rested on a platform consisting of a 5-ft.-square section of  $\frac{3}{4}$ -in. plywood, with a 1-ft.-diam. hole in the center, permitting the column to be positioned in the center. The platform was attached to the angle-iron support structures by means of elevating screws, which enabled the platform to be raised or lowered and thus permitted a scanning of the column at various vertical positions.

In addition, rollers attached to the underside of the counter mounting allowed it to be revolved for a circumferential scan of the extraction column.

### Chemical Form of Iodine-131

For this investigation iodine-131 was required to be in a chemical form which was soluble in toluene and completely insoluble in water, to permit "tagging" of the toluene droplets. After a survey of the available forms of the isotope, it was decided that a radioiodinated triolein supplied by the Abbott Laboratories of North Chicago, Illinois, was satisfactory. This compound was prepared from molecularly distilled 99.5% triolein and had iodine-131 attached to the double-bonded carbon groups.

Experiments with a DuNoüy Tensiometer revealed that iodinated triolein and its triolein carrier had no effect on the interfacial tension of the toluene-water system.

### Column Packings

Four different sizes of nonporous unglazed-porcelain Raschig rings were used:  $\frac{1}{2}$ -,  $\frac{3}{8}$ -,  $\frac{1}{4}$ -, and 1 in. The packing was carefully sorted to remove all broken or irregular pieces and was initially cleaned by washing in a 1-1 hydrochloric acid-water solution. The column was packed by slowly dropping several rings at a time into the column, which was filled with water. The method proposed by Wicks (7), that of passing an air stream up through the column at a rate high enough to flood the column was utilized to settle the packing; this is the method generally accepted for a packed absorption column.

## EXPERIMENTAL PROCEDURE

The holdup of the dispersed-solvent phase, toluene, passing countercurrent to the continuous-solvent phase, water, was investigated. Before operation was started, the liquids in the feed drums *A* (Figure 1)

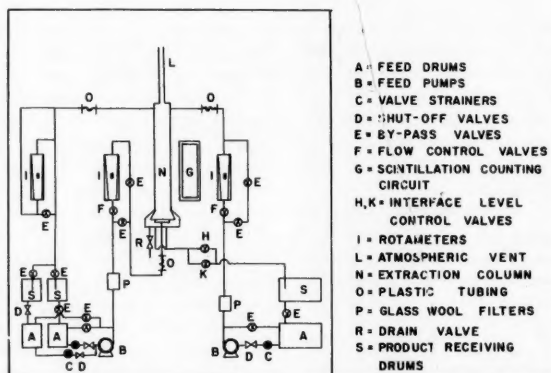


Fig. 1. Schematic flow diagram of experimental equipment.

were mutually saturated with the opposite solvent, and the radioiodinated triolein containing iodine-131 (about 6 mcurie.) was placed in the toluene feed drum A. The liquids were circulated through the column for a period of about 6 hr. to insure that all of the isotope was uniformly distributed throughout the solvent phase.

For a run the by-pass line valves *E* were partially closed and the shut-off valve *D* in the water feed line at the entrance to the tower was opened. The flow rate of the aqueous phase was set by adjusting the flow control valve, *F*. This value was indicated by reading the rotameter *I* in the water feed line. The shut-off valve *D* in the toluene feed line was opened, and the flow rate of the toluene phase was set by adjusting the toluene flow-control valve *F*. Toluene entered the column via the dispersed-phase distributor and rose through the packing as drops. Valve *K* was adjusted until the two-phase interface was located approximately 3 in. above the top of the packing. By means of the finer control valve *H*, the interface was located at the exact mark, 3 in. above the packing. Operation was held constant and the flow rates were observed on the rotameters *I*.

The scintillation counter was oriented so that the front end was approximately 6¼ in. from the outer edge of the column. It was so positioned that the counter and the cross section of the column were symmetrical; i.e., the axis of the probe passed through the center of the cross section of the column. The platform was elevated to a position where the scintillation counter viewed the middle section of the column at a point equidistant from the entrance and exit sections.

When a count was taken, the rotameter (Figure 2) was turned on and the high voltage adjusted. After a period of approximately 20 min. both the toluene-water system and the rate meter came to equilibrium. At this point the Esterline-Angus recorder was turned on to give a permanent record of the counting rate.

At a given vertical position the counter was revolved around the column to four different positions 90 deg. apart, and a separate counting record was obtained for each. For the larger packing, i.e., ¾- and 1-in. rings, two and sometimes three different vertical positions were also investigated. This produced eight and even twelve

separate counting rates for averaging purposes at a given dispersed- and continuous-phase flow rate. These horizontal planes were 3 in. apart.

To calibrate these radiation rates in terms of holdup, i.e., the fractional part of the total void volume within the column that is occupied by the dispersed-phase droplets, the column was filled only with a stationary column of toluene. Correspondingly, all the void volume in the column was occupied by the normally dispersed "tagged" phase. The radiation emitted under these conditions was recorded as outlined above. The ratio of the two radiation intensities (with suitable corrections) yielded directly the fractional holdup within the column under operating conditions.

In the investigations to determine whether all or a fraction of the total holdup had a net movement through the column, both a tagged and an "isotope-free" toluene phase were employed.

Initially equilibrium holdup was generated in the column by the method previously outlined, only the water and tagged toluene phases being used. When equilibrium conditions were reached, the flow of the tagged toluene was stopped and replaced by the flow of an isotope-free toluene phase. This was accomplished by closing valves *D* and *E* (Figure 1) corresponding to the tagged toluene feed and receiving tanks *S* and *A* and opening valves *D* and *E* corresponding to the isotope-free toluene-phase feed and receiving tanks *S* and *A*. Consequently the radiation rates detected by the scintillation-counting circuit *G* were indicative of the rate at which the dispersed phase was being displaced and of the quantity of the total holdup that had a net movement through the column, resulting from collisions with succeeding toluene droplets.

The quantity of radioiodinated triolein used was generally 6 mcurie. when it was initially placed in the system. Because of decay, fresh batches of isotope had to be introduced into the system every 3 or 4 weeks.

#### TYPES OF DISPERSED-PHASE HOLDUP

Gaylor and Pratt (3) and Wicks (7) have presented data and correlations for the dispersed-phase holdup within a

packed extraction column. The total dispersed-phase holdup was defined as the sum of the free holdup and the permanent holdup. The free holdup was measured by determining the number of dispersed-phase droplets that would rise to the interface and coalesce when all entry and exit streams to and from the column were stopped. The permanent holdup was then determined by draining and washing the column free of all the remaining dispersed phased trapped within the packing.

Gaylor and Pratt (3) presumed that the permanent holdup was permanently locked in the packing and that, becoming saturated, it has no influence on mass transfer. Wicks (7) however, presumed that some of this permanent holdup had a net movement through the column, resulting from collisions with succeeding droplets, and consequently tentatively defined an "operational" holdup. This holdup consisted of the free holdup plus a fraction of the permanent holdup presumably having a net movement through the column. Wicks endeavored to free these temporarily held droplets by means of pulsations of the continuous phase, although he realized that this procedure only approximated the actual droplet behavior.

By using a tagged toluene phase, as well as an isotope-free toluene phase, these studies revealed that besides the free holdup all the permanent holdup had a net movement through the column. Although all these droplets comprising the permanent holdup have an over-all movement, this movement is not uniform. A range of different retention times in the packing exists for these permanent holdup droplets.

In addition, this investigation revealed a new type of holdup, which is termed *hysteresis holdup*. As the name implies, it was noted that total holdup experienced a hysteresis cycle when the continuous-phase velocity was varied from a given value to a maximum terminal value and back again to the original value at a given dispersed-phase velocity. This hysteresis did not exist for variations of the dispersed-phase velocity at a given continuous-phase velocity in the region below loading. Although the free holdup is the same for the given  $V_D$  and  $V_C$ , this hysteresis is actually experienced by the permanent holdup and consequently influences the total holdup of the dispersed phase. As a result, four types of holdup were studied:

1. *Permanent holdup*—the volume of dispersed phase which is trapped in the packing and does not rise freely to the interface because of difference in density.

2. *Total holdup*—the total volume of dispersed phase within the effective packing volume at any time, i.e., free holdup plus permanent holdup.

3. *Hysteresis holdup*—the volume of

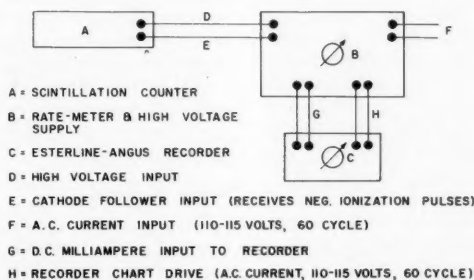


Fig. 2. Diagram of scintillation-counting circuit.

dispersed phase which is permanently trapped in the packing as a consequence of the prior history of the column with respect to variations of the continuous phase. At a given dispersed-phase velocity the same curve does not define the variation of permanent holdup with increasing and decreasing continuous-phase velocity. The difference between these two curves at a given  $V_C$  represents the hysteresis holdup.

4. *Operational holdup*—the volume of dispersed phase which Wicks (7) considered to be the active portion of the dispersed phase taking part in mass transfer.

#### EXPERIMENTAL HOLDUP RESULTS

Values of permanent and total holdup, reported as volume percentage of the total void, were obtained and grouped in series to illustrate the hysteresis effect. The range of data covered a 6-in. I.D. column packed with  $\frac{1}{2}$ -,  $\frac{5}{8}$ -,  $\frac{3}{4}$ -, and 1-in. Raschig rings and an unpacked spray column. Table 1 lists typical experimental results obtained for  $\frac{5}{8}$ -in. rings in the 6-in. I.D. column.

The total-holdup data obtained were checked for consistency by plotting the percentage of total holdup vs. the dispersed-phase velocity at an constant continuous-phase velocity. A typical illustration of the consistency obtained is presented in Figure 4.

The total-holdup results obtained for a specific packed bed were reproducible within 8 to 9% on a relative basis. The results for the runs with the  $\frac{1}{2}$ - and  $\frac{5}{8}$ -in. packings were reproducible within 5 to 6%, owing to the larger magnitude of the holdup values. The holdup data for the  $\frac{3}{4}$ - and 1-in. rings, as well as for the spray column, however, were reproducible within 9 to 10%. Similar trends in reproducibility existed for the permanent holdup, although, because of the smaller range of magnitudes involved, the percentages tend to be a little higher.

#### Channeling of the Dispersed Phase

As mentioned in the description of the experimental procedure, in order to obtain an average holdup at a given vertical position in the packing, the scintillation counter was revolved around the column. A typical illustration of the variation encountered is presented in Figure 5. For the 1-in. rings the variation

is quite pronounced, with the maximum value deviating 33% from the minimum value. This deviation is about 25% for the  $\frac{3}{4}$ -in. rings and only 9% for the  $\frac{5}{8}$ - and  $\frac{1}{2}$ -in. rings. It would thus appear that the 25 and 33% deviations represent channeling or maldistribution of the dispersed-phase droplets. The 1- and  $\frac{3}{4}$ -in. rings in the 6-in. I.D. column represent a column diameter to packing size ratio of 6.0 and 8.0 respectively, and in the other two cases the ratio is 9.6 and 12.0. The criterion, therefore, to eliminate channeling in a packed extraction column would be that the ratio of column diameter to packing size should be maintained larger than 8.0 and preferably about 10.0.

The tabulated values of total holdup shown on Figure 5 represent the average of the four values obtained through

circumferentially scanning the column. Various other methods of averaging were analyzed, including ones postulated by radiation-counting theory. It was found, however, that the circumferential deviation was not of sufficient magnitude to permit other averaging methods to yield results which were different from the arithmetic average; consequently the experimental results of holdup represent arithmetic averages.

#### Holdup Hysteresis

The dispersed-phase-holdup results were obtained by setting  $V_D$  and increasing  $V_C$  from zero in intervals as outlined by the data to a terminal  $V_C$ . When the variation was reversed, i.e.,  $V_C$  decreased from its maximum value back to zero again, the data did not fall on the original curve. In other words there was a hys-

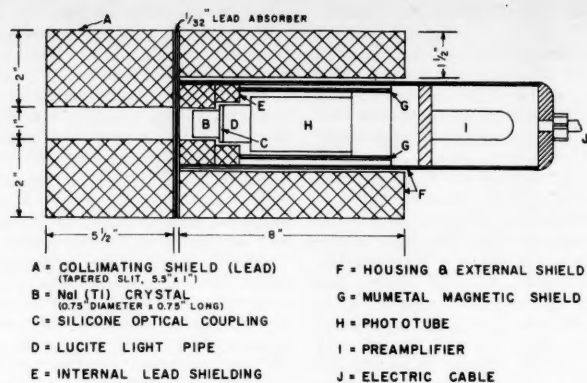


Fig. 3. Scintillation-counter specifications.

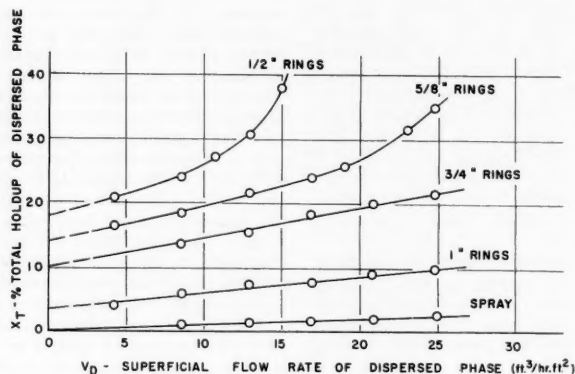


Fig. 4. Percentage of total holdup at zero continuous-phase flow.

TABLE 1. COEFFICIENTS FOR CORRELATION OF HOLDUP DATA

Packings size, in.	$A_1$	$B_1$	$C_1$	$D_1$
$\frac{1}{2}$	17.5	0.402	0.768	0.0914
$\frac{5}{8}$	13.5	0.080	0.658	0.00682
$\frac{3}{4}$	10.5	0.038	0.480	~0.001
1	3.8	~0.0	0.201	~0.0008
Spray	0.0	0.0	0.099	~0.0



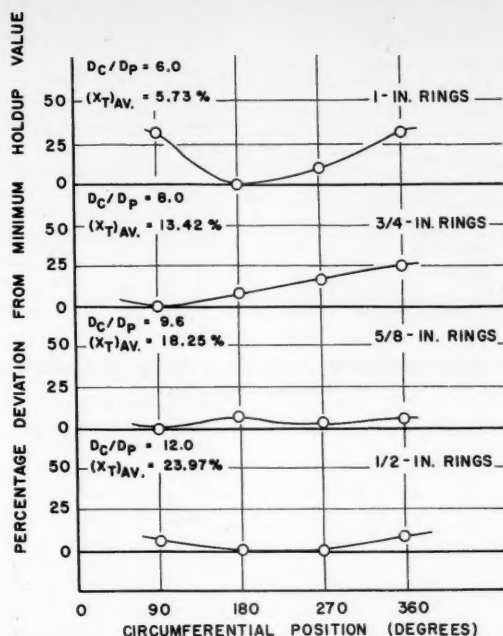


Fig. 5. Circumferential variation of holdup at midpoint of packed height;

$$V_D = 8.51 \text{ cu. ft./hr. (sq. ft.)}, V_C = 0.$$

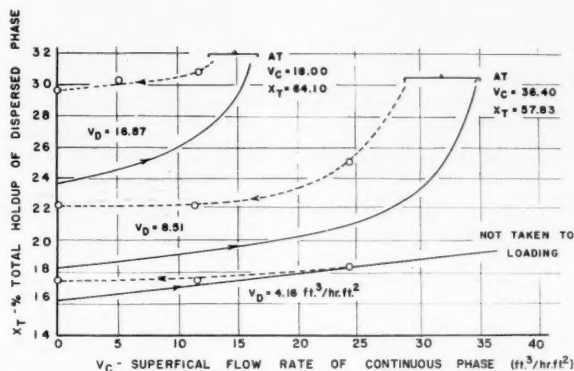


Fig. 6. Percentage of total holdup for 5/8-in. rings with hysteresis of holdup.

ally, the tagged toluene phase was taken to loading and then returned to a continuous-phase flow rate of zero; i.e., a hysteresis cycle was executed. The flow of the tagged toluene was stopped, and the flow of the isotope-free toluene was simultaneously started.

Such an operating procedure disclosed the quantity of toluene droplets which had a net movement through the packing. Figure 7 illustrates the results of such an operation performed with 5/8-in. Raschig rings. The "normal" 100% mark on the ordinate axis denotes the total holdup of the dispersed phase corresponding to the lower portion, or base line, of the hysteresis curve. The other horizontal line designates the total holdup corresponding to the upper portions of the hysteresis curve.

The results reveal that during operation on the lower portion of the total-holdup hysteresis curve all the total holdup has a net movement through the packing. On the upper portion, however, only the holdup corresponding to the lower portion of the curve will be displaced. The hysteresis holdup, i.e., the difference between the upper and lower portions of the curve, is permanently trapped in the packing.

#### Entrance Effects

During the course of this investigation the column was completely scanned vertically as well as horizontally, and thus were permitted the determination of vertical variations of the holdup of the dispersed phase (Figure 8). As this run was performed at a rather large continuous-phase flow rate, entrance effects were quite pronounced.

In the region of the top of the packing there is an appreciable increase in holdup. This increase is due to back-circulating toluene droplets. In Figure 1 it will be noted that the water phase enters the column via two water-inlet pipes located about 3 in. from the top of the packing. At higher water flow rates the downward thrust of the incoming phase causes many of the rising toluene droplets to back circulate into the packing. For this column height and for the given flow rates, Figure 8 reveals that there is over a 100% increase in holdup in a region constituting about 15% of the packed height. For larger packed heights this region will, of course, represent a smaller percentage of the packed height of the column.

#### CORRELATION OF HOLDUP DATA

The primary criteria used in developing equations suitable for correlating the various holdup effects were simplicity of ultimate use and the interrelation of any coefficients for the three types of holdup reported. Accordingly, the following empirical equations were used to correlate the data. It should be kept in mind that

teresis effect. To validate these results, runs were performed which lasted 3 to 4 hours, revealing that hysteresis actually was present; the effect was not due to unsteady state conditions. Figure 6 represents an illustration of this effect for the 5/8-in. Raschig rings. The lower curve with  $V_D = 4.16$  as a parameter corresponds to data taken in the region below loading; the hysteresis holdup (difference between upper and lower positions of curve) is rather small. For  $V_D = 8.51$  and  $V_D = 16.87$ , however, the hysteresis holdup is quite large, because these data consist of runs taken to the region of loading and back again. Experimentally it was found that the free

holdup remains the same for both the upper and lower portions of the hysteresis curve; it is actually the permanent holdup that undergoes hysteresis and produces this effect in the total holdup results. Below the region of loading, however, no hysteresis existed for variations of the dispersed-phase velocity at a constant continuous-phase flow rate.

#### Operational Holdup Conclusions

In order to discover which type of holdup constituted the active area of mass transfer and to obtain an insight into Wicks's operational holdup, a series of runs was performed on both a tagged and an isotope-free toluene phase. Ini-

the equations developed are for the specific packings used, for flow conditions below loading, for the system toluene-water, and for the specific mode of tower operation and packing herein reported.

#### Permanent Holdup

The permanent holdup in the region below loading can be represented by

$$X_P = A_1 + B_1(V_C) \quad (3)$$

where  $X_P$  = permanent holdup and  $V_C$  = continuous-phase flow rate, cu. ft./ (hr.) (sq. ft.)

#### Total Holdup

The experimental data on total holdup have been correlated by

$$X_{T0} = A_1 + C_1(V_D) \quad (4)$$

where  $X_{T0}$  = the total holdup at zero continuous-phase flow rate and

$$X_T = A_1 + B_1(V_C) + C_1(V_D) \quad (5)$$

where  $X_T$  = the total holdup of the dispersed phase. Equation (5) was found to represent about 95% of the total holdup within the column, and an additional term was required to account for the remaining 5%. Accordingly, an additional term was added to Equation (5) to account for all the total holdup:

$$X_T = A_1 + B_1(V_C) + C_1(V_D) + D_1(V_C)(V_D) \quad (6)$$

The free holdup present within the packing is obtained as the difference between Equations (6) and (3):

$$X_F = C_1(V_D) + D_1(V_C)(V_D) \quad (7)$$

where  $X_F$  = the free holdup.

#### Holdup with Hysteresis

The equations for correlating the hysteresis holdup were obtained in an analogous manner on the assumption that the permanent holdup of the dispersed phase was defined by the maximum continuous-phase velocity employed during the continuous operation of the packed column. The equations obtained were

$$X_P^* = A_1 + B_1(V_{Cm}) \quad (8)$$

where  $X_P^*$  = the permanent holdup corresponding to the upper portion of the hysteresis curve and  $V_{Cm}$  = the maximum continuous-phase flow rate that has been employed in the continuous operational history of the column.

The total holdup, with hysteresis, is given by

$$X_T^* = X_P^* + X_F \quad (9)$$

Substitution of Equations (7) and (8) into (9) yields

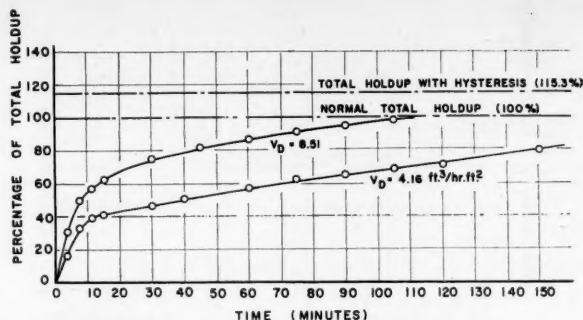


Fig. 7. Relative displacement of dispersed-phase holdup for 5/8-in. rings at zero continuous-phase flow.

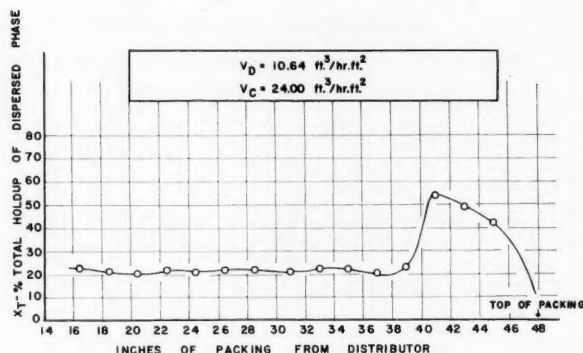


Fig. 8. Vertical variation of dispersed-phase holdup for 5/8-in. Raschig rings:

$$V_D = 10.64 \text{ cu. ft./ (hr.) (sq. ft.)}, V_C = 24.00 \text{ cu. ft./ (hr.) (sq. ft.)}.$$

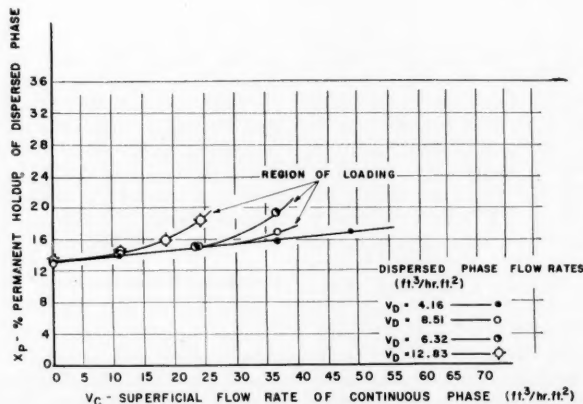


Fig. 9. Percentage of permanent holdup for 5/8-in. Raschig rings.

$$X_T^* = A_1 + B_1(V_{cm}) + C_1(V_D) + D_1(V_C)(V_D) \quad (10)$$

Table 2 presents the values of the coefficients  $A_1$ ,  $B_1$ ,  $C_1$ , and  $D_1$  obtained from the experimental data. It was generally found that the equations presented permitted the calculation of the holdup to within 8% of the observed data with the exception of the data in the vicinity of loading.

#### SUMMARY

This investigation involved the study of the effect of flow rates and packing size upon the holdup of a toluene-dispersed phase flowing countercurrent to a continuous water phase in packed columns. Four different packings were used:  $\frac{1}{2}$ -,  $\frac{5}{8}$ -,  $\frac{3}{4}$ -, and 1-in. nonporous, unglazed Raschig rings, in an experimental column of 6 in. I.D. The results of the investigation are as follows:

Consistent data were obtained for three different types of holdup: permanent, total, and hysteresis. The

permanent holdup includes the dispersed phase droplets, which do not rise freely to the water face. The total holdup is the total volume of dispersed phase within the effective packing volume at any time. The hysteresis holdup is the volume of dispersed phase permanently trapped in the packing as a consequence of executing a hysteresis cycle with variations of the continuous-phase velocity. This holdup represents the difference between the upper and lower portions of a total-holdup hysteresis curve.

The holdup data below the loading point have been correlated by the equations

$$X_P = A_1 + B_1(V_C)$$

$$X_T = A_1 + B_1(V_C) + C_1(V_D) + D_1(V_C)(V_D)$$

$$X_P^* = A_1 + B_1(V_{cm})$$

Tabulated values for the coefficients are given.

When operating procedure is defined by the lower portion of the hysteresis

curve, all the dispersed-phase droplets, free and permanent, have a net movement through the column. All the permanent holdup droplets are normally freed during the course of operation by impact from succeeding droplets. Hysteresis holdup, however, represents permanently trapped solvent droplets that have not net movement through the column.

Channeling, i.e., maldistribution of the dispersed phase occurs when the ratio of column diameters to packing size is 8.0 or less.

The effect of packing size on holdup is in agreement with the findings of previous investigators (3, 4, 7). The holdup of the dispersed phase increases as the packing size decreases.

Two distinct zones of flow were found to occur. The increase in holdup with increasing continuous- and dispersed-phase velocities was different in each zone. In the zone below loading, the holdup was found to increase linearly with the dispersed-phase flow at a constant continuous-phase flow rate. In addition, the increase of holdup with continuous-phase flow was approximately linear at a constant dispersed-phase flow rate in the region below loading.

TABLE 2

Run	6 in. I.D. Packed height: 48 in.		$\frac{5}{8}$ -in. rings Void fraction: 0.680			
	Flow rates, cu. ft./ (hr.) (sq. ft.)		Stream temperature °F.		Holdup data, vol. % of total voids	
	Toluene in	Water in	Toluene inlet	Water inlet	Permanent	Total
2-1	4.16	0.0	91	87	14.83	16.17
-2	4.16	11.50	92	90	13.88	17.18
-3	4.16	24.00	92	94	14.92	18.26
-4	4.16	36.40	93	97	15.75	19.35
-5	4.16	48.00	92	98	16.79	21.75
-6	4.16	24.00	93	99	16.12	18.01
-7	4.16	11.50	94	100	—	17.33
-8	4.16	0.0	96	95	16.08	17.67
-9	6.32	0.0	91	88	12.65	16.05
-10	6.32	11.50	91	91	13.98	17.52
-11	6.32	24.00	93	94	14.66	19.58
-12	6.32	36.40	94	97	16.88	22.40
-13*	6.32	48.00	94	98	18.32	29.56
-14	6.32	24.00	95	100	16.49	22.38
-15	6.32	11.50	93	100	—	21.86
-16	6.32	0.0	95	95	17.70	20.75
-17	8.51	0.0	85	87	13.28	18.25
-18	8.51	11.50	86	87	14.38	19.33
-19	8.51	24.00	86	90	15.01	21.09
-20*	8.51	36.40	91	91	19.38	57.83
-21	8.51	24.00	90	93	18.71	25.13
-22	8.51	11.50	92	95	18.06	22.53
-23	8.51	0.0	92	92	17.06	22.30
-24	12.83	0.0	89	87	13.33	21.41
-25	12.83	4.90	89	88	13.49	22.02
-26	12.83	11.50	91	92	14.84	22.73
-27	12.83	18.00	93	94	15.80	24.34
-28	12.83	24.00	93	95	18.32	27.46
-29*	12.83	30.25	94	97	16.93	58.44
-30	12.83	24.00	94	99	18.44	29.46
-31	12.83	11.50	94	100	19.30	26.91
-32	12.83	0.0	94	95	16.71	24.50

\*Flow rates in vicinity or in excess of loading-point velocities.

#### NOTATION

$A_1$  = coefficient in holdup correlation  
 $B_1$  = coefficient in holdup correlation  
 $C_1$  = coefficient in holdup correlation  
 $D_1$  = coefficient in holdup correlation  
 $V$  = superficial liquid velocity, cu. ft./ (hr.) (sq. ft. of column cross section)  
 $X$  = fractional holdup of the dispersed phase in that portion of the column volume which may be occupied by liquid

#### Subscripts

$C$  = continuous phase  
 $D$  = dispersed phase  
 $F$  = free  
 $P$  = permanent  
 $T$  = total

#### LITERATURE CITED

1. Allerton, Joseph, B. O. Strom, and R. E. Treybal, *Trans. Am. Inst. Chem. Engrs.*, **39**, 361 (1943).
2. Dell, F. R., and H. R. C. Pratt, *Trans. Inst. Chem. Engrs. (London)*, **29**, 89 (1951).
3. Gayler, R., and H. R. C. Pratt, *ibid.*, **29**, 110, (1950).
4. Gayler, R., N. W. Roberts, and H. R. C. Pratt, *ibid.*, **31**, 57 (1953).
5. Gier, T. E., and J. O. Hougen, *Ind. Eng. Chem.*, **45**, 1362 (1953).
6. Row, S. B., J. H. Koffolt, and J. R. Withrow, *Trans. Am. Inst. Chem. Engrs.*, **37**, 559 (1941).
7. Wicks, C. E., and R. B. Beckmann, *A. I. Ch. E. Journal*, **1**, 426 (1955).

Presented at A.I.Ch.E. Boston meeting

# Reaction Kinetic Studies: Catalytic Dehydrogenation of Sec-butyl Alcohol to Methyl Ethyl Ketone

JOSEPH J. PERONA and GEORGE THODOS

Northwestern Technological Institute, Evanston, Illinois

Reaction kinetics for the catalytic dehydrogenation of sec-butyl alcohol to methyl ethyl ketone has been investigated at atmospheric pressure and temperatures ranging from 650° to 750°F. in the presence of solid brass spheres, 1/8 in. in diameter. The nature of this catalyst permitted a direct evaluation of the surface involved in this reaction and allowed the definition of a surface-feed ratio to be expressed as  $S/F$  in place of the conventional weight-feed ratio  $W/F$  commonly used in catalytic studies. Feed compositions ranged from sec-butyl alcohol to mixtures containing high percentages of methyl ethyl ketone and hydrogen.

In these studies mass transfer effects were found to be significant and, for a proper representation of conditions at the catalyst surface, must be taken into account. The effect of feed compositions on the initial rates of reaction showed that the rate-controlling step was the desorption of hydrogen involving a single-site mechanism.

In addition, the results of these studies have been used to produce values of height of reactor unit HRU which have been found to correlate with mass velocity and temperature. The HRU provides a simple means of calculating the depth of catalyst necessary to effect a designated conversion.

The design of catalytic reactors according to fundamental principles requires an exacting background knowledge of the reaction mechanism taking place on the surface of the catalyst. Although empirical approaches have proved expedient for the design of commercial units, a more fundamental approach to the solution of such problems becomes increasingly significant. As a result of the developments of the reaction-rate mechanisms proposed by Hougen and Watson (2) and involving the participation of active centers on the catalytic surfaces, it is now possible to associate the rate of reaction with the behavior of the reactants and products on these active centers. Several possible mechanisms have been produced, and to date these constitute the fundamental background for comprehension of the various steps taking place in the course of a reaction. The possible rate mechanisms are numerous, and the development of the corresponding rate equations is presented elsewhere (2).

The preponderance of catalytic reactions has been carried out in the presence of porous catalysts which provide an extensive network through which the reactants and products must diffuse in order for the reaction to proceed. The variables influencing the diffusional phenomena occurring within the catalyst pores have been considered theoretically by Thiele (12). These diffusional effects have been shown to decrease with the size of the catalytic particles and to become insignificant for fluidized beds. For larger particles in fixed beds, diffusion

to or from the interior of the catalyst may be significant and presents an additional variable in the fundamental study of reaction mechanisms. The use of solid brass as catalyst for the dehydrogenation of sec-butyl alcohol, besides eliminating this possible variable, also permits the direct calculation of the surface taking part in the reaction. Since it is possible to account for the surface participating in the reaction, the relationship of space velocity and conversion  $dx_A$  taking place in an elementary section of reactor volume whose surface is  $dS$  may be expressed as

$$F dx_A = r_A dS \quad (1)$$

From Equation (1) the surface-feed ratio  $S/F$ , which is directly related to space velocity, now can be defined in terms of conversion and reaction rate as follows:

$$\frac{S}{F} = \int_0^{x_A} \frac{dx_A}{r_A} \quad (2)$$

The surface-feed ratio  $S/F$  is a more direct relationship and is used in these studies rather than the conventional weight-feed ratio  $W/F$ . For porous catalysts the use of the weight-feed ratio  $W/F$  proves more expedient and is found to be specific to the type of catalyst, method of preparation, and size. On the other hand, the ratio  $S/F$  is more fundamental in this application since it deals only with the specific nature of the reaction and not the method of preparation and size of the catalyst. Therefore, whenever the surface of the catalyst can be conveniently obtained, the surface-feed ratio  $S/F$  may be applied.

## EXPERIMENTAL EQUIPMENT

The experimental unit used in these studies, which is presented diagrammatically in Figure 1, consisted of a small continuous pilot plant having a stainless steel tubular reaction heated by an electric furnace. Liquid mixtures of sec-butyl alcohol and methyl ethyl ketone were pumped into the reactor from a calibrated feed tank. The introduction of hydrogen, nitrogen, and air to the system was regulated by means of a needle valve, and the flow rates were measured with a rotameter. The reactor effluent was passed through a water-cooled condenser to a phase separator, from which noncondensable gases could be collected over salt water in the gas-sampling bottle or passed through the wet-test meter to measure the rate of production.

### Reactor

Figure 2 shows the details of the reactor, which was fabricated from 1½-in., type-304 stainless steel pipe and was 40 in. long. Two stainless steel sleeves, 1 and ½ in. I.D., provided a variation of cross-sectional area of the catalyst bed. In this manner greater ranges of mass velocity through the catalyst were conveniently obtained with the equipment available. Thermowells provided on the top flange and bottom plug permitted the establishment of temperature profiles over the full length of the reactor. The entire volume of the reactor, with the exception of the catalyst zone, was filled with 3- to 5-mm. glass shot. The glass shot above the catalyst bed provided adequate heat transfer surface and insured a uniform fluid flow pattern; whereas this packing below the catalyst bed acted as a support and also decreased the void volume of the reactor, causing the rapid removal of the effluents.

## PRELIMINARY INVESTIGATIONS

The catalytic dehydrogenation of secondary alcohols to ketones was first reported by Ipatieff (4) with metals such as iron, zinc, brass, manganese, and nickel. No significant dehydrogenation was noted with aluminum, lead, tin, bismuth, antimony, or magnesium. Balandin and Liberman (1) and Neish (9) showed that copper has initial dehydrogenating properties which gradually diminish owing to irreversible poisoning effects. Ivannikov, Tatarskaya, and Gavrilova (5) showed that uranium acts as a promoter to copper, which did not

Joseph J. Perona is at present with the Oak Ridge National Laboratory, Oak Ridge, Tennessee.



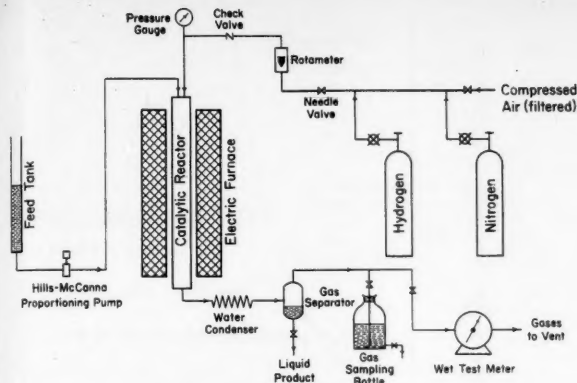


Fig. 1. Flow diagram of experimental equipment.

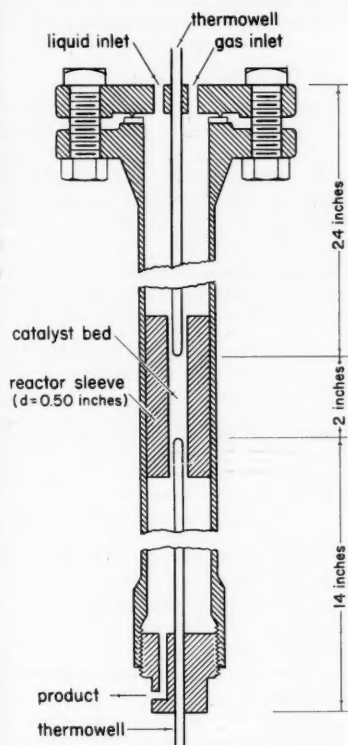


Fig. 2. Experimental reactor.

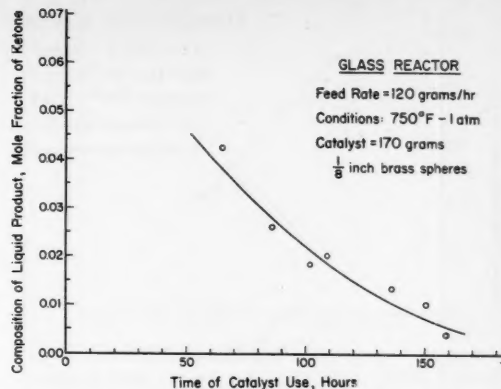


Fig. 3. Activity of catalyst in glass reactor vs. time.

attached to the use of brass for the commercial production of methyl ethyl ketone. The technical information in the literature involving the use of brass for the production of ketones is essentially nonexistent despite the current commercial interest and activity on this subject. Therefore, it was found necessary to conduct a series of exploratory investigations in order to study the behavior of this catalyst under varying conditions of operation.

Brass ball bearings  $\frac{1}{8}$ -in. in diameter having a tolerance of  $\pm 0.001$  in. and composed of 65% copper and 35% zinc were used throughout this study.

Brass spheres in a glass reactor packed with glass shot showed a continued decrease in activity with time as indicated in Figure 3. Inspection showed a

A typical analysis of the effluent gases was found by mass spectrometer measurements to have the following composition:

	Mole fraction
Hydrogen	0.959
Methane	0.033
Ethane	0.001
Ethylene	0.007
	1.000

This indicates that the reaction in the absence of catalyst is basically of a cracking nature with a preponderance of hydrogen resulting in the effluent gases while no ketone was noted in the effluent liquid. In all cases the alcohol involved in this decomposition reaction consumed less than 1% of the alcohol introduced into the reactor.

Experimentation with the stainless steel reactor revealed that blank runs following a regeneration period with air produced relatively high rates of cracked gases which decreased rapidly with time. Average rates of gas production in the course of a run were measured and are expressed as the zigzag lines presented in Figure 5. Instantaneous rates of gas production can be established from the straight-line relationship drawn through these average rates and presented in Figure 5. These observations strongly suggest that the cracking reactions might have been catalyzed to some extent by the metallic oxides produced during the regeneration period and that the decrease in gas rate was due to the reduction of the metallic oxides by the product hydrogen. In order to test this theory, a regeneration period with air was followed by a nitrogen purge and then hydrogen was passed through the reactor at 800°F. for 10 hr. before the start of a run with sec-butyl alcohol and without a catalyst. The rate of cracked gases produced under these conditions was found to be only about 25 cc./hr. in comparison with a rate of about 400

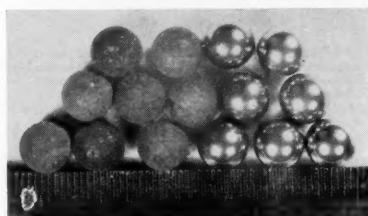


Fig. 4. Appearance of new and used brass ball bearings as catalyst.

show poisoning effects after 60 hr. of use. Several dehydrogenating catalysts of the zinc oxide type are reported in the literature (7, 8, 10). Iron, manganese, and nickel, although capable of dehydrogenating secondary alcohols to ketones, have the added catalytic ability to decompose the ketones produced into olefins and oxides of carbon (4). In addition, Ipatieff (4) noted that zinc tended to oxidize in the course of the reaction involving the dehydrogenation of alcohols.

Considerable importance has been

black carbonaceous deposit on both the brass catalyst and the glass spheres which was completely removed by the passage of air at approximately 800°F. The appearance of the oxidized catalyst is essentially black and is compared with a new catalyst in Figure 4.

Several blank runs were made with the glass reactor without a catalyst. With a temperature of 750°F. in the zone ordinarily occupied by the catalyst, an effluent gas rate of approximately 300 cc./hr. was observed for sec-butyl alcohol feed rates of 200 to 600 g./hr.

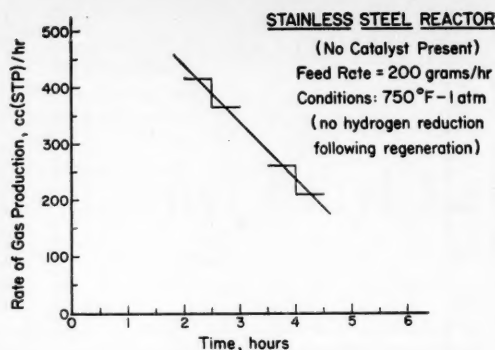


Fig. 5. Cracking activity of blank reactor after regeneration (no hydrogen reduction).

cc./hr. found initially with the stainless steel reactor and no hydrogen reduction following regeneration.

The rate of the cracking reaction was found to increase sharply with temperature, as shown by Figure 6. Therefore, in order to keep the rate of cracking as low as possible and at the same time to obtain a reasonable conversion, a temperature of 750°F. was selected as the maximum to be investigated.

A 24-hr. cycle of 5 hr. of reaction time, 5 hr. of regeneration with air at 800°F., and 14 hr. of reduction with hydrogen at 800°F. was found to yield consistent and reproducible data. The first 2 hr. of feed introduction was used to bring the reactor up to reaction temperature and to allow the reactants to attain chemical equilibrium with the catalyst. Hourly liquid samples were collected, and product gas rates were observed during the last 3 hr. of the reaction time. The decrease in conversion over the 3-hr. period, due to loss in catalyst activity, was of the same order as conversion changes due to slight

temperature variations ( $\pm 5^\circ\text{F}$ ). Values of conversion and temperature over the 3-hr. period were averaged for each run.

#### EXPERIMENTAL RESULTS AND INTERPRETATION OF DATA

Rate data were taken at 650° and 700°F. for four different feed compositions and at 750°F. for five different feed compositions. All runs were made at atmospheric pressure. The extent of conversion was calculated from the composition of the liquid samples, which were analyzed in a Baird infrared spectrophotometer, and from the effluent gases, which were considered to be hydrogen. The material balances resulting from the liquid composition and gases produced were always in good agreement. The experimental data obtained from these studies are presented in Table 1.\*

\*Tabular material has been deposited as document 5219 with the American Documentation Institute, Photoduplication Service, Library of Congress, Washington 25, D. C., and may be obtained for \$1.25 for photoprints or 35-mm. microfilm.

TABLE 2. CALCULATED INITIAL RATES OF REACTION

Temperature, °F.	Feed composition, mole fraction			Partial pressures of feed components, atm.			$r_0$ , Initial rate of reaction, lb.-moles alcohol converted/(hr.)(sq. ft.)
	Alcohol	Ketone	Hydrogen	Average pressure	Alcohol	Ketone	
650	1.000			0.988 atm	0.988		0.00620
650	0.594	0.406		0.978	0.581	0.397	0.00415
650	0.196	0.804		0.979	0.192	0.787	0.00178
650	0.550		0.450	0.990	0.545		0.00640
700	1.000			0.978	0.978		0.0255
700	0.594	0.406		0.962	0.571	0.391	0.0150
700	0.196	0.804		0.979	0.192	0.787	0.0061
700	0.529		0.471	0.986	0.521		0.0254
750	1.000			0.984	0.984		0.0425
750	0.594	0.406		0.985	0.585	0.400	0.0233
750	0.394	0.606		0.965	0.380	0.585	0.0174
750	0.196	0.804		0.978	0.192	0.786	0.0100
750	0.607		0.393	0.987	0.600		0.0425

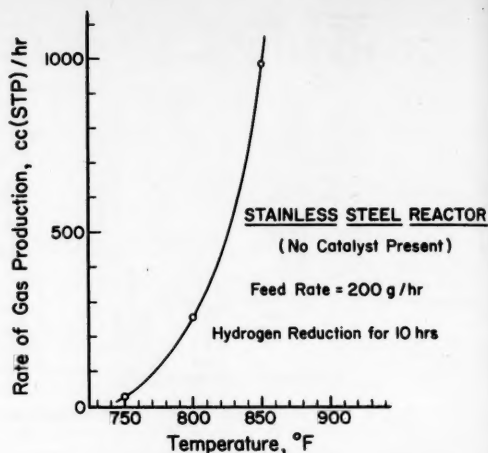


Fig. 6. Cracking activity of blank reactor vs. temperature after regeneration followed by hydrogen reduction.

Plots of conversion  $x_A$  vs. the surface-feed ratio  $S/F$  were produced for all feed compositions at 650°, 700°, and 750°F. and graphically differentiated to obtain the initial rate of reaction corresponding to conversion,  $x_A = 0$ , and surface-feed ratio,  $S/F = 0$ . A plot of  $x_A$  vs.  $S/F$  at 700°F. is presented in Figure 7 for the following four different feed compositions.

	Feed Compositions for 700°F., Mole Fraction			
	1	2	3	4
Alcohol	1.000	0.594	0.196	0.529
Ketone		0.406	0.804	
Hydrogen				0.471
	1.000	1.000	1.000	1.000

The initial rate obtained through these means is directly related to the composition of the feed; at the value  $S/F = 0$  any mass transfer contributions are eliminated, thus permitting a direct association of the initial rate only with the composition of the incoming feed. A summary of initial reaction rates is presented in Table 2 for the different compositions at 650°, 700°, and 750°F.

#### Establishment of Surface Mechanism

The data presented in Table 2 were subjected to a rigorous analysis along the lines proposed by Hougen and Watson (2) in order to establish the reaction mechanism at the catalyst surface controlling this dehydrogenation step. Equilibrium constants  $K$  used in this investigation were calculated from the relationship

$$\log K = -\frac{2,790}{T} + 1.510$$

$$\cdot \log T + 1.865 \quad (3)$$

where  $T$  is expressed in degrees Kelvin. This equation was developed by Kolb

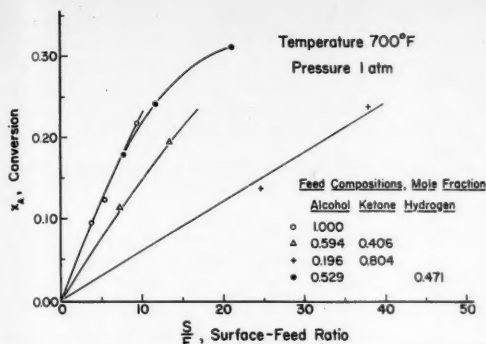


Fig. 7. Experimental results of conversion vs. surface-feed ratio at 700°F. and atmospheric pressure.

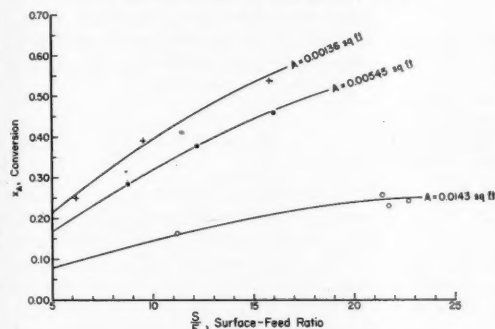


Fig. 9. Effects of mass transfer associated in the catalytic dehydrogenation of sec-butyl alcohol in the presence of brass at 750°F. and 1 atm.

and Burwell (6), who approached equilibrium for this reaction from both directions. Altogether, ten possible reaction model mechanisms were assumed to apply, and the corresponding rate equations were derived for them. The resulting equations are presented in Table 3\*, along with the corresponding calculated constants. The solution of simultaneous equations involving the feed compositions and initial rates of reaction produced the rate constants summarized in Table 3. A review of these constants shows that the desorption of hydrogen from a single site is the only mechanism for which the constants were all positive at 650°, 700°, and 750°F. Therefore, the rate of reaction for the dehydrogenation of sec-butyl alcohol to methyl ethyl ketone in the presence of brass becomes

$$r_A = \frac{C \left[ p_{Ai} - \frac{p_{Ki} p_{Hi}}{K} \right]}{p_{Ki} \left[ 1 + K_A p_{Ai} + K_{AK} \frac{p_{Ai}}{p_{Ki}} \right]} \quad (4)$$

For the derivation of this equation the reaction was assumed to take place in three steps: (1) the adsorption of the alcohol onto an active site, (2) decomposition of the alcohol-active site com-

plex to form methyl ethyl ketone in the vapor phase and adsorbed molecular hydrogen, (3) desorption of the hydrogen in the vapor phase. The first two steps were assumed to be at equilibrium, with the third step controlling the rate of

the reaction. In Equation (4)  $K_A$  is the adsorption equilibrium constant for step 1, and  $K_{AK}$  is the product of  $K_A$  and the equilibrium constant for step 2.

The constants  $C$ ,  $K_A$ , and  $K_{AK}$  are summarized in Table 3 and are correlated

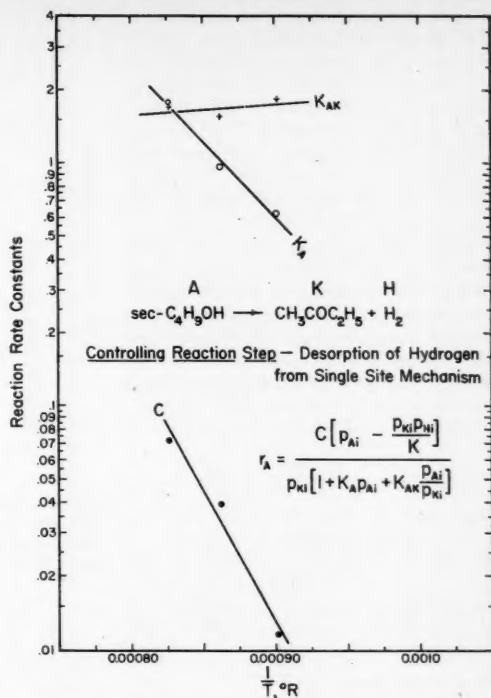


Fig. 8. Relationships of rate constants and temperature.

TABLE 4. COMPARISON OF CALCULATED AND EXPERIMENTAL REACTION RATES AT 700°F.

Run	$(x_A)_{avg}$ Con-	$S/F$ at $(x_A)_{avg}$	Average partial pressures In main gas stream, atm.			Average reaction rate, lb.-moles/ (hr.)(sq. ft.)			Calcu- lated	Experi- mental
			Alcohol	Ketone	Hydro- gen	Alcohol	Ketone	Hydro- gen		
M-1	0.0476	1.9	0.879	0.042	0.042	0.859	0.056	0.056	0.0236	0.0246
M-4	0.097	6.4	0.490	0.419	0.049	0.472	0.426	0.052	0.0137	0.0150
M-8	0.089	3.7	0.453	0.042	0.489	0.445	0.052	0.491	0.0230	0.0233
M-13	0.068	11.3	0.177	0.791	0.013	0.172	0.792	0.014	0.0057	0.0061

TABLE 6. PERTINENT DATA FOR THE CALCULATION OF REACTION RATES OF ILLUSTRATIVE EXAMPLE

Con- version $x_A$	Partial pressure of components in main gas stream, atm.			Mass transfer coefficients, lb.-moles/(hr.) (sq. ft.)(atm.)			Partial pressures of components at catalyst surface, atm.			Reaction rate, lb.-moles/ (hr.)(sq. ft.)
	$p_A$	$p_K$	$p_H$	$k_{gA}$	$k_{gK}$	$k_{gH}$	$p_{Ai}$	$p_{Ki}$	$p_{Hi}$	
0.00	1.000	0.000	0.000							0.000
0.0471	0.910	0.045	0.045	0.720	1.015	3.72	0.859	0.081	0.055	0.0371
0.1285	0.772	0.114	0.114	0.788	1.167	4.07	0.727	0.144	0.123	0.0352
0.229	0.626	0.187	0.187	0.892	1.420	4.63	0.593	0.208	0.193	0.0297
0.310	0.526	0.237	0.237	0.970	1.640	5.05	0.498	0.253	0.242	0.0270
0.600	0.251	0.375	0.375	1.275	2.86	6.70	0.236	0.381	0.378	0.0181
0.800	0.113	0.444	0.444	1.490	4.47	7.83	0.105	0.446	0.445	0.0106
0.900	0.052	0.474	0.474	1.600	6.05	8.46	0.048	0.475	0.475	0.00578

\*See footnote on page 232.

with reciprocal temperature to produce the linear relationships presented in Figure 8. The positive temperature coefficient exhibited with  $K_A$ , the adsorption equilibrium constant of the alcohol, may appear inconsistent with present concepts which point out that this variation should be negative. The majority of catalytic reactions found in the literature show these constants to have a negative temperature coefficient; however, a few exceptions have been reported. In the hydrogenation studies of Sussman and Potter (11) over a copper-magnesia catalyst a positive temperature coefficient for the adsorption equilibrium constant of propylene is similarly reported. These constants can be expressed in equation form with temperature as follows:

$$\log C = -\frac{10,735}{T} + 7.776 \quad (5)$$

$$\log K_A = -\frac{6165}{T} + 5.327 \quad (6)$$

$$\log K_{AK} = \frac{486}{T} - 0.1968 \quad (7)$$

#### Mass Transfer Effects

The establishment of the rate-controlling step on the surface of the catalyst involved initial rates at  $S/F = 0$  corresponding to infinite feed flow rates. At these conditions mass transfer contributions are eliminated, and the partial pressures of the components in the main gas stream become identical to those existing at the solid-gas interface. Therefore, the reaction rate taking place at the surface of the catalyst and expressed by Equation (4) becomes applicable only when the partial pressures of the components are known at the interface.

The effects of mass transfer on this reaction were studied by varying the cross-sectional area of the reactor and observing the influence of the surface-feed ratio  $S/F$  on the conversion  $x_A$ . These investigations were conducted at 750°F. with a feed consisting only of sec-butyl alcohol. The results of these observations, presented in Figure 9, indicate that mass transfer contributions at this temperature are significant and must be accounted for in the proper design of a reactor. The details involving mass transfer calculations to permit evaluation of the partial pressures of the components at the interface are presented by Hougen and Watson (2) and utilize mass transfer coefficients for these components that were produced from the mass transfer factor:

$$j_d = \frac{k_g M_m p_f}{G} \left[ \frac{\mu}{\rho D_m} \right]^{2/3} \quad (8)$$

where  $\mu/\rho D_m$  = Schmidt group, dimensionless. Through these means it becomes possible to evaluate the partial pressure difference of a component across the gas

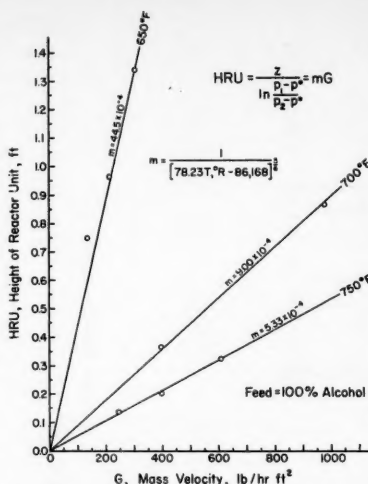


Fig. 10. Relationships of height of reactor unit and mass velocity for the dehydrogenation of sec-butyl alcohol at 650°, 700°, and 750°F. (catalyst: brass spheres 1/8 in. in diameter).

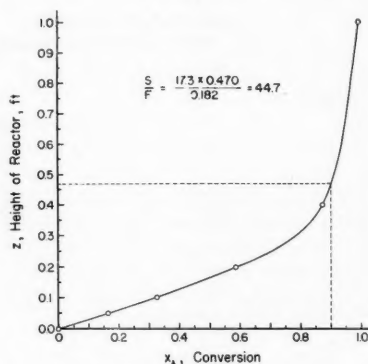


Fig. 11. Reactor height vs. conversion relationship for illustrative example (HRU approach).

film, thus permitting the use of the rate equation, which becomes applicable to conditions existing at the surface of the catalyst. Partial pressures at the interface were calculated for four runs at 700°F. and covered a wide range of compositions of alcohol, ketone, and hydrogen. The reaction rates calculated from these interfacial partial pressures are presented in Table 4 and compared with the average experimental rates obtained from the  $x_A$  vs.  $(S/F)$  curves at conditions of average conversion. The approach involving mass transfer calculations, illustrated in a later section, is found to be, although rigorous, somewhat unwieldy for expediency.

#### Height of Reactor Unit

The combined contributions of mass transfer effects and the reaction at the surface are conveniently represented by the height of reactor unit, HRU. For a reaction which is unimolecular in both directions and for which the partial-

pressure changes of the components across the film are equal and the adsorption terms in the denominator of the rate equation are negligible, Hurt (3) defines the height of a catalytic reactor through the expression

$$z = (HCU + HTU)N_R = (HRU)N_R \quad (9)$$

where  $HCU$  represents the height of catalytic unit resulting from the surface reaction;  $HTU$ , the height of transfer unit due to mass transfer effects; and  $HRU$ , the height of reactor unit, which represents the contribution of both mass transfer and surface-reaction effects.

Although Hurt in the development of these concepts has postulated a unimolecular reaction, these units have been assumed to apply in the dehydrogenation of sec-butyl alcohol, where

$$N_R = \ln \frac{p_1 - p^*}{p_2 - p^*} \quad (10)$$

From the data of Table 1,  $HRU$  values have been calculated for a feed consisting of sec-butyl alcohol at 650°, 700°, and 750°F. The resulting  $HRU$  values and data from which they were derived appear in Table 5† and are plotted in Figure 10 as straight lines against mass velocity which pass through the origin. Consequently this relationship of  $HRU$  becomes

$$HRU = mG \quad (11)$$

where  $G$  represents the mass velocity, pounds per hour per square feet, and  $m$  is a constant which may be expressed in terms of temperature through the relationship

$$m = \frac{1}{(78.23T - 86,168)^{5/6}} \quad (12)$$

in which  $T$  is the reaction temperature in degrees Rankine. Although the theoretical background involving the definition of  $HRU$  for this reaction is not rigorous, the relationships resulting from the application of Equation (11) to produce the straight lines of Figure 10 affords an expedient means for the design of reactors which incorporate the simultaneous contribution of both mass transfer and the reaction taking place on the surface of the catalyst. This approach eliminates the unavoidable and laborious trial-and-error procedure resulting from the application of the multiconstant rate equation and necessary mass transfer calculations for the establishment of the proper rate of reaction.

#### Illustrative Example

The catalytic dehydrogenation of secondary butyl alcohol to methyl ethyl ketone is to be carried out at 750°F. and atmospheric pressure in a cylindrical reactor 3 in. in diameter and packed with 1/8-in. brass spheres. A feed stream of 2 gal./hr. of

†See footnote on page 232.



secondary butyl alcohol is introduced to the reactor.

Calculate the reactor height required to effect a 90% conversion using the following:

- the height-of-reactor-unit (HRU) approach
- the reaction-rate equation with associated mass transfer calculations

#### Solution

Feed rate =  $2 \times 6.7 = 13.4$  lb./hr. = 0.182 lb.-moles/hr.

Cross-sectional area of reactor =  $\pi/4(3/12)^2 = 0.0490$  sq. ft.

Mass velocity =  $13.4/0.0490 = 275$  lb./hr.(sq. ft.)

Catalyst surface: For a void volume fraction,  $\epsilon = 0.40$ , the catalyst surface becomes 17.3 sq. ft./ft. of reactor height

PART A. From Figure 10,  $HRU = 0.147$  ft. at  $G = 275$  lb./hr.(sq. ft.) and  $750^\circ\text{F}$ . The equilibrium constant at this temperature  $K_p = 95.94$  was used to calculate the equilibrium composition, which is

	Mole fraction
Alcohol	0.0026
Ketone	0.4987
Hydrogen	0.4987
	1.0000

The height of the reactor required when sec-butyl alcohol is charged to the reactor becomes

$$z = (HRU)N_R = (HRU) \ln \frac{p_{A_1} - p_A^*}{p_{A_2} - p_A^*}$$

$$= 0.147 \ln \frac{1.000 - 0.0026}{0.0026} = 0.147 \ln 1.000 = 0.0026$$

Assumed values of  $z$  produced the following partial pressures of alcohol leaving the reactor  $p_{A_2}$ , corresponding to conversions  $x_A$ .

$z$ , ft.	$p_{A_2}$ , atm.	$x_A$
0.00	1.000	0.000
0.05	0.713	0.168
0.10	0.508	0.326
0.20	0.259	0.588
0.40	0.0682	0.872
1.00	0.0037	0.993

The relationship of reactor height  $z$  vs. conversion  $x_A$  is presented in Figure 11. From this figure a reactor height of  $z = 0.47$  ft. is required to effect a 90% conversion.

PART B. A rigorous solution to this problem involving the use of the reaction-rate equation and mass transfer contributions necessitates a trial-and-error procedure, in which the composition of alcohol, ketone, and hydrogen must be established at the catalyst surface in order to produce the proper rate. For a designated conversion  $x_A$  a preliminary rate of reaction was calculated by using the component compositions of the main gas stream. Mass transfer calculations involving the use of  $j_d$  factors for granular packings (2) permitted the evaluation of mass transfer coefficients  $k_g$  for alcohol, ketone, and hydrogen from which the partial-pressure differences of these components across the gas film were calculated. With the composition of these components defined at the interface, a new reaction rate was calculated and the mass transfer calculations repeated until the reaction rate no longer changed. The final

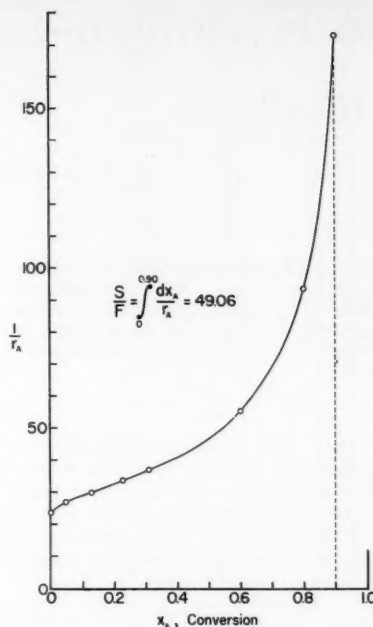


Fig. 12. Reciprocal rate-conversion relationship for illustrative example (rigorous approach involving reaction rate and mass transfer effects).

rates taking place at the catalyst surface are presented in Table 6 along with their corresponding conversions  $x_A$  and other pertinent data.

A plot of reciprocal rates and conversions is presented in Figure 12, which upon integration between the limits of conversion,  $x_A = 0$  to  $x_A = 0.90$ , yields a value of

$$\frac{S}{F} = \int_0^{0.90} \frac{dx_A}{r_A} = 49.06$$

The height of the reactor required to effect a 90% conversion therefore becomes

$$\frac{S}{F} = \frac{(17.3)(h)}{0.182} = 49.06$$

$$h = 0.51 \text{ ft.}$$

The results produced by both methods are in fair agreement. The method involving the use of the rate equation and mass transfer contribution is rigorous and accurate but is quite demanding from a calculation point of view. On the other hand, the approach involving the use of the height of reactor unit proves somewhat less exact, but far less time consuming for a reasonable conclusion. This inexactness is inherently associated in the proper number of reactor units  $N_R$  as reflected in the differences involved in the logarithmic expression at high conversions.

#### NOTATION

- $C$  = constant in rate equation  
 $D_m$  = diffusivity of transferable component, sq. ft./hr.  
 $F$  = feed rate, lb.-moles of alcohol/hr.  
 $G$  = mass velocity of gas stream, lb./hr.(sq. ft.)

- $HCU$  = height of catalytic unit, ft.  
 $HRU$  = height of reactor unit, ft.  
 $HTU$  = height of transfer unit, ft.  
 $j_d$  = mass transfer factor  
 $k_g$  = mass transfer coefficient, lb.-moles/(hr.) (sq. ft.) (atm.)  
 $K$  = chemical equilibrium constant  
 $K_A$  = adsorption equilibrium constant for sec-butyl alcohol  
 $K_{AK}$  = constant in rate equation  
 $m$  = slope of  $HRU$  vs.  $G$   
 $M_m$  = mean molecular weight of gas stream  
 $N_R$  = number of reactor units  
 $p^*$  = partial pressure of alcohol at thermodynamic equilibrium, atm.  
 $p_1$  = partial pressure of alcohol entering reactor, atm.  
 $p_2$  = partial pressure of alcohol leaving reactor, atm.  
 $p_f$  = partial pressure of non-transferable component, atm.  
 $p_{A_i}$  = partial pressure of alcohol at interface, atm.  
 $p_{K_i}$  = partial pressure of ketone at interface, atm.  
 $p_{H_i}$  = partial pressure of hydrogen at interface, atm.  
 $r_A$  = reaction rate, lb.-moles of alcohol converted/(hr.) (sq. ft.)  
 $S$  = surface area of catalyst, sq. ft.  
 $T$  = absolute temperature,  $^\circ\text{K}$  or  $^\circ\text{R}$ .  
 $W$  = weight of catalyst, lb.  
 $x_A$  = conversion, lb.-moles of alcohol converted/lb.-mole of alcohol in feed  
 $z$  = height of catalyst bed, ft.  
 $\mu$  = viscosity of gas, lb./hr.(ft.)  
 $\rho$  = density of gas, lb./cu. ft.

#### LITERATURE CITED

- Balandin, A. A., and A. L. Liberman, *Compt. rend. acad. sci. (U.S.S.R.)*, **28**, 794 (1940).
- Hougen, O. A., and K. M. Watson, "Chemical Process Principles," pp. 902-926 and 982-990, John Wiley and Sons, New York (1947).
- Hurt, D. M., *Ind. Eng. Chem.*, **35**, 522 (1943).
- Ipatieff, V. N., "Catalytic Reactions at High Pressures and Temperatures," pp. 16-18, The Macmillan Company, New York (1936).
- Ivannikov, P. Y., M. G. Tatarkaya, and E. Y. Gavrilova, *Sintet. Kauchuk*, **9**, 16 (1936).
- Kolb, H. J., and R. L. Burwell, Jr., *J. Am. Chem. Soc.*, **67**, 1084 (1945).
- Mottern, H. O., U. S. Pat. 2,586,694 (February 19, 1952).
- McNeil, Donald, and F. R. Charlton, British Pat. 636,743 (May 3, 1950).
- Neish, A. C., *Can. J. Research*, **23B**, 49 (1945).
- Padovani, Carlo, and Giuseppe Salvi, *Riv. combustibili*, **5**, 81 (1951).
- Sussman, M. V., and Charles Potter, *Ind. Eng. Chem.*, **46**, 457 (1954).
- Thiele, E. W., *Ind. Eng. Chem.*, **31**, 916 (1939).

Presented at A.I.Ch.E. Seattle meeting

# Phase Behavior of Hydrogen-light-hydrocarbon Systems

A. L. BENHAM, D. L. KATZ, and R. B. WILLIAMS

University of Michigan, Ann Arbor, Michigan

The decreasing solubility of hydrogen in hydrocarbons with decreasing temperature continues down to the freezing point of the hydrocarbons, around  $-300^{\circ}\text{F}$ . This behavior is shown to be an enlargement of phenomena exhibited by normal hydrocarbon mixtures. Methods of predicting equilibrium-phase compositions are presented for hydrogen in light-hydrocarbon systems. The correlations are satisfactory for binary and certain ternary systems, but are not reliable for complex mixtures.

The phase behavior of hydrogen-hydrocarbon systems is interesting because of the need for predicting their behavior in processing operations and because of the unusual region of reverse-order solubility described by Kay (11). This paper shows that the reverse-order solubility for hydrogen systems is different from that for hydrocarbon systems by only a matter of degree, no doubt because of the high volatility of the hydrogen. Methods of correlating vapor-liquid equilibria data (references in Table 1) are discussed for binary, ternary, and complex systems.

## REVERSE-ORDER AND NORMAL SOLUBILITY

In 1941 Kay (11) published some of the first results of a vapor-liquid-phase study of a hydrogen-hydrocarbon system, which show reverse-order solubility over a considerable range of temperatures and pressures. Reverse-order solubility is defined as the phenomenon occurring when the solubility of a constituent decreases with a decrease in temperature while all other variables are held constant.

A. L. Benham is at present with the Ohio Oil Company, Littleton, Colorado.

Aroyan (1) has shown that the hydrogen-hydrocarbon systems differ from normal phase behavior in degree but not in kind.

The ethane-*n*-heptane binary system (12) which may be taken as typical of many hydrocarbon systems, may be said to exhibit normal behavior. Reverse-order solubility occurs in the cross-hatched area (Figure 1) where the bubble-point portion of the phase envelope has a negative slope.

Figure 2 contains both the experimental pressure-temperature behavior of the hydrogen-methane system (3 and 4) and a hypothetical continuation of the phase envelopes drawn by comparison with the normal-type phase behavior. This figure shows that the region of negative slopes for bubble-point curves has been enlarged and reaches down to a temperature where the hydrocarbon separates as a solid phase. No vapor-liquid equilibria can be obtained in that portion of the phase envelope which would have a positive slope owing to the appearance of the solid phase. Thus hydrogen-hydrocarbon systems are different only to the extent that they have an enlarged region where reverse-order solubility occurs.

## GENERALIZED CORRELATION OF BINARY SYSTEMS

An expression first used by Krichevsky and Kasarnovsky (15) for extrapolating the solubility data of slightly soluble gases in liquids has been used to describe the solubility of hydrogen in light-hydrocarbon solvents. The expression as modified by Kobayashi and Katz (14) and applied in this work contains the assumption that the molal volume does not change with pressure and the approximation that the fugacity of a mixture of a liquid and a slightly soluble gas is predicted by a pseudo Henry's law constant,  $Q$

$$\log_{10} (f^{\circ}y/x)_2 = \log Q + \bar{V}_2 P / 2.303 RT \quad (1)$$

where

- $f_2^{\circ}$  = fugacity of hydrogen at  $T$  and  $P$
- $y_2$  = mole fraction of hydrogen in vapor phase
- $x_2$  = mole fraction of hydrogen in liquid phase
- $Q$  = modified Henry's-law constant at  $T$
- $\bar{V}_2$  = molal volume of hydrogen in liquid phase at  $T$
- $P$  = pressure of system
- $R$  = gas constant
- $T$  = temperature of system

This expression was used by Krichevsky and Kasarnovsky to predict the solubility of nitrogen in water up to 1,000 atm. pressure, by Wiebe and Gaddy (20) for carbon dioxide in water, and by Kobayashi and Katz (14) for hydrocarbons in water. Fastowsky and Gonikberg (9) used this expression for the description of their hydrogen-methane system.

An idealized description of the solubility behavior of a slightly soluble substance is shown in the sketch in Figure 3, which is a three-dimensional plot of the logarithm of  $f^{\circ}y/x$  as a function of  $P/2.303 RT$  and the temperature. The idealized case shown is for a substance displaying a molal volume which is a function of temperature only and which has a modified Henry's-law

TABLE 1. SOURCES OF HYDROGEN-HYDROCARBON EQUILIBRIUM DATA

System	Reference	Temperature range, $^{\circ}\text{F}$ .
Hydrogen-methane	(16)	-140 to -175
Hydrogen-methane	(9)	-230 to -298
Hydrogen-methane	(10)	-295 to -310
Hydrogen-methane	(3, 4)	-150 to -250
Hydrogen-ethylene	(17)	-120 to -175
Hydrogen-ethylene	(21, 22)	0 to -250
Hydrogen-ethane	(16)	-120 to -175
Hydrogen-ethane	(21, 22)	50 to -275
Hydrogen-propylene	(21, 22)	75 to -275
Hydrogen-propane	(21, 22)	75 to -300
Hydrogen-propane	(5)	40 to 190
Hydrogen-isobutane	(6)	100 to 250
Hydrogen- <i>n</i> -butane	(1, 2)	75 to -200
Hydrogen- <i>n</i> -butane	(18)	75 to 240
Hydrogen-methane-ethylene	(17)	-120 to -175
Hydrogen-methane-ethane	(16)	-120 to -175
Hydrogen-methane-propylene	(3, 4)	-100
Hydrogen-methane-propane	(3, 4)	0 to -200
Hydrogen-methane-ethylene-ethane-propylene-propane	(3, 4)	0 to -100

TABLE 2. FUGACITY OF HYDROGEN

Fugacity, lb./sq. in. abs., at

Pressure, lb./sq. in. abs.	0°F.	-50°F.	-100°F.	-150°F.	-200°F.	-250°F.	-275°F.	-300°F.
250	252.5	252.8	252.8	252.8	252.5	251.0	249.4	247.0
500	510.5	511.0	512.0	511.0	510.0	504.5	499.5	489.5
1,000	1,044	1,046	1,049	1,049	1,045	1,025	1,007	972
2,000	2,186	2,196	2,208	2,216	2,204	2,154	2,094	1,994
3,000	3,441	3,468	3,498	3,525	3,522	3,459	3,369	3,213
4,000	4,816	4,872	4,940	5,012	5,036	5,004	4,908	4,720
5,000	6,320	6,435	6,555	6,675	6,785			
6,000	7,974	8,148	8,352	8,592	8,814			
7,000	9,779	10,120	10,370	10,770	11,100			
8,000	11,750	12,140	12,620	13,240				
10,000	16,310	17,060	17,950					

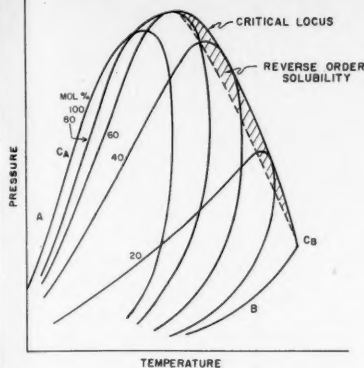


Fig. 1. Pressure-temperature phase behavior for the ethane-n-heptane system.

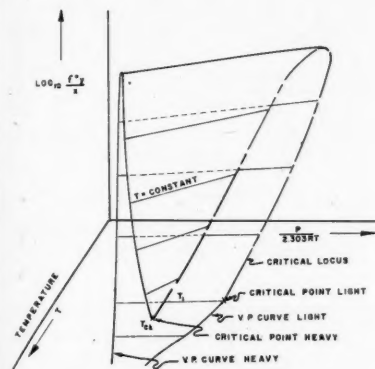


Fig. 3. Idealized behavior of a slightly soluble substance.

constant as is a function of temperature only. With these limitations Figure 3 would contain a family of straight lines having parameters of constant temperature, which in the three-dimensional figure result in a curved surface extending from the critical temperature of the heavy component down to lower limit of the coexistence of vapor and liquid for the particular system. At low temperatures (temperatures below the critical temperature of the slightly soluble component) the line extends between the vapor pressure of the two substances and will have a positive slope. For a temperature  $T_1$  equal to the critical temperature of the slightly soluble substance, the line will exist between the vapor pressure of the solvent and the critical pressure of the solute. Most substances show an increase in molal volume with an increase in temperature; therefore, the constant temperature lines in Figure 3 exhibit greater positive slopes at the higher temperature. The preceding analogy may be extended to higher temperatures up to the limit of the critical temperature of the solvent  $T_{c,s}$ , where a single point would be shown.

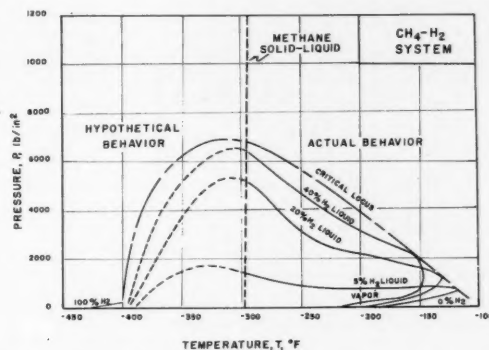


Fig. 2. Actual and hypothetical extension of pressure-temperature phase behavior for the hydrogen-methane system.

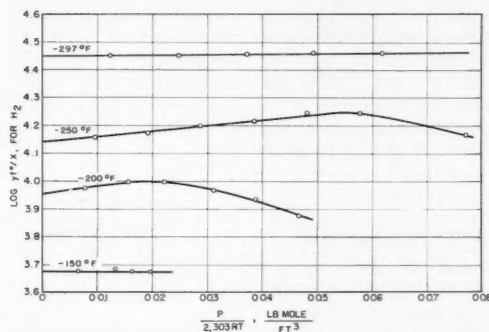
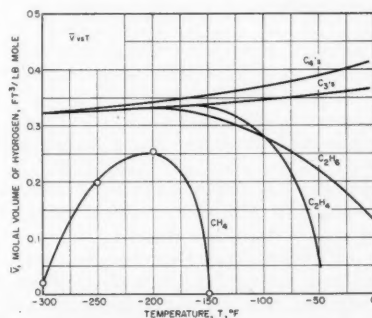
Fig. 4.  $K_f$  for hydrogen as a function of pressure for the hydrogen-methane system.

Fig. 5. Molal volume for hydrogen in the hydrogen-hydrocarbon system as a function of temperature.

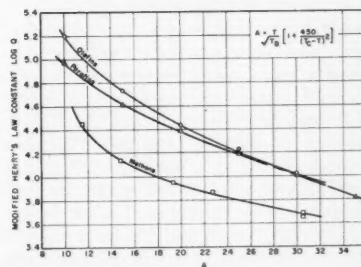


Fig. 6. Modified Henry's-law constant for hydrogen in the hydrogen-hydrocarbon system as a function of temperature.

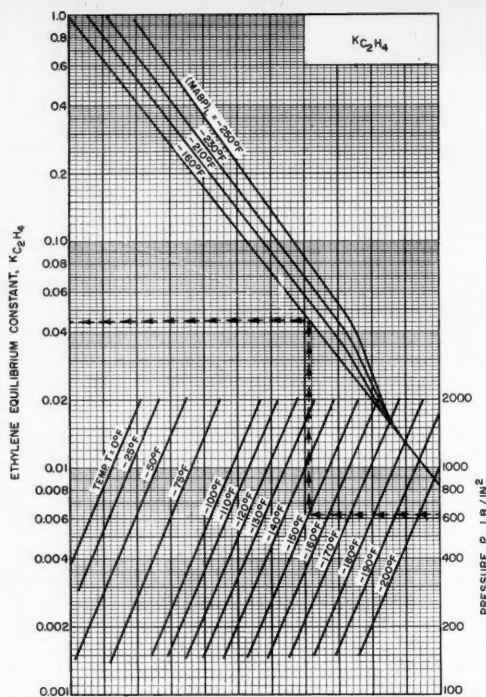


Fig. 7. Nomographic correlation of ethylene equilibrium constants in the hydrogen-methane-ethylene system.

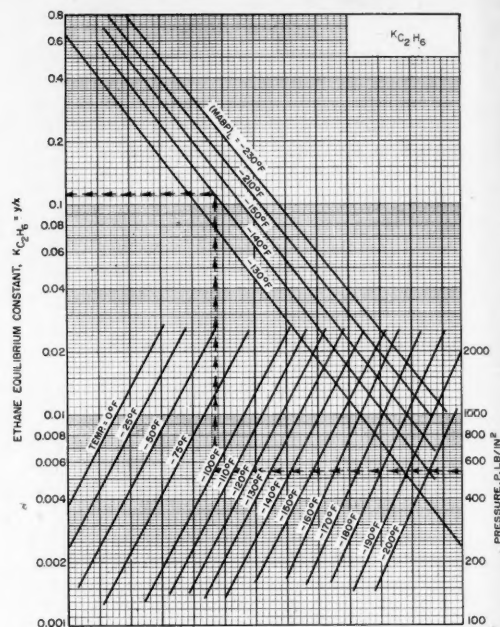


Fig. 8. Nomographic correlation of ethane equilibrium constants in the hydrogen-methane-ethane system.

Before the solubility relationship could be applied to hydrogen binary systems, it was necessary to have fugacity data for pure hydrogen. These data were obtained from Deming and Shupe (7) or were computed at low temperatures and high pressures (8, 21) from the compressibility data of Woolley et al. (23). Since these fugacity values do not appear to have been published elsewhere, they are given in Table 2.

From Equation (1) it may be seen that if one knows the fugacity, molal volume, and modified Henry's-law constant for the temperature, pressure, and system in question, the equilibrium constant ( $y/x$ ) for hydrogen may be calculated.

Figure 4 shows how the molal volume and the modified Henry's law-constant are evaluated. In these plots given for the hydrogen-methane systems the slope of the straight-line portion is equal to the molal volume of hydrogen and the intercept is equal to the modified Henry's-law constant. These molal volumes have been obtained for the available hydrogen-hydrocarbon binary systems and are shown as a function of temperature and solvent in Figure 5. Excluding methane, the limiting value of the molal average volume is about 0.32 cu. ft./mole near the freezing point of the light hydrocarbon solvent. The values of  $\bar{V}$  obtained here may not agree with experimentally determined values, owing to the previous assumptions used in obtaining Equation (1).

It was found that a plot of the logarithm of the modified Henry's-law constant as a function of an empirical temperature function gave a reasonably good grouping of the values of modified Henry's-law constant.

$$A = T/\sqrt{T_B}[1 + 450/(T_c - T)^2] \quad (2)$$

where

$T$  = temperature, °R.

$T_B$  = normal boiling point of the solvent, °R.

$T_c$  = critical temperature of the solvent, °R.

It will be seen in Figure 6 that the data are grouped principally into three lines representing the Henry's-law constant for hydrogen in paraffins, olefins, and methane, an indication of a different solubility dependence for hydrogen in each of these three types of solvents.

For systems containing more than one hydrocarbon, it is recommended that the solubility of hydrogen be calculated for each hydrocarbon as though it were present alone. The solubilities are then averaged in the ratio of the mole fraction of each hydrocarbon present.

An evaluation of the hydrogen binary systems reveals the following general characteristics. The equilibrium constant for hydrogen increases with a decrease in temperature at constant pressure except for a limited range of conditions close to the vapor-pressure curve for the hydro-

carbon solvent. A second characteristic is that the equilibrium constant for hydrogen increases as the hydrocarbon solvent is changed from methane to butane. A similar effect may be noted for the olefinic solvents. These observations would tend to indicate that the hydrogen equilibrium constant increases as the molecular weight of the solvent increases; however, consideration of both paraffinic and olefinic systems shows that neither the molecular weight nor the boiling point of the solvent are a good criterion for determining the effect of a different solvent. The equilibrium constant for hydrogen in propylene is sometimes greater than in propane, and likewise that in ethylene is sometimes greater than in ethane. Paraffinic and olefinic compounds are not interchangeable based on boiling point or molecular weight.

#### CORRELATION OF TERNARY SYSTEMS

According to the phase rule, a ternary system may be described in terms of three variables, such as temperature, pressure, and one concentration variable. Consideration of the available ternary-system data showed that the hydrogen systems definitely required the use of the phase-rule variables; i.e., consideration of data for a given temperature and pressure showed that the equilibrium constants for all three components varied as the composition of the liquid or vapor phase was changed.

A generalized correlation of equilibrium



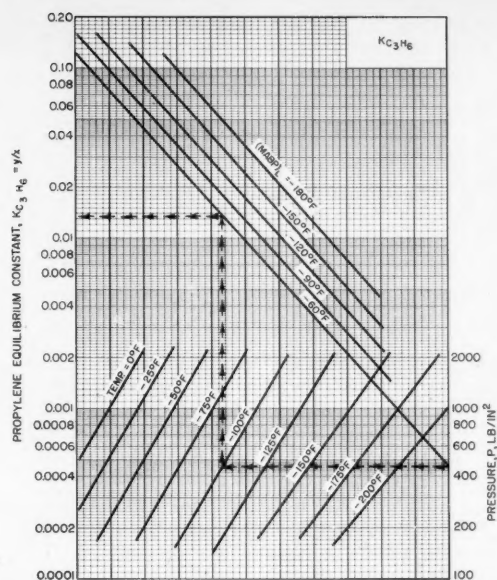


Fig. 9. Nomographic correlation of propylene equilibrium constants in the hydrogen-methylene-propylene system.

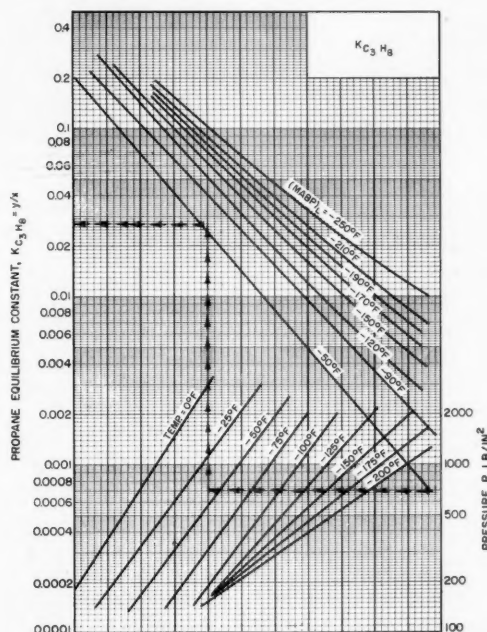


Fig. 10. Nomographic correlation of propane equilibrium constants in the hydrogen-methane-propane system.

constants must contain variables which exist or may be obtained for any system regardless of its particular components

or complexity. Some concentration variables which fulfill these requirements are the molal average properties of each

phase such as the boiling points, molecular weights, critical temperatures, and critical pressures. The mole fraction of hydrogen in either phase would also be a universal property of hydrogen systems.

The hydrogen-methane ternary systems with ethylene, ethane, propylene, and propane were examined, and it was found that the equilibrium constants for the constituents could be correlated by use of the temperature, pressure, and a single generalized concentration variable such as the molal average boiling point of the liquid phase  $MABP_L$ .

Examination of the equilibrium constants for ethylene, ethane, propylene, and propane in the corresponding hydrogen-methane ternary systems revealed a regularity which was represented by nomographs as shown in Figures 7, 8, 9, and 10. These nomographs, which make use of the required number of phase-rule variables as represented by the temperature, pressure, and molal average boiling point of the liquid phase, represent the data for the hydrogen-hydrocarbon binary as well as for the corresponding hydrogen-methane-hydrocarbon ternary system. The nomographical correlations should not be expected to apply for conditions in the critical region.

#### TERNARY PAIR CORRELATIONS

Simple methods of correlating the equilibrium constants found in any hydrogen binary or ternary system were considered in the search for a correlation involving the temperature, pressure, and one or two concentration variables which could be used later for the description of complex systems.

The possibility of correlating the equilibrium constant for hydrogen in terms of the temperature, pressure, and the molal average boiling point of the liquid phase  $MABP_L$  was considered as a means of describing any hydrogen binary, ternary, or complex system. Figure 11 contains a semilogarithmic plot of the equilibrium constant for hydrogen in various systems as a function of  $MABP_L$  at  $-100^\circ\text{F}$ . and 500 and 1,000 lb./sq. in. This plot shows that use of those three variables is inadequate for the unique specification of the equilibrium constant for hydrogen in any binary, ternary, or complex system. The plot does show that these three variables are sufficient to describe any single hydrogen three-component system and also that there exists a simple straight-line relationship which describes the variation of the hydrogen equilibrium constant with  $MABP_L$  in a (hydrogen)-(saturated-hydrocarbon)-(corresponding-unsaturated-hydrocarbon) ternary system.

From the phase rule it may be shown that a four-component system may be described by use of four variables such as temperature, pressure, and two concentration variables. It follows that those

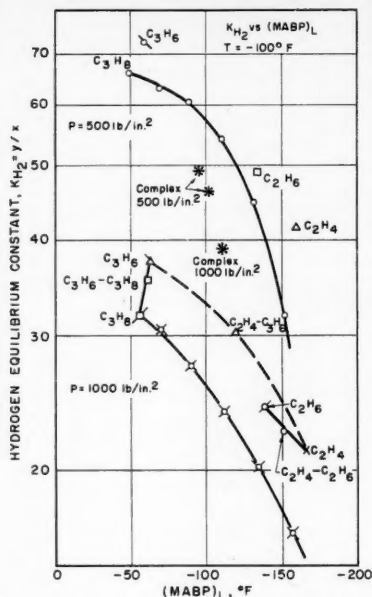


Fig. 11. Equilibrium constants for hydrogen at  $-100^\circ\text{F}$ . and 500 and 1,000 lb./sq. in. vs. the liquid molal average boiling point.

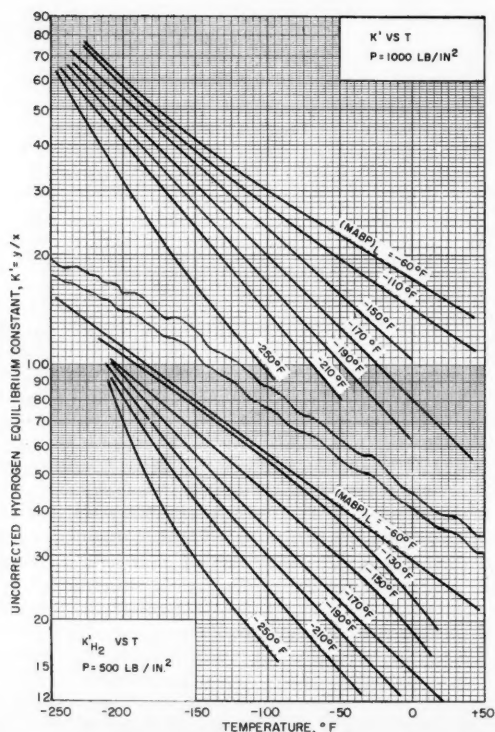


Fig. 12.  $(MABP)_L - y_{H_2}$  correlation for hydrogen equilibrium constants at 500 and 1,000 lb./sq. in.

four variables should describe the behavior of the four possible ternary systems derived from the four components.

Methods of correlating the data from the ternary systems of both hydrogen-methane-ethylene and hydrogen-methane-propane in terms of two concentration variables in addition to the temperature and pressure were considered. Among those tried were two schemes which have proved useful for the correlation of paraffinic hydrocarbon systems.

The first method used was similar to that of the Kellogg (13) correlation of hydrocarbon equilibrium constants. From all the possible variables which could be used to correlate the hydrogen equilibrium constants the two which proved to be the best were  $MABP_L$  and the mole fraction of hydrogen in the vapor phase  $y_{H_2}$ . Figures 12, 13, and 14 contain the plots which predict the equilibrium constants for hydrogen in either the hydrogen-methane-ethylene system or in the hydrogen-methane-propane system. In Figure 12 the uncorrected equilibrium constant for hydrogen  $K_{H_2}'$  has been plotted as a function of temperature for pressures of 500 and 1,000 lb./sq. in. and

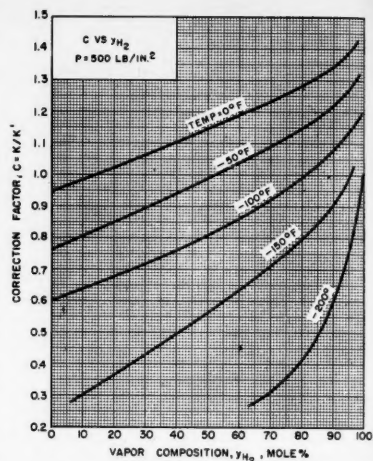


Fig. 13. Correction factor for Figure 14 at 500 lb./sq. in.

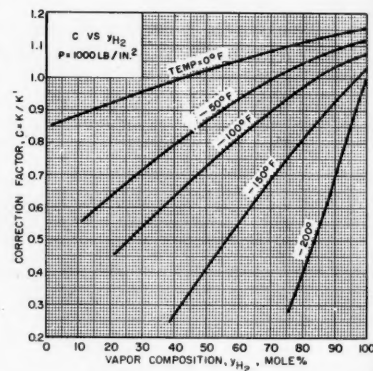


Fig. 14. Correction factor for Figure 12 at 1,000 lb./sq. in.

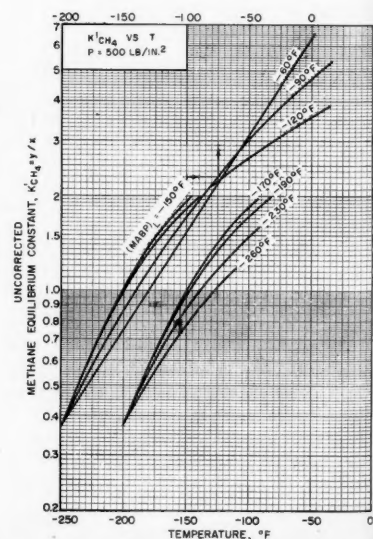


Fig. 15.  $(MABP)_L - (MABP)_V$  correlation for methane equilibrium constants at 500 lb./sq. in.

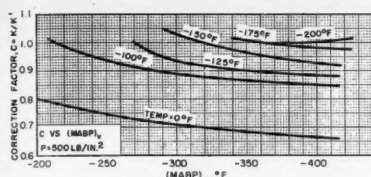


Fig. 16. Correction factor for Figure 17.

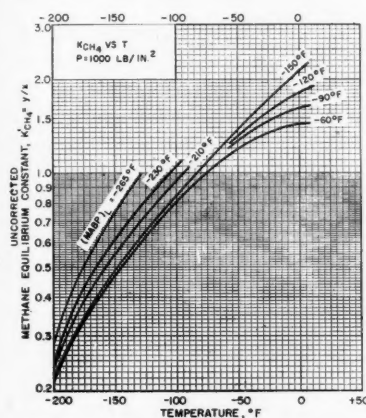


Fig. 17.  $(MABP)_L - (MABP)_v$  correlation for methane equilibrium constants at 1,000 lb./sq. in.

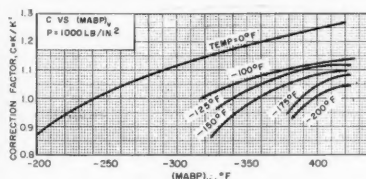


Fig. 18. Correction factor for Figure 17.

for  $MABP_L$ 's between values of  $-60^\circ$  to  $-250^\circ\text{F}$ . Figures 13 and 14 contain correction factors to be applied to  $K_{H_2}$ , which are shown as functions of the mole percentage of hydrogen in the vapor phase  $yH_2$ .

The methane equilibrium constants for the same systems have been correlated as functions of the temperature, pressure,  $MABP_L$ , and  $MABP_v$  as shown in Figures 15, 16, 17, and 18.

The correlations given for hydrogen and methane equilibrium constants were used to predict equilibrium constants for the hydrogen-methane-ethane and hydrogen-methane-propylene systems. A comparison with the actual data showed large deviations which implied that either the best correlation involving the use of four variables had not been found or that it was going to be necessary to use more variables.

The "convergence pressure method," used by Organick (19) to describe the equilibrium constants of the paraffinic hydrocarbons in terms of the temperature, pressure, and convergence pressure, was applied with little or no success.

#### COMPLEX SYSTEMS

A limited number of vapor-liquid data for a six-component system composed of hydrogen, methane, ethylene, ethane, propylene, and propane are available from which it was possible to consider the application of the foregoing correlations for ternary-system equilibrium constants. Three data points are shown in Figure 11 which demonstrate the inability of the three variables of pressure, temperature, and  $MABP_L$  to determine uniquely the equilibrium constant for hydrogen in a six-component system.

The  $MABP_L$ - $yH_2$  correlation of hydrogen equilibrium constants was used to predict the constants for hydrogen in the six-component system and was found to give results which were in error from

3 to 35%. The  $MABP_L$ - $MABP_v$  correlation of methane equilibrium constants was compared with the six-component data, and errors from 3 to 30% were obtained.

This lack of agreement shows the inability of four variables, including temperature, pressure, and two molal average properties, to predict six-component system behavior. Table 3 gives the comparison of the equilibrium constants in the two systems with almost identical values of the molal average of boiling points, molecular weights, critical temperatures, and critical pressures and at the same temperature and pressure. The comparison indicates that at least five variables and probably the full-phase-rule set of six variables is required to obtain an adequate correlation of a six-component system involving hydrogen and light hydrocarbons.

#### LITERATURE CITED

1. Aroyan, H. J., Ph.D. thesis, Univ. Mich., Ann Arbor (1949).
2. —, and D. L. Katz, *Ind. Eng. Chem.*, **43**, 185 (1951).
3. Benham, A. L., Ph.D. thesis, Univ. Mich., Ann Arbor (1956).
4. —, and D. L. Katz, *A. I. Ch. E. Journal*, **3**, 33 (1957).
5. Burris, W. L., N. T. Hsu, H. H. Reamer, and B. H., Sage, *Ind. Eng. Chem.*, **45**, 210 (1953).
6. Dean, M. R., and J. W. Tooke, *Ind. Eng. Chem.*, **38**, 389 (1946).
7. Deming, W. E., and L. E. Shupe, *Phys. Rev.*, **40**, 848 (1934).
8. Dodge, B. F., "Chemical Engineering Thermodynamics," p. 238, McGraw-Hill Book Company, Inc., New York (1944).
9. Fastowsky, M. G., and V. G. Gonikberg, *J. Phys. Chem. (U.S.S.R.)*, **14**, 427 (1940).
10. Freeth, F. A., and T. T. H. Verschöyle, *Proc. Roy. Soc. (London)*, **130A**, 453 (1931).
11. Kay, W. B., *Chem. Revs.*, **29**, 501 (1941).
12. —, *Ind. Eng. Chem.*, **30**, 459 (1938).
13. "Kellogg Equilibrium Constants," The M. W. Kellogg Company, New York.
14. Kobayashi, Riki, and D. L. Katz, *Ind. Eng. Chem.*, **45**, 440 (1953).
15. Krichevsky, I. R., and J. S. Kasarnovsky, *J. Am. Chem. Soc.*, **57**, 2168 (1935).
16. Levitskaya, E. P., *J. Tech. Phys. (U.S.S.R.)*, **11**, 197 (1941).
17. Likhter, A. I., and N. P. Tikhonovich, *ibid.*, **10**, 1201 (1940).
18. Nelson, E. E., and W. S. Bonnell, *Ind. Eng. Chem.*, **35**, 204 (1943).
19. Organick, E. I., and G. G. Brown, *Chem. Eng. Progr. Symposium Ser. No. 2*, **48**, 97 (1952).
20. Wiebe, Richard, and V. L. Gaddy, *J. Am. Chem. Soc.*, **61**, 315 (1939).
21. Williams, R. B., Ph.D. thesis, Univ. Mich., Ann Arbor (1954).
22. —, and D. L. Katz, *Ind. Eng. Chem.*, **46**, 2512 (1954).
23. Woolley, H. W., R. B. Scott, and F. G. Brickmedde, *J. Research Natl. Bur. Standards*, **41**, No. 5, 379 (1948).

TABLE 3. COMPARISON OF EQUILIBRIUM CONSTANTS IN A SIX-COMPONENT SYSTEM WITH THOSE IN A THREE-COMPONENT SYSTEM HAVING SIMILAR MOLAL AVERAGE PROPERTIES

(Temperature =  $-100^\circ\text{F}$ .; pressure = 500 lb./sq. in.)

	System	
	$\text{H}_2\text{—CH}_4\text{—C}_3\text{H}_8$	Six-component
$(MABP)_L$ , °F	-96	-96
$(MABP)_v$ , °F	-362	-362
$(MW)_L$ , lb./lb. mole	37	37
$(MW)_v$ , lb./lb. mole	7.1	7.4
$(T_c)_L$ , °F	127	130
$(T_c)_v$ , °F	-300	-295
$(P_c)_L$ , lb./sq. in.	626	638
$(P_c)_v$ , lb./sq. in.	377	355
$K$ for $\text{H}_2 = y/x$	57.0	49.1
$K$ for $\text{CH}_4 = y/x$	1.50	2.05
$K$ for $\text{C}_3\text{H}_8 = y/x$	0.014	0.0136

# Effect of Wall Roughness on Convective Heat Transfer in Commercial Pipes

J. W. SMITH and NORMAN EPSTEIN

University of British Columbia, Vancouver, British Columbia

Heat transfer and fluid friction measurements were made for air flow through a smooth copper pipe and six other commercial pipes, with a ratio of diameter to equivalent sand roughness varying from 640 to 64. The Reynolds number range was 10,000 to 80,000. Though some increase in heat transfer coefficients with roughness was found, the heat transmission per unit power loss always decreased.

The momentum-heat-transfer analogies of Reynolds and Colburn are shown to be inadequate for handling the experimental data. Those of Prandtl and Taylor, von Kármán, and Pinkel fail to show a required Reynolds number dependence of  $j_h$  when friction factor has become independent of Reynolds number for a rough pipe. Martinelli's equation shows such dependence and, even in approximate form, gives good prediction of the experimental results.

Although the effect of wall roughness on fluid friction in pipes has received extensive study, investigation of the corresponding effect on convective heat transfer has been restricted to artificially roughened pipes (7, 8, 25). Published studies by Cope (7) and Sams (25), the latter summarized by Pinkel (21), at Reynolds numbers exceeding 2,000 indicated that the increase in heat transfer due to machined roughness elements on the inside of tubes is considerably smaller than the accompanying increase in frictional pressure drop for the same fluid velocity. Furthermore, for a given pressure drop roughened pipes showed smaller heat-transmission rates than smooth tubes, and this was also true if the comparison was made for equal power consumption. Apparently the form drag caused by machined roughness projections produces an inefficient type of turbulence from the heat transfer point of view.

The foregoing two studies, however, also indicated that the shape and configuration of the roughness projections are as important as the height of these projections in determining their effect on fluid friction and heat transfer. Moreover, Colburn (5) and later Pratt (23) analyzed data on metallic turbulence promoters placed within pipes (14, 19) to show that in certain instances the heat-transmission performance for a given power loss is increased by such promoters, and Drexel and McAdams (10) have shown similar results for wavy surfaces.

This leaves open the possibility that for wall roughness as found in commercial pipes the large frictional pressure-drop increase over that for smooth tubes is accompanied by a substantial increase in convective heat transfer. In the present work seven commercial pipes were investigated, covering a large range of roughness ratio  $D/e$ .

## EXPERIMENTAL APPARATUS AND PROCEDURE

A horizontal double-pipe heat exchanger, illustrated in Figure 1, was used for making the experimental measurements. A controlled and orifice-metered air flow through the inside of the test pipe was heated by pressure-regulated 20 lb./sq. in. gauge saturated steam condensing on the outside

of the pipe. To eliminate the steam-film heat transfer resistance, the outside of the test pipe was polished on an emery sander and frequently coated with oleic acid, thus ensuring that condensation of the steam as drops, rather than as a continuous film, always prevailed. This procedure was visually observed by placing the test pipe in a glass tube, into which steam was admitted, before and after the pipe was placed in the experimental steam jacket. Since the test pipes were all new, clean, scale-free, and metallic, no pretreatment was given the inside of the pipes and it was assumed that the only appreciable resistance to heat transfer was in the air film. The measured steam temperature was therefore taken as the temperature of the inside pipe surface.

The orifice assembly, with *vena contracta* taps, was constructed according to A.S.M.E.

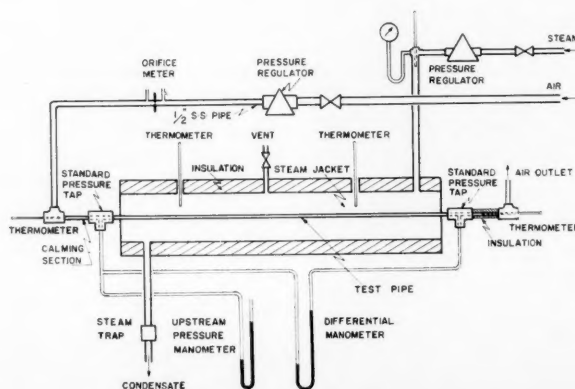


Fig. 1. Schematic diagram of apparatus.

J. W. Smith is at present with DuPont of Canada Ltd., Kingston, Ontario.



specifications (1), as were the static pressure taps at the entrance and exit of the test pipes. The bore of the taps was made to conform as closely as possible to the actual inside diameter of the pipe in which they were placed. Orifice plates were calibrated against a diaphragm gas meter. Calibrated thermometers were used to measure inlet-air temperature to 0.1°F., mixed-outlet-air temperature to 0.2°F., and steam temperature to 0.2°F. The steam jacket was vented to ensure release of noncondensables. Pressure drop and upstream pressure manometers were filled with water, carbon tetrachloride, or mercury, depending on the flow rate.

A calming length of 8 in., corresponding to 16-30 inside diameters for the pipes, preceded the heat exchange section. Since  $L/D$  of the test pipes was in the range 124-231, this length was, according to Latzko (16) and Boelter et al. (3) as summarized by McAdams (18), sufficient to reduce entrance effects to negligible proportions. A 4-in. unheated mixing section followed the heater, the mixing being accentuated by the fact that the exit thermometer bulb itself was only a little smaller than the small pipe diameters investigated. The heated length of pipe was 5.17 ft. and the distance between pressure taps was 5.55 ft. The seven pipes investigated, together with their inside diameters, are listed in Table 1.

Eighty nonheating and a similar number of heating runs were performed on the pipes. Barometer, manometer, and thermometer readings were recorded at the steady state, which was maintained for at least 15 min. A Reynolds number range of 10,000 to 80,000 was covered. For three of the runs the inlet steam was carefully dried and the condensate from the steam trap was carefully collected through a water-cooled condenser, so that an energy balance might be made on the system.

#### Data Processing

In all calculations the inside diameter of a pipe was taken as that specified by the manufacturer. Caliper measurements confirmed this assumption. As a further check, the diameter of the 1/4-in. standard steel pipe was measured by volumetric displacement of mercury, the deviation of this value from that of the manufacturer being only 0.5%.

For both heating and nonheating runs the frictional pressure drop was related to the measured pressure drop by the following form of the Bernoulli equation for a horizontal pipe:

$$\Delta p_f = p_1 - p_2 - \frac{G^2(v_2 - v_1)}{g_c} \quad (1)$$

For the nonheating runs the temperature change through the test section rarely exceeded 3°F. and was usually much less. These runs were therefore treated as isothermal at the average air temperature and the data used to calculate the conventional Reynolds number and Fanning friction factor. Correlation of the rough pipe data was achieved by means of Colebrook's (6) equation for sand-roughened pipes in the transitional

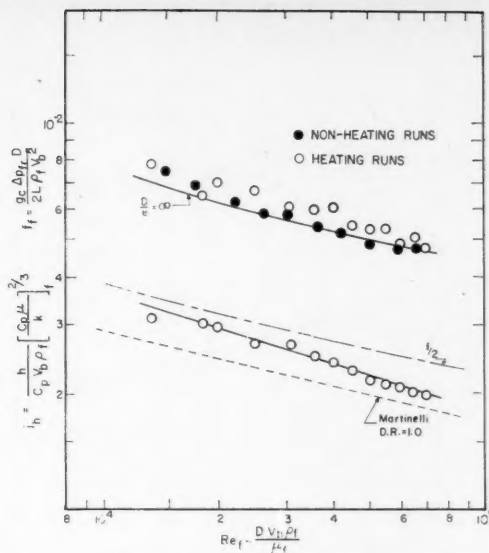


Fig. 2. Copper pipe, 1/4 in.; fluid friction and heat transfer data.

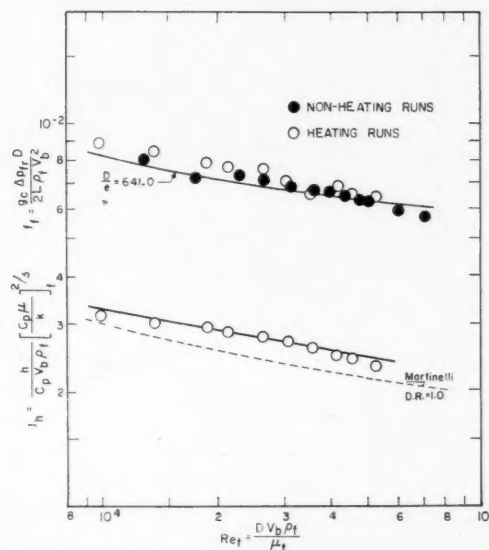


Fig. 3. Standard steel pipe, 3/8 in.; fluid friction and heat transfer data.

TABLE 1. PROPERTIES AND EMPIRICAL CONSTANTS FOR VARIOUS PIPES\*

Pipe	D, ft.	D/e, Eq'n. (2)	a, Eq'n. (7)	n, Eq'n. (7)	a.d., %
1/4-in. Copper	0.0313	—	0.0585	0.302	±2.1
3/8-in. Standard steel	0.0411	641 ± 32	0.0175	0.183	±1.8
1/2-in. Standard steel	0.0303	463 ± 51	0.0365	0.257	±3.2
3/8-in. Galvanized	0.0411	211 ± 12	0.0218	0.205	±1.5
1/2-in. Karbate	0.0417	189 ± 6	0.0258	0.209	±1.0
1/4-in. Galvanized	0.0303	112 ± 2.5	0.0142	0.156	±3.7
3/8-in. Galvanized	0.0224	63.4 ± 1.8	0.00611	0.0714	±3.8

\*Complete tabular data are on file as document 5213 with the American Documentation Institute, Photoduplication Service, Library of Congress, Washington 25, D. C., for \$2.50 for photoprints or \$1.75 for 35-mm. microfilm.

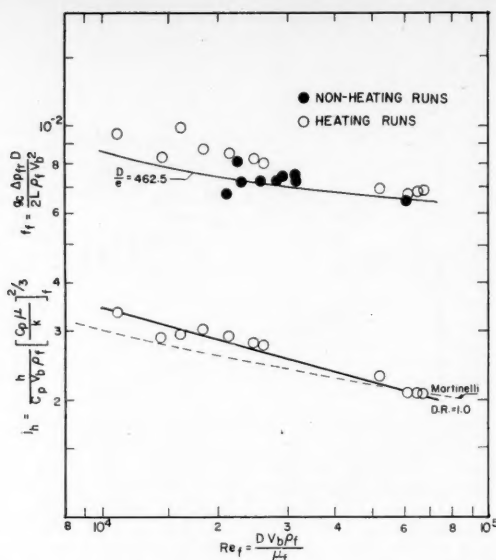


Fig. 4. Standard steel pipe, 1/4 in.; fluid friction and heat transfer data.

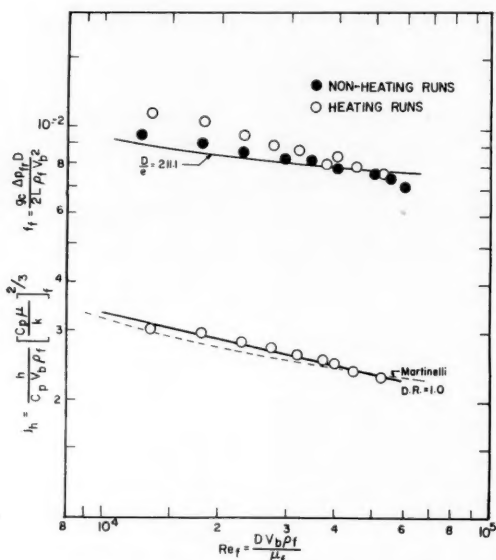


Fig. 5. Galvanized pipe, 3/8 in.; fluid friction and heat transfer data.

region between laminar and completely turbulent flow:

$$\frac{1}{\sqrt{f}} = 4 \log (D/e) + 2.28 - 4 \log \left( 1 + \frac{4.67 D/e}{Re \sqrt{f}} \right) \quad (2)$$

which reduces to the von Kármán-Nikuradse (12, 20) equation for rough pipes when turbulence is fully developed. The geometric mean value of the ratio

$D/e$ , as calculated from Equation (2), was determined for each rough pipe and is recorded in Table 1, in conjunction with the corresponding "probable error of the mean" (27). Correlation of the data for the smooth copper pipe, however, could not be achieved by Equation (2), and therefore these data were handled by the von Kármán-Nikuradse (12, 20) equation for smooth tubes:

$$\frac{1}{\sqrt{f}} = 4.0 \log Re \sqrt{f} - 0.40 \quad (3)$$

Physical properties of air were those used in several N.A.C.A. reports (11, 25, 29).

Fluid friction data for the heating runs were correlated, after Humble, Lowdermilk, and Desmon (11), by evaluating all fluid properties at the film temperature  $t_f$ , defined as midway between the average bulk temperature  $t_b$  and the inside wall temperature  $t_s$ . The film Reynolds number is defined by

$$Re_f = \frac{D V_b \rho_f}{\mu_f} \quad (4)$$

and the film Fanning friction factor by

$$f_f = \frac{\Delta p_f D g_c}{2 L \rho_f V_b^2} \quad (5)$$

Humble et al. found that heating data correlated in this manner lay on the curve representing isothermal data, except at  $Re_f$  less than 20,000, where the method appeared to overcompensate for radial temperature gradients.

The three energy-balance runs showed an average excess of less than 5% heat lost by the steam over that gained by the air. This was accounted for by heat loss to the surroundings through the insulation. Since the kinetic energy increase of the air was negligible in relation to the enthalpy increase, the heat transfer coefficients were based on the rate of enthalpy increase of the air. Logarithmic mean terminal temperature difference was used in evaluating  $h$ .

The heat transfer data were correlated by the film Reynolds number, defined by Equation (4), and the  $j_h$  factor of Colburn (4), modified according to the method of Humble et al. (11):

$$j_h = \frac{h}{C_p V_b \rho_f} \left( \frac{C_p \mu}{k} \right)^{2/3} \quad (6)$$

The film Prandtl number for the heating runs deviated little from 0.69. The two dimensionless groups were related by equations of the form

$$j_h = a Re_f^{-n} \quad (7)$$

The constants  $a$  and  $n$ , evaluated by the method of least squares, are listed in Table 1 for the various pipes. The average deviation (a.d.) of  $j_h$  calculated by these equations from the measured values of  $j_h$  is also recorded in Table 1 for each pipe.

## SUMMARY AND INTERPRETATION OF RESULTS

The processed fluid friction and heat transfer data for the various pipes are plotted in the form of dimensionless groups in Figures 2 through 8. The curve through the friction-factor points for the copper pipe is based upon Equation (3), and the friction-factor curves for the other pipes are based on Equation (2), the geometric mean value of  $D/e$  calculated from the nonheating data being used. In accordance with Humble et al. (11), the correlation of the heating data,

using film Reynolds number and friction factor, with the nonheating data, is better at high than at low Reynolds numbers, where film friction factors for heating tend to exceed isothermal friction factors. The agreement is good, nevertheless, and shows that no significant changes occurred in the pipe surfaces in the intervals between nonheating and heating runs.

The solid lines through the heat transfer points are plotted according to Equation (7), with the constants as determined by least squares. For purposes of comparison, all the curves, without the corresponding data points, are replotted in Figure 9, where it is seen that a percentage increase in  $f$  at a given Reynolds number over that for a smooth pipe is never accompanied by more than one-third the corresponding percentage increase in  $j_h$ , and usually the increase in  $j_h$  is even smaller. This agrees with the data of Sams (25) for square-thread-type roughness and with most of Cope's (7) data for pyramid-shaped roughness. In practice, the relatively small increase in heat transfer due to surface roughness will usually be negated by fouling, and so for design purposes the equations for a smooth pipe are recommended.

A replot of the heat transfer curves according to Equation (7a)

$$\frac{hD}{k_f} (Pr)_f^{-1/3} = a Re_f^{1-n} \quad (7a)$$

is given in Figure 10. This method of plotting has the advantage of showing the heat transfer coefficient as a function of velocity, if pipe dimensions and fluid properties are assumed fixed, and allows comparison with the curves of both Cope and Sams. All the curves for the rough pipes in Figure 10 show a tendency to diverge from that for the smooth copper pipe at the higher Reynolds numbers. This divergence is again in agreement with the data of Sams but is at odds with those of Cope, who noted a tendency to converge at higher Reynolds numbers (7, 15). The  $D/e$  ratios for the  $1/8$ - and  $1/4$ -in. galvanized pipes are in the range of square-thread-type roughness ratios studied by Sams, and the heat transfer data are in substantial agreement. The Karbate pipe shows somewhat higher heat transfer coefficients at the lower Reynolds numbers than the other pipes. Such a tendency at the lower Reynolds numbers was also noted by Cope for his pyramid-roughened pipes, but not by Sams. Under a microscope, the surface of the Karbate pipe bore some resemblance to Cope's pipe-surface photographs. It appears, therefore, that although the steel and galvanized pipes behave more like square-thread-roughened pipes, the Karbate is closer to pyramid-shaped roughness.

At the lower Reynolds numbers, the steel and galvanized pipes show heat

Fig. 6. Karbate pipe, 1/2 in.; fluid friction and heat transfer data.

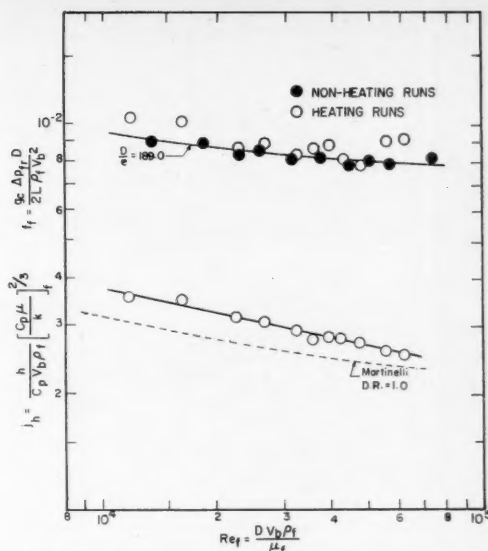


Fig. 7. Galvanized pipe, 1/4 in.; fluid friction and heat transfer data.

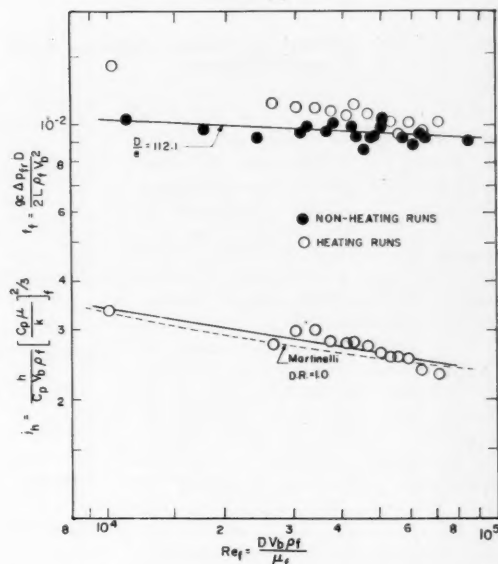
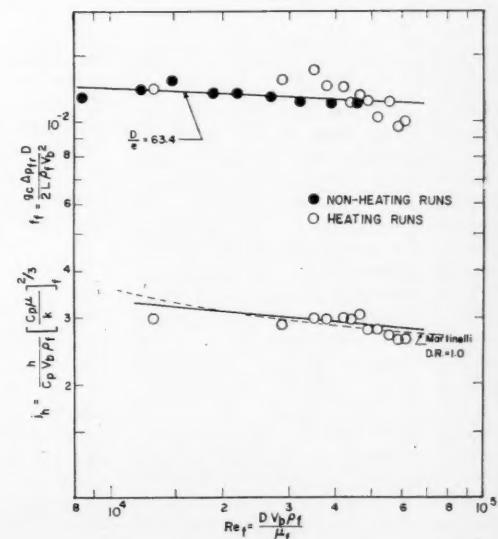


Fig. 8. Galvanized pipe, 1/8 in.; fluid friction and heat transfer data.



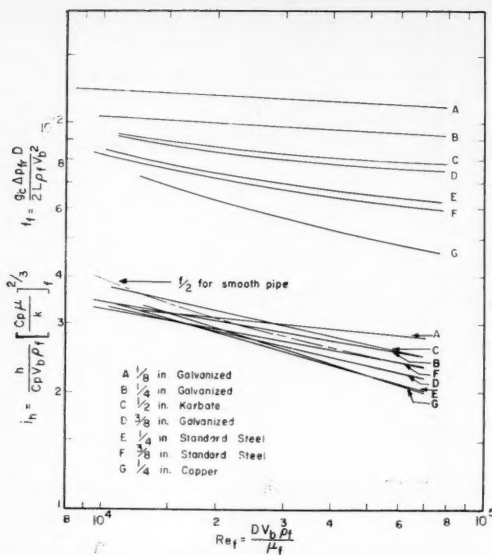


Fig. 9. Fluid-friction and heat-transfer curves for seven commercial pipes.

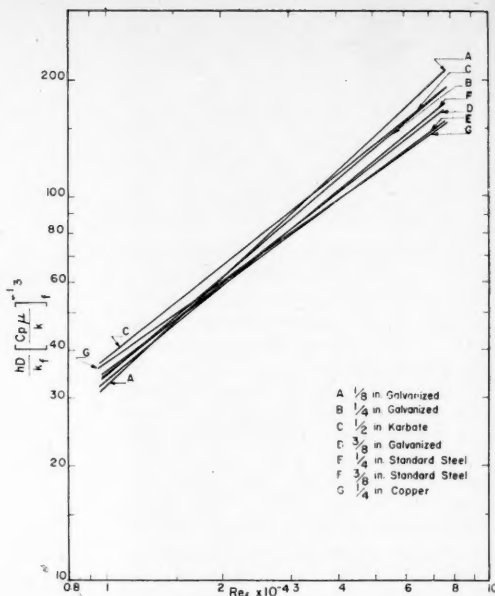


Fig. 10. Heat-transmission curves for various pipes.

transfer coefficients slightly smaller than for the smooth copper pipe, an effect also noted by Cope for one of his pipes, even lower in equivalent sand-roughness ratio  $D/e$  than that of the  $1/8$ -in. galvanized pipe studied here. The possible experimental error for the lower velocity points in the case of the rougher pipes is, however, estimated to be as high as  $-10\%$ , compared with an estimated average experimental error of  $-4\%$  for all the runs. This decrease in accuracy for the low-velocity runs through the rougher pipes is primarily attributable to the considerably smaller exit terminal temperature differences measured for these runs and may account for the anomaly in the present investigation.

The dimensionless group  $j_h/fRe_f$  may be arranged as follows:

$$\frac{j_h}{fRe_f} = \frac{h}{\Delta p_{fr} g_c D^2} \cdot \frac{\mu_f}{C_p \rho_f} \quad (8)$$

For pipes of equal dimensions through which flow the same fluid at the same film temperature, the modulus  $j_h/Re_f f$  thus represents the relative heat transfer coefficients per unit pressure drop. This group is therefore used to compare heat-transmission performance of three pipes on a unit pressure drop basis, in Figure 11. It is apparent that over the entire range of Reynolds number studied, the smooth copper pipe is on this basis more efficient than the rougher Karbate pipe, which, in turn, is more efficient than the still rougher galvanized pipe. A similar result is shown in Figure 12, where the comparison is made on the basis of unit power loss with the modulus  $j_h/Re_f^2 f$ . This group represents heat transfer coefficient per unit frictional power loss:

$$\frac{j_h}{fRe_f^2} = \frac{h}{\Delta p_{fr} V_b \pi D^2} \cdot \frac{\pi L}{2g_c D} \cdot \frac{\mu_f^2}{C_p \rho_f^2} \quad (9)$$

As predictable, the differences between pipes on the unit power basis are somewhat smaller than on the unit pressure-drop basis.

#### MOMENTUM-HEAT TRANSFER ANALOGIES

The data on rough pipes offer a critical test of the many analogies between turbulent momentum and heat transfer which have been proposed.

Dealing with a turbulent system, and one in which  $Pr$  is near unity, Reynolds (24) originally argued that

$$j_h Pr^{-2/3} = \frac{h}{C_p V_b \rho} = \frac{\alpha f}{2} \quad (10)$$

The dimensionless constant  $\alpha$  has commonly been taken as unity (15, 18). In the present study, for which  $Pr_f$  was essentially constant at 0.69, Equation (10) says that  $j_h$  is directly proportional to  $f$ . A similar result arises from Colburn's (4) empirical modification of the Prandtl-Taylor analogy:

$$j_h = \frac{f}{2} \quad (11)$$

This proportionality between  $j_h$  and  $f$ , either at a fixed Reynolds number for varying roughness or for fixed roughness at varying Reynolds number, is at complete odds with the data of Figure 9. Equation (11) is suitable for smooth pipes, as in Figure 2, and is even applicable for approximate prediction of rough-pipe heat transfer if the  $f$  is for a smooth tube, as in Figure 9, but should

not be applied when rough-pipe friction factors are used. Equation (10), with  $\alpha = 1$ , is a reasonable first approximation for pipes of intermediate roughness.

The equations of Taylor (28) and Prandtl (22), who developed the laminar sublayer concept, of von Kármán (13), who introduced the concept of a buffer layer between the laminar sublayer and the turbulent core, and of Pinkel (21), who based his work on the analyses of von Kármán and of Deissler (9), as well as on the empirical data of Sams (25), all lead in the present instance of a fixed Prandtl number to an equation of the form

$$j_h = \frac{\sqrt{f/2}}{b + c \cdot \sqrt{f/2}} \quad (12)$$

where  $b$  is a constant which depends upon the Prandtl number and  $c$  is a constant which depends both on the Prandtl number and the wall roughness. Although Equation (12), unlike (10) and (11), does not imply direct proportionality between  $j_h$  and  $f$  at fixed Reynolds number, it does imply that where  $f$  becomes independent of  $Re$  for a rough pipe,  $j_h$  also becomes independent of  $Re$ . Reference to Figures 2 to 9 shows that this contradicts the experimental facts. After the friction factor curves for the rougher pipes have become practically horizontal, the  $j_h$  curves continue to slope downward. The artificial roughness data of Cope and of Sams show the same effect.

A momentum-heat-transfer analogy equation which does show a dependence of  $j_h$  with  $Re$  even after  $f$  has become independent of  $Re$ , is that developed by Boelter, Martinelli, and Jonassen (2) as



an extension of von Kármán's work. This was further refined by Martinelli (17) to include the effect of the diffusivity ratio  $D.R.$  Martinelli's equation, with equality of momentum and thermal eddy diffusivities assumed, may be written as

$$j_h = \frac{\sqrt{f/2} (Pr)^{2/3} \frac{\Delta t_{max}}{\Delta t_{mean}}}{5 \left[ Pr + \ln(1 + 5Pr) + 0.5 D.R. \ln \frac{Re}{60} \sqrt{f/2} \right]} \quad (13)$$

In the present instance no temperature profiles were measured and hence  $\Delta t_{max}/\Delta t_{mean}$ , which is a function of the radial temperature gradients, was not evaluated. However, since the density and other fluid properties have been evaluated at the "film" temperature, an empirical factor  $T_f/T_b$  has in effect been applied for handling such temperature gradients. If  $Pr_f$  is assigned its value for the present study 0.69, and if  $D.R.$  is taken as unity, Equation (13) reduces to

$$\frac{\sqrt{f_f}}{j_h} = 10.425 \cdot \log Re_f \sqrt{f_f} - 0.3395 \quad (13a)$$

By use of the friction factor curves of Figures 2 to 8, plots of  $j_h$  vs.  $Re_f$  have been calculated according to Equation (13a) and are reproduced in the same figures. Agreement with the experimental data is good, particularly with several of the rougher pipes. Equation (13a) also indicates a straight-line relationship between  $\sqrt{f_f}/j_h$  and  $\log Re_f \sqrt{f_f}$ . All the heating data were thus plotted in Figure 13, where again reasonably good agreement between the data and the Martinelli line occurs.

Except for the Karbate pipe, which, as already noted, displays its distinctive type of roughness, the greatest deviations between the experimental data and the Martinelli equation occur for the smoother pipes and for the lower Reynolds numbers, i.e., for low values of  $Re \sqrt{f_f}$ . These are precisely the points where the assumption of  $D.R. = 1.0$  is in greatest error. Correct values of  $D.R.$  for these cases, since they are less than unity, would raise the Martinelli lines of Figures 2 to 8, particularly those for the smoother pipes at low  $Re$ .

A more rigorous test of the Martinelli equation with the present data is planned for the future. This will involve evaluation of  $D.R.$  by use of the formula developed by Martinelli (17, 18), accounting for radial temperature gradients by estimation and application of the factor  $\Delta t_{max}/\Delta t_{mean}$ , rather than by  $T_f/T_b$ , and applying the factor of Seban and Shimazaki (26) to convert the Martinelli derivation for uniform heat flux to the present case of uniform wall temperature.

Use of roughness Reynolds number and shear Stanton number as correlating parameters is currently under trial.

#### ACKNOWLEDGMENT

The authors are indebted to the National Research Council of Canada and to the U.B.C. President's Committee on Research for grants-in-aid of this study. Thanks are

also due to B. C. Almaula, who initiated the construction of the apparatus.

#### NOTATION

- $a$  = constant in Equation (7), dimensionless  
 $a.d.$  = average deviation between measured  $j_h$  and  $j_h$  calculated by Equation (7), %

- $b$  = constant in Equation (12), dimensionless  
 $c$  = constant in Equation (12), dimensionless  
 $C_p$  = heat capacity of fluid, B.t.u./  
 (lb.) (°F.)  
 $D$  = inside diameter of pipe, ft.  
 $D.R.$  = diffusivity ratio =  $E_H/(E_H + k/\rho C_p)$ , dimensionless  
 $e$  = equivalent sand roughness, ft.  
 $E_H$  = eddy diffusivity of heat, sq. ft./hr.  
 $f$  = Fanning friction factor,  $\Delta p_f D g_c/2LV^2\rho$ , dimensionless  
 $g_c$  = conversion factor =  $4.17 \times 10^8$   
 (lb.) (ft.) / (hr.)<sup>2</sup> (lb.-force)  
 $G$  = mass velocity, lb./ (hr.) (sq. ft.)  
 $h$  = coefficient of heat transfer between fluid and surface, B.t.u./  
 (hr.) (sq. ft.) (°F.)  
 $j_h$  = heat transfer factor =  $(h/C_p V \rho) (Pr)^{2/3}$

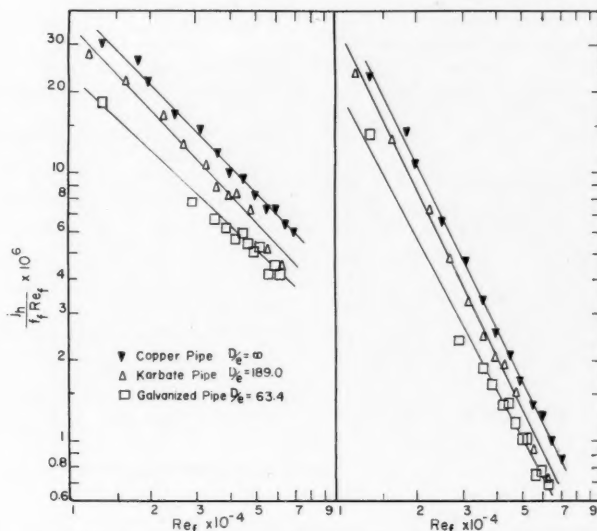


Fig. 11. Heat transmission per unit pressure drop for three pipes.

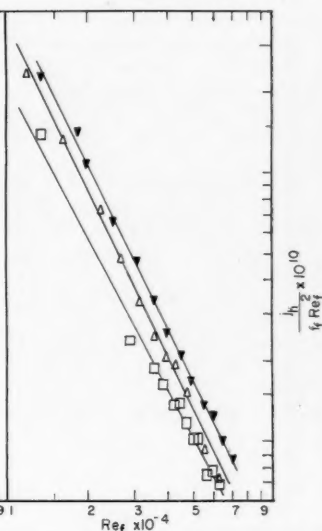


Fig. 12. Heat transmission per unit power loss for three pipes.

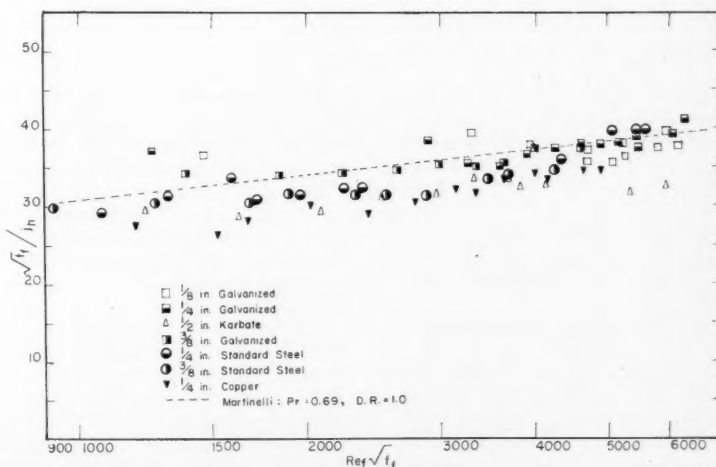


Fig. 13. Test of Martinelli's analogy.

$k$  = thermal conductivity of fluid, (B.t.u.)(ft.)/(hr.)(sq. ft.)(°F.)  
 $L$  = length of pipe, ft.  
 $n$  = constant in Equation (7) = slope of  $j_h$  vs.  $Re$ , curves in Figure 9 = 1 - slope of curves in Figure 10, dimensionless  
 $p$  = absolute pressure, lb.-force/sq. ft.  
 $\Delta p_{fr}$  = frictional pressure drop, lb. force/sq. ft.  
 $Pr$  = Prandtl number =  $C_p \mu / k$ , dimensionless  
 $Re$  = Reynolds number =  $DV\rho/\mu$ , dimensionless  
 $t$  = temperature of fluid, °F.  
 $t_b$  = average bulk temperature of fluid =  $(t_1 + t_2)/2$ , °F.  
 $t_f$  = film temperature =  $(t_b + t_s)/2$ , °F.  
 $t_s$  = inside surface temperature of pipe, °F.  
 $\Delta t_{maz}$  = temperature difference between inside surface of pipe and axis of pipe, °F.  
 $\Delta t_{mean}$  = temperature difference between inside surface of pipe and bulk of fluid, °F.  
 $T$  = absolute temperature, °R.  
 $V$  = velocity of fluid, ft./hr.  
 $V_b$  = velocity of fluid defined by  $G/\rho_{avg}$   
 $v$  = specific volume of fluid, cu. ft./lb.  
 $w$  = weight rate of air flow, lb./hr.  
 $\alpha$  = ratio of total diffusivity of heat to total diffusivity of momentum, dimensionless  
 $\mu$  = viscosity of fluid, lb./(ft.)(hr.)  
 $\rho$  = density of fluid, lb./cu. ft.  
 $\rho_{avg}$  = density of fluid evaluated at  $(p_1 + p_2)/2$  and  $t_b$ , lb./cu. ft.  
 $\rho_f$  = density of fluid evaluated at  $(p_1 + p_2)/2$  and  $t_f$ , lb./cu. ft.

#### Subscripts

- 1 = test pipe entrance (slightly different for pressure drop than for heat transfer)  
 2 = test pipe exit (slightly different for pressure drop than for heat transfer)  
 $b$  = bulk, evaluated at temperature  $t_b$   
 $f$  = film, fluid properties evaluated at temperature  $t_f$

#### LITERATURE CITED

- Am. Soc. Mech. Engrs., "Rept. of A.S.M.E. Special Research Committee on Fluid Meters," 4 ed. (1937).
- Boelter, L. M. K., R. C. Martinelli, and Finn Jonassen, *Trans. Am. Soc. Mech. Engrs.*, **63**, 447 (1941).
- Boelter, L. M. K., C. Young, and H. W. Iversen, *Natl. Advisory Comm. Aeronaut. Tech. Note* 14-51 (1948).
- Colburn, A. P., *Trans. Am. Inst., Chem. Engrs.*, **29**, 174 (1933).
- , *Purdue Univ. Eng. Bull. Research Ser.*, **84**, p. 52 (1942).
- Colebrook, C. F., *J. Inst. Civil Engrs.*, **11**, 133 (1938-39).
- Cope, W. F., *Proc. Inst. Mech. Engrs.*, **145**, 99 (1941).
- Chu, H., and V. L. Streeter, III, *Inst. Technol. Proj.* 4918 (Aug. 1949).
- Deissler, R. G., *Trans. Am. Soc. Mech. Engrs.*, **76**, 73 (1954).
- Drexel, R. E., and W. H. McAdams, *Natl. Advisory Comm. Aeronaut. War-time Rept.* 108 (1945).
- Humble, L. V., W. H. Lowdermilk, and L. C. Desmon, *Natl. Advisory Comm. Aeronaut. Rept.* 1020 (1951).
- Kármán, T. von, *Natl. Advisory Comm. Aeronaut. Tech. Mem.* 611 (1931).
- , *Trans. Am. Soc. Mech. Engrs.*, **61**, 705 (1939).
- King, W. J., and A. P. Colburn, *Ind. Eng. Chem.*, **23**, 919 (1931).
- Knudsen, J. G., and D. L. Katz, "Fluid Dynamics and Heat Transfer," p. 177, Univ. Mich. Press, Ann Arbor (1954).
- Latzko, H., *Natl. Advisory Comm. Aeronaut. Tech. Mem.* 1068 (1944).
- Martinelli, R. C., *Trans. Am. Soc. Mech. Engrs.*, **69**, 947 (1947).
- McAdams, W. H., "Heat Transmission," 3 ed., McGraw-Hill Book Company, Inc., New York (1954).
- Nagaoka, J. and A. Watanabe, *Proc. 7 Intern. Congr. Refrig., The Hague-Amsterdam*, **3**, No. 16, 221 (1937).
- Nikuradse, J., *Forschungsheft*, **361**, 1 (1933).
- Pinkel, Benjamin, *Trans. Am. Soc. Mech. Engrs.*, **76**, 305 (1954).
- Prandtl, L., *Physik, Z.*, **11**, 1072 (1910); **29**, 487 (1928).
- Pratt, H. R. C., *Trans. Inst. Chem. Engrs. (London)*, **28**, 177 (1950).
- Reynolds, Osborne, *Proc. Manchester Lit. Phil. Soc.*, **14**, 7 (1874).
- Sams, E. W., *Natl. Advisory Comm. Aeronaut. Research Mem.* E52 D17 (1952).
- Seban, R. A., and T. T. Shimazaki, *Trans. Am. Soc. Mech. Engrs.*, **73**, 803 (1951).
- Sherwood, T. K., and C. E. Reed, "Applied Mathematics in Chemical Engineering," 1 ed., McGraw-Hill Book Company, Inc., New York (1939).
- Taylor, G. I., *Brit. Advisory Comm. Aeronaut. Rept. and Memo.* 272 (1917).
- Tribus, Myron, and L. M. K. Boelter, *Natl. Advisory Comm. Aeronaut. A.R.R.* (Oct. 1942).

Presented at A.I.Ch.E. Boston meeting

# Control of Continuous-flow Chemical Reactors

OLEGH BILOUS, H. D. BLOCK, and EDGAR L. PIRET

University of Minnesota, Minneapolis, Minnesota

## I. Frequency-response Relations for a Continuously Stirred Tank Reactor

Although applications of frequency-response techniques to the control of processes are well known in electrical engineering and in the instrumentation field, relatively little has been done to develop in a quantitative manner the employment of these techniques in the control of chemical reactions. As a result the control characteristics of chemical reactors are today being come upon either in the pilot plant or in the field. This study was motivated by the fact that processes designed on the basis of steady state operation may sometimes prove inadequate for automatic control.

Oleg Bilous is with Laboratoire Centrale des Poudres, Paris, France, and H. D. Block at Cornell University, Ithaca, New York.

It is the purpose of this paper then to show how frequency-response analysis may be used to develop the theory of control of continuous-flow chemical reactors. The response equations are developed for simple and complex reactions of any order, and, for clarity, their applications are illustrated with selected numerical examples and by the use of polar plots.

The effects on the reactor-product stream which are considered in the equations include variations in feed-stream composition and temperature, the heat input or cooling of the reactor by coils, and the effect of temperature level on the rates of reaction and of heat release. How automatic-control requirements may

influence proper reactor design is also illustrated. Only single-stage reactors are considered here. Chains of reactors will be treated in Part II.

The transient behavior of continuous reactor systems has been considered by Mason and Piret (7) and the self-regulation properties of chains of reactors by Devyatov and Bogshv (3); Kramers and Alberda (6) have applied the method of complex amplitudes to the study of mixing and residence times in reactors. These investigations are all limited to first-order processes with no temperature effects. Transient equations for second-order processes in continuous reactors with no temperature effects were recently treated by Acton and Lapidus (1). The

general theory of frequency-response analysis has, of course, long been developed.

## THE PROBLEM

In the continuous operation of a stirred tank reactor the product obtained must be of uniform quality. Thus composition of the outlet stream from the reactor should be maintained within given limits around the steady state value, the width of the permissible band being determined by the severity of specifications. As the product composition depends on many variables, such as feed concentration and reactor temperature, one part of the problem is to find the effect of variations in these upon the product composition. When this effect is known, one can calculate the limits which should be imposed upon feed concentration and reactor temperature to hold the subsequent variation in outlet-stream composition within the allowable range.

In practice the fluctuations externally imposed on the reactor are likely to be highly irregular. For analytical purposes however sinusoidal variations are usually assumed. Thus results remain general and the mathematics is more tractable. The results are general because in a linear system an arbitrary fluctuation can, at least theoretically, be resolved into its harmonic components and the response functions of these integrated to find the total effect.

A second problem concerns more specifically the design of the control system. Process characteristics being known from the first part of the study, the control characteristics best suited to the problem are examined, especially the effects of the different types of control on the behavior of the continuous process. A specific question which arises at this point is the effect of dead time in the control loop on the cycling tendencies of the process. This question is briefly examined in Part II for the limiting case of a tubular reactor.

## THEORY

The first problem may be restated as follows. Given a small periodic variation in the parameters defining reactor operation, find the resulting periodic variation in composition of the effluent stream from the reactor.

### The Basic Equations

As is usually done in the theory of continuously stirred tank reactors, uniformity of conditions will be assumed throughout the reactor space. The steady state performance is then readily predictable for either simple or complex reactions, as shown in reference 2 and reference 4. Two chemical components, A in the feed and B in the product, will

be considered, component B representing the product of interest. The theory could of course be developed in general for any number of components, but consideration of only two components of interest is sufficient for most of the actual applications. For simplicity, developments presented here are for the case where

$$\frac{dB}{dt} = -\frac{1}{\alpha} \frac{dA}{dt} = R(x, T)$$

The reaction rate  $R(x, T)$  is a function of  $x$ , the concentration of A, and the temperature  $T$ . The stoichiometric coefficient is  $\alpha$ . No assumption is made about the order of the reaction, and so the case examined remains quite general. The mass balances across the reactor give the basic transient equations

$$[\text{accumulation}] = [\text{input}] - [\text{output}] - [\text{reacted}]$$

$$\theta \frac{dx}{dt} = x_0 - x - \alpha \theta R(x, T) \quad (1)$$

$$\theta \frac{dy}{dt} = y_0 - y + \theta R(x, T) \quad (2)$$

and from the heat balance

$$\theta \frac{dT}{dt} = T_0 - T + \theta h(T) + Q \alpha \theta R(x, T) + \theta H(t) \quad (3)$$

where

$\theta = V/F$  = reactor holding time, hr.

$T, T_0$  = temperature in the reactor and in the feed stream, °K.

$Q = -\Delta H_R/c_p$  = change in temperature caused by adiabatic reaction per mole of component A reacted in a unit volume of reacting mixture, (°K.)(liter)/mole.  $Q$  is positive for an exothermic reaction. The specific heat per unit volume,  $c_p$ , is taken constant and the same for the feed and product.

$h(T)$  = heat input to the reactor volume expressed as change in temperature, °K./hr., due to heat input from sources which depend on  $T$  only.  $h(T)$  is equal to the rate of heat input to the whole reactor due to temperature-dependent sources, divided by the total reactor heat capacity,  $Vc_p$ .

$H(t)$  = heat input, °K./hr., from independent time-varying sources such as would be caused by the manipulation of a steam valve

The notations of this section are illustrated in Figure 1. For convenience  $Q$  has been assumed to be a constant independent of concentration and temperature. All other factors are considered either negligible or remaining constant in this analysis. The heat input  $h(T)$  covers heat losses by the reactor surface

and heat inputs (due to heat transfer from heating or cooling coils or jackets operating at constant temperatures for example). The equations will first be linearized and then solved by methods commonly used in the analysis of electrical networks.

### Linearization

The three equations [(1), (2), (3)] where the derivatives are set equal to zero define the steady state conditions

$$x_s, y_s, T_s$$

related by

$$x_0 - x_s - \alpha \theta R(x_s, T_s) = 0 \quad (4)$$

$$y_0 - y_s + \theta R(x_s, T_s) = 0 \quad (5)$$

$$T_0 - T_s + \theta h(T_s) + \theta H_s + Q \alpha \theta R(x_s, T_s) = 0 \quad (6)$$

For nonsteady operations the variables  $X, Y, Z$  defined by

$$x = x_s + X \quad (7)$$

$$y = y_s + Y \quad (8)$$

$$T = T_s + Z \quad (9)$$

are introduced. They represent variations around the steady state. This study will be concerned with small variations only; that is, second-order terms in  $X, Y, Z$  will be assumed negligible. Under this assumption the reaction rate  $R(x, T)$  may be written as follows:

$$R(x, T) = R(x_s, T_s) + R_x'(x_s, T_s)X + R_T'(x_s, T_s)Z \quad (10)$$

$R_x'(x_s, T_s)$  and  $R_T'(x_s, T_s)$  being the partial derivatives of the rate with respect to concentration of A and temperature.

In order to simplify the problem, the derivative  $h_T'(T_s)$  of the heat-input function will be neglected. Thus instead of  $h(T) = h(T_s) + h_T'(T_s)Z$  one may write

$$h(T) = h(T_s) \quad (11)$$

Also  $H(t) \equiv H_s + \Delta H(t)$ . Replacing  $(x_0, y_0, T_0)$  by  $(X_0 + x_s, Y_0 + y_s, Z_0 + T_s)$  and introducing (7), (8), (9) and (10), (11) in the three transient equations (1), (2), (3) gives

$$\theta \frac{dX}{dt} + (1 + \alpha \theta R_x')X + \alpha \theta R_T'Z = X_0 \quad (12)$$

$$\theta \frac{dY}{dt} - \theta R_x'X + Y - \theta R_T'Z = Y_0 \quad (13)$$

$$\theta \frac{dZ}{dt} - Q\alpha\theta R_x'X + (1 - Q\alpha\theta R_T')Z = \theta\Delta H + Z_0 \quad (14)$$

These are now linear first-order differential equations. The forcing functions  $X_0$ ,  $Y_0$  and  $\theta\Delta H + Z_0$ , where  $X_0$ ,  $Y_0$  and  $Z_0$  are the varying parts of the feed concentrations in  $A$  and  $B$  and of the feed temperature, will be later assumed to be periodic functions.

#### Method of Complex Amplitudes

The method of complex amplitudes is rigorously based on Fourier transforms, but the simple presentation given below is sufficient here. A more detailed treatment may be found in reference 5.

In all this section the existence of a steady state response of the system to the periodic forcing functions is assumed. Thus the calculated response will have no physical significance if the system is unstable. System stability may be discussed by consideration of the roots of its characteristic equation.

The periodic functions used in this treatment will be represented by the form

$$\chi(t) \equiv X e^{j\omega t} \quad (15)$$

where  $\chi(t)$  is the periodic function, for instance a variation in concentration or temperature,  $X$  is a complex number, and  $e^{j\omega t} = \cos \omega t + j \sin \omega t$ . The frequency of oscillation in radians/hour is represented by  $\omega$  and  $j$  stands for  $\sqrt{-1}$ . The derivative of  $\chi(t)$  is

$$\frac{d\chi(t)}{dt} = X \frac{d}{dt} e^{j\omega t} = j\omega X e^{j\omega t} = j\omega \chi(t) \quad (16)$$

and therefore in this case, that is to say for periodic functions of Form (15), the operation of taking the time derivative is equivalent to the operation of multiplication by  $j\omega$ .

Since the solutions will therefore be of the same form as the forcing functions, the system of linear differential equations (12), (13), and (14) may be written as follows:

$$(1 + j\omega\theta + \theta\alpha R_x')X + \theta\alpha R_T'Z = X_0 \quad (17)$$

$$-\theta R_x'X + (1 + j\omega\theta)Y - \theta R_T'Z = Y_0 \quad (18)$$

$$-Q\alpha\theta R_x'X + (1 + j\omega\theta - Q\alpha\theta R_T')Z = \theta\Delta H + Z_0 \quad (19)$$

The applications below are based on these three equations. For present purposes the feed concentration of  $B$  and the inlet-feed temperature will usually be held constant and thus in the forms above  $Y_0$  and  $Z_0$  become zero.

In the first case, discussed below, temperature effects will for clarity be

This may be written as follows, by putting the complex number  $Y/X_0$  in the polar form (15):

$$Y = \frac{\theta R_x'}{\sqrt{(1 + \alpha\theta R_x' - \omega^2\theta^2)^2 + \omega^2\theta^2(2 + \theta\alpha R_x')^2}} e^{j\phi} X_0 \quad (21)$$

with the angle  $\phi$  defined by

$$\tan \phi = \frac{-\omega\theta(2 + \alpha\theta R_x')}{1 + \theta\alpha R_x' - \omega^2\theta^2} \quad (22)$$

Therefore, the ratio of the magnitude of the variation in product concentration  $|Y|$  to the magnitude of the variation in feed concentration  $|X_0|$  is

$$\left| \frac{Y}{X_0} \right| = \frac{|\theta R_x'|}{\sqrt{(1 + \theta\alpha R_x' - \omega^2\theta^2)^2 + \omega^2\theta^2(2 + \theta\alpha R_x')^2}} \quad (23)$$

considered negligible so that only the variations in concentration of the feed will affect the concentration of the products. One way in which this can come about is the case where the temperature of the reactor is maintained steady; i.e.,  $Z$  equals zero when heat input balances output,  $-Q\alpha R_x'X = \Delta H$ , in particular if the heat of reaction  $Q$  is zero and there is no heat input. Another way occurs if the rate of reaction is not strongly temperature dependent over the control range and so  $R_T' = 0$ .

In the second case the internal reactor temperature will be allowed to vary with the heat of the reaction. Finally, the third case will concern variations in product concentrations and reactor temperature caused by heat input alone when the feed concentration is constant, that is to say, with  $X_0 \equiv 0$ .

#### First Case: Variations in Concentration Alone

For the case where there is no temperature effect,

$$(1 + j\omega\theta + \alpha\theta R_x')X = X_0$$

$$-\theta R_x'X + (1 + j\omega\theta)Y = 0$$

from which is found

$$Y = \frac{\theta R_x'}{(1 + j\omega\theta)(1 + j\omega\theta + \alpha\theta R_x')} X_0 \quad (20)$$

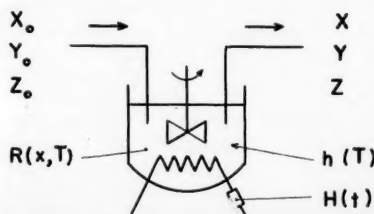


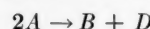
Fig. 1. Illustration of nomenclature.

and this result is valid whatever the order of the reaction, provided that the amplitudes of the variations are small.

Inspection of (23) shows that the reactor is stable in all cases, because the denominator of the transfer function cannot be zero for real values of  $\omega$ . Furthermore the homogeneous system has the solution  $Y = Ce^{-t/\theta}$ .

#### Illustration I

The second-order reaction is



with a rate expressed by

$$\frac{dB}{dt} = -\frac{1}{2} \frac{dA}{dt} = k[A]^2$$

The kinetic rate constant  $k$  is

$$k = 1.165 \cdot 10^{14} e^{-10,000/T} \text{ mole}^{-1} \text{ hr.}^{-1}$$

The reactor is operated with a holding time

$$\theta = 20 \text{ min.}$$

and a feed containing 1.75 moles/liter of  $A$ . The reactor temperature is  $80^\circ\text{C}$ . The effect of variations in the concentration of  $A$  in the feed upon the concentration of product  $B$  in the effluent are calculated. At  $80^\circ\text{C}$ , the value of the rate constant is  $k = 1.165 (10^{14}) e^{-10,000/T} = 58.10 \text{ mole}^{-1} \text{ hr.}^{-1}$  and the steady state composition of the reacting mixture is given by the following mass balances:

on component  $A$

$$x_s - 1.75 + 2\left(\frac{20}{60}\right)(58.1)x_s^2 = 0$$

on component  $B$

$$y_s - \left(\frac{20}{60}\right)(58.1)x_s^2 = 0$$

The solutions are

$$x_s = 0.20 \text{ mole/liter,}$$

$$y_s = 0.775 \text{ mole/liter}$$

The equations, similar to (20), (21), (22), which must be used in this case to determine the effect of variations in the concentration of  $A$  in the feed upon the concentration of product  $B$  in the effluent are



$$Y = \frac{\theta R_x'}{(1 + j\omega\theta)(1 + j\omega\theta + 2\theta R_x')} X_0$$

$$Y = \frac{\theta R_x'}{\sqrt{(1 + 2\theta R_x' - \omega^2\theta^2)^2 + 4\omega^2\theta^2(1 + \theta R_x')^2}} e^{j\phi} X_0$$

with the angle  $\phi$  defined by

$$\tan \phi = -\frac{2\omega\theta(1 + \theta R_x')}{1 + 2\theta R_x' - \omega^2\theta^2}$$

where

$$R(x) = kx^2$$

and therefore

$$\theta R_x' = 2k\theta x = 2 \times 58.10$$

$$\times \frac{1}{3} \times 0.20 = 7.750$$

For the numerical data of the illustration the following values of the variation  $|Y/X_0|$  and the phase angle  $\phi$  are obtained for different values of frequency.

$\omega\theta$	0.01	0.10	0.50
$\omega$	0.03	0.30	1.50
$ Y/X_0 $	0.470	0.467	0.419
$\phi$	-0.6	-6	-28

The frequency  $\omega$  is expressed in radians per hour and the phase angle  $\phi$  in degrees.

#### Second Case: Variations in Concentration and Temperature

In the derivation of (20) it has been assumed that the temperature effects on the process could be neglected. In the case where there is an appreciable temperature effect the variations in product concentration due to variation in feed concentration of component A alone are related through the equations

$$(1 + j\omega\theta + \alpha\theta R_x')X + \alpha\theta R_T'Z = X_0$$

$$-\theta R_x'X + (1 + j\omega\theta)Y - \theta R_T'Z = 0$$

$$-\alpha Q\theta R_x'X + (1 + j\omega\theta$$

$$- \alpha Q\theta R_T')Z = 0$$

which are a special case of Equations (17), (18), (19) with no independent time-varying heat input,  $\Delta H = 0$ .

The expression corresponding to (20) for the present use is

$$Y = \frac{\theta R_x'}{(1 + j\omega\theta)(1 + j\omega\theta + \theta\alpha R_x' - Q\alpha\theta R_T')} X_0 \quad (24)$$

which may be written, similarly to (21):

$$Y = \frac{\theta R_x' e^{j\phi}}{\sqrt{(1 + \theta\alpha R_x' - \alpha Q\theta R_T' - \omega^2\theta^2)^2 + \omega^2\theta^2(2 + \alpha\theta R_x' - \alpha Q\theta R_T')^2}} X_0 \quad (25)$$

where the phase angle  $\phi$  is given by

$$\tan \phi = -\frac{\omega\theta(2 + \alpha\theta R_x' - \alpha Q\theta R_T')}{1 + \alpha\theta R_x' - \alpha Q\theta R_T' - \omega^2\theta^2} \quad (26)$$

The stability and the relative sensitivity of reaction systems may be more readily evaluated by factoring out a nonfrequency term from the response equations. For instance, Equation (24) may be rewritten as

$$\frac{Y}{X_0} = \frac{\theta R_x'}{1 + \alpha\theta R_x' - Q\alpha\theta R_T'} \frac{1}{(1 + j\omega\theta) \left(1 + j\omega \frac{\theta}{1 + \theta\alpha R_x' - Q\alpha\theta R_T'}\right)}$$

The first or amplification factor describes the response of the system to a steady perturbation, whereas the second factor indicates its dynamic behavior and thus

1.00	2.00	10.0	100
3.00	6.00	30.00	300
0.331	0.203	0.040	0.001
-49	-70	-115	-170

the controllability.

It is seen that the condition of stability is

$$1 + \theta\alpha R_x' - Q\alpha\theta R_T' > 0$$

hence in terms of the heat of reaction the system is unstable when

$$Q > \frac{1 + \theta\alpha R_x'}{\alpha\theta R_T'}$$

Since  $R_T'$ , the temperature coefficient of the reaction rate, is usually positive, this means that instability may occur for exothermic reactions with a sufficiently high value of the heat of reaction. Expressed in terms of the holding time the condition of stability yields

$$\theta < \frac{1}{(QR_T' - R_x')\alpha}$$

where

$$Q > \frac{R_x'}{R_T'}$$

Thus, when a reaction is sufficiently

exothermic ( $Q > R_x'/R_T'$ ), reactor operation as described by the linearized model will be stable only when the holding time  $\theta$  does not exceed a certain value. There is no limitation on the holding time for the case of an endothermic reaction.

This discussion is an example of a case when control requirements may place limitations on reactor design.

#### Illustration 2

In order to give an idea of the magnitude

of the temperature effect the variation in product concentration due to a variation in feed concentration will be calculated, the temperature effect being taken into account with the data used in Illustration 1.

With the introduction of the stoichiometric coefficient  $\alpha = 2$ , Expression (25) for the present case becomes

$$Y = \frac{\theta R_x' e^{j\phi}}{\sqrt{(1 + 2\theta R_x' - 2Q\theta R_T' - \omega^2\theta^2)^2 + 4\omega^2\theta^2(1 + \theta R_x' - Q\theta R_T')^2}} X_0$$

with

$$\tan \phi = -\frac{2\omega\theta(1 + \theta R_x' - Q\theta R_T')}{1 + 2\theta R_x' - 2Q\theta R_T' - \omega^2\theta^2}$$

The data of Illustration 1 gives

$$k = 1.165 \cdot 10^{14} e^{-10,000/T_s}$$

$$x_s = 0.200 \text{ mole/liter,}$$

$$T_s = 80^\circ\text{C.}$$

$$\theta = 20 \text{ min.}$$

Assuming that the reacting mixture has the density and heat capacity of water and that the heat of reaction is

$$\Delta H_R = -50,000 \text{ cal./mole of A}$$

yields

$$Q = 50 (^\circ\text{K.})(\text{liter})/\text{mole}$$

Then

$$\theta R_x' = 7.750$$

$$Q\theta R_T' = 3.112$$

Reactor operation is stable since

$$1 + 2\theta R_x' - 2Q\theta R_T' = 10.28 > 0$$

The values of the variation amplitude ratio  $|Y/X_0|$  and the phase angle  $\phi$  have been calculated for different values of the variation frequency  $\omega$  and are presented below:

Second-order exothermic reaction:  $Q = 50^\circ\text{K.}$

$\omega\theta$	0.01	0.10	0.50	1.00	2.00	10.0	100
$\omega$	0.03	0.30	1.50	3.00	6.00	30.0	300
$ Y/X_0 $	0.755	0.751	0.673	0.531	0.331	0.054	0.0008
$\phi$	-0.6	-6	-29	-51	-74	-128	-174

The calculations have also been made for the case of an endothermic second-order reaction, with  $Q = -75^\circ\text{K}$ , for the data used in Illustration 1.

Second-order endothermic reaction:  $Q = -75^\circ\text{K}$ .

$\omega\theta$	0.01	0.10	0.50	1.00	2.00	10.0	100
$\omega$	0.03	0.30	1.50	3.00	6.00	30.0	300
$ Y/X_0 $	0.300	0.298	0.268	0.211	0.1334	0.0278	0.001
$\phi$	-0.6	-6	-28	-47	-68	-105	-165

The values resulting from the calculations of Illustrations 1 and 2 are represented in Figure 2, which is called a Nyquist polar plot. If  $M$  is a point of the plot which represents a particular operating condition for the reactor, the length of the vector joining the origin to  $M$  is  $|Y/X_0|$  and the angle of the vector with the positive direction of the horizontal axis is the phase angle  $\phi$ . The lower half of the curve corresponds to positive frequencies, the upper half being a reflection of those on the real axis.

On the polar plot of Figure 2 are represented the values of Illustration 1, where the reaction is assumed to have a negligible temperature dependence, by the locus  $Q = 0$ . The data of Illustration 2, where the reaction considered is exothermic, are shown by the locus  $Q = 50(^\circ\text{K})$ (liter)/mole. Also presented is the case of an endothermic reaction, with  $Q = -75(^\circ\text{K})$ (liter)/mole. Several values of  $\omega\theta$  are shown in Figure 2 to indicate how the curves are prepared from the foregoing tables.

It is apparent from the polar plots of Figure 2 that the outgoing concentrations of endothermic reactions and temperature-insensitive reactions are less sensitive toward variations in feed composition than are those of exothermic reactions.

This fact is easily understood in a qualitative way, as a concentration increase in the feed reactant for the case of an endothermic reaction brings about a temperature decrease which counteracts the effect of increased feed concentration on the reaction rate. An endothermic reaction thus possesses a certain degree of self-regulation. On the contrary, an exothermic reaction is autocatalyzed through its heat output: an increase in feed concentration increases the reaction rate and the heat of reaction only serves further to increase the rate. Thus exothermic reactions may be expected to present some instability; however, an increased rate burns out the excess reactant and the process tends to normal. The equation developed here of course take these simultaneous effects into account.

It appears from Figure 2 that the Nyquist plots for variations in concentration are nearly circular and may be approximated by a family of circles. A system with a single time lag, called a first-order system, has a circular Nyquist plot. The approximation is usually possible because of the preponderance of

the holding-time lag over the other lags in the system.

As a final result of the Nyquist plots

for Illustrations 1 and 2, it may be observed that the maximum amplitude ratio of the concentration variations is given by

$$\left| \frac{Y}{X_0} \right|_{\max} = \left| \frac{\theta R_z'}{1 + 2\theta R_z' - 2Q\theta R_T'} \right| \quad (27)$$

Expression (27) shows that the maximum amplitude ratio is infinite when

$$Q = \frac{1 + 2\theta R_z'}{2\theta R_T'} = 132.7(^\circ\text{K})\text{(liter)/mole.}$$

This represents a limiting case of stability in the example. Reactions with  $Q \geq 132.7(^\circ\text{K})$ (liter)/mole would be unstable under the conditions of Illustration 2.

### Third Case: Heat-input Variations

Coming back to the more general case chosen for the exposition of the theory, one may now examine the nature of the influence of independent variations in heat input to the reactor  $H$  upon product concentration and reactor temperature. A constant feed composition and temperature will be assumed in order to isolate clearly the results of interest. Knowledge of the effect of heat-input variations on reactor temperature is necessary in order to determine later the sensitivity, rate of response, and other characteristics of the instruments and elements in a reactor heat-control loop which will provide an adequate degree of control.

Equations (17), (18), and (19) will be used, with the assumption that  $X_0 = 0$ , which corresponds to a constant feed composition

$$(1 + j\omega\theta + \alpha\theta R_z')X + \alpha\theta R_T'Z = 0 \quad (17')$$

$$-\theta R_z'X + (1 + j\omega\theta)Y - \theta R_T'Z = 0 \quad (18')$$

$$-\alpha Q\theta R_z'X + (1 + j\omega\theta - \alpha Q\theta R_T')Z = \theta\Delta H \quad (19')$$

The solutions are

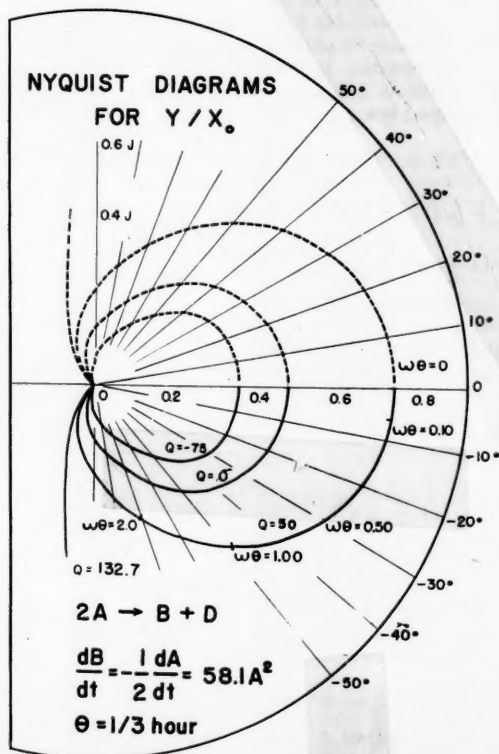


Fig. 2. Nyquist-type diagrams for concentration variations in a C.S.T.R. Data of illustrations 1 and 2 for the second-order reaction  $2A \rightarrow B + D$ .

the quantity  $\theta\Delta H$  being replaced by  $Z_0$ , variation in feed temperature.

#### GENERALIZATION

For simplicity the previous theory was developed on the basis of a reaction involving a feed reactant  $A$  and a product  $B$  with rate dependent on the concentration of  $A$  and the temperature. If several reactants determine the rate, then an additional material-balance equation appears for each of these reactants. The resulting set of simultaneous differential equations is then most conveniently expressed by the use of matrices. The form of the solution for reactions where several components affect the rate will now be shown. A tabulation will also be presented of the specific frequency-response functions for typical complex reaction systems. It should be kept in mind that, since linearization has been used, the frequency-response functions obtained are valid for only small variation amplitudes, such as are usually present under automatic control.

Considered first is the case of  $m$  reactants:  $A_1, A_2, \dots, A_m$ . It is assumed that the effect of temperature variations can be ignored\*, and so the rate of increase of  $x_i$ , the concentration of  $A_i$ , can be written as  $R_i(x_1, \dots, x_m)$ . Proceeding just as before, one finds that the frequency-response functions  $X_1, X_2, \dots, X_m$  to perturbations  $X_1^0, X_2^0, \dots, X_m^0$ , of frequency  $\omega$ , in the feed concentrations satisfy the equations

$$[(1 + j\omega\theta)I - \theta R] \begin{bmatrix} X_1 \\ \vdots \\ X_m \end{bmatrix} = \begin{bmatrix} X_1^0 \\ \vdots \\ X_m^0 \end{bmatrix}$$

where  $I$  is the identity matrix and  $R$  is a matrix whose element in the  $i$ th row and  $j$ th column is  $\partial R_i / \partial x_j$ , evaluated at the steady state values. The equations may then be solved by the usual Cramers' rule. The solutions appear as the quotient of two determinants, the denominator being  $\det [(1 + j\omega\theta)I - \theta R]$  and the

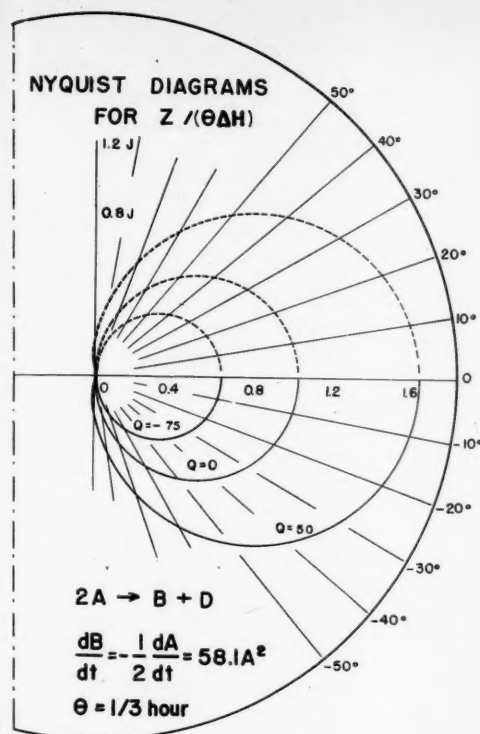


Fig. 3. Nyquist diagrams for temperature variations in a C.S.T.R. Data of illustration 3 for the second-order reaction  $2A \rightarrow B + D$ .

$$\frac{Z}{\theta\Delta H} = \frac{(1 + \alpha\theta R_z' + j\omega\theta)}{(1 + j\omega\theta)(1 + \alpha\theta R_z' - \alpha Q\theta R_T' + j\omega\theta)} \quad (28)$$

for the relation between reactor temperature variations  $Z$  and heat-input variations  $\Delta H$  and

$$\frac{Y}{\theta\Delta H} = \frac{\theta R_T'}{(1 + j\omega\theta)(1 + \alpha\theta R_z' - \alpha Q\theta R_T' + j\omega\theta)} \quad (29)$$

for the relation between variations in product concentration  $Y$  and heat-input variations. It is seen that Expression (29), giving the relationship  $Y/(\theta\Delta H)$ , has the same structure as (24), which gives  $Y/X_0$ . The polar plots corresponding to these expressions will therefore have the same shape, and the discussion of system stability made in the second case will apply.

#### Illustration 3

The plots of  $Z/(\theta\Delta H)$ , which express the dependence of reactor temperature on reactor heat input, are presented in Figure 3, for the data of the preceding illustration. The plots representing  $Y/(\theta\Delta H)$  are similar to those of Figure 2, differing only by the scale factor  $R_T'/R_z'$ , and therefore have not been redrawn. The values used for Figure 3 which represents  $Z/(\theta\Delta H)$ , are tabulated below.

In the case of the second-order reaction, which we assume, Expressions (28) and (29) take the form

Results of the calculation of the absolute value and phase angle of  $Z/(\theta\Delta H)$  are presented below for different values of the heat of reaction parameter  $Q$ .

$Q = 50(^{\circ}\text{K})(\text{liter})/\text{mole}$  (exothermic reaction)

$\omega\theta$	0.01	0.10	0.50	1.00	2.00	10.0	100.
$\omega$	0.03	0.30	1.50	3.00	6.00	30.0	300.
$ Z/(\theta\Delta H) $	1.608	1.600	1.436	1.132	0.710	0.1338	0.0101
$\phi$	-0.6	-6.	-28.	-47.	-68.	-97.	-93.

$Q = -75(^{\circ}\text{K})(\text{liter})/\text{mole}$  (endothermic reaction)

$\omega\theta$	0.01	0.10	0.50	1.00	2.00	10.0	100.
$\omega$	0.03	0.30	1.50	3.00	6.00	30.0	300.
$ Z/(\theta\Delta H) $	0.638	0.635	0.571	0.452	0.286	0.0692	0.0098
$\phi$	-0.6	-6.	-26.	-44.	-61.	-74.	-84.

In this case too the diagrams appear as nearly circular. Indeed, for  $Q = 0$  the Nyquist diagram for  $Z/(\theta\Delta H)$  is a circle.

It should be remarked that variations in reactor concentration or temperature caused by variations in feed temperature are exactly the same as those examined above,

numerator being the same but with the appropriate column being replaced by

\*When temperature effects are included, the results are very similar to those shown here, but for the sake of brevity they are not presented.

TABLE 1. CLASSIFICATION OF REACTIONS ACCORDING TO THEIR RATE DEPENDENCE

Group	Example	Rate functions	General rate-function type
Single Irreversible Reactions	(1) $A \rightarrow B$ (2) $2A \rightarrow 2B$ (3) $A + C \rightarrow B$	$R_1 = -R_2 = -kx, R_3 = R_4 = 0$ $R_1 = -R_2 = -kx^2, R_3 = R_4 = 0$ $R_1 = R_3 = -R_2 = -kxu, R_4 = 0$	$R_2 = -R_1 = R(x), R_3 = R_4 = 0$ $R_2 = -R_1 = R(x), R_3 = R_4 = 0$ $R_2 = -R_1 = -R_3 = R(x, u), R_4 = 0$
Single Reversible Reactions	(4) $A \rightleftharpoons B$ (5) $2A \rightleftharpoons 2B + C$ (6) $A + C \rightleftharpoons B + D$	$R_1 = -R_2 = k_1y - k_2x, R_3 = R_4 = 0$ $R_1 = k_1uy - k_2x^2 = -R_2 = -2R_3, R_4 = 0$ $R_1 = R_3 = -R_2 = -R_4 = k_1vy - k_2ux$	$R_2 = -R_1 = R(x, y), R_3 = R_4 = 0$ $R_2 = -R_1 = 2R_3 = R(x, y, u), R_4 = 0$ $R_2 = R_4 = -R_1 = -R_3 = R(x, y, u, v)$
Consecutive reactions	(7) $A \rightarrow B \rightarrow C$	$R_1 = -k_1x, R_2 = k_1x - k_2y, R_3 = k_2y, R_4 = 0$	$R_2 = R_2(x, y), R_1 = R_1(x),$ $R_3 = R_3(y), R_4 = 0$
Competing Reactions	(8) $\begin{cases} 2A \rightarrow B + D \\ B + C \rightarrow E \end{cases}$	$R_1 = -2k_1x^2, R_2 = k_1x^2 - k_2uy$ $R_3 = -k_2uy, R_4 = k_1x^2$	$R_2 = R_2(x, y, u), R_1 = R_1(x)$ $R_3 = R_3(y, u), R_4 = R_4(x)$
Consecutive and reversible Reactions	(9) $\begin{cases} 2A \rightleftharpoons B + C \\ B \rightarrow D \end{cases}$	$R_1 = 2k_1uy - 2k_2x^2,$ $R_2 = k_2x^2 - k_1uy - k_3y$ $R_3 = k_2x^2 - k_1uy, R_4 = k_3y$	$R_1 = R_1(x, y, u), R_2 = R_2(x, y, u)$ $R_3 = R_3(x, y, u), R_4 = R_4(y)$
Competing Reactions	(10) $\begin{cases} A \rightleftharpoons B + C \\ B + A \rightarrow D \end{cases}$	$R_1 = k_1uy - k_2x - k_3xy$ $R_2 = k_2x - k_1uy - k_3xy$ $R_3 = k_2x - k_1uy, R_4 = k_3xy$	$R_1 = R_1(x, y, u)$ $R_2 = R_2(x, y, u)$ $R_3 = R_3(x, y, u)$ $R_4 = R_4(x, y)$

NOTE: Letters  $x, y, u, v$  stand for the concentrations of  $A, B, C, D$ . The  $k$ 's are rate constants.

$$\begin{bmatrix} X_1 \\ \vdots \\ X_m \end{bmatrix}$$

For example, there are four reactants  $A_1 = A, A_2 = B, A_3 = C, A_4 = D$  with concentrations  $x_1 = x, x_2 = y, x_3 = u, x_4 = v$ . The frequency response  $Y$  of the variations in the concentration of  $B$  due to a perturbation  $X_0$  in the feed concentration of  $A$  is given by

$Y =$

$$\theta \begin{vmatrix} R_{2x}' & R_{2u}' & R_{2v}' \\ -\theta R_{3x}' & 1 + j\omega\theta - \theta R_{3u}' & -\theta R_{3v}' \\ -\theta R_{4x}' & -\theta R_{4u}' & 1 + j\omega\theta - \theta R_{4v}' \end{vmatrix} X_0$$

$$\begin{vmatrix} 1 + j\omega\theta - \theta R_{1x}' & -\theta R_{1y}' & -\theta R_{1u}' & -\theta R_{1v}' \\ -\theta R_{2x}' & 1 + j\omega\theta - \theta R_{2y}' & -\theta R_{2u}' & -\theta R_{2v}' \\ -\theta R_{3x}' & -\theta R_{3y}' & 1 + j\omega\theta - \theta R_{3u}' & -\theta R_{3v}' \\ -\theta R_{4x}' & -\theta R_{4y}' & -\theta R_{4u}' & 1 + j\omega\theta - \theta R_{4v}' \end{vmatrix}$$

where  $R_{ix}'$  denotes  $\partial R_i / \partial x$  at the steady state value, etc.

If only the reactants  $A, B, C$  affect the rates of reaction, then  $\partial R_1 / \partial v = \partial R_2 / \partial v = \partial R_3 / \partial v = \partial R_4 / \partial v = 0$  and the frequency response takes the form

$$Y = \theta \begin{vmatrix} R_{2x}' & R_{2u}' \\ -\theta R_{3x}' & 1 + j\omega\theta - \theta R_{3u}' \end{vmatrix} X_0$$

$$\begin{vmatrix} 1 + j\omega\theta - \theta R_{1x}' & -\theta R_{1y}' & -\theta R_{1u}' \\ -\theta R_{2x}' & 1 + j\omega\theta - \theta R_{2y}' & -\theta R_{2u}' \\ -\theta R_{3x}' & -\theta R_{3y}' & 1 + j\omega\theta - \theta R_{3u}' \end{vmatrix}$$

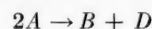
For the cases where the reaction rates depend on neither  $C$  nor  $D$  one has

$$Y = \frac{\theta R_{2x}' X_0}{1 - \theta(R_{2y}' + R_{1x}') + \theta^2(R_{1x}'R_{2y}' - R_{1y}'R_{2x}' - \omega^2) + j\omega\theta[2 - \theta(R_{2y}' + R_{1x}')]}$$

In Table 1 are listed ten types of reactions, giving the specific rate functions for each case and also the general type to which the example belongs. In Table 2 various general types are listed and the frequency-response function is given for each of these. The material in these tables is by no means exhaustive and is offered only for convenience and as an indication of the general nature of the results. In Table 2 the notation

#### NONLINEARITY OF REACTOR EQUATIONS

Chemical rate equations which occur in industrial practice are usually nonlinear. In this work they have been treated by the method of linearization, which was justified by the fact that the deviations from the steady state which are considered are small. Nonlinear-system response for large deviations from equilibrium is usually treated by approximation methods, and the results are obtained in the form of series. As a test of the degree of approximation obtained by linearization, the case of the second-order reaction chosen in Illustration 1, has been treated below, any temperature effect being neglected. The reaction is



with the rate

$$\frac{dB}{dt} = -\frac{1}{2} \frac{dA}{dt} = kx^2$$

The equations, similar to (12) and (13) which give the variations in composition  $X$  and  $Y$ , are

$$\theta \frac{dX}{dt} + (1 + 4k\theta x_s)X + 2\theta kX^2 = X_0 \quad (30)$$

$$\theta \frac{dY}{dt} + Y = 2k\theta x_s X + k\theta X^2 \quad (31)$$

Here, however, the second-order terms have not been neglected.

For simplicity, in the first equation

$$A = 1 + 4k\theta x_s$$

$$\lambda = \omega\theta$$



TABLE 2. FREQUENCY-RESPONSE FUNCTIONS  $Y/X_0$ , FOR ISOTHERMAL CONCENTRATION VARIATIONS IN A CONTINUOUS STIRRED TANK REACTOR

Rate-function type	Frequency-response function $Y/X_0$
$R_2 = -R_1 = R(x), R_3 = R_3(x, y),$ $R_4 = R_4(x, y, u)$	$\frac{\theta R_x'}{1 + \theta R_x' - \omega^2 \theta^2 + j\omega \theta (2 + \theta R_x')}$
$R_2 = -R_1 = -R_3 = R(x, u),$ $R_4 = R_4(x, y, u)$	$\frac{\theta R_x'}{(1 + j\omega \theta)(1 + j\omega \theta + \theta[R_x' + R_x'])}$
$R_2 = -R_1 = R(x, y), R_3 = R_3(x, y),$ $R_4 = R_4(x, y, u)$	$\frac{\theta R_x'}{(1 + j\omega \theta)(1 + j\omega \theta + \theta[R_x' - R_y'])}$
$R_2 = -R_1 = -R_3 = R_4 = R(x, y, u, v)$	$\frac{\theta R_x'}{(1 + j\omega \theta)(1 + j\omega \theta + \theta[R_x' + R_y' - R_v' - R_v'])}$
$R_1 = R_1(x, y), R_2 = R_2(x, y)$ $R_3 = R_3(x, y), R_4 = R_4(x, y, u)$	$\frac{\theta R_{2x}'}{1 - \theta(R_{2y}' + R_{1x}') + \theta^2(R_{1x}'R_{2y}' - R_{1y}'R_{2x}' - \omega^2) + j\omega \theta[2 - \theta(R_{2y}' + R_{1x}')]}$
$R_1 = R_1(x), R_2 = R_2(x, y, u)$ $R_3 = R_3(y, u), R_4 = R_4(x, y, u)$	$\frac{\theta R_{2x}'(1 + j\omega \theta - \theta R_{3u}')}{[1 + j\omega \theta - \theta R_{1x}'] [1 - \theta(R_{2y}' + R_{3u}') + \theta^2(R_{2y}'R_{3u}' - R_{3y}'R_{2u}' - \omega^2) + j\omega \theta(2 - \theta[R_{2y}' + R_{3u}'])]}$

Its steady state solution in the first-order approximation is, as before,

$$X_1 = \frac{X_0}{A + j\lambda}$$

$X_0$  being a cyclic quantity of frequency  $\omega$ . To obtain a series expansion in powers of  $X_0$  one writes

$$X = X_1 + X_2$$

Substituting into (30) gives

$$\begin{aligned} \theta \frac{dX_2}{dt} + AX_2 &= (X_0 - \theta \frac{dX_1}{dt} - AX_1) - (2\theta kX_2^2 + 4\theta kX_1X_2) - 2\theta kX_1^2 \end{aligned}$$

The first bracket on the right vanishes from the definition of  $X_1$ . The second contains second-order terms, which are neglected. The final equation for  $X_2$  is therefore

$$\theta \frac{dX_2}{dt} + AX_2 = -\frac{2\theta k}{(A + j\lambda)^2} X_0^2$$

where  $X_0^2$  is a cyclic quantity of frequency  $2\omega$ .

The steady-response term  $X_2$  therefore is

$$X_2 = \frac{-2\theta k}{(A + j\lambda)^2(A + 2j\lambda)} X_0^2 \quad (32)$$

In the same way

$$X_3 = \frac{8\theta^2 k^2 X_0^3}{(A + j\lambda)^3(A + 2j\lambda)(A + 3j\lambda)} \quad (33)$$

The general term may be easily found, but for the present purposes the second-order approximation will be sufficient.

$$\begin{aligned} X &= \frac{X_0}{A + j\lambda} \left[ 1 - \frac{2\theta k X_0}{(A + j\lambda)(A + 2j\lambda)} \right] \quad (34) \end{aligned}$$

Similarly, as  $Y = Y_1 + Y_2$  in (31),

$$\begin{aligned} Y &= \frac{2k\theta x_s X_0}{(A + j\lambda)(1 + j\lambda)} \\ &\cdot \left[ 1 + \frac{(1 + j\lambda)X_0}{2x_s(A + j\lambda)(A + 2j\lambda)} \right] \quad (35) \end{aligned}$$

The corrective factors depend on the input signal  $X_0$ . This dependence may be illustrated graphically by drawing a series of Nyquist polar diagrams of  $Y/X_0$  for different values of the input signal amplitude  $X_0$ . However, since the correction factors are usually small, only the amplitude of the correction factor for  $Y/X_0$  has been calculated as an example,

$$\epsilon = \frac{(1 + j\lambda)X_0}{2x_s(A + j\lambda)(A + 2j\lambda)} \quad (36)$$

at vanishing frequency  $\omega = 0$  for the data of Illustration 1. In the results presented below, the variation amplitude  $|X_0|$  has been expressed in percentage of the feed concentration  $x_0$ .

$$\begin{aligned} A &= 1 + 4k\theta x_s = 1 + 4 \times \frac{1}{3} \\ &\times 58.10 \times 0.20 = 16.49 \end{aligned}$$

and

$$\epsilon_{\omega=0} = \frac{1.75}{200 \times 0.20 \times 16.49^2} |X_0| \%$$

$$\epsilon_{\omega=0} = 0.000161 |X_0| \%$$

A few values are given below

$ X_0 $	0%	10%	20%	40%
$\epsilon_{\omega=0}$	0.0000	0.0016	0.0032	0.0064

Thus for an input signal amplitude of 10% of the steady state value of the feed

concentration, the error in outlet amplitude  $Y$  at vanishing frequency, calculated from Equation (36), will be only 0.16%. The correction is therefore small.

#### COMMENT

The equations developed herein are mathematical consequences of the theories of continuously stirred tank reactors and of frequency-response analysis. Each theory can be verified separately by the proper means. Hence it is felt that an attempt to verify experimentally the response equations obtained would amount largely to a study of the approach to ideal performance of the entire system, including control valves, sensing elements, signal transmission lines, and degree of mixing and of the chemical reaction, etc., which might be chosen to make up the experimental system.

An alternate procedure, advantageous in selected cases, is to use frequency-response experiments, with the specific purpose of studying the transient behavior of the particular reaction, of the stirred reactor itself, of concentration sensing elements, or of other components used in the control-loop system. For such purposes the continuous-chemical-reactor-control theory presented in this paper, which allows for complex reactions and temperature effects, would prove useful in the analysis of the experimental results.

The relations describing the characteristics of several typical loop systems including the control elements will be presented in Part II. The use of analogue computers to solve the equations will also be considered as well as the response functions for reactor chains and for a tubular reactor.

## ACKNOWLEDGMENT

The authors are indebted to Professor Hans Kramers for several valuable suggestions made in the final preparation of these papers on control while he was Minnesota Mining and Manufacturing—Visiting Professor of Chemical Engineering at the University of Minnesota.

## NOTATION

$A$	= a chemical compound or its concentration (mole/liter)
$B$	= same
$c$	= specific heat of the reacting mixture, calories/g.
$C$	= concentration, mole/liter
$e$	= volumetric C.S.T.R. (continuously stirred tank reactor) to batch efficiency ratio
$F$	= flow rate, liters/hr.
$h$	= reactor heat input, °K./hr.
$H$	= reactor heat input, °K./hr.
$\Delta H_R$	= heat of reaction, calories/mole of $A$
$I$	= control quality
$j$	= pure imaginary, $\sqrt{-1}$
$k$	= reaction-rate constant, different units.

$K$	= proportionality constant for a proportional controller
$M$	= a matrix
$n$	= mole fraction, or number of reactors in a chain or reaction order
$Q$	= modified heat of reaction, (°K.) (mole)/liter of $A$
$R$	= general reaction rate
$t$	= time, hr.
$T$	= temperature, °K., or controller time constant
$V$	= reactor volume, liters or variation vector
$x$	= concentration of feed component, mole/liter
$X$	= variation in concentration of feed component, mole/liter
$y$	= concentration of product component, mole/liter
$Y$	= variation in concentration of product component, mole/liter
$Z$	= variation in reactor temperature, °K.
$\alpha, \beta, \gamma$	= stoichiometric coefficients
$\Delta$	= fractional control quality
$\theta$	= C.S.T.R. holding time, hr.
$\rho$	= density of reacting mixture, g./liter

$\tau$	= reaction time for a tubular reactor, hr.
$\omega$	= signal frequency, radians/hr.

## Subscripts

0, 1	= C.S.T.R. feed and product streams
$D$	= derivative controller
$I$	= integral controller
$n$	= reactor number in a chain
$P$	= proportional controller
$s$	= steady state

## LITERATURE CITED

1. Acton, F. S., and Leon Lapidus, *Ind. Eng. Chem.*, **47**, 706 (1955).
2. Bilous, Oleg, and E. L. Piret, *Chem. Eng. Progr.* (to be published).
3. Devyatov, B. N., and G. N. Bogashev, *Zhuy. Priklad. Khim.*, **24**, 807 (1951).
4. Eldridge, J. W., and E. L. Piret, *Chem. Eng. Progr.*, **46**, 290 (1950).
5. James, H. M., N. B. Nichols, and R. S. Phillips, "Theory of Servomechanisms," McGraw-Hill Book Company, Inc., New York (1947).
6. Kramers, Hans, and G. Alberda, *Chem. Eng. Sci.*, **2**, 173 (1953).
7. Mason, D. R., and E. L. Piret, *Ind. Eng. Chem.*, **42**, 817 (1950); **43**, 1210 (1951).

## II. Frequency-response Relations for Reactor Chains, Tubular Reactors, and Unit Reactor Control Loops

### REACTOR CHAINS

The results which were obtained in Part I for a single reactor can be used to calculate step by step the response of a chain of reactors. Interest in these calculations is twofold. First the safe operation of the whole chain may put upon a reactor in the chain more stringent control requirements than would individual operation, especially in the case of reactions highly sensitive to temperature. Second, these calculations can be used to determine simpler modes of control for the whole chain. In some cases, for instance, the feed flow is controlled by inlet sampling and the whole heating system by a sampling of the final product, the individual heat-control loop on each reactor thus being eliminated. The calculations are straightforward and the theory is easily developed with the introduction of matrices. It will be developed here on the basis of the example used previously, of a reaction involving components  $A$  and  $B$ , with a rate  $R(x, T)$ .

#### First Case: Variations in Concentration Only

Equations (17) and (18) of Part I are

used with the feed concentration variations  $X_0$  and  $Y_0$

$$(1 + \alpha\theta R_x' + j\omega\theta)X = X_0 \quad (1)$$

$$-\theta R_x'X + (1 + j\omega\theta)Y = Y_0 \quad (2)$$

These may be written in matrix form, the variation vector  $V_i$  representing the variations in the composition of the feed to reactor  $i + 1$ :

$$V_i = \begin{bmatrix} X_i \\ Y_i \end{bmatrix}$$

and the matrix  $M_i$  of the variation coefficients being introduced.

In matrix notation Equations (1) and (2) may be written

$$\begin{bmatrix} 1 + \alpha\theta R_x' + j\omega\theta, & 0 \\ -\theta R_x', & 1 + j\omega\theta \end{bmatrix} \begin{bmatrix} X \\ Y \end{bmatrix} = \begin{bmatrix} X_0 \\ Y_0 \end{bmatrix}$$

and for the reactor  $i$  in a chain

$$\begin{bmatrix} 1 + \alpha\theta R_{xi}' + j\omega\theta_i, & 0 \\ -\theta_i R_{xi}', & 1 + j\omega\theta_i \end{bmatrix} \begin{bmatrix} X_i \\ Y_i \end{bmatrix} = \begin{bmatrix} X_{i-1} \\ Y_{i-1} \end{bmatrix}$$

or

$$V_{i-1} = M_i V_i \quad (3)$$

with

$$M_i = \begin{bmatrix} 1 + \alpha\theta_i R_{xi}' + j\omega\theta_i, & 0 \\ -\theta_i R_{xi}', & 1 + j\omega\theta_i \end{bmatrix} \quad (4)$$

Therefore, the relation between product and feed variations in composition is

$$V_n = (M_1 M_2 \cdots M_i \cdots M_n)^{-1} V_0 \quad (5)$$

This formula gives the desired result, namely that the product composition varies as a function of feed-composition variations.

#### Illustration 4

The foregoing formula will be applied to the case of a first-order reaction



performed isothermally in a chain of reactors of equal size. The rate of the reaction is

$$R(x) = \frac{dB}{dt} = -\frac{dA}{dt} = kx$$

Therefore  $R_x'(x) = k$  and the quantity  $\theta R_x' = \theta k$  is constant for all reactors. All the matrices  $M_i$  are therefore the same, and Formula (5) may be written as  $V_n = M^{-n} V_0$  or

$$\begin{bmatrix} X_n \\ Y_n \end{bmatrix} = \begin{bmatrix} 1 + \theta k + j\omega\theta & 0 \\ -\theta k & 1 + j\omega\theta \end{bmatrix}^{-n} \begin{bmatrix} X_0 \\ Y_0 \end{bmatrix} \quad (6)$$

Matrix multiplication and division yields

$$= \begin{bmatrix} 1 + \theta k + j\omega\theta & 0 \\ -\theta k & 1 + j\omega\theta \end{bmatrix}^{-n} = \begin{bmatrix} \frac{1}{(1 + \theta k + j\omega\theta)^n} & 0 \\ \Omega & \frac{1}{(1 + j\omega\theta)^n} \end{bmatrix}$$

the term  $\Omega$  being

$$\Omega = \theta k \sum_{\lambda=0}^{n-1} (1 + \theta k + j\omega\theta)^{\lambda-n} \cdot (1 + j\omega\theta)^{-1-\lambda} \quad (7)$$

Developing matrix expression (6) shows the relation between variations in concentration of  $A$  in the feed and product streams to be

$$X_n = \frac{1}{(1 + \theta k + j\omega\theta)^n} X_0 \quad (8)$$

and the variation in the concentration of  $B$  in the product stream  $Y_n$ , caused by concentration variations  $X_0, Y_0$  in the feed stream,

$$Y_n = \Omega X_0 + \frac{1}{(1 + j\omega\theta)^n} Y_0$$

Usually  $Y_0 = 0$ , no product being present in the feed stream, and thus

$$Y_n = \Omega X_0,$$

or

$$Y_n = \theta k \sum_{\lambda=0}^{n-1} (1 + \theta k + j\omega\theta)^{\lambda-n} \cdot (1 + j\omega\theta)^{-1-\lambda} X_0 \quad (9)$$

or, summing the geometric series,

$$\frac{Y_n}{X_0} = (1 + j\omega\theta)^{-n} - (1 + j\omega\theta + \theta k)^{-n}$$

This is an interesting result, as it relates the variations in product composition to those in feed composition for a reactor chain. To illustrate this relationship better, a numerical example is presented. A chain of  $n$  equal-sized reactors operates on the first-order reaction

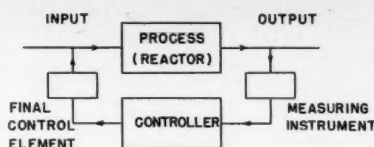


Fig. 4. Block diagram of a control system.

with a 95% conversion of compound  $A$ . The inlet and outlet concentrations are compound  $A$   $x_0 = 1.00$  mole/liter,  $x_n = 0.05$  mole/liter product  $B$   $y_0 = 0.00$  mole/liter,  $y_n = 0.95$  mole/liter

The operation is isothermal, with a rate constant

$$k = 19.0 \text{ hr.}^{-1}$$

The holding time,  $\theta$ , for a reactor of the chain is found from a mass balance over the system, given by

$$\theta = \frac{1}{k} \left[ \left( \frac{x_0}{x_n} \right)^{1/n} - 1 \right] \quad (10)$$

The maximum amplitude ratio is attained at vanishing frequency. Its value, calculated from Formula (9) for  $\omega = 0$ , is

$$\begin{aligned} \left| \frac{Y_n}{X_0} \right|_{\max} &= 1 - \frac{1}{(1 + \theta k)^n} \\ &= 1 - \frac{x_n}{x_0} = 0.95 \end{aligned}$$

It is therefore a constant, independent of the number of reactors.

While vanishing frequency results are the easiest to calculate, more information about system behavior may be derived from the values of the phase angle and amplitude ratio of the concentration variations at a frequency physically related to system properties, that is, for instance, such as  $\omega\theta = 1$ . Such results, calculated by means of Equation (9), are presented in the accompanying table.

POLAR-PLOT DATA FOR A REACTOR CHAIN, FOR  $\omega\theta = 1$

Number of reactors, $n$	Unit holding time, $\theta$	Total holding time, $n\theta$	Amplitude ratio $ Y_n/X_0 $ for $\omega\theta = 1$	Phase angle for $\omega\theta = 1$ , deg.
1	1.000 hours	1.000 hours	0.671	-48
2	0.183	0.366	0.763	-56
3	0.090	0.271	0.813	-57
5	0.043	0.216	0.861	-58
10	0.018	0.184	0.904	-58
$\infty$	0.000	0.158	0.950	-57.3

These values give an indication of the transformation of the shape of the Nyquist plot with reactor number. From a nearly circular plot touching the imaginary axis at the origin for a single reactor, the plots evolve toward a circle centered at the origin for the limiting case of the tubular reactor.

Formula (5) gives the relation between

feed- and product-composition variations for a chain of  $n$  stirred-flow reactors. It may be interesting to examine what happens when the number of reactors increases indefinitely, the total holding time remaining constant. This limiting case is represented by a tubular reactor with uniform conditions in a cross section.

#### Limiting Case of the Tubular Reactor

All holding times are assumed equal and  $\tau = n\theta$  is the tubular-reactor holding time. Therefore

$$\theta_i = \frac{\tau}{n} = \Delta\tau_i$$

where the increment  $\Delta\tau_i$  is thus defined. Then Expression (4) of the matrix  $M_i$  may be written

$$M_i = \begin{bmatrix} 1 & 0 \\ 0 & 1 \end{bmatrix} + \begin{bmatrix} \alpha R_{xi}' + j\omega & 0 \\ -R_{xi}', & j\omega \end{bmatrix} \Delta\tau_i$$

Neglecting second-order terms in  $\Delta\tau_i$  gives

$$M_i = \exp \left\{ \begin{bmatrix} \alpha R_{xi}' + j\omega & 0 \\ -R_{xi}', & j\omega \end{bmatrix} \Delta\tau_i \right\}$$

Therefore

$$V_0 = M_1 M_2 \cdots M_i \cdots M_n V_n$$

$$V_0 = \exp \left\{ \sum_{i=1}^{n-1} \begin{bmatrix} \alpha R_{xi}' + j\omega & 0 \\ -R_{xi}', & j\omega \end{bmatrix} \Delta\tau_i \right\} V_n$$

Passing to the limit gives

$$V_n = \exp \left\{ - \begin{bmatrix} \alpha \int_0^\tau R_x' dt + j\omega\tau & 0 \\ - \int_0^\tau R_x' dt, & j\omega\tau \end{bmatrix} \right\} V_0 \quad (11)$$

The exponential form of the transfer functions characterizing the behavior of

systems with dead time may be recognized. The matrices

$$\begin{bmatrix} j\omega\tau & 0 \\ 0 & j\omega\tau \end{bmatrix} \quad \text{and} \quad \begin{bmatrix} \alpha \int_0^\tau R_x' dt & 0 \\ - \int_0^\tau R_x' dt & 0 \end{bmatrix}$$

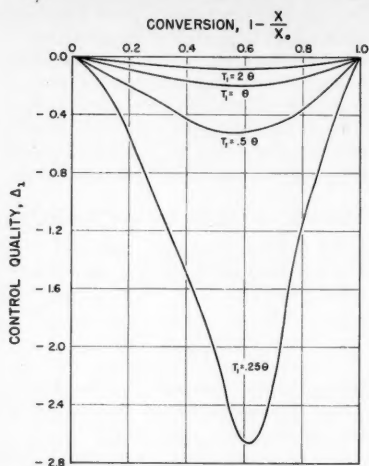


Fig. 5. Fractional control quality against conversion for integral control of a first-order reaction in a C.S.T.R.

commute; therefore Expression (11) may be written

$$V_n = \exp \left\{ - \begin{bmatrix} j\omega\tau & 0 \\ 0 & j\omega\tau \end{bmatrix} \right\} \cdot \exp \left\{ - \begin{bmatrix} \alpha \int_0^\tau R_x' dt & 0 \\ - \int_0^\tau R_x' dt & 0 \end{bmatrix} \right\} V_0$$

or

$$V_n = \exp \{-j\omega\tau\} \begin{bmatrix} \exp \left\{ -\alpha \int_0^\tau R_x' dt \right\} & 0 \\ 1 - \exp \left\{ -\int_0^\tau R_x' dt \right\} & 1 \end{bmatrix} V_0 \quad (12)$$

Developing this matrix expression one finds the formula for a tubular reactor (with any order reaction) which corresponds to Expression (9) for a reactor chain:

$$Y_n = \left( 1 - \exp \left\{ -\int_0^\tau R_x' dt \right\} \right) \cdot \exp \{-j\omega\tau\} X_0 \quad (13)$$

The Nyquist diagram, which represents  $Y_n/X_0$ , is a circle centered at the origin of the complex plane.

#### Second Case: Variation in Concentration and Temperature with a Steady Heat Input

The treatment for this case is similar to that above, the equations to be considered being

$$(1 + \alpha\theta R_x' + j\omega\theta)X + \alpha\theta R_T'Z = X_0 \\ -\theta R_x'X + (1 + j\omega\theta)Y \\ -\theta R_T'Z = Y_0$$

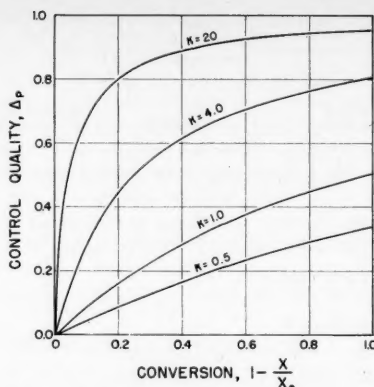


Fig. 6. Fractional control quality against conversion for proportional control of a first-order reaction in a C.S.T.R.

$$-\alpha Q\theta R_x'X + (1 + j\omega\theta \\ -\alpha Q\theta R_T')Z = Z_0$$

obtained from the basic expressions (17), (18), (19) of Part I.

The matrix  $M_i$  similar to (4) is now

$$M_i = \begin{bmatrix} 1 + \alpha\theta_i R_{xi}' + j\omega\theta_i & 0 & \alpha\theta_i R_{Ti}' \\ -\theta_i R_{xi}' & 1 + j\omega\theta_i & -\theta_i R_{Ti}' \\ -\alpha Q\theta_i R_{xi}' & 0 & 1 - \alpha Q\theta_i R_{Ti}' + j\omega\theta_i \end{bmatrix} \quad (14)$$

and the relation between feed and product variations for a chain of  $n$  reactors is as before

$$V_n = (M_1 M_2 \cdots M_i \cdots M_n)^{-1} V_0 \quad (15)$$

where the vectors  $V_i$  are defined now as

$$V_i = [X_i, Y_i, Z_i]$$

Numerical calculations on Formula (15) are best carried out step by step. The determinant of Matrix (14) is

$$D_i \equiv (1 + j\omega\theta_i)^2 [1 + \alpha\theta_i (R_{xi}' - QR_{Ti}') + j\omega\theta_i]$$

The factor

$$1 + \alpha\theta_i (R_{xi}' - QR_{Ti}') + j\omega\theta_i$$

is recognized as one that appeared in Expression (24) of Part I.

The stability of the reactor chain is obtained when all units of the chain are stable. Following the discussion in Part I the condition on the holding times

$$\theta_i < \frac{1}{(QR_{Ti}' - R_{xi}')\alpha}$$

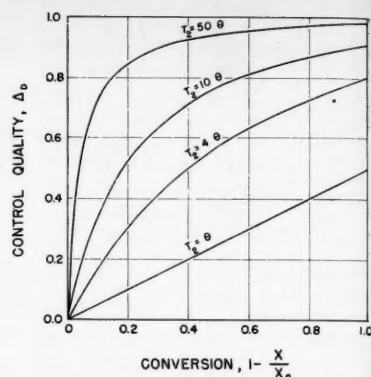


Fig. 7. Fractional control quality against conversion for derivative control of a first-order reaction in a C.S.T.R.

is obtained, which must be satisfied in the case of a highly exothermic reaction ( $Q > R_{xi}'/R_{Ti}'$ ) in order to have stable operation. This is again an example of the restrictions which control requirements may impose on reactor design.

#### REACTOR CONTROL

In the preceding page only the calculation of the frequency response of continuously stirred tank reactors has been considered. This section will combine for illustrative purposes, the frequency-response functions thus obtained with different controller-response functions to find the quality of the control circuit formed by reactor and controller. The control system considered may be represented by Figure 4.

A variable in the reactor outlet stream, for instance product concentration, is measured and is compared with the desired value in the controller which sends out a signal acting on the controlled variable in the reactor inlet stream, for instance feed concentration, through a final control element. Detailed information about such diagrams and control theory in general may be found in references 1 and 2.

A negligible lag is assumed in measurement and in the final control element, in order to isolate the effect of controller-response characteristics on the system. For present purposes the three usual idealized types of controllers are examined (1). Actual controllers often approach combinations of these and can be treated in the same manner; such a case will be illustrated in the analogue example.



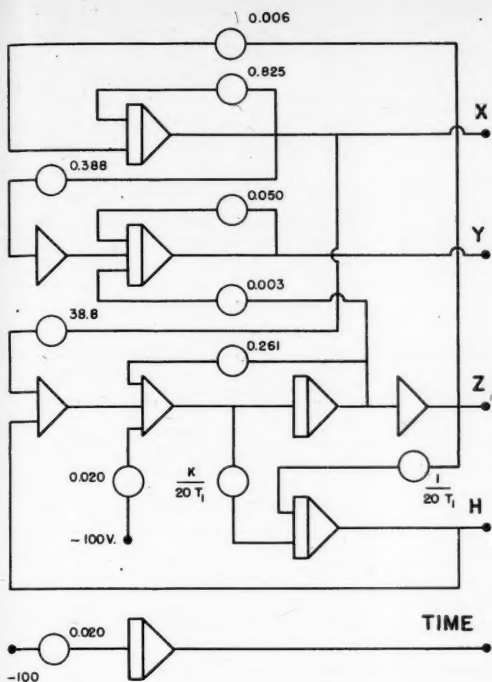


Fig. 8. R.E.A.C. circuit for temperature control in a C.S.T.R. Data of illustration 3.

$G_n(j\omega)$  is the frequency-response function for the reactor chain without control.

For the controlled system (Figure 4) the input to the reactor is equal to the input to the system  $X_0$  minus the output of the final controller. The input to the controller is the output of the reactor  $Y_n$ . Hence if  $G(j\omega)$  represents the frequency-response function for the controller, the output of the controller is  $G(j\omega)Y_n$ ; the input to the reactor is  $X_0 - G(j\omega)Y_n$ ; and the output of the reactor is  $Y_n = G_n(j\omega)[X_0 - G(j\omega)Y_n]$ . Solving this for  $Y_n$  yields

$$Y_n = \frac{G_n(j\omega)}{1 + G(j\omega)G_n(j\omega)} X_0 \quad (19)$$

The frequency-response function for the system with control is therefore

$$Y(j\omega) = \frac{Y_n}{X_0} = \frac{G_n(j\omega)}{1 + G(j\omega)G_n(j\omega)} \quad (20)$$

Control quality may then be determined from formula (18), where  $Y(j\omega)$  is replaced by its expression (20).

The case of a single reactor will be examined in more detail. The expression of control quality for a single reactor with different controllers or no control are, from the foregoing development,

Controller	Frequency response $G(j\omega)$
Integral	$-P/E = 1/j\omega T_1$
Proportional	$-P/E = K$
Derivative	$-P/E = j\omega T_2$

In the preceding expressions of controller response to a cyclic disturbance of frequency  $\omega$ ,  $E$  designates the error signal and  $P$  the controller output. The quantities  $T_1$ ,  $K$ ,  $T_2$  are constants characteristic of controller operation.

Control quality may be expressed by the quantity

$$I = \int_0^\infty |W(t)|^2 dt \quad (16)$$

where  $W(t)$  is the system response to a unit impulse applied to system input at time zero. The choice of this criterion takes into consideration the importance of the deviation amplitude caused by the perturbation and also the length in time of the deviation. This expression will be used in the study of control quality.

The integral  $I$  may be evaluated in terms of the frequency-response function of the controlled system  $Y(j\omega)$ . From reference 2

$$W(t) = \frac{1}{2\pi} \int_{-\infty}^{+\infty} d\omega e^{j\omega t} Y(j\omega) \quad (17)$$

Therefore

$$I = \int_0^\infty |W(t)|^2 dt = \frac{1}{\pi} \int_0^\infty Y(j\omega) Y(-j\omega) d\omega \quad (18)$$

integral control

$$I_I = \frac{1}{\pi} \int_0^\infty \frac{\theta^2 k^2 \omega^2 T_1^2 d\omega}{k^2 \theta^2 - 2\omega^2 k T_1 \theta^2 (2 + \theta k) + \omega^2 T_1^2 (1 + \omega^2 \theta^2) [(1 + \theta k)^2 + \omega^2 \theta^2]}$$

proportional control

$$I_P = \frac{1}{\pi} \int_0^\infty \frac{\theta^2 k^2 d\omega}{K^2 \theta^2 k^2 + 2K(1 + \theta k - \omega^2 \theta^2) \theta k + (1 + \omega^2 \theta^2) [(1 + \theta k)^2 + \omega^2 \theta^2]}$$

derivative control

$$I_D = \frac{1}{\pi} \int_0^\infty \frac{\theta^2 k^2 d\omega}{k^2 \theta^2 \omega^2 T_2^2 + 2\omega^2 \theta^2 T_2 (2 + \theta k) k + (1 + \omega^2 \theta^2) [(1 + \theta k)^2 + \omega^2 \theta^2]}$$

These expressions are valid only for stable systems. The value of  $I$  would be infinite for an unstable system, as in this case response  $W(t)$  is undamped or ever increasing in amplitude.

#### Example

A control loop will be considered on the basis of measurement of product concentration in the outlet stream and control of feed concentration in the inlet stream. Reactor operation is assumed to be isothermal and data of Illustration 4 are used. Thus the frequency-response function for a chain of  $n$  equal-sized reactors is given by Expression (9):

$$G_n(j\omega) = \frac{Y_n}{X_0} = \theta k \sum_{\lambda=0}^{\lambda=n-1} (1 + \theta k + j\omega \theta)^{\lambda-n} (1 + j\omega \theta)^{-1-\lambda}$$

When there is no control, that is to say,

$$\frac{1}{T_1} = K = T_2 = 0$$

these integrals reduce to

$$I_0 = \frac{1}{\pi} \int_0^\infty \frac{\theta^2 k^2 d\omega}{(1 + \omega^2 \theta^2) [(1 + \theta k)^2 + \omega^2 \theta^2]} = \frac{\theta k^2}{2(1 + \theta k)(2 + \theta k)}$$

The integrals expressed above are calculated by integration in the complex plane or use of tables in the appendix of reference 2. The results have been expressed here in terms of the system with no control in fractional form:

$$\Delta = 1 - \frac{I}{I_0}$$

which better shows the gain in control quality due to the controller. The value of  $\Delta$  when the control loop is broken is zero and reaches unity for perfect control. The expressions for the respective fractional control qualities are for integral control

$$\Delta_I = \frac{k\theta^2}{k\theta^2 - (1 + \theta k)(2 + \theta k)T_1},$$

for  $T_1 > \frac{k\theta^2}{(2 + \theta k)(1 + \theta k)}$

for proportional control

$$\Delta_P = \frac{K\theta k}{1 + \theta K + K\theta k}$$

for derivative control

$$\Delta_D = \frac{T_2 k}{2 + \theta k + T_2 k}$$

Fractional control quality has been represented for the different modes of control  $\Delta_I$ ,  $\Delta_P$ ,  $\Delta_D$  against conversion in Figures 5, 6, and 7. Curves are given for different values of the characteristic control parameters  $T_1$ ,  $K$ , and  $T_2$ . Conversion in this case is

$$1 - \frac{x}{x_0} = \frac{\theta k}{1 + \theta k}$$

where  $x_0$ ,  $x$  are the concentrations of reactant A in the feed and the product.

The plots of Figures 5, 6, and 7 show an increase in control quality by the same instrument when the conversion decreases, which is evident *a priori*, since at low conversion a disturbance on the feed will have only a small effect on outlet product concentration. The plots are characteristic of the three simplified modes of control examined. Idealized components have been used in this loop analysis and the results in practice must be tempered with a knowledge of the performance of the components and system actually available.

#### ANALOGUE SIMULATION OF CONTROLLED SYSTEMS

The equations describing the operation of the three types of controllers which have been considered in this study are

Integral control

$$E = -T_1 \frac{dP}{dt}$$

Proportional control

$$E = -\frac{1}{K} P$$

Differential control

$$P = -T_2 \frac{dE}{dt}$$

These equations, written for an appropriate control loop, may be associated with the linearized equations describing reactor behavior: [Equations (12), (13), (14) of Part I].

$$\theta \frac{dX}{dt} + (1 + \alpha\theta R_x')X + \alpha\theta R_T'Z = X_0 \quad (21)$$

$$\theta \frac{dY}{dt} - \theta R_x'X + Y - \theta R_T'Z = Y_0 \quad (22)$$

$$\theta \frac{dZ}{dt} - \alpha Q\theta R_x'X + (1 - \alpha Q\theta R_T')Z = \theta\Delta H + Z_0 \quad (23)$$

The system thus obtained may be solved to obtain the response of the controlled

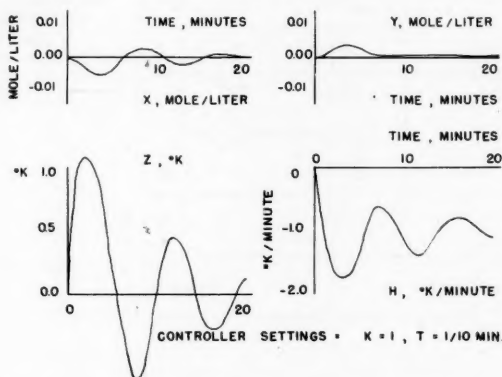


Fig. 9. Example of C.S.T.R. temperature control (underdamped case).

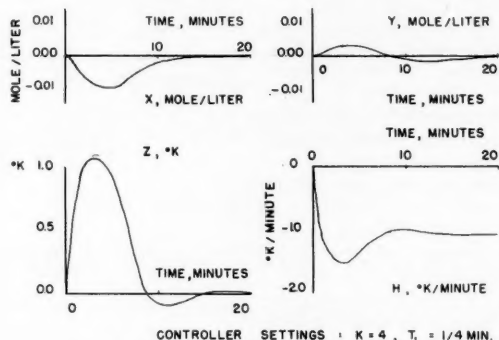


Fig. 10. Example of C.S.T.R. temperature control (correct controller settings).

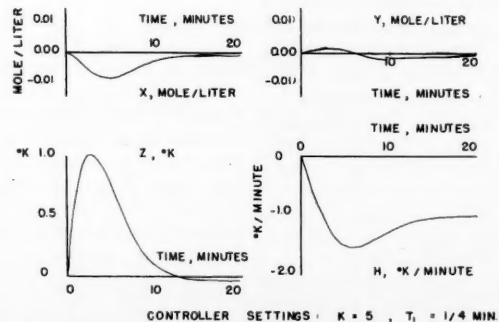


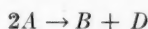
Fig. 11. Example of C.S.T.R. temperature control (overdamped case).

reactor to a given disturbance. The analytical solution will, however, in many cases be cumbersome and in practice, especially when more complex performance functions are needed, the use of an analogue computer is of great advantage. An example will be solved with the analogue technique.

Considered here is the case of a temperature-control loop with a controller combining the proportional and integral control modes. A constant feed composition is assumed, that is to say  $X_0 = Y_0 = 0$ , and a disturbance caused by a change in feed temperature,  $Z_0$ . The equations which describe this system are (21), (22), (23) and the controller equation for the temperature-control loop becomes

$$\frac{dH}{dt} = -K \frac{dZ}{dt} - \frac{1}{T_1} Z \quad (24)$$

With the values of Illustration 2 for a second-order exothermic reaction



with  $\Delta H_R = -50,000$  cal./mole of  $A$  these equations take the following form:

$$0.33 \frac{dX}{dt} + 16.50X + 0.1245Z = 0$$

$$0.33 \frac{dY}{dt} - 7.750X + Y - 0.0622Z = 0$$

$$0.33 \frac{dZ}{dt} - 775.X - 5.224Z = 0.33\Delta H + Z_0$$

$$0.33 \frac{dH}{dt} = -0.33K \frac{dZ}{dt} - \frac{0.33}{T_1} Z$$

The analogue circuit which represents these equations with a time scale changed from hours to minutes is given as an illustration on Figure 8. The symbols of the circuit diagram are standard and may be found in reference 3.

This circuit was used to determine the response of the controlled reactor to a change in feed temperature

$$Z_0 = 1^\circ\text{C.}$$

for three different settings of the controller characteristics  $K$  and  $T_1$ . The results are given on Figures 9, 10, and 11. Figure 9 represents a case with low damping ( $K = 1$ ,  $T_1 = 1/10$  min.). The system oscillates around the steady state. Figure 10 represents a more damped case ( $K = 4$ ,  $T_1 = 1/4$  min.), which would be acceptable in practice. The system represented in Figure 11 is overdamped ( $K = 5$ ,  $T_1 = 1/4$  min.) but may still be acceptable in practice. Such examples could be multiplied for various combinations of controller types. Discussion of them is easy, and they will not be developed further here.

## CYCLING IN SYSTEMS WITH DEAD TIME

If the number of stirred flow reactors in a chain is increased indefinitely, the over-all holding time remaining constant, at the limit the case of a tubular reactor is obtained. The frequency-response functions for the isothermal tubular reactor without volume change have been obtained in Expression (12). For the case of a first-order reaction the expression of the frequency-response function relating product-concentration variations  $Y_n$  to feed concentration variations  $X_0$  has been found:

$$Y_n = (1 - e^{-k\tau})e^{-j\omega\tau} X_0$$

The presence of the imaginary exponential in the expression of the frequency-response function is characteristic of systems with dead time. Thus a measuring instrument placed at the reactor outlet will perceive feed perturbations only a time after they happen and any corrective action will be delayed by that much. This dead time in the reactor system increases with the number of reactors in the chain and approaches a maximum time in a tubular reactor, and so in the latter design control may be more difficult than in a continuously stirred tank reactor (C.S.T.R.). Also control by stages may more readily be applied to the selected elements of a chain.

Dead time may easily lead to cycling of the controlled system if the control is improperly designed. Only an example of such a case will be given, for proportional control applied to a tubular reactor by measurement of product concentration at the outlet and control of inlet-feed concentration.

If  $A(t)$  designates the disturbance on the feed concentration at the reactor inlet, the disturbance on product concentration at the outlet is  $(1 - e^{-k\tau})A(t - \tau)$  and the equation of the proportional-control loop is

$$A(t) + K(1 - e^{-k\tau})A(t - \tau) = 0 \quad (25)$$

where  $K$  is the characteristic constant of the proportional controller. Equation (25) is of the difference type, and methods of solution are well known. Thus introducing a solution

$$A(t) = e^{st}$$

into Equation (25) results in a characteristic equation which gives the values of  $s$  for which  $e^{st}$  is a solution of (25):

$$1 + K(1 - e^{-k\tau})e^{-s\tau} = 0$$

It is found that

$$s = \frac{1}{\tau} [\ln K(1 - e^{-k\tau}) + j\pi(1 + 2\lambda)]$$

where  $\lambda$  may take any integer value. The system is stable if the exponential  $e^{st}$  is damped:

$$\frac{1}{\tau} \ln K(1 - e^{-k\tau}) < 0$$

or

$$K(1 - e^{-k\tau}) < 1$$

Thus a limitation exists on the values of the proportional factor  $K$  which may be used. If controller action is too powerful (high  $K$ ), cycling may develop.

## COMMENT

It should be realized that in the practice of automatic control the results of frequency-response analyses can today be used to advantage principally for guidance rather than for the exact prediction of the performance to be expected of a practical control system. In the first place the disturbances occurring in an industrial operation will not usually be regular or periodic, although of course the typically random disturbance will excite all frequencies. Furthermore, the differences found between theory and practice are often the result of deviations from the simplified characteristics which are usually assumed for the sensing and the control elements. Furthermore largely indeterminate lags often occur in industrial installations. Nevertheless the equations obtained as a result of the application of frequency response theory offer real advantages in simplicity of treatment and clarity of exposition, have proved extremely helpful in understanding the control process itself, and have guided the engineer to practical solutions to automatic-control problems. As more precise characterizations of modern commercial instruments and of lag systems become available, better predictions are to be expected.

Numerical examples have been worked out in this paper and especially in Part I in order to demonstrate clearly the method of application of frequency-response analysis to continuous-flow reactions. These should also serve to clarify the characteristics of the chemical reactor control process itself. It was shown for example that such important factors as temperature-sensitive rates of reaction can be readily analyzed by these methods.

## NOTATION

See page 256.

## LITERATURE CITED

1. Eckman, D. P., "Principles of Industrial Control," John Wiley and Sons, Inc., New York (1948).
2. James, H. M., N. B. Nichols, and R. S. Phillips, "Theory of Servomechanisms," McGraw-Hill Book Company, Inc., New York (1947).
3. Korn, G. A., and T. M. Korn, "Electronic Analog Computers," McGraw-Hill Book Company, Inc., New York (1952).

# Volumetric and Phase Behavior in the Hydrogen-*n*-hexane System

W. B. NICHOLS, H. H. REAMER, and B. H. SAGE

California Institute of Technology, Pasadena, California

In spite of the importance of hydrogenation processing operations in the refining of petroleum there are only limited experimental volumetric and phase equilibrium data concerning mixtures of hydrocarbons and hydrogen. An investigation of the volumetric and phase behavior of the hydrogen-*n*-hexane system was therefore undertaken.

The experimental study involved measurements of the specific volume of four mixtures of hydrogen and *n*-hexane at eight temperatures between 40° and 460°F. for pressures up to 10,000 lb./sq. in. In addition, the composition of the gas phase in heterogeneous mixtures was determined at six temperatures within the interval mentioned above for pressures as high as 10,000 lb./sq. in.

Little about this system was found to be qualitatively unusual except that the critical pressure exceeded 10,000 lb./sq. in. at all temperatures below 340°F. As would be expected, the dew-point gas was rather lean in *n*-hexane for temperatures below 220°F. and at pressures above 100 times the vapor pressure of *n*-hexane throughout the pressure range covered by this study.

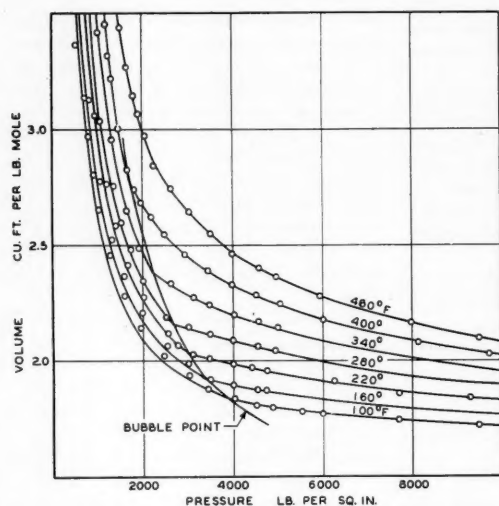


Fig. 1. Sample experimental volumetric measurements for mixture containing 0.1895 mole fraction hydrogen.

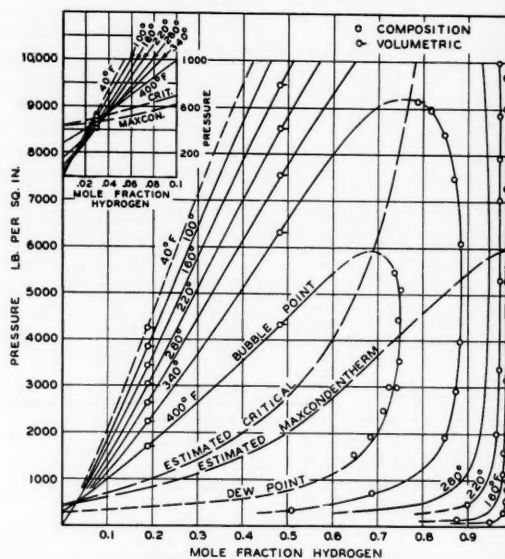


Fig. 2. Composition of coexisting phases in hydrogen-*n*-hexane system.

Only results from limited investigations of the volumetric and phase behavior of binary systems involving hydrogen and hydrocarbons at high pressures are available. The phase behavior of the hydrogen-propane system has been investigated (2) and the solubility of hydrogen has been determined in a number of hydrocarbons (4, 5), but these limited data do not permit a general correlation of the effect of the characteristics of the hydrocarbon components upon the phase behavior of such systems or of the partial volume (?) of hydrogen in hydrocarbon liquids.

TABLE 1. MOLAL VOLUMES FOR MIXTURES OF HYDROGEN AND *n*-HEXANE

Pressure lb./sq. in.	40° F.	100° F.	160° F.	220° F.	280° F.	340° F.	400° F.	460° F.
Mole fraction hydrogen = 0.1895								
Dew point	(9)*	(17)	(40)	(77)	(127)	(220)	(425)	
Bubble Point	(4,240)*	(3,840)	(3,430)	(3,030)	(2,640)	(2,225)	(1,705)	
	1.770	1.844	1.924	2.030	2.166	2.381	2.792	
200	6.78†							
400	4.09	4.47	4.87	5.51	6.34			
600	3.25	3.40	3.65	4.05	4.59	5.30		
800	2.758	2.920	3.10	3.40	3.72	4.20	4.96	
1,000	2.500	2.641	2.782	3.02	3.19	3.53	4.00	5.01
1,250	2.304	2.406	2.537	2.681	2.840	3.07	3.36	3.98
1,500	2.170	2.275	2.367	2.487	2.617	2.784	2.985	3.48



TABLE 1. (Cont.)

Pressure lb./sq. in.	40° F.	100° F.	160° F.	220° F.	280° F.	340° F.	400° F.	460° F.
1,750	2.080	2.170	2.260	2.363	2.458	2.607	2.778	3.20
2,000	2.010	2.092	2.168	2.256	2.352	2.473	2.679	3.01
2,250	1.960	2.034	2.109	2.185	2.267	2.382	2.605	2.879
2,500	1.919	1.985	2.052	2.128	2.200	2.347	2.542	2.790
2,750	1.885	1.946	2.007	2.076	2.163	2.319	2.493	2.714
3,000	1.861	1.918	1.973	2.037	2.148	2.289	2.451	2.649
3,500	1.820	1.870	1.917	2.008	2.114	2.240	2.384	2.548
4,000	1.788	1.833	1.893	1.984	2.084	2.200	2.330	2.472
4,500	1.762	1.808	1.877	1.966	2.063	2.166	2.283	2.416
5,000	1.756	1.791	1.859	1.946	2.039	2.135	2.244	2.365
6,000	1.737	1.770	1.833	1.909	1.992	2.082	2.174	2.275
7,000	1.722	1.756	1.812	1.886	1.954	2.039	2.124	2.214
8,000	1.706	1.742	1.796	1.861	1.931	2.006	2.084	2.162
9,000	1.693	1.726	1.778	1.844	1.910	1.980	2.049	2.117
10,000	1.678	1.711	1.764	1.828	1.892	1.954	2.021	2.077

Mole fraction hydrogen = 0.4833

Dew point	(34)*	(40)	(85)	(140)	(221)	(336)	(738)
Bubble point			(9,500)*	(8,575)	(7,560)	(6,320)	(4,330)
			1.424	1.497	1.597	1.756	2.193
200							
400							
600							
800	4.28†	4.70					
1,000	3.63	3.97	4.23	4.86			
1,250	3.11	3.36	3.65	3.98	4.34	4.93	
1,500	2.768	2.997	3.22	3.48	3.78	4.21	4.80
1,750	2.522	2.724	2.913	3.13	3.37	3.73	4.15
2,000	2.341	2.517	2.678	2.863	3.08	3.36	3.74
2,250	2.202	2.361	2.506	2.670	2.857	3.09	3.39
2,500	2.091	2.226	2.361	2.513	2.678	2.879	3.12
2,750	1.996	2.127	2.250	2.384	2.531	2.707	2.912
3,000	1.923	2.041	2.150	2.278	2.411	2.562	2.740
3,500	1.800	1.901	2.004	2.108	2.222	2.343	2.471
4,000	1.716	1.800	1.898	1.981	2.077	2.181	2.286
4,500	1.641	1.733	1.804	1.889	1.963	2.052	2.152
5,000	1.585	1.662	1.738	1.806	1.874	1.948	2.050
6,000	1.506	1.565	1.627	1.683	1.738	1.796	1.903
7,000	1.443	1.497	1.549	1.595	1.642	1.702	1.801
8,000	1.397	1.442	1.486	1.528	1.567	1.638	1.724
9,000	1.348	1.399	1.437	1.475	1.519	1.590	1.665
10,000	1.338	1.367	1.396	1.433	1.485	1.558	1.619

Mole fraction hydrogen = 0.7878

Dew point	(61)*	(79)	(127)	(292)	(494)
Bubble point					
200					
400					
600					
800					
1,000					
1,250	3.95†	4.35			
1,500	3.38	3.74	4.09	4.49	
1,750	2.977	3.28	3.60	3.92	4.30
2,000	2.681	2.949	3.21	3.50	3.83
2,250	2.448	2.683	2.920	3.18	3.46
2,500	2.266	2.478	2.686	2.917	3.17
2,750	2.109	2.309	2.504	2.702	2.926
3,000	1.986	2.165	2.335	2.526	2.727
3,500	1.787	1.926	2.087	2.248	2.413
4,000	1.636	1.763	1.898	2.037	2.182
4,500	1.520	1.638	1.757	1.890	1.999
5,000	1.427	1.528	1.640	1.749	1.860
6,000	1.288	1.369	1.470	1.552	1.642
7,000	1.184	1.258	1.336	1.409	1.489
8,000	1.109	1.177	1.240	1.308	1.375
9,000	1.051	1.121	1.167	1.224	1.280
10,000	1.018	1.065	1.118	1.158	1.212

\*Values in parentheses represent pressures expressed in pounds per square inch absolute.

†Volume expressed in cubic feet per pound mole.

In order to extend the knowledge of the volumetric and phase behavior of hydrogen-hydrocarbon systems, an experimental study of the hydrogen-*n*-hexane system was carried out at temperatures between 40° and 460°F. and for pressures up to 10,000 lb./sq. in. The investigation included a direct evaluation of the composition of the gas phase in heterogeneous mixtures of these components, as well as measurements of the specific volume of four mixtures as a function of pressure and temperature.

The volumetric behavior of hydrogen has been investigated in detail, but it is beyond the scope of the present discussion to present a review of these data. For present purposes the measurements of Wiebe and Gaddy (15) and Deming and Shupe (3) were employed. The latter data appeared to describe the volumetric behavior of hydrogen with an uncertainty of less than 0.2%. A recent study of the volumetric behavior of *n*-hexane (14) is in good agreement with the earlier measurements of Kelso and Felsing (6). Volumetric behavior of *n*-hexane in the liquid phase is known throughout the range of pressures and temperatures of interest with an uncertainty of approximately 0.25%. There is no experimental information available at higher than atmospheric pressure to describe the volumetric behavior of *n*-hexane in the gas phase, except for states at temperatures above 482°F., where some measurements are reported by Kelso and Felsing (6).

The foregoing experimental information concerning the volumetric behavior of hydrogen and *n*-hexane suffices for present needs and aids in the smoothing of the present data with respect to composition. The behavior of hydrogen and *n*-hexane is not reported here.

#### METHODS AND APPARATUS

This investigation will determine specific volume as a function of pressure and temperature for a series of mixtures of hydrogen and *n*-hexane of chosen compositions. In principle the experimental methods involved the confinement of a sample mixture of known composition and weight in a stainless steel pressure vessel over mercury.

Effective volume of this chamber was varied by the introduction or withdrawal of mercury. Mechanical agitation was provided to hasten the attainment of physical equilibrium within and between the phases. The details of the experimental apparatus used for this purpose have been described (13). Pressures were measured by means of a balance utilizing a piston-cylinder combination (13), which was calibrated against the vapor pressure of carbon dioxide (1). Recent experience with such an instrument (11) indicates that the pressures within the apparatus relative to the vapor pressure of carbon

dioxide at the ice point were known within 0.2 lb./sq. in. or 0.10%, whichever was the larger measure of uncertainty.

The stainless steel vessel containing the hydrocarbons under investigation was immersed in an agitated liquid bath, the temperature of which was controlled with a resistance thermometer through a modulating electronic circuit (10). This temperature was related to the international platinum scale by means of a strain-free platinum resistance thermometer of the coiled-filament type (8), which was compared with the indications of a similar instrument that had been calibrated by the National Bureau of Standards. The temperature of the contents of the pressure vessel was known within 0.02°F. of the international platinum scale throughout the temperature interval between 40° and 460°F.

The *n*-hexane was introduced by weighing-bomb techniques (13) and the hydrogen by volumetric methods involving a measured change in the volume in an auxiliary reservoir at constant pressure under isothermal conditions.

The weight of the mixtures was known within 0.05% for all four compositions investigated. Experience with the equipment indicates that the relative probable error in specific volume at pressures below 5,000 lb./sq. in. was approximately 0.25%. This probable error increased gradually at the higher pressure to a relative value of 0.5% at 10,000 lb./sq. in. The larger uncertainties at the higher pressures resulted from difficulties in obtaining reproducible calibrations of the volumetric equipment under these conditions.

Some difficulty was experienced from thermal rearrangement of the *n*-hexane at temperatures of 400° and 460°F., indicated by comparison of the equilibrium volumetric behavior near the bubble point for samples at 100°F. which had and had not been subjected to investigation at 400° and 460°F. An increase in bubble-point pressure of as much as 10 lb./sq. in. was experienced in the case of the mixtures rich in *n*-hexane. It therefore should be emphasized that in the vicinity of bubble point, measurements at 400° and 460°F. are subject to an additional uncertainty beyond that just described. However, this thermal rearrangement did not significantly modify the volumetric behavior in the condensed liquid or in the heterogeneous region at specific volumes several times the volume of bubble point. Some difficulty was experienced in obtaining molal volumes in the heterogeneous region with as small an uncertainty as would be estimated from the accuracy of the evaluation of the individual variables. This uncertainty apparently resulted from difficulties in attaining equilibrium between the phases in the heterogeneous region. For this reason it is probable that the molal volumes of the heterogeneous mixtures

may involve uncertainties as large as 1%. These uncertainties are probably largest and most frequently encountered at the lower temperatures.

In order to establish the composition of the gas phase of heterogeneous mixtures of hydrogen and *n*-hexane, it was found desirable to determine the mole fraction of each of the components by direct measurement. It was not found

desirable to utilize volumetric measurements at constant composition to obtain these data. The small change in composition which was experienced at dew point with large changes in pressure throughout the greater part of the temperature interval covered by this investigation renders measurements at constant composition ineffective.

As a result of the marked difference in

TABLE 2. PROPERTIES OF THE COEXISTING GAS AND LIQUID PHASES IN THE HYDROGEN-*n*-HEXANE SYSTEM

Pressure, lb./sq. in.	Mole fraction hydrogen	Volume, cu. ft./lb. mole Dew point	Mole fraction hydrogen	Volume, cu. ft./lb. mole Bubble point	Equilibrium ratio	
					Hydrogen	<i>n</i> -Hexane
40° F.						
1.107*	0	—	0	2.064	—	1.0000
500	0.996	—	0.028	2.022	35.19	0.0041
1,000	0.998	—	0.054	1.980	18.53	0.0026
1,500	0.998	3.80†	0.078	1.945	12.88	0.0023
2,000	0.998	2.914	0.099	1.912	10.04	0.0022
2,500	0.998	2.381	0.120	1.880	8.288	0.0023
3,000	0.998	2.023	0.140	1.850	7.103	0.0023
3,500	0.998	1.768	0.160	1.818	6.238	0.0024
4,000	0.998	1.577	0.179	1.790	5.562	0.0024
4,500	0.998	1.429	0.199	1.754	5.024	0.0025
5,000	0.998	1.311	0.218	1.721	4.588	0.0026
6,000	0.998	1.132	0.256	1.659	3.904	0.0027
7,000	0.998	1.007	0.294	1.598	3.391	0.0028
8,000	0.998	0.9150	0.334	1.531	2.988	0.0030
9,000	0.998	0.8449	0.376	1.472	2.654	0.0032
10,000	0.998	0.7920	0.422	1.414	2.365	0.0035
100° F.						
4.954*	0	—	0	2.148	—	1.0000
500	0.986	—	0.031	2.095	31.81	0.0144
1,000	0.992	—	0.059	2.050	16.81	0.0085
1,500	0.994	4.24†	0.084	2.015	11.83	0.0066
2,000	0.995	3.24	0.108	1.975	9.209	0.0061
2,500	0.995	2.643	0.131	1.940	7.595	0.0058
3,000	0.995	2.242	0.153	1.900	6.503	0.0061
3,500	0.995	1.958	0.175	1.870	5.686	0.0061
4,000	0.995	1.744	0.196	1.830	5.077	0.0062
4,500	0.995	1.578	0.217	1.800	4.585	0.0064
5,000	0.995	1.445	0.238	1.772	4.181	0.0066
6,000	0.995	1.245	0.279	1.698	3.566	0.0069
7,000	0.995	1.104	0.322	1.620	3.090	0.0074
8,000	0.995	1.000	0.366	1.545	2.719	0.0079
9,000	0.995	0.9221	0.412	1.461	2.415	0.0085
10,000	0.995	0.8607	0.461	1.390	2.158	0.0093
160° F.						
15.82*	0	—	0	2.256	—	1.0000
500	0.961	—	0.034	2.195	28.69	0.0403
1,000	0.978	—	0.064	2.140	15.28	0.0235
1,500	0.983	4.66†	0.092	2.090	10.68	0.0187
2,000	0.986	3.56	0.119	2.041	8.286	0.0159
2,500	0.987	2.902	0.144	2.000	6.854	0.0152
3,000	0.988	2.460	0.169	1.960	5.846	0.0144
3,500	0.988	2.147	0.193	1.920	5.119	0.0149
4,000	0.988	1.912	0.216	1.880	4.574	0.0153
4,500	0.988	1.728	0.239	1.840	4.134	0.0158
5,000	0.988	1.581	0.262	1.798	3.770	0.0163
6,000	0.988	1.359	0.309	1.710	3.197	0.0174
7,000	0.988	1.202	0.356	1.630	2.775	0.0186
8,000	0.988	1.084	0.405	1.543	2.440	0.0202
9,000	0.988	0.9968	0.456	1.460	2.167	0.0221
10,000	0.988	0.9290	0.511	1.380	1.933	0.0245

TABLE 2. (Cont.)

Pressure, lb./sq. in.	Mole	Volume,	Mole	Volume,	Equilibrium ratio	
	fraction hydrogen	cu. ft./lb. mole Dew point	fraction hydrogen	cu. ft./lb. mole Bubble point	Hydrogen	n-Hexane
220° F.						
39.87*	0	—	0	2.391	—	1.0000
500	0.904	—	0.036	2.321	25.11	0.0996
1,000	0.946	—	0.070	2.256	13.51	0.0581
1,500	0.960	5.07†	0.102	2.195	9.412	0.0445
2,000	0.966	3.87	0.132	2.137	7.318	0.0392
2,500	0.969	3.16	0.160	2.082	6.056	0.0369
3,000	0.971	2.677	0.187	2.032	5.193	0.0357
3,500	0.973	2.334	0.215	1.984	4.526	0.0344
4,000	0.974	2.078	0.241	1.931	4.041	0.0343
4,500	0.974	1.898	0.267	1.882	3.634	0.0355
5,000	0.974	1.718	0.293	1.835	3.324	0.0368
6,000	0.974	1.475	0.345	1.740	2.823	0.0397
7,000	0.974	1.300	0.396	1.648	2.460	0.0430
8,000	0.974	1.170	0.450	1.552	2.164	0.0473
9,000	0.974	1.070	0.508	1.448	1.917	0.0528
10,000	0.973	0.9990	0.570	1.347	1.707	0.0628
280° F.						
84.93*	0	—	0	2.565	—	1.0000
500	0.797	—	0.038	2.489	20.97	0.2110
1,000	0.886	—	0.078	2.400	11.36	0.1236
1,500	0.914	—	0.115	2.321	7.948	0.0972
2,000	0.927	4.17†	0.149	2.250	6.221	0.0858
2,500	0.934	3.40	0.181	2.185	5.160	0.0806
3,000	0.939	2.887	0.213	2.120	4.408	0.0775
3,500	0.942	2.520	0.244	2.060	3.861	0.0767
4,000	0.944	2.240	0.274	2.000	3.445	0.0771
4,500	0.945	2.025	0.304	1.940	3.109	0.0790
5,000	0.946	1.854	0.334	1.882	2.832	0.0811
6,000	0.946	1.595	0.393	1.765	2.407	0.0890
7,000	0.945	1.411	0.451	1.660	2.095	0.1002
8,000	0.944	1.270	0.511	1.545	1.847	0.1145
9,000	0.941	1.168	0.576	1.440	1.634	0.1392
10,000	0.931	1.095	0.649	1.332	1.435	0.1966
340° F.						
160.28*	0	—	0	2.806	—	1.0000
500	0.606	—	0.037	2.726	16.22	0.4091
1,000	0.772	—	0.086	2.615	8.977	0.2495
1,500	0.826	—	0.132	2.510	6.258	0.2005
2,000	0.851	4.45†	0.172	2.423	4.948	0.1800
2,500	0.865	3.63	0.210	2.340	4.119	0.1709
3,000	0.873	3.08	0.249	2.254	3.506	0.1691
3,500	0.878	2.690	0.285	2.170	3.081	0.1706
4,000	0.882	2.394	0.322	2.096	2.739	0.1740
4,500	0.884	2.166	0.359	2.020	2.462	0.1810
5,000	0.885	1.986	0.394	1.942	2.246	0.1898
6,000	0.884	1.720	0.461	1.800	1.918	0.2152
7,000	0.880	1.539	0.528	1.657	1.667	0.2542
8,000	0.865	1.410	0.597	1.522	1.449	0.3350
9,000	0.815	1.325	0.691	1.382	1.179	0.5987
9,200‡	0.768	1.333	0.768	1.333	1.000	1.0000
400° F.						
277.53*	0	—	0	3.23	—	1.0000
500	0.310	—	0.032	3.15	9.688	0.7128
1,000	0.568	—	0.103	2.980	5.515	0.4816
1,500	0.656	—	0.165	2.840	3.967	0.4120
2,000	0.700	4.61†	0.224	2.700	3.125	0.3866
2,500	0.722	3.78	0.283	2.581	2.551	0.3877
3,000	0.736	3.22	0.341	2.460	2.158	0.4006
3,500	0.745	3.82	0.396	2.355	1.881	0.4222
4,000	0.749	2.523	0.448	2.250	1.672	0.4547
4,500	0.750	2.292	0.500	2.147	1.500	0.5000
5,000	0.747	2.105	0.555	2.060	1.346	0.5685
5,920‡	0.688	1.870	0.688	1.870	1.000	1.0000

\*Vapor pressure of *n*-hexane.

†Volumes at dew point, calculated.

‡Critical state.

volatility between the components, partial condensation at liquid-nitrogen temperatures was employed. The sample of the gas phase was removed from the heterogeneous mixture under isobaric-isothermal conditions and passed through a special weighing bomb (13) which was maintained at liquid-nitrogen temperatures. To ensure that all the *n*-hexane was removed the hydrogen was passed through a second weighing bomb also maintained at liquid-nitrogen temperatures. The total quantity of hydrogen in the sample was determined by volumetric measurement in a large glass vessel maintained at 100°F. The change in pressure within this vessel was determined by means of a mercury-in-glass manometer used in conjunction with a cathetometer. The *n*-hexane and a small quantity of dissolved hydrogen were permitted to warm to room temperature in the weighing bombs and then were recooled to liquid-nitrogen temperatures and the hydrogens were removed by prolonged evacuation. No difficulty was experienced in obtaining measurements reproducible within 0.001 mole fraction *n*-hexane. Measurements upon samples of known compositions yielded results within this error. The techniques developed for partial condensation should have permitted the composition of the gas phase in heterogeneous mixtures of hydrogen and *n*-hexane to be determined within 0.002 mole fraction.

#### MATERIALS

The hydrogen, obtained from a commercial manufacturer, was prepared electrolytically and contained 0.005 mole fraction oxygen and, reportedly, less than 0.002 mole fraction of material other than hydrogen and water. The gas was passed through liquid nitrogen, through a chamber containing platinum wire heated to approximately 800°F., and again through a coil immersed in liquid nitrogen. This treatment was followed by contact with activated charcoal and anhydrous calcium sulfate. These processes were carried out at pressures of over 500 lb./sq. in. Mass spectrographic analysis of hydrogen so purified indicated that it contained less than 0.001 mole fraction of material other than hydrogen.

The *n*-hexane was obtained as research grade from the Phillips Petroleum Company, which reported it to contain not more than 0.003 mole fraction of material other than *n*-hexane. The hydrocarbon was dried over metallic sodium and solidified at liquid-nitrogen temperatures. It was maintained at a relatively high vacuum in the solid state for an extended period to complete the removal of noncondensable gases. A value of 40.8707 lb./cu. ft. for the specific weight at 77°F. was obtained for the air-free sample of liquid as compared with 40.878 lb./cu. ft. reported by Rossini (12) for an air-saturated sample at the same temperature. The index of refraction relative to the *D* lines of sodium at 77°F. was 1.37225, as compared with 1.37226 reported by Rossini (12) for air-saturated *n*-hexane. It is

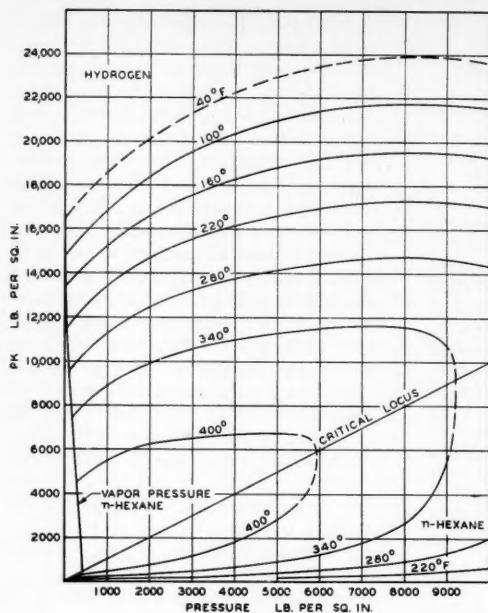


Fig. 3. Equilibrium ratios for hydrogen and *n*-hexane.

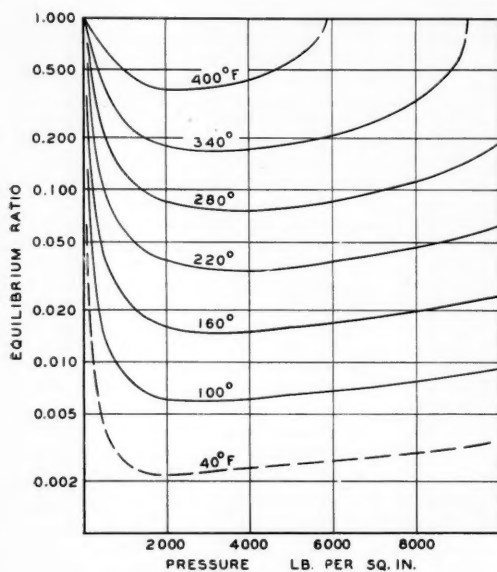


Fig. 4. Equilibrium ratio for *n*-hexane.

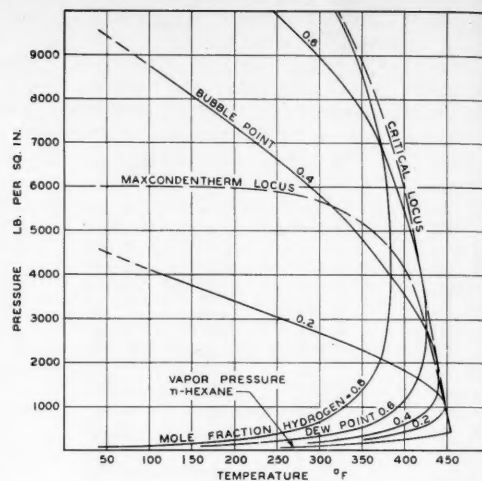


Fig. 5. Pressure-temperature diagram for hydrogen-*n*-hexane system.

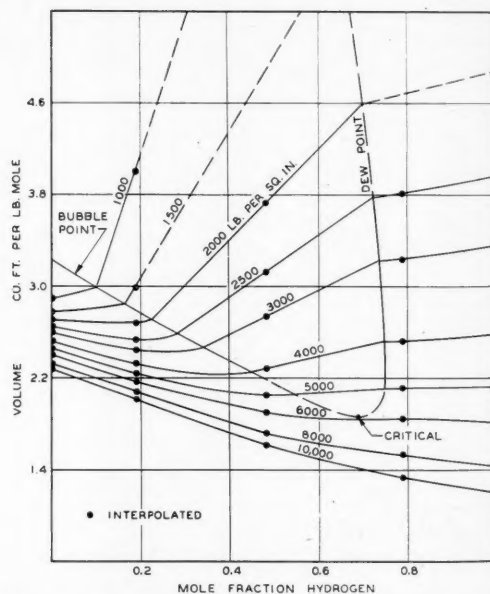


Fig. 6. Molal volume as a function of composition at 400°F.



probable that the material used in this investigation contained less than 0.001 mole fraction of impurities.

## EXPERIMENTAL RESULTS

Measurements of the volumetric behavior of four mixtures of hydrogen and *n*-hexane were investigated. A large sample of each mixture was introduced and measurements were made for pressures from approximately 1,000 to 10,000 lb./sq. in. The sample was then brought to a single-phase state and approximately 80% of it removed. The remaining smaller sample was then investigated over the same temperature interval to obtain data for pressures below 1,000 lb./sq. in. Figure 1 shows the experimental information obtained for a mixture containing 0.1895 mole fraction hydrogen. It is clear that at 100°F. the specific volumes smoothed with respect to composition deviated somewhat from the experimental data for this mixture. Similar experimental information was obtained for each of the three other samples investigated. The detailed record of experimental data obtained in the course of this volumetric study is available (9). One mixture containing 0.0298 mole fraction hydrogen did not differ significantly as to volumetric behavior in the liquid phase from pure *n*-hexane and was not used directly in the smoothing of the volumetric data in this region.

The composition of the coexisting phase as determined from condensation analysis of samples withdrawn under isobaric-isothermal conditions from the gas phase of heterogeneous mixtures of hydrogen and *n*-hexane is shown in Figure 2. The scale of the figure in the vicinity of pure *n*-hexane was enlarged markedly in order to illustrate the behavior of the gas phase in somewhat greater detail. The points shown for the liquid phase were obtained from discontinuities in the isothermal first deriva-

tive of specific volume as a function of pressure. The data obtained in the course of the measurement of the composition of the gas phase in heterogeneous mixtures of hydrogen and *n*-hexane are also available (9).

Figure 3 presents the product of the molal gas-liquid equilibrium ratios and pressure for hydrogen and for *n*-hexane as a function of pressure for each of the several temperatures investigated. The use of the product of pressure and the equilibrium ratio made it possible to present the behavior in greater detail than when the equilibrium ratio alone is employed.

The equilibrium ratio for *n*-hexane is presented in Figure 4 for each of the temperatures investigated. The values for 40°F. are included by extrapolation and indicated by dotted curves. The dew- and bubble-point curves are shown for the four mixtures on a pressure-temperature diagram in Figure 5, the loci of the critical and maxcondentherm states being included. The two-phase pressure exceeds 10,000 lb./sq. in. at temperatures below 320°F.

The variation in volume with composition at 400°F. is presented in Figure 6, which includes the behavior for *n*-hexane (14) and hydrogen (3). The molal volumes for even values of pressure were interpolated from the experimental data for each mixture. The agreement with the data for *n*-hexane and hydrogen appears satisfactory and was comparable with that shown in Figure 6 for all the temperatures investigated.

Table 1 records the molal volume for even values of pressure and temperature for three experimentally studied compositions. A standard deviation of 0.000036 cu. ft./lb. was found for the experimental data in the liquid phase from the smooth curves from which the tabular information of Table 1 was obtained. The standard deviation of the data in the two-phase region was 0.00044 cu. ft./lb. The much larger deviation in

the heterogeneous region probably results from a lack of strict attainment of equilibrium between the phases. The deviation was random, as measurements were obtained upon both increase and decrease in the total volume of the system. The standard deviation cited assumed that all the uncertainty existed in specific volume and that none was associated with the evaluation of pressure, temperature, and composition. The data of Table 1 are smooth with respect to composition within the small uncertainty associated with graphical operations involving volumetric data for *n*-hexane, hydrogen, and the four experimental mixtures investigated.

Table 2 presents the compositions and molal volumes of the liquid and gas phases of heterogeneous mixtures of hydrogen-*n*-hexane for seven temperatures between 40° and 400°F. In addition, the molal equilibrium ratios for hydrogen and *n*-hexane and estimates of the critical state were included. Table 3 records a number of the properties at the unique states in the heterogeneous region.

## ACKNOWLEDGMENT

This work was in part supported by the General Petroleum Corporation through scholarship grants to W. B. Nichols, D. E. Stewart, C. H. Viens, and W. C. Windham. June Gray assisted with the calculations and preparation of the figures. W. N. Lacey reviewed the manuscript.

## LITERATURE CITED

1. Bridgeman, O. C., *J. Am. Chem. Soc.*, **49**, 1174 (1927).
2. Burriss, W. L., N. T. Hsu, H. H. Reamer, and B. H. Sage, *Ind. Eng. Chem.*, **45**, 210 (1953).
3. Deming, W. E., and L. E. Shupe, *Phys. Rev.*, **40**, 848 (1932).
4. Ipatieff, V. V., Jr., V. P. Teodorovich, and I. M. Levine, *Oil Gas J.*, **32**, 14 (1933).
5. Kay, W. B., *Chem. Revs.*, **29**, 501 (1941).
6. Kelso, E. A., and W. A. Felsing, *J. Am. Chem. Soc.*, **62**, 3132 (1940).
7. Lewis, G. N., *Proc. Am. Acad. Arts Sci.*, **43**, 259 (1907).
8. Meyers, C. H., *J. Research Natl. Bur. Standards*, **9**, 807 (1932).
9. Nichols, W. B., H. H. Reamer, and B. H. Sage, *Am. Doc. Inst.*, Washington, D. C., Doc. No. 5215, \$2.50 for photoprints or \$1.75 for 35-mm. microfilm.
10. Reamer, H. H., and B. H. Sage, *Rev. Sci. Instr.*, **24**, 362 (1953).
11. *Ibid.*, **26**, 592 (1955).
12. Rossini, F. D., et al., "Selected Values of Physical and Thermodynamic Properties of Hydrocarbons and Related Compounds," Carnegie Press, Pittsburgh (1953).
13. Sage, B. H., and W. N. Lacey, *Trans. Am. Inst. Mining Met. Engrs.*, **136**, 136 (1940).
14. Stewart, D. E., B. H. Sage, and W. N. Lacey, *Ind. Eng. Chem.*, **46**, 2529 (1954).
15. Wiebe, Richard, and V. L. Gaddy, *J. Am. Chem. Soc.*, **60**, 2300 (1938).

TABLE 3. ESTIMATED PROPERTIES AT THE UNIQUE STATES IN THE HYDROGEN-*n*-HEXANE SYSTEM\*

Mole fraction hydrogen	Pressure, lb./sq. in.	Temperature, °F.	Pressure, lb./sq. in.	Temperature, °F.
	Critical		Maxcondentherm	
0.0	433.9†	454.6†	433.9	454.6
0.1	690	452	620	452
0.2	1000	449	840	449
0.3	1430	445	1150	446
0.4	2000	439	1500	441
0.5	2790	432	2010	435
0.6	4050	419	2750	425
0.7	6300	396	3660	411
0.8	—	277	4590	382
0.9	—	—	5450	327
1.0	188.1‡	-399.8‡	188.1	-399.8

\*These data are much more uncertain than the directly measured quantities.

†Critical of *n*-hexane.

‡Critical of hydrogen.

# Flow of Steam-water Mixtures in a Heated Annulus and Through Orifices

JOHN W. HOOPES, JR.

Columbia University, New York, New York

Values of total pressure drop are presented for the flow of vaporizing water in an internally heated 1-in. I.D. by 1½-in. O.D. annulus at mass velocities of 270 to 1,440 lb./sq. ft., pressures of 9 to 180 lb./sq. in., and up to 0.34 fraction by weight vaporized. The total heated length over which boiling took place was as large as 6 ft. There is no evidence of "sonic" pressure jumps at the outlet. The results for the annulus mentioned lie within +30 to -11% of the Lockhart-Martinelli curve at higher qualities and with  $\pm 45\%$  of the correlation at lower qualities where the actual quality is more uncertain. A simplified correlation in terms of quality and volume fraction of liquid predicted the two-phase frictional pressure drops with an average error of 41%.

It was found that the ratio of the two-phase pressure drop through a 0.3-in. orifice to the drop with no vaporization was approximately a linear function of the quality in the *vena contracta* but was only one tenth to one third as great as would be predicted if the mixture were to expand as a homogeneous fluid. Prediction of orifice pressure drops is improved if slip between vapor and liquid is considered.

Pressure drop accompanying the flow of mixtures of steam and water is of importance in forced- and natural-circulation evaporators, condensate return lines carrying flashing liquids, steam boilers, and certain nuclear reactors. Two-phase flow is also encountered in the simultaneous transport of oil and gas in wells and gathering systems and in air lifts for the pumping of liquids. The resistance offered by restrictions such as valves or orifices, also of interest, has been studied much less than has been flow through uniform conduits. It has commonly been assumed that "critical," or "sonic," conditions occur in vaporizing liquids at surprisingly low flow rates, with large over-all pressure drops resulting because of the accompanying pressure "jump."

This paper discusses two-phase pressure drop data taken in the boiling region

of a flow channel in which water was pumped downward through a concentric annulus with an electrically heated core (Figure 1).

## APPARATUS

Deionized water was circulated through an air-operated flow-control valve and a measuring orifice and into a 6-in.-diam. header, which served essentially as a high-pressure reservoir at about 250 lb./sq. in. gauge. Flow to the test section, measured by a Potter turbine-type flow meter, was controlled by manually operated valves immediately downstream of the flow meter. The effluent from the test section was quenched by a metered stream of by-pass water, and the combined streams were sent to a booster pump, shell-and-tube heat exchangers, and thence back to the main circulating pump. The pressure in the quench tank was held constant by a standpipe leading to an open drum.

The heated section consisted of an inner tube of 2S aluminum approximately 1 in. O.D., pressurized internally with nitrogen, and an outer aluminum housing tube of an outside diameter to give a ½- or ¼-in. annulus between them. The annulus concentricity was maintained by spacer ribs

made of a silicone-Fiberglas laminate. The ribs were held in broached slots in the housing tube and were in tight contact with the core tube. The resulting annulus, therefore, consisted essentially of three identical subchannels as shown in Figure 2. The heated length over which boiling took place depended on the inlet water temperature but was as long as 6 ft. There was at least an equal length in which liquid was being heated to the boiling point.

The core was heated with direct currents of up to 20,000 amp. In some runs cores having a uniform 0.035-in. wall were used to provide a nearly uniform heat flux over the length of the flow channel. In others cores having a varying wall thickness were used, giving a cosine distribution of heat flux chopped at the ends to about 10% of that at the maximum flux.

At the end of the heated section the annulus was expanded to form the chamber shown in Figure 3. The effluent from the annulus entered the quench tank from the chamber through orifice holes 0.38 in. in diameter. The number of holes could be varied from one to five. Some runs were made with the chamber removed. The annulus effluent then discharged directly into the quench tank.

Pressure taps were located in the quench tank, in the chamber, at the end of the

John W. Hoopes, Jr., is at present with Atlas Powder Company, Wilmington, Delaware.

\*Tabular material has been deposited as document 5212 with the American Documentation Institute, Photoduplication Service, Library of Congress, Washington 25, D. C., and may be obtained for \$2.50 for photoprints or \$1.75 for 35-mm. microfilm.

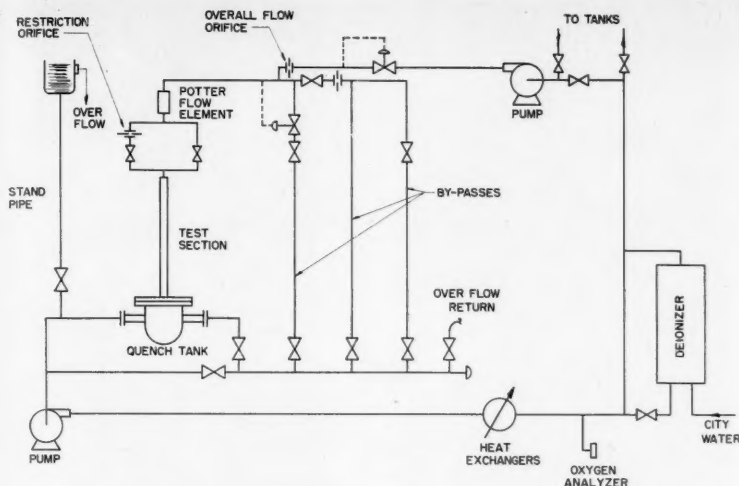


Fig. 1. Sketch of flow loop.

enlarged section just before the chamber proper, at the annulus outlet, 0.2 ft. upstream, and about every 0.5 ft. for several feet upstream from the outlet. The gauge lines, filled with water at room temperature, led to the manifold shown in Figure 4. All pressures were read on the same 12-in. precision Bourdon gauge shown. [Also visible in the figure are (a) the housing tube, (b) standpipe, (c) nitrogen cylinder, (d) bus duct, (e) window in quench tank at "4 o'clock" behind the large pressure gauge, (f) by-pass.]

Voltage drop and inside wall temperatures were measured over the heated length at cross sections spaced 1.15 ft. apart by use of a rod with thermocouple and voltage probes. This rod was inserted inside the core and manipulated from the top electrical contact assembly. The current, supplied by two generators in parallel, was obtained from the voltage drop across standard shunts. During a given run the current was held constant within  $\pm 0.1\%$  by means of an electronic excitation regulator.

The air content of the water during a run was between 2 and 10 p.p.m., usually between 2 and 5 p.p.m.

Accuracy of the important variables is estimated as follows:

Power	$\pm 0.25\%$
Mass velocity	$\pm 11$ lb.-mass/ (sec.)(sq. ft.)
Inlet temperature	$\pm 0.5^\circ\text{C.}$
Pressures	$\pm 0.5$ lb.-force/sq. in.

Mixture qualities calculated from the preceding data are uncertain by about 0.002. Only results for locations having qualities over about 0.0075 are given here.

The runs reported\* were made over the following range of conditions:

Liquid (inlet) velocity, ft./sec.	5.1-19.7
Mass velocity in annu- lus, lb./(sec.)(sq. ft.)	317-1,230
Outlet quality (uncor- rected for kinetic energy)	0.026-0.34

Pressure at start of boil- ing, lb.-force/sq. in. abs.	41-180
Pressure at annulus out- let, lb.-force/sq. in. abs.	23-83
Pressure in quench tank, lb.-force/sq. in. abs.	23-24
Heat flux at start of boil- ing (Uniform heat flux runs), B.t.u./ (hr.)(sq. ft.)	347,000-864,000

In delineating the two-phase flow region, boiling was assumed to commence at the point where the total energy of the fluid (calculated from the inlet temperature, flow, current, and voltage) was equal to the saturation enthalpy as determined from a plot of pressure and the corresponding enthalpy of saturated liquid along the channel. With the  $\frac{1}{4}$ -in. annulus subcooled or local boiling occurred upstream of this point, and a few observations with a glass housing tube with an  $\frac{1}{8}$ -in. annulus have shown that boiling starts near the ribs before the entire liquid is heated to its boiling point. These phenomena cause the pressure gradients to increase above the gradients for all liquid flow before the nominal boiling point is reached but will not be discussed further.

#### QUALITY

Qualities along the heated section were calculated by setting up a total energy balance between the inlet and the point in question. The total energy  $E$  per pound of fluid is given by

$$E = E_i + Q = h_i + \frac{G^2 v_i^2}{2g_c J} + \frac{Z_i g}{g_c J} + Q = h + \frac{Zg}{g_c J} + KE$$

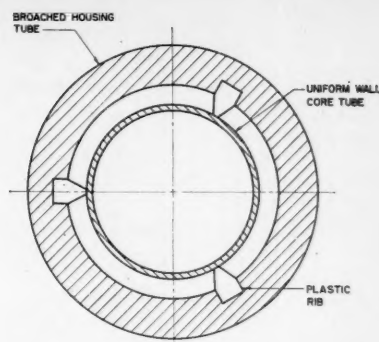


Fig. 2. Cross section of annulus tested.

$$= h + \frac{Zg}{g_c J} + \frac{(1-x)G^2 v_f^2}{2g_c J} + \frac{xG^2 v_g^2}{2g_c J} \quad (1)$$

$Q$  is the heat added per pound of fluid and was calculated from the flow, current, and voltage drop. Because there may be slip between the two phases of a boiling mixture, with the vapor phase moving faster, the kinetic energies of the liquid and vapor phases are expressed separately in the equation.

If the mixture behaved as a homogeneous fluid—which requires that  $V_f = V_g$  and thermodynamic equilibrium exist between the phases—the kinetic energy of the stream could be expressed by a single term similar to that for a pure liquid of specific volume  $v = (1-x)v_f + xv_g$ . The kinetic energy term is then merely  $(G^2 v^2)/2g_c$ .

The most convenient way of taking slip velocity into account is to use experimentally measured values of the holdup of liquid and vapor. If this is done, the ratio of the total kinetic energy with slip to that for the homogeneous case is given by

$$\frac{KE}{(KE)_{hom}} = \frac{\frac{(1-x)^3 v_f^2}{R_f^2} + \frac{x^3 v_g^2}{R_g^2}}{[(1-x)v_f + xv_g]^2} \quad (2)$$

$R_f$  and  $R_g$  are the volume fractions of liquid and vapor respectively and have been correlated by Lockhart and Martinelli (7) in terms of the quantity

$$X_{tt} = \sqrt{\frac{(dp/dL)_L}{(dp/dL)_G}} = X_{tt}^{0.9}$$

Figure 5a was calculated from Equation (2) by use of their correlation; the presence of slip reduces the total kinetic energy by up to 93% at 25 lb./sq. in. abs. The actual kinetic energy may be higher because of the entrainment of some of the liquid in the faster moving gas phase, which has been measured by Alves (1).

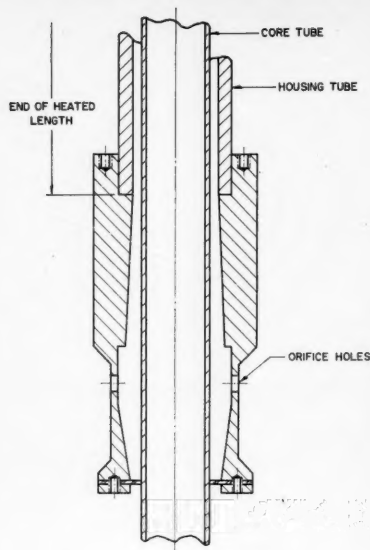


Fig. 3. Annulus outlet and orifice chamber.

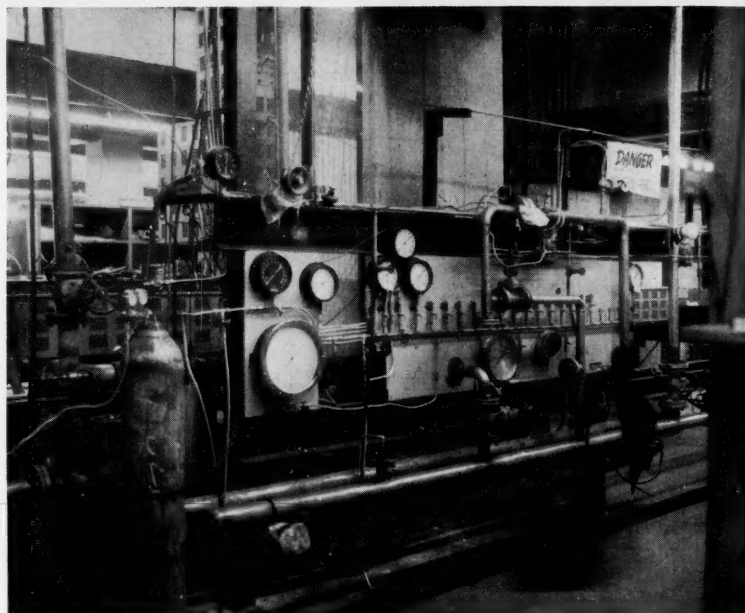


Fig. 4. Photograph of bottom of test section, including pressure manifold.

In general, successive approximations made with Equations (1) and (2) are required to calculate  $x$ ; however, the kinetic energy terms are small enough to be neglected except at very high mass velocities and low pressures (large  $v_g$ ). The elevation terms  $(Z_g)/(g_c J)$  and  $(Z_l)/(g_c J)$  can almost always be neglected.

#### TYPE OF FLOW

The flow was characterized from the flow-pattern regions given by Baker (2) for horizontal flow. As can be seen from Figure 6, at the lowest flow rates the flow pattern theoretically changes in about 2 ft. of channel through the following types of flow: slug, annular, dispersed\*. Most of the two-phase pressure drop occurs in the dispersed region. At higher flows with greater turbulence the flow changes from bubble or froth flow directly to dispersed flow.

The conclusions based on Figure 6 are supported by motion pictures of one run, taken through a glass housing tube. Conditions corresponding roughly to the point labeled A on Figure 6 were visually confirmed as bubble or possibly

slug flow; however, there were no violent pressure fluctuations commonly attributed to slug flow.

#### PRESSURE GRADIENTS

The total pressure gradient at any point  $dp/dL$  was obtained by taking the slope of a plot of the measured pressures as a function of heated length. By the method of Martinelli and Nelson (8), it was then separated by calculation into the following three components:

1. The contribution due to changes in elevation,  $(dp/dL)_{EL}$ . For downward flow  $(dp/dL)_{EL} = -[(R_f/v_f) + (R_g/v_g)]$  which is obtained merely by considering the weight of mixture in a unit height of vertical channel. Since the quantity is small, it was approximated by its value under conditions of homogeneous flow,

$$-\frac{1}{(1-x)v_f + xv_g} = -\frac{1}{v}$$

2. The pressure gradient due to the acceleration or rate of change of momentum of the stream,  $(dp/dL)_{ACC}$ . A momentum balance for flow patterns typified by annular flow gives

$$\begin{aligned} \left(\frac{dp}{dL}\right)_{ACC} &= \frac{G^2}{g_c} \frac{d}{dL} \left[ \frac{(1-x)^2}{R_f} v_f + \frac{x^2}{R_g} v_g \right] \\ &= \frac{G^2}{g_c} \frac{dr}{dL} \quad (4) \end{aligned}$$

The values of  $r$ , which is a function of quality and pressure, were computed at

each point by use of a nomographic chart, plotted, and  $(dp/dL)_{ACC}$  was calculated by taking slopes. If the flow were homogeneous,

$$\left(\frac{dp}{dL}\right)_{ACC, hom} = \frac{G^2}{g_c} \frac{d}{dL} [(1-x)v_f + xv_g] \quad (5)$$

The ratio of the acceleration pressure drop with slip to that for homogeneous flow is plotted in Figure 5b, again by use of the Lockhart and Martinelli correlation for  $R_f$  and  $R_g$ .

3. Frictional pressure gradient  $(dp/dL)_{TFP}$  was found by difference. Figure 7 is a typical plot of  $x$ ,  $dp/dL$ ,  $(dp/dL)_{ACC}$ , and  $(dp/dL)_{TFP}$  as functions of heated length. Elevation pressure gradients, which ranged from 0.004 to 0.15 lb.-force/(sq. in.)(ft.), are too small to be observable. The fraction of the total pressure drop due to acceleration increases rapidly with increasing quality.

It should be pointed out that at high total pressure gradients the accuracy of the computed frictional drops depends on the accuracy of  $(dp/dL)_{ACC}$ , which in turn requires accurate values of  $R_f$  and  $R_g$ . For example, if the acceleration pressure drop had been calculated by Equation (5), the values of  $(dp/dL)_{TFP}$  would have been much smaller—or even negative. Thus correlation of two-phase frictional pressure drop under such conditions is a necessary but not sufficient test of the method of calculating  $(dp/dL)_{ACC}$  as well as of the correlation method itself. Unfortunately, if correlations fail it is difficult to isolate the cause.

\*Baker in his review summarizes various investigators' definitions of these types of flow as follows: *slug flow*, flow in which a wave is picked up periodically by the more rapidly moving gas to form a frothy slug which passes through the pipe at a much greater velocity than the average liquid velocity; *annular flow*, flow in which the liquid forms in a film around the inside wall of the pipe and the gas flows at a high velocity as a central core; *dispersed flow*, flow in which most or nearly all of the liquid is entrained as spray by the gas.



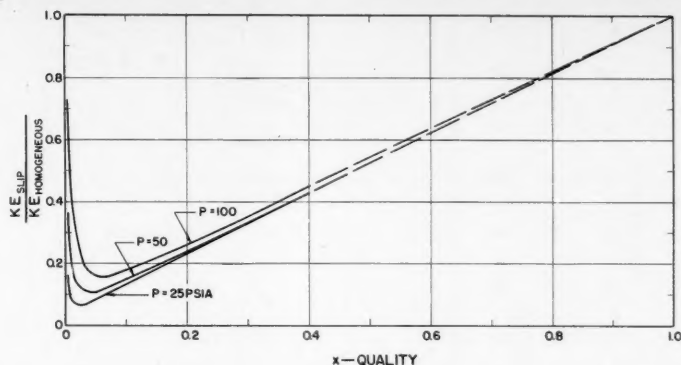


Fig. 5a. Ratio of kinetic energy, slip velocity being taken into account, to the kinetic energy for homogeneous flow.

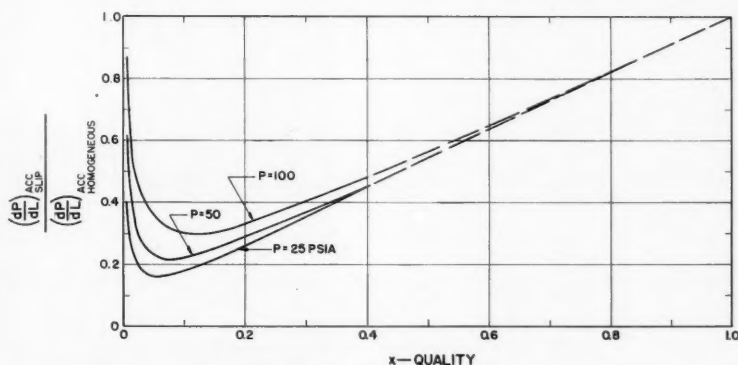


Fig. 5b. Ratio of acceleration pressure gradient, slip velocity being taken into account, to the acceleration pressure gradient, homogeneous flow being assumed.

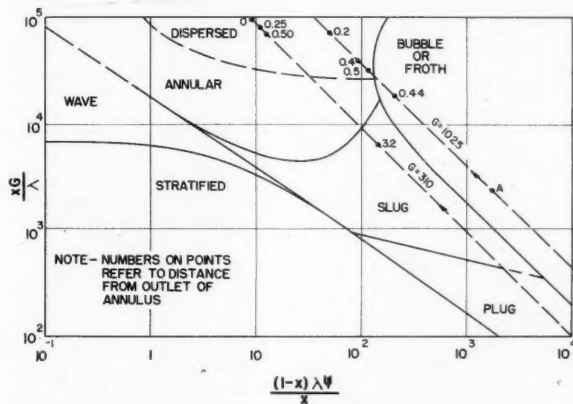


Fig. 6. Flow-pattern regions for results reported (correlation of Baker).

#### LOCKHART AND MARTINELLI CORRELATION FOR TWO-PHASE FRICTIONAL PRESSURE DROP

Values of  $(dp/dL)_{TPF}$  were calculated from several points along the tube for twenty-two different runs. They were converted to the Lockhart and Martinelli parameter  $\phi_L = [(dp/dL)_{TPF}/(dp/dL)_L]^{1/2}$  by no-power liquid-pressure-drop data for

calculating  $(dp/dL)_L$  and were plotted as a function of  $\chi_{li}$ . Figure 8 shows that the results for the  $1/8$ -in. annulus lie within  $\pm 30$  to  $-11\%$  of the Lockhart-Martinelli curve at higher qualities (lower  $\chi_{li}$ ) and within  $\pm 45\%$  of the correlation at lower qualities (higher  $\chi_{li}$ ), where the actual quality is in doubt by as much as 20 to 30%. It should be

remembered that errors of  $\pm 30$  or  $\pm 45\%$  in  $\phi_L$  correspond to  $\pm 70$  or  $\pm 110$  to  $-70\%$  error in the calculated pressure drop respectively. No satisfactory explanation for the higher deviation of the two  $1/4$ -in. runs has been advanced.

#### SIMPLIFIED CORRELATION FOR VAPORIZATION PROCESSES

Calculation of two-phase frictional-pressure drop when a liquid is being heated and vaporized in the same conduit is more convenient if the frictional-pressure gradient is expressed as the ratio  $(dp/dL)_{TPF}/(dp/dL)_f$ ; where  $(dp/dL)_f$  is the pressure gradient that would be obtained if all the mixture were liquid at the same temperature, and it is very nearly constant along the tube. The Lockhart and Martinelli  $(dp/dL)_L$  is approximately equal to  $(dp/dL)_f (1-x)^{1.8}$ .

The results of Linning (6) indicate that in annular flow, which is closely related to dispersed flow, the vapor-liquid-interface velocity is approximately equal to that of the average liquid velocity. Thus in downward flow in a pipe the liquid near the wall behaves essentially as a falling film whose flow is aided by the more rapidly moving gas but whose "wetted perimeter" for friction is the conduit wall perimeter, the same as it would be if the channel were full of liquid. It seems reasonable therefore to consider the pressure drop due to the "actual" liquid velocity. In a narrow annular passage or closely spaced parallel plates the wetted area may decrease as the quality increases, as vapor may tend to flow near to one wall of the passage.

If a friction factor  $f_{TPF}$  for the liquid phase alone is defined by the usual Fanning equation, the equation for frictional pressure gradient can be written for the liquid phase and for the total flow if it were all liquid. Division of the two equations gives

$$\frac{(dp/dL)_{TPF}}{(dp/dL)_f} = \left( \frac{f_{TPF} r_{HTPF}}{f_f r_H} \right) \left( \frac{1-x}{R_f} \right)^2 \quad (6)$$

where  $r_{HTPF}$  and  $r_H$  are the hydraulic radii (ratio of cross-sectional area to wetted perimeter) of the liquid phase in the mixture and of the completely filled flow channel. Calvert and Williams (9) have treated this problem more elegantly by considering the shear forces in the liquid phase.

Presumably the product  $f_{TPF} r_{HTPF}$  is a function of the flow pattern, slip velocity, and quality. On the other hand the plot of the pressure-gradient ratio in Figure 9 as a function of  $[(1-x)/R_f]^2$  shows that the results with the  $1/8$ -in. annulus can be correlated with an average deviation of 41% by assuming  $(f_{TPF} r_{HTPF})/(f_f r_H) = 1$  in Equation (6).

Since the ratio  $r_{HTF}/r_H$  would be equal to  $R_f$  if the wetted perimeter were to remain unchanged during the vaporization, this assumption could hold true only if the walls were becoming partially nonwetted as quality increased.

Figure 9 is also interesting in that the published values of  $R_f$  and  $R_g$  are used to estimate phase velocities in the annular- and dispersed-flow region and indicate that a large part of the increased pressure drops in two-phase flow can be accounted for by the increased velocities of the phases. The effect of wave formation as found by Bergelin *et al.* (5) for stratified flow is probably not a factor here in the annular and dispersed region, although entrainment is the analogous effect in annular flow.

Those points on the right of Figure 9, in which the observed pressure drop is greater than 200% of that predicted correspond to runs with medium flow ( $G = 400$  to  $1,000$  lb.-mass/(sec.) (sq. ft.) and of fairly high quality (greater than 0.1) and to locations only about 0.25 ft. from the annulus outlet. At this location the pressure gradient is quite steep, about 100 lb.-force/(sq. in.) ft.  $(dp/dL)_{TPF}$  is probably high for two reasons: (1) the calculated  $(dp/dL)_{ACC}$  is probably too low because entrainment of some of the liquid in faster moving vapor is not taken into account [if  $(dp/dL)_{ACC}$  were higher, then  $(dp/dL)_{TPF}$  would be smaller] and (2) the extra energy required to detach and accelerate liquid droplets from the bulk of the liquid undoubtedly shows as added pressure drop.

The two very low points on the right half of Figure 9 are for two runs of high flow [ $G > 1,100$  lb.-mass/(sec.) (sq. ft.)] and low quality (less than 0.05). Along a large part of the heated length  $(dp/dL)_{ACC}$ , as calculated by Equation (4), is greater than  $dp/dL$ . The calculated acceleration pressure drops may be high because of a failure to maintain thermodynamic equilibrium at these high flows. If this were true, the calculated rate of change of quality would be too high, which would be reflected in a too-high  $(dp/dL)_{ACC}$ .

Since the Lockhart-Martinelli parameter  $\chi_{it}$  must be evaluated in order to find  $R_f$ , the utility of the correlation rests primarily in the convenience of using the ratio  $(dp/dL)_{TPF}/(dp/dL)_f$  where the quality is changing.

#### SONIC OR CRITICAL VELOCITY

The pressure at the annulus outlet was found to be very near that of the orifice chamber (or of the quench tank if the chamber were removed) in every boiling run. There was no evidence of sonic choking at the outlet, even at the highest flows and very steep pressure gradients. The flows were up to four times as high as the critical mass velocity calculated

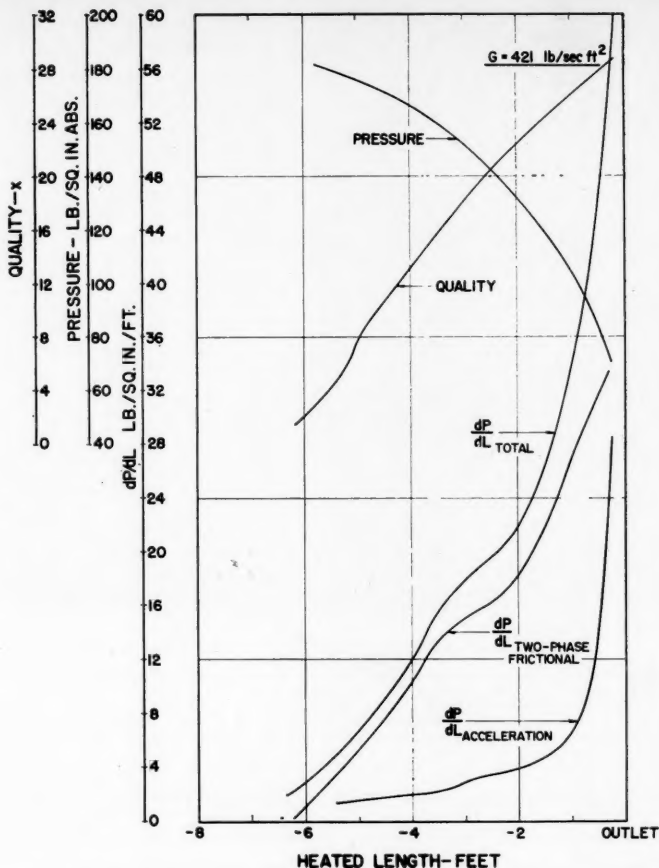


Fig. 7. Plot of quality, total pressure gradient, and acceleration pressure gradient as a function of heated length.

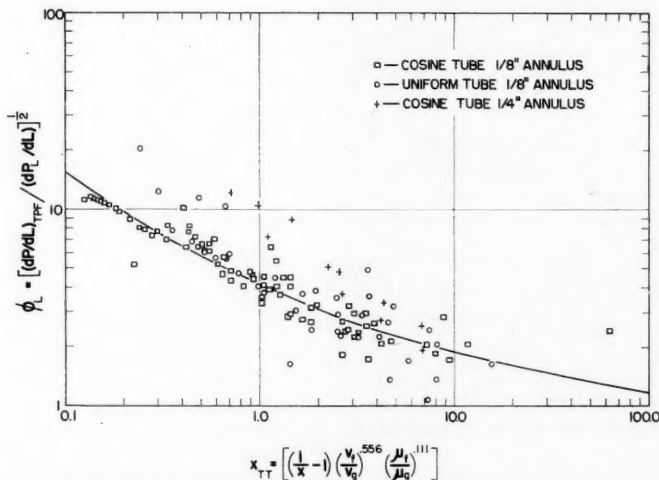


Fig. 8. Plot of Martinelli parameter  $\phi_L$  as a function of  $\chi_{it}$ .

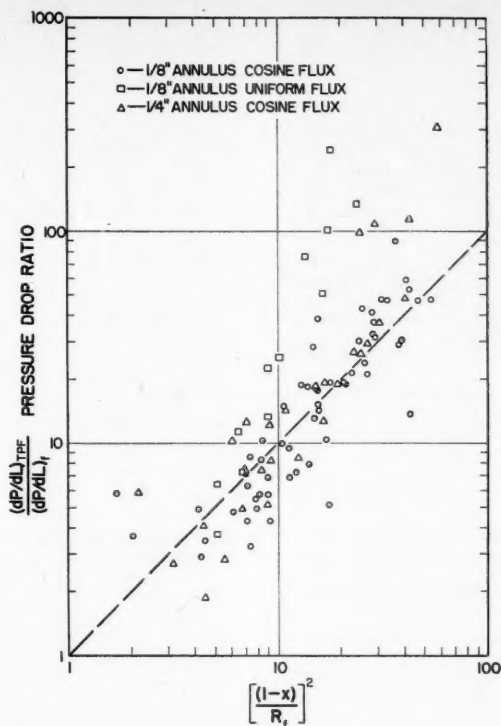


Fig. 9. Plot of two-phase frictional pressure-drop ratio  $(dp/dL)_{TPF}/(dp/dL)_f$  as a function of  $(1-x)^2/R_f^2$ .

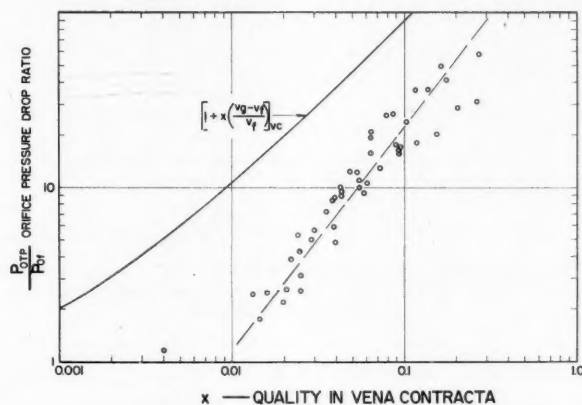


Fig. 10. Plot of two-phase orifice pressure-drop ratio  $\Delta p_{OTP}/\Delta p_{of}$  as a function of  $x_{VC}$ , homogeneous flow being assumed.

when a homogeneous fluid was assumed at outlet conditions:

$$G_{crit} = \sqrt{-g_c \left( \frac{\partial p}{\partial [(1-x)v_f + xv_g]} \right)} \quad (7)$$

The very steep pressure gradients at the outlet may have been interpreted by previous investigators as a choking due to critical flow. Indeed, the practical effect may be considered to be the same

as if a "jump" had occurred, as the over-all pressure drop for a given flow and power input was essentially unaffected by removal of the chamber, i.e., by a change in annulus discharge pressure. In calculating over-all pressure drops by steps or by graphical integration using the equation

$$p_1 - p_2 = \int_{L_1}^{L_2} (dp/dL)_{TPF} dL$$

$$+ \int_{L_1}^{L_2} (dp/dL)_{ACC} dL + \int_{L_1}^{L_2} (dp/dL)_{EL} dL \quad (8)$$

one can assume the outlet pressure to be that at which Equation (7) applies. A graphical representation of Equation (7) is available for steam-water mixtures (10).

#### PRESSURE DROP THROUGH ORIFICES

The pressure drop across an orifice discharging into a large chamber is the acceleration pressure drop between the upstream side and the *vena contracta*. For homogeneous flow this would be equal to  $G^2 v / 2g_c$ , evaluated at the *vena contracta* conditions. There is no regain of pressure because the energy of the jet is completely lost in turbulence.

If the upstream velocity in the direction of the orifice is negligible, the ratio of the pressure drop for a homogeneous two-phase mixture to that for liquid at the same mass velocity and temperature is given by

$$\frac{\Delta p_{OTP, hom}}{\Delta p_{of}} = \frac{(1-x)v_f + xv_g}{v_f} = 1 + \frac{x(v_g - v_f)}{v_f} \quad (9)$$

If slip is taken into account, the pressure drop is equal to  $r(G^2/g_c)$  where  $r$  is defined in Equation (4). Expressed as a pressure-drop ratio,

$$\frac{\Delta p_{OTP}}{\Delta p_{of}} = \frac{(1-x)^2}{R_f} + \frac{v_g x^2}{v_f R_g} \quad (10)$$

Values of  $\Delta p_{of}$  were obtained from the results of runs with cold water, suitably corrected to the saturation temperature at the quench tank (*vena contracta*) pressure. The cross-sectional area of the *vena contracta* was taken as 61% of the orifice area, as determined by these measurements. With this value of the area, kinetic energy corrections were applied to the total energy when qualities were calculated.

Figure 10 is a plot of the orifice-pressure-drop ratio as a function of quality evaluated at quench-tank conditions. Since the quench-tank pressure was essentially the same for all runs,  $v_g$  and  $v_f$  are the same, and Equation (9) can be shown as a single curve. The assumption of homogeneous flow leads to predicted pressure drops from 400 to 900% of those observed. Quality alone serves to correlate the results well; however, the points from a series of runs at a quite different quench-tank pressure would probably have fallen on a different line.

Figure 11a shows that Equation (10) agrees much better with the experimental results than does Equation (9). Qualities

are calculated by use of Equations (1) and (2) to evaluate the kinetic energy in Figure 11a. The predicted pressure drops are progressively lower at higher powers, i.e., at higher flow rates for a given quality. In Figure 11b the homogeneous kinetic energy was used in the energy balance at higher flows to calculate the qualities. It is seen that the effect of power is eliminated. The average error is 31%. The very low points are for low qualities (about 0.02) where quality may be in error by 10% and flow patterns may not be the same as for higher degrees of vaporization. In any case the agreement is surprisingly good considering that the values of  $R_o$  and  $R_f$  used were those for horizontal flow of air and water or air and kerosene through a uniform pipe.

There was apparently no "sonic choking" due to critical flow. This agrees with the results of Benjamin and Miller (4), who passed steam-water mixtures through orifices at pressure differences up to 145 lb./sq. in. gauge.

## CONCLUSIONS

The results indicate that the relationships given by Martinelli and Nelson (8) for calculating local two-phase pressure gradients of vaporizing water are satisfactory for a small annulus and downward flow in the dispersed and slug-annular flow regions and the relatively low pressures used in this study. More data are desirable on larger diameter flow channels in vertical conduits.

The correlation of Lockhart and Martinelli for volume fraction vapor and liquid in horizontal flow can be used to estimate pressure drops for flow of flashing mixtures through orifices with an average error of 31%. At qualities over about 0.05, the error is about 20%. The correlation is also useful in calculating frictional pressure drop in pipes, an indication that the individual phase velocities are the chief factor determining the frictional pressure drop in the flow regions studied.

A better understanding of the phenomena involved, which will presumably result in an ability to predict pressure drops more accurately, can best be obtained by measurements of flow pattern with visual observations and of local slip velocities or holdup.

## ACKNOWLEDGMENT

The author wishes to acknowledge the help of Martin Gutstein and William Begell in performing many of the calculations and of Henry Hyman in preparing the drawings.

## NOTATION

$E$  = total specific energy of stream, B.t.u./lb. mass  
 $f$  = Fanning friction factor

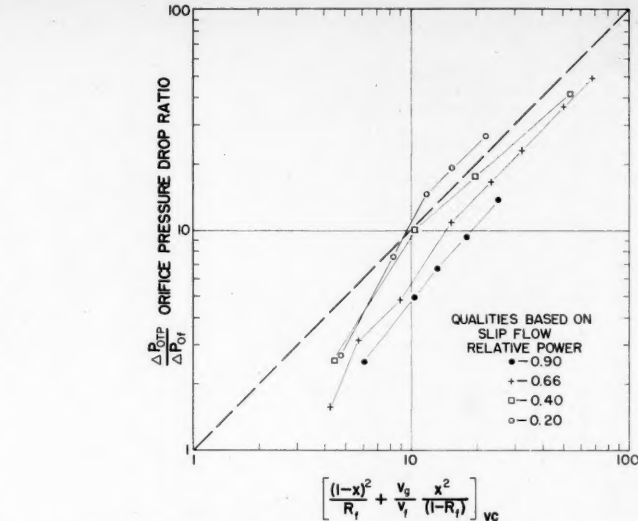


Fig. 11a. Plot of two-phase orifice pressure-drop ratio  $\Delta p_{OTP}/\Delta p_{OF}$  as a function of  $[(1-x)^2/R_f] + (v_g/v_f)(x^2/R_g)$ , qualities based on slip flow at vena contracta conditions.

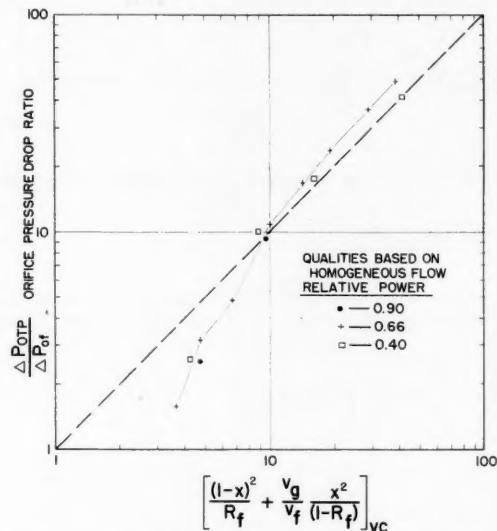


Fig. 11b. Plot of two-phase orifice pressure-drop ratio  $\Delta p_{OTP}/\Delta p_{OF}$  as a function of  $[(1-x)^2/R_f] + (v_g/v_f)(x^2/R_g)$ , qualities based on homogeneous flow at vena contracta conditions.

$\frac{(dp/dL)_F}{r_H V^2 / 2g_c}$	$r_H$	= hydraulic radius, cross sectional area divided by wetted perimeter, ft.
$G$	$R$	= fraction of cross section occupied by a phase
$g_c$	$s$	= entropy, B.t.u./[(lb.-mass)(°F.)]
$g$	$S$	= cross section perpendicular to flow, sq. ft.
$h$	$v$	= specific volume, cu. ft./lb.-mass
$J$	$V$	= velocity, ft./sec.
$L$	$W$	= mass rate of flow, lb.-mass/sec.
$p$	$x$	= quality ( $W_g/W$ )
$Q$	$X_{tt}$	= Lockhart and Martinelli correlating parameter = $\sqrt{\frac{(dp/dL)_L}{(dp/dL)_G}}$
		for both phases turbulent
		$Z$ = elevation above arbitrary datum, ft.



- $X_{ii}$  = Lockhart and Martinelli correlating parameter =  $X_{ii}^{1/1.9}$   
 $\phi_L$  = Lockhart and Martinelli parameter =  

$$\sqrt{\frac{(dp/dL)_{TPF}}{(dp/dL)_L}}$$
  
 $\lambda$  =  $[(0.075v_g)(62.3v_f)]^{-1/2}$   
 $\Psi$  =  $(73/v)[\mu_f(62.3v_f)^2]^{1/3}$   
 $\nu$  = surface tension of liquid phase, dynes/cm.

#### Subscripts

- $f$  = saturated liquid phase  
 $g$  = saturated vapor phase  
 $i$  = initial (subcooled) conditions  
 Absence of a subscript usually denotes an average property for the whole stream, such as  
 $W = W_f + W_g$   
 $v = (1-x)v_f + xv_g$   
 $O$  = orifice (used with other subscripts)  
 $TP$  = two phase  
 $hom$  = homogeneous flow  
 $crit$  = critical or sonic conditions  
 $vc$  = vena contracta

#### Pressure Gradients, lb.-force/(sq. ft./ft.)

- $dp/dL$  = static pressure gradient  
 $(dp/dL)_{ACC}$  = acceleration pressure gradient  
 $(dp/dL)_{EL}$  = gradient due to elevation differences  
 $(dp/dL)_{TPF}$  = two-phase frictional pressure gradient for whole stream ( $W$  lb.-mass/sec.)  
 $(dp/dL)_L$  = pressure gradient if only the liquid phase were flowing ( $W_f$  lb.-mass/sec., as a liquid)  
 $(dp/dL)_G$  = pressure gradient if only the vapor phase were flowing ( $W_g$  lb.-mass/sec., as a vapor)  
 $(dp/dL)_f$  = pressure gradient if the whole stream were flowing as a liquid ( $W$  lb.-mass/sec.)  
 $\Delta p_{OTP}$  = two-phase orifice pressure drop ( $W$  lb.-mass/sec.)  
 $\Delta p_{of}$  = orifice pressure drop if  $W$  lb. mass/sec. of liquid were flowing

#### LITERATURE CITED

- Alves, G. E., *Chem. Eng. Progr.*, **50**, 449 (1954).
- Baker, Ovid, *Oil Gas J.*, p. 185 (July 26, 1954).
- Begell, William, and J. W. Hoopes, Jr., "Acceleration Pressure Drops in Two-phase Flow," internal report (April 1954).
- Benjamin, M. W., and J. G. Miller, *Trans. Am. Soc. Mech. Engrs.*, **63**, 419 (1941).
- Bergelin, O. P., P. K. Kegel, F. G. Carpenter, and Carl Gazley, Jr., "Heat Transfer and Fluid Mech. Institute," p. 19, *Am. Soc. Mech. Engrs.* (1949).
- Linning, D. L., *Proc. Inst. Mech. Engrs.*, (London), **1B**, 64 (1952).

- Lockhart, R. W., and R. C. Martinelli, *Chem. Eng. Progr.*, **45**, 39 (1949).
- Martinelli, R. C., and D. B. Nelson, *Trans. Am. Soc. Mech. Engrs.*, **70**, 695 (1948).
- Calvert, Seymour, and B. C. Williams, *A.I.Ch.E. Journal*, **1**, 78 (1955).
- "The Reactor Handbook," vol. 2, p. 77, AECD-3546, Govt. Printing Office, Washington, D. C. (March 1955).

#### APPENDIX

##### Derivation of Equations

##### Kinetic Energy

The kinetic energy per pound of a homogeneous fluid or of a single phase of a mixture can be expressed by

$$KE = \frac{V^2}{2g_c J} = \frac{G^2 v^2}{2g_c J} = \frac{W^2 v^2}{S^2 2g_c J} \quad (10)$$

if the velocity profile is sufficiently flat. The average specific volume  $v$  of a two-phase mixture at rest or with phases moving at the same velocity is given by

$$v = (1-x)v_f + xv_g \quad (11)$$

Thus the expression for kinetic energy becomes for homogeneous flow

$$KE = \frac{G^2 [(1-x)v_f + xv_g]^2}{2g_c J} \quad (12)$$

In general, if  $V_f \neq V_g$ ,

$$V_f = \frac{W_f v_f}{R_f S} = \frac{(1-x)W v_f}{S R_f} \\ = (1-x) \frac{v_f}{R_f} G \quad (13a)$$

$$V_g = \frac{W_g v_g}{R_g S} = \frac{xW v_g}{S R_g} = x \frac{v_g}{R_g} G \quad (13b)$$

and the total kinetic energy per pound of mixture for flow with slip is then [from Equation (1)]

$$KE = \frac{G^2}{2g_c J} \left[ (1-x)^3 \frac{v_f^2}{R_f^2} + x^3 \frac{v_g^2}{R_g^2} \right] \quad (14)$$

Division of Equation (14) by (12) gives Equation (2).

##### Elevation Head

The head drop due to a change in elevation is calculated from the weight of the mixture which is included within cross sections  $\Delta Z$  apart.

The mass of liquid included in a length  $\Delta L$  is equal to  $R_f S \Delta L / v_f$ , and the mass of vapor is  $R_g S \Delta L / v_g$ . The component of the force of gravity acting in the direction of flow is then equal to

$$\left[ \frac{R_f}{v_f} + \frac{R_g}{v_g} \right] S \Delta L \frac{g}{g_c} \left( \frac{\Delta Z}{\Delta L} \right)$$

Expressed as a pressure gradient by dividing by  $S \Delta L$  and letting  $\Delta L$  become very small

$$\left( \frac{dp}{dL} \right)_{EL} = \left[ \frac{R_f}{v_f} + \frac{R_g}{v_g} \right] \frac{g}{g_c} \left( \frac{\Delta Z}{\Delta L} \right) \quad (15)$$

$g/g_c$  is equal to unity. For vertically downward flow

$$\frac{\Delta Z}{\Delta L} = -1$$

and Equation (3) results.

For a homogeneous fluid the mass of fluid included between the sections is merely  $S \Delta L / v$ , where  $v$  is given by Equation (11). Reasoning analogous to that used in deriving Equation (3) gives the expression

$$\left( \frac{dp}{dL} \right)_{EL, hom} = - \frac{1}{(1-x)v_g + xv_g} \quad (16)$$

##### Acceleration Pressure Drop

The pressure gradient due to acceleration is the rate of change with distance of the rate of momentum carried by the fluid, divided by the cross section. For a homogeneous fluid, momentum is carried past a cross section at a rate given by

$$\frac{W V}{g_c} = \frac{W G v}{g_c} \quad (17)$$

measured in pounds force. The acceleration pressure drop is obtained by taking the rate of change of this momentum flow with distance and dividing by the cross section. Equation (5) is obtained if  $v$  is evaluated by Equation (11).

The total rate of flow of momentum carried by a two-phase mixture is similarly found to be

$$\frac{W_f V_f}{g_c} + \frac{W_g V_g}{g_c} \quad (18)$$

Substitution of

$$W_f = (1-x)W \quad (19)$$

$$W_g = xW \quad (20)$$

$$V_f = \frac{(1-x)W v_f}{R_f S}$$

$$= (1-x) G \frac{v_f}{R_f} \quad (21)$$

$$V_g = \frac{xG v_g}{R_g} \quad (22)$$

differentiating and dividing by  $S$  gives Equation (4).

##### Application of Fanning Equation to Individual Phases

The Fanning equation for all liquid flow can be written as

$$\left( \frac{dp}{dL} \right)_f = \frac{f_f r_H V^2}{2g_c v_f} = \frac{f_f r_H W^2 v_f}{2g_c S^2} \quad (23)$$

A similar equation can be written for the liquid phase alone in two-phase flow

$$\left( \frac{dp}{dL} \right)_{TPf} = \frac{f_{TPf} r_{HTPf} V^2}{2g_c v_f} \\ = \frac{f_{TPf} r_{HTPf} (1-x)^2 W^2 v_f}{2g_c (R_f S)^2} \quad (24)$$

Thus the two-phase-pressure-drop ratio is obtained by division of Equation (24) by Equation (23).

# Hydraulics of Wetted-wall Columns

E. R. MICHALIK

Mellon Institute, Pittsburgh, Pennsylvania

On the assumption of laminar Newtonian flow, flow profiles are developed for both the vertical plate and cylindrical column by use of classical equations. From the flow profiles the mass transport, vertical pressure gradient, and optimal design parameters are calculated. With the Reynolds-number criterion used to ascertain the maximum nonturbulent velocity, minimal values for the plate distance and column radius can be calculated. An example is included for each case.

Where laminar Newtonian flow prevails, the flow profiles of both liquid and vapor streams can be computed by elementary classical methods. From these profiles one can find all other hydraulic characteristics of flow. The following development considers the wetted-wall column for two cases, the vertical flat plate and the cylindrical column, where it is assumed that laminar Newtonian flow prevails.

The development in each of the two cases can be broken up into three areas of interest. The first two sections in both cases deal with obtaining the differential equation in terms of velocity from equilibrium of forces and solving this differential equation by use of boundary conditions. These sections may or may not be of interest to most engineers. The third section in both cases deals with concepts of mass transport and pressure gradient in wetted-wall columns, which are obtained directly from the velocity equations. The developments in the three sections can stand alone.

The fourth section introduces the use of the Reynolds number of the vapor to determine a so-called "critical plate distance," or radius. The expression for velocity in the vapor stream as predicted by the Reynolds number contains the vapor-stream width, or diameter (hydraulic diameter), and if one assumes that the average velocity over the vapor-stream width is to remain less than that predicted by the use of Reynolds number, a simple mathematical manipulation will yield an upper boundary on plate distance, or radius, for any fixed ratio of vapor-stream width to plate width, or radius. Only the upper bound is of interest here, since for any fixed ratio a decrease in the plate width or radius would lessen both total mass flow and mass flow per unit area. The lower limit of plate distance or radius based upon vapor transport per unit area for all ratio values from 1 to 0 is of value, as it forms a lower boundary for design purposes. This expression is developed, and two examples showing the

use of the expressions developed are included. A three-dimensional graph is also included to show what the author has accomplished with the foregoing development.

It is hoped that the results of the fourth section can be used to interpret flow in packed columns after experimental verification, as it would otherwise be of no value. This might be accomplished by considering the packed column as an aggregate of small individual cylinders or large concentric cylinders.

## VERTICAL FLAT PLATES

### Basic Equations

The column is bounded by two vertical parallel planes separated by the distance  $2x_0$ . The reflux liquid flows downward by gravity as film on the walls and is symmetrically divided between them. Cartesian coordinates are taken with the  $yz$  plane parallel to and midway between the walls with the  $z$  axis vertically upward. The linear velocity of flow upward is  $W$  and horizontal components are zero. Further, for a given mass flow  $W$  is a function of  $x$  alone. The two interfaces are the planes  $x = \pm x_0$ , where  $x_0$ , the half thickness of the vapor path, is to be determined from the given operating conditions.

The fluids are both assumed to be Newtonian; that is, the tractive force per unit area is assumed to be equal to the product of the viscosity  $\eta$ , a constant property of the material, and the shear rate  $dW/dx$ . This law provides the starting point for the derivation of the flow distribution.

An element of volume in the liquid has width  $\Delta x$ , a unit length in  $y$  direction, and a thickness  $\Delta z$  in  $z$  direction. Steady state conditions in the liquid are defined as

$$F_1 + F_2 + F_3 = 0$$

where

$F$  = gravitational force =  $\Delta x \cdot \Delta z \cdot 1 \cdot \rho_l g$

$F_2$  = pressure gradient force =  $(\Delta p / \Delta z) \cdot \Delta z \cdot \Delta x \cdot 1$

$$F_3 = \text{shear force} = \Delta F_x = \eta_l (\Delta / \Delta x) (dW/dx) \Delta z \cdot \Delta x \cdot 1$$

Simplifying and passing to the limit, one gets the basic differential equation

$$\eta_l \frac{d^2 W_l}{dx^2} + Q = 0 \quad (1)$$

where  $Q = (dp/dz) + \rho_l g$

The corresponding vapor equation can be written as

$$\eta_v \frac{d^2 W_v}{dx^2} + \frac{dp}{dz} = 0 \quad (2)$$

since density term can be neglected.

If it is assumed that pressure gradient is only a function of height  $z$  ( $dp/dz$  is independent of  $x$ ), integration of Equation (1) twice yields

$$\eta_l W_l + \frac{x^2}{2} Q = C_1 x + C_2 \quad (3)$$

Integrating Equation (2) once gives

$$\eta_v \frac{dW_v}{dx} + x \frac{dp}{dz} = C_3 \quad (4)$$

( $dp/dz$  is independent of  $x$ )

and another integration yields

$$\eta_v W_v + \frac{x^2}{2} \frac{dp}{dz} = C_3 x + C_4 \quad (5)$$

### Boundary Conditions

In the vapor stream  $dW_v/dx = 0$  at  $x = 0$ ; hence from Equation (4)  $C_3 = 0$ , and in the liquid stream, since a no-slip condition at the walls is assumed,

$$W_l = 0 \text{ for } x = x_0 \text{ and } x = -x_0$$

Equation (3) therefore becomes

$$\eta_l W_l = \frac{Q}{2} (x_0^2 - x^2) \quad (6)$$

When a no-slip assumption is made at the interface, the limiting liquid and vapor velocities on the respective opposite sides of that plane are assumed equal, i.e.,  $W_l = W_v$  at  $x = x_0$ , and one gets upon substituting from Equation (5) with

E. R. Michalik is now with the Pittsburgh Plate Glass Company, Creighton, Pennsylvania.

$C_1 = 0$  into Equation (6) a value for  $C_1$  so that finally Equation (5) may be written as

$$\eta_s W_s = \frac{1}{2} \left[ \frac{\eta_s}{\eta_l} Q (x_0^2 - x_s^2) + \frac{dp}{dz} (x_s^2 - x^2) \right] \quad (7)$$

This completes the calculation of the flow profiles, Equation (6) expressing the velocity of the liquid in any plane  $x$  where  $x_s \leq x \leq x_0$  and Equation (7) giving the vapor velocity for  $x$  where  $0 \leq x \leq x_s$ .

#### Expressions for $dp/dz$ and Mass Transport

The velocities  $W_s$  and  $W_l$  calculated for the liquid and vapor streams are point functions and consequently are inherently dependent variables of only indirect engineering importance. The total mass flow rates, however, are of primary importance and can be calculated from the velocities by integrating them over the cross-sectional area of the streams. Thus

$$M_l = 2\rho_l \int_{x_s}^{x_0} W_l dx = \frac{\rho_l}{3\eta_l} Q(2x_0^3 - 3x_s x_0^2 + x_s^3) \quad (8)$$

and

$$M_s = 2\rho_s \int_0^{x_s} W_s dx = \frac{2\rho_s}{3\eta_s} x_s^3 \frac{dp}{dz} + \frac{\rho_s}{\eta_l} Q(x_0^2 x_s - x_s^3) \quad (9)$$

In practice the total mass flow rates are usually regarded as related to each other by an independent parameter, the reflux ratio  $R$ , where

$$R = (M_s - M_l)/M_s$$

The liquid holdup in the unit-area column is given by

$$H_l = \rho_l (x_0 - x_s)$$

Unfortunately, this is not uniquely determined for  $x_s$  and  $x_0$  independently, as it depends on the ratio  $x_s/x_0$ . Use of the Reynolds number to determine the onset of turbulence does fix the maximum value for  $x_0$  for any given ratio  $x_s/x_0$  when the system just reaches the turbulent stage. That there is a minimum value for  $x_0$  will also be shown. For the important case of  $M_s = M_l$ , equating Equation (9) to the negative of Equation (8) gives for the pressure gradient

$$\frac{dp}{dz} = -\rho_l g \frac{(3k_1 - 1)u^3 + 3(1 - k_1)u - 2}{(1 - 3k_1 + 2k_2)u^3 - 3(1 - k_1)u + 2} \quad (10)$$

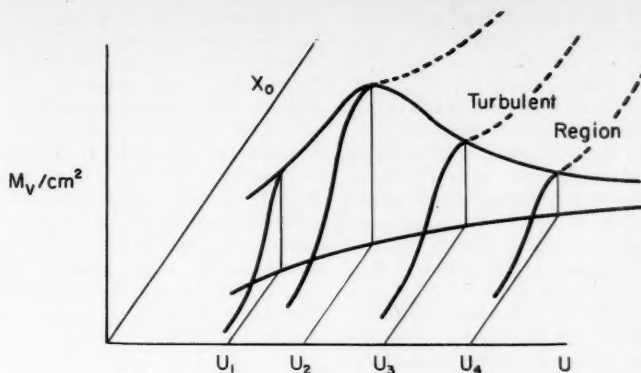


Fig. 1.

where

$$u = x_s/x_0, \quad k_1 = \rho_s/\rho_l, \quad k_2 = k_1\eta_l/\eta_s$$

This relation can be plotted graphically, and from such a curve  $u$  can be determined for values of  $dp/dz$ .  $[(1/\rho_l)g(dp/dz)]$  is monotonic and is  $-1$  when  $u = 0$  and equal to zero when  $u = 1$ . To determine  $x_0$  another criterion is necessary.

Equation (9), for use in the fourth section, can be written as

$$M_s = \rho_s x_0^3 u \left[ \frac{2}{3\eta_s} \frac{dp}{dz} u^2 + \frac{Q}{\eta_l} (1 - u^2) \right] \quad (10a)$$

which is in gram seconds<sup>-1</sup>, and the average mass transport in (gram centimeters<sup>-2</sup>)(second<sup>-1</sup>) is

$$\frac{M_s}{2x_s} = \rho_s \frac{x_0^2}{2} \left[ \frac{2}{3\eta_s} \frac{dp}{dz} u^2 + \frac{Q}{\eta_l} (1 - u^2) \right] \quad (10b)$$

where again  $u = x_s/x_0$

#### Critical Values for Plate Distance

An expression for the average velocity in the vapor stream can be obtained from the integral of the expression for the velocity equation (7). Thus

$$\bar{W}_s = \frac{1}{x_s} \int_0^{x_s} W_s dx = \frac{x_s^2}{3\eta_s} \frac{dp}{dz} + \frac{Q}{2\eta_l} (x_0^2 - x_s^2) \quad (11)$$

If it is assumed that the average velocity must be less than (or equal to) the velocity determined by the Reynolds number, then  $\bar{W}_{Rs} \geq \bar{W}_s$ ,

where

$$\bar{W}_{Rs} = \frac{Re\eta_s}{D\rho_s} = \frac{Re\eta_s}{4x_s\rho_s} \geq \bar{W}_s \quad (11a)$$

since  $4x_s = D$  (hydraulic diameter) and  $Re$  = Reynolds number.

Substituting expression (11) for  $\bar{W}_s$  in (11a) and solving the inequality for  $x_0^3$  one gets

$$x_0^3 \leq \frac{Re\eta_s}{2\rho_s u \left[ \frac{2}{3\eta_s} \frac{dp}{dz} u^2 + \frac{Q}{\eta_l} (1 - u^2) \right]} \quad (12)$$

where again  $u = x_s/x_0$ .

From simple considerations of the denominator in (12), it is obvious that  $x_0$  satisfies the inequality

$$x_0^3 \geq \frac{Re\eta_s}{2\rho_s \text{Max } u \left[ \frac{2}{3\eta_s} \frac{dp}{dz} u^2 + \frac{Q}{\eta_l} (1 - u^2) \right]} \quad (13)$$

This denominator in (13) has a maximum, as it is 0 for both  $u = 0$  and  $u = 1$  since  $(dp/dz) = 0$  when  $u = 1$ . It is positive throughout the range  $0 \leq u \leq 1$ .

To interpret the inequalities (12) and (13) an expression for mass vapor transport is required. This has been developed as Equation (10a). If the equality for  $x_0^3$  in Equation (12) is substituted in (10a), then the mass vapor transport in gram-seconds<sup>-1</sup> at the average critical velocity becomes

$$M_s = \frac{Re\eta_s}{2} \quad (14)$$

The inequality (12) states that for a fixed  $u$ ,  $x_0$  cannot exceed the right member as the critical velocity would be exceeded, and Equation (10a) clearly states that the mass vapor transport would decrease with decreasing  $x_0$  and fixed  $u$ . The inequality (13) forms an absolute lower bound for  $x_0$  for all  $u$  (Figure 1).

The following example illustrates the development. Values of  $u$  were arbitrarily chosen and the values of the pressure gradient from Equation (10) were calculated as shown in the second column in Table 1. To show that the denominator of the right member of (13) has a maximum, the third column of Table 1 was calculated by use of the results of columns 1 and 2 in the same table.

Table 2 was then readily obtained from Equations (12) and (14) and the results in Table 1. The last column in Table 2 is merely the third column divided by  $2x_s$ , sq. cm., as an area element of one unit in depth and  $2x_s$  units wide is assumed.

Since all the calculations are based upon operating just at the critical velocity range, the interpretation of the results in Table 2 is as follows. If, for example,  $x_0$  is chosen larger than 0.06757 cm., the value of  $u$  must be larger than 0.95 if turbulence is to be avoided. Or, if  $x_0$  is fixed at 0.06757 cm., then any increase in the liquid layer (decreasing  $u$ ) would cause the system to exceed the average critical velocity and enter the turbulent stage, since the table shows that a decreasing  $u$  must be associated with a decreasing  $x_0$ .

From an inspection of column 3 in Table 1, it is clear that the value of  $u = 0.74$  and corresponding  $x_0 = 0.03195$  in Table 2 form the lower bound on the half-plate distance.

Figure 1 is a three-dimensional graph of the surface with planes  $u = \text{constant}$  cutting the surface in the curves of which only the maximum ordinate is of interest in each slice. The graph is not intended to be used numerically but only as an aid to explaining the development.

#### Example

$$\begin{aligned}\rho_l &= 0.66 \text{ g./ml.} & \eta_l &= 0.0027 \text{ poise} \\ \rho_v &= 0.0036 \text{ g./ml.} & \eta_v &= 0.00011 \text{ poise} \\ Re \text{ of the vapor} &= 2,1000 \\ g &= 980.65 \text{ dynes/sq. cm.}\end{aligned}$$

TABLE 1

$u = x_s/x_0$	$1/(\rho_l g) \frac{dp}{dz}$	$1/(\rho_l g) M_v/x_0^3$
1	0	0
0.95	-0.03728	-0.57853
0.90	-0.14008	-2.03201
0.85	-0.29250	-3.69666
0.80	-0.45984	-4.92946
0.75	-0.61075	-5.45134
0.74	-0.63736	-5.47316
0.73	-0.66263	-5.47081
0.72	-0.68656	-5.44619

TABLE 2

$u = x_s/x_0$	$x_0$ , cm.	$M_v$ , g./sec.	$M_v$ , g./sq. cm. (sec.)
0.95	0.06757	0.1155	0.900
0.90	0.04445	0.1155	1.444
0.85	0.03642	0.1155	1.865
0.80	0.03308	0.1155	2.182
0.75	0.03198	0.1155	2.408
0.74	0.03195	0.1155	2.442

The results of the example can be interpreted pictorially as in Figure 1. The vertical ordinate is mass transport per unit area, and the two variables in the horizontal plane are  $x_0$  and  $u$ . The planes  $u_1, u_2, u_3$ , and  $u_4$  cut out curves on the surface. The values for  $M_v$ /sq. cm. in Table 1 correspond to the maximum ordinates on these curves. The largest

ordinate of this set of ordinates is represented on the curve with an  $x_0$  coordinate which corresponds to minimum  $x_0$  in the table and maximum value for  $M_v$ /sq. cm. For any fixed value of  $u$ , there is a value of  $x_0$  which corresponds to the maximum ordinate in the slice. If in this slice ( $u$  fixed)  $x_0$  were chosen smaller, then the  $M_v$ /sq. cm. would decrease. If the  $x_0$  were chosen larger, the system would no longer be in laminar flow but turbulent, and hence the mass transport per unit area would no longer be predictable with this model. This region on each slice is dashed.

#### CYLINDRICAL COLUMNS

##### Basic Equations

As in the vertical-plate system, laminar Newtonian flow is assumed to prevail in vapor and liquid streams. The flow profiles can be computed by elementary classical methods and hence all other hydraulic characteristics of the column can be found.

The cylinder radius is  $x_0$  and the radius of the vapor column  $x_s$ . The reflux liquid is assumed to flow downward under force of gravity as films on the walls. The liquid stratum is annular in form with width equal to  $x_0 - x_s$ .

The liquid and vapor are assumed, again, to be Newtonian; that is, the tractive force per unit area is assumed to be equal to the product of viscosity,  $\eta$ , a constant, and the shear rate  $dW/dx$ .

The elemental strip considered in this discussion is an annulus with an area of  $2\pi x \Delta x$ . Basic equations are developed from considerations of equilibrium of forces. As in the vertical-plate case, equilibrium conditions in the liquid layer are expressed by

$$\frac{d}{dx} \left( \eta_v x \frac{dW_v}{dx} \right) + xQ = 0 \quad (1')$$

This equation is analogous to Equation (1) in the vertical-plate case but since the elemental strip is an annulus the form of the equation is necessarily different.

The corresponding vapor equation, with the assumption of negligible density, is

$$\frac{d}{dx} \left( \eta_v x \frac{dW_v}{dx} \right) + x \frac{dp}{dz} = 0 \quad (2')$$

Integrating Equation (1') twice, one gets

$$\eta_v W_l = \frac{-x^2 Q}{4} + C_1 \ln x + C_2 \quad (3')$$

The corresponding vapor equation becomes after the first integration

$$\eta_v x \frac{dW_v}{dx} = \frac{-x^2 dp}{2 dz} + C_3 \quad (4')$$

and a second integration yields

$$\eta_v W_v = \frac{-x^2 dp}{4 dz} + C_3 \ln x + C_4 \quad (5')$$

##### Boundary Conditions

In the vapor stream, since the velocity profile is symmetric,  $dW_v/dx = 0$  at  $x = 0$ . Therefore, Equation (4') yields  $C_3 = 0$ , and so Equation (5') becomes

$$\eta_v W_v = \frac{-x^2 dp}{4 dz} + C_4 \quad (5'a)$$

In the liquid layer  $W_l = 0$  for  $x = x_0$  (no slip condition at walls); hence Equation (3') gives

$$C_2 = \frac{x_0^2 Q}{2} - C_1 \ln x_0$$

and so Equation (3') can be written as

$$\eta_l W_l = \frac{Q}{4} (x_0^2 - x^2) + C_1 \ln x/x_0 \quad (6')$$

Further, since  $W_l$  is finite for any  $x$  such that  $0 \leq x \leq x_0$ ,  $C_1$  must be 0 and Equation (6') for velocity in the liquid layer becomes

$$\eta_l W_l = \frac{Q}{4} (x_0^2 - x^2) \quad (6'a)$$

This corresponds to Equation (6) in the vertical-plate case.

In the vapor stream, since the limiting velocities at the interface of the liquid and vapor streams are assumed equal, one can write  $W_v = W_l$  at  $x = x_s$  so that Equation (6'a) may be set equal to (5'a) when  $x = x_s$ , whence a solution for  $C_4$  gives

$$C_4 = \frac{x_s^2 dp}{4 dz} + \frac{\eta_v}{4 \eta_l} Q (x_0^2 - x_s^2)$$

Finally the expression for vapor becomes

$$\begin{aligned}\eta_v W_v &= \frac{1}{4} \frac{\eta_v}{\eta_l} Q (x_0^2 - x_s^2) \\ &+ \frac{dp}{dz} (x_s^2 - x^2) \quad (7')\end{aligned}$$

which is similar to Equation (7) in the vertical-plate case.

This completes the velocity-profile developments. Equations (6'a) and (7') are quite essential in all that follows.

##### Expressions for Pressure Gradient and Mass Transport

Here, as in the vertical plate, explicit expressions will be obtained for the pressure gradient and mass transport by merely assuming an equilibrium state. Both the vapor mass transport and liquid mass transport per unit time are obtained by merely integrating over the velocity profiles. Then under assumption of equilibrium these two are set equal and the resulting equality yields an expression for pressure gradient.



Since

$$M_l = 2\pi\rho_l \int_{x_s}^{x_0} W_l x dx$$

$$= \frac{2\pi}{4} \frac{\rho_l}{\eta_l} Q \int_{x_s}^{x_0} x(x_0^2 - x^2) dx$$

$$= \frac{\pi}{2} \frac{\rho_l}{\eta_l} Q \left( \frac{x_0^2 - x_s^2}{2} \right)^2 \quad (8')$$

and

$$M_v = 2\pi\rho_v \int_0^{x_s} W_v x dx$$

$$= \frac{2\pi\rho_v}{4\eta_v} \int_0^{x_s} \left[ \frac{dp}{dz} (x_s^2 x - x^3) \right. \\ \left. + \frac{\eta_v}{\eta_l} Q (x_0^2 - x_s^2) x \right] dx$$

$$= \frac{\pi\rho_v}{2\eta_v} \left[ \frac{x_s^4}{4} \frac{dp}{dz} \right. \\ \left. + \frac{Q}{2} \frac{\eta_v}{\eta_l} (x_0^2 - x_s^2) x_s^2 \right] \quad (9')$$

Then setting  $M_v = -M_l$  and manipulating, one gets

$$\frac{dp}{dz} = -\rho_l g \frac{(1-u^2)^2 + k_1(1-u^2)u^2}{(1-u^2)^2 + k_2u^4 + 2k_1u^2(1-u^2)} \quad (10')$$

where  $k_1 = \rho_v/\rho_l$ ;  $k_2 = k_1\eta_l/\eta_v$  and  $u = x_s/x_0$ .

Here, too,  $dp/dz$  is monotonic, varying from 0 to  $-\rho_l g$  for  $1 \geq u \geq 0$ .

For calculation purposes it is better to write Equation (9') as

$$M_v = \frac{\pi\rho_v x_0^4 u^2}{8\eta_v} \cdot \left[ \left( \frac{2\eta_v Q}{\eta_l} - \frac{dp}{dz} \right) u^2 + \frac{2\eta_v Q}{\eta_l} \right] \quad (10'a)$$

whence the average mass transport per (centimeter square<sup>-1</sup>)(second<sup>-1</sup>), is

$$\frac{M_v}{\pi x_s^2} = \frac{\rho_v x_0^2}{8\eta_v} \cdot \left[ \left( \frac{2\eta_v Q}{\eta_l} - \frac{dp}{dz} \right) u^2 + \frac{2\eta_v Q}{\eta_l} \right] \quad (10'b)$$

Expression (10'b) has the value 0 at  $u = 0$  since  $dp/dz = -\rho_l g$  at  $u = 0$ . It has the value 0 at  $u = 1$  since  $dp/dz = 0$  at  $u = 1$ . Since the function is positive throughout  $0 \leq u \leq 1$ , it has a maximum for any assigned value of  $x_0$ .

#### Critical Values of Radius

As in the vertical-plate case, if one uses the Reynolds number to determine a critical velocity, certain limitations on the values of  $u$  and  $x_0$  will exist when this critical velocity is interpreted as the onset of turbulence. Values of the velocity (average velocity) in excess of the critical velocity would lead to turbulence. The critical velocity is given by  $W_{Re} = (Re \eta_v)/(2x_0\rho_v)$  where  $Re$  is Reynolds

number and  $2x_0$  is hydraulic diameter. The average velocity in the vapor stream is

$$\bar{W}_v = \frac{1}{x_s} \int_0^{x_s} W_v dx \quad (11')$$

$$= \frac{1}{4\eta_v} \left[ \frac{2}{3} x_s^2 \frac{dp}{dz} + \frac{\eta_v Q}{\eta_l} (x_0^2 - x_s^2) \right]$$

If one assumes nonturbulent flow, then  $\bar{W}_v \leq W_{Re}$ ; hence using (11') and the expression for  $W_{Re}$ , one gets as an inequality for  $x_0$

$$x_0^3 \leq \frac{6\eta_v \eta_l Re}{\rho_v \left[ 2 \frac{k_2}{k_1} \frac{dp}{dz} u^3 + 3Qu(1-u^2) \right]} \quad (12')$$

TABLE 1'

$u$	$1/(\rho_l g) dp/dz$	$x_0$	$M_v$ , g./sec.	$M_v$ , g./sq. cm. (sec.)
0.95	-0.0876	0.0776	$1.933 \times 10^{-2}$	1.132
0.90	-0.3008	0.0537	$1.305 \times 10^{-2}$	1.778
0.85	-0.5312	0.0468	$1.074 \times 10^{-2}$	2.160
0.80	-0.7007	0.0451	$0.971 \times 10^{-2}$	2.374
0.79	-0.7340	0.0451	$0.938 \times 10^{-2}$	2.354
0.75	-0.8209			

In Table 1'  $dp/dz$  was calculated for selected values of  $u$  by use of Equation (10') and  $x_0$  was calculated by use of Equation (12'). In the calculation of  $x_0$  from (12') the denominator of the right member had a maximum in the range of  $u = 0.80$  to  $0.79$ . This value then determines the optimum value for  $x_0$  from Equation (13'). The last column shows that the optimum value for mass transport per unit area results for an  $x_0 = 0.0451$  cm.

The interpretation of these results is identical to interpretation in the vertical-plate case, and Figure 1 is again applicable in a general sense.

#### NOTATION

$C_1, C_2, C_3, C_4$  = arbitrary constants in differential equations

$D$  = hydraulic diameter

$dp/dz$  = vertical pressure gradient

$dW/dx$  = shear rate

$g$  = gravitational constant

$H_l$  = liquid holdup

$k_1 = \rho_v/\rho_l$

$k_2 = k_1\eta_l/\eta_v$

$M_l$  = mass liquid flow, g./sec.

$M_v$  = mass vapor flow, g./sec.

$Q$  =  $dp/dz + \rho_l g$

$Re$  = Reynolds number (in vapor stream)

$u = x_s/x_0$

$W_l$  = linear velocity in liquid

$W_v$  = linear velocity in vapor

$\bar{W}_v$  = average linear velocity in vapor

$x_0$  = half-plate distance, or radius of cylinder

$x_s$  = half-vapor width, or radius of vapor stream

$\Delta$  = incremental operator

$\eta_l$  = viscosity of liquid

$\eta_v$  = viscosity of vapor

$\rho_l$  = density of liquid

$\rho_v$  = density of vapor

#### LITERATURE CITED

1. Lamb, Horace, "Hydrodynamics," Cambridge University Press (1924).
2. Prandtl, Ludwig, "Essentials of Fluid Dynamics," Hofner Publishing Company (translation of 1949 German ed.), New York (1952).

# Some Remarks on Longitudinal Mixing or Diffusion in Fixed Beds

RUTHERFORD ARIS and NEAL R. AMUNDSON

University of Minnesota, Minneapolis, Minnesota

It has been shown both theoretically and experimentally that the radial Peclet number in a packed bed approaches about 11. If it is assumed that the interstitial volume of the bed forms mixing cells, then a comparison of the solutions obtained from the mixing and turbulent diffusive mechanisms shows that the axial Peclet number for agreement of the two must be about 2, as a limiting case for high Reynolds numbers. This is substantiated by experiment.

The mechanism by which heat or mass is dispersed in a packed bed through which a fluid is flowing has been given a great deal of attention. It is assumed that the dispersion of heat or mass both axially and radially is a diffusional process superimposed upon a convective flow and that the whole is described by the partial differential equation

$$-\text{div}(-D \text{grad } c + \bar{V}c) = \frac{\partial c}{\partial t}$$

This equation is usually simplified further so that for the case of radial symmetry about the axis of mean flow

$$-V \frac{\partial c}{\partial x} + D_r \left( \frac{\partial^2 c}{\partial r^2} + \frac{1}{r} \frac{\partial c}{\partial r} \right) + D_a \frac{\partial^2 c}{\partial x^2} = \frac{\partial c}{\partial t} \quad (1)$$

with a similar equation for heat flow. The substitutions  $x = D_p y$ ,  $r = D_p \rho$ ,  $t = (D_p \tau)/V$  reduce Equation (1) to

$$-\frac{\partial c}{\partial y} + \frac{1}{Pe_r} \left( \frac{\partial^2 c}{\partial \rho^2} + \frac{1}{\rho} \frac{\partial c}{\partial \rho} \right) + \frac{1}{Pe_a} \frac{\partial^2 c}{\partial y^2} = \frac{\partial c}{\partial \tau}$$

where  $Pe_r = (VD_p)/D_r$  and  $Pe_a = (VD_p)/D_a$  which are the radial and axial Peclet numbers, respectively.

Considerable effort has been expended to relate the Peclet numbers to the fluid dynamical character of the problem. In particular, Bernard and Wilhelm (1) and Singer and Wilhelm (2) have shown that for sufficiently high Reynolds numbers and sufficiently high tube-to-particle-diameter ratio,  $Pe_r$  must be about 11. Baron (3) from a random-walk analogy in one dimension estimated  $Pe_r$  to be between 5 and 13, and Ranz (6) in a detailed analysis of the flows in a rhombohedrally packed bed of spheres showed that  $Pe_r$  is 11.2. For some time it was thought that packed-bed diffusion should be isotropic; however, recent measurements by Kramers and Alberda (5) indicated that the longitudinal Peclet number should be about 1 with a mixing-

cell model, and Wilhelm and his coworkers (10) showed that  $Pe_a$  must be about 2. (Perhaps the difference in the two results may be explained on the basis of bypassing, as different kinds of packing were employed.) Hence the diffusional process is anisotropic, the diffusional effect in the axial direction being considerably greater than anticipated.

It is the purpose of this paper to hypothesize a rather simple mechanism and to show on the basis of this mechanism that the Peclet number  $Pe_a$  must be about 2 for sufficiently high Reynolds numbers and for spherical packing material.

For the sake of definiteness it will be supposed that the bed is packed with spheres in a rhombohedral blocked-passage arrangement. The spheres are then in layers, each layer having a thickness of  $\gamma D_p$ ,  $\gamma = \sqrt{2}/3$ . The void fraction in such a bed is 0.2595, which may be assumed to be the average free area in the bed open to flow. If one examines the free area open to flow from a plane through the centers of a layer of spheres to a plane through the centers in the next layer, it is found that if the layer is divided into thirds, the first third has an average free area of 0.1827, the middle third 0.4132, and the top third 0.1827. The free area in a plane through sphere centers is 0.0933. Thus there are planes in the bed through which the velocity of the fluid is very high followed by regions in which the velocity is considerably less. It will be assumed therefore that the free volume in each layer, that is the layer between planes passing through sphere centers, serves as mixing cells for the fluid, the influent to a cell acting as a jet mixer and thereby increasing the turbulence in the free volume. The effluent from a cell will have the composition of the cell. This situation should certainly be approximated at high Reynolds numbers, and therefore the theory is a limiting one only. Since there is no lag assumed in the fluid flow from one cell to the next, a concentration signal will be instantaneously propagated in attenuated form through

the bed just as there is in conventional diffusion theory.

If, following Kramers and Alberda (5), one considers a series of well-agitated cells, numbered from 0 to  $n$ , initially free of solute, having a volume  $v$ , being fed with a stream  $q$ , and having introduced into the zeroth cell a solution with a concentration of  $c_f(t)$ , with  $t > 0$ , the system is described by

$$qc_{n-1} - qc_n = v \frac{\partial c_n}{\partial t}$$

$$c_n = 0, \quad t = 0$$

$$qc_f - qc_0 = v \frac{\partial c_0}{\partial t}, \quad t > 0$$

The Laplace transform  $\bar{c}_n$  of the solution  $c_n$  is

$$\bar{c}_n = \left( \frac{q}{v} \right)^{n+1} \frac{\bar{c}_f}{\left( \frac{q}{v} + p \right)^{n+1}}$$

and the inverse is

$$c_n = \frac{1}{n!} \left( \frac{q}{v} \right)^{n+1} \int_0^t c_f(\theta) (t - \theta)^n e^{-(q/v)(t-\theta)} d\theta$$

giving the concentration in the  $n$ th cell at time  $t$  due to a varying input.

If one defines  $\bar{c}_n$  by

$$\bar{c}_n = \frac{1}{n!} \left( \frac{q}{v} \right)^{n+1} \int_0^t c_f(\theta) (t - \theta)^n e^{-(q/v)(t-\theta)} d\theta$$

then  $\bar{c}_n$  is that part of the concentration in the  $n$ th cell at time  $t$  which results from  $q c_f(\theta) d\theta$  molecules having been introduced into the zeroth cell at time  $\theta$ . Therefore

$$\frac{\bar{c}_n(\theta) v}{q c_f(\theta) d\theta} = \left( \frac{q}{v} \right)^n \frac{1}{n!} (t - \theta)^n e^{-(q/v)(t-\theta)}$$

is the fraction of those molecules introduced at time  $\theta$  over a time interval  $d\theta$

which are in the  $n$ th cell at time  $t$  or, alternatively, by Bernoulli's theorem

$$P_p = \frac{\left(\frac{q}{v}t\right)^n e^{-(q/v)t}}{n!}$$

is the probability that a molecule introduced into the bed at time  $t = 0$  is in the  $n$ th layer at time  $t$ . One immediately recognizes this as a Poisson probability density function with a mean and dispersion given respectively by (1)

$$\mu_p = \frac{q}{v}t$$

$$D_p = \frac{q}{v}t$$

If one considers the corresponding problem phrased in diffusion language, the required equations are

$$-V \frac{\partial c}{\partial x} + D \frac{\partial^2 c}{\partial x^2} = \frac{\partial c}{\partial t} \quad (2)$$

$$Vc_f(t) = Vc - D \frac{\partial c}{\partial x},$$

$$x = 0, \quad t > 0 \quad (3)$$

$$c = 0, \quad t < 0 \quad (4)$$

where  $D$  is used for  $D_a$ . It will be shown that probability considerations dictate the use of Equation (3) rather than the condition  $c = c_f(t)$  at  $x = 0$ . This has been discussed in some detail by Kramers and Alberda (5), Danckwerts (3), Wehner and Wilhelm (9), and others. The Laplace transform  $\bar{c}$  of the solution  $c$  to Equations (2), (3), and (4) is

$$\bar{c} = \bar{c}_f \frac{V \exp\left\{\frac{Vx}{2D}\right\} \exp\left\{-\frac{x}{\sqrt{D}} \sqrt{\frac{V^2}{4D} + p}\right\}}{D\left(\frac{V}{2D} + \frac{1}{\sqrt{D}} \sqrt{\frac{V^2}{4D} + p}\right)}$$

The inverse transform may be obtained to give

$$c(t) = V \int_0^t c_f(\theta) P_d(x, t - \theta) d\theta$$

where

$$P_d(x, \theta) = \frac{1}{\sqrt{\pi D \theta}} \exp\left\{-\frac{(x - V\theta)^2}{4D\theta}\right\}$$

$$- \frac{V}{2D} \exp\left\{\frac{Vx}{D}\right\} \operatorname{erfc}\left(\frac{x + V\theta}{2\sqrt{D\theta}}\right).$$

$$\frac{\bar{c}(\theta) dx}{Vc_f(\theta) d\theta} = P_d(x, t - \theta) dx$$

is the fraction of those molecules introduced at time  $\theta$  over an interval of time  $d\theta$  which are in a volume element  $1 \cdot dx$  at  $x$  at time  $t$ . In other words

$$P_d(x, t) dx \quad (5)$$

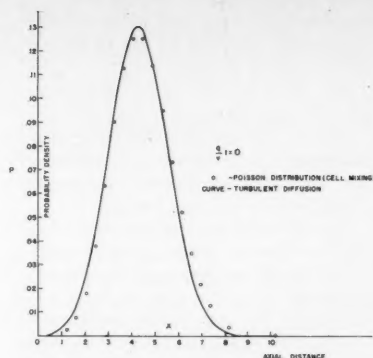


Fig. 1. Comparison of cell mixing and diffusional mechanisms with data as given in the numerical example  $(q/v)t = 10$ .

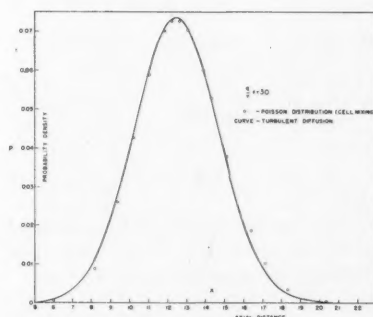


Fig. 2. Comparison of cell mixing and diffusional mechanisms with data as given in the numerical example  $(q/v)t = 30$ .

is the probability that a molecule introduced into the bed at  $x = 0$  at time  $t = 0$  is in a volume  $1 \cdot dx$  at  $x$  at time  $t$ .  $P_d(x, t)$  is then the probability density function. In order to make this quantity dimensionless it is desirable to let

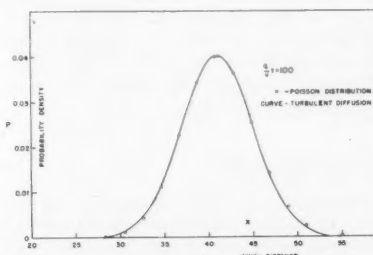


Fig. 3. Comparison of cell mixing and diffusional mechanisms with data as given in the numerical example  $(q/v)t = 100$ .

$x = \gamma D_p z$  so that the probability density function becomes

$$\gamma D_p P_d(\gamma D_p z, t) \quad (6)$$

This analysis could have been carried out by a random walk with a suitable bias on the steps as in reference 8.

In order to show that this is a real probability function it is essential to show that

$$\int_0^\infty P_d(x, t) dx = 1$$

This is rather tedious but may be carried out with ease in the  $p$  plane to give

$$\int_0^\infty \bar{P}_d(x, p) dx = \frac{1}{p}$$

where  $\bar{P}_d$  is the Laplace transform of  $P_d$ , and since the Laplace transform of 1 is  $1/p$  the particle is certainly somewhere in the bed. Thus the use of boundary condition (3) ensures that a molecule once admitted remains in the bed.

Thus the two alternative mechanisms produce two different probability density functions  $P_p$  and  $P_d$ . It is well known that the Poisson probability density may be approximated by the normal density function

$$P_p \cong \frac{1}{\sqrt{4\pi Dt}} \exp\left\{-\frac{(x - Vt)^2}{4Dt}\right\}$$

The function  $P_d$  may be written in the form

$$\frac{1}{\sqrt{\pi Dt}} \exp\left\{-\frac{(x - Vt)^2}{4Dt}\right\} \left[1 - \frac{Vt}{x + Vt} \left(1 - \frac{2Dt}{(x + Vt)^2} + \frac{12D^2t^2}{(x + Vt)^4} \dots\right)\right]$$

by making use of the asymptotic expansion for the erfc. For large values of  $x + Vt$  and in particular for  $x$  in the neighborhood of  $Vt$ , this expression reduces to

$$P_d(x, t) = \frac{1}{\sqrt{4\pi Dt}} \exp\left\{-\frac{(x - Vt)^2}{4Dt}\right\}$$

and hence  $P_d$  approaches, in the neighborhood of the mean at least, the normal density function. The mean and dispersion of the dimensionless normal density function are (4)

$$\mu_n = Vt/\gamma D_p$$

$$D_n = 2Dt/\gamma^2 D_p^2$$

If these density functions are to give the same distribution of solute in the bed, the means and dispersions must be equal so that

$$\frac{Vt}{\gamma D_p} = \frac{q}{v}t$$

$$\frac{2Dt}{(\gamma D_p)^2} = \frac{q}{v} t$$

where the dimensionless form of the normal density function is

$$P_n(x, t) = \frac{\gamma D_p}{\sqrt{4\pi Dt}} \exp \left\{ -\frac{(\gamma D_p z - Vt)^2}{4Dt} \right\}$$

Hence there results

$$\frac{VD_p}{D} = \frac{2}{\gamma}$$

For rhombohedral close packing

$$\frac{VD_p}{D} = \frac{2}{0.815} = 2.46 \quad (7)$$

and for random packing  $\gamma$  is about 1 or less, and thus

$$\frac{VD_p}{D} \cong 2$$

as was to be shown.

In this analysis it was shown that the Poisson distribution and diffusional distribution each approached the normal distribution some distance from the bed entrance. It was then suggested that the means and dispersions of the Poisson and normal distributions should be the same. In order to make the analysis complete one should compare all the moments of the Poisson and diffusional distributions. This is tedious, however, and leads to integrals which are difficult to evaluate or estimate. Since the purpose here has been to show the possibility that intracellular mixing obtained in the bed, it is instructive perhaps to exhibit some numerical comparisons of the distribution functions.

A rhombohedrally packed blocked-passage bed with spheres 5 mm. in diameter will be considered. The interstitial average velocity of the fluid is 2 cm./sec. A bed cross section of 1 sq. cm. is taken as a unit.

$$\begin{aligned} D_p &= 0.5 \text{ cm.} \\ \alpha &= 0.2595 \\ \gamma &= 0.817 \\ v &= 0.106 \text{ cc./sq. cm. of bed cross section} \\ V &= 2 \text{ cm./sec.} \\ Pe_a &= VD_p/D = 2.46 \\ D &= (2)(0.5)/2.46 = 0.408 \text{ sq. cm./sec.} \end{aligned}$$

Thus the turbulent diffusivity must be chosen as 0.408 if the two mechanisms are to agree. Also

$$\begin{aligned} q &= \alpha V = 0.519 \text{ (cc./sec.) / sq. cm. of bed cross section} \\ V/D &= 4.908 \text{ cm.}^{-1} \end{aligned}$$

It should be noted that  $q$  and  $v$  are defined for 1 sq. cm. of bed cross section. Thus  $q$  is identical with the superficial

velocity in the bed and  $v$  is the volume of a cell contained in 1 sq. cm. of bed cross section and is  $\gamma D_p$  cm. deep.

Figures 1, 2, and 3 were then plotted,  $(qt/v)$  being chosen as a parameter. For  $(q/V)t = 100$  the two mechanisms give distribution plots which are indistinguishable. In all cases, however, the agreement is satisfactory and convincing.

Earlier in the paper some mention was made of the use of the proper boundary condition. If one assumes the boundary condition to be  $c = c_f$  where  $c_f$  is a constant for  $t > 0$ , it is then a simple matter to show that the diffusive mechanism gives as the Laplace transform of the solution

$$\bar{c} = \frac{c_f}{p} \exp \left\{ \frac{Vx}{2iD} \right\} \cdot \exp \left\{ -\frac{x}{\sqrt{D}} \sqrt{\frac{V^2}{4D} + p} \right\}$$

the inverse of which is

$$c = c_f \int_0^t \frac{x}{\sqrt{4\pi D\theta^3}} \cdot \exp \left\{ -\frac{(x - V\theta)^2}{4D\theta} \right\} d\theta$$

In order to calculate the total number of molecules in the bed at any time, one may form the quantity

$$\Sigma = \int_0^\infty c(x, t) dx$$

It is somewhat easier to integrate the Laplace transform of  $c(x, t)$  from zero to infinity and then to invert the transform to give

$$\begin{aligned} \Sigma &= c_f \int_0^\infty \left[ \frac{\sqrt{D}}{\sqrt{\pi t}} \exp \left\{ -\frac{V^2}{4D} \right\} \right. \\ &\quad \left. + \frac{V}{2} + \frac{V}{2} \operatorname{erf} \left( \frac{V\theta}{2\sqrt{D}} \right) \right] d\theta \quad (8) \end{aligned}$$

The boundary condition  $c = c_f$  might be expected to ensure that the number of molecules in the bed would increase linearly with the time. However, Equation (8) does not indicate this, and hence molecules once admitted to the bed have back mixed out of the bed. If one accepts the hypothesis that the packing is responsible for the mixing, this hardly seems possible, and  $c = c_f$  at  $x = 0$  appears to be an improper boundary condition. This diffusion involves only turbulent, and not molecular, diffusion.

#### ACKNOWLEDGMENT

The authors are indebted to R. L. Storrer, who made the calculations for Figures 1, 2, and 3.

It should be pointed out that the authors, after the first review of this paper, had the advantage of examining a paper by Wilhelm and McHenry (10).

#### NOTATION

- $c$  = concentration in diffusive mechanism, moles/cc.
- $c_n$  = concentration in  $n$ th cell, moles/cc.
- $c_f$  = influent concentration, moles/cc.
- $\bar{c}$  = fractional concentration as defined in text
- $D$  = diffusion or mixing coefficient, sq. cm./sec.
- $D_p$  = particle packing diameter, cm.
- $D_a$  = axial diffusion coefficient, sq. cm./sec.
- $D_r$  = radial diffusion coefficient, sq. cm./sec.
- $d$  = dispersion of a distribution about the mean
- $\operatorname{erf}(x) = \frac{2}{\sqrt{\pi}} \int_0^x e^{-\alpha^2} d\alpha$
- $\operatorname{erfc}(x) = 1 - \operatorname{erf}(x)$
- $P$  = symbol for a probability density function
- $Pe_r, Pe_a$  = Peclet numbers as defined in text
- $q$  = flow rate, cc./sec. (sq. cm.) of bed cross section
- $r$  = radius variable, cm.
- $\rho$  = dimensionless radius variable
- $t$  = time, sec.
- $V$  = interstitial velocity, cm./sec.
- $V_0$  = superficial velocity =  $\alpha V$ , cm./sec.
- $v$  = volume of a cell =  $\alpha \gamma D_p$ , cc./sq. cm. of bed cross section
- $x$  = axial variable, cm.
- $y$  = dimensionless axial variable
- bars in general indicate Laplace transform

#### Subscripts

- $p$  = Poisson
- $d$  = diffusion
- $n$  = normal

#### Greek Letters

- $\alpha$  = fractional void volume
- $\gamma$  = distance between successive layers of spheres
- $\mu$  = mean of a distribution
- $\tau$  = time (dimensionless) =  $V_0 t / D_p \alpha$
- $\theta$  = time, sec.

#### LITERATURE CITED

1. Bernard, R. A., and R. H. Wilhelm, *Chem. Eng. Progr.*, **46**, 233 (1950).
2. Baron, Thomas, *ibid.*, **48**, 118 (1952).
3. Danckwerts, P. V., *Chem. Eng. Sci.*, **2**, 1 (1953).
4. Fry, T. C., "Probability and Its Engineering Uses," D. Van Nostrand and Company, New York (1928).
5. Kramers, H., and G. Alberda, *Chem. Eng. Sci.*, **2**, 173 (1953).
6. Ranz, W. E., *Chem. Eng. Progr.*, **48**, 247 (1952).
7. Singer, E., and R. H. Wilhelm, *ibid.*, **46**, 343 (1950).
8. Wax, N., Editor, "Noise and Stochastic Processes," Dover Publications, New York (1954).
9. Wehner, J. F., and R. H. Wilhelm, prepublication manuscript.
10. Wilhelm, R. H., and K. W. McHenry, *A. I. Ch. E. Journal*, **3**, 83 (1957).



# Mass Transfer in a Continuous-flow Mixing Vessel

D. W. HUMPHREY and H. C. VAN NESS

Purdue University, Lafayette, Indiana

Mass transfer coefficients have been determined for the dissolution of  $\text{Na}_2\text{S}_2\text{O}_5 \cdot 5\text{H}_2\text{O}$  crystals in water under conditions of turbulent agitation in a mixing vessel. The dissolution was carried out in a steady-flow process in which the area of salt crystals and the concentration of the solution in the mixing vessel were constant during each run. A comparison is made with previously unpublished results for batch runs in a similar system, and a method is developed for calculating the surface area of salt particles suspended in the mixing vessel under steady-flow conditions.

Relatively little attention has been given in recent years to the problem of determining mass transfer coefficients for the dissolution of solids in liquids in agitated systems. A major portion of the work reported on this subject has been done by Hixson and coworkers (1 to 5), and Wilhelm, Conklin, and Sauer (10) and Mack and Marriner (8) have also published experimental results. Most recently Johnson and Huang (7) described a series of experiments designed for a basic study of rates of dissolution of solids from a flat surface into liquids under turbulent agitation in a mixing tank.

All these experiments have been carried out in batch systems wherein the agitated liquid is brought in contact with an initial quantity of salt. As dissolution occurs, the surface area of the solid phase and the concentration of the agitated solution change continuously from the beginning to the end of a run. Since the rate of mass transfer from solid to liquid depends on both surface area and concentration, it also varies continuously with time. This obviously complicates the taking of data and the calculation of mass transfer coefficients for such systems, and it may partly explain why so few experimental investigations have been made of this subject.

One method of obviating these difficulties is to design a steady-flow system in which salt and solvent are continuously added to an agitated solution in a mixing tank while the solution is continuously withdrawn. At steady state the surface area of the solid and the concentration of the solution remain constant. The concentration of the solution can then be readily measured, and the surface area of the solid can be calculated by a method to be described. The objective of the present research was to investigate the use of such a system for the purpose of determining mass transfer coefficients.

D. W. Humphrey is at present with Research Laboratories, Standard Oil Company of Indiana, Whiting, Indiana, and H. C. Van Ness is at Rensselaer Polytechnic Institute, Troy, New York.

the salt crystals from a bin and dumped them into the tank. In a steady state system the feed rate is, of course, equal to the rate of solution.

The approximate experimental conditions are given in Table 1. Original experimental data are given by Humphrey (6).

## THE MASS TRANSFER COEFFICIENT

According to the film theory, the mass transfer of salt from the surface of a salt particle to the main body of a turbulent liquid is treated as if it occurred by molecular diffusion through a laminar layer of liquid surrounding the salt particle, the layer being thick enough to contain all the concentration gradient. Since the degree of agitation affects the rate of mass transfer, it is assumed to control the thickness of this laminar layer. The rate of mass transfer by diffusion through the laminar layer is given by the equation

$$(N_s)_d = -D_s A_s \frac{dC_s}{dy} \quad (1)$$

Mass transfer by bulk flow also occurs in the laminar film, however, because the solvent diffuses toward the solid-liquid interface under the influence of the concentration gradient and can be removed only by bulk flow of solution from the interface to the main body of the liquid. The rate of diffusion of solvent toward the interface is given by an equation analogous to Equation (1):

$$(N_f)_d = D_f A_s \frac{dC_f}{dy} \quad (2)$$

The picture is further complicated by the fact that the salt used in this work ( $\text{Na}_2\text{S}_2\text{O}_5 \cdot 5\text{H}_2\text{O}$ ) contained water of hydration, which can be transferred to the main body of the aqueous solution only by bulk flow. Bulk flow refers only to the movement of solution as a unit away from the interface, and thus it accomplishes transfer of salt as well as solvent from the interface to the main body of the solution. The total rate of transfer of salt is the sum of the rates of transfer by molecular diffusion and by bulk flow:

$$(N_s)_t = (N_s)_d + (N_s)_b \quad (3)$$

Similarly, the rate of transfer of water from the interface to the main body of solution is

$$(N_f)_t = (N_f)_b - (N_f)_d \quad (4)$$

TABLE 1. APPROXIMATE EXPERIMENTAL CONDITIONS

	Propeller	Turbine
Impeller speed, rev./min.	From 400 to 1,300	From 200 to 600
Water-flow rate, gal./min.	1.3	1.3
Feed rate of hydrated salt, g./min.	105	From 75 to 125
Initial surface area of salt, sq. ft./lb.	15.6	From 9.0 to 15.6

The salt used for this purpose was sodium thiosulfate pentahydrate ( $\text{Na}_2\text{S}_2\text{O}_5 \cdot 5\text{H}_2\text{O}$ ) in the form of commercial *Hypo rice*, and tap water was used as the solvent. *Hypo rice* was selected because of its ready availability, its regular crystalline form, and the relative ease with which it may be suspended in water.

## EXPERIMENTAL

A schematic diagram of the equipment is shown in Figure 1. The mixing vessel was a flat-bottomed, cylindrical can, 1 ft. in diameter and 15 in. high. It contained four symmetrically located baffles which extended 1 in. from the side of the vessel. Two impellers were used, one a three-blade, 4-in.-diam., marine-propeller type and the other a six-blade (flat), 4-in., radial-flow turbine manufactured by The Mixing Equipment Company. Both were mounted centrally and vertically in the mixing tank three in. from the bottom, speed control being obtained by a pulley system between the shaft and the motor. The liquid depth in the tank was maintained at 12 in.

Water was fed to the mixing vessel from a constant-head tank. Solution flowed from the mixing tank through an overflow tap in the side of the tank. The outlet was covered with a 40-mesh screen to prevent salt particles from leaving the tank. The water line and the overflow line were fitted with quick-closing valves so that flow in both might be stopped simultaneously. The overflow line also contained an orifice and a conductivity cell for indicating flow rate and concentration, which were used merely to show when steady state was reached.

The salt feeder consisted of a rotating wheel fitted with small buckets, which lifted

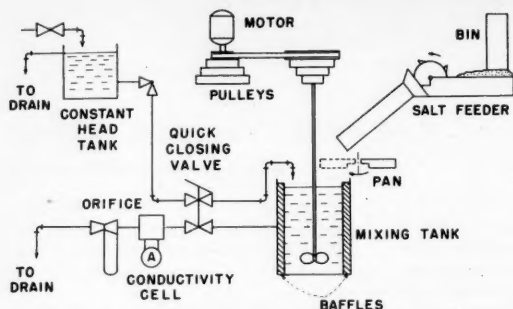


Fig. 1. Schematic diagram of equipment.

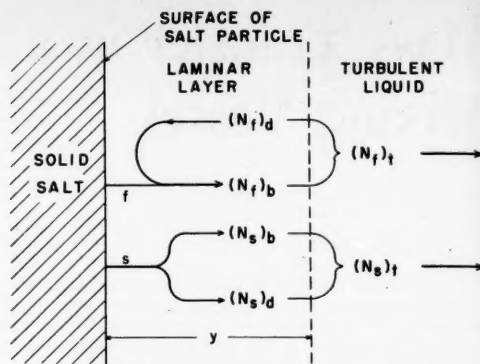


Fig. 2. Mechanisms of mass transfer.

These various transfer mechanisms are illustrated schematically in Figure 2.

Since bulk flow amounts to transporting the solution as a whole, the total rate of bulk flow of salt plus water at any point in the laminar film is

$$\frac{(N_f)_b}{1 - x_s} = \frac{(N_s)_b}{x_s} \quad (5)$$

where  $x_s$  is the mole fraction of salt in the laminar film at any point.

Furthermore, the over-all result of all transfer operations is to put the hydrated salt in solution. Thus:

$$\frac{(N_s)_i}{z_s} = \frac{(N_f)_i}{1 - z_s} \quad (6)$$

where  $z_s$  is the fraction of the total transfer that is salt, i.e., the mole fraction of salt ( $\text{Na}_2\text{S}_2\text{O}_3$ ) in the hydrate ( $\text{Na}_2\text{S}_2\text{O}_3 \cdot 5\text{H}_2\text{O}$ ).

Equations (1) through (6) may be combined to give the total rate of transfer of salt at any point in the laminar film:

$$(N_s)_i = \frac{z_s A_s}{z_s - x_s} \left[ x_s D_f \left( \frac{dC_f}{dy} \right) - (1 - x_s) D_s \left( \frac{dC_s}{dy} \right) \right] \quad (7)$$

If the concentrations in Equation (7) are replaced by

$C_s = (\rho/M)x_s$  and  $C_f = (\rho/M)(1 - x_s)$  after suitable rearrangement it becomes

$$(N_s)_i = -\frac{z_s A_s D_s (\rho/M)}{(z_s - x_s)} \left( \frac{dx_s}{dy} \right) + \frac{z_s A_s x_s (D_f - D_s)}{z_s - x_s} \left[ (1 - x_s) \frac{d(\rho/M)}{dy} + (\rho/M) \frac{dx_s}{dy} \right] \quad (8)$$

In most instances the second term on the right of Equation (8) is small compared with the first term, and in the interest of simplicity it may be neglected. The reason for this is that  $x_s$  is usually small even for saturated solutions, and for sodium thiosulfate its maximum value at room temperature is 0.065.

Also, this term will vanish if  $D_f$  and  $D_s$  are the same. Although this is true for ideal gases, it is not necessarily true for liquids. Neglecting this term, leads to an equation analogous to that used for gaseous diffusion:

$$(N_s)_i = -\frac{z_s A_s D_s (\rho/M)}{(z_s - x_s)} \left( \frac{dx_s}{dy} \right) \quad (9)$$

Since  $(N_s)_i$  is constant, integration of Equation (9) from the interface to the bulk conditions gives

$$(N_s)_i = \frac{z_s A_s D_s (\rho/M)_m}{y} \cdot \ln \left[ \frac{z_s - (x_s)_2}{z_s - (x_s)_1} \right] \quad (10)$$

where the subscript 2 indicates bulk conditions and 1, the saturation value at the interface. If the mass transfer coefficient is defined as  $K' = D_s/y$ , Equation (10) becomes

$$(N_s)_i = K' z_s A_s (\rho/M)_m \cdot \ln \left[ \frac{z_s - (x_s)_2}{z_s - (x_s)_1} \right] \quad (11)$$

where  $(\rho/M)_m$  is the arithmetic mean of the values at the interface and in the bulk of the solution. Equation (11) was used in this work for the calculation of values of  $K'$ . For  $\text{Na}_2\text{S}_2\text{O}_3 \cdot 5\text{H}_2\text{O}$ ,  $z_s$  has a value of  $1/6$ . If  $z_s$  is unity and if  $(x_s)_2$  and  $(x_s)_1$  are small, this equation reduces to the more common form:

$$(N_s)_i = K(\rho/M) A_s (x_{s1} - x_{s2}) = K A_s (C_{s1} - C_{s2})$$

#### SURFACE AREA DETERMINATION

The calculation of mass transfer coefficients by Equation (11) requires that the surface area of the suspended salt particles be known. This area was calculated from the weight of suspended salt particles and their initial area, the weight being determined by stopping all flows simultaneously at the end of a run and measuring the increase in concentration of the solution caused by the dissolution of the suspended salt. In all cases con-

centrations were determined by titration with a standardized iodine solution.

Consider the dissolution of a single salt particle having an instantaneous weight  $W_i$  and area  $A_i$ . If it is assumed that the shape of the particle does not change as it dissolves, then

$$W_i = E^3 Q^3 \quad (12)$$

and

$$A_i = \alpha E^2 Q^2 \quad (13)$$

where  $Q$  = equivalent diameter of the particle, i.e., the diameter of a sphere equal in volume to the salt particle, and  $E$  and  $\alpha$  = constants depending on the density and shape of the particle.

Equation (11) may be written for an individual salt particle as it dissolves in a system at steady state:

$$\frac{1}{M_s} \left( \frac{dW_i}{d\theta} \right) = A_i (\rho/M)_m K' z_s \cdot \ln \left[ \frac{z_s - (x_s)_2}{z_s - (x_s)_1} \right] \quad (14)$$

If  $W_i$  and  $A_i$  are eliminated by Equations (12) and (13) and the resulting equation is integrated for steady-flow conditions, the result is

$$Q = Q_0 - \frac{\theta \alpha M_s (\rho/M)_m K' z_s}{3E} \cdot \ln \left[ \frac{z_s - (x_s)_2}{z_s - (x_s)_1} \right] \quad (15)$$

This equation shows that the equivalent diameter of a single salt particle  $Q$  is a linear function of the time after it was introduced, as all other quantities in the equation are independent of time.

Therefore at any time during the steady-flow process a series of sizes of salt particles will be present in the mixing tank, one size for each different moment a particle was added to the tank. Since the salt particles were added at a regular period, and all were of approximately the same size initially, the sizes which exist in the tank at the moment a particle is added are

$$\frac{Q_0}{s}, \frac{2Q_0}{s}, \frac{3Q_0}{s}, \dots, \frac{jQ_0}{s}, \dots, \frac{sQ_0}{s}$$

Of course, at other times the sizes will be slightly different, but this series of sizes is adequate for an excellent approximation of the surface area when  $s$  is large. The area of all salt particles in the mixing tank is calculated by summing the areas of all sizes of the series. For this purpose it is convenient to relate the total area of the salt particles suspended in the mixing tank to some collective property such as their total weight:

$$A_s = BW_s \quad (16)$$

The coefficient  $B$  was evaluated from Equations (16), (12), and (13) as follows:

$$B = \frac{A_s}{W_s} = \frac{\sum_{j=0}^s \alpha E^2 (jQ_0/s)^2}{\sum_{j=0}^s E^3 (jQ_0/s)^3}$$

$$= \frac{\alpha \sum_{j=0}^s j^2}{EQ_0 \sum_{j=0}^s j^3}$$

$$B = \left( \frac{\alpha}{EQ_0} \right) \left[ \frac{(s)(s+1)(2s+1)/6}{s^2(s+1)^2/4} \right]$$

$$= \frac{2\alpha}{3EQ_0} \left( 2 - \frac{1}{s+1} \right)$$

For large values of  $s$  (In the present work  $s$  was about 500.) this becomes

$$B = \frac{4}{3} \left( \frac{\alpha}{EQ_0} \right) \quad (17)$$

but

$$\frac{A_0}{W_0} = \frac{\alpha E^2 Q_0^2}{E^3 Q_0^3} = \frac{\alpha}{EQ_0} \quad (18)$$

Equations (16), (17), and (18) may be combined to give

$$A_s = (4/3)(A_0/W_0)W_s \quad (19)$$

The equation for the surface area of suspended salt particles at steady state was developed on the assumption that all salt particles added to the solution were initially of the same size and shape. Actually this was only approximately true. However, Equation (19) should be valid for a small range of initial particle sizes and shapes if a representative mean value is used for  $A_0/W_0$ . Since the crystals used in this work were approximately cylindrical in shape, the initial area was determined from their average linear dimensions.

## RESULTS

The mass transfer coefficients as calculated by Equation (11) were correlated by an equation of the type suggested by Hixson and Baum (2):

$$\frac{K'd}{D_s} = a \left( \frac{\mu}{\rho D_s} \right)^{0.5} \left( \frac{nd^2 \rho}{\mu} \right)^b \quad (20)$$

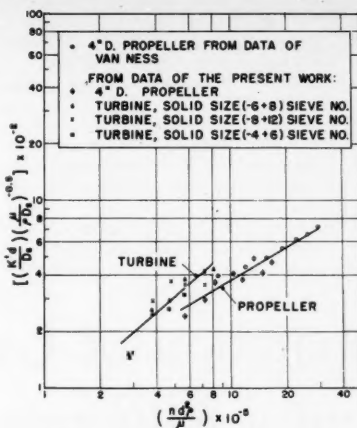


Fig. 3. Correlation of mass transfer coefficients.

The 0.5 power on the Schmidt group has been established both by Hixson and Baum (2) and by Johnson and Huang (7). The power  $b$  on the Reynolds number varies from system to system, as does the coefficient  $a$ . In the present work the results for the propeller showed  $a$  to be 0.13 and  $b$  to be 0.58. Results for the turbine gave  $a$  as 0.0032 and  $b$  as 0.87. These results were determined from the lines shown on Figure 3.

Included on this plot are some results obtained a number of years ago by one of the authors (9) for batch experiments in an identical system with the same propeller that was employed in the present work. No runs were made at that time with the turbine. It is seen that the results for the batch runs with this propeller correlate well with the results of the steady-flow runs of the present investigation for the same propeller.

## DISCUSSION

The most significant result of this research is the agreement of the steady-flow results with the batch results reported by Van Ness (9) for the same system. This appears to demonstrate the validity of the method used to calculate surface area in the steady-flow experiments.

Only one size of salt particle was used for the propeller runs: particles passing a 6-mesh screen and collecting on an 8-mesh screen. For the turbine runs several sizes of particles were used, as shown on Figure 3. While the results scatter somewhat, there is no correlation of  $K'$  with respect to particle size. This further confirms similar conclusions reached by Wilhelm, Conklin, and Sauer (10) and by Van Ness (9).

The rather poor precision of results shown in Figure 3 is caused by a fundamental difficulty in making steady-flow runs. The weight of salt suspended under steady conditions was calculated from a difference between two very nearly equal

concentrations. Thus small errors in concentration measurements can cause rather large errors in the value of  $W_s$ , and hence  $A_s$ , the weight and area of suspended salt. Precision could no doubt be improved by refinements in technique. The only other disadvantage of the flow method is that rather large quantities of salt are used.

The anticipated advantages of the steady-flow method were well demonstrated in practice. Sampling of the solution is a simple matter, and the necessity of integrating the rate equation with time is avoided.

## NOTATION

- $a$  = coefficient in Equation (20)
- $A_s$  = surface area of suspended salt at steady state, sq. ft.
- $A_i$  = instantaneous surface area of a single salt particle dissolving under steady state conditions, sq. ft.
- $A_0$  = initial surface area of an individual salt particle, sq. ft.
- $b$  = exponent in Equation (20)
- $B$  = coefficient in Equation (16)
- $C_f$  = concentration of solvent, lb. moles/cu. ft.
- $C_s$  = concentration of salt, lb. moles/cu. ft.
- $d$  = size factor, taken as tank diameter, ft.
- $D_f$  = diffusivity of the solvent, sq. ft./hr.
- $D_s$  = diffusivity of the salt, sq. ft./hr.
- $E$  = a constant in Equations (12) and (13)
- $K'$  = mass transfer coefficient in Equation (11), lb. moles/(hr.)(sq. ft.)/(lb. mole/cu. ft.)
- $M$  = molecular weight of solution
- $M_s$  = molecular weight of the salt as the solid hydrate
- $n$  = rotational velocity of impeller, rev./min.
- $(N_s)_t$  = total rate of mass transfer of salt, lb. moles/hr.
- $(N_f)_t$  = total rate of mass transfer of solvent, lb. moles/hr.
- $(N_s)_d$  = rate of mass transfer of salt by diffusion, lb. moles/hr.
- $(N_f)_d$  = rate of mass transfer of solvent by diffusion, lb. moles/hr.
- $(N_s)_b$  = rate of mass transfer of salt by bulk flow, lb. moles/hr.
- $(N_f)_b$  = rate of mass transfer of solvent by bulk flow, lb. moles/hr.
- $Q$  = equivalent diameter of salt particle, ft.
- $Q_0$  = initial equivalent diameter of salt particle, ft.
- $s$  = number of different sizes of salt particles suspended at steady state
- $W_s$  = weight of suspended salt particles at steady state, lb.
- $W_i$  = instantaneous weight of a single salt particle dissolving under steady state conditions, lb.

$W_0$  = initial weight of a single salt particle, lb.  
 $x_s$  = mole fraction of salt in solution  
 $y$  = thickness of the laminar film, ft.  
 $z_s$  = fraction of total mass transfer which is salt, mole basis  
 $\alpha$  = constant in Equation (13)  
 $\theta$  = time, hr.  
 $\mu$  = viscosity of solution, lb./hr. (ft.)  
 $\rho$  = density of solution, lb./cu. ft.

#### LITERATURE CITED

1. Hixson, A. W., and G. A. Wilkens, *Ind. Eng. Chem.*, **25**, 1196 (1933).
2. Hixson, A. W., and S. J. Baum, *ibid.*, **33**, 478 (1941).
3. *Ibid.*, **34**, 120 (1942).
4. *Ibid.*, **194** (1942).
5. Hixson, A. W., T. B. Drew, and K. L. Knox, *Chem. Eng. Progr.*, **50**, 592 (1954).
6. Humphrey, D. W., M.S. thesis, Purdue University, Lafayette, Ind. (1956).

7. Johnson, A. I., and C. J. Huang, *A. I. Ch. E. Journal*, **2**, 412 (1956).
8. Mack, D. E., and R. A. Marriner, *Chem. Eng. Progr.*, **45**, 545 (1949).
9. Van Ness, H. C., M.S. thesis, Univ. Rochester, Rochester, N. Y., (1946).
10. Wilhelm, R. H., L. H. Conklin, and T. C. Sauer, *Ind. Eng. Chem.*, **33**, 453 (1941).

Presented at A.I.Ch.E. Pittsburgh meeting

# Ion Exchange Separation of Gram Quantities of Americium from a Kilogram of Lanthanum

D. E. ARMSTRONG, L. B. ASPREY, J. S. COLEMAN, T. K. KEENAN, L. E. LaMAR, and R. A. PENNEMAN

Los Alamos Scientific Laboratory, University of California, Los Alamos, New Mexico

The separation of 4.5 g. of americium from approximately a kilogram of light rare earths (primarily lanthanum) was achieved on a pilot plant scale by chromatographic displacement of the mixture from Dowex-50 resin with 0.1% ammonium citrate at pH 8 into hydrogen-form Dowex-50. The americium collected into a narrow band and was eluted free from lanthanum but contained an equal weight of cerium. A 6- and a 2-in.-diam. column were used in tandem. Use of a final column with a much smaller diameter would have permitted a cleaner separation from cerium, but this was left for a laboratory-scale separation by a different process. Precipitation, which was observed in the columns during the first runs, was later avoided entirely by use of high flow rates both initially and during the transfer between columns. No adverse effects were noted from ~15 curies of alpha activity.

The success of Spedding and Powell (1, 2) in separating kilogram quantities of rare earths by displacement from Dowex-50 using 0.1% ammonium citrate at pH 8 suggested that this technique could be applied advantageously to the separation of americium from gross quantities of lanthanum, provided that gram amounts of trivalent americium behaved like a rare earth of intermediate atomic number and, in addition, that several curies of alpha activity would not interfere. Tracer-scale work (3) had shown that americium eluted at about the same position as promethium in the elution analysis of a mixture of trivalent rare earths and americium using ammonium citrate and Dowex-50. Thus, in the displacement of a mixture of americium and lanthanum from Dowex-50 using 0.1% ammonium citrate at pH 8, the elution positions should be in the aforementioned order after attainment of equilibrium. Furthermore, one would expect that moving the rare earth-americium band through a relatively few equivalent lengths of resin would achieve separation since the problem is essentially that of separating two light rare earths separated by four atomic numbers.

When a macro mixture of rare earths is displaced from Dowex-50 resin with 0.1% ammonium citrate at pH 8 into additional hydrogen-form Dowex-50, a series of head-to-tail bands develops, each band containing a substantially pure rare earth with overlap only at the boundaries (1, 2). Furthermore, after

equilibrium band lengths are attained, the length of a band is invariant, and elution through additional resin achieves no further separation. Obviously therefore it is preferable to have rare earth bands long with respect to their width, so that cross-contamination by overlap is minimized. This behavior is quite different from that of a mixture of rare earths under elution analysis conditions, where bell-shaped rather than flat bands develop and increasing the length of the column increases the distance between adjacent elution peaks.

#### EXPERIMENTAL

A limit of  $\frac{1}{2}$  kg. of lanthanum per run was imposed for several reasons: (1) there were restrictions due to the neutron and gamma activity from the americium associated with this amount of lanthanum; (2)  $\frac{1}{2}$  kg. of lanthanum would load a 2½-ft. resin bed, 6 in. in diameter, to 25% capacity originally and to half its length when the rare earth band had stretched out to equilibrium; (3) some such limit was suggested by the reported (1) formation of a precipitate when the initial loading of light rare earths exceeded 1.2 g./sq. cm. of column cross section; (4) exploratory work with a 5-cm. I.D. column and a resin-bed height of 70 cm. showed that lanthanum and americium were separated when the column was loaded to 22% capacity with a portion of the lanthanum-americium

mixture to be separated. However, near the leading edge of the original absorbed band precipitation occurred, causing a portion of the americium to be held up. This precipitate dissolved and caught up with the main americium band before its elution.

It has been reported (2) that precipitation of the heavier rare earths can be avoided even with very high loading of the resin bed if high initial flow rates are used during spreading out of the rare earth band. After the rare earth band is spread out to its equilibrium length, the flow rate can be lowered. With 0.1% ammonium citrate at pH 8 used, the attainment of this equilibrium length involves lengthening of the band from its original absorbed length, in which nearly all the exchange sites are occupied by rare earth, to approximately twice this length (1).

There was available about a kilogram of light rare earths, consisting primarily of lanthanum with 5% cerium, in which americium was present to ~0.5 wt. % (4.5 g. of Am<sup>241</sup>). Consequently,  $\frac{1}{2}$  kg. of lanthanum would contain only 1.5 g. of americium or ~18.5 meq. of trivalent americium. On a 2-in.-diam. column (20 sq. cm. area), with a resin capacity of 2 meq./cc., the final americium band would theoretically be only ~0.9 cm. long. (With 0.1% ammonium citrate, pH 8, the composition of the resin within the equilibrium band is divided about equally between ammonium and rare earth form.) Obviously, with such a length-to-width ratio, one could not anticipate a clean separation from the beginning edge of the rare earth immediately following. Nevertheless, if banding of the americium were obtained comparable to that reported for the rare earths, then adequate separation of the americium from the bulk of impurities would be achieved.

The combination of a 6- and a 2-in.-



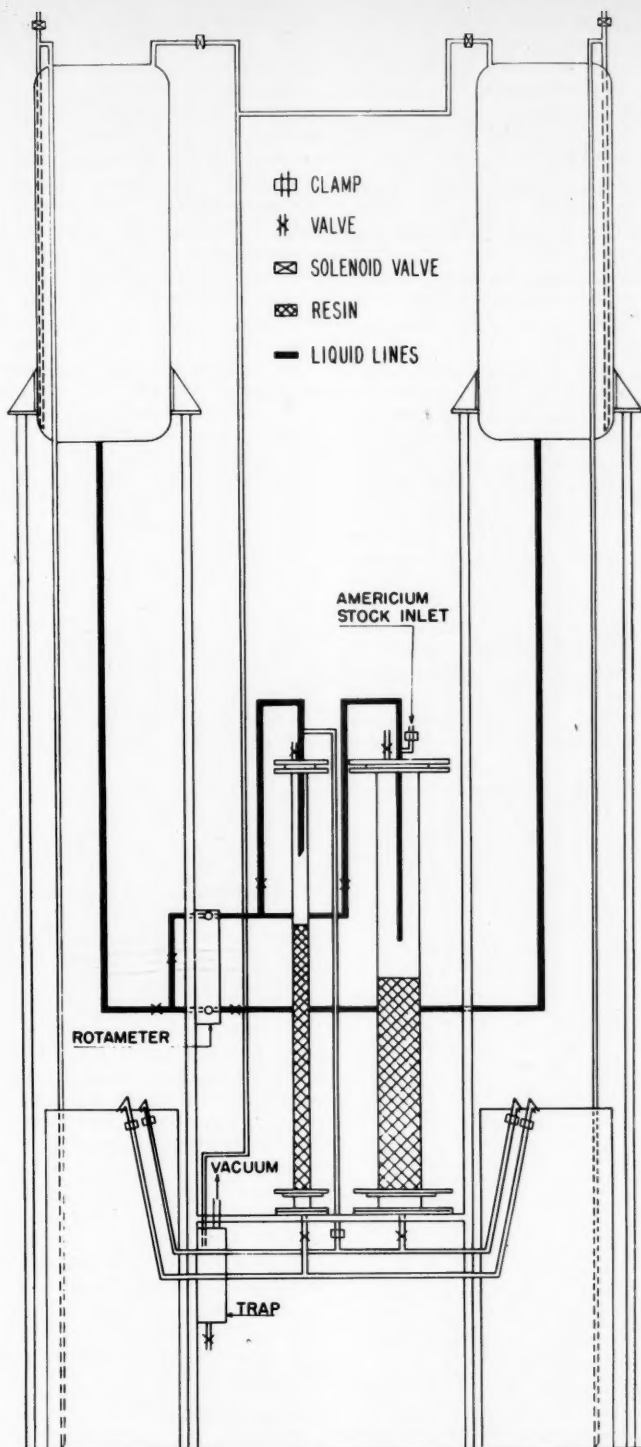


Diagram of apparatus.

diam. column was chosen, as if a 10-to-1 concentration of americium to rare earth was achieved on the 6-in. column, then use of a following 2-in. column would permit nearly the same loading/sq. cm. (9 to 1 area ratio) and should be sufficiently narrow to permit adequate banding of the americium and consequent

separation from the bulk of the rare earths when the americium band was eluted.

#### Equipment

Two 5-ft. Pyrex pipes (one 2- and one 6-in. I.D.) were installed and connected to two 60-gal. overhead feed tanks and two

60-gal. floor tanks with 1/4-in. stainless steel pipe. The two columns were connected so that the effluent from the 6-in. column might be fed to either of the floor tanks or to the top of the 2-in. column. A valve manifold allowed the use of any combination of feed and collecting tanks with either column. For recycling, the effluent solution was adjusted to pH 8 in the collecting tanks and was then vacuum-lifted (through 3/4-in. polyethylene pipe) to the overhead feed tanks. Tygon tubing was used for all other connections.

Because floor space was at a premium, the entire apparatus was placed along the wall of a room with an 18-ft. ceiling and occupied a space only 2 by 8 by 17 ft. The two 60-gal. overhead tanks were strapped to the back wall and each stood on two 12-ft. lengths of 1 1/2-in. standard pipe, bolted to a gusseted flange which was welded to the tank bottoms. The two floor tanks were placed between these pipe legs. The two glass columns were mounted between the two sets of pipe legs and were enclosed in a wooden box with Lucite front; this enclosure was connected to the exhaust system to prevent alpha contamination of the laboratory air. (See figure.)

The feed solution was gravity fed at constant head to the columns through a rotameter. Since continuous feed was necessary, the overhead feed tanks were used alternately. At ~25 gal./hr., the fastest feed rate used, there was adequate time to adjust the pH of a tank of effluent and vacuum-lift it into the overhead tank before the other feed tank was empty. Air motors and stirrers with 3-in. propellers were used for mixing.

#### Resin

The ion exchanger was Dowex-50, a sulfonated styrene-divinylbenzene copolymer (8% DVB). Although the mesh size was given as 60 to 100, sieve analysis of the air-dried resin showed that ~20% of the particles were finer than 100 mesh and ~12% were coarser than 60 mesh. Resin for the columns was prepared by slurring this stock with five times its volume of water and rejecting fractions that settled slower than 7 to 8 in./min. This remaining fraction contained resin coarser than 100 mesh. The effectiveness of water grading was demonstrated by the total retention of this resin by the 100-mesh screen at the base of the columns even after repeated back washing. Although the resin was finer than the -20 + 30 mesh size used by Spedding (2), it was sufficiently coarse to permit linear flow rates of 6 cm./min. with the effective head (10 ft.). Flow rates up to 9 cm./min. were maintained by connecting the column outlets to partially evacuated 12-gal. carboys.

The capacity of the water-settled, hydrogen-form resin was determined to be 1.95 meq./ml. Resin was loaded into the columns under water to a height of 80 cm. in the 6-in.-diam. column and to 100 cm. in the 2-in.-diam. column. The resin was supported on a 100-mesh stainless steel screen which was held in an inner slot cut partially through a neo-

prene washer. The gasket was held between a 2-in. glass spacer and the end plate of the column. The resin was conditioned by converting it to the ammonium form with 5% ammonium citrate solution, pH 8. It was then washed with water and converted to the hydrogen form with 2% sulfuric acid (until the effluent tested free from  $\text{NH}_3$ ). The columns were washed with water to remove sulfate, and then the freeboard liquid over the resin was made 0.2N in hydrochloric acid.

#### Preparation of Feed Stock

One third of the americium-lanthanum stock solution was filtered to remove silica, drawn into an 18-liter overhead feed bottle (wrapped with 1/16-in.-lead sheet to reduce the americium gamma radiation), and diluted to 15 liters with hydrochloric acid. Water washes were used to rinse the lines. The resulting clear pink solution was then 0.17M in hydrochloric acid,  $4 \times 10^{-4}$ M in americium, and  $\sim 0.15$ M in rare earth.

The remaining two thirds of the americium stock was passed through chloride-form anion resin to remove an unknown constituent that caused precipitation when the original stock was diluted with water. It was then diluted and placed in the feed bottle in the same manner as the first one third had been handled.

#### Loading of 6-in. Column

The americium-lanthanum solution was siphoned onto the 6-in. column at a rate of  $\sim 1$  to 2 cm./min. (3 to 6 gal./hr.). Absorption of americium on the resin was essentially complete, as the effluent contained much less than 1  $\mu\text{g.}/\text{liter}$ . The column was washed with water until a negative test for chloride ion was obtained. During the addition of the americium feed stock a large cavity in the center of the resin bed was noticed. This had evidently been dug by the stream of entering liquid. In the light of an ultraviolet lamp americium-lanthanum-form resin can be distinguished from the hydrogen form. Prominent spikes 2 to 3 in. long could be seen ahead of the main body of americium-lanthanum-form resin, an indication that absorption was not uniform.

For the two subsequent runs the loading technique was modified as follows. A length of closed-end stainless steel tubing  $\frac{1}{2}$  in. O.D. was suspended centrally from the feed pipe by use of Tygon tubing. Two rows of 0.04-in. holes were drilled radially near the closed end of this tube. This "shower-head" arrangement worked better than a baffle plate with the feed liquid jetting out symmetrically to the walls, even at low feed rates, as long as the holes were kept beneath the surface of the liquid over the resin. The dense rare-earth-americium feed solution formed a readily visible layer over the resin, and

the less dense washes pushed the feed layer uniformly down into the resin. Absorbing the rare-earth-americium material by this technique gave a flat band with sharp boundaries.

#### Elution of Americium

Each of the overhead tanks was filled with 55 gal. of 0.1% ammonium citrate, 0.2% phenol, at pH 8. The water used had a conductivity corresponding to 2 p.p.m. (as salt). An auxiliary tank containing 50 gal. of citrate solution was held in reserve for emergency use. Each run required about 400 gal. of eluant; recycling made it possible to work with only 110 gal.

For the first run the 6-in. column was eluted at a linear flow rate of 5.2 cm./min. (15 gal./hr.). Part of the americium precipitated near the top of the column, but the remainder moved down the column as expected. (Later very slow citrate elution of the precipitate on the 6-in. column was successful.) When americium activity appeared in the effluent from the 6-in. column, the stream was diverted onto the 2-in. column at 1.5 gal./hr. Again a portion of the americium gamma activity was found to lag at the top of the 2-in. column, presumably by precipitate formation; however, before the main band of americium reached the bottom of this column, this lagging activity diminished and caught up with the main americium band. During the elution down the 2-in. column the americium formed a sharp, visible band about 1 cm. in length, which advanced at a linear rate down the 2-in. column, allowing accurate prediction of its elution time.

During the second run the flow rate through the large column was increased to 25 gal./hr. (8.6 cm./min.) to spread out the rare-earth-americium band and then maintained at 17 gal./hr. until the americium gamma activity was 10 cm. from the bottom. The flow rate was then cut to 8 gal./hr. to sharpen the bands. The 6-in. column (which had been loaded by use of the "shower head" in a very even band) eluted cleanly without perceptible lag of americium activity. However, when the flow rate was dropped to 1 gal./hr. during the passage of americium activity from the 6-in. column onto the 2-in. column, some of the americium activity again lagged at the top of the smaller column behind the main portion. This was avoided during the third run by transferring from the 6-in. column onto the 2-in. column at an increased flow rate, 9 cm./min. (3 gal./hr.) until the americium band had neared the bottom of the second column. The flow rate was then reduced to 0.34 cm./min. to sharpen the americium band prior to its elution.

As long as there is hydrogen-form resin in the column ahead of the eluting bands, ammonium ion (and any americium or

rare earth ions) is removed from the 0.1% ammonium citrate and develops ammonium-form resin, leaving citric acid in the effluent, which can be adjusted to pH 8 and reused. Consequently the rate of band front advance is a linear function of the number of millequivalents of ammonium ion passed through each square centimeter of this front. The time rate of band advance depends on flow rate and column area. The time rate of the americium band advance varied with flow rate as predicted. Even with various flow-rate changes, as listed above, the rate of americium band advance per liter of eluant was time independent, as predicted by theory.

Ideally, there would have been americium activity only in the particular effluent fraction from the 2-in. column that contained the main batch of americium. However, in practice it was found that a few micrograms of americium activity was found in all effluent fractions, the amount building the closer americium came toward the bottom of the columns. Furthermore, it was not desirable to switch the effluent from the 6-onto the 2-in. column too soon because of the concomitant lowering in flow rate. Some americium activity therefore leaked through into the effluent stream prior to switching onto the 2-in. column.

#### RESULTS AND DISCUSSION

High pH citrate elution of an americium-light rare earth mixture from Dowex-50, with  $\text{H}^+$  used as a retaining ion, has been demonstrated to be applicable for concentrating gram amounts of americium from amounts of rare earth more than 200 times greater. Formation of precipitate can be avoided by the use of high flow rates. Detailed analysis of the narrow americium band on elution showed that it was a small, flat-topped band, eluting along with the leading edge of the cerium band. Because of its dilution with cerium, americium did not reach its theoretical elution concentration of 8 to 9 meq./liter and required about 2 gal. for elution. No detectable lanthanum was found, but a trace amount of yttrium and ytterbium, too small to form finite-width bands, eluted with the beginning of the americium band. These materials had not been detected in a spectrographic analysis of the feed material but were concentrated along with the americium.

#### ACKNOWLEDGMENT

This work was sponsored by the U. S. Atomic Energy Commission.

#### LITERATURE CITED

1. Spedding, F. H., and J. E. Powell, *J. Am. Chem. Soc.*, **76**, 2545 (1954); *ibid.*, **76**, 2550 (1954).
2. ———, *Chem. Eng. Progr. Symposium Ser. No. 14*, **50**, 7 (1954).
3. Thompson, S. G., B. B. Cunningham, and G. T. Seaborg, *J. Am. Chem. Soc.*, **72**, 2798 (1950).

# Approximate Operational Calculus in Chemical Engineering

STUART W. CHURCHILL

University of Michigan, Ann Arbor, Michigan

Approximations are suggested to extend the usefulness of operational calculus in solving boundary-value problems of interest to the chemical engineer. General approximations are outlined and specific ones illustrated. The use of computing machines with operational calculus is also considered.

Operational calculus has been found useful in many characteristic problems in chemical engineering. The applications considered by Marshall and Pigford (8) and those noted in recent annual reviews (8 to 11) include diffusion, conduction, convection, distillation, kinetics, and process control.

Unfortunately, present operational techniques are not always adequate for the very problems for which, in principle, operational calculus holds the most promise. These limitations are aggravated by the notorious difficulty encountered by the mathematician in establishing proofs in operational calculus for procedures that he suspects to be valid.

Approximation can be used to surmount some of the limitations in operational theory. In addition to permitting solution of complex and otherwise intractable problems, approximation may indicate useful simplifications that are not apparent from an exact solution. The use of approximation has been rather slighted in the literature of operational calculus, presumably because of the taint imposed by lack of rigor. Although numerous specific examples having a physical or mathematical basis have been reported, only McLachlan (7) and Doetsch (3) have attempted to generalize the use of approximation, and then only for the limiting conditions of long and short times in transient problems.

Since the purpose of this paper is to acquaint the chemical engineer with the possibilities and advantages of a mathematical technique, rather than to develop new mathematics, all proofs and most details will be omitted. Approximations will generally be justified on physical grounds. The engineer is seldom disturbed by his inability to establish rigorously the validity or uniqueness of a solution if it satisfies physical tests.

Consideration will be limited to the Laplace transformation, which is the most extensively used form of operational calculus. The use of approximation with other transforms is also advantageous, and equivalent procedures are readily developed.

## THE LAPLACE TRANSFORMATION

If a function  $F(t)$  is multiplied by  $e^{-st}$  and integrated with respect to  $t$  from zero to infinity, a new function,  $f(s)$ , is obtained. This operation is called the Laplace transformation of  $F(t)$ , and  $f(s)$  is called the Laplace transform; i.e.,

$$\mathcal{L}\{F(t)\} = \int_0^\infty e^{-st} F(t) dt = f(s) \quad (1)$$

The inverse operation is designated

$$F(t) = \mathcal{L}^{-1}\{f(s)\} \quad (2)$$

Operational calculus was developed empirically by Heaviside as a set of rules of procedure. Subsequently an extensive theory was developed, and the mathematical foundations, limitations, and formal applications are well treated in modern texts (2, 7, 14). Although transforms have been derived and tabulated for many functions and mathematical operations (4), problems of interest more often than not yield functions not to be found in such tables.

Letting the transform variable,  $s$ , be a complex variable permits expression of the inverse transformation in terms of the complex inversion integral.

$$F(t) = \frac{1}{2\pi i} \lim_{\beta \rightarrow \infty} \int_{\gamma-i\beta}^{\gamma+i\beta} e^{st} f(s) ds \quad (3)$$

where

$$s = x + iy$$

$\gamma$  = a sufficiently large, fixed value of  $x$ .

The theory of residues and line integrals can be used to evaluate the foregoing integral. In many cases the problem is reduced to one of finding the singularities in  $f(s)$ .

The complex inversion integral can be written as a real integral,

$$F(t) = \frac{e^{\gamma t}}{\pi} \int_0^\infty [u(\gamma, y) \cos yt - v(\gamma, y) \sin yt] dy \quad (4)$$

where  $u$  = real part of  $f(s)$ , and  $v$  = imaginary part of  $f(s)$ , but in this form the integration is generally too difficult to be performed analytically.

The most important operational property of the Laplace transformation arises from the derivative

$$\mathcal{L}\{F'(t)\} = sf(s) - F(+0) \quad (5)$$

Differentiation of  $F(t)$  thus corresponds to multiplication of the transform  $f(s)$  by  $s$  and subtraction of  $F(+0)$ . Equation (5) in turn leads to an expression for the transform of the  $n$ th derivative:

$$\mathcal{L}\{F^n(t)\} = s^n f(s) - s^{n-1} F(+0) - s^{n-2} F'(+0) - \dots - F^{(n-1)}(+0) \quad (6)$$

Linear ordinary differential equations with constant coefficients are thus transformed into algebraic equations, solution of which followed by inversion then yields a solution to the differential equation. Other operational properties permit simplification and solution of a few more complex types of differential equations.

The transformation of simple partial differential equations yields ordinary differential equations, which may be easier to solve. The solution of the ordinary differential equation involving a transformed function may possibly be solvable by a second transformation.

Multiplication of the transforms of two functions corresponds to a particular integration

$$\mathcal{L}^{-1}\{f_1(s) \cdot f_2(s)\} = \int_0^t F_2(t-\lambda) F_1(\lambda) d\lambda \quad (7)$$

This property permits solution of certain integral equations as well as additional differential equations.

The operation

$$\mathcal{L}\{F(t-m)\} = e^{-ms} f(s) \quad (8)$$

where

$$F(t) = 0 \text{ for } t < 0$$

permits solution of certain finite-difference equations and finite-difference-differential equations such as those encountered in equilibrium-stage operations.

From these examples, several limitations on the usefulness of the operational method are apparent or implied:

1. The functions encountered in the equations and boundary conditions must be transformable.
2. The transformed equations and boundary conditions must be solvable.
3. It must be possible to invert the transformed solution.

The mathematical restrictions on the transformation are not very serious and are satisfied by most functions encountered in engineering problems. On the other hand, the class of equations which are simplified by transformation is rather limited. With such equations the relative

advantage of the operational method over other classical methods depends largely on the nature of the boundary conditions. In particular, if the values of the dependent variable to be transformed and its derivatives at  $t = +0$  are known, the operational method is at least worth looking into. The simplification gained by transformation is often negated by difficulties in inverting the transformed solution.

#### APPROXIMATE INVERSION

The inversion process may be simplified or expedited by the following methods, one or more of which are applicable in most problems.

1. The transformed function may be expanded in series. The entire series may then be inverted or appropriate terms may be discarded before inversion. Frequently several different expansions are feasible, yielding solutions or indicating approximations of different utility. The use of series expansion is illustrated in Problems I, II, and III, which follow.

2. A complicated function may be represented empirically by some arbitrary function which is more readily inverted, as indicated in Problem III. This method of approximation can seldom be justified mathematically but is worth trying if the solution can be tested. (Similarly, boundary conditions and generating functions may be approximated by other functions more susceptible to transformation, as illustrated in Problem IV.)

3. The inversion may be carried out only for particular or limiting values of a parameter, as indicated in Problems I and III, or of a nontransformed independent variable, as indicated in Problem II. This procedure may be expressed mathematically as

$$\begin{aligned} F(x_0, t) &= [F(x, t)]_{x=x_0} \\ &= \{ \mathcal{L}^{-1}[f(x, s)] \}_{x=x_0} \quad (9) \\ &= \mathcal{L}^{-1}[f(x_0, s)] \end{aligned}$$

4. Approximate inversions for large and small values of  $t$  can sometimes be obtained by letting  $s$  assume small and large values, respectively; i.e.,

$$F(t) \underset{t \rightarrow \infty}{\cong} \mathcal{L}^{-1}\{f(s)\}_{s \rightarrow 0} \quad (10)$$

and

$$F(t) \underset{t \rightarrow 0}{\cong} \mathcal{L}^{-1}\{f(s)\}_{s \rightarrow \infty} \quad (11)$$

One or both of these approximations are illustrated in Problems I, II, and III. Equation (10) is not valid if any of the singularities in  $f(s)$  occur in the half of the complex plane where the real value of  $s$  is positive. Thus formal use of this approximation may lead to error; however, it is usually easier to detect an erroneous solution than to find the singularities.

5. The real form of the inversion

integral, Equation (4), can be evaluated graphically, numerically, or by quadrature, as suggested in Problem III.

6. Approximate values may be used for the singularities when residue theory is used to carry out the inversion. This approximation is not used in any of the illustrative problems.

#### ILLUSTRATIVE PROBLEMS

Four problems were chosen to illustrate the use of approximation with the Laplace transformation. The equations in the problems are streamlined by the implicit inclusion of physical factors and constants in generalized variables.

Although the greatest utility of approximation is in complex problems that cannot be solved rigorously, relatively simple problems were deemed best for illustration. In several cases the nature and validity of the approximations are apparent by direct comparison with a rigorous solution. The techniques used in these simple problems are of course directly applicable in more complex ones.

##### Problem I

Jeffreys (5) has indicated the use of approximation in the solution of the set of simultaneous rate equations describing a radioactive decay series. He also discusses the physical interpretation of the approximate results in some detail. The general problem is represented by the equations

$$\frac{dC_1}{dt} = -k_1 C_1 \text{ with } C_1 = C_0 \text{ at } t = 0 \quad (12)$$

$$\frac{dC_2}{dt} = -k_2 C_2 + k_1 C_1 \quad (13)$$

$$\frac{dC_3}{dt} = -k_3 C_3 + k_2 C_2 \quad (14)$$

etc., and finally

$$\frac{dC_n}{dt} = k_{n-1} C_{n-1} \quad (15)$$

for the end product, which does not decompose.

Transformation yields the corresponding equations

$$C_1 = \frac{C_0}{s + k_1} \quad (16)$$

$$C_2 = \frac{k_1 C_0}{(s + k_2)(s + k_1)} \quad (17)$$

$$C_3 = \frac{k_2 k_1 C_0}{(s + k_3)(s + k_2)(s + k_1)} \quad (18)$$

and

$$C_n = \frac{k_{n-1} k_{n-2} \cdots k_1 C_0}{s(s + k_{n-1})(s + k_{n-2}) \cdots (s + k_1)} \quad (19)$$

The corresponding exact solutions are

$$C_1 = C_0 e^{-k_1 t} \quad (20)$$

$$C_2 = k_1 C_0 \left[ \frac{e^{-k_1 t}}{k_2 - k_1} + \frac{e^{-k_2 t}}{k_1 - k_2} \right] \quad (21)$$

$$\begin{aligned} C_3 = k_2 k_1 C_0 & \left[ \frac{e^{-k_1 t}}{(k_3 - k_1)(k_2 - k_1)} \right. \\ & + \frac{e^{-k_2 t}}{(k_3 - k_2)(k_1 - k_2)} \\ & \left. + \frac{e^{-k_3 t}}{(k_2 - k_3)(k_1 - k_3)} \right] \quad (22) \end{aligned}$$

and

$$\begin{aligned} C_n = C_0 - k_{n-1} k_{n-2} \cdots k_1 C_0 & \cdot \left[ \frac{e^{-k_1 t}}{k_1(k_{n-1} - k_1)(k_{n-2} - k_1) \cdots (k_2 - k_1)} \right. \\ & \left. + \cdots \right] \quad (23) \end{aligned}$$

In the following approximations  $s$  will be treated as a real variable.

##### Short-time Approximation

For very short times  $|s|$  will be very large with respect to all the rate constants. Then

$$C_1 \rightarrow \frac{C_0}{s} \quad (24)$$

$$C_2 \rightarrow \frac{k_1 C_0}{s^2} \quad (25)$$

$$C_3 \rightarrow \frac{k_2 k_1 C_0}{s^3} \quad (26)$$

$$C_n \rightarrow \frac{k_{n-1} k_{n-2} \cdots k_1 C_0}{s^n} \quad (27)$$

and

$$C_1 \rightarrow C_0 \quad (28)$$

$$C_2 \rightarrow k_1 C_0 t \quad (29)$$

$$C_3 \rightarrow \frac{k_2 k_1 C_0 t^2}{2!} \quad (30)$$

$$C_n \rightarrow \frac{k_{n-1} k_{n-2} \cdots k_1 C_0 t^{n-1}}{(n-1)!} \quad (31)$$

##### Moderate-time Approximation

Expanding the transforms in series by division yields a useful form for moderately short times corresponding to  $|s|$  greater than any  $k$ . Thus

$$C_1 = \frac{C_0}{s} \left[ 1 - \left( \frac{k_1}{s} \right) + \left( \frac{k_1}{s} \right)^2 + \cdots \right] \quad (32)$$

$$\begin{aligned} C_2 = \frac{k_1 C_0}{s^2} & \left[ 1 - \frac{(k_1 + k_2)}{s} \right. \\ & \left. + \frac{(k_1^2 + k_1 k_2 + k_2^2)}{s^2} + \cdots \right] \quad (33) \end{aligned}$$



$$c_3 = \frac{k_2 k_1 C_0}{s^3} \left[ 1 - \frac{(k_1 + k_2 + k_3)}{s} + \dots \right] \quad (34)$$

$$c_n = \frac{k_{n-1} k_{n-2} \dots k_1 C_0}{s^n} \left[ 1 - \frac{k_1 + k_2 + \dots + k_{n-1}}{s} + \dots \right] \quad (35)$$

$$C_1 = C_0 \left[ 1 - k_1 t + \frac{(k_1 t)^2}{2!} - \frac{(k_1 t)^3}{3!} + \dots \right] \quad (36)$$

$$C_2 = k_1 C_0 t \left[ 1 - \frac{(k_1 + k_2) t}{2!} + \frac{(k_1^2 + k_2 k_1 + k_2^2) t^2}{3!} - \dots \right] \quad (37)$$

$$C_3 = \frac{k_2 k_1 C_0 t^2}{2!} \left[ 1 - \frac{(k_1 + k_2 + k_3) t}{3!} + \dots \right] \quad (38)$$

$$C_n = \frac{k_{n-1} k_{n-2} \dots k_1 C_0 t^{n-1}}{(n-1)!} \left[ 1 - \frac{(k_1 + k_2 + \dots + k_{n-1}) t}{n!} + \dots \right] \quad (39)$$

The first terms of the series solutions are the very short-time solutions. The series themselves are obviously those obtained from series expansion of the exact solutions. Thus in this problem a short-time approximation of any desired accuracy can be obtained by letting  $|s| \rightarrow \infty$  and dropping higher order terms.

#### Long-time Approximation

For long times  $s$  will be small with respect to some of the rate constants. If it is assumed that all the rate constants except  $k_2$  are much larger than  $|s|$

$$c_1 \rightarrow \frac{C_0}{k_1} \text{ and } C_1 \rightarrow 0 \quad (40, 41)$$

$$c_2 \rightarrow \frac{C_0}{s + k_2}, \text{ and } C_2 \rightarrow C_0 e^{-k_2 t} \quad (42, 43)$$

$$c_3 \rightarrow \frac{k_2 C_0}{k_3(s + k_2)}, \text{ and } C_3 \rightarrow \frac{k_2 C_0}{k_3} e^{-k_3 t} \quad (44, 45)$$

$$c_n \rightarrow \frac{k_2 C_0}{s(s + k_2)}, \text{ and } C_n \rightarrow C_0 [1 - e^{-k_2 t}] \quad (46, 47)$$

Equation (41) does not follow directly from Equation (40) but is apparent from Equation (12) or (20). These approximate solutions can, of course, be obtained from the exact solution. Thus the formal procedure used to obtain the approximations is substantiated in this case even though it is not in general rigorous.

#### Problem II

The representation of a transformed solution by an asymptotic series to expedite inversion or to yield a more satisfactory solution upon inversion has been used widely. The following example from Carslaw and Jaeger (1) also illustrates inversion at a single value of the untransformed variable.

The transformed solution for the temperature in a long cylindrical rod, initially at zero temperature but maintained at unit temperature at the surface after time zero, can be written in generalized terms as

$$u(r, s) = \frac{I_0(\sqrt{s}r)}{s I_0(\sqrt{s})} \quad (48)$$

The details of the derivation of Equation (48) are given in reference 1. The exact solution is

$$T(r, t) = 1 - 2 \sum_{n=1}^{\infty} \frac{J_0(\alpha_n r)}{\alpha_n J_1(\alpha_n)} e^{-\alpha_n^2 t} \quad (49)$$

$$u(s) = \frac{1}{s \left[ 1 - \sqrt{s} \frac{1 + \left( \frac{1 - L\sqrt{s}}{1 + L\sqrt{s}} \right) e^{2\sqrt{s}(L-1)}}{1 - \left( \frac{1 - L\sqrt{s}}{1 + L\sqrt{s}} \right) e^{2\sqrt{s}(L-1)}} + \phi s \right]} \quad (55)$$

where  $\alpha_n$  are the roots of  $J_0(\alpha_n) = 0$ .

#### Short-time Approximation

Equation (49) is inconvenient for  $t < 0.02$  because the series converges very slowly. For short times and large  $s$  only the positive exponentials of the asymptotic series

$$I_0(x) = \frac{e^x}{\sqrt{2\pi x}} \left[ 1 + \frac{1}{8x} + \frac{9}{128x^2} + \dots \right] + \frac{e^{-x+1/2\pi i}}{\sqrt{2\pi x}} \left[ 1 - \frac{1}{8x} + \frac{9}{128x^2} - \dots \right] \quad (50)$$

are significant. Introducing these terms

into Equation (48) and simplifying gives

$$u(r, s) \cong \frac{e^{-\sqrt{s}(1-r)}}{s\sqrt{r}} \left[ 1 + \frac{1-r}{8r\sqrt{s}} + \frac{9-2r-7r^2}{128sr^2} + \dots \right] \quad (51)$$

Although all the terms of Equation (51) could be inverted, only the first term need be considered for short times if  $r$  is not too small:

$$T(r, t) \cong \frac{1}{\sqrt{r}} \operatorname{erfc} \left( \frac{1-r}{2\sqrt{t}} \right) \quad (52)$$

#### Short-time Approximation for Center

Putting  $r = 0$  in Equation (48) and then introducing the positive exponentials of the asymptotic series only in the denominator gives

$$u(0, s) \cong \frac{\sqrt{2\pi}}{s^{3/4}} e^{-\sqrt{s}} \left[ 1 - \frac{1}{8\sqrt{s}} - \dots \right] \quad (53)$$

For short times, only the first term needs to be inverted and

$$T(0, t) \cong \frac{e^{-1/8t}}{\sqrt{\pi t}} K_{1/4} \left( \frac{1}{8t} \right) \quad (54)$$

#### Problem III

Sleicher and Churchill (12) used a number of techniques to invert the following expression for the transient temperature of a sphere in a dispersion of spheres exposed to a radiant flux

The details of the derivation of Equation (55) and the physical significance of the variables are given in the foregoing reference.

#### Short-time Approximation

For large  $s$  and  $L > 1$

$$u(s) \rightarrow \frac{1}{s(1 + \sqrt{s} + \phi s)} \quad (56)$$

Equation (56) is also obtained by letting  $L \rightarrow \infty$ , which corresponds to reduction of the problem to one of a single sphere in an infinite medium.

#### Integral Inversion

The inverse transform of Equation (56) can be written in terms of the real integral

$$T = 1 - \frac{2}{\pi \sqrt{\phi}}$$

$$\int_0^\infty \frac{e^{-(t/\phi)y^2} dy}{1 - \left(2 - \frac{1}{\phi}\right)y^2 + y^4} \quad (57)$$

The integral can be evaluated graphically for a series of values of  $t$  and  $\phi$ . Accurate evaluation at small values of  $t/\phi$  is difficult owing to a sharp peak in the integrand at  $y = \sqrt{1 - (1/2\phi)}$ . This difficulty can be minimized by rearranging Equation (57) as

$$T = 1 - e^{-t/\phi} \left[ 1 - \frac{2}{\pi\sqrt{\phi}} \int_0^\infty \frac{1 - e^{-(t/\phi)(y^2-1)}}{1 - \left(2 - \frac{1}{\phi}\right)y^2 + y^4} dy \right] \quad (58)$$

or by taking a mean value of the exponential at the peak; i.e.,

$$T \cong 1 - \exp\left\{-\frac{t}{\phi}\left(1 - \frac{1}{2\phi}\right)\right\} \quad (59)$$

As an example of the difficulty that can arise from an improper approximation, it will be noted that neglecting  $1/\phi$  with respect to 2 in the denominator of the integrand produces a zero in the denominator at  $y = 1$  and thus makes the integrand infinite.

#### Series Inversion

Formally carrying out the division indicated in Equation (56) yields

$$u = \frac{1}{s^2} \left[ 1 - \frac{1}{\phi\sqrt{s}} - \frac{(\phi-1)}{\phi^2 s} + \dots \right] \quad (60)$$

and inversion gives

$$T = \frac{t}{\phi} \left[ 1 - \frac{4}{3\phi} \sqrt{\frac{t}{\pi}} - \frac{(\phi-1)}{2\phi^2} t + \dots \right] \quad (61)$$

Unfortunately, Equation (61) converges slowly except for very small  $t$ .

#### Parametric Approximation

Practical values of the parameter  $\phi$  were found to exceed 400. For  $\phi > 400$ ,  $\sqrt{s}$  is never more than 2.5% of  $(1 + \sqrt{s} + \phi s)$  for all real values of  $s$  from zero to infinity. If  $\sqrt{s}$  is neglected in  $(1 + \sqrt{s} + \phi s)$ , the inversion is readily performed and gives

$$T = 1 - e^{-t/\phi} \quad (62)$$

Equation (62), which can also be obtained by physical reasoning, is found to differ from Equation (57) by less than 3% for all  $t$  at  $\phi = 400$ . This is an example of a formal procedure which is

quite unsound mathematically, but which leads to a useful and verifiable result. Due caution should be exercised in using this formal procedure because a very small error in representing  $f(s)$  may lead to a much larger error in  $F(t)$ .

#### Long-time Approximation

For long times and  $L^3 \gg 3\phi$ , as  $s \rightarrow 0$

$$u \rightarrow \frac{3}{L^3 s^2} \quad (63)$$

and

$$T \rightarrow \frac{3t}{L^3} \quad (64)$$

The form of Equation (64) and hence of Equation (63) can also be rationalized physically.

#### General Approximation

It is apparent that the expression

$$u = \frac{1}{s} \left( \frac{1}{1 + \phi s} + \frac{3}{L^3 s} \right) \quad (65)$$

yields asymptotic solutions for both long and short times provided that  $\phi > 400$  and  $L^3 \gg 3\phi$ . Direct numerical comparison shows that Equation (65) differs from Equation (55) by no more than 8%, even in the intermediate range of real values of  $s$  where both the long- and short-time terms are appreciable. Inversion of Equation (65) yields

$$T = 1 - e^{-t/\phi} + \frac{3t}{L^3} \quad (66)$$

Again an approximation which is unjustifiable mathematically appears to give a physically acceptable solution.

#### Problem IV

Transient conduction in a semiinfinite slab with radiation and convection from the surface and generation of energy due to a chemical reaction at the surface can be used to illustrate the approximation of boundary conditions. The boundary-value problem can be written

$$k \frac{\partial^2 T}{\partial z^2} = \rho c \frac{\partial T}{\partial t} \quad (67)$$

$$h[T_s - T] + \sigma(T_s^4 - T^4) + Ae^{-B/T} + k \frac{\partial T}{\partial z} = 0 \quad \text{at } z = 0 \quad (68)$$

and

$$T = 0 \quad \text{at } t = 0 \quad (69)$$

#### Approximate Representation of Radiation

The awkward radiation term can be replaced by a linear expression

$$h_r[T_s - T] = \sigma[T_s^4 - T^4] \quad (70)$$

where

$$h_r = \sigma[T_s + T][T_s^2 + T^2] \quad (71)$$

For any limited range of  $T$  the variation of  $h_r$  will be slight and a mean value can be selected which leads to only a slight error.

#### Approximate Representation of Generation

Similarly, over a moderate range of temperature the exponential expression can be replaced by a linear expression

$$Ae^{-B/T} \cong a + bT \quad (72)$$

with the coefficients  $a$  and  $b$  chosen empirically.

#### Solution

After introduction of the approximate boundary conditions the problem can be rewritten in the following simplified form:

$$\frac{\partial T}{\partial t} = \frac{\partial^2 T}{\partial Z^2} \quad (73)$$

$$T = 0 \quad \text{at } \theta = 0 \quad (74)$$

$$T_0 - T + \frac{\partial T}{\partial Z} = 0 \quad \text{at } Z = 0 \quad (75)$$

where

$$Z = (h + h_r - b)z/k \quad (76)$$

$$\sqrt{\theta} = (h + h_r - b)\sqrt{t/k\rho c} \quad (77)$$

and

$$T_0 = [a + (h_r + h)T_s]/(h + h_r - b) \quad (78)$$

The rewritten problem can be transformed and the transformed problem solved to give

$$u = \frac{T_0 e^{-\sqrt{s}Z}}{s(\sqrt{s} + 1)} \quad (79)$$

Equation (79) is then inverted to give

$$\frac{T}{T_0} = \operatorname{erfc}\left(\frac{Z}{2\sqrt{\theta}}\right) - e^{Z+\theta} \operatorname{erfc}\left(\frac{Z}{2\sqrt{\theta}} + \sqrt{\theta}\right) \quad (80)$$

#### MACHINE INVERSION

A general card program has been developed (13) for the inversion of the Laplace transform of functions which can be expressed as a rational algebraic function  $a(s)/b(s)$  with a numerator of any order up to fifteen and a denominator of any order up to sixteen. A further restriction is that the poles of the function be of the following types: first-order poles, real or complex; second-order poles, real only; and first-, second-, or third-order poles at the origin. The process described requires that the poles be known in advance. However, the roots of such equations can also be found to any desired degree of accuracy by routine machine computation, and so the entire operation can be programmed.

Obviously, any function which can be approximated by a function of this form can be inverted on a computing machine. A program to evaluate the constants in such an empirical equation can also be written. Thus the entire process of empirical representation, evaluation of singularities, and inversion can be carried out formally by machine. Since the use of the empirical representation is not rigorous, the solution would have to be tested.

#### CONCLUSIONS

Complex Laplace transforms can be inverted approximately by a number of simple techniques. Although the validity of the techniques is not easy to establish rigorously, the results can usually be tested by physical reasoning. By the use of empirical representations, almost any function can be inverted on a computing machine. These techniques extend the usefulness of operational calculus to many complex problems in chemical engineering.

#### ACKNOWLEDGMENT

Invaluable advice and assistance were provided by J. H. Chin.

#### NOTATION

$c$	= heat capacity
$C_0$	= original concentration of component 1
$C_n(t)$	= concentration of $n$ th component

$c(s)$	= transformed concentration of $n$ th component
$\text{erfc}(x)$	= complementary error function of $x$
$h$	= heat transfer coefficient for convection
$h_r$	= heat transfer coefficient for radiation
$J_0(x)$	= $J_0(ix)$
$J_0(x)$	= Bessel function of first kind and zero order of $x$
$J_1(x)$	= Bessel function of first kind and first order of $x$
$K_{1/4}(x)$	= modified Bessel function of second kind and one-quarter order of $x$
$k$	= thermal conductivity
$k_n$	= rate constant for $n$ th reaction
$L$	= dimensionless distance between spheres
$r$	= fraction of radius
$s$	= variable of transformation
$t$	= time
$T$	= temperature or dimensionless temperature
$T_s$	= temperature of surroundings
$u(s)$	= transformed temperature or dimensionless temperature
$z$	= distance from surface
$\phi$	= dimensionless parameter
$\rho$	= density

#### LITERATURE CITED

1. Carslaw, H. S., and J. C. Jaeger, "Conduction of Heat in Solids," Oxford

- University Press, London (1947).
2. Churchill, R. V., "Modern Operational Mathematics in Engineering," McGraw-Hill Book Company, Inc., New York (1944).
3. Doetsch, G., *J. reine u. angew. Math.*, **167**, 274 (1932).
4. Erdélyi, Arthur, "Tables of Integral Transforms," vol. I, McGraw-Hill Book Company, Inc., New York (1954).
5. Jeffreys, H., "Operational Methods in Mathematical Physics," Cambridge University Press, London (1931).
6. Marshall, W. R., Jr., and R. L. Pigford, "The Application of Differential Equations to Chemical Engineering Problems," Univ. of Delaware, Newark, Del. (1947).
7. MaLachlan, N. W., "Complex Variable Theory and Transform Calculus," Cambridge University Press, London (1953).
8. Rose, Arthur, J. A. Schilk, and R. C. Johnson, *Ind. Eng. Chem.*, **45**, 933 (1953).
9. Rose, Arthur, R. L. Heiny, R. C. Johnson, and J. A. Schilk, *ibid.*, **46**, 916 (1954).
10. Rose, Arthur, R. C. Johnson, and R. L. Heiny, *ibid.*, **47**, 626 (1955).
11. Rose, Arthur, R. C. Johnson, R. L. Heiny, and T. J. Williams, *ibid.*, **48**, 622 (1956).
12. Sleicher, C. A., Jr., and S. W. Churchill, *Ind. Eng. Chem.*, **48**, 1819 (1956).
13. Titus, C. K., *J. Assoc. Computing Machines*, **2**, 18 (1955).
14. Widder, D. V., "The Laplace Transform," Princeton University Press, Princeton, N. J. (1946).

## Fluidization and Sedimentation of Spherical Particles

THOMAS J. HANRATTY and ABDEMANNAN BANDUKWALA

University of Illinois, Urbana, Illinois

Data are presented in support of an expression describing the relation between the sedimenting velocity or the fluidizing velocity and the fraction voids. This expression which contains no empirical constants may be obtained by considering a particle in a fluid having the average properties of the suspension. Stokes's law is used to calculate the force on the particle, and an equation derived by Vand is used to describe the viscosity of the suspension. The equation based on this model is valid for particle Reynolds numbers less than 0.07. The model may be used as an approximation of bed behavior at higher Reynolds numbers by application of a correction to Stokes's law.

The steady state settling rate of a single particle in a fluid or the fluid velocity necessary to suspend a single particle may be described by equating the force of gravity to the viscous drag of the fluid. For spherical particles

Drag force on particle

$$= C_D \frac{1}{2} \rho U_0^2 \left( \frac{\pi D_p^2}{4} \right) \quad (1)$$

Force of gravity

$$= (\rho_s - \rho) g \left( \frac{\pi D_p^3}{6} \right) \quad (2)$$

$$U_0 = \sqrt{\frac{4gD_p(\rho_s - \rho)}{3\rho C_D}} \quad (3)$$

For low settling rates ( $Re_p < 0.1$ ) the drag coefficient  $C_D$  may be described by Stokes's law, and Equation (3) becomes

$$U_0 = \frac{(\rho_s - \rho)gD_p^2}{18\mu} \quad (4)$$

Abdemannan Bandukwala is with Standard Oil Company (Indiana), Whiting, Indiana.

At high settling rates experimental measurements of  $C_D$  reported in the literature may be used. Equations (3) and (4) are not valid to predict the rate of settling of a bed of particles or the velocity necessary to suspend a bed of particles at a given voidage. The surrounding particles affect the flow field, and therefore the experimental conditions under which  $C_D$  is determined for single particles are not reproduced.

A number of derivations have been presented in the literature to describe the settling velocity or the fluidization velocity of beds of particles. Most of these have been empirical. Two derivations, which contain no empirical constants, describe the behavior of fluidizing or sedimenting beds at low Reynolds numbers. Brink-

man (2), who calculated the force on a particle embedded in a porous mass, described the flow through the mass by Darcy's equation. The following equation for the sedimenting velocity is obtained if the viscosity term in his derivation is assumed to be that of the pure liquid:

$$\frac{U_c}{U_0} = 1 + \frac{3}{4}c \left( 1 - \sqrt{\frac{8}{c} - 3} \right) \quad (5)$$

Hawksley (3) applied a derivation presented by Vand (4) for the viscosity of concentrated suspensions of spherical particles:

$$\mu_c = \mu \exp \left( 2.5c/1 - \frac{39}{64}c \right) \quad (6)$$

He describes the force on each of the particles in the system with Stokes's law. However the properties of the fluid are altered to account for the presence of the other particles. The viscosity is given by Equation (6), and the density is that of the suspension

$$\rho_c = c\rho_s + (1 - c)\rho \quad (7)$$

The relative velocity between the fluid and the particles of the suspension is equal to the settling velocity divided by the void fraction:

$$U = \frac{U_c}{1 - c} \quad (8)$$

Hawksley substituted for  $U_0$ ,  $\rho$ , and  $\mu$  in

Equation (4) the expressions given by Equations (6), (7), and (8).

$$U_c = \frac{(\rho_s - \rho)gD_p^2(1 - c)^2}{18\mu \exp(2.5c/1 - \frac{39}{64}c)} \quad (9)$$

$$\frac{U_c}{U_0} = (1 - c)^2 \exp(-2.5c/1 - \frac{39}{64}c)$$

Equations (5) and (9) are plotted in Figure 1. It can be seen that the results of the derivation of Brinkman and of that of Vand and Hawksley are quite different. Data have been presented in the literature to support both theories (3, 5).

The experimental investigation reported in this paper was undertaken to examine the validity of these two models. Measurements of the effect of void fraction upon the settling rate and the fluidization velocity were made for beds of spherical particles. By varying the viscosity of the fluid, experiments could be conducted over a large range of  $Re_p$ .

## DESCRIPTION OF EXPERIMENTS

The fluidization and sedimentation of 0.022-in. steel spheres ( $\rho_s = 7.43$  g./cc.) and of 0.028-in. glass spheres ( $\rho_s = 2.88$  g./cc.) in glycerine-water solutions were studied. The bed was contained in a 4-in.-diam. glass column and the liquor was circulated through the column from a holding tank, as indicated in Figure 2.

The behavior of the bed was dependent on the type of calming section employed.

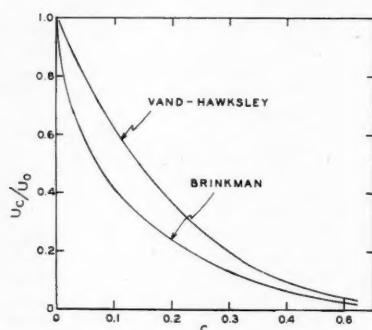


Fig. 1. Comparison of derivations of Brinkman and Hawksley.

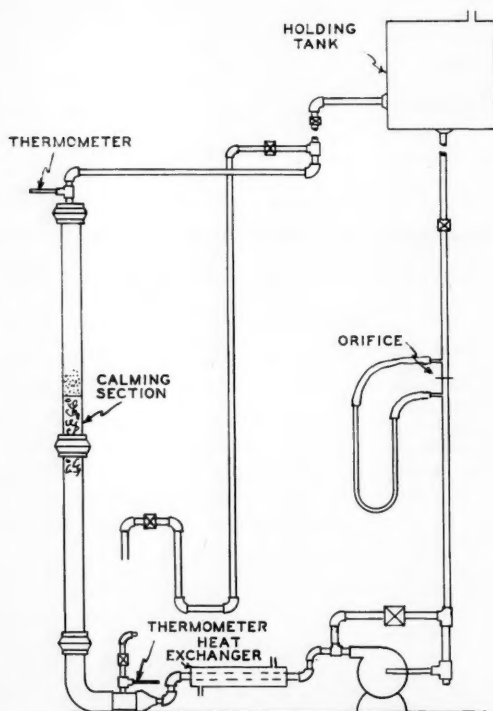


Fig. 2. Equipment used in experiments.

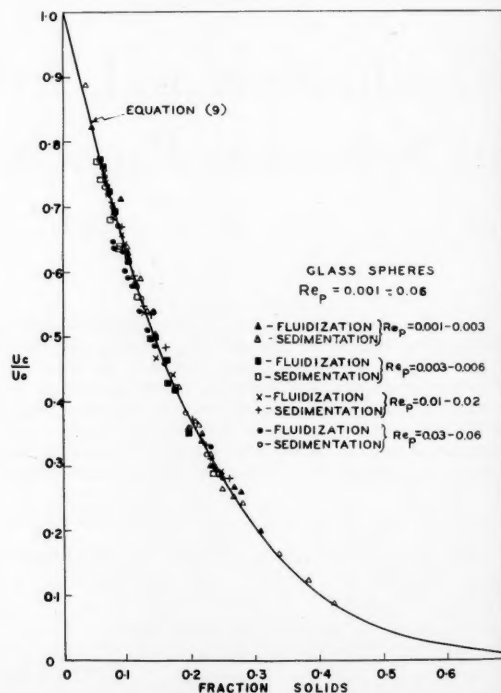


Fig. 3. Fluidization and sedimentation data for glass spheres;  $Re_p = 0.001 - 0.06$ .



n by

(9)  
3.4 c)

ed in  
results  
d of  
quite  
ed in  
ories

re-  
en to  
odels.  
void  
the  
beds  
the  
ould  
ep.

n of  
(cc.)  
2.88  
were  
4-in.-  
was  
hold-

dent  
oyed.

003

006

02

06

class

957

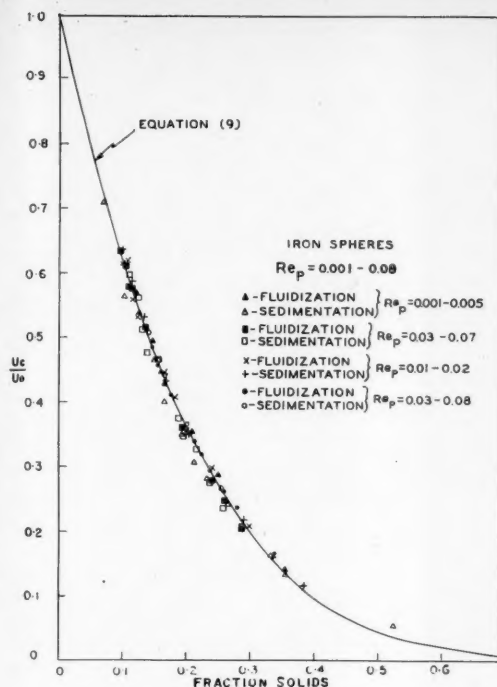


Fig. 4. ↑ Fluidization and sedimentation data for iron spheres;  
 $Re_p = 0.008 - 0.07$ .

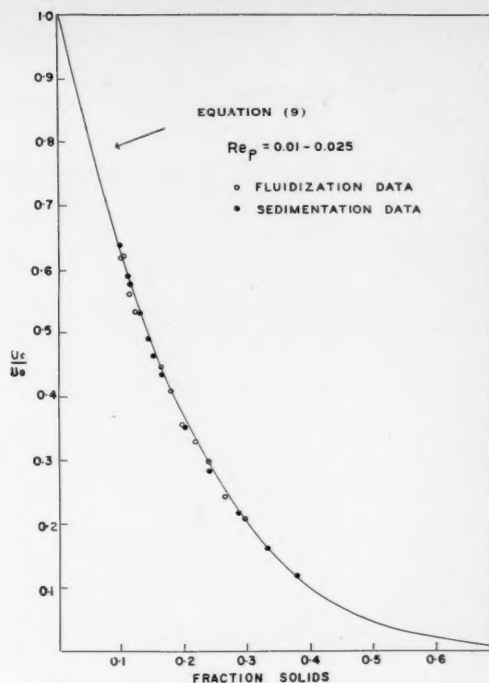
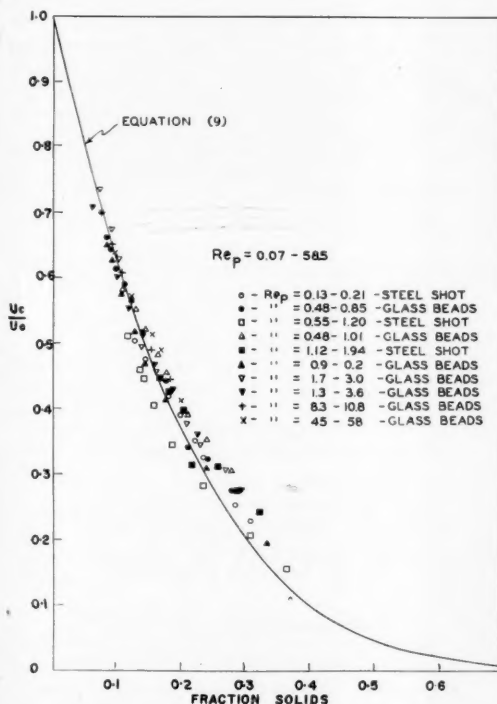


Fig. 5. Comparison of sedimentation and fluidization data for a typical run. ↑



← Fig. 6. Fluidization and sedimentation data at high Reynolds numbers;  
 $Re_p = 0.07$  to 58.5.

Company and the steel shot by the Wheelabrator and Equipment Corporation. Particles retained between Tyler sieves 20 and 35 were screened through specially designed equipment. A number of highly polished soft-steel slabs were supported on two threaded screws. By means of positioning and locking nuts the gaps between the slabs could be accurately adjusted, and the particles were sieved through these openings. After the sieving the particles were rolled down an 18-in. incline of 10°. Nonspherical particles stuck to the incline and were discarded. The process was repeated with an incline of 5°.

Data were taken over a viscosity range of 1 to 390 centipoise and a density range of 1.00 g. to 1.25 g./cc. The particle Reynolds number  $Re_p$  varied between 0.001 and 58.2; the Reynolds number of the liquid in the empty column before entry into the bed varied from 0.12 to 7,700. Fluidization data were taken over the entire range, whereas it was possible to perform sedimentation experiments only at the lower Reynolds numbers.

## RESULTS

Data obtained at particle Reynolds numbers less than 0.07 agreed with the Vand-Hawksley theory. In Figures 3 and 4 the results for low Reynolds numbers are presented as a plot of  $U_c/U_0$  vs. fraction solids. In fluidization runs  $U_c$  is the fluid velocity based on the empty tube. In sedimentation runs  $U_c$  is the rate at which the bed settles. The solid line in Figures 3 and 4 is Equation (9).

In runs where both fluidization and sedimentation data were obtained no difference could be noted, even at higher

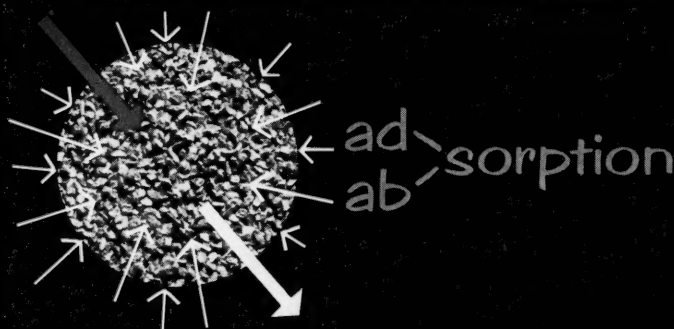
A uniform flow into the bed was necessary in order to obtain meaningful results. This was especially true at high void fractions. In order to obtain uniform flow a 7-in. section of copper turnings was introduced below the bed support and metal baffles were placed in the elbow. The bed support consisted of a copper screen soldered to a thin metal plate which was shaped to fit snugly in the column. A gravity feed was

employed for low flow rates, and at high throughputs a centrifugal pump was used. As fluids of high viscosity heated upon being circulated through the system, a heat exchanger controlled the temperature of the inlet fluid before it reached the column.

Special precautions were undertaken to obtain uniform spherical particles. The glass beads were manufactured by the Minnesota Mining and Manufacturing

## MIN CHEMISTRY at work

**case:** how M & C materials and methods get the job done by sorption processing



Ad- or ab-... whichever prefix to sorption you prefer... M & C works with you to get the right balance of medium, efficiency, purity, treating conditions and economy.

**Sorptive Mineral Report:** M & C offers many grades for many jobs.

**Molecules Out**—you can refine, purify, decolorize; remove odors, colors, taste, moisture, acids, sulfur compounds, fluorides, unsaturates, many others.

**Molecules In**—other grades serve as carriers in scores of processes.

**Anti-Caking**—often 1% or less of specific sorptive grades make sticky, waxy, hygroscopic chemicals free flowing.

**Drying**—M & C desiccants dry air, hydrogen, CO<sub>2</sub>, hydrocarbons, other fluids and gases.

Our business is to supply low-cost, nature-given materials that are process-engineered to make things go smooth in your plant... good in your markets. Use the coupon.

MINERALS & CHEMICALS CORPORATION OF AMERICA  
3058 Essex Turnpike, Menlo Park, N. J.

I'm interested in a natural mineral product for \_\_\_\_\_

Send: ☐ Detailed adsorbent literature ☐ Free samples

name \_\_\_\_\_ title \_\_\_\_\_

company \_\_\_\_\_

address \_\_\_\_\_

city \_\_\_\_\_ zone \_\_\_\_\_ state \_\_\_\_\_

For more data, see  
*Chemical Materials  
Catalog*  
Pages 330-334



## MINERALS & CHEMICALS

CORPORATION OF AMERICA  
3058 Essex Turnpike, Menlo Park, N. J.

*Leaders in creative use of non-metallic minerals*

ATTAPULGITE (Attapulgis)  
ACTIVATED BAUXITE (Porocel)  
KAOLIN (Edgar • ASPs)  
LIMESTONE (Chemstone)  
SPEEDI-DRI FLOOR ABSORBENTS

Reynolds numbers. Data from a typical run are shown in Figure 5.

Data at higher Reynolds numbers are presented in Figure 6, the terminal velocity  $U_0$  being calculated by the use of Equation (3). Data from reference 6 were used to evaluate  $C_D$ , and the Reynolds number used was  $Re_p = (D_p U_0 \rho) / (1 - c) \mu$ . The curve drawn in Figure 6 was calculated from Equation (9). The trend of individual runs did not agree too well with the Vand-Hawksley theory; however, the theory appears to be an approximation of the data obtained in this research at Reynolds numbers between 0.07 and 58.5.

A complete tabulation of the data and results of this research is contained in reference 1.

### VISUAL OBSERVATIONS

At particle Reynolds numbers below 0.8 the bed had a uniform appearance, with no large mass movements of the particles. The particles, however, were continually coming together in small groupings and then dispersing. At particle Reynolds numbers above 2 there became evident mass movements of groups of particles. At the highest Reynolds numbers for both the iron shot and the glass spheres the particle flow pattern consisted of a random eddying motion. There were large variations in the solids concentration, and the motion was quite similar to that obtained in gas-solid systems.

### NOTATION

- $c$  = fraction solids
- $C_D$  = particle drag coefficient
- $D_p$  = particle diameter
- $g$  = acceleration of gravity
- $Re_p$  = particle Reynolds number =  $D_p U_0 \rho / (1 - c) \mu$
- $U_0$  = free fall velocity of a single particle
- $U_c$  = settling velocity of a sedimenting bed; velocity of the fluid based on the empty tube cross section
- $U$  = actual fluid velocity
- $\mu$  = fluid viscosity
- $\mu_c$  = viscosity of a suspension
- $\rho$  = fluid density
- $\rho_s$  = solid density
- $\rho_c$  = density of a suspension

### LITERATURE CITED

1. Bandukwala, A. K., M.S. thesis, Univ. Illinois (1956).
2. Brinkman, H. C., *Appl. Sci. Res.*, **A1**, 27 (1947).
3. Hawksley, P. G. W., "Some Aspects of Fluid Flow," Arnold Press, New York (1950).
4. Vand, Vladimir, *J. Phys. & Colloid Chem.*, **52**, 277 (1948).
5. Verschoor, H., *Appl. Sci. Res.*, **A2**, 155 (1949-51).
6. Perry, J. H., ed., "Chemical Engineers' Handbook," 3 ed., McGraw-Hill Book Company, Inc., New York (1950).

typical  
s are  
minal  
e use  
nce 6  
the  
=  
wn in  
ation  
d not  
ksley  
rs to  
ained  
s be-  
and  
d in

elow  
ance,  
the  
were  
small  
par-  
here  
s of  
chest  
shot  
flow  
ying  
s in  
tion  
d in

article  
ating  
d on

Univ.

A1,

ts of  
York

olloid

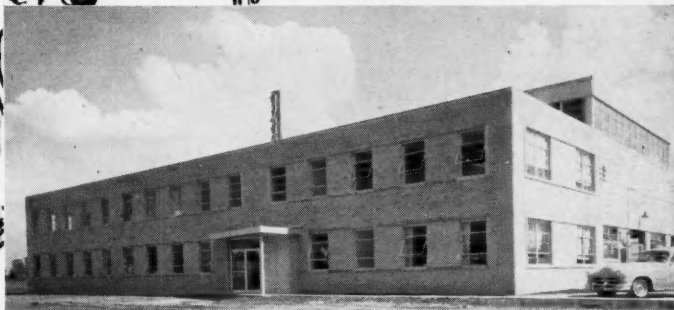
155

ers'  
Book

957



EIMCO RESEARCH AND DEVELOPMENT CENTER



PORTABLE TEST EQUIPMENT DOES RESEARCH WORK



**MODERN EQUIPMENT IS ESSENTIAL...**

## **BUT RESEARCH AND DEVELOPMENT DEPEND ON PEOPLE**

Modern equipment and machinery are very important . . . but notable gains in research and development still depend primarily on people.

Realizing this, Eimco exercised great care in selecting a staff of highly competent men interested in long-range research and development to guide the Eimco Research and Development Center at Palatine, Illinois.

The staff includes men who have received their training in the foremost educational institutions of the United States . . . men with informative backgrounds secured through many years of close association with the Process Industry and its problems.

With specialized equipment to enable them to

utilize more efficiently their knowledge and understanding of problems involved in liquids-solids separation through filtration . . . these men are (1) providing accurate conclusions fundamental to proper filter selection for a wide variety of chemical and metallurgical processes; (2) conducting critical examinations into existing filtration techniques and filter equipment and (3) undertaking comprehensive analytical research projects to develop new methods and designs.

Arrange today to have your Eimco sales engineer conduct a preliminary investigation into your process problem. He walks into your plant confident that — upon request — he has the support of skilled technologists using modern, complete test and research facilities.

**THE EIMCO CORPORATION**  
SALT LAKE CITY, UTAH

Research and Development Division, Palatine, Illinois

Export Offices: Eimco Building, 51-52 South Street, New York 5, N. Y.

Process Engineers Inc. Division, San Mateo, California

BRANCHES AND DEALERS IN PRINCIPAL CITIES THROUGHOUT THE WORLD



B-266

# COMMUNICATIONS TO THE EDITOR

## A Rate Equation for Molecular Diffusion in a Dispersed Phase

STANLEY H. JURY, University of Tennessee, Knoxville, Tennessee

Clarification appears necessary for the rate equation for molecular diffusion within a dispersed phase such as that of a granular solid or a relatively stagnant drop of fluid. One encounters, in connection with theoretical developments concerning this type of diffusion, statements that it has been "assumed" that a rate equation of the form

$$\text{rate} = \text{constant} (W^* - W) \quad (1)$$

is applicable. Here

$W$  = average concentration of a solute in a dispersed phase

$W^*$  = average concentration on the dispersed-phase side of the interface between dispersed and continuous phase

An effort is made in this note to elucidate the conditions under which Equation (1) is applicable. The constant in Equation

(1) is normally represented by the symbol  $ka$  with the units of reciprocal time. Specification of the true physical composition of  $ka$  follows as a by-product of the foregoing effort. Further a substitute rate equation is given for the shorter time intervals wherein rate equation (1) fails.

Wicke (1) in his treatment of a similar problem regarding an adsorbent granule came close to clarifying the situation without actually having recognized a basic conclusion of his work.

The governing equation for diffusion in a sphere of dispersed phase is

$$\frac{\partial C_s}{\partial t} = D \left[ \frac{\partial^2 C_s}{\partial r^2} + \frac{2}{r} \frac{\partial C_s}{\partial r} \right] \quad (2)$$

where

$C_s$  = point concentration of a solute in the sphere, mole/cu. ft.

$D$  = molecular diffusivity of mass, sq. ft./hr.

$r$  = radial position in sphere, ft.

$t$  = time, hr.

The limiting conditions are

$$C_s(r, 0) = C_i, \text{ a constant}$$

$$C_s(0, t) = \text{a maximum or minimum} \quad (3)$$

$$C_s(R, t) = C_s^*(t)$$

where

$$R = \text{radius of the sphere, ft.}$$

If for convenience one defines

$$U(r, t) = rC_s(r, t) \quad (4)$$

then

$$\frac{\partial U}{\partial t} = D \frac{\partial^2 U}{\partial r^2} \quad (5)$$

and

$$U(r, 0) = rC_i$$

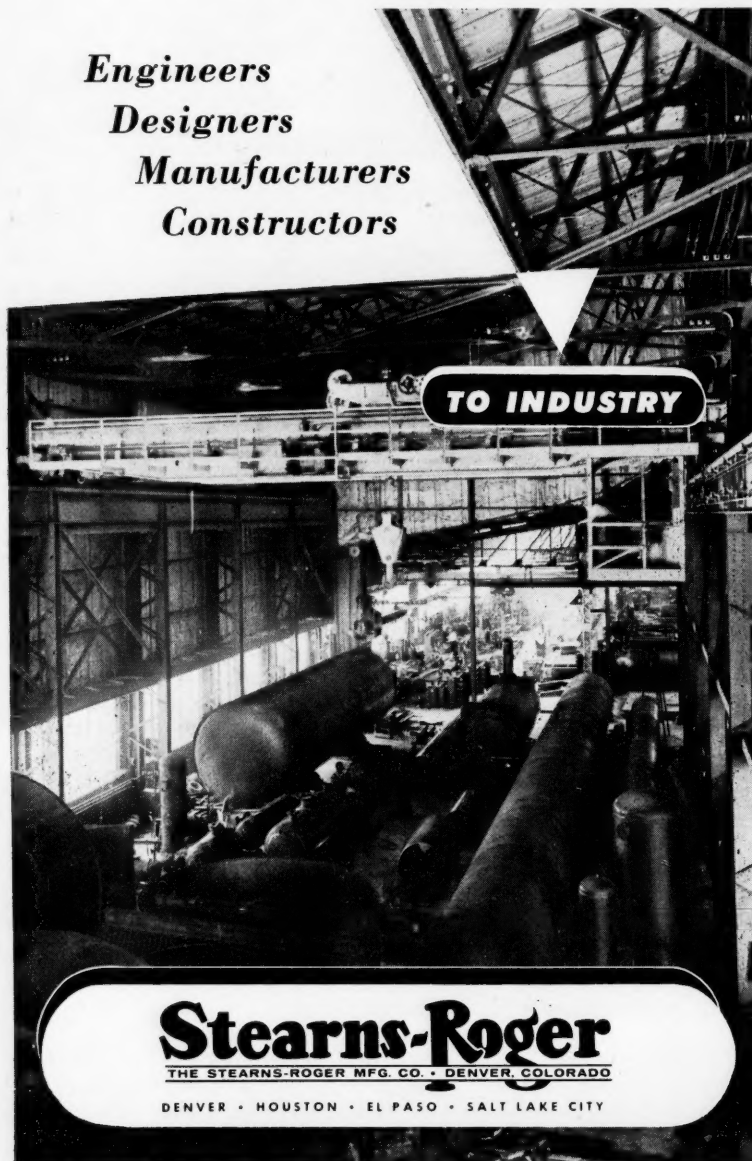
$$U(0, t) = 0 \quad (6)$$

$$U(R, t) = RC_s^*(t)$$

The solution to this problem and consequently to the original set out in Equations (2) and (3) is

$$C_s(r, t) - C_s^*(t) = \frac{2R}{\pi r} \int_0^1 \frac{dC_s^*(\phi)}{d\phi} \cdot \sum_{n=1}^{\infty} (-1)^n \frac{\sin n\pi \frac{r}{R}}{n} \cdot \exp \left\{ -\frac{Dn^2\pi^2}{R^2} (t - \phi) \right\} d\phi \quad (7)$$

**Engineers  
Designers  
Manufacturers  
Constructors**



**TO INDUSTRY**

**Stearns-Roger**  
THE STEARNS-ROGER MFG. CO. • DENVER, COLORADO  
DENVER • HOUSTON • EL PASO • SALT LAKE CITY



By definition

$$\frac{4}{3} \pi R^3 W(t) = \int_0^R 4\pi r^2 C_s(r, t) dr \quad (8)$$

and so if one substitutes for  $C_s(r, t)$  from (7) it is found that

$$W(t) = C_s^*(t) - \frac{6}{\pi^2} \sum_1^{\infty} \frac{1}{n^2} \cdot \exp \left\{ -\frac{D n^2 \pi^2 t}{R^2} \right\} \int_0^t \frac{dC_s^*(\phi)}{d\phi} \cdot \exp \left\{ \frac{n^2 \pi^2 D \phi}{R^2} \right\} d\phi \quad (9)$$

The time derivative of Equation (9), i.e., the rate equation for the dispersed phase, is

$$\frac{dW}{dt} = \frac{6D}{R^2} \sum_1^{\infty} \int_0^t \frac{dC_s^*(\phi)}{d\phi} \cdot \exp \left\{ -\frac{n^2 \pi^2 D(t - \phi)}{R^2} \right\} d\phi \quad (10)$$

The numerical value of the terms of the exponential series in Equations (9) and (10) drops rapidly for large values of  $n^2 \pi^2 D t / R^2$ , and so the first term of the series adequately represents the function. Under these circumstances one may write for Equation (9)

$$W(t) = W^*(t) - \frac{6}{\pi^2} \int_0^t \frac{dC_s^*(\phi)}{d\phi} \cdot \exp \left\{ -\frac{\pi^2 D}{R^2} (t - \phi) \right\} d\phi \quad (11)$$

and for (10)

$$\frac{dW}{dt} = \frac{6D}{R^2} \int_0^t \frac{dC_s^*(\phi)}{d\phi} \cdot \exp \left\{ -\frac{\pi^2 D}{R^2} (t - \phi) \right\} d\phi \quad (12)$$

Eliminating the integral expression between Equations (11) and (12) leads to the conclusion for longer times or in general larger values of  $\pi^2 D t / R^2$  that

$$\frac{dW}{dt} = \frac{\pi^2 D}{R^2} (W^* - W) \quad (13)$$

Further under these circumstances

$$ka = \frac{\pi^2 D}{R^2} \quad (14)$$

As the dimensionless group  $\pi^2 D t / R^2$  decreases in value to the point where terms involving  $n = 2, 3, \dots$  become significant, then one must return to the use of rate equation (10) since (13) will fail under these circumstances. These conclusions are independent of the distribution relation between  $C_s^*(t)$  and its continuous-phase counterpart, as this distribution relation has not been used in the derivation.

#### LITERATURE CITED

1. Wicke, E. von, *Kolloid Z.*, 93, 139 (1940).



## HEVI DUTY "MULTIPLE UNIT" MUFFLE FURNACE For Temperatures To 2000° F.

This furnace has been designed for general laboratory requirements such as drying of precipitates, ash determinations, fusions, ignitions, heating metals and alloys, enameling, heat treating, and experimental test work.

The efficient Hevi Duty Muffle Furnace shown is housed in a cylindrical shell mounted on a pyramidal type base with practically line contact between them . . . allowing for free circulation of air and eliminating trapped heat in the base. Available in four standard sizes.

For complete details, construction, and specifications, see your Laboratory Supply Dealer, or write for Bulletin LAB-849.

### "MULTIPLE UNIT"

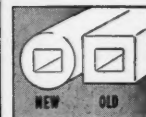
#### HEVI DUTY ELECTRIC COMPANY

MILWAUKEE 1, WISCONSIN

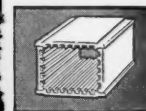
Heat Treating Furnaces... Electric Exclusively  
Dry Type Transformers Constant Current Regulators



Instruments and Controls operate at approximately room temperature . . . there is no trapped heat.



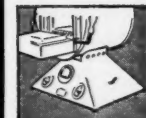
As a result of correct insulation design, you can shift rapidly to desired operating temperatures.



Reversible and easily replaceable Multiple Units, time-tested for 30 years, have been retained.



36 steps of control through a Hevi Duty Tap-Changing Transformer allows maximum flexibility of control.



Controls are mounted in a recessed position for safety and at correct angle for proper vision.



Rear panel is removable for access to terminal board. Release of front panel permits control assembly to slide forward.



measuring  
space and  
matter  
in microns

to give  
you better

# SPRAY NOZZLES

The microscopic structure of a spray is a world of spherical bodies in motion with "wide" spaces in between. This is one of the levels of observation where our research engineers obtain important data for better spray nozzle design and performance.

For complete information, write for Catalog 24.

**SPRAYING SYSTEMS CO.**  
3210 RANDOLPH • BELLWOOD, ILLINOIS

ADVANCED SPRAY NOZZLE DESIGN FOR NEW  
DIMENSIONS IN CONTROL AND PERFORMANCE

## INDEX OF ADVERTISERS

Beckman Instruments, Inc. . . . . Inside Back Cover	Ohaus Scale Corporation . . . . . 5J
Bowen Engineering, Inc. . . . . 146	Spraying Systems Company . . . . . 10J
Eimco Corporation, The . . . . . 7J	Stearns Rodger Mfg. Company . . . . . 8J
Hevi Duty Electric Company . . . . . 9J	Titanium Alloy Mfg. Div. . . . . 6J
Minerals & Chemicals Corp. of America 296	Wiley & Sons, Inc., John . . . . . 4J
Mixing Equipment Co. . . . . Outside Back Cover	York Process Equipment Corp. Inside Front Cover

## Advertising Offices

New York 36—Lansing T. Dupree, Adv. Mgr.; John M. Gaede, Asst. Adv. Mgr.; Paul A. Jolcuvar, Dist. Mgr.; Donald J. Stroop, Dist. Mgr.; Hale H. Carey, Dist. Mgr.; 25 W. 45th St., Columbus 5-7330.

Chicago 11—Richard R. Quinn, Dist. Mgr., 612 North Michigan Ave., Room 507, Superior 7-0385.

Cleveland 15—Eugene B. Pritchard, Dist. Mgr., 1836 Euclid Ave., Superior 1-3315.

Pasadena 1—Richard P. McKey, Dist. Mgr., 465 East Union St., Ryan 1-8779.

Dallas 28—Richard E. Hoierman, Dist. Mgr., 2831 El Capitan Drive, Davis 7-3630.

Birmingham 9, Ala.—Fred W. Smith, Dist. Mgr., 1201 Forest View Lane—Vesthaven, Tremont 1-5762.

## EXCHANGE

Articles recently published in *Chemical Engineering Progress* that may be of interest to *Journal* readers will be listed regularly in these columns. *C. E. P.* is published monthly by the American Institute of Chemical Engineers, 25 West 45 Street, New York 36, New York, and is available on subscription for \$6.00 for one year, \$10.00 for two years; foreign subscriptions are \$8.00 annually, except in Canada, where the price is \$6.50, and in the Pan American Union, where it is \$7.50. Single copies are 75 cents unless more than a year old.

### VOLUME 53, NUMBER 2 (FEBRUARY, 1957)

Decontamination of Irradiated Uranium by a Fluoride Volatility Process, William J. Mecham, Robert C. Liimatainen, Robert W. Kessie, and Waldemar B. Seefeldt.

Volume Reduction of Radioactive Waste by Carrier Precipitation, R. E. Burns and M. J. Stedwell

Fuel Cycles in Single-region Thermal Reactors, Manson Benedict and Thomas H. Pigford

### VOLUME 53, NUMBER 3 (MARCH, 1957)

Recent Findings on Dust Explosions, Irving Hartmann

The Role of Air Contaminants in Formulating Oxygen Plant Safety Principles, Clyde McKinley and Franklin Himmelberger

The Falling-film Hydrochloric Acid Absorber, W. M. Gaylord and M. A. Miranda

### VOLUME 53, NUMBER 4 (APRIL, 1957)

The Mechanism of Hot-surface Drying of Fibrous Sheets, Arthur C. Dreshfield, Jr.

Safety Aspects of Modern Air-separation Plant Cycles, F. G. Kerry

Status of Electric Membrane Demineralization, William E. Katz

For those of our readers interested in chemical engineering papers published abroad, we shall from time to time note the table of contents of a current issue of *Chemical Engineering Science*, published by the Pergamon Press, Ltd., 4 and 5 Fitzroy Square, London W. 1, England. In volume 6, number 4/5, appear

K. J. Cannon and K. G. Denbigh, Studies on Gas-solid Reactions:

I. The Oxidation Rate of Zinc Sulphide 145

II. Causes of Thermal Instability 155

E. Wicke, Einige neue Verfahrensprinzipien mit Wirbelschichten 160

Owen E. Potter, Mass Transfer between Co-current Fluid Streams and Boundary Layer Solutions 170

H. E. Hoelscher, Temperature Stability of Fixed-bed Catalytic Converters 183

P. M. Heertjes, Studies in Filtration. Blocking Filtration 190

R. W. Maxwell and J. Anderson Storow, Mercury Vapour Transfer Studies: I 204

J. J. Keyes, Jr., and R. L. Pigford, Diffusion in a Ternary Gas System with Application to Gas Separation 215

Octave Levenspiel and W. K. Smith, Notes on the Diffusion-type Model for the Longitudinal Mixing of Fluids in Flow 227

chemical  
be of  
e listed  
. P. is  
a Insti-  
vest 45  
and is  
for one  
n sub-  
cept in  
d in the  
\$7.50.  
s more

957)  
ium by  
liam J.  
Robert  
feldt.  
aste by  
ns and  
al Re-  
mas H.

osions,  
rmulat-  
nciples,  
immel-  
d Ab-  
M. A.

ying of  
eld, Jr.  
aration  
eraliza-

ted in  
blished  
e note  
ssue of  
blished  
and 5  
nd. In

h,  
ul-  
145  
155  
n-  
160  
ee-  
nd  
170  
a-  
n-  
183  
n.  
190  
or-  
er  
204  
d,  
m  
on 215  
h,  
el  
ds  
227

1957